frontiers | Research Topics

Fish molecular innate immunity and innate immune responses against pathogens

Edited by
Jun Li, Sun Yun, Heng Chi, Mofei Li and Chunsheng Liu

Published in
Frontiers in Immunology

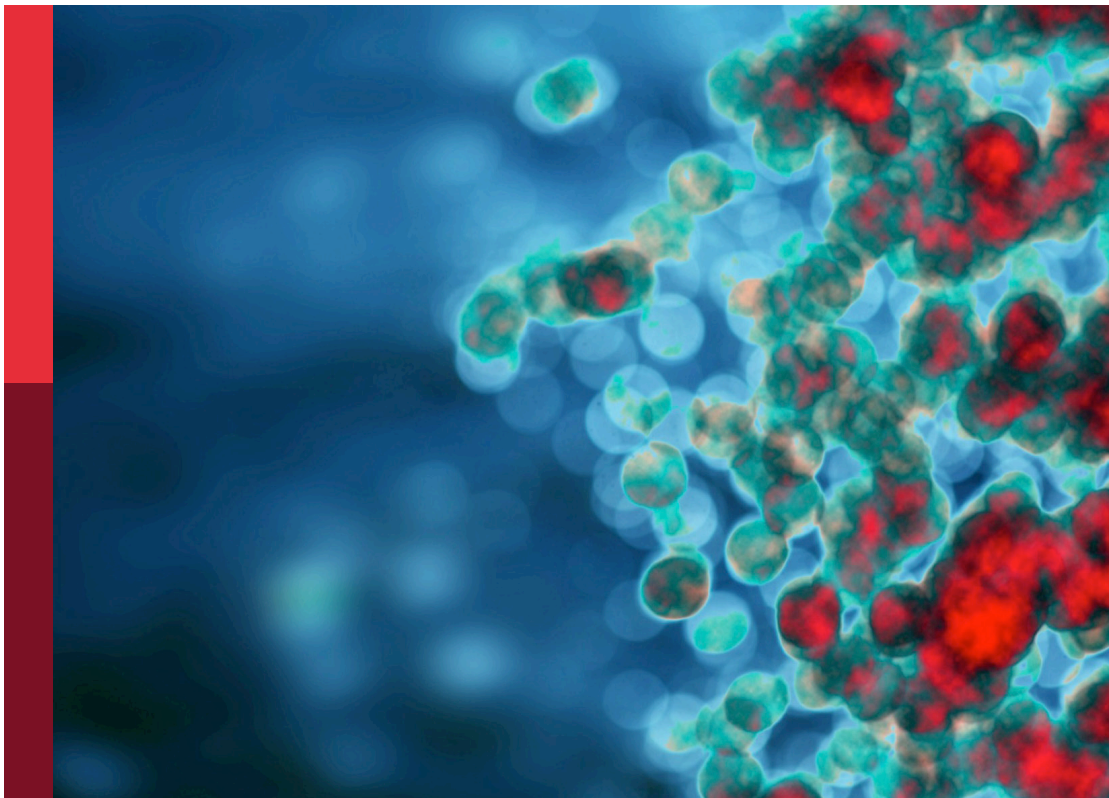

ISSN 1664-8714
ISBN 978-2-8325-3313-0
DOI 10.3389/978-2-8325-3313-0

About Frontiers

Frontiers is more than just an open access publisher of scholarly articles: it is a pioneering approach to the world of academia, radically improving the way scholarly research is managed. The grand vision of Frontiers is a world where all people have an equal opportunity to seek, share and generate knowledge. Frontiers provides immediate and permanent online open access to all its publications, but this alone is not enough to realize our grand goals.

Frontiers journal series

The Frontiers journal series is a multi-tier and interdisciplinary set of open-access, online journals, promising a paradigm shift from the current review, selection and dissemination processes in academic publishing. All Frontiers journals are driven by researchers for researchers; therefore, they constitute a service to the scholarly community. At the same time, the *Frontiers journal series* operates on a revolutionary invention, the tiered publishing system, initially addressing specific communities of scholars, and gradually climbing up to broader public understanding, thus serving the interests of the lay society, too.

Dedication to quality

Each Frontiers article is a landmark of the highest quality, thanks to genuinely collaborative interactions between authors and review editors, who include some of the world's best academicians. Research must be certified by peers before entering a stream of knowledge that may eventually reach the public - and shape society; therefore, Frontiers only applies the most rigorous and unbiased reviews. Frontiers revolutionizes research publishing by freely delivering the most outstanding research, evaluated with no bias from both the academic and social point of view. By applying the most advanced information technologies, Frontiers is catapulting scholarly publishing into a new generation.

What are Frontiers Research Topics?

Frontiers Research Topics are very popular trademarks of the *Frontiers journals series*: they are collections of at least ten articles, all centered on a particular subject. With their unique mix of varied contributions from Original Research to Review Articles, Frontiers Research Topics unify the most influential researchers, the latest key findings and historical advances in a hot research area.

Find out more on how to host your own Frontiers Research Topic or contribute to one as an author by contacting the Frontiers editorial office: frontiersin.org/about/contact

Fish molecular innate immunity and innate immune responses against pathogens

Topic editors

Jun Li — Lake Superior State University, United States
Sun Yun — Hainan University, China
Heng Chi — Ocean University of China, China
Mofei Li — Tianjin Normal University, China
Chunsheng Liu — Hainan University, China

Citation

Li, J., Yun, S., Chi, H., Li, M., Liu, C., eds. (2023). *Fish molecular innate immunity and innate immune responses against pathogens*. Lausanne: Frontiers Media SA.
doi: 10.3389/978-2-8325-3313-0

Table of contents

frontiers | Frontiers in Immunology

TYPE Original Research
PUBLISHED 18 October 2022
DOI 10.3389/fimmu.2022.1027064

OPEN ACCESS

EDITED BY
Heng Chi,
Ocean University of China, China

REVIEWED BY
Houguo Xu,
Yellow Sea Fisheries Research Institute (CAFS), China
Yunji Xiu,
Qingdao Agricultural University, China

*CORRESPONDENCE
Xiao-Qiu Zhou
zhouxq@sicau.edu.cn
Lin Feng
fenglin@sicau.edu.cn

†These authors have contributed equally to this work

SPECIALTY SECTION
This article was submitted to Molecular Innate Immunity, a section of the journal Frontiers in Immunology

RECEIVED 24 August 2022
ACCEPTED 26 September 2022
PUBLISHED 18 October 2022

CITATION
He X-N, Zeng Z-Z, Wu P, Jiang W-D, Liu Y, Jiang J, Kuang S-Y, Tang L, Feng L and Zhou X-Q (2022) Dietary Aflatoxin B1 attenuates immune function of immune organs in grass carp (Ctenopharyngodon idella) by modulating NF-κB and the TOR signaling pathway.
Front. Immunol. 13:1027064.
doi: 10.3389/fimmu.2022.1027064

Dietary Aflatoxin B1 attenuates immune function of immune organs in grass carp (Ctenopharyngodon idella) by modulating NF-κB and the TOR signaling pathway

Xiang-Ning He[1†], Zhen-Zhen Zeng[1†], Pei Wu[1,2,3], Wei-Dan Jiang[1,2,3], Yang Liu[1,2,3], Jun Jiang[1,2,3], Sheng-Yao Kuang[4], Ling Tang[4], Lin Feng[1,2,3*] and Xiao-Qiu Zhou[1,2,3*]

[1]Animal Nutrition Institute, Sichuan Agricultural University, Chengdu, China, [2]Fish Nutrition and Safety Production University Key Laboratory of Sichuan Province, Sichuan Agricultural University, Chengdu, China, [3]Key Laboratory for Animal Disease-Resistance Nutrition, Ministry of Education, Ministry of Agriculture and Rural Affairs, Key Laboratory of Sichuan Provence, Chengdu, China, [4]Animal Nutrition Institute, Sichuan Academy of Animal Science, Chengdu, China

Aflatoxin B1 (AFB1) is kind of a common mycotoxin in food and feedstuff. Aquafeeds are susceptible to contamination of AFB1. In teleost fish, the spleen and head kidney are key immune organ. Moreover, the fish skin is a critical mucosal barrier system. However, there was little study on the effects of dietary AFB1 on the immune response of these immune organs in fish. This study aimed to explore the impacts of oral AFB1 on the immune competence and its mechanisms in the skin, spleen, and head kidney of grass carp. Our work indicated that dietary AFB1 reduced antibacterial compounds and immunoglobulins contents, and decreased the transcription levels of antimicrobial peptides in grass carp immune organs. In addition, dietary AFB1 increased the transcription levels of pro-inflammatory cytokines and reduced the transcription levels of anti-inflammatory cytokines in the grass carp immune organs, which might be regulated by NF-κB and TOR signaling, respectively. Meanwhile, we evaluated the content of AFB1 in the grass carp diet should not exceed 29.48 μg/kg diet according to the levels of acid phosphatase and lysozyme. In summary, dietary AFB1 impaired immune response in grass carp skin, spleen, and head kidney.

KEYWORDS

AFB1, spleen, head kidney, skin, immune

Introduction

As the plant raw materials gradually in place of animal raw materials, the contamination of agriculture products by mycotoxin is a worldwide concern problem, which caused a problem of feed safety, including aquafeed (1). Aflatoxin B1 (AFB1) is a kind of common mycotoxin, which could induce inflammatory response in mutton sheep muscle (2). It was found that AFB1 could be detected in fish feed in most areas, and up to 150 μg/kg (3). Fish that consume AFB1-contaminated feed experience detrimental health effects, and even endanger human health (4). The only study found that AFB1 induced intestinal inflammation by upregulating *TNF-α* and *IL-1β* mRNA expression in rainbow trout (5). Previous research demonstrated that AFB1 stunted the growth of grass carp (6). It has been known that the growth of fish is associated with its immunity (7). As central immune organs in teleost fish, the spleen and head kidney are responsible for regulating immune response (8), containing large numbers of lymphocytes and macrophages (9, 10). As we all know, lymphocytes and macrophages are an essential part of the immune system (11). The fish's skin, an important mucosal defense organ, has developed a mature immune barrier to protect the whole body from pathogens invasion (12, 13). Currently, there is no study has been conducted on how AFB1 affects fish skin, spleen, and head kidney immunity. According to a previous report, organs' function is closely related to their structural integrity (14). Huang et al. (15) study found that deoxynivalenol (DON) damaged the structural integrity of grass carp intestinal, which resulted in a decrease in the intestinal immune function (16). Another previous research exhibited that AFB1 disrupted the structure of the spleen and head kidney, causing tissue vacuolar degeneration, melanoma macrophage center, and cell necrosis (6). The above studies indicate that the reduction of fish immunity by AFB1 may be related to the destruction of mucosal immunity and central immune, which is worthy of further study.

The spleen and head kidney are the heart of systemic immunity, which are involved in the process of systemic immune response (17, 18). When inflammation occurs, the spleen and head kidney usually respond by secreting antimicrobial substances and cytokines (19). It is well known that skin serves as the first line of defense against invading pathogens (12). It has been shown that in fish skin, goblet cells and lymphocytes secrete antibacterial compounds and immunoglobulin (20). In addition, skin is a crucial immunological organ in fish, which forms a better immune barriers system to protect the body from attacks. Our previous studies found that obvious yellowing of surface was observed on grass carp skin with the increasing AFB1 concentration. We hypothesized that AFB1 might aggravate inflammation in grass carp skin. However, there is no report about the effect of AFB1 on antibacterial compounds and cytokines in the skin, spleen, and head kidney of fish. Yang et al. (21) found that AFB1 decreased the immune parameters (e.g. IgM, C3, and C4) in juvenile turbot serum. In addition, AFB1 decreased the viability and induced an inflammatory response in macrophages (22). Meanwhile, one study found that AFB1 upregulated the gene levels of *IL-1β* in the intestine mucosa of the broiler (23), but another study suggested that dietary AFB1 did not change *IL-1β* gene expression in sheep muscle (2). The above results indicated that different animal tissues have different immune responses to AFB1. However, beyond this, Guo et al. (24) found that AFB1 upregulated significantly the mRNA levels of pro-inflammatory cytokines *IL-6*, *IL-8*, and *TNF-α* in kidney cells of chicken embryos. And Cao et al. (2) found that AFB1 downregulated the mRNA level of anti-inflammatory cytokine *IL-10* in mutton sheep muscle. Studies conducted above indicated that AFB1 could induce inflammation in animals. However, there is no relevant report on the immune response of AFB1 to fish skin, spleen, and head kidney. So it is necessary to study the impacts of AFB1 on the immune competence of the skin, spleen, and head kidney of fish.

It is well known that an important transcription factor nuclear factor kappa B p65 (NF-κB p65) is involved in inflammatory responses (25). When the NF-κB is activated, it increases the transcription of proinflammatory cytokines (26). It has not been reported that AFB1 regulates the immune response of fish immune organs through NF-κB and target of rapamycin (TOR) signaling pathways. It was reported that AFB1 activated NF-κB signaling pathways and induced inflammatory responses in ducks' ileum (27). Another study found that AFB1 upregulated *NF-κB p65* mRNA expression and induced inflammatory responses in chicken embryos' primary intestinal epithelium (24). These results indicated that AFB1 could induce inflammatory responses in animals by activating the NF-κB signaling pathway. Furthermore, the TOR pathway has a significant role to play in immunoregulation (28). It was reported that anti-inflammatory cytokines in the skin, spleen, and head kidney of fish are regulated by the TOR signaling pathway (12, 29). Ivanovics et al. (30) found that AFB1 exposure significantly reduced the arginine level in zebrafish larvae lysates. Chen et al. (31) reported that arginine deficiency downregulated TOR mRNA expression in Jian carp (*Cyprinus carpio* var. *Jian*) spleen and head kidney. Following the above reports, we speculate that AFB1 might induce inflammatory responses through NF-κB p65 and mTOR signaling pathways, which needs further in-depth studies.

Grass carp is a kind of important economic freshwater fish in China, accounting for more than 18% of total freshwater aquaculture production in 2017 (32). It is well known that grass carp belong to herbivorous fish, it is usually with plant protein raw materials in the majority of commercial feed (33). Thus, in the process of large-scale commercial production of fish feed, it is very likely that there is a problem with excess AFB1 residue. Our research has focused on the immune components

and cytokines and its relative signaling of grass carp skin, spleen, and head kidney. Furthermore, we evaluated the AFB1 safe upper dose for grass carp according to the ACP and LZ, to provide a practical reference for production.

Materials and methods

Composition of test feeds

The feed formulation was identical to our previous research (6). A basal experimental diet was prepared using casein, gelatin, and fish meal as protein sources, soybean oil, and fish oil as lipid sources. All feed ingredients contain no AFB1. The relative diet's nutrition levels met the growing need for juvenile grass crap. AFB1 (purity > 98%) was bought from Pribolab Pte. Ltd. (Singapore). There were six different concentrations [0 (un-supplement), 30, 60, 90, 120, and 150 μg/kg diet, respectively] of AFB1 in the feed. We used high-performance liquid chromatographic (HPLC) to measure the actual concentration, which were 0.04 (un-supplement), 29.48, 58.66, 85.94, 110.43 and 146.92 μg/kg diet, respectively.

Feeding trial

The use of animals in experiments was under the regulations established by the Sichuan Agricultural University Animal Care Advisory Committee. After purchase, the grass carp were adapted to the environment for 28 days before the experiment. The average weight of the grass carp was 12.96 ± 0.03 g. They were randomly allocated into 6 groups of three replicated cages. Our experiment was conducted outdoor. The average water temperature is 28.5 ± 2°C. The pH value was around 7.5 ± 0.3. We maintained the dissolved oxygen in water > 6.0 mg/L by adjusting the oxygenator. The experiment was carried out under a natural light cycle.

Challenge test and sample collection

The grass carp was challenged with *A. hydrophila* for 2 weeks after the growth experiment. *A. hydrophila* infection is a serious problem in aquaculture (34), which is usually used to evaluate the effect on the immunity of fish (35). Our *A. hydrophila* was generously gifted by the College of Veterinary Medicine, Sichuan Agricultural University. 15 fish were treated with an intraperitoneal injection of *A. hydrophila* (1.0 *ml*, $2.5x10^6$ colony-forming units (CFU)/ml) for every treatment. And the control group was infected with 1.0 ml saline.

All the fish were anesthetized with benzocaine (50 mg/L) after the challenge test. The samples were selected and flash frozen on liquid nitrogen, a portion of the samples was quickly frozen in a -20°C freezer for the analysis of immune components, and the other part of the samples were removed in a -80°C freezer for PCR and Western blot analysis.

Immune components analysis

The sample preparation for immune components determination was referenced by Lu et al. (12). The immunoglobulin M (IgM), ACP, and Lysozyme (LZ) activity, complement component 3 (C3), and component 4 (C4) contents were tested by assay kit (Nanjing Jiancheng, Chain). According to the kit instructions, the specific operation was performed.

Real-time PCR

The RNAiso Plus kit (TaKaRa, China) was used to extract total RNA. RNA concentrations were obtained by spectrophotometry, and RNA quality was confirmed by agarose gel electrophoresis (1%). Then, cDNA synthesis was performed with a cDNA synthesis Kit (Takara, China). The quantitative real-time PCR primers were indicated in Table 1. The β-actin was used as an internal reference gene.

Western blot

An aliquot of the homogenates was used for protein measurement, the method was performed as our lab method (36). For each sample, total proteins (40 μg) were extracted and separated on sodium dodecyl sulfate-polyacrylamide gel electrophoresis (8%) and then transferred to polyvinylidene-fluoride membrane immunoblotting membranes. The membranes were incubated overnight in the primary antibody at 4°C. Then the membranes were washed and incubated with the secondary antibodies at room temperature for 90 min. Immunocomplexes were visualized by enhanced chemiluminescence reagents (Beyotime Biotechnology Inc., China), then quantifications were performed in Image 1.63 software. The information of antibodies was listed in Supplementary Table 1.

Statistical analysis

All data were represented as the mean ± standard deviation (SD). Significance differences among groups were determined by using one-way analysis of variance (ANOVA). The significant difference among the different groups' means was tested by using Duncan's multiple ranges, and data were analyzed by SPSS 18.0 (SPSS Inc., Chicago, IL, USA). The experiment data were visualized by GraphPad 8.0 software and the Hiplot platform (12).

10.3389/fimmu.2022.1027064

TABLE 1 Characteristics of different expression genes related to immune function.

Target gene	Primer sequence Forward (5'→3')	Primer sequence Reverse (5'→3')	Temperature(°C)	Accession number
hepcidin	AGCAGGAGCAGGATGAGC	GCCAGGGGATTTGTTTGT	59.3	JQ246442.1
LEAP-2A	TGCCTACTGCCAGAACCA	AATCGGTTGGCTGTAGGA	59.3	FJ390414
LEAP-2B	TGTGCCATTAGCGACTTCTGAG	ATGATTCGCCACAAAGGGG	59.3	KT625603
β-defensin-1	TTGCTTGTCCTTGCCGTCT	AATCCTTTGCCACAGCCTAA	58.4	KT445868
Mucin2	GAGTTCCCAACCCAACACAT	AAAGGTCTACACAATCTGCCC	60.4	KT625602
IFN-γ2	TGTTTGATGACTTTGGGATG	TCAGGACCCGCAGGAAGAC	60.4	JX657682
TNF-α	CGCTGCTGTCTGCTTCAC	CCTGGTCCTGGTTCACTC	58.4	HQ696609
IL-1β	AGAGTTTGGTGAAGAAGAGG	TTATTGTGGTTACGCTGGA	57.1	JQ692172
IL-6	CAGCAGAATGGGGGAGTTATC	CTCGCAGAGTCTTGACATCCTT	62.3	KC535507.1
IL-8	ATGAGTCTTAGAGGTCTGGGT	ACAGTGAGGGCTAGGAGGG	60.3	JN663841
IL-10	AATCCCTTTGATTTTGCC	GTGCCTTATCCTACAGTATGTG	61.4	HQ388294
IL-12p35	TGGAAAAGGAGGGGAAGATG	AGACGGACGCTGTGTGAGTGTA	55.4	KF944667.1
IL-12p40	ACAAAGATGAAAAACTGGAGGC	GTGTGTGGTTTAGGTAGGAGCC	59.0	KF944668.1
IL-15	CCTTCCAACAATCTCGCTTC	AACACATCTTCCAGTTCTCCTT	61.4	KT445872
IL-17D	GTGTCCAGGAGAGCACCAAG	GCGAGAGGCTGAGGAAGTTT	62.3	KF245426.1
IL-4/13A	CTACTGCTCGCTTTCGCTGT	CCCAGTTTTCAGTTCTCTCAGG	55.9	KT445871
IL-4/13B	TGTGAACCAGACCCTACATAACC	TTCAGGACCTTTGCTGCTTG	55.9	KT625600
TGF-β1	TTGGGACTTGTGCTCTAT	AGTTCTGCTGGGATGTTT	55.9	EU099588
TGF-β2	TACATTGACAGCAAGGTGGTG	TCTTGTTGGGGATGATGTAGTT	55.9	KM279716
NF-κB p52	TCAGTGTAACGACAACGGGAT	ATACTTCAGCCACACCTCTCTTAG	58.4	KM279720
NF-κB p65	GAAGAAGGATGTGGGAGATG	TGTTGTCGTAGATGGGCTGAG	62.3	KJ526214
c-Rel	GCGTCTATGCTTCCAGATTTACC	ACTGCCACTGTTCTTGTTCACC	59.3	KT445865
IκBα	TCTTGCCATTATTCACGAGG	TGTTACCACAGTCATCCACCA	62.3	KJ125069
IKKα	GGCTACGCCAAAGACCTG	CGGACCTCGCCATTCATA	60.3	KM279718
IKKβ	GTGGCGGTGGATTATTGG	GCACGGGTTGCCAGTTTG	60.3	KP125491
IKKγ	AGAGGCTCGTCATAGTGG	CTGTGATTGGCTTGCTTT	58.4	KM079079
TOR	TCCCACTTTCCACCAACT	ACACCTCCACCTTCTCCA	61.4	JX854449
S6K1	TGGAGGAGGTAATGGACG	ACATAAAGCAGCCTGACG	54.0	EF373673
4E-BP1	GCTGGCTGAGTTTGTGGTTG	CGAGTCGTGCTAAAAAGGGTC	60.3	KT757305
4E-BP2	TGTGCCATTAGCGACTTCTGAG	ATGATTCGCCACAAAGGGG	59.3	KT625603
β-actin	GGCTGTGCTGTCCCTGTA	GGGCATAACCCTCGTAGAT	61.4	M25013

Results

Skin phenotype

It is well known that skin rot is the typical symptom of *Aeromonas hydrophila* infection in fish. Our previous study found that obvious yellowing of surface were observed on grass carp skin with the increasing AFB1 concentration, which is the typical symptom of skin rot (6). As shown in Figure 1, compared to the control group (0.04 μg/kg diet), the skin rot was increased with the increase of AFB1 (58.66-146.92 μg/kg diet), and showed a highly positive correlation.

Immune parameters in skin, spleen, and head kidney of grass carp

The immune-related parameters of skin, spleen, and head kidney were given in Figure 2. In the skin, the C3, C4, and IgM content and the LZ, ACP activities were reduced when the dose of AFB1 reached 58.66, 58.66, 29.48, 58.66, and 58.66 μg/kg diet ($P < 0.05$), respectively. But in the spleen and head kidney, the above immune parameters were decreased with the level of AFB1 up to 58.66, 29.48, 85.94, 58.66, and 58.66 μg/kg diet ($P < 0.05$), respectively. The immune components reached the lowest level in the 146.92 μg/kg diet groups in the immune organs of grass carp.

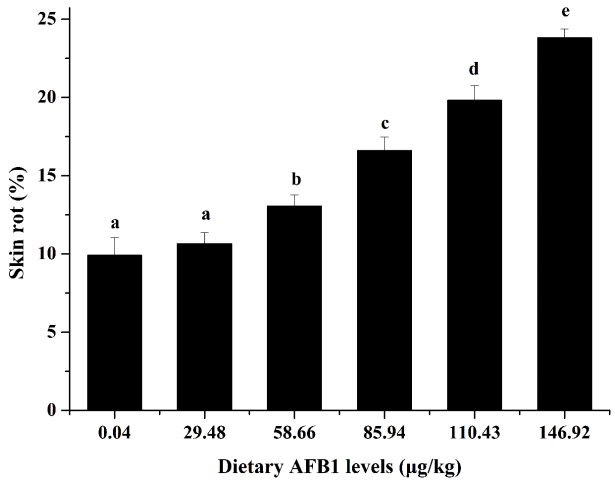

FIGURE 1
Effects of dietary AFB1 (μg/kg) on skin rot of grass carp after challenged with *A. hydrophila*. n=6 (six fish in each group). Different letters indicate significant differences ($P < 0.05$).

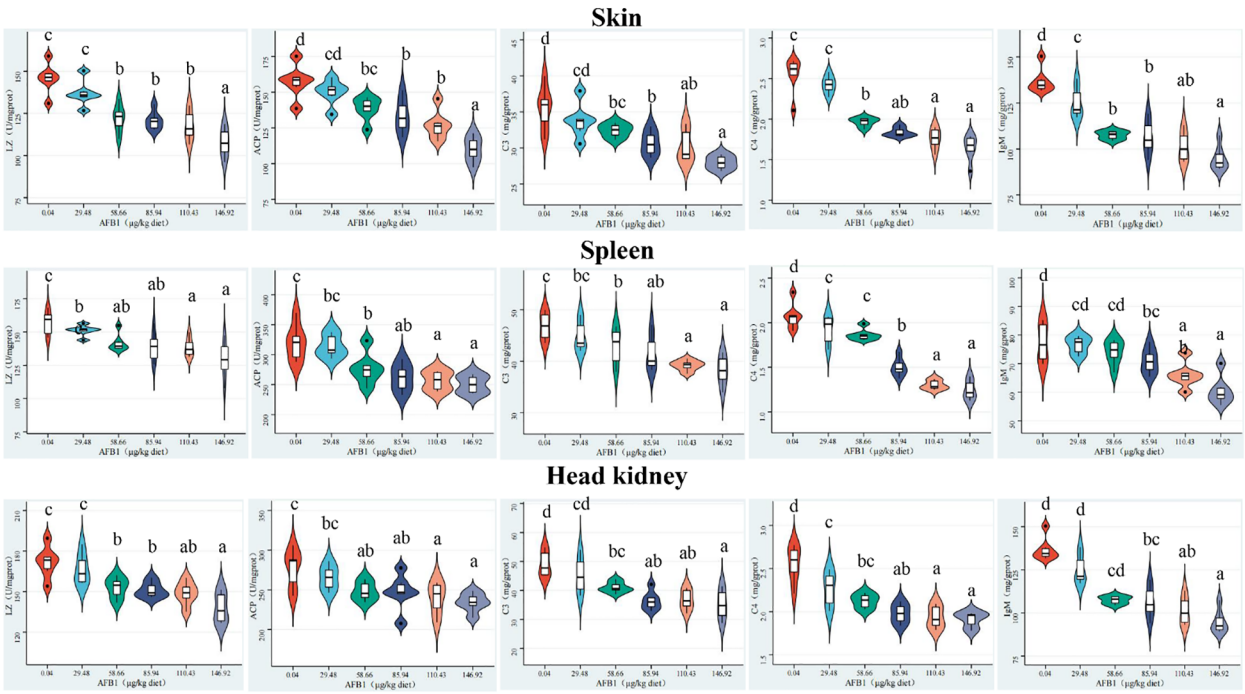

FIGURE 2
Effects of dietary AFB1 (μg/kg) on the immune parameters (LZ, ACP, C3, C4, IgM) of skin, spleen, and head kidney of grass carp after challenged with *A. hydrophila*. n=6 (six fish in each group). Different letters represent a significance difference ($P < 0.05$).

The transcription levels of antimicrobial peptides and mucin in skin, spleen, and head kidney of grass carp

In Figure 3, in the skin, the gene expression of *hepcidin*, *β-defensin-1*, *LEAP-2A*, *Mucin2*, and *LEAP-2B* were significantly downregulated with the dose of AFB1 up to 85.94, 85.94, 58.66, 85.94, and 85.94μg/kg diet ($P < 0.05$), respectively. In the spleen, there was a significantly decreased in *β-defensin-1*, *LEAP-2A*, *Mucin2*, and *LEAP-2B* gene expression when the dietary AFB1 dose was up to 58.66, 85.94, 85.94, and 85.94 μg/kg diet ($P < 0.05$), respectively. In the head kidney, the gene expression of *β-defensin-1*, *LEAP-2A*, *Mucin2*, and *LEAP-2B* were significantly decreased when the dose of AFB1 reached 58.66, 85.94, 58.66, and 58.66 μg/kg diet ($P < 0.05$), respectively. Interestingly, in the spleen and head kidney, *hepcidin* mRNA expression had not changed at any level of AFB1.

The transcription levels of inflammatory cytokines and inflammatory response-related signal molecules in skin, spleen, and head kidney of grass carp

The pro-inflammatory cytokines were shown in Figure 4. In the skin, the gene expression of *IL-8*, *IL-15*, *IL-6*, *IL-17D*, tumor necrosis factor α (*TNF-α*), interferon γ2 (*IFN-γ2*), and *IL-12p40* were significantly upregulated with the AFB1 levels up to 58.66, 110.43, 58.66, 85.94, 85.94, 58.66, and 85.94 μg/kg diet ($P < 0.05$), respectively. In the spleen, the gene expression of the above pro-inflammatory cytokines was significantly upregulated with the AFB1 levels up to 85.94, 58.66, 85.94, 58.66, 85.94, 58.66, and 85.94 μg/kg diet ($P < 0.05$), respectively. In the head kidney, the gene expression of the above pro-inflammatory cytokines was significantly upregulated with the AFB1 levels up to 85.94, 85.94, 58.66, 85.94, 85.94, 110.43, and 85.94 μg/kg diet ($P < 0.05$),

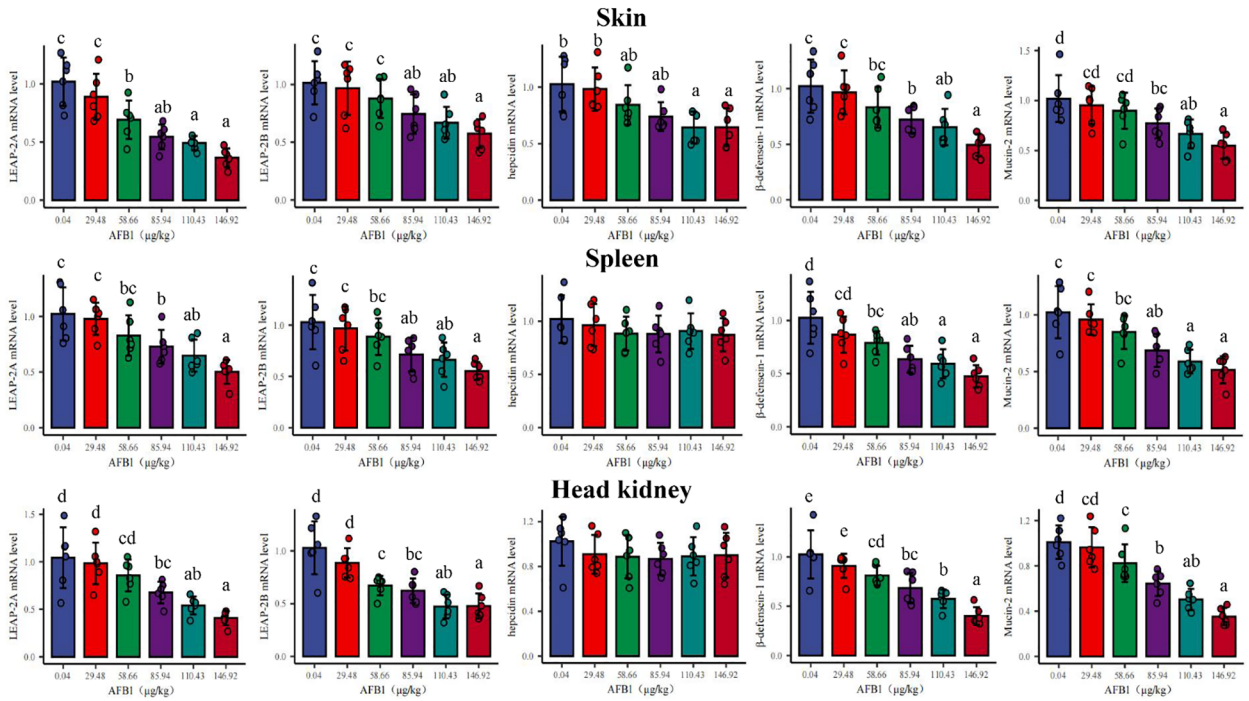

FIGURE 3
Effects of dietary AFB1 (μg/kg) on the mRNA levels of antibacterial peptides (*LAEP-2A*, *LEAP-2B*, *hepcidin*, *β-defenscin-1*) and *Mucin-2* of skin, spleen, and head kidney of grass carp after challenged with *A. hydrophila*. n=6 (six fish in each group). Different letters represent a significance difference (P < 0.05).

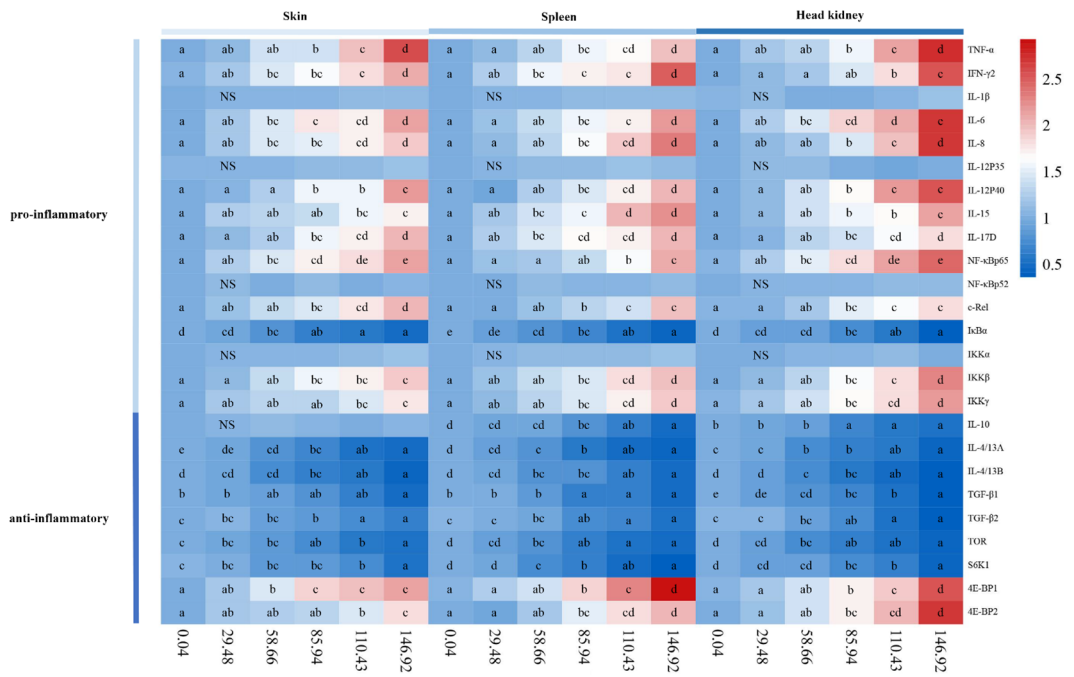

FIGURE 4
Heat-map of AFB1-changed mRNA levels of pro-inflammatory cytokines, anti-inflammatory cytokines, and inflammatory response related signal molecules in skin, spleen and head kidney of grass carp after *A. hydrophila* infection. n=6 (six fish in each group). Different letters indicate significant differences (P < 0.05).

respectively. Interestingly, in the skin, spleen, and head kidney, *IL-1β* and *IL-12p35* mRNA expression were insignificantly (*P*>0.05) at any levels of AFB1.

The anti-inflammatory cytokines were shown in Figure 4. In the skin, *TGF-β1*, *IL-4/13A*, *TGF-β2*, and *IL-4/13B* gene expression were significantly downregulated with the AFB1 levels up to 146.92, 58.66, 85.94, and 85.94 μg/kg diet (*P* < 0.05), respectively. In the spleen, the above anti-inflammatory cytokines gene expression was significantly downregulated with the AFB1 levels up to 85.94, 58.66, 58.66, 85.94, and 85.94 μg/kg diet (*P* < 0.05), respectively. In the head kidney, the transcription levels of *IL-10*, *IL-4/13A*, *IL-4/13B*, *TGF-β1*, and *TGF-β2* were significantly downregulated (*P* < 0.05), when the AFB1 dose reached 85.94, 58.66, 58.66, 58.66, and 85.94 μg/kg diet, respectively. Interestingly, the transcription level of *IL-10* has not been changed at any levels of AFB1 in the skin, spleen, and head kidney of grass carp.

The inflammatory signaling molecules were shown in Figure 4. In the skin, *c-Rel*, *NF-κBp65*, *IKK-β*, *IKK-γ*, *4E-BP1*, and *4E-BP2* genes expression were significantly upregulated when the AFB1 dose reached 85.94, 58.66, 85.94, 110.43, 58.66, and 110.43 μg/kg diet (*P* < 0.05), respectively. *IκBα*, *TOR*, and *S6K1* gene expression were significantly downregulated when the AFB1 levels were up to 58.66, 85.94, and 110.43 μg/kg diet (*P* < 0.05), respectively. In the spleen, *NF-κBp65*, *c-Rel*, *IKK-β*, *IKK-γ*, *4E-BP1*, and *4E-BP2* genes expression were upregulated when the AFB1 dose reached 110.43, 85.94, 85.94, 85.94, 85.94, and 85.94 μg/kg diet (*P* < 0.05), respectively. But *IκBα*, *TOR*, and *S6K1* gene expression were all significantly downregulated when the AFB1 dose reached 58.66 μg/kg diet (*P* < 0.05). In the head kidney, *NF-κBp65*, *c-Rel*, *IKK-β*, *IKK-γ*, *eIF4E-binding protein 1* (*4E-BP1*), and *4E-BP2* genes expression were significantly upregulated when the AFB1 dose reached 58.66, 85.94, 85.94, 85.94, 85.94, and 85.94 μg/kg diet (*P* < 0.05), respectively. While *IκBα*, *TOR*, and *S6K1* transcription levels were significantly reduced, when the AFB1 levels were up to 85.94, 58.66, and 85.94 μg/kg diet (*P* < 0.05), respectively. Interestingly, *NF-κBp52* and *IKKα* gene expression had no significant effect on the immune organs at any levels of AFB1.

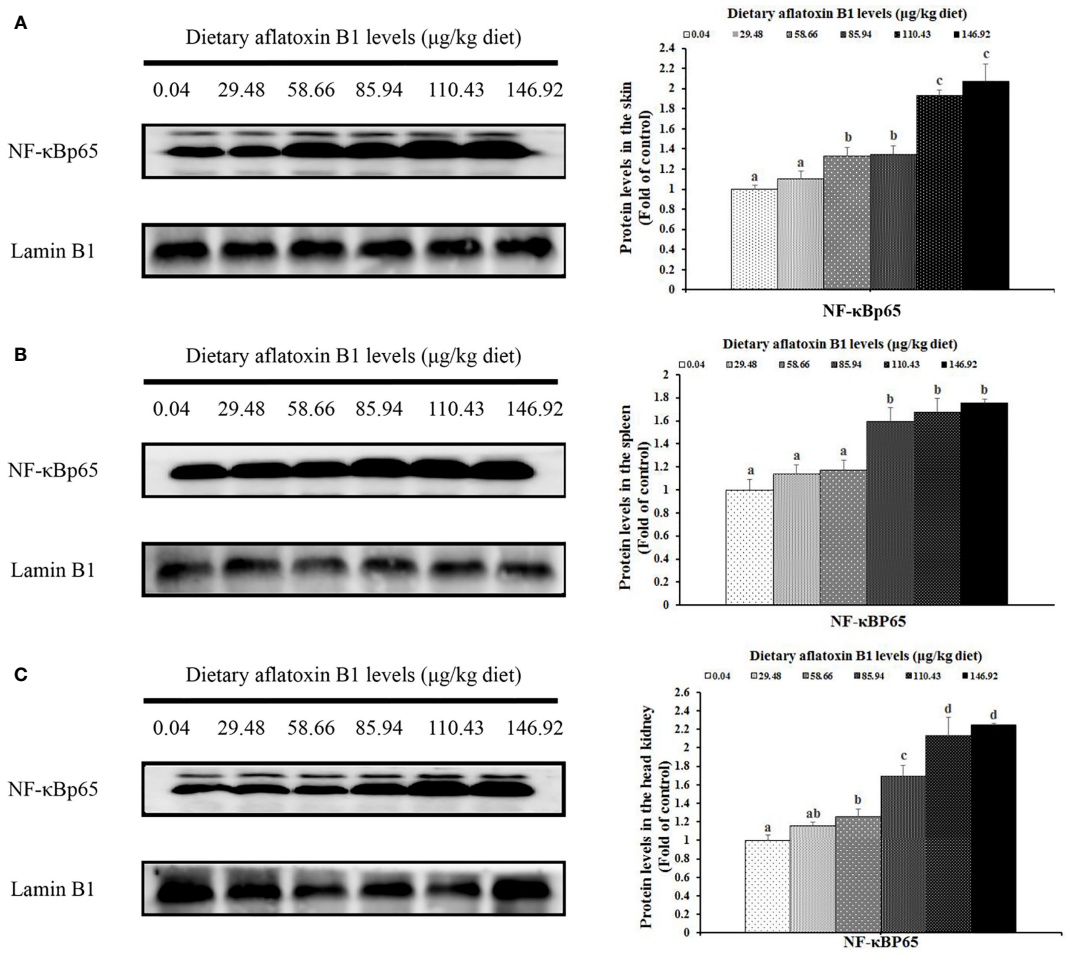

FIGURE 5
The protein levels NF-kB p65 in the skin **(A)**, spleen **(B)** and head kidney **(C)** of grass carp after infection of *A hydrophila*. n=6 (six fish in each group). Different letters indicate significant differences (P < 0.05).

Protein expression levels of nuclear factor-κB p65 (NF-κB p65) and phosphorylation of TOR in skin, spleen, and head kidney of grass carp

In Figure 5, dietary AFB1 led to the decrease of nuclear NF-κB p65 in a dose-dependent manner in the immune organs of grass carp. In the skin, spleen, and head kidney, the levels of NF-κB p65 protein were significantly upregulated when the AFB1 levels reached 58.66, 85.94, and 58.66 μg/kg diet ($P < 0.05$), respectively. In Figure 6, dietary AFB1 led to the decrease of the protein in a dose-dependent manner in the grass carp skin, spleen, and head kidney. Western blot analysis indicated that grass carp had significantly decreased both the levels of p-TOR Ser^{2448} and T-TOR protein when the dietary AFB1 levels reached 85.94 μg/kg diet ($P < 0.05$) in the skin, spleen, and head kidney, respectively. Both the levels of p-TOR Ser^{2448} and T-TOR protein reached the lowest levels in the 146.92 μg/kg diet groups in the skin, spleen, and head kidney.

Discussion

Using the same growth test as our previous study, we conducted research as part of a larger project to evaluate the immune function of AFB1 on the immune organs (skin, spleen, and head kidney) of grass carp (6). It has been confirmed that dietary AFB1 inhibited fish growth and disrupted the physical barrier of grass carp spleen and head kidney in our previous study (6). However, in addition to physical barriers, fish immune organ health also depends on immune barriers (37). It was the primary aim of this study to determine whether AFB1 affected

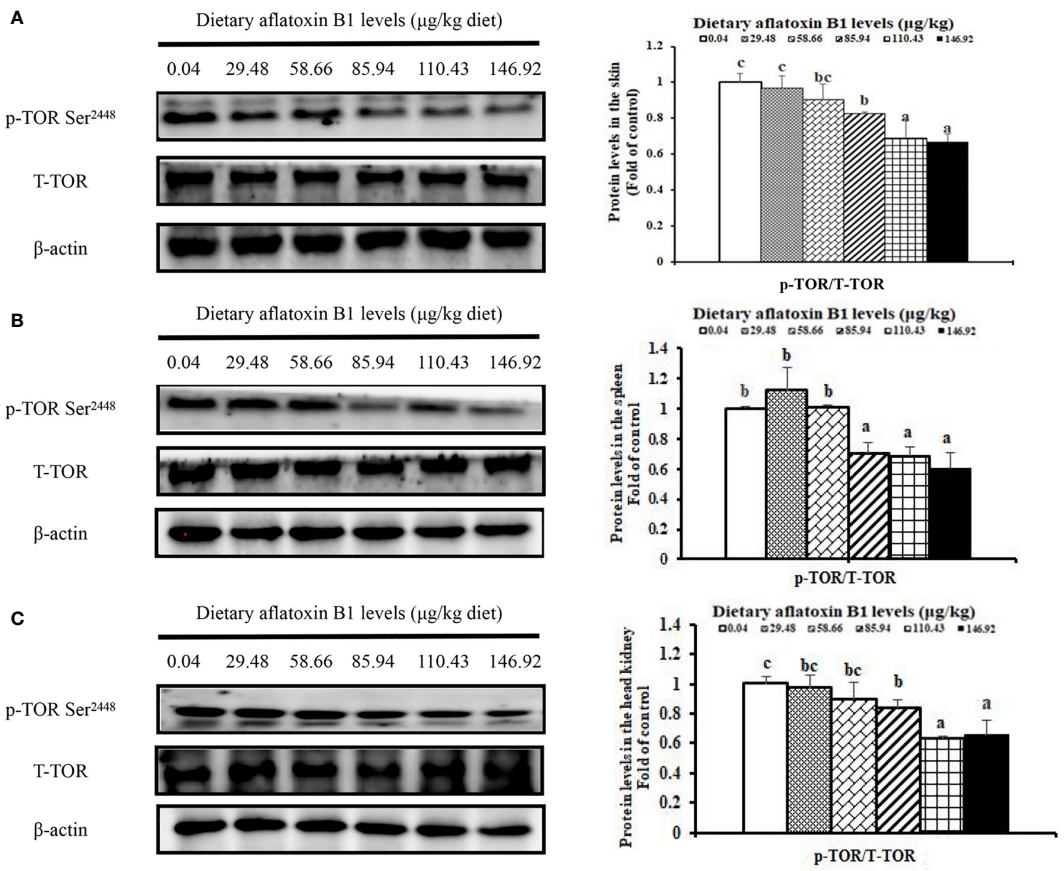

FIGURE 6
The protein levels phosphorylation of TOR at Ser2448 in the skin **(A)**, spleen **(B)** and head kidney **(C)** of grass carp after infection of *A hydrophila*. n=6 (six fish in each group). Different letters indicate significant differences ($P < 0.05$).

inflammation in fish immune organs (head kidney, spleen and skin) after infection with *A. hydrophila*.

AFB1 attenuated immunological parameters of immune organs

As is well known that the function of the immune barrier of fish is mediated by immune substances, which include ACP and LZ activities, C3, C4, and immunoglobulins contents, and the antibacterial peptides gene expression (38). As an important component of innate immune response, ACP and LZ have excellent bactericidal effects, whereas complement system is involved in the recognition and elimination of pathogens in fish (39, 40). In addition, antimicrobial peptides are also important components of fish innate immunity, mainly including β-defensin1, LEAP-2A, LEAP-2B, etc. (14). Our results found that AFB1 decreased the activities of LZ, ACP, the contents of C3, C4, and IgM, and downregulated *β-defensin1*, *LEAP-2A*, *LEAP-2B*, and *Mucin2* gene expression in skin, spleen, and head kidney of grass carp. Similarly, Sahoo et al. (35) found that AFB1 decreased LZ activity in rohu serum, and another research also confirmed that AFB1 significantly decreased the contents of immune components (e.g. C3, C4) in juvenile turbot serum (21), which were consistent with our results, suggesting that AFB1 could suppress the immune function of the skin, spleen, and head kidney partly referring to decrease immune components in fish. The reason for the inhibition of AFB1 on immunological parameters may be attributed to the reduction of the number of immune cells. It is well known that lymphocytes could produce immune components (40), such as LZ, IL-4, and IL-8, etc. A study observed that AFB1 reduced lymphocyte proliferation in rainbow trout (41). The present study showed that AFB1 could decrease the content of LZ. As far as we know, lysozyme is derived from monocytes and neutrophils, which were a large number of distributions in the spleen and head kidney. Although the above evidence has been presented, a large number of

experimental data are still needed to further confirm. Furthermore, it should be noted that, the spleen and head kidney of grass carp did not exhibit any changes in *hepcidin* transcription levels due to AFB1. The reason may be partially related to the *IL-1β* mRNA levels. Research on murine exhibited that *IL-1β* participates in the regulation of *hepcidin* in primary hepatocytes (42). Coincidentally, our results found that AFB1 had no impact on *IL-1β* mRNA expression. Nevertheless, the mechanisms involved in this process need to be studied in greater detail.

AFB1 attenuated inflammatory response of immune organs

Cytokines-mediated inflammation response is a hallmark of immune system up-regulation (43, 44). It is largely acknowledged that the inflammation could be aggravated by increasing the transcription levels of pro-inflammatory cytokines and decreasing the transcription levels of anti-inflammatory cytokines in fish, which were regulated by NF-κB and TOR (45, 46). Generally, adverse external stress can usually lead to drastic changes in immune homeostasis, mainly manifested as dynamic changes in inflammatory cytokines. The current research demonstrated that dietary AFB1 increased the pro-inflammatory cytokines transcription levels and decreased the anti-inflammatory cytokines transcription levels in the skin, spleen, and head kidney of grass carp. Similarly, one research demonstrated that dietary AFB1 increased the transcription levels of TNF-α and IL-1β in rainbow trout intestinal (5), another study found that dietary AFB1 significantly increased IFN-γ content in the broiler jejunum mucosa (23); in addition, dietary AFB1 downregulated *IL-10* mRNA expression in chicken livers (47), which were consistent with the above results. Combining the above mentioned evidences, AFB1 induced inflammatory responses in fish immune organs has been observed. Based on our assumptions, there might be a connection between AFB1 and immune cells. A variety of inflammatory cytokines are released by macrophages and immune cells during the inflammatory process (48). The *in vitro* study revealed that AFB1 inhibits the growth of murine macrophages and decreases various secretory cytokines found in these cells (49). Furthermore, we observed two interesting findings. Firstly, AFB1 had not changed the transcription levels of *IL-1β* in the skin, spleen, and head kidney of grass carp. The possible reason may be that the contact time and dose of AFB1 to grass carp were insufficient. Similarly, Dugyala and Sharma et al. (50) found that 0.145 mg AFB1/kg body weight induced *IL-6* and *TNF-α* higher expression in rat peritoneal macrophages at 2 weeks, nevertheless Rossano et al. (51) found that 1.0 pg/ml AFB1 downregulated *IL-6* and *TNF-α* mRNA expression in and human monocytes at 2h and 12h. The possible reason accounting for the different results is that the time and dose of AFB1 exposed to macrophages were different. This might support our hypothesis, but the clear mechanisms need further investigation. Secondly, in the present experiment, AFB1 only upregulated *IL-12p40* rather than *IL-12p35* in the skin, spleen, and head kidney of grass carp. It was reported that the stable expression of different subtypes of mRNA may be different in different tissues (52). Pandit et al. (53) found that the mRNA of *IL-12p40* is high expression in immune tissues (such as the spleen and head kidney) of grass carp during *A. hydrophila* infection, while the mRNA of *IL-12p35* is mostly expressed in the central nervous system. This might support our hypothesis. Its exact mechanism of action needs to be determined through further research.

AFB1 modulates immune response related signaling pathways

As we have known, the activation of the IKK complex promotes the degradation of IκBα and then activates NF-κB, whose activation could increase the pro-inflammatory cytokines transcription levels in humans (54). In humans, the level of nuclear NF-κB protein could be a symbol of activating NF-κB signaling (55). In the current work, we observed that AFB1 upregulated the mRNA levels of nuclear NF-κB protein in grass carp skin, spleen, and head kidney. Correlation analyses displayed that *IFN-γ2*, *TNF-α*, *IL-6*, *IL-8*, *IL-12p40*, *IL-15*, and *IL-17D* gene expression were positively correlated with the NF-κBp65 protein levels (Table 2), suggesting that AFB1 aggravated spleen and head kidney inflammation partially related to activation of NF-κBp65 signaling in grass carp. The reason for the activation of NF-κB signaling by AFB1 was still not clarified in the immune organs of fish. Probably two reasons contributed to this. Firstly, this is partially related to IkBα, IKKβ, and IKKγ. Studies suggested that IKKβ, γ could activate NF-κB nuclear translocation, and IκBα could inhibit NF-κB nuclear translocation (55). Our results found that AFB1 upregulated *IKKβ*, and *IKKγ* genes expression and downregulated *IκBα* gene expression in the skin, spleen, and head kidney of grass carp, which supports our hypothesis. Secondly, it is might associated with the mRNA levels of the *NF-κB*. Takahashi et al. (56) found that upregulating the *NF-κB* mRNA levels could increase the levels of the NF-kBp65 protein level. Our results indicated that AFB1 upregulated the *NF-κB p65* gene expression in grass carp skin, spleen, and head kidney, which is consistent with the results of the protein expression from the current study. Interestingly, the results from our study found that AFB1 had not changed *NF-κBp52* transcription level in grass carp skin, spleen, and head kidney. The possible reason is linked to the stably *IKKα* gene expression. It was shown that *NF-κBp52* could be specifically activated by *IKKα* in mammalian cells (57). The

10.3389/fimmu.2022.1027064

TABLE 2 Correlation coefficient of parameters in the immune organs of grass carp[1].

Independent parameters	Dependent parameters	Spleen Correlation coefficients	P	Head kidney Correlation coefficients	P
NF-κB p65 protein level	TNF-α	+0.970	<0.01	+0.957	<0.01
	IFN-γ2	+0.885	<0.01	+0.920	<0.05
	IL-6	+0.935	<0.01	+0.969	<0.01
	IL-8	+0.951	<0.01	+0.936	<0.01
	IL-12P40	+0.936	<0.01	+0.983	<0.01
	IL-15	+0.941	<0.01	+0.943	<0.01
	IL-17D	+0.947	<0.01	+0.971	<0.01
c-Rel mRNA level	TNF-α	+0.937	<0.01	+0.955	<0.01
	IFN-γ2	+0.968	<0.01	+0.933	<0.01
	IL-6	+0.972	<0.01	+0.986	<0.01
	IL-8	+0.961	<0.01	+0.939	<0.01
	IL-12P40	+0.960	<0.01	+0.983	<0.01
	IL-15	+0.928	<0.01	+0.978	<0.01
	IL-17D	+0.914	<0.01	+0.988	<0.01
IκBα mRNA level	NF-κB p65 protein level	-0.965	<0.01	-0.978	<0.01
	c-Rel	-0.926	<0.01	-0.982	<0.01
IKKβ mRNA level	NF-κB p65 protein level	+0.940	<0.01	+0.970	<0.01
	IκBα	-0.992	<0.01	-0.996	<0.01
IKKγ mRNA level	NF-κB p65 protein level	+0.944	<0.01	+0.972	<0.01
	IκBα	-0.989	<0.01	-0.995	<0.01
p-TOR protein level	IL-4/13A	+0.964	<0.01	+0.932	<0.01
	IL-4/13B	+0.870	<0.01	+0.963	<0.05
	IL-10	+0.941	<0.01	+0.959	<0.01
	TGF-β1	+0.980	<0.01	+0.957	<0.01
	TGF-β2	+0.973	<0.01	+0.954	<0.01

[1]"+" means positive correlation; "-" means negative correlation.

current results showed that AFB1 had not changed the *IKKα* transcription level in the skin, spleen, and head kidney of grass carp, which supported our assumption.

Studies in mammalian have found that activation of mTOR signaling promotes the production of anti-inflammatory cytokines (e.g., IL-10, TGF-β1). According to previous study, S6K1 and 4E-BP are key signaling molecules downstream of mTOR protein (46). A study has revealed that phosphorylation of TOR Ser2448 can reflect TOR signaling activation in Jian carp (*Cyprinus carpio* var. *Jian*) (58). Our results demonstrated that AFB1 reduced p-TOR Ser2448 transcription level in the skin, spleen, and head kidney of grass carp, which demonstrated that AFB1 inhibited the activation of TOR signaling. Correlation analyses displayed that *TGF-β1*, *TGF-β2*, *IL-10*, *IL-4/13A*, and *IL-4/13B* gene expression were positively correlated with the p-TOR Ser2448 (Table 2), suggesting that AFB1 aggravated spleen and head kidney inflammation partly be associated with the inhibition of TOR signaling in fish. The reason for the inhibition signaling of TOR by AFB1 may be related, in part to TOR transcription and translation. Kew et al. (57) indicated that the level of p-TOR Ser2448 protein was in contact with its transcription and translation. Our present result showed that AFB1 could decrease *TOR* transcription level in the grass carp skin, spleen, and head kidney, which support our hypothesis. Our results indicated that AFB1 aggravated inflammation might related to the activation of NF-κBp65 signaling and inhibition of TOR signaling.

AFB1 safe upper dose for grass carp

Intensive farming poses health-threatening to fish. However, the health of fish is associated with its immunity. The increase in morbidity is used to assess the adverse effects of harmful substances on the body. ACP and LZ activities, as important immune indicators, often used to evaluate the health of fish immune organs (59). Therefore, in order to maintain the skin, spleen, and head kidney health of grass carp, we selected the dose with no significant effect of AFB1 on ACP and LZ as the safe upper dose. Finally, we determined that AFB1 not exceeding 29.48 μg/kg diet could maintain the health of immune organs.

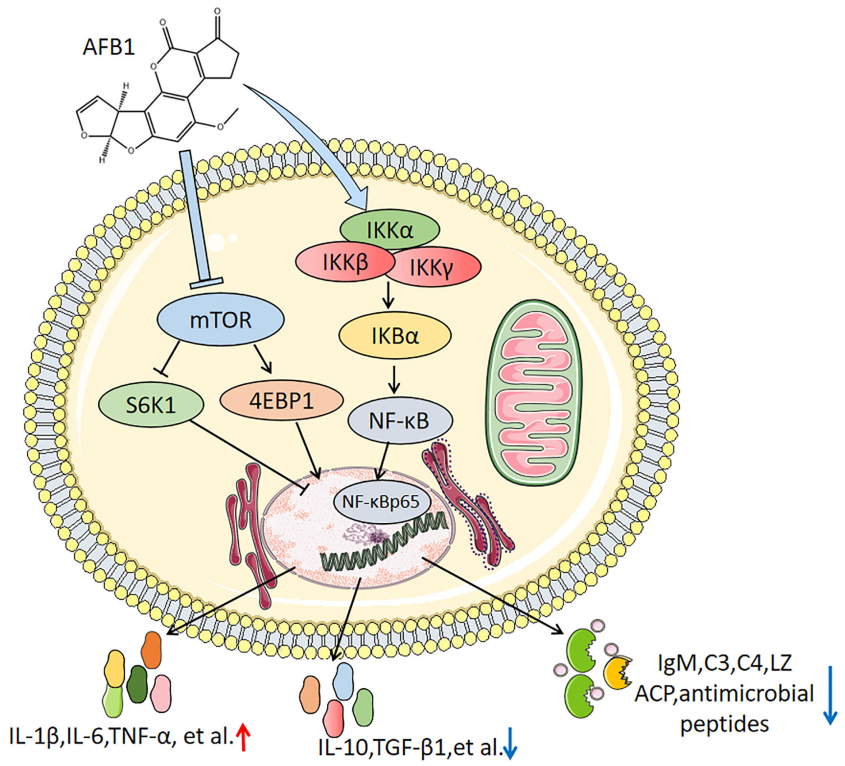

FIGURE 7
The mechanism of AFB1 on immune function of immune cells in the skin, spleen and head kidney of grass carp.

Conclusion

In conclusion, as shown in Figure 7, the results of our study demonstrate that AFB1 destructed immune competent of grass carp skin, spleen, and head kidney (1). Dietary AFB1 decreased C3, C4, and IgM contents, LZ and ACP activities, and downregulated *β-defensin1*, *Mucin2*, *LEAP-2A*, and *LEAP-2B* gene expression in skin, spleen, and head kidney of grass carp (2). Dietary AFB1 promoted inflammatory responses related to the activation of [(*IKKβ* and *IKKγ* rather than *IKKα*)/*IκBα*/*NF-κB* (*p65* and *c-Rel* rather than *p52*) to upregulate the pro-inflammatory cytokines genes expression (except *IL-1β* and *IL-12p35*), and inhibition of [*TOR*/(*S6K1*, *4E-BP1*)] signaling to downregulate the anti-inflammatory cytokines genes expression in grass carp skin, spleen, and head kidney. Moreover, the content of AFB1 in the grass carp diet should not exceed 29.48 μg/kg diet according to the activities of LZ and ACP.

Data availability statement

The original contributions presented in the study are included in the article/Supplementary Material. Further inquiries can be directed to the corresponding authors.

Ethics statement

The animal study was reviewed and approved by Sichuan Agricultural University Animal Care Advisory Committee.

Author contributions

X-NH: Writing-Original draft preparation, Formal analysis, Investigation. Z-ZZ: Formal analysis, Investigation. LF: Data Curation. W-DJ, PW: Methodology. YL, JJ: Validation. S-YK, LT: Resources. X-QZ: Conceptualization, Writing-Reviewing and Editing, Project administration. All authors contributed to the article and approved the submitted version.

Funding

This research was financially supported by National Key Research and Development Program of China (2019YFD0900200, 2018YFD0900400), National Natural Science Foundation of China for Outstanding Youth Science Foundation (31922086), Supported by Earmarked found for China Agriculture Research System

(CARS-45), and supported by Sichuan Science and Technology Program (2019YFN0036).

Acknowledgments

The authors would like to express theirsincere thanks to the personnel of these teams for theirkind assistance.

Conflict of interest

The authors declare that the research was conducted in the absence of any commercial or financial relationships that could be construed as a potential conflict of interest.

Publisher's note

Supplementary material

The Supplementary Material for this article can be found online at: https://www.frontiersin.org/articles/10.3389/fimmu.2022.1027064/full#supplementary-material

References

1. Jensen T, de Boevre M, Preußke N, de Saeger S, Birr T, Verreet J, et al. Evaluation of high-resolution mass spectrometry for the quantitative analysis of mycotoxins in complex feed matrices. *Toxins* (2019) 11(9):531. doi: 10.3390/toxins11090531

2. Cao Q, Lin L, Xu T, Lu Y, Zhang C, Yue K, et al. Aflatoxin B1 alters meat quality associated with oxidative stress, inflammation, and gut-microbiota in sheep. *Ecotoxicology Environ Saf* (2021) 225:112754. doi: 10.1016/j.ecoenv.2021.112754

3. Marijani E, Kigadye E, Okoth S. Occurrence of fungi and mycotoxins in fish feeds and their impact on fish health. *Int J Microbiol* (2019) 2019:6743065. doi: 10.1155/2019/6743065

4. Mokubedi S, Phoku J, Changwa R, Gbashi S, Njobeh P. Analysis of mycotoxins contamination in poultry feeds manufactured in selected provinces of south Africa using uhplc-Ms/Ms. *Toxins* (2019) 11(8):452. doi: 10.3390/toxins11080452

5. Ghafarifarsani H, Kachuei R, Imani A. Dietary supplementation of garden thyme essential oil ameliorated the deteriorative effects of aflatoxin B1 on growth performance and intestinal inflammatory status of rainbow trout (Oncorhynchus mykiss). *Aquaculture* (2021) 531:735928. doi: 10.1016/j.aquaculture.2020.735928

6. Zeng Z-Z, Jiang W-D, Wu P, Liu Y, Zeng Y-Y, Jiang J, et al. Dietary aflatoxin B1 decreases growth performance and damages the structural integrity of immune organs in juvenile grass carp (Ctenopharyngodon idella). *Aquaculture* (2019) 500 (1):1–17. doi: 10.1016/j.aquaculture.2018.09.064

7. Yu Y, Wang Q, Huang Z, Ding L, Xu Z. Immunoglobulins, mucosal immunity and vaccination in teleost fish. *Front Immunol* (2020) 11:567941. doi: 10.3389/fimmu.2020.567941

8. Taysse L, Chambras C, Marionnet D, Bosgiraud C, Deschaux P. Basal level and induction of cytochrome P450, erod, udpgt, and gst activities in carp (*Cyprinus carpio*) immune organs (Spleen and head kidney). *Bull Environ contamination Toxicol* (1998) 60(2):300–5. doi: 10.1007/s001289900625

9. Jalili M, Gerdol M, Greco S, Pallavicini A, Buonocore F, Scapigliati G, et al. Differential effects of dietary supplementation of krill meal, soybean meal, butyrate, and bactocell on the gene expression of Atlantic salmon head kidney. *Int J Mol Sci* (2020) 21(3):886. doi: 10.3390/ijms21030886

10. Zaritsky L, Dery A, Leong W, Gama L, Clements J. Tissue-specific interferon alpha subtype response to siv infection in brain, spleen, and lung. *J Interferon Cytokine research: Off J Int Soc Interferon Cytokine Res* (2013) 33(1):24–33. doi: 10.1089/jir.2012.0018

11. Yaron J, Zhang L, Guo Q, Awo E, Burgin M, Schutz L, et al. Myxoma virusrecombinant -derived immune modulator m-T7 accelerates cutaneous wound healing and improves tissue remodeling. *Pharmaceutics* (2020) 12(11):1003. doi: 10.3390/pharmaceutics12111003

12. Lu Z, Feng L, Jiang W, Wu P, Liu Y, Jiang J, et al. Aeromonas hydrophilamannan oligosaccharides application: Multipath restriction from infection in the skin barrier of grass carp. *Front Immunol* (2021) 12:742107. doi: 10.3389/fimmu.2021.742107

13. Pietrzak E, Mazurkiewicz J, Slawinska A. Innate immune responses of skin mucosa in common carp (*Cyprinus carpio*) fed a diet supplemented with galactooligosaccharides. *Animals* (2020) 10(3):438. doi: 10.3390/ani10030438

14. Jiang W, Zhang L, Feng L, Wu P, Liu Y, Kuang S, et al. Flavobacterium columnarenew insight on the immune modulation and physical barrier protection caused by vitamin a in fish gills infected with. *Front Immunol* (2022) 13:833455. doi: 10.3389/fimmu.2022.833455

15. Huang C, Wu P, Jiang W, Liu Y, Zeng Y, Jiang J, et al. Deoxynivalenol decreased the growth performance and impaired intestinal physical barrier in juvenile grass carp (Ctenopharyngodon idella). *Fish shellfish Immunol* (2018) 80:376–91. doi: 10.1016/j.fsi.2018.06.013

16. Huang C, Feng L, Jiang W, Wu P, Liu Y, Zeng Y, et al. Deoxynivalenol decreased intestinal immune function related to nf-Kb and tor signalling in juvenile grass carp (Ctenopharyngodon idella). *Fish shellfish Immunol* (2019) 84:470–84. doi: 10.1016/j.fsi.2018.10.039

17. Chaklader M, Siddik M, Fotedar R, Howieson J. Insect larvae, hermetia illucens in poultry by-product meal for barramundi, lates calcarifer modulates histomorphology, immunity and resistance to vibrio harveyi. *Sci Rep* (2019) 9 (1):16703. doi: 10.1038/s41598-019-53018-3

18. Seong H, Jeong Y, Lee W, Kim J, Kim J, Ahn J, et al. Splenic uptake on fdg Pet/Ct correlates with kikuchi-fujimoto disease severity. *Sci Rep* (2021) 11 (1):10836. doi: 10.1038/s41598-021-90350-z

19. Hu Y, Feng L, Jiang W, Wu P, Liu Y, Kuang S, et al. Ctenopharyngodon idellalysine deficiency impaired growth performance and immune response and aggravated inflammatory response of the skin, spleen and head kidney in grown-up grass carp. *Anim Nutr (Zhongguo xu mu shou yi xue hui)* (2021) 7(2):556–68. doi: 10.1016/j.aninu.2020.07.009

20. Vargas D, Vallejos-Vidal E, Reyes-Cerpa S, Oyarzún-Arrau A, Acuña-Castillo C, Imarai M, et al. The analysis of live-attenuated piscirickettsia salmonis vaccine reveals the short-term upregulation of innate and adaptive immune genes in Atlantic salmon (Salmo salar): An in situ open-Sea cages study. *Microorganisms* (2021) 9(4):703. doi: 10.3390/microorganisms9040703

21. Yang J, Wang T, Lin G, Li M, Zhu R, Yiannikouris A, et al. Scophthalmus maximusthe assessment of diet contaminated with aflatoxin b in juvenile turbot () and the evaluation of the efficacy of mitigation of a yeast cell wall extract. *Toxins* (2020) 12(9):597. doi: 10.3390/toxins12090597

22. Ma J, Liu Y, Guo Y, Ma Q, Ji C, Zhao L. Transcriptional profiling of aflatoxin B1-induced oxidative stress and inflammatory response in macrophages. *Toxins* (2021) 13(6):401. doi: 10.3390/toxins13060401

23. Sarker M, Wan X, Yang H, Wang Z. Dietary lycopene supplementation could alleviate aflatoxin b induced intestinal damage through improving immune function and anti-oxidant capacity in broilers. *Animals: an Open Access J MDPI* (2021) 11(11):3165. doi: 10.3390/ani11113165

24. Guo H-W, Chang J, Wang P, Yin Q-Q, Liu C-Q, Xu X-X, et al. Effects of compound probiotics and aflatoxin-degradation enzyme on alleviating aflatoxin-

induced cytotoxicity in chicken embryo primary intestinal epithelium, liver and kidney cells. *AMB Express* (2021) 11(1):1–12. doi: 10.1186/s13568-021-01196-7

25. Chen Y, Zhang X, Yu C, Huang S, Xie Y, Dou X, et al. Artesunate exerts protective effects against ulcerative colitis *Via* suppressing Toll–Like receptor 4 and its downstream nuclear Factor–Kb signaling pathways. *Mol Med Rep* (2019) 20 (2):1321–32. doi: 10.3892/mmr.2019.10345

26. Cordaro M, Trovato Salinaro A, Siracusa R, D'Amico R, Impellizzeri D, Scuto M, et al. Hidrox roles in neuroprotection: Biochemical links between traumatic brain injury and alzheimer's disease. *Antioxidants (Basel Switzerland)* (2021) 10(5):818. doi: 10.3390/antiox10050818

27. Jin S, Yang H, Jiao Y, Pang Q, Wang Y, Wang M, et al. Anas platyrhynchosdietary curcumin alleviated acute ileum damage of ducks () induced by Afb1 through regulating Nrf2-are and nf-Kb signaling pathways. *Foods (Basel Switzerland)* (2021) 10(6):1370. doi: 10.3390/foods10061370

28. Wu W, Deng H, Rao N, You N, Yang Y, Cao M, et al. Neoadjuvant everolimus plus letrozole versus fluorouracil, epirubicin and cyclophosphamide for er-positive, Her2-negative breast cancer: Study protocol for a randomized pilot trial. *Trials* (2017) 18(1):497. doi: 10.1186/s13063-017-2228-5

29. Jiang W, Zhang L, Feng L, Wu P, Liu Y, Jiang J, et al. Inconsistently impairment of immune function and structural integrity of head kidney and spleen by vitamin a deficiency in grass carp (Ctenopharyngodon idella). *Fish shellfish Immunol* (2020) 99:243–56. doi: 10.1016/j.fsi.2020.02.019

30. Ivanovics B, Gazsi G, Reining M, Berta I, Poliska S, Toth M, et al. Embryonic exposure to low concentrations of aflatoxin B1 triggers global transcriptomic changes, defective yolk lipid mobilization, abnormal gastrointestinal tract development and inflammation in zebrafish. *J hazardous materials* (2021) 416:125788. doi: 10.1016/j.jhazmat.2021.125788

31. Chen G, Liu Y, Jiang J, Jiang W, Kuang S, Tang L, et al. Effect of dietary arginine on the immune response and gene expression in head kidney and spleen following infection of jian carp with aeromonas hydrophila. *Fish shellfish Immunol* (2015) 44(1):195–202. doi: 10.1016/j.fsi.2015.02.027

32. He L, Zhang A, Pei Y, Chu P, Li Y, Huang R, et al. Differences in responses of grass carp to different types of grass carp reovirus (Gcrv) and the mechanism of hemorrhage revealed by transcriptome sequencing. *BMC Genomics* (2017) 18 (1):452. doi: 10.1186/s12864-017-3824-1

33. Aanyu M, Carpaij C, Widmer M. Effect of diets with graded levels of inclusion of cotton and sunflower seed cakes on the growth performance and feed utilization of Nile tilapia, oreochromis niloticus. livestock rese arch for rural development. *Livestock Res Rural Dev* (2012) 24(5):35–40. doi: 10.1016/0166-9834(83)80238-3

34. Ma S, Dong Y, Wang N, Liu J, Lu C, Liu Y. Identification of a new effector-immunity pair of aeromonas hydrophila type vi secretion system. *Veterinary Res* (2020) 51(1):71. doi: 10.1186/s13567-020-00794-w

35. Sahoo P, Mukherjee S. Immunomodulation by dietary vitamin c in healthy and aflatoxin B1-induced immunocompromised rohu (Labeo rohita). *Comp immunology Microbiol Infect Dis* (2003) 26(1):65–76. doi: 10.1016/s0147-9571(01)00038-8

36. Dong Y, Jiang W, Liu Y, Wu P, Jiang J, Kuang S, et al. Threonine deficiency decreased intestinal immunity and aggravated inflammation associated with nf-Kb and target of rapamycin signalling pathways in juvenile grass carp (Ctenopharyngodon idella) after infection with aeromonas hydrophila. *Br J Nutr* (2017) 118(2):92–108. doi: 10.1017/s0007114517001830

37. Chen K, Jiang W, Wu P, Liu Y, Kuang S, Tang L, et al. Effect of dietary phosphorus deficiency on the growth, immune function and structural integrity of head kidney, spleen and skin in young grass carp (Ctenopharyngodon idella). *Fish shellfish Immunol* (2017) 63:103–26. doi: 10.1016/j.fsi.2017.02.007

38. Tort L, Balasch J, Mackenzie S. Fish immune system. a crossroads between innate and adaptive responses. *Inmunologia* (2003) 22(3):277–86.

39. Lu Y, Liang X-P, Jin M, Sun P, Ma H-N, Yuan Y, et al. Effects of dietary vitamin e on the growth performance, antioxidant status and innate immune response in juvenile yellow catfish (Pelteobagrus fulvidraco). *Aquaculture* (2016) 464:609–17. doi: 10.1016/j.aquaculture.2016.08.009

40. Magnadottir B, Lange S, Gudmundsdottir S, Bøgwald J, Dalmo R. Ontogeny of humoral immune parameters in fish. *Fish shellfish Immunol* (2005) 19(5):429–39. doi: 10.1016/j.fsi.2005.03.010

41. Ottinger C, Kaattari S. Sensitivity of rainbow trout leucocytes to aflatoxin B1. *Fish Shellfish Immunol* (1998) 8(7):515–30. doi: 10.1006/fsim.1998.0154

42. Lee P, Peng H, Gelbart T, Wang L, Beutler E. Regulation of hepcidin transcription by interleukin-1 and interleukin-6. *Proc Natl Acad Sci United States America* (2005) 102(6):1906–10. doi: 10.1073/pnas.0409808102

43. Choi A, Ryter S. Inflammasomes: Molecular regulation and implications for metabolic and cognitive diseases. *Molecules Cells* (2014) 37(6):441–8. doi: 10.14348/molcells.2014.0104

44. Sang R, Liu Y, Kong L, Qian L, Liu C. Effect of acellular amnion with increased tgf-B and bfgf levels on the biological behavior of tenocytes. *Front bioengineering Biotechnol* (2020) 8:446. doi: 10.3389/fbioe.2020.00446

45. Chen S, Zhu J, Chen G, Zuo S, Zhang J, Chen Z, et al. 1,25-dihydroxyvitamin D3 preserves intestinal epithelial barrier function from tnf-A induced injury *Via* suppression of nf-kb P65 mediated mlck-P-Mlc signaling pathway. *Biochem Biophys Res Commun* (2015) 460(3):873–8. doi: 10.1016/j.bbrc.2015.03.125

46. Weichhart T, Costantino G, Poglitsch M, Rosner M, Zeyda M, Stuhlmeier K, et al. The tsc-mtor signaling pathway regulates the innate inflammatory response. *Immunity* (2008) 29(4):565–77. doi: 10.1016/j.immuni.2008.08.012

47. Wang X, Li W, Wang X, Han M, Muhammad I, Zhang X, et al. Water-soluble substances of wheat: A potential preventer of aflatoxin B1-induced liver damage in broilers. *Poultry Sci* (2019) 98(1):136–49. doi: 10.3382/ps/pey358

48. Zhou Y, Chen R, Liu D, Wu C, Guo P, Lin W. Asperlin inhibits lps-evoked foam cell formation and prevents atherosclerosis in apoe–/– mice. *Mar Drugs* (2017) 15(11):358. doi: 10.3390/md15110358

49. Moon E, Rhee D, Pyo S. *In vitro* suppressive effect of aflatoxin B1 on murine peritoneal macrophage functions. *Toxicology* (1999) 133:171–9. doi: 10.1016/s0300-483x(99)00023-2

50. Dugyala R, Sharma R. The effect of aflatoxin B1 on cytokine mrna and corresponding protein levels in peritoneal macrophages and splenic lymphocytes. *Int J Immunopharmacol* (1996) 18(10):599–608. doi: 10.1016/s0192-0561(96)00066-5

51. Rossano F, Ortega De Luna L, Buommino E, Cusumano V, Losi E, Catania M. Secondary metabolites of aspergillus exert immunobiological effects on human monocytes. *Res Microbiol* (1999) 150(1):13–9. doi: 10.1016/s0923-2508(99)80042-4

52. Everett L, Cleuren A, Khoriaty R, Ginsburg D. Murine coagulation factor viii is synthesized in endothelial cells. *Blood* (2014) 123(24):3697–705. doi: 10.1182/blood-2014-02-554501

53. Pandit N, Shen Y, Xu X, Yu H, Wang W, Wang R, et al. Differential expression of interleukin-12 P35 and P40 subunits in response to aeromonas hydrophila and aquareovirus infection in grass carp, ctenopharyngodon idella. *Genet Mol research: GMR* (2015) 14(1):1169–83. doi: 10.4238/2015.February.6.20

54. Bollrath J, Greten F. Ikk/Nf-kappab and Stat3 pathways: Central signalling hubs in inflammation-mediated tumour promotion and metastasis. *EMBO Rep* (2009) 10(12):1314–9. doi: 10.1038/embor.2009.243

55. Zandi E, Rothwarf D, Delhase M, Hayakawa M, Karin M. The ikappab kinase complex (Ikk) contains two kinase subunits, ikkalpha and ikkbeta, necessary for ikappab phosphorylation and nf-kappab activation. *Cell* (1997) 91(2):243–52. doi: 10.1016/s0092-8674(00)80406-7

56. Takahashi N, van Kilsdonk J, Ostendorf B, Smeets R, Bruggeman S, Alonso A, et al. Tumor marker nucleoporin 88 kda regulates nucleocytoplasmic transport of nf-kappab. *Biochem Biophys Res Commun* (2008) 374(3):424–30. doi: 10.1016/j.bbrc.2008.06.128

57. Kew R, Penzo M, Habiel D, Marcu K. The ikkα-dependent nf-Kb P52/Relb noncanonical pathway is essential to sustain a Cxcl12 autocrine loop in cells migrating in response to Hmgb1. *J Immunol (Baltimore Md: 1950)* (2012) 188 (5):2380–6. doi: 10.4049/jimmunol.1102454

58. Hu K, Zhang J, Feng L, Jiang W, Wu P, Liu Y, et al. Effect of dietary glutamine on growth performance, non-specific immunity, expression of cytokine genes, phosphorylation of target of rapamycin (Tor), and anti-oxidative system in spleen and head kidney of jian carp (*Cyprinus carpio* var. *Jian). Fish Physiol Biochem* (2015) 41(3):635–49. doi: 10.1007/s10695-015-0034-0

59. Zheng L, Feng L, Jiang W, Wu P, Tang L, Kuang S, et al. Selenium deficiency impaired immune function of the immune organs in young grass carp (Ctenopharyngodon idella). *Fish shellfish Immunol* (2018) 77:53–70. doi: 10.1016/j.fsi.2018.03.024

frontiers | Frontiers in Immunology

TYPE Original Research
PUBLISHED 06 January 2023
DOI 10.3389/fimmu.2022.1110322

OPEN ACCESS

EDITED BY
Heng Chi,
Ocean University of China, China

REVIEWED BY
Jingguang Wei,
South China Agricultural University, China
Xue Qiao,
Dalian Ocean University, China

*CORRESPONDENCE
Xianghui Kong
xhkong@htu.cn

†These authors have contributed equally to this work and share first authorship

SPECIALTY SECTION
This article was submitted to Molecular Innate Immunity, a section of the journal Frontiers in Immunology

RECEIVED 28 November 2022
ACCEPTED 19 December 2022
PUBLISHED 06 January 2023

CITATION
Zhao Y, Zhang J, Qiao D, Gao F, Gu Y, Jiang X, Zhu L and Kong X (2023) *Cc*GSDMEa functions the pore-formation in cytomembrane and the regulation on the secretion of IL-1β in common carp (*Cyprinus carpio haematopterus*). *Front. Immunol.* 13:1110322. doi: 10.3389/fimmu.2022.1110322

*Cc*GSDMEa functions the pore-formation in cytomembrane and the regulation on the secretion of IL-1β in common carp (*Cyprinus carpio haematopterus*)

Yanjing Zhao†, Jie Zhang†, Dan Qiao, Feng Gao, Yanlong Gu, Xinyu Jiang, Lei Zhu and Xianghui Kong*

Engineering Lab of Henan Province for Aquatic Animal Disease Control, College of Fisheries, Henan Normal University, Xinxiang, Henan, China

GSDME is the only direct executor of caspase-dependent pyroptosis in both canonical and non-canonical inflammasomes known to date in fish, and plays an important role in anti-bacterial infection and inflammatory response. In order to determine the regulation of GSDMEa on antibacterial infection in innate immune response, the *CcGSDMEa* gene in common carp (*Cyprinus carpio haematopterus*) was first identified and characterized, and then its function related to immune defense was investigated. Our results showed that the expressions of *Cc*GSDMEa at the mRNA and protein levels were both significantly increased after *Aeromonas hydrophila* intraperitoneal infection at the early stage than that in the control group. We found that *Cc*GSDMEa could be cleaved by inflammatory caspase (*Cc*Caspase-1b) and apoptotic caspases (*Cc*Caspase-3a/b and *Cc*Caspase-7a/b). Interestingly, only the *Cc*GSDMEa-NT (1-252 aa) displayed bactericidal activity to *Escherichia coli* and could punch holes in the membrane of HEK293T cells, whereas *Cc*GSDMEa-FL (1-532 aa) and *Cc*GSDMEa-CT (257-532 aa) showed no above activity and pore-forming ability. Overexpression of *Cc*GSDMEa increased the secretion of *Cc*IL-1β and the release of LDH, and could reduce the *A. hydrophila* burdens in fish. On the contrary, knockdown of *Cc*GSDMEa reduced the secretion of *Cc*IL-1β and the release of LDH, and could increase the *A. hydrophila* burdens in fish. Taken together, the elevated expression of *Cc*GSDMEa was a positive immune response to *A. hydrophila* challenge in fish. *Cc*GSDMEa could perform the pore-formation in cell membrane and the regulation on the secretion of IL-1β, and further regulate the bacterial clearance *in vivo*. These results suggested that *Cc*GSDMEa played an important role in immune defense against *A. hydrophila* and could provide a new insight into understanding the immune mechanism to resist pathogen invasion in teleost.

KEYWORDS

common carp, *Aeromonas hydrophila*, GSDMEa, caspases, gasdermin pore, IL-1β secretion

Introduction

The common carp (*Cyprinus carpio haematopterus*), as an important economic species, is famous for rich nutrition, fast growth rate and long-standing history of breeding, and contributes a lot to freshwater aquaculture (1). The expansion of farming scale and the emergence of intensive rearing bring economic benefits, but also lead to the outbreaks of various diseases at the meantime. Bacterial hemorrhagic septicemia caused by *Aeromonas hydrophila* is one of the main diseases, which is ferocious and causes fish massive die-offs in severe case. *A. hydrophila* is a Gram-negative short rod-shaped bacterium, which is widely distributed in various water and can cause severe diseases in fish, reptiles, amphibians and humans under certain conditions (2). In aquaculture, when environmental factors suddenly change and water quality deteriorates, *A. hydrophila* can infect various fish species, such as Indian major carp, mrigal *Cirrhinus mrigala* (3), rainbow trout *Oncorhynchus mykiss* (4), common carp *C. carpio* (5, 6), crucian carp *Carassius auratus* (7, 8), grass carp *Ctenopharyngodon idellus* (9), zebrafish *Danio rerio* (10), channel catfish *Ictalurus punctatus* (11–13), and tilapia *Oreochromis niloticus* (14), and lead to the outbreaks of bacterial hemorrhagic septicemia. This bacterial septicemia disease affected the quality and safety of the aquatic products, seriously restricted the sustainable development of healthy aquaculture, and resulted in considerable economic losses (2, 15). Hence, it is particularly important to determine the immune response of fish to the *A. hydrophila* infection, and to provide an effective strategy for controlling and preventing this bacterial septicemia.

In fish, innate immunity is considered as the major form of host defense, and it is also the efficient first line to resist invading pathogen (8). After the infection of *A. hydrophila*, the innate immune response is activated to improve the immune ability in teleost, and effectively eliminate pathogenic bacteria. Studies have shown that gasdermin E (GSDME) plays an indispensable role in combatting pathogen invasion through its NT-domain in teleost (16–20). The GSDME is composed of a conserved N-terminal pore-forming domain (N-PFD), a C-terminal auto-inhibitory domain (C-AID), and an intermediate linker region with a caspase hydrolysis site (18, 19, 21, 22). Under the normal condition, GSDME exists in inactive form with the full-length sequence *in vivo*, but under the stimulation of pathogen-associated molecular patterns (PAMPs) or damage-associated molecular patterns (DAMPs), Caspase-1/3/7 are activated and cleave GSDME in the linker region to release the NT domain, and then GSDME-NT oligomerization can penetrate cellular membrane, destroy cytomembrane integrity and lead to pyroptosis. Finally, the membrane rupture cells, as well as PAMPs and DAMPs, are phagocytosed by neutrophils to clear pathogenic bacteria and damaged cells (18, 19, 23–26).

Accompanying pyroptosis occurrence, massive cytoplasmic contents such as interleukin-1β (IL-1β), tumor necrosis factor-α (TNF-α), lactate dehydrogenase (LDH) and ATP were released into the extracellular area at the same time (27, 28). As a key pro-inflammatory cytokine, IL-1β can trigger an inflammatory reaction at the site of pathogenic infection to clear pathogens (29–32). However, IL-1β, without signal peptide, could not be directly secreted to the outside of cell. Previous studies have shown that the predicted maximum diameter of IL-1β was 4.5 nm, and the intracellular IL-1β could be released to the extracellular through the pores formed by gasdermin (33, 34). However, LDH could not pass through the gasdermin pore because the predicted maximum diameter of LDH tetramer was 9.6 nm, and it could only be released upon membrane rupture (35). Hence, only IL-1β, not LDH, is released from intracellular area to extracellular area, which can be used as biological indicator of membrane pore formed by GSDME in fish (35). Both IL-1β and LDH are released into the extracellular simultaneously, and it is indicated that cell membrane rupture and pyroptosis appear.

Previous studies have shown that zebrafish *Dr*GSDMEa and *Dr*GSDMEb, turbot (*Scophthalmus maximus*) *Sm*GSDMEb and tongue sole (*Cynoglossus semilaevis*) *Cs*GSDME could be cleaved by caspases and formed the membrane pores to cause pyroptosis (16–19). However, up to now, the function of GSDMEa in common carp is still unclear. Herein, we investigated the roles of *Cc*GSDMEa in the pore-formation of cellular membrane and regulation of IL-1β secretion after *A. hydrophila* infection. This study aims to clarify the roles of *Cc*GSDMEa in immune response of common carp and provide a new insight into protecting fish against pathogen infection.

Materials and methods

Experimental animals and cell culture

Experiments involving live animals were conducted in accordance with the "Regulations for the Administration of Affairs Concerning Experimental Animals" promulgated by the State Science and Technology Commission of Henan Province. This study was approved by the Animal Care and Use Ethics Committee of the Henan Normal University.

The healthy common carp (23 ± 2 g, 11 ± 1 cm) were from the aquaculture base in Zhengzhou, Henan province. Before the experiment, the fish were randomly grouped with 50 fish in each group, and then acclimated in 200 L tanks for two weeks. During acclimation, the fish were maintained at 25 ± 2 °C, and pH 7.0 ± 0.2, with the dissolved oxygen concentration of 6.0 ± 0.2 mg/L and natural light/dark cycle, and 1/3 water in tank was exchanged with the fresh aerated water twice a week. The fish were fed with pellets at 5% body weight. The common carp (4% of stock) were randomly sampled for bacterial or virus detection, and no pathogen was detected in the sampled fish, the experimental fish were considered to be healthy (36).

Mycoplasma-free Human Embryonic Kidney (HEK) 293T cells were cultured in DMEM medium (Hyclone, USA) supplemented with 10% (v/v) Fetal bovine serum (FBS, Gibco, USA), 2 mM L-Glutamine, and 4.5 g Glucose, at 37 °C in a 5% CO_2 incubator. For mycoplasma-free *Epithelioma papulosum cyprini* (EPC) cell, the M199 medium (Hyclone, USA) supplemented with 10% FBS, 1000 mg D-Glucose, 2200 mg $NaHCO_3$, and 100 mg L-Glutamine was used, and cultured at 25°C in an incubator with 5% CO_2. The cells were passaged every 2-3 d at a split ratio of 1:3 when the cells reached 90% confluency.

Bacterial strain culture

A. hydrophila, which was stored in our laboratory and isolated from common carp (15), cultured on Luria-Bertani broth (LB) plates at 28°C overnight, and single colony of each strain was then inoculated into 5 mL LB medium at 28 °C with constant shaking (180 rpm), and then sub-cultured in 100 mL LB medium with the ratio of 1:100 at 28 °C at 180 rpm until the absorbance values (OD_{600}) was 0.6 (37). The half lethal concentration (LC_{50}) of bacteria was 7×10^7 CFU/mL. The bacteria were harvested by centrifugation at 8000 rpm at 4 °C for 10 min, washed three times with 0.75% physiological saline (0.75% NaCl), and then resuspended in 0.75% NaCl with the concentration of 7×10^6 CFU/mL.

RNA extraction and cDNA synthesis

Total RNA was extracted from the samples using RNA extraction reagent RNAiso (TaKaRa, Japan) on the basis of the protocol of manufacture. Total RNA was dissolved in the RNase free water (Sangon, China). The concentration was determined by NanoDrop 2000 spectrophotometer (Thermo company, USA), and the purity was detected through 1% agarose gel electrophoresis. First-strand cDNA used for gene cloning was synthesized using the PrimeScript™ II 1st Strand cDNA Synthesis Kit (TaKaRa, Japan), and the PrimeScript™ RT Master Mix was used to synthesize cDNA template for quantitative Real Time PCR (qRT-PCR) (Vazyme, China). The reverse transcription products were stored at -20°C until used.

Gene cloning and bioinformatics analysis

The open reading frame (ORF) amplification of *CcGSDMEa* was performed in a 20 μL reaction system, which was made up of 1 μL cDNA template, 1 μL forward primer, 1 μL reverse primer, 10 μL 2 × Taq Master Mix, and 7 μL ddH_2O. The PCR procedure was set as follows: 5 min at 94 °C for pre-denaturation, 34 cycles (30 s at 94°C for denaturation, 30 s at 58 °C for annealing, and 120 s at 72 °C for extension), and 10 min at 72°C for final extension. The products were analyzed on 1.5% agarose electrophoresis and purified by DNA gel extraction kit (Omega, USA). The purified DNA was ligated into the pMD-19T vector (Takara, Japan), and then transformed into *Escherichia coli* DH5α (Biomed, China). Positive clones were sequenced in Sangon Biotech Company (Shanghai, China).

The rapid amplification of cDNA end (RACE) method was used to amplify the 3' and 5' end sequences of *CcGSDMEa*. According to the instruction of PrimeScript™ II 1st Strand cDNA Synthesis Kit, the Oligo dT Primer was replaced by the 3' RACE Olig(T)-adaptor for reverse transcription to obtain the 3' RACE template. With regard to 5' RACE amplification template, the obtained cDNA product was purified with E.Z.N.A. Cycle-pure Kit (Omega, USA), and Poly (A) tail was added at the 3' end after purification. A total of 50 μL reaction system was as follows: cDNA 10 μL, 5 × TdT buffer 10 μL, 1% BSA 5 μL, dATP (10 mmol/L) 2.5 μL, TdT enzyme 1 μL, and ddH_2O 21.5 μL. Reaction condition was at 37 °C for 30 min and at 80 °C for 3 min. The obtained final product was 5' RACE template. The PCR amplification was performed using the primers of 3'/5' -Out and 3' RACE Adaptor/5' RACE Olig(T)-Adaptor for the first round PCR, and then followed by the nested PCR with the primers of 3'/5' -In and 3'/5' RACE Adaptor using the first round PCR products (diluted 50 times) as the template. The reaction system and PCR procedure were same as ORF amplification, except only 20 cycles for first round PCR. The primers used for gene cloning were shown in Table 1.

The amplified ORF was overlapped with the 3'/5' terminal sequences to obtain the full length of *CcGSDMEa* cDNA sequence, implemented in software DNAMAN. CLC Main Workbench 6.8 was used to translate the amino acid sequences. Theoretical isoelectric point (*pI*) and molecular weight (MW) were respectively calculated on the basis of deduced amino acid sequences by the Compute *pI*/MW software (https://web.expasy.org/compute_pi/). The domains were predicted and annotated with Simple Modular Architecture Research Tool-SMART (http://smart.embl-heidelberg.de/), and the three-dimensional structure of protein was predicted by I-TASSER (https://zhanggroup.org/I-TASSER). Homologous sequences were searched and analyzed by the BLAST algorithm of NCBI (http://blast.ncbi.nlm.nih.gov/Blast.cgi). Multiple sequence alignments were carried out using the DNAMAN 8.0, and phylogenetic tree was constructed using the neighbor-joining method, implemented in MEGA 7.0 program with a bootstrap test of 1000 replicates.

Spatial expression analysis by qRT-PCR

Various tissues including gill, liver, spleen, head kidney, trunk kidney, heart, intestine, brain, muscle, and skin were taken aseptically from six healthy fish (23 ± 2 g), respectively.

TABLE 1 Primers used for gene cloning and qRT-PCR in this study.

Primer names	Sequences (5′-3′)	Usage
CcGSDMEa ORF-F	ATGTTTGATAAAGCGACAAAG	ORF amplification
CcGSDMEa ORF-R	TCATGCAGCAACAAAGGATGC	
CcGSDMEa 5'-Out	CATTGAGTTTGAATCCTGTGGGTC	5' RACE
CcGSDMEa 5'-In	CACCACCGCAAGCACCTG	
CcGSDMEa 3'-Out	GGATGCTGGACTGGACCTGC	3' RACE
CcGSDMEa 3'-In	CAATGTTTTGCTACGGAAAGAGAATG	
5' RACE Olig(T)-Adaptor	GACTCGAGTCGACATCG$(T)_{17}$	Adaptor primer for RACE
5' RACE Adaptor	GACTCGAGTCGACATCG	
3' RACE Olig(T)-Adaptor	CTGATCTAGAGGTACCGGATCC$(T)_{14}$	
3' RACE Adaptor	CTGATCTAGAGGTACCGGATCC	
CcGSDMEa qRT-PCR-F	TGCTTTGGTGGATAGACTTGAGA	qRT-PCR
CcGSDMEa qRT-PCR-R	GTGGTAAGTCCACTCTTGTCAAG	
CcIL-1β qRT-PCR-F	CAGAGCAACAAACTAAGTGACGAG	
CcIL-1β qRT-PCR-R	GTGACCCGAATGACAGCCTC	
18S qRT-PCR-F	GAGACTCCGGCTTGCTAAAT	
18S qRT-PCR-R	CAGACCTGTTATTGCTCCATCT	

Total RNA extraction and cDNA synthesis were performed as described above. The AceQ qPCR SYBR Green Master Mix (Vazyme, China) and LightCycler® 480 II instrument (Roche, Switzerland) were used for qRT-PCR to detect gene expression at mRNA level. The qRT-PCR was performed in a 20 μL reaction system (10 μL 2 × AceQ qPCR SYBR Green Master Mix, 1 μL specific primers, 3 μL cDNA template and 6 μL ddH_2O), and cycling program (180 s at 95 °C for pre-incubation, followed by 40 cycles of 95 °C for 10 s and 60 °C for 30 s for amplification). The amplification efficiency of qRT-PCR primers for *CcGSDMEa* and *CcIL-1β* gene was 97.34% and 99.07%, respectively. The *18S* was used as the reference gene, and the amplification efficiency was 100.8% (Table 1). The results were analyzed by the $2^{-\Delta\Delta Ct}$ method.

A. hydrophila challenge and sampling

The healthy common carp (23 ± 2 g) were randomly divided into two groups (the treated group and the control group), with 50 fish each group. Fish were injected intraperitoneally with 100 μL *A. hydrophila* suspension at a concentration of 7×10^6 CFU/mL in treated group. In the control group, the fish were injected with 0.75% NaCl in the same volume. The experiments were carried out in triplicate. The fish were not fed during the experiment period and maintained under the same conditions with those during the acclimation period. The mortality of fish was observed and recorded every day. After *A. hydrophila* challenge, six fish from each group were randomly selected at 0 h, 3 h, 6 h, 12 h, 24 h, 48 h and 96 h, respectively, which were anesthetized with ethyl 3-aminobenzoate (MS-222, Sigma, USA), and then sampled. Blood was collected from the caudal vein and centrifuged at 3000 rpm at 4 °C for 10 min to collect serum, which was used for Enzyme-Linked Immunosorbent Assay (ELISA). The tissues (gill, liver, spleen, head kidney, intestine and skin) were sampled immediately and stored in liquid nitrogen. Total RNA extraction, cDNA synthesis, and qRT-PCR were carried out as described above.

Plasmid construction

The different forms of *Cc*GSDMEa were cloned into His-tagged pET-32a vector or GFP-tagged pEGFP-C1 vector through Hind III and KpnI sites to generate r*Cc*GSDMEa-FL (1-532 aa) or GFP-*Cc*GSDMEa-FL, r*Cc*GSDMEa-NT (1-252 aa) or GFP-*Cc*GSDMEa-NT and r*Cc*GSDMEa-CT (257-532 aa) or GFP-*Cc*GSDMEa-CT recombinant plasmids. *Cc*Caspase-1a/1b/3a/3b/7a/7b sequences were inserted into N-DmrB-pcDNA3.1-3HA expression vector through EcoR I and KpnI sites, respectively. The *Cc*GSDMEa, *Cc*Caspase-1a/1b/3a/3b/7a/7b, pET-32a (+) vector, pEGFP-C1 vector and N-DmrB-pcDNA3.1-3HA vector were digested by restriction enzymes (New England Biolabs, USA), and then they were purified and

ligated together by the T4 ligation enzyme (TakaRa, Japan). The recombinant plasmids were transferred into *E. coli* strain DH5α, and the positive clones were verified by sequencing. The primers used to construct plasmids were listed in Table 2. To remove the endotoxin, the constructed recombinant eukaryotic plasmids were extracted with an EndoFree Plasmid Kit following the instruction of manufacturer (Omega, USA).

*Cc*GSDMEa cleavage assay

A total of 5×10^6 EPC cells were seeded per well in six-well plates for 16 h, then co-transfected with GFP-*Cc*GSDMEa-FL (2.5 μg) and *Cc*Caspase-1a/1b/3a/3b/7a/7b (2.5 μg) plasmids using Lipofectamine 3000 Reagent (Thermo Fisher Scientific, USA) according to the instructions when the cells reached 90% confluency. 36 h later, the EPC cells were exposed to 1 μM AP20187 (a chemical inducer of dimerization, which could penetrate the cell membrane and induce the DmrB fusion protein to dimerize. Selleck, China) for 6 h to mediate *Cc*Caspase-1a/1b/3a/3b/7a/7b dimerization (38, 39). Next, the cells were collected, and the total proteins were extracted using the protein extraction kit (Solarbio, China) according to the specification. In detail, the EPC cells were lysed in lysis buffer supplemented with 1% PMSF, protease inhibitor and phosphatase inhibitor on ice for 15 min, and then centrifuged at 12000 rpm at 4 °C for 10 min. Protein concentration was detected by BCA assay kit (Solarbio, China). Subsequently, the protein was mixed with 5 × protein loading buffer (Solarbio, China) and boiled for 10 min, and then used for western blotting.

Immunocytochemical staining

The HEK293T cells (5×10^5 cells/well) were seeded on coverslips into 6-well cell culture plates overnight, and the plasmids expressing GFP-*Cc*GSDMEa-FL, GFP-*Cc*GSDMEa-NT and GFP-*Cc*GSDMEa-CT (1000 ng/well) were transfected with Lipofectamine 3000 Reagent when the cells reached 70% confluency, and the pEGFP-C1 vector was used as the control.

At 24 h after transfection, the cells were collected, and washed three times with sterile 1 × PBS buffer (Solarbio, China), and then fixed with 4% paraformaldehyde at room temperature for 1 h, washed three times. The cells were incubated with 0.1% Hoechst 33342 (Invitrogen, USA) for ten minutes for the sake of nucleus staining, or incubated with 0.1% DiI (Beyotime, China) for 10 min for the sake of cell plasma membrane staining, and then washed three times. The cell coverslips were mounted on glass slides with Antifade Mounting Medium (Beyotime, China) and air-dried at room temperature. The fluorescence images of cells were observed under a fluorescence microscope (Zeiss, Germany). In addition, the HEK293T cells were fixed with 2.5% glutaraldehyde at 4 °C overnight, and dehydrated using series gradient alcohol and tertiary butanol, and then the integrity of cytomembrane was observed under a biotypic scanning electron microscope (JEOL, Japan).

TABLE 2 Primers used for plasmid construction in this study.

Primer names	Sequences (5′-3′)
r*Cc*GSDMEa-F	GGGGTACCATGTTTGATAAAGCGAC (KpnI)
r*Cc*GSDMEa-NT-R	CCCAAGCTTGGGATGGGGATTCTGGGAAAT (Hind III)
r*Cc*GSDMEa-CT-F	GGGGTACCGGTCAGTGGCCACTGATC (KpnI)
r*Cc*GSDMEa-R	CCCAAGCTTTCATGCAGCAACAAAGG (Hind III)
GFP-*Cc*GSDMEa-F	CCCAAGCTTCGATGTTTGATAAAGCGAC (Hind III)
GFP-*Cc*GSDMEa-NT-R	GGGGTACCGAAAGTGGGATGGGGATT (KpnI)
GFP-*Cc*GSDMEa-CT-F	CCCAAGCTTCGGGTCAGTGGCCACTGATC (Hind III)
GFP-*Cc*GSDMEa-R	GGGGTACCTCATGCAGCAACAAAGGATGC (KpnI)
*Cc*Caspase-1a-3HA-F	CGGGTACCATGGCGAAGAGTACTAAGGAG (KpnI)
*Cc*Caspase-1a-3HA-R	GGGAATTCTGAGAGTCCGGGGAACAGGTAG (EcoR I)
*Cc*Caspase-1b-3HA-F	GGGGTACCATGGACATCAAAAGAGTTATG (KpnI)
*Cc*Caspase-1b-3HA-R	CGGAATTCTTACATGAGTCCAGGGAACAGG (EcoR I)
*Cc*Caspase-3a-3HA-F	GGGGTACCATGGATTCGTATCTCACAG (KpnI)
*Cc*Caspase-3a-3HA-R	CGGAATTCTTATTTAGAGAAATAGAG (EcoR I)
*Cc*Caspase-3b-3HA-F	CCAAGCTTATGAACGGAGACTGCGTG (Hind III)
*Cc*Caspase-3b-3HA-R	CGGAATTCTCAAGCAGTGAAGTACATC (EcoR I)
*Cc*Caspase-7a-3HA-F	GGGGTACCATGATGTCTTGTAAATTTC (KpnI)
*Cc*Caspase-7a-3HA-R	CGGAATTCTCAGCTGATGGAGCTCTTC (EcoR I)
*Cc*Caspase-7b-3HA-F	GGGGTACCATGGTTTCGCTTTCTCCG (KpnI)
*Cc*Caspase-7b-3HA-R	CGGAATTCTCAGTTGAAGTAGAGCTC (EcoR I)

The underlined letters indicated restriction enzyme site.

Assay for antibacterial effect and cytotoxicity

The different forms of r*Cc*GSDMEa recombinant plasmids were transferred into *E. coli* strain BL21 (DE3), and the transformants were cultured in LB with 100 μg/mL Ampicillin (Amp), shaken at 200 rpm at 37 °C until OD_{600} to 0.6. The bacteria diluted at 10^4 times, were evenly spread with 50 μL on LB agar plates with or without 0.1 mM IPTG, and then cultured at 37 °C overnight. The CFU on the plates was counted and statistically calculated. At the same time, the growth curve of *E. coli* was tested by measuring the OD_{600} after induction by IPTG.

The cytotoxicity was monitored by evaluating the release of LDH from cells. The cell culture medium was centrifuged at 400 g for 5 min at 4°C, and the supernatant was collected. The LDH content released from the cells was detected according to the instruction of the Lactate Dehydrogenase Cytotoxicity Detection Kit (Beyotime, China). The untransfected cells were used as the blank background control, and the LDH released from the cells treated with LDH release agent was used as the positive control with maximum enzyme activity. Each sample was tested in triplicate. Cytotoxicity (%) = (treated sample A_{490} - blank background control A_{490})/(maximum enzyme activity A_{490} - blank background control A_{490}) × 100.

Assay for bacterial clearance

The healthy fish (9 ± 0.5 g) were randomly divided into five groups (i.e., Control group: PBS; Knockdown groups: siControl group and si*Cc*GSDMEa group; Overexpression groups: pEGFP-C1 group and GFP-*Cc*GSDMEa-FL group). The primers of siRNAs (si*Cc*GSDMEa-F/R, 5'-GGA UCU AUA GAG UUG GGA ATT-3', 5'-UUC CCA ACU CUA UAG AUC CTT-3'; siControl-F/R, 5'-UUC UCC GAA CGU GUC ACG UTT-3', 5'-ACG UGA CAC GUU CGG AGA ATT-3') were designed and synthesized by Sangon Biotech Company (Shanghai, China). For the different knockdown groups, the fish were intramuscularly injected with 100 μL (10 μg) siControl or si*Cc*GSDMEa, respectively. The fish were intramuscularly injected with 100 μL (10 μg) GFP-*Cc*GSDMEa-FL or pEGFP-C1 plasmid in different overexpression groups, respectively (29, 40). In the control group, the fish were injected with 100 μL PBS by the same method. The experiments were carried out in triplicate. After 3 and 7 d, the tissues (gill, liver, spleen, trunk kidney and head kidney) were sampled in the aseptic condition and used for analyzing the efficiency of knockdown or overexpression by RT-qPCR.

In knockdown groups, overexpression groups and the control group, the fish were intraperitoneally injected with 100 μL *A. hydrophila* suspension (7× 10^6 CFU/mL) after knockdown or overexpression 3 d. The experiments were carried out in triplicate. After challenge for 24 h, the tissues were sampled respectively in the aseptic condition, and used to count the bacterial number in samples by plate count and detect the expression of *CcIL-1β* by RT-qPCR. Blood was collected from the caudal vein and centrifuged at 3000 rpm at 4 °C for 10 min to collect the serum, which was used for ELISA to measure the content of *Cc*IL-1β.

Assay for *Cc*IL-1β secretion

EPC cells (5 × 10^6 cells/well) were seeded into 6-well cell culture plates overnight, and then the siControl, si*Cc*GSDMEa, pEGFP-C1 and GFP-*Cc*GSDMEa-FL plasmids (1000 ng/well) were transfected when the cells reached 90% confluency, respectively. The untransfected cells were used as the control. The efficiency of knockdown or overexpression *in vitro* was analyzed after 24 h and 48 h, respectively. The untransfected cells and the cells transfected successfully with the above plasmids were divided into two subgroups, respectively. One group was stimulated by 10 μL *A. hydrophila* (1×10^4 CFU/well), and the other group was added with isometric PBS. After 3 h, the content of LDH and *Cc*IL-1β in cell culture medium was assessed to determinate the role of *Cc*GSDMEa in regulating IL-1β secretion.

ELISA

The levels of *Cc*GSDMEa and *Cc*IL-1β in serum were measured according to the method of ELISA (6, 40). Briefly, 96-well Immuno-Maxisorp plates were coated with the serum (1:1) in 2× coating buffer (0.05 M carbonate buffer, pH 9.6) overnight at 4 °C. Next, 10% skimmed milk powder was used as the blocking agent at 37 °C for 2 h, and then were subsequently washed three times (wash buffer: 20 mM PBST, 274 mM NaCl, 5.4 mM KCl, 20 mM Na_2HPO_4, 3.6 mM KH_2PO_4, 0.5 mL Tween-20, PH 7.4). Polyclonal antibodies against *Cc*GSDMEa or *Cc*IL-1β (1: 500, prepared in our laboratory) were added to the wells to incubation at 37 °C for 2 h and an addition wash. After incubation with horseradish peroxidase labeled Goat anti-Mouse IgG/HRP (Solarbio, China) at 37 °C for 1 h, the plates were washed again. 3,3',5,5' -tetramethylbenzidine (TMB, Sigma, USA) was used as the substrate for color development at 37 °C for 30 min. The reaction was terminated by adding 50 μL of termination solution (2M H_2SO_4). The OD_{450} absorbance value was detected in a microplate reader (PerkinElmer, USA) within 10 min, and the amount of excretive *Cc*GSDMEa and *Cc*IL-1β (pg/mL) was estimated by comparing to reference curves constructed using the corresponding standards.

Western blotting analysis

The protein samples (30 μg) were separated by SDS-PAGE before being transferred to a PVDF membrane (Millipore, USA)

according to traditional protocol. The membranes were blocked in 5% w/v nonfat dry milk in TBST and then washed three times using TBST for 10 min every time. The mouse anti-GFP Ab (1:10,000, GenScript, China) or mouse anti-β-actin Ab (1:10,000, Beyotime, China) was incubated overnight at 4°C and washed another three times, then followed by incubation with the appropriate secondary goat anti-mouse IgG-HRP Ab (1:5000; Solarbio, China) and washed three times again, whereafter detected by super ECL detection reagent (Millipore, USA) using gel imaging system (Biorad, USA).

Statistical analysis

All values in this study were presented as means ± standard deviation (M ± SD) (n=3). The data statistical analysis was performed by SPSS 20.0 and GraphPad Prism 5.0. The statistical significance was determined using Student's *t* test and one-way ANOVA followed by Tukey's test. Significant difference was set as P <0.05 (*), P <0.01 (**), or P <0.001 (***).

Result

Structural analysis of *Cc*GSDMEa

In this study, *CcGSDMEa* (GenBank accession number: ON981707), a homologous *GSDME* gene, was obtained from common carp, which is distributed within 7320 bp genomic fragment on chromosome A19 with 9 exons and 8 introns. The location and transcription direction of the adjacent genes to *CcGSDMEa* were consistent with those of *DrGSDMEa* and *HsGSDME*, and it was suggested that genes adjacent to *CcGSDMEa* loci shared an overall conserved chromosome synteny with those of humans and zebrafish (Figure 1A). The full length of *CcGSDMEa* cDNA sequence is 2736 bp with a 1599 bp ORF, a 177 bp 5'-untranslated region and a 960 bp 3'-untranslated region (Figure S1). The ORF encoded 532 amino acids was predicted with molecular weight of 58.57 kDa and theoretical isoelectric point of 4.92. It displayed high identities (58.9%) and similarities (76.0%) to zebrafish *DrGSDMEa*, but low identities (29.3% and 24.2%) and similarities (51.2% and 45.8%) to zebrafish *DrGSDMEb* and human *HsGSDME*, respectively (Table 3).

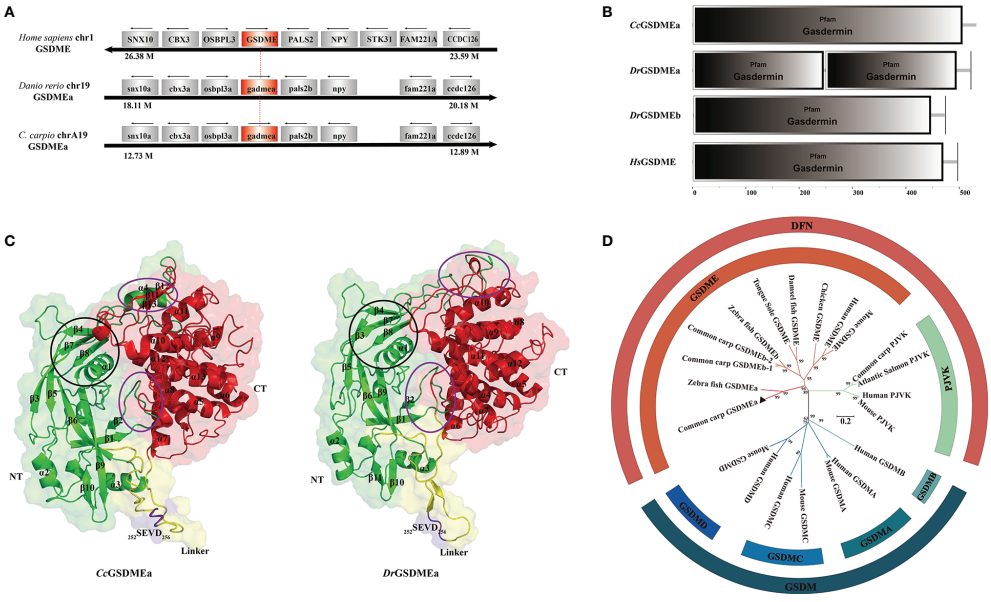

FIGURE 1
Structural feature and phylogenetic evolution of *Cc*GSDMEa. **(A)** Gene synteny and chromosomal location analysis of *CcGSDMEa*. The genes adjacent to GSDME loci on human chromosome 1, zebrafish chromosome 19, common carp chromosome A19 are shown. Arrows indicate gene orientation. The small arrows above the gene indicate the direction in which the gene is transcribed. **(B)** Structure domains of *Cc*GSDMEa, *Dr*GSDMEa/b, and *Hs*GSDME predicted by SMART. **(C)** The tertiary structures of *Cc*GSDMEa and *Dr*GSDMEa modeled by I-TASSER. The NT domains and CT domains are colored green and red, respectively. The motifs of tetrapeptide $_{252}$SEVD$_{256}$ specifically recognized by caspases are marked in purple, and the linker regions are labeled in yellow. Secondary structure element α-helices and β-strands are indicated in images. The inter-domain interfaces are highlighted by purple ellipses. The α1, β3, β4, β7 and β8 marked by the black circle form the structure of the membrane inserted N-terminal domain. **(D)** Phylogenetic relationships of GSDM family members. The phylogenetic tree was constructed by MEGA (version 7.0) using the neighbor-joining method. The reliability of each node was estimated by bootstrap test with 1000 replications. The accession numbers of selected GSDM protein sequences from the National Center for Biotechnology Information Reference Sequence database (http://www.ncbi.nlm.nih.gov/RefSeq/) are shown in Table 3.

10.3389/fimmu.2022.1110322

To better understand the function of *Cc*GSDMEa, the features of domain and tertiary architecture were characterized. The *Cc*GSDMEa contained one gasdermin domain, which is consistent with the other GSDM family members except for *Dr*GSDMEa (Figure 1B). In addition, the *Cc*GSDMEa shared highly conserved tertiary architectures with zebrafish *Dr*GSDMEa, which had a conserved N-terminal pore-forming domain, C-terminal auto-inhibitory domain and a flexible and pliable hinge region (Figure 1C). In linker regions, the predicted tetrapeptide motif, which was specifically recognized by caspases, was $_{252}$SEVD$_{256}$. This was the same as the cleavage site of *Dr*GSDMEa. Phylogenetic tree revealed that *Cc*GSDMEa was grouped with zebrafish *Dr*GSDMEa with a high score of bootstrap tests. Interestingly, *Cc*GSDMEa was not grouped with GSDMEb of common carp, but was clustered into a separate clade (Figure 1D), which provided us a better clue for future analysis of GSDME evolutionary function in teleost. In addition, both members of the deafness-associated gene (i.e., GSDME and PJVK) were clustered together, and they were distant from the other members (GSDMA, GSDMB, GSDMC and GSDMD).

TABLE 3 Identity and similarity between *Cc*GSDMEa and other species GSDM sequences.

Gene name	Gene bank No.	Identities	Similarities
*Cc*GSDMEa	ON981707		
*Cc*GSDMEb-1	OP046437	31.9%	52.5%
*Cc*GSDMEb-2	OP046436	30.0%	50.7%
*Dr*GSDMEa	XP_005170134.1	58.9%	76.0%
DrGSDMEb	NP_001001947.1	29.3%	51.2%
*Cs*GSDME	XP_016893587.1	25.9%	52.1%
*Ap*GSDME	XP_022071512.1	27.0%	49.4%
*Gd*GSDME	NP_001006361.2	25.3%	44.6%
*Hs*GSDME	NP_004394.1	24.2%	45.8%
*Mm*GSDME	NP_061239.1	21.9%	45.3%
*Cc*PJVK	XP_018961188.2	15.0%	30.9%
*Ss*PJVK	XP_045556351.1	13.0%	27.0%
*Hs*PJVK	AAI46939.1	24.2%	29.9%
*Mm*PJVK	NP_001074180.1	21.9%	30.4%
*Hs*GSDMD	AAH69000.1	15.4%	32.2%
*Mm*GSDMD	AAH29813.1	13.4%	32.1%
*Hs*GSDMC	AAH35321.1	12.1%	29.8%
MmGSDMC	NP_113555.1	14.0%	32.1%
HsGSDMB	KAI4049241.1	11.7%	30.1%
*Hs*GSDMA	AAI09198.1	14.3%	31.7%
*Mm*GSDMA	NP_067322.1	14.7%	32.3%

Expression profile of *Cc*GSDMEa after *A. hydrophila* challenge

CcGSDMEa was widely expressed in the tested tissues and exhibited a tissue-specific spatial expression pattern. *CcGSDMEa* was highly expressed in the skin and gill, followed by the head kidney and trunk kidney, and the lowest expression was in brain (Figure 2A). Moreover, the expression levels in immune-related tissues (head kidney, spleen, skin, intestine and gill) were markedly higher than those in heart, liver and brain.

To further analyze the expression profile of *Cc*GSDMEa in response to bacterial infection, *A. hydrophila* was chosen to stimulate the juvenile common carp. The peaks of *CcGSDMEa* expression were at 3 h in liver, at 6 h in gill, head kidney and spleen, and at 12 h in intestine and skin (Figures 2C-H). Although the peaks of mRNA expression levels were different in various tissues and appeared at the different time points, the expression levels of *CcGSDMEa* were increased after *A. hydrophila* infection, compared with the control. The protein expression level of *Cc*GSDMEa showed a trend of increasing at first and then decreasing with the time prolongation in serum, and the expression peak was observed at 12 h (Figure 2B). The expression levels among different time points showed significant differences. Meanwhile, the protein expression levels of *Cc*GSDMEa were notably increased at the different time points compared with the control.

*Cc*GSDMEa-NT was produced from *Cc*GSDMEa cleavage by *Cc*Caspase-1/3/7

To better understand the cleavage mechanism of *Cc*GSDMEa, each of the *Cc*Caspase-1a, *Cc*Caspase-1b, *Cc*Caspase-3a, *Cc*Caspase-3b, *Cc*Caspase-7a and *Cc*Caspase-7b plasmids was co-transfected with *Cc*GSDMEa-FL into EPC cells, and then treated with the dimerizing drug AP20187 for 6 h. The results showed that *Cc*Caspase-1b, *Cc*Caspase-3a, *Cc*Caspase-3b, *Cc*Caspase-7a and *Cc*Caspase-7b could cleave *Cc*GSDMEa to produce *Cc*GSDMEa-NT, except for *Cc*Caspase-1a (Figure 3A). The LDH released from cells co-transfected *Cc*Caspase-1b/3a/3b and *Cc*GSDMEa, were dramatically higher than that released from cells only transfected *Cc*GSDMEa (Figure 3B). HEK293T cells were co-transfected with *Cc*Caspase-1a/1b/3a/3b/7a/7b and *Cc*GSDMEa, and the morphology of cell membrane was observed. The results showed that, except for the co-

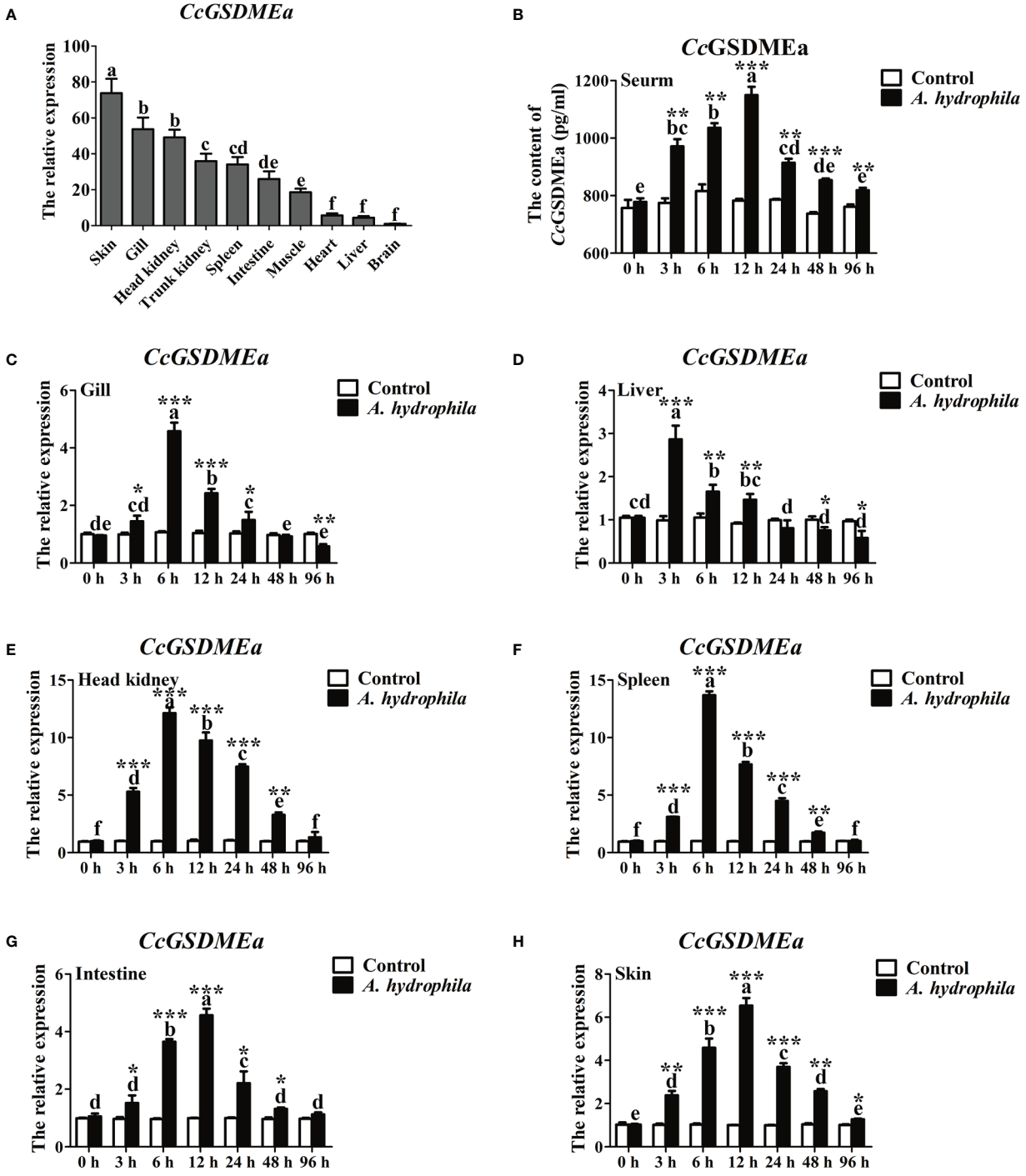

FIGURE 2
Expression profile of *Cc*GSDMEa after *A. hydrophila* challenge. **(A)** Tissues distribution of *CcGSDMEa* in healthy *C. carpio*. The lowest expression level in brain was chosen as calibration (set as 1), and the relative expression of *CcGSDMEa* in other tissues was represented as fold-changes to the calibration. **(B)** The protein expression levels of *Cc*GSDMEa in serum after *A. hydrophila* challenge. **(C-H)** The mRNA expression levels of *CcGSDMEa* in different tissues after *A. hydrophila* challenge. The control group was chosen as calibration (set as 1). The data were expressed as mean ± SD (n = 3). Significant difference between the different time points were analyzed using one-way ANOVA followed by Tukey's test, and presented with the different lowercase letters in the group challenged by *A. hydrophila* ($P<0.05$), and the same letter was indicated no significant difference ($P > 0.05$). The significant differences between the *A. hydrophila* challenge group and the control group at the same time point were analyzed by student's *t* test and indicated with asterisks (*, $P < 0.05$; **, $P < 0.01$, ***, $P < 0.01$).

10.3389/fimmu.2022.1110322

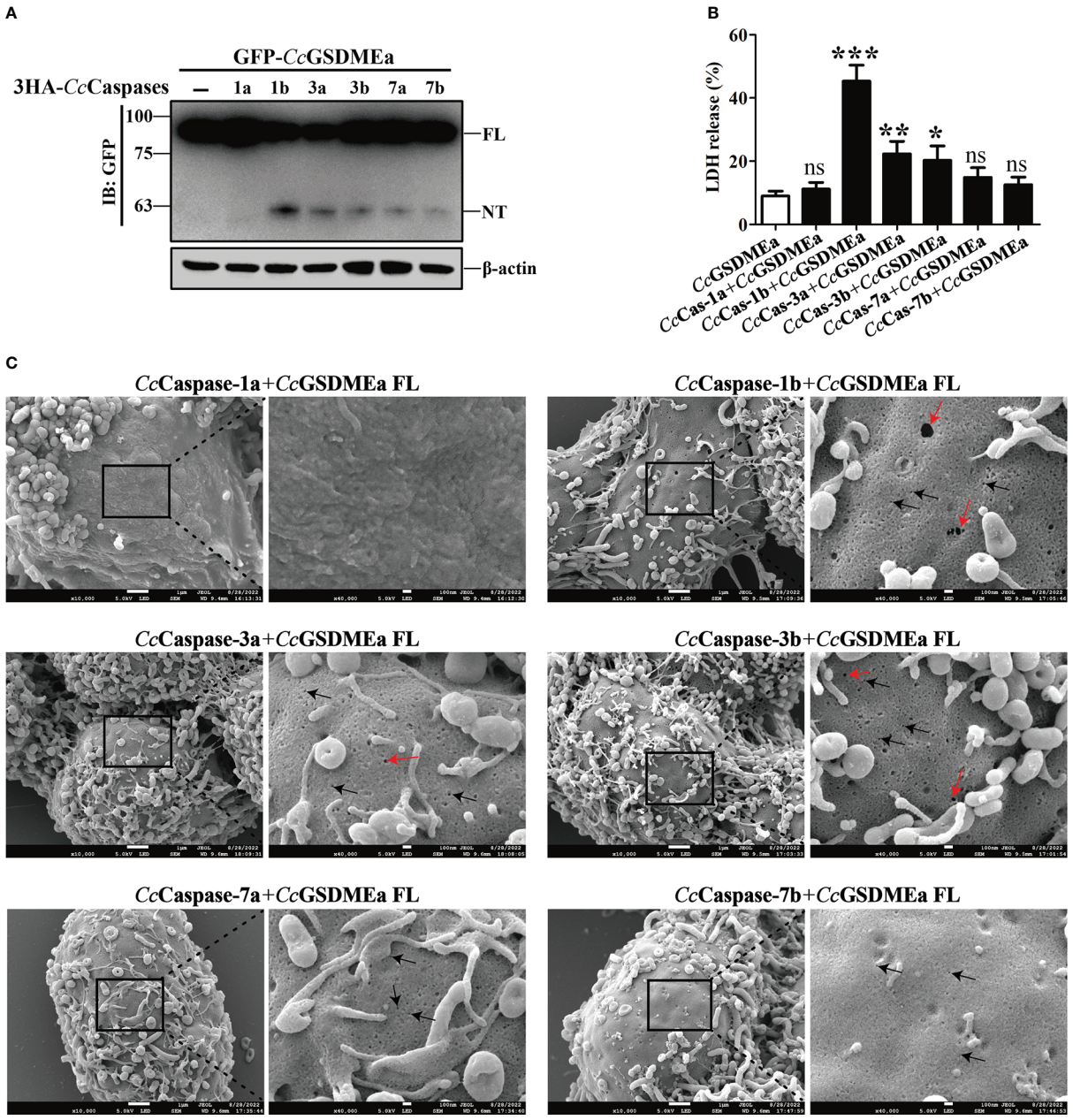

FIGURE 3
*Cc*GSDMEa-NT was produced from *Cc*GSDMEa cleavage by *Cc*Caspase-1/3/7. **(A)** The western bolting result that *Cc*GSDMEa was cleaved by *Cc*Caspase-1b/3a/3b/7a/7b. **(B)** LDH release from the EPC cells co-transfected with *Cc*GSDMEa and the *Cc*Caspase-1a/1b/3a/3b/7a/7b plasmids. **(C)** Morphological observation of HEK293T cells co-transfected with *Cc*GSDMEa and the *Cc*Caspase-1a/1b/3a/3b/7a/7b plasmids. Red arrows display cell plasma membrane rupture, and dark arrows indicate the gasdermin membrane pores. Values are shown as mean ± SD (n = 3). The LDH release from the cells only transfected with *Cc*GSDMEa was set as control. The significance difference of LDH release between the control cells and the co-transfected cells was analyzed by student's *t* test and shown as: ns, $P > 0.05$; *, $P < 0.05$; **, $P < 0.01$; ***, $P < 0.001$.

transfection of *Cc*Caspase-1a and *Cc*GSDMEa, membrane pores could be observed in the co-transfected cells (Figure 3C). It was indicated that any one of *Cc*Caspase-1b/3a/3b/7a/7b could cleave *Cc*GSDMEa to generate *Cc*GSDMEa-NT, which could oligomerize on the cell membrane and penetrate the plasma membrane.

The membrane pore formation induced by *Cc*GSDMEa-NT

To explore the pore forming function of *Cc*GSDMEa, the *Cc*GSDMEa-FL/NT/CT recombinant plasmids with GFP-tag were constructed (Figure 4A). The different recombinant

10.3389/fimmu.2022.1110322

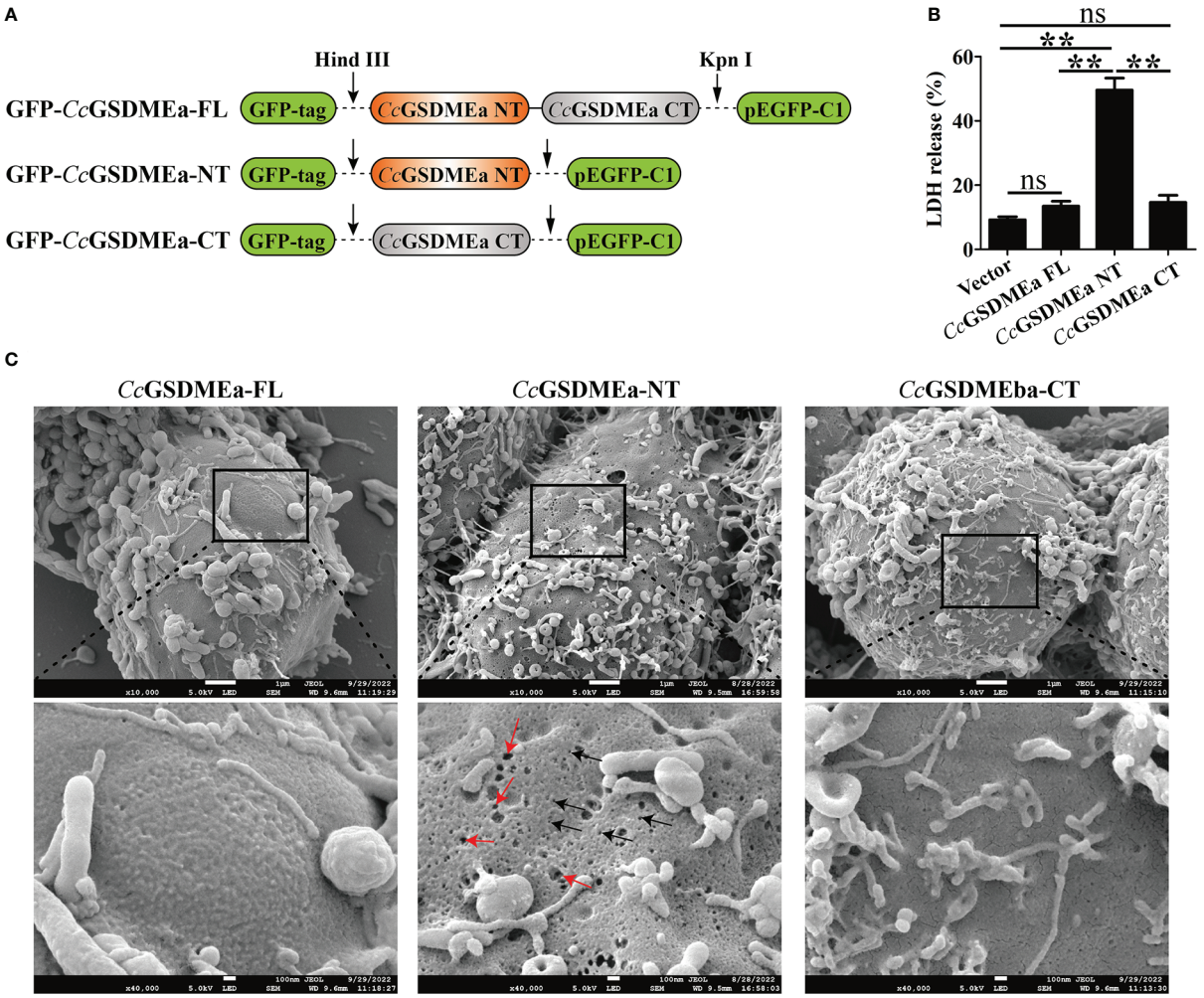

FIGURE 4
Membrane pore formation induced by *Cc*GSDMEa-NT in HEK293T cells. **(A)** Schematic diagram of the recombinant plasmids of *Cc*GSDMEa-FL (1-532 AA), *Cc*GSDMEa-NT (1-250 AA), *Cc*GSDMEa-CT (257-532 AA) and pEGFP-C1. **(B)** LDH release from cells transfected with 1000 ng of different forms of *Cc*GSDMEa recombinant plasmids. **(C)** Morphological observation of HEK293T cells transfected with different forms of *Cc*GSDMEa recombinant plasmids. Red arrows display cell plasma membrane rupture, and dark arrows indicate the membrane pores induced by *Cc*GSDMEa-NT. The LDH release values are shown as M ± SD (n = 3). The significant differences were analyzed by student's *t* test, "**" means $P < 0.01$, "ns" means no significant difference.

plasmids of *Cc*GSDMEa were transfected into HEK293T cells to observe the morphological changes and LDH release. The results showed that the release of LDH from cells expressing *Cc*GSDMEa-NT was markedly higher than that of cells expressing *Cc*GSDMEa-FL or *Cc*GSDMEa-CT and pEGFP-C1 vector (Figure 4B). Cytomembrane pores and rupture phenomenon were also observed only in the transfected cells with *Cc*GSDMEa-NT plasmids (Figure 4C). It was suggested that only *Cc*GSDMEa could punch holes in the membrane and disrupt the integrity of cytomembrane through its NT domain.

In addition, the subcellular localizations of *Cc*GSDMEa-FL, NT and CT in HEK293T cells were varied (Figure 5A). The *Cc*GSDMEa-FL was localized in the cytoplasm and cytomembrane, the *Cc*GSDMEa-NT was only situated in the cytomembrane, and the *Cc*GSDMEa-CT was distributed in the whole cells. We also found that *Cc*GSDMEa-NT and DiI-labeled cytomembrane were completely colocalized (Figure 5B), and it was indicated that *Cc*GSDMEa-NT could accumulate on the cellular membrane.

Bactericidal activity of *Cc*GSDMEa to *E. coli*

In order to detect the bactericidal activity of *Cc*GSDMEa, *Cc*GSDMEa-FL, *Cc*GSDMEa-NT and *Cc*GSDMEa-CT were subcloned into pET-32a vector, respectively (Figure 6A). The recombinant plasmids r*Cc*GSDMEa-FL/NT/CT were expressed

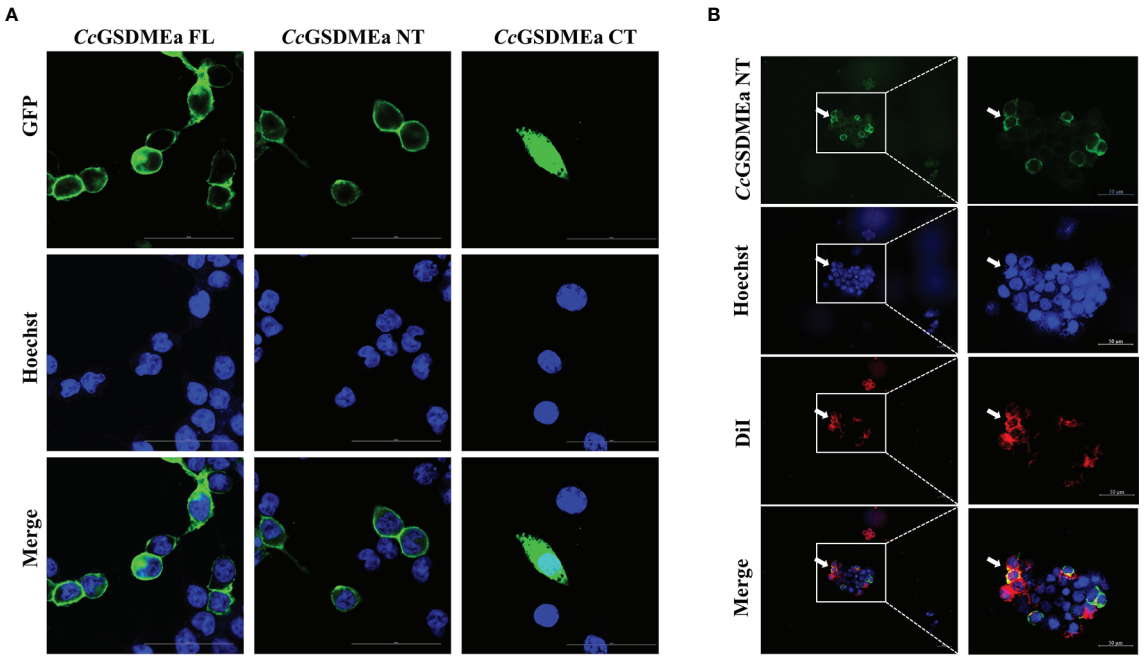

FIGURE 5
Subcellular localizations of *Cc*GSDMEa different forms. **(A)** Subcellular localizations of *Cc*GSDMEa-FL/NT/CT and Hoechst-stained nucleus in HEK293T cells. **(B)** Subcellular localization of *Cc*GSDMEa-NT, Hoechst-stained nucleus and DiI-stained cytomembrane in HEK293T cells (white arrowheads). The original microscope images were on the left and the locally enlarged images were on the right in **(B)**.

in *E. coli* by IPTG-induced manner. Of note, the number of *E. coli* expressing r*Cc*GSDMEa-NT was markedly reduced compared with that of expressing r*Cc*GSDMEa-FL or r*Cc*GSDMEa-CT after IPTG induction (Figures 6B, C). The growth curves of *E. coli* expressing different recombinant plasmids of *Cc*GSDMEa were also been analyzed. The OD_{600} of *E. coli* expressing r*Cc*GSDMEa-NT indicated little change at different time points after IPTG induction, but the OD_{600} values of *E. coli* expressing r*Cc*GSDMEa-FL, r*Cc*GSDMEa-CT and pET-32a vector showed an increasing trend with time prolongation after IPTG induction (Figure 6D). It was demonstrated that *Cc*GSDMEa-NT could perform bactericidal function.

*Cc*GSDMEa promotes the expression of *Cc*IL-1β *in vivo*

To better understand the role of *Cc*GSDMEa in regulating *Cc*IL-1β, the *Cc*GSDMEa in fish was knocked down or overexpressed, and the expression of *Cc*IL-1β at the mRNA and protein levels were detected. The knockdown and overexpression of *Cc*GSDMEa were confirmed based on the results of *CcGSDMEa* mRNA expression levels *in vivo*. Figure 7 showed that the *CcGSDMEa* mRNA expression levels in GFP-*Cc*GSDMEa group were markedly increased compared with the levels in pEGFP-C1 group at 3 d and 7 d (Figures 7A, B). However, the expression levels of *CcGSDMEa* in si*Cc*GSDMEa group were lower than those in siControl group (Figures 7C, D).

In *Cc*GSDMEa overexpression group, the *Cc*IL-1β expressions at the mRNA and protein levels were notably higher compared with the expression levels in pEGFP-C1 group (Figures 7E, G). In *Cc*GSDMEa knockdown group, the expression levels of *Cc*IL-1β decreased compared with the siControl group (Figures 7F, H). These results suggested that *Cc*GSDMEa could promote *Cc*IL-1β expression.

*Cc*GSDMEa prevents *A. hydrophila* colonization *in vivo*

As mentioned above, the expression of *Cc*GSDMEa increased in fish when stimulated by *A. hydrophila* (Figure 2). After *Cc*GSDMEa was overexpressed or knocked down, the bacterial burdens were examined in tissues of fish after *A. hydrophila* challenge for 24 h. As shown in Figure 8, the bacterial burdens were obviously lower in head kidney, spleen, gill, liver and trunk kidney in GFP-*Cc*GSDMEa overexpression group than those in the pEGFP-C1 group. While, in si*Cc*GSDMEa group, the bacterial burdens were observably increased in head kidney, gill, liver, spleen and trunk kidney, compared with those in siControl group. It was indicated that the *Cc*GSDMEa could prevent the colonization of *A. hydrophila* and minish the bacterial burdens in fish.

10.3389/fimmu.2022.1110322

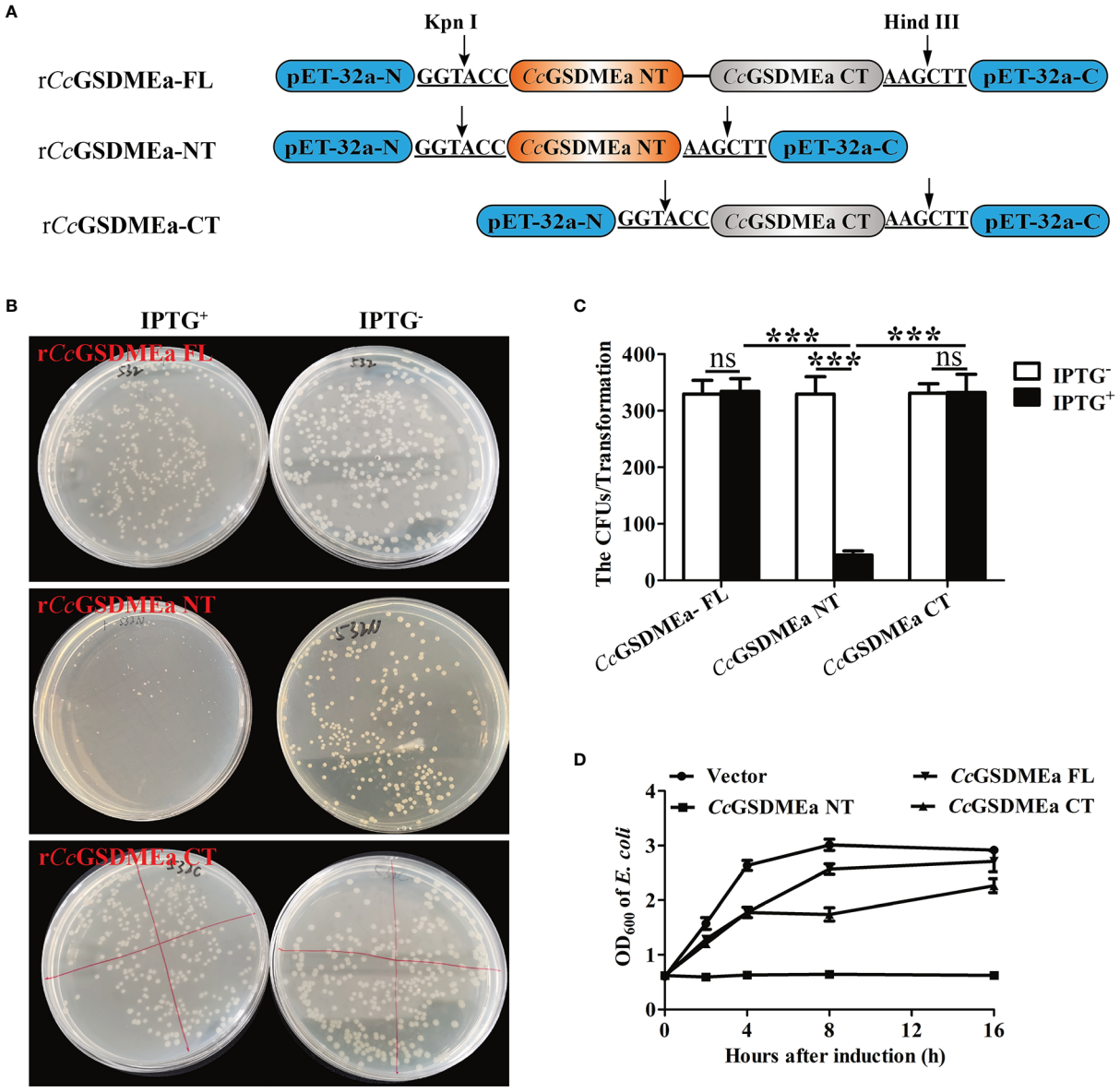

FIGURE 6
Bactericidal activity of *Cc*GSDMEa to *E. coli*. **(A)** Schematic diagram of the recombinant plasmids of r*Cc*GSDMEa-FL, r*Cc*GSDMEa-NT and r*Cc*GSDMEa-CT. **(B)** Colony growth of *E. coli* expressing r*Cc*GSDMEa-FL/NT/CT. **(C)** Calculation of CFUs on the plates. **(D)** Growth curves of *E. coli* expressing r*Cc*GSDMEa-FL/NT/CT after IPTG induction. Values are expressed as M ± SD (n = 3). The statistical difference was analyzed by student's *t* test (***, $P < 0.001$; ns, no significant difference).

*Cc*GSDMEa promotes the secretion of *Cc*IL-1β in EPC cells

After EPC cells challenged with *A. hydrophila*, the expression levels of *CcGSDMEa* and *CcIL-1β* significantly increased, compared with the control group (Figure 9A), it was suggested that *A. hydrophila* could trigger the innate immune responses of EPC cells. Similarly, the contents of *Cc*IL-1β protein in the cell culture medium were also increased after *A. hydrophila* challenge compared with the control group (Figure 9B), and it was manifested that *A. hydrophila* challenge could promote the secretion of *Cc*IL-1β. Moreover, the LDH released from EPC cells treated by *A. hydrophila* were observably higher than that in the control group (Figure 9C), and indicted that *A. hydrophila* challenge might destroy cytomembrane integrity of EPC cells.

To clarify the effect of *Cc*GSDMEa on *Cc*IL-1β secretion, the *Cc*GSDMEa was overexpressed or knocked down in EPC cells, and then the contents of *Cc*IL-1β protein in cell culture medium were examined after *A. hydrophila* stimulation. As shown in

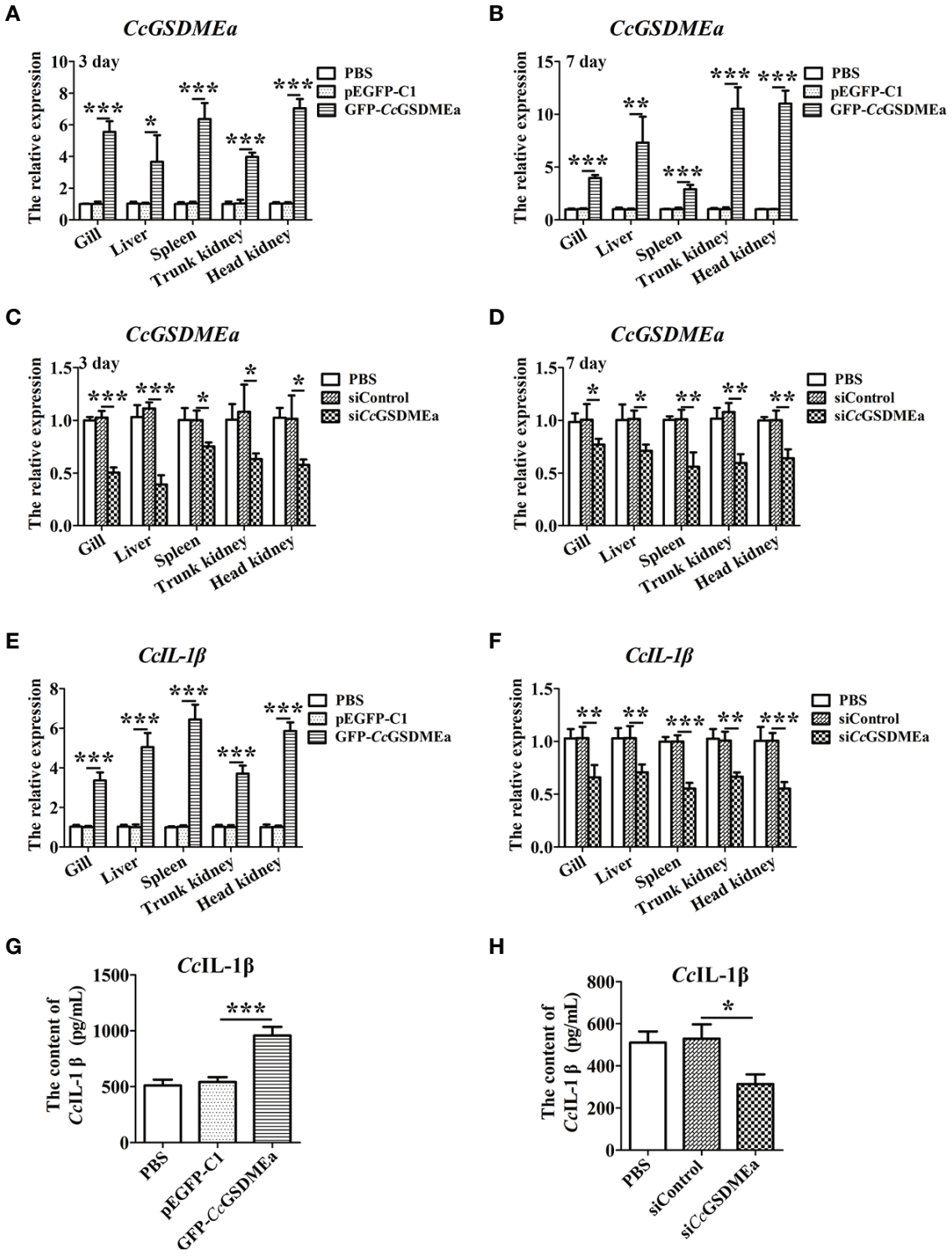

FIGURE 7
*Cc*GSDMEa promotes the expression of *Cc*IL-1β *in vivo*. **(A-D)** Overexpression efficiency and knockdown efficiency of *Cc*GSDMEa in gill, liver, spleen, trunk kidney and head kidney of *C. carpio*. **(E, F)** The mRNA expression levels of *Cc*IL-1β in the different groups after *A. hydrophila* challenge. **(G, H)** The protein expression levels of *Cc*IL-1β in the different groups after *A. hydrophila* challenge. In each case, the mRNA expression level in the PBS group was chosen as calibration (set as 1). The statistical difference was analyzed by student's *t* test (*, $P < 0.05$; **, $P < 0.01$; ***, $P < 0.001$).

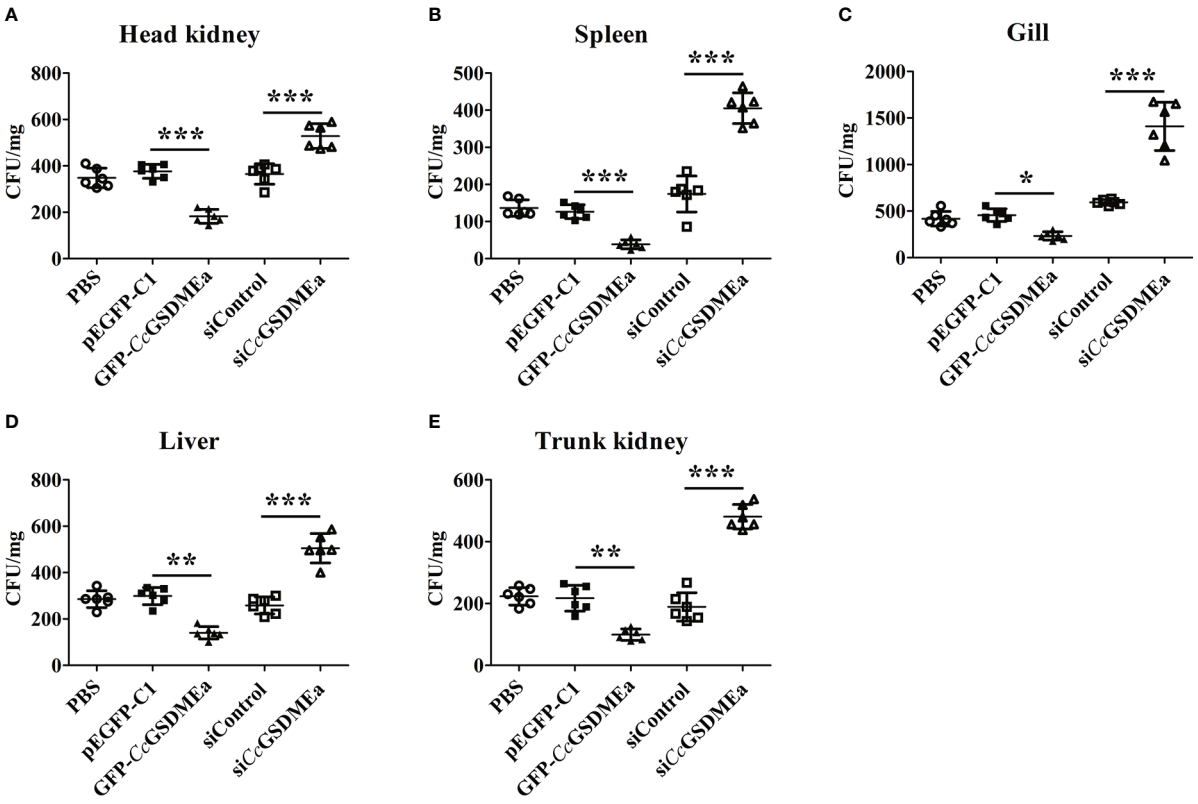

FIGURE 8
*Cc*GSDMEa prevents *A. hydrophila* colonization *in vivo*. Bacterial burdens in head kidney **(A)**, spleen **(B)**, gill **(C)**, liver **(D)** and trunk kidney **(E)** of different groups infected with *A. hydrophila*. The data are expressed as mean ± SD (n = 3) and analyzed statistically by student's *t* test (*, $P < 0.05$; **, $P < 0.01$; ***, $P < 0.001$).

Figures 9D, E, the overexpression and knockdown of *Cc*GSDMEa were both affirmed. After *A. hydrophila* challenge, in the *Cc*GSDMEa overexpression group, expression level and secretion content of *Cc*IL-1β and the release of LDH were significantly increased, compared with the pEGFP-C1 group (Figures 9F-H). It was illustrated that the overexpression of *Cc*GSDMEa could intensify the effect of *A. hydrophila* challenge on *Cc*IL-1β secretion and LDH release. However, in si*Cc*GSDMEa group, after *A. hydrophila* challenge, the expression level and secretion content of *Cc*IL-1β and the release of LDH were notably decreased compared with the siControl group. It was implied that the knockdown of *Cc*GSDMEa could retard the effect of *A. hydrophila* on *Cc*IL-1β secretion and LDH release. Taken together, these results revealed that *Cc*GSDMEa played an important role in regulating the secretion of *Cc*IL-1β.

Discussion

The different types of cell death, such as apoptosis, autophagy, necrosis or pyroptosis, mainly depend on the inducing factors and the different stages of the cell cycle. Among these types of programmed cell death, pyroptosis is a newly defined inflammatory programmed cell death that plays an important role in fighting bacterial infections and inflammatory diseases (41). Previous studies have shown that the gasdermin family members were the executors of pyroptosis and played key roles in the innate immunity (18, 42, 43). However, in teleost, only two members of gasdermin family (GSDME and PJVK) have been identified to date, and they were considered as the ancient members of the GSDM family (19, 21, 44). Since PJVK does not perform immune-related functions (35, 45), GSDME is considered to be the only executor of pyroptosis in teleost, and its role of innate immune to resist pathogen invasion has become a research hotspot.

In this study, the *CcGSDMEa* identified from common carp shares conserved chromosomal colinearity and tertiary structure with GSDME in other fish and human (17–19, 24). Similar to the structure of mouse GSDMA3, α1, α4 helix and β1-β2 hairpin in NT domain of *Cc*GSDMEa provide the main surface for binding to the CT domain and then form the major autoinhibitory interactions (44). In addition, α1, β3, β4, β7 and β8 can form the N-terminal structure that inserts into cytomembrane. The

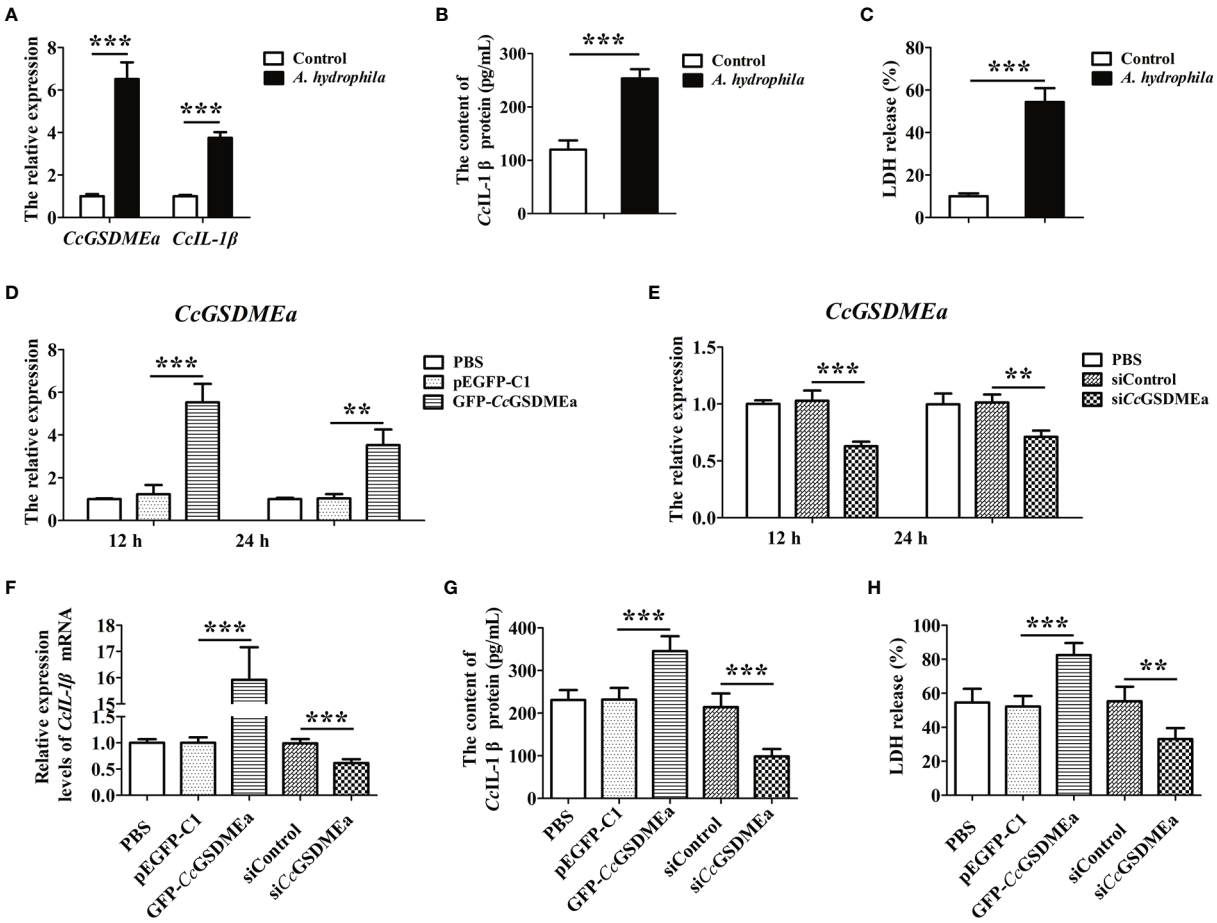

FIGURE 9
*Cc*GSDMEa promotes the secretion of *Cc*IL-1β *in vitro*. **(A)** The mRNA expression levels of *CcGSDMEa* and *CcIL-1β* in EPC cells after *A. hydrophila* challenge. **(B)** The content of *Cc*IL-1β protein in the cell culture medium after *A. hydrophila* challenge. **(C)** The LDH release in EPC cells after *A. hydrophila* challenge. **(D, E)** The overexpression and knockdown efficiency of *Cc*GSDMEa in EPC cells at 12 h and 24 h. **(F-H)** The mRNA expression levels of *CcIL-1β*, protein secretion contents of *Cc*IL-1β and the LDH release from cells in overexpression or knockdown group after *A. hydrophila* challenge. The data were expressed as mean ± SD (n = 3). The significant differences were analyzed using student's *t* test (**, $P < 0.01$; ***, $P < 0.001$).

α1 is the first α-helix that specifically interacts with phospholipids, and β3, β4, β7 and β8 are four parallel β-strands, which can insert into the membrane. These structural properties of *Cc*GSDMEa might provide the basis for its functional role.

CcGSDMEa was ubiquitously expressed in all tested tissues, although the expression levels are different in the varied tissues. In zebrafish, *DrGSDMEa* was highly expressed in intestine, gill, head kidney and spleen, but lowly expressed in brain, heart and muscle (19). The same situation was found in common carp. The high expression of *CcGSDMEa* in immune-related tissues indicated that it played an important role in the immune surveillance system. Studying the expression changes of *Cc*GSDMEa after *A. hydrophila* challenge is helpful to understand the immune response of fish to pathogen infection and provide new insights into the formulation of effective measures to prevent the occurrence of disease. The increased expression levels of *Cc*GSDMEa (mRNA and protein) suggested that *Cc*GSDMEa played an important role in immune response against the invasion of *A. hydrophila*. The peaks of *Cc*GSDMEa expression levels appeared at the early stage of infection, indicated that fish immune response was more active and stronger at the early stage of pathogen infection, and it suggested that the early stage of infection was the best period to clear pathogens in fish.

GSDME could be cleaved by caspases to cause pyroptosis in teleost. For instance, *Dr*GSDMEa could be cleaved by inflammatory caspases (caspase-B and caspase-19b) and apoptotic caspases (caspase-3a/b, caspase-7 and caspase-8a) in zebrafish (16), the *Sm*GSDME could be cleaved by *Sm*caspase in turbot, and *Cs*GSDME could be cleaved by caspase-1/3/7 in tongue sole (18). Similarly, *Cc*GSDMEa was cleaved by inflammatory caspases (*Cc*Caspase-1b) and apoptotic caspases (caspase-3a/b and caspase-7a/b) to release its N-terminal

domain to form the pores on cell membrane. Moreover, *Cc*GSDMEa cleaved by *Cc*Caspase-1b/3a/3b also could disrupt the cell membrane. The different LDH release and the different degree of cell membrane destruction of the cells might be due to the different cleavage efficiency of *Cc*GSDMEa by *Cc*Caspase-1b/3a/3b/7a/7b. The tongue sole *Cs*GSDME was cleaved with high efficiency by inflammatory Caspase-1, and with comparatively low efficiency by apoptotic Caspase-3/7 (18). To be different from this result, zebrafish *Dr*GSDMEa was cleaved with high efficiency by Caspase-1/3b and with low efficiency by Caspase-3a/7 (17, 19). This suggested that the efficiency of GSDME being cleaved in fish was not only related to the different of Caspases, but also related to the specificity of species.

Studies have shown that the NT-domain of GSDME could punch holes in the cell membrane and induced pyroptotic bubble formation and membrane lysis (18, 19, 28, 33). The membrane pore formation, cytomembrane rupture and LDH release from cells were observed only in transfected cells with *Cc*GSDMEa-NT plasmid, which was consistent with that found in zebrafish *Dr*GSDMEa and turbot *Sm*GSDMEb (16, 17). In addition, the number of *E. coli* expressing r*Cc*GSDMEa-NT was markedly reduced after IPTG induction, this was consistent with the findings in tongue sole, turbot and zebrafish (16–18). Accumulating evidence suggested that *Cc*GSDMEa-NT could not only punch holes in the membrane of HEK293T cells, but also directly destroy the integrity of bacterial membrane of *E. coli*, and showed that the *Cc*GSDMEa exerted its bactericidal activity and cytotoxicity through its NT domain.

The antibacterial infection mechanism of GSDME remains to be poorly understood in fish at present. In this research, the increased bacterial burdens in various tissues in *Cc*GSDMEa-knockdown group demonstrated that the ability to eliminate the invading bacteria was reduced in host. With respect to *Cc*GSDMEa-overexpression group, it was shown that bacterial loads were obviously decreased in different tissues. These results mentioned above provided the direct evidence that *Cc*GSDMEa played a key role in regulating bacterial clearance in fish. As a key node in the immune and inflammatory networks, IL-1β performs antibacterial defenses through involving in inflammation reaction in innate immunity (29, 30, 32, 46). Our results showed that *Cc*GSDMEa could promote the expression and secretion of *Cc*IL-1β, involve in inflammation reaction, and then help the host eliminate invading pathogens.

To sum up, *Cc*GSDMEa could be cleaved by *Cc*Caspase-1b/3a/3b/7a/7b to generate *Cc*GSDMEa-NT domain, which could oligomerize and translocate to the plasma membrane, where it could form pores to promote pyroptosis. *Cc*GSDMEa was involved in innate immune defense against *A. hydrophila* infection in common carp, through regulating the secretion of *Cc*IL-1β, and it was indicated that *Cc*GSDMEa played an important role in combating bacterial invasion (Figure 10). These results will provide a reference for us to further study the immune mechanism to defense against bacterial infection in fish, and also provide new strategies to prevent and control fish diseases for healthy and continuous aquaculture.

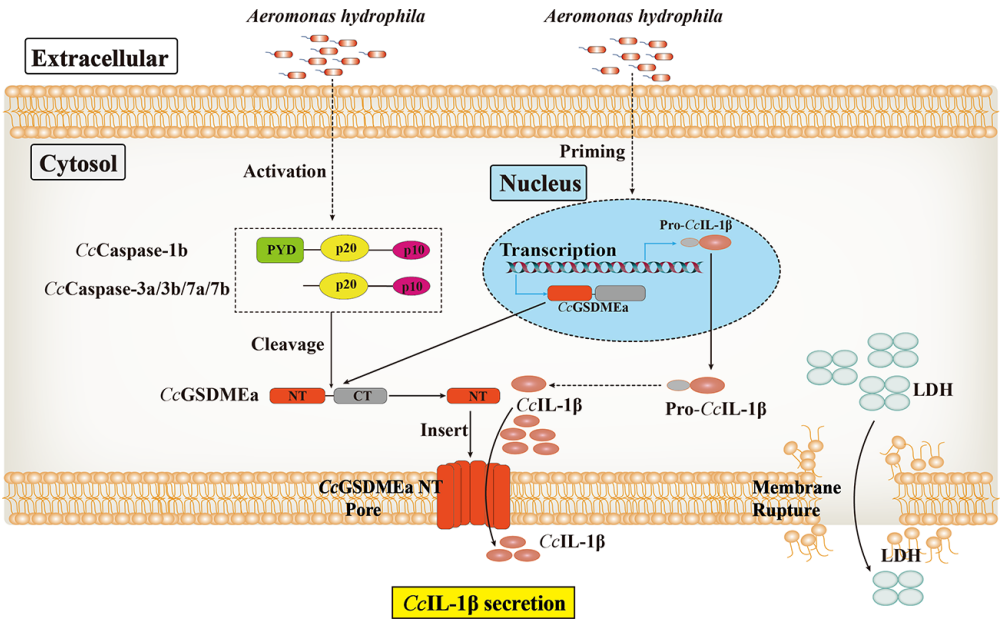

FIGURE 10
The proposed mode of the regulation role of *Cc*GSDMEa on *Cc*IL-1β secretion in common carp.

Data availability statement

The datasets presented in this study can be found in online repositories. The names of the repository/repositories and accession number(s) can be found in the article/ Supplementary Material.

Ethics statement

The animal study was reviewed and approved by Animal Care and Use Ethics Committee of the Henan Normal University.

Author contributions

YZ and JZ: conceived, designed and performed the experiments, and analyzed data, as well as wrote the draft manuscript and submitted the manuscript. DQ, FG and YG: carried out the experiments and analyzed data. XJ and LZ: performed data interpretation and acquired finding. XK: designed this study and provided a critical editing of the manuscript and was responsible for forming the finalizing manuscript. All authors contributed to the article and approved the submitted version.

Funding

This work was sponsored by the National Natural Science Foundation of China (U2004154).

Acknowledgments

We thank the Engineering Lab of Henan Province for Aquatic Animal Disease Control and Engineering Technology Research Center of Henan Province for Aquatic Animal Cultivation (Henan Normal University, Xinxiang, China) for providing instruments.

Conflict of interest

The authors declare that the research was conducted in the absence of any commercial or financial relationships that could be construed as a potential conflict of interest.

Publisher's note

Supplementary material

The Supplementary Material for this article can be found online at: https://www.frontiersin.org/articles/10.3389/fimmu.2022.1110322/full#supplementary-material

References

1. Nakajima T, Hudson MJ, Uchiyama J, Makibayashi K, Zhang J. Common carp aquaculture in neolithic China dates back 8,000 years. *Nat Ecol Evol* (2019) 3 (10):1415–8. doi: 10.1038/s41559-019-0974-3

2. Lafferty KD, Harvell CD, Conrad JM, Friedman CS, Kent ML, Kuris AM, et al. Infectious diseases affect marine fisheries and aquaculture economics. *Ann Rev Mar Sci* (2015) 7:471–96. doi: 10.1146/annurev-marine-010814-015646

3. Basu M, Swain B, Maiti NK, Routray P, Samanta M. Inductive expression of toll-like receptor 5 (TLR5) and associated downstream signaling molecules following ligand exposure and bacterial infection in the Indian major carp, mrigal (*Cirrhinus mrigala*). *Fish Shellfish Immunol* (2012) 32(1):121–31. doi: 10.1016/j.fsi.2011.10.031

4. Orozova P, Sirakov I, Austin DA, Austin B. Recovery of bacillus mycoides, b. pseudomycoides and *Aeromonas hydrophila* from common carp (*Cyprinus carpio*) and rainbow trout (*Oncorhynchus mykiss*) with gill disease. *J Fish Dis* (2018) 41 (1):125–9. doi: 10.1111/jfd.12686

5. Di G, Li H, Zhang C, Zhao Y, Zhou C, Naeem S, et al. Label-free proteomic analysis of intestinal mucosa proteins in common carp (*Cyprinus carpio*) infected with aeromonas hydrophila. *Fish Shellfish Immunol* (2017) 66:11–25. doi: 10.1016/j.fsi.2017.04.025

6. Feng JC, Cai ZL, Zhang XP, Chen YY, Chang XL, Wang XF, et al. The effects of oral rehmannia glutinosa polysaccharide administration on immune responses, antioxidant activity and resistance against *Aeromonas hydrophila* in the common carp, cyprinus carpio l. *Front Immunol* (2020) 11:904. doi: 10.3389/fimmu.2020.00904

7. Podok P, Xu L, Xu D, Lu L. Different expression profiles of interleukin 11 (IL-11), intelectin (ITLN) and purine nucleoside phosphorylase 5a (PNP 5a) in crucian carp (*Carassius auratus gibelio*) in response to cyprinid herpesvirus 2 and aeromonas hydrophila. *Fish Shellfish Immunol* (2014) 38(1):65–73. doi: 10.1016/j.fsi.2014.03.001

8. Zhang J, Wang L, Zhao Y, Kong X, Wu F, Zhao X. Molecular characterization and expression analysis of toll-like receptors 5 and 22 from natural triploid carassius auratus. *Fish Shellfish Immunol* (2017) 64:1–13. doi: 10.1016/j.fsi.2017.03.004

9. Weifeng M, Yaping W, Wenbo W, Bo W, Jianxin F, Zuoyan Z. Enhanced resistance to *Aeromonas hydrophila* infection and enhanced phagocytic activities in human lactoferrin-transgenic grass carp (*Ctenopharyngodon idellus*). *Aquaculture* (2004) 242(1-4):93–103. doi: 10.1016/j.aquaculture.2004.07.020

10. Lu AJ, Hu XC, Wang Y, Zhu AH, Shen LL, Tian J, et al. Skin immune response in the zebrafish, *Danio rerio (Hamilton)*, to *Aeromonas hydrophila* infection: a transcriptional profiling approach. *J Fish Dis* (2015) 38(2):137–50. doi: 10.1111/jfd.12214

11. Bebak J, Wagner B, Burnes B, Hanson T. Farm size, seining practices, and salt use: risk factors for aeromonas hydrophila outbreaks in farm-raised catfish, Alabama, USA. *Prev Vet Med* (2015) 118(1):161–8. doi: 10.1016/j.prevetmed.2014.11.001

12. Mu X, Pridgeon JW, Klesius PH. Comparative transcriptional analysis reveals distinct expression patterns of channel catfish genes after the first infection and re-infection with aeromonas hydrophila. *Fish Shellfish Immunol* (2013) 35(5):1566–76. doi: 10.1016/j.fsi.2013.08.027

13. Peatman E, Mohammed H, Kirby A, Shoemaker CA, Yildirim-Aksoy M, Beck BH. Mechanisms of pathogen virulence and host susceptibility in virulent *Aeromonas hydrophila* infections of channel catfish (*Ictalurus punctatus*). *Aquaculture* (2018) 482:1–8. doi: 10.1016/j.aquaculture.2017.09.019

14. Pachanawan A, Phumkhachorn P, Rattanachaikunsopon P. Potential of psidium guajava supplemented fish diets in controlling *Aeromonas hydrophila* infection in tilapia (*Oreochromis niloticus*). *J Biosci Bioeng* (2008) 106(5):419–24. doi: 10.1263/jbb.106.419

15. Zhao XL, Jin ZH, Di GL, Li L, Kong XH. Molecular characteristics, pathogenicity and medication regimen of *Aeromonas hydrophila* isolated from common carp (Cyprinus carpio l.). *J Vet Med Sci* (2019) 81(12):1769–75. doi: 10.1292/jvms.19-0025

16. Chen H, Wu X, Gu Z, Chen S, Zhou X, Zhang Y, et al. Zebrafish gasdermin e cleavage-engaged pyroptosis by inflammatory and apoptotic caspases. *Dev Comp Immunol* (2021) 124:104203. doi: 10.1016/j.dci.2021.104203

17. Chen S, Jin P, Chen H, Wu D, Li S, Zhang Y, et al. Dual function of a turbot inflammatory caspase in mediating both canonical and non-canonical inflammasome activation. *Dev Comp Immunol* (2021) 121:104078. doi: 10.1016/j.dci.2021.104078

18. Jiang S, Gu H, Zhao Y, Sun L. Teleost gasdermin e is cleaved by caspase 1, 3, and 7 and induces pyroptosis. *J Immunol* (2019) 203(5):1369–82. doi: 10.4049/jimmunol.1900383

19. Li JY, Wang YY, Shao T, Fan DD, Lin AF, Xiang LX, et al. The zebrafish NLRP3 inflammasome has functional roles in ASC-dependent interleukin-1beta maturation and gasdermin e-mediated pyroptosis. *J Biol Chem* (2020) 295 (4):1120–41. doi: 10.1074/jbc.RA119.011751

20. Song Z, Zou J, Wang M, Chen Z, Wang Q. A comparative review of pyroptosis in mammals and fish. *J Inflammation Res* (2022) 15:2323–31. doi: 10.2147/JIR.S361266

21. Daskalov A, Glass NL. Gasdermin and gasdermin-like pore-forming proteins in invertebrates, fungi and bacteria. *J Mol Biol* (2022) 434(4):167273. doi: 10.1016/j.jmb.2021.167273

22. Feng S, Fox D, Man SM. Mechanisms of gasdermin family members in inflammasome signaling and cell death. *J Mol Biol* (2018) 430(18 Pt B):3068–80. doi: 10.1016/j.jmb.2018.07.002

23. Chen J, Ge L, Shi X, Liu J, Ruan H, Heng D, et al. Lobaplatin induces pyroptosis in cervical cancer cells *via* the caspase-3/GSDME pathway. *Anticancer Agents Med Chem* (2022) 22(11):2091–7. doi: 10.2174/1871520621666211018100532

24. Dong S, Shi Y, Dong X, Xiao X, Qi J, Ren L, et al. Gasdermin e is required for induction of pyroptosis and severe disease during enterovirus 71 infection. *J Biol Chem* (2022) 298(5):101850. doi: 10.1016/j.jbc.2022.101850

25. Rogers C, Fernandes-Alnemri T, Mayes L, Alnemri D, Cingolani G, Alnemri ES. Cleavage of DFNA5 by caspase-3 during apoptosis mediates progression to secondary necrotic/pyroptotic cell death. *Nat Commun* (2017) 8:14128. doi: 10.1038/ncomms14128

26. Wang Y, Gao W, Shi X, Ding J, Liu W, He H, et al. Chemotherapy drugs induce pyroptosis through caspase-3 cleavage of a gasdermin. *Nature* (2017) 547 (7661):99–103. doi: 10.1038/nature22393

27. Aglietti RA, Estevez A, Gupta A, Ramirez MG, Liu PS, Kayagaki N, et al. GsdmD p30 elicited by caspase-11 during pyroptosis forms pores in membranes. *Proc Natl Acad Sci U.S.A.* (2016) 113(28):7858–63. doi: 10.1073/pnas.1607769113

28. Sborgi L, Ruhl S, Mulvihill E, Pipercevic J, Heilig R, Stahlberg H, et al. GSDMD membrane pore formation constitutes the mechanism of pyroptotic cell death. *EMBO J* (2016) 35(16):1766–78. doi: 10.15252/embj.201694696

29. Chen S, Ma X, Wu D, Yang D, Zhang Y, Liu Q. *Scophthalmus maximus* interleukin-1beta limits *Edwardsiella piscicida* colonization in vivo. *Fish Shellfish Immunol* (2019) 95:277–86. doi: 10.1016/j.fsi.2019.10.050

30. Dinarello CA. Immunological and inflammatory functions of the interleukin-1 family. *Annu Rev Immunol* (2009) 27:519–50. doi: 10.1146/annurev.immunol.021908.132612

31. Fabiani C, Sota J, Tosi GM, Franceschini R, Frediani B, Galeazzi M, et al. The emerging role of interleukin (IL)-1 in the pathogenesis and treatment of inflammatory and degenerative eye diseases. *Clin Rheumatol* (2017) 36(10):2307–18. doi: 10.1007/s10067-016-3527-z

32. Munoz-Wolf N, Lavelle EC. A guide to IL-1 family cytokines in adjuvanticity. *FEBS J* (2018) 285(13):2377–401. doi: 10.1111/febs.14467

33. Ding J, Wang K, Liu W, She Y, Sun Q, Shi J, et al. Pore-forming activity and structural autoinhibition of the gasdermin family. *Nature* (2016) 535(7610):111–6. doi: 10.1038/nature18590

34. Liu X, Zhang Z, Ruan J, Pan Y, Magupalli VG, Wu H, et al. Inflammasome-activated gasdermin d causes pyroptosis by forming membrane pores. *Nature* (2016) 535(7610):153–8. doi: 10.1038/nature18629

35. Kovacs SB, Miao EA. Gasdermins: Effectors of pyroptosis. *Trends Cell Biol* (2017) 27(9):673–84. doi: 10.1016/j.tcb.2017.05.005

36. Zhou ZX, Zhang BC, Sun L. Poly(I:C) induces antiviral immune responses in Japanese flounder (*Paralichthys olivaceus*) that require TLR3 and MDA5 and is negatively regulated by Myd88. *PloS One* (2014) 9(11):e112918. doi: 10.1371/journal.pone.0112918

37. Zhang J, Li L, Kong X, Wu F, Zhou C, Nie G, et al. Expression patterns of toll-like receptors in natural triploid *Carassius auratus* after infection with aeromonas hydrophila. *Vet Immunol Immunopathol* (2015) 168(1-2):77–82. doi: 10.1016/j.vetimm.2015.08.009

38. Wang Z, Gu Z, Hou Q, Chen W, Mu D, Zhang Y, et al. Zebrafish GSDMEb cleavage-gated pyroptosis drives septic acute kidney injury in vivo. *J Immunol* (2020) 204(7):1929–42. doi: 10.4049/jimmunol.1901456

39. Boucher D, Monteleone M, Coll RC, Chen KW, Ross CM, Teo JL, et al. Caspase-1 self-cleavage is an intrinsic mechanism to terminate inflammasome activity. *J Exp Med* (2018) 215(3):827–40. doi: 10.1084/jem.20172222

40. Chen H, Ding S, Tan J, Yang D, Zhang Y, Liu Q. Characterization of the Japanese flounder NLRP3 inflammasome in restricting *Edwardsiella piscicida* colonization in vivo. *Fish Shellfish Immunol* (2020) 103:169–80. doi: 10.1016/j.fsi.2020.04.063

41. Bergsbaken T, Fink SL, Cookson BT. Pyroptosis: host cell death and inflammation. *Nat Rev Microbiol* (2009) 7(2):99–109. doi: 10.1038/nrmicro2070

42. He WT, Wan H, Hu L, Chen P, Wang X, Huang Z, et al. Gasdermin d is an executor of pyroptosis and required for interleukin-1beta secretion. *Cell Res* (2015) 25(12):1285–98. doi: 10.1038/cr.2015.139

43. Shi J, Zhao Y, Wang K, Shi X, Wang Y, Huang H, et al. Cleavage of GSDMD by inflammatory caspases determines pyroptotic cell death. *Nature* (2015) 526 (7575):660–5. doi: 10.1038/nature15514

44. Broz P, Pelegrin P, Shao F. The gasdermins, a protein family executing cell death and inflammation. *Nat Rev Immunol* (2020) 20(3):143–57. doi: 10.1038/s41577-019-0228-2

45. Xia S. Biological mechanisms and therapeutic relevance of the gasdermin family. *Mol Aspects Med* (2020) 76:100890. doi: 10.1016/j.mam.2020.100890

46. Garlanda C, Dinarello CA, Mantovani A. The interleukin-1 family: back to the future. *Immunity* (2013) 39(6):1003–18. doi: 10.1016/j.immuni.2013.11.010

frontiers | Frontiers in Immunology

TYPE Original Research
PUBLISHED 02 February 2023
DOI 10.3389/fimmu.2023.1128196

OPEN ACCESS

EDITED BY
Mofei Li,
Tianjin Normal University, China

REVIEWED BY
Weiwei Zhang,
Ningbo University, China
Jian Zhang,
Yantai University, China
Min Zhang,
Qingdao Agricultural University, China

*CORRESPONDENCE
Ying Wu
wuying0947009@126.com
Yongcan Zhou
zychnu@163.com

†These authors have contributed equally to this work

SPECIALTY SECTION
This article was submitted to Molecular Innate Immunity, a section of the journal Frontiers in Immunology

RECEIVED 20 December 2022
ACCEPTED 23 January 2023
PUBLISHED 02 February 2023

CITATION
Sun Y, Cao Z, Zhang P, Wei C, Li J, Wu Y and Zhou Y (2023) IFN regulatory factor 3 of golden pompano and its NLS domain are involved in antibacterial innate immunity and regulate the expression of type I interferon (IFNa3). *Front. Immunol.* 14:1128196. doi: 10.3389/fimmu.2023.1128196

IFN regulatory factor 3 of golden pompano and its NLS domain are involved in antibacterial innate immunity and regulate the expression of type I interferon (IFNa3)

Yun Sun[1,2†], Zhenjie Cao[1,3†], Panpan Zhang[1,2], Caoying Wei[1,3], Jianlong Li[1,2], Ying Wu[1,3*] and Yongcan Zhou[1,2*]

[1]State Key Laboratory of Marine Resource Utilization in South China Sea, Hainan University, Haikou, China, [2]Collaborative Innovation Center of Marine Science and Technology, Hainan University, Haikou, China, [3]Hainan Provincial Key Laboratory for Tropical Hydrobiology and Biotechnology, College of Marine Science, Hainan University, Haikou, China

Introduction: The transcription factor interferon regulatory factor 3 (IRF3) plays an important role in host defence against viral infections. However, its role during bacterial infection in teleosts remains unclear. In the present study, we evaluated the antibacterial effects of *Trachinotus ovatus* IRF3 (TroIRF3) and how it regulates type I interferon (IFN).

Methods: Subcellular localisation experiments, overexpression, and quantitative real-time PCR (qRT-PCR) were performed to examine the nuclear localisation signal (NLS) of TroIRF3 and its role in the antibacterial regulatory function of TroIRF3. We assessed the binding activity of TroIRF3 to the IFNa3 promoter by luciferase reporter assay.

Results and Discussion: The results showed that TroIRF3 was constitutively expressed at high levels in the gill and liver. TroIRF3 was significantly upregulated and transferred from the cytoplasm to the nucleus after *Vibrio harveyi* infection. By overexpressing TroIRF3, the fish were able to inhibit the replication of *V. harveyi*, whereas knocking it down increased bacterial replication. Moreover, the overexpression of TroIRF3 increased type I interferon (IFNa3) production and the IFN signalling molecules. The NLS, which is from the 64–127 amino acids of TroIRF3, contains the basic amino acids KR74/75 and RK82/84. The results proved that NLS is required for the efficient nuclear import of TroIRF3 and that the NLS domain of TroIRF3 consists of the key amino acids KR74/75 and RK82/84. The findings also showed that NLS plays a key role in the antibacterial immunity and upregulation of TroIFNa3 induced by TroIRF3. Moreover, TroIRF3 induces TroIFNa3 promoter activity, whereas these effects are inhibited when the NLS domain is deficient. Overall, our results suggested that TroIRF3 is involved in the antibacterial immunity and regulation of type I IFN in *T. ovatus* and that the NLS of TroIRF3 is vital for IRF3-mediated antibacterial responses, which will aid in understanding the immune role of fish IRF3.

KEYWORDS

IRF3, *Trachinotus ovatus*, antimicrobial immunity, nuclear localization signal, IFNa3

1 Introduction

Innate immunity is the first line of defence against invading viruses and bacteria. The innate antiviral mechanism in mammals involves interferon (IFN), which induces the expression of IFN-relative genes (1–3). IFN can be divided into two major categories based on its cysteine residues. In all teleost fish lineages, type I IFNs contain two cysteine residues; however, type II IFNs contain four cysteine residues in a few species (4–7). In both vertebrates and invertebrates, interferon regulatory factors (IRFs) regulate type I and II IFN transcriptional activation (8).

Thus far, nine IRF family members have been found in mammals, 10 in birds and 11 in fish (9). The N-terminal DNA binding domain (DBD), consisting of five tryptophan repeats, is highly homologous between IRF members. The DBD forms a helix-turn-helix structure that binds specifically to IFN-stimulated response element (ISRE) sequences in the promoters of IFNβ and IFN-stimulated genes (ISGs) (10). Except for IRF1 and IRF2, the C-terminal of each IRF has an IRF association domain (IAD), which is used to interact with other IRFs and other factors (11–13). IRF3 and IRF7 contain a serine-rich region (SRD) at the C-terminus that controls their transcriptional activities when phosphorylated by viruses (11–14). Two transcription factors, IRF3 and IRF7 control the expression of type I IFNs (15, 16). The antiviral effects of several innate immune receptors, including retinoic acid-inducible gene I (RIG-I)-like receptors (RLRs), toll-like receptors (TLRs) and DNA sensors, are mediated by IRF3 (17–19). All TLRs in mammals (except TLR3) transduce signals through the MyD88-dependent pathway using molecules such as the TNFR-associated factor 6 (TRAF6) (17, 20–22). In general, pathogen invasion initiates an immune response by activating the immune signalling pathways. As a member of the IRF family, IRF3 plays an important role in immune signalling. Following bacterial infection, IRF3 is responsible for controlling the expression of IFNs and ISGs (23). ISGs include ISG15, MAX interactor I (MXI) and Viperin1 (24).

Accurate cellular localization plays a crucial role in the effective function of most signaling proteins, the ability of IRF3 to translocate into the nucleus is essential for its biological activity. Nuclear localization signals (NLSs) and nuclear export signals (NESs) are intrinsic targeting signals required to facilitate the shuttle between the nucleus and the cytoplasm for proteins larger than 45 kDa (25). IRF3 accumulates in the cytoplasm under resting conditions and adopts an auto-inhibited conformation, which is mediated by the NES. When infected, IRF3 enters the nucleus *via* NLS after being phosphorylated and dimerized at its C-terminus. IRF3 and the coactivator CBP/p300 form a complex and then bind the IFN-α/β promoters and the ISRE sequences of the targeted genes (14, 26, 27). Several studies have found that bacterial products, such as lipopolysaccharide (LPS), can activate toll-like receptors to induce type I IFN expression through IRF3 signalling (28–31). However, the role of IRF3 in bacterial infection is less understood.

The characteristics and functions of IRF3s have been reported in several species of teleost fish, such as *Epinephelus coioides*, *Cynoglossus semilaevis*, *Carassius auratus* L., *Salmo salar*, *Larimichthys crocea*, and *Paralichthys olivaceus* (32–37). In a previous study, red-spotted grouper nervous necrosis virus replication was significantly decreased in *E. coioides* when IRF3 was overexpressed (32). For *C. auratus* L., fish IFN or polyinosinic-polycytidylic acid (poly I:C) induced the phosphorylation of IRF3 and translocation from the cytoplasm to the nucleus. In addition, *C. auratus* L. IRF3 overexpression induced IFN production, which subsequently triggered ISG transcription *via* signal transducer and activator of transcription 1 (STAT1) (33). Moreover, viral and bacterial stimulation significantly induced *C. semilaevis* IRF3 (34). Although some studies have investigated IRF3 in fish, its function, particularly its role in antibacterial immunity, remains largely unknown.

Vibrio harveyi is a gram-negative opportunistic pathogenic bacterium of many commercially farmed fish species (38, 39). *Trachinotus ovatus* (golden pompano) is one of the most economically important aquaculture species in China that suffers from *V. harveyi*, resulting in serious economic losses (40). IFNa3 is a member of type I IFNs in *T. ovatus*. Previous study demonstrated that IRF1, IRF2, IRF5, and IRF7 positively regulate IFNa3 expression in *T. ovatus* (41, 42). The purpose of this study was to assess the antibacterial immune effects of IRF3 in *T. ovatus* (TroIRF3) and its role in the regulation of IFNa3. Based on these investigations, we further examine the NLS in TroIRF3 and its role in the host antibacterial immune response induced by TroIRF3.

2 Materials and methods

2.1 Fish, cell lines and bacteria

T. ovatus were purchased from a commercial fish farm in Hainan, China. Before the experiment, the fish were acclimated at 26°C in a flow-through water system for one week. All animal experiments conducted during this study were approved by the Animal Care and Use Committee at Hainan University. Human embryonic kidney (HEK293T) cells were cultured at ambient CO_2 and 37°C in Dulbecco's modified Eagle's medium (DMEM, USA), the DMEM contained 1% penicillin and streptomycin (Pen Strept) and 10% foetal bovine serum (FBS). Golden pompano snout (GPS) cells were generously donated by the South China Sea Institute of Oceanology Chinese Academy of Sciences. The GPS cells were grown at 26°C with Leibovitz's L-15 medium containing 10% FBS (Gibco, USA) (42, 43). *V. harveyi* was grown at 28°C in Luria-Bertani broth (38).

2.2 TroIRF3 cloning

Based on the transcriptome data, the primers TroIRF3-F/TroIRF3-R were used to clone the open reading frame (ORF) of TroIRF3 by polymerase chain reaction (PCR) amplification (Table S1). Sequencing was performed following gel purification of the PCR products into the pEASY®-T1Simple Vector (Transgen, Beijing, China). A homology search of the TroIRF3 protein sequence was conducted using BLAST programs on NCBI (http://www.ncbi.nlm.nih.gov/blast). Signal peptide prediction was performed using SignalP 5.1. Thereafter, DNAMAN (Lynnon Biosoft, USA) was used to align the amino acid sequences. SWISS-MODEL was used to predict the TroIRF3's tertiary structure. A phylogenetic analysis was performed using neighbour-joining methods through MEGA 6.0.

2.3 Expression profiles of TroIRF3 in normal tissues and when challenged with *V. harveyi*

A total of 11 tissues were obtained from 15 healthy *T. ovatus* (blood, head kidney, liver, intestine, spleen, gill, muscle, skin, brain, stomach and heart). To avoid the affection of the individual difference of fish, the fish tissues were mixed aseptically into a sample with five identical samples. The tissue samples were stored at −80°C until RNA extraction was performed. The *T. ovatus* were divided into two groups: control and bacterial challenge. The challenge group received 0.1 ml of *V. harveyi* (2×10^6 CFU/ml), while the control group received the same volume of PBS. At 6, 9, 12 and 24 hours post-injection (hpi), 15 individuals in each group were randomly sacrificed, and the liver, spleen and head-kidney were sampled. Five identical tissues from each group were mixed aseptically to form a sample. The total RNA was extracted from the harvested samples using the Total RNA Extraction Kit (Promega, China). The cDNA was synthesised using the Reverse Transcription System (Promega, China). An SYBR ExScript qRT–PCR kit (LS2062, Promega, China) was used to perform quantitative real-time PCR (qRT-PCR) on a qTOWER3 Real-Time PCR (qPCR) system (Analytik Jena, Germany). The internal reference gene was *β-2 microglobulin* (*B2M*), and the relative expression levels of *TroIRF3* were calculated using the $2^{-\Delta\Delta CT}$ method (44). The primers are summarised in Table S1.

2.4 TroIRF3 overexpression and *V. harveyi* infection *in vivo*

The eukaryotic expression vector pTroIRF3 was constructed for TroIRF3 overexpression *in vivo*. TroIRF3 was cloned into the pCN3's *Sma* I site and transformed into *Escherichia coli*, DH5α. pTroIRF3 was extracted using the Endo Free Plasmid Kit (Tiangen, China). The fish (weight 15.2 ± 3.1 g) were randomised into three groups (N=12), with each receiving a 0.1 ml injection of pTroIRF3 (150 μg/ml), pCN3 (empty vector, 150 μg/ml) or PBS (control). To detect the expression level of TroIRF3, the liver, spleen and head-kidney of three fish from each group were collected after five days of intramuscular injection of plasmids. After the isolation of total RNA and cDNA synthesis, TroIRF3 expression was detected by qRT-PCR with primer TroIRF3-RT-F/R (Table S1). *B2M* was used as the internal reference gene. *V. harveyi* (10^5 CFU/fish) was injected into the remaining fish. The liver, spleen and head-kidney of three fish in each group were homogenised at 6, 9 and 12 hpi for bacterial count analysis.

2.5 TroIRF3 knockdown and *V. harveyi* infection *in vivo*

The small interfering RNA (siRNA) of TroIRF3 was synthesised using the T7 RiboMAX™ Express RNAi System (Promega, USA). The primers used for siRNA synthesis are listed in Table S1. A total of 36 fish were randomly divided into three groups of 12 each and injected with 0.1 ml of PBS (control), siRNA-C (control, 15 μg/fish) or siRNA-TroIRF3 (15 μg/fish). At 12 h after intramuscular injection of siRNA, three fish were sacrificed for liver, spleen and head-kidney collection. Then, qRT–PCR was performed to detect the TroIRF3 expression levels. The rest of the fish were infected with *V. harveyi* (10^5 CFU/fish). The liver, spleen and head-kidney of three fish in each group were homogenised at 6, 9, and 12 hpi for bacterial count analysis.

2.6 Subcellular localisation

The eukaryotic expression vector pTroIRF3-N3 was created by cloning TroIRF3's ORF into the *Bgl* II and *Sal* I sites of pEGFP-N3. Subcellular localisation experiments were performed to examine TroIRF3 localisation in the cell with or without *V. harveyi* infection. The cells were seeded on 24-well plates and grown overnight, and then Lipofectamine 2000 (Invitrogen, USA) was used to transfect pEGFP-N3 or pTroIRF3-N3 into the GPS cells. At 48 h post-transfection, the cells transfected with pTroIRF3-N3 were treated with 0.1 ml PBS (control) or *V. harveyi* (1×10^5 CFU/ml) for 6 h. The GPS cells were washed, stained and visualised with fluorescence microscopy (Leica, Wetzlar, Germany) after fixing in 4% paraformaldehyde.

Different PCR fragments of TroIRF3 were inserted into *Bgl* II and *Sal* I sites of pEGFP-N3 vector to constructe TroIRF3-GFP truncation mutants: pTroIRF3-(△NES)-N3, pTroIRF3-1-165-N3, pTroIRF3-1-417-(△NES)-N3, pTroIRF3-64-466-(△NES), or pTroIRF3-127-466-(△NES). Various plasmids were transfected into the GPS cells to detect the NLSs of TroIRF3. The cells were fixed, washed, stained and visualised under fluorescence microscopy at 48 h post-transfection.

Two TroIRF3 variants (KR74/75NG and RK82/84LQ) were designed to further detect the NLSs of IRF3 within the aa 64–127 region. The PCR fragments of KR74/75NG and RK82/84LQ were inserted into *Bgl* II and *Sal* I sites of pEGFP-N3 vector to construct two recombinant plasmids: pTroIRF3-KR74/75NG-N3 and pTroIRF3-RK82/84LQ-N3. The primers used are listed in Table S1. The GPS cells were transfected with plasmids (pTroIRF3-KR74/75NG-N3 or pTroIRF3-RK82/84LQ-N3). After 48 h, the cells were treated with 0.1 ml *V. harveyi* (1×10^5 CFU/ml) or PBS (control) for 6 h. Afterwards, the cells were fixed, washed, stained and visualised under fluorescence microscopy.

2.7 Role of NLSs sites in immune response *in vivo*

2.7.1 Role of NLSs in the antibacterial regulatory function of TroIRF3

To further investigate the role of these basic amino acids in TroIRF3's antibacterial regulation, two recombinant plasmids (pTroIRF3-KR74/75NG and pTroIRF3-RK82/84LQ) were constructed by inserting the variants into the *Sma* I sites of the pCN3 vectors. The fish were randomised into four groups (12 fish per group) and injected with PBS (control), pTroIRF3 (15 μg/fish), pTroIRF3-KR74/75NG (15 μg/fish), or pTroIRF3- RK82/84LQ (15 μg/fish), respectively. After five days, the liver, spleen and head-kidney of three fish from each group were collected to detect the expression level of TroIRF3 or it mutants. The remaining fish were

intraperitoneally infected with *V. harveyi* (2×10^6 CFU/fish). The liver, spleen and head-kidney of three fish in each group were homogenised at 6, 9 and 12 hpi for bacterial count analysis.

2.7.2 Role of NLSs in immune gene expression induced by TroIRF3

Twelve fish were randomised into four groups and injected with PBS (control), pTroIRF3, pTroIRF3-KR74/75NG or pTroIRF3-RK82/84LQ, respectively. After five days of injection, the spleens were collected, followed by RNA isolation and cDNA synthesisation. The relative transcription level of *IFNa3*, *MXI*, *TRAF6*, *Viperin1* and mitochondrial antiviral signalling (*MAVS*) was detected by qRT-PCR. The primers are listed in Table S1.

2.8 Luciferase reporter assay

The TroIRF3 binding site in the promoter of TroIFNa3 was evaluated by luciferase reporter assay. Three truncation mutants of the TroIFNa3 promoter (−1649 to +1, −896 to +1 and −722 to +1) were amplified and inserted into the *Kpn* I and *Xho* I restriction sites of the pGL4-basic luciferase reporter plasmid (Promega, USA) to obtain the recombinant plasmid pGL4-TroIFNa3-p1, pGL4-TroIFNa3-p2 and pGL4-TroIFNa3-p3. The primers used are summarised in Table S1. Lipofectamine 2000 (Invitrogen, USA) was used to cotransfect pRL-TK (0.025 μg), pGL4-TroIFNa3-p1/p2/p3 (0.25 μg) and pTroIRF3 (0.25 μg) into the HEK293T cells. pRL-TK was used as an internal control. After 36 h of transfection, the firefly and renilla luciferase activities were measured using a dual-luciferase reporter assay system (Promega, USA). The activity ratio between the firefly luciferase and the renilla luciferase was used to calculate the luciferase activity. The effect of *V. harveyi* stimulation on the TroIFNa3 promoter activation mediated by TroIRF3 was detected. After 24 h of transfection, the transfected HEK293T cells were treated with PBS or *V. harveyi* (1×10^2 CFU/ml) for 12 h. Luciferase activity was measured in the lysed cells as described above.

Luciferase reporter assay was performed to detect whether the activation of the TroIFNa3 promoter was dependent on the pTroIRF3 concentration. The HEK293T cells were cotransfected with pRL-TK (0.025 μg), pGL4-TroIFNa3-p2 (0.25 μg) and different concentrations of pTroIRF3 (0, 0.01, 0.05, 0.1 or 0.2 μg). After 24 h, the transfected HEK293T cells were treated with *V. harveyi* (1×10^2 CFU/ml) for 12 h. Luciferase activity was measured in the lysed cells as described above.

Luciferase reporter assay was performed to detect the role of the basic amino acids (KR74/75 and RK82/84) in the TroIRF3-triggered TroIFNa3-p2 activation. The HEK293T cells were cotransfected with pGL4-TroIFNa3-p2, wild-type TroIRF3 or its variants (pTroIRF3-KR74/75NG or pTroIRF3-RK82/84LQ) and pRL-CMV. After 24 h, the cells were treated with *V. harveyi* (1×10^2 CFU/ml) for 12 h. Afterwards, the relative luciferase activity was tested as described above.

2.9 Statistical analysis

All data were analysed by SPSS 16.0 (SPSS, IL, USA) and GraphPad Prism 5 (GraphPad, CA, USA). The statistical significance level of this study was set at 0.05.

3 Results

3.1 Cloning and sequence analysis of TroIRF3

The full length of TroIRF3 cDNA contains a 1398 bp ORF encoding 465 amino acids (GenBank Accession No. AWY04222.1). In theory, it has a molecular mass of 52 kDa and an isoelectric point of 4.89. According to the amino acid alignments, TroIRF3 contains three conserved domains, namely, DBD, IAD and SRD (Figure 1A). Among the selected IRF3 sequences, TroIRF3 was closest to that of *Seriola lalandi dorsalis* (85.95%), followed by those of *Siniperca chuatsi* and *Lateolabrax japonicus* (81.94% and 82.37%, respectively) (Figure 1A). According to the SWISS-MODEL online software, TroIRF3 has a similar three-dimensional structure to human IRF3 (Figure 1B). In addition, the IRF3 from fish and mammals were located in two separate branches, while TroIRF3 was inserted in the fish cluster. TroIRF3 shows a close evolutionary relationship with *S. lalandi dorsalis* IRF3 (Figure 1C).

3.2 Expression pattern of TroIRF3 with or without bacterial challenge

The expression level of *TroIRF3* was detected in 11 normal tissues (spleen, head-kidney, skin, muscle, gill, heart, liver, brain, stomach, blood and intestine) by qRT-PCR. *TroIRF3* was constitutively distributed in all the tissues examined. *TroIRF3* expression was high in the gill and liver but low in the spleen and blood (Figure 2A).

The level of *TroIRF3* expression following *V. harveyi* infection was detected using qRT-PCR (Figure 2B). The level of *TroIRF3* expression in the liver was increased from 6 hpi to 24 hpi (4.1-, 30.9-, 4.1-, and 2.7-folds at 6, 9, 12, and 24 hpi, respectively), the expression level of *TroIRF3* in the spleen was increased from 6 hpi to 24 hpi (3.5-, 40.2-, 6.5-, and 7.8-folds at 6, 9, 12, and 24 hpi, respectively), and the expressions of *TroIRF3* in the head-kidney were increased from 9 hpi to 24 hpi but manifested no difference at 6 hpi (35.5-, 8.8-, and 4.0-folds at 9, 12, and 24 hpi, respectively). Based on these results, TroIRF3 may contribute to antibacterial immunity.

3.3 Overexpression of TroIRF3 decreases *V. harveyi* replication *in vivo*

To clarify TroIRF3's role in antibacterial immunity, we assessed the effects of TroIRF3 overexpression on the fish's antibacterial ability. An increase in *TroIRF3* expression was observed in fish treated with pTroIRF3, indicating the overexpression of TroIRF3 (Figure S1A). Compared with the control group, the number of bacteria in the tissues decreased in the TroIRF3-overexpressing fish (Figure 3A). The bacterial load in the liver was significantly decreased in the TroIRF3-overexpressing fish compared with the control fish by 7.1- and 8.3-fold at 6 and 9 hpi, respectively. The pattern of bacterial load in the spleen of the pTroIRF3-overexpressing fish was similar to that in the liver, which decreased significantly with 5.0- and 10.9-fold

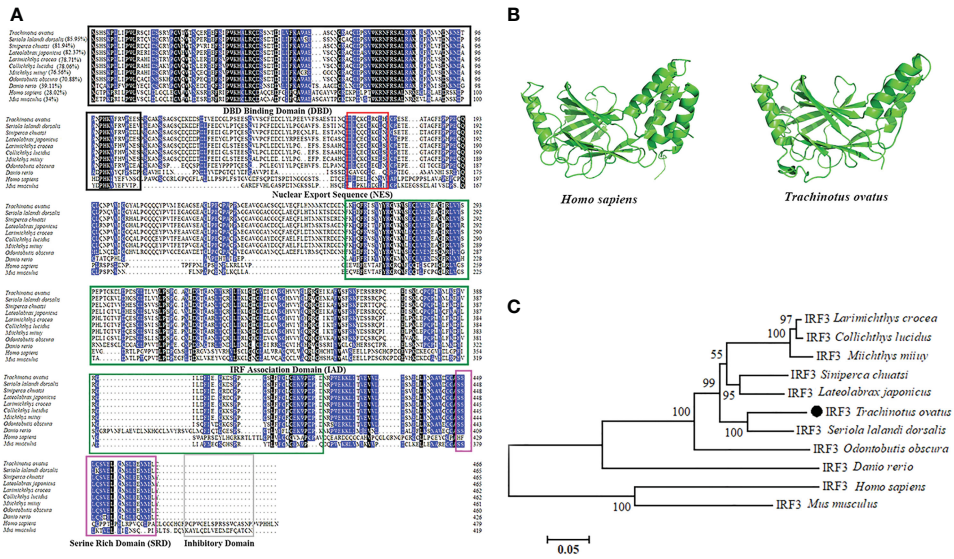

FIGURE 1
Sequence characteristics of TroIRF3. **(A)** Alignment of amino acid sequences from TroIRF3 and other IRF3 homologs. Identities between TroIRF3 and the compared sequences are shown in brackets. The background color of amino acid residues corresponds to the conservation degree (blue > 75%, black = 100%). The conserved DBD domain is boxed in black, the conserved IAD domain is boxed in green, the conserved SRD domain is boxed in purple, and the conserved inhibitory domain is boxed in gray. The nuclear export sequences (NES) are marked with the red box. **(B)** Analysis of the SWISS-MODEL prediction for TroIRF3 (SWISS-MODEL Template ID: 5jek.2) compared to human IRF3. **(C)** Phylogenetic analysis of TroIRF3. MEGA 6.0 was used to construct a phylogenetic tree based on neighbor-joining (NJ). The sequences of TroIRF3 genes used in this study were obtained from GenBank, a list of GenBank accession numbers can be found in Table S2.

at 6 and 9 hpi, respectively. Compared with the control fish, TroIRF3 overexpression significantly reduced the number of bacterial colonies in the head-kidney by 6.8- and 9.6-fold at 9 and 12 hpi, respectively. No significant difference in bacterial loads was observed between the empty vector-injected fish and the control fish, which showed that the vector had no effect on the fish's antibacterial immune responses.

3.4 Knockdown of TroIRF3 increases *V. harveyi* replication *in vivo*

The effects of TroIRF3 on antibacterial immune responses were further investigated, and TroIRF3 was knocked down using siRNA administration. The *TroIRF3* gene was decreased *in vivo* using siRNA

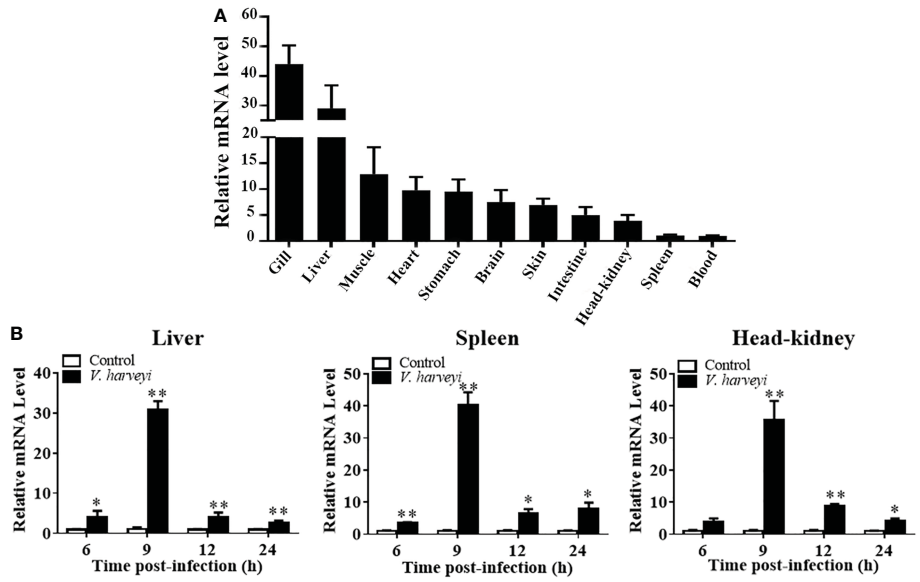

FIGURE 2
Expression profiles of TroIRF3 in normal tissues and when challenged with *V. harveyi*. **(A)** TroIRF3 expression levels in different tissues. **(B)** Expression of TroIRF3 in the liver, spleen, and head-kidney in response to the *V. harveyi* challenge. At every time point, control fish were set to have an average expression level of 1. Error bars display means ± SD (N = 3). N, indicates parallel experiments. *$P < 0.05$, **$P < 0.01$.

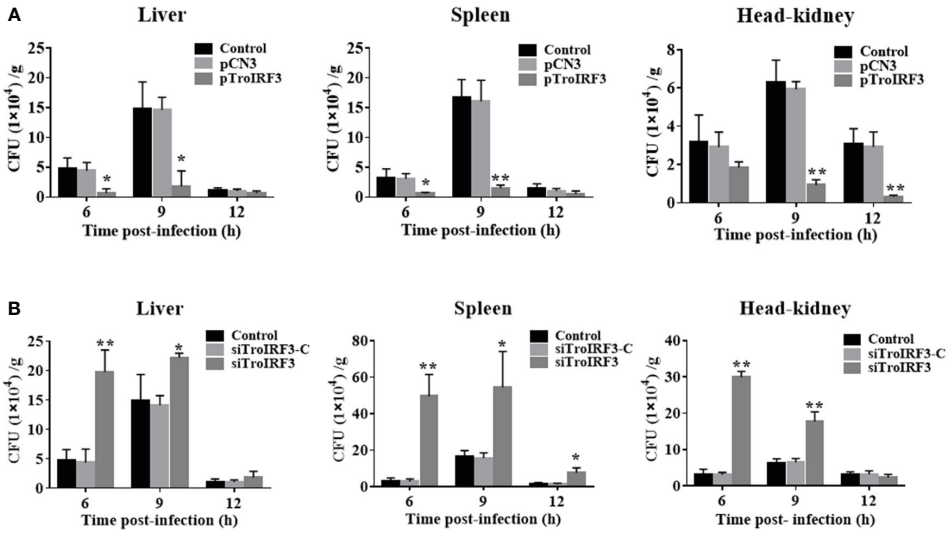

FIGURE 3
Effects of TroIRF3 on bacterial infection. **(A)** At five days after injection with PBS (Control), pCN3, and pTroIRF3, *T. ovatus* was infected with *V. harveyi*, and their liver, spleen, and head-kidney bacteria were determined at 6, 12, and 24 hpi. **(B)** *T. ovatus* was injected with siTroIRF3, siTroIRF3-C, or PBS (Control) for 12 h, then infected with *V. harveyi*, and their liver, spleen, and head-kidney bacteria were determined at 6, 12, and 24 hpi. The data are shown as the means ± SD (N =3), N, the number of fish used at each time point per group. $^{*}P < 0.05$, $^{**}P < 0.01$.

(Figure S1B). Compared with the control fish, the number of bacteria in the tissues obviously increased in the siTroIRF3-treated fish (Figure 3B). Compared with the control fish, the TroIRF3 knockdown fish exhibited an increased number of bacteria in the liver by 4.2- and 1.5-fold at 6 and 9 hpi, respectively. At 6, 9 and 12 hpi, the siTroIRF3-treated fish had higher bacterial colony counts in the spleen (15.4-, 3.3- and 4.9-fold). Compared with the control group, the siTroIRF3-treated fish had 9.5- and 2.8-fold higher bacterial loads in the head-kidneys at 6 and 9 hpi, respectively. The PBS-treated group and siTroIRF3-C-treated group (siRNA-C) showed similar bacterial loads, which indicated that the siRNA-C had no effect on the fish's antibacterial immune responses. Together, TroIRF3 was involved in the antibacterial response against *V. harveyi in vivo*.

3.5 Mapping of the NLS domain of IRF3

The subcellular localisation of TroIRF3 with or without *V. harveyi* stimulation was studied using a fluorescence microscope. EGFP is detected in both cytoplasm and nucleus, TroIRF3 was located exclusively in the cytoplasm in the uninfected cells and translocated to the nucleus after infection with *V. harveyi* (Figure 4A). Given the presence of both NLS and NES in IRF3, its predominant cytoplasmic localisation suggested constitutive activities of NES before virus infection, nuclear exports dominated nuclear imports (45). The regulation function of IRF3 was dependent on its nuclear location. To define the TroIRF3's NLS domain, the NES was inactivated to prevent interference. The protein of TroIRF3 (△NES) was located in the nucleus and cytoplasm of the GPS cells, suggesting that TroIRF3 is capable of entering and staying in the nucleus without NES (Figure 4C). To produce different mutants, TroIRF3's N-terminal and C-terminal regions were truncated (Figure 4B). The C-terminal truncations (aa 1–417 and 1–165) and N-terminal truncations (aa 64–466) fused with GFP retained translocation into the nuclei, but the aa 127-466 did not (Figure 4C). According to these experiments, the TroIRF3's NLS domain is located at the N-terminus of aa 64–127.

3.6 Mutational analysis of IRF3 NLS

According to a previous study, mice IRF3 nuclear import requires both basic residue clusters (KR77/78 and RK86/87) (45). The TroIRF3's NLS domain lies between amino acids 64 and 127. Site-directed mutagenesis was then constructed to determine whether they contribute to the nuclear accumulation of TroIRF3. In TroIRF3 mutants (KR74/75NG and RAK82/84LAQ), basic amino acids (KR74/75 and RK82/84) were replaced with uncharged amino acids (Figure 5A). The results of the subcellular localisation assays showed that *V. harveyi* infection caused TroIRF3, but not KR74/75NG and RK82/84LQ, to be localized in the nucleus (Figures 4A, 5B). Therefore, the NLS of TroIRF3 is composed of amino acid residues KR74/75 and RK82/84, which are critical in TroIRF3 nuclear accumulation.

3.7 Antibacterial function of TroIRF3 requires NLS

To determine whether NLS affects TroIRF3-mediated antibacterial defences, the number of *V. harveyi* in the fish treated with pTroIRF3 or the indicated TroIRF3 mutants (pTroIRF3-KR74/75NG and pTroIRF3-RK82/84LQ) was tested. TroIRF3 overexpression significantly suppressed *V. harveyi* replication in the fish, which was in line with our previous observations (Figure 6). However, the number of invaded bacteria in pTroIRF3-KR74/75NG- or pTroIRF3-RK82/84LQ-treated fish was enhanced compared with that in the wild-type pTroIRF3-treated fish (Figure 6). These results

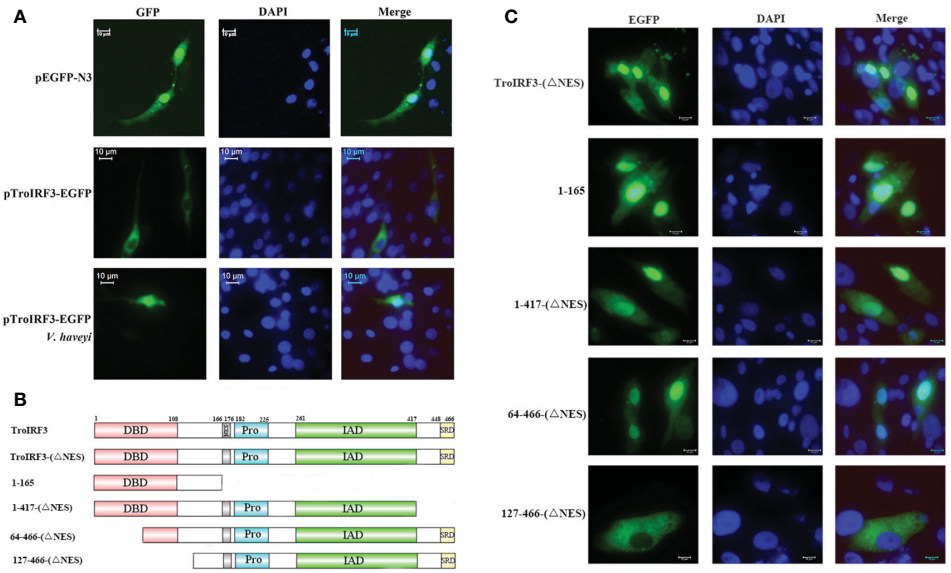

FIGURE 4
Mapping of the TroIRF3 NLS domain. **(A)** GPS cells were transfected with pEGFP-N3 or pTroIRF3-N3 for 48 h, and the cell transfected with pTroIRF3-N3 were incubated with PBS or *V. haveyi* for six hours, followed by inverted fluorescence microscopy imaging. DAPI was used to stain the nuclei of cells. **(B)** Schematic presentation of TroIRF3-GFP truncation mutants. **(C)** GPS cells were transfected with TroIRF3-GFP truncation mutant plasmids for 48 h before examination by an inverted fluorescence microscope.

showed that basic amino acids KR74/75 and RK82/84 are required for the efficient antibacterial function of TroIRF3.

3.8 TroIRF3-mediated immune gene expression requires an intact NLS

To investigate the effects of NLS on the TroIRF3-mediated immune gene expression, the expression levels of immune genes (*IFNa3*, *MXI*, *TRAF6*, *Viperin1* and *MAVS*) in the spleen of the fish treated with pTroIRF3 or the indicated TroIRF3 mutants (pTroIRF3-KR74/75NG and pTroIRF3-RK82/84LQ) were tested. In the pTroIRF3-, pTroIRF3-KR74/75NG- and pTroIRF3-RK82/84LQ-treated fish, the expression level of *TroIRF3* and modified TroIRF3 mutants were significantly upregulated compared with the control fish (Figure S2). TroIRF3 remarkably enhanced the production of *IFNa3*, *MXI*, *TRAF6*, *Viperin1* and *MAVS*. However, the expression level of the immune genes (*IFNa3, MXI, TRAF6, Viperin1* and *MAVS*) in the pTroIRF3-KR74/75NG- or pTroIRF3-RK82/84LQ-treated fish was significantly reduced compared with that in the pTroIRF3-treated fish (Figure 7). Furthermore, the fish treated with pCN3, pTroIRF3- KR74/75NG or pTroIRF3-RK82/84LQ showed the same expression level of immune genes (Figure 7). These results showed that basic amino acids KR74/75 and RK82/84 are required for immune gene induction by TroIRF3.

3.9 TroIFNa3 activation mediated by TroIRF3

Based on the predicted binding sites, consecutive truncated mutants of the TroIFNa3 promoter were constructed to investigate the TroIRF3-binding region in the TroIFNa3 promoter (Figure 8A). TroIFNa3-p2 had a higher response to TroIRF3 than the other mutants, suggesting that the region consists of –896 bp to +1 bp from the transcriptional start site, which contains the binding site for IRF3 (Figure 8A). The activation of the TroIFNa3 promoter by TroIRF3 was further enhanced by *V. harveyi* stimulation (Figure 8B). Furthermore, the activation of TroIFNa3-p2 is dependent on the TroIRF3 concentration (Figure 8C).

Subsequently, the potential effects of NLS on TroIRF3-mediated TroIFNa3-p2 activation were investigated using the luciferase reporter assay. TroIRF3 exhibited remarkably enhanced TroIFNa3-p2 activation following *V. harveyi* infection, whereas the other variants (pTroIRF3-KR74/75NG and pTroIRF3-RK82/84LQ) did not exhibit TroIFNa3-p2 activation under the same conditions (Figure 8D).

4 Discussion

IRF3 activates type I IFN and ISGs, which function as defences against viral and bacterial infections (46). TroIRF3 was identified and characterised in the present study. In addition, the functions of TroIRF3 were investigated, including the intracellular localisation of TroIRF3 and the ability of TroIRF3 to be an activator in antibacterial response and initiator of the transcription of TroIFNa3.

From fish to mammals, the DBD, IAD and SRD domains are conserved in vertebrate IRF3. The DBD domain consists of highly conserved tryptophan residues and forms a helix-turn-helix motif that binds to the ISRE in target promoters (33, 47, 48). After activation, the IRF3 molecules homodimerise through the IAD motif (49). SRD is critical for the phosphorylation IRF3 (12, 14). As with the other IRF3, TroIRF3 has a DBD on the N-terminus and IAD and SRD at the C-terminus. In the phylogenetic analysis, IRF3 from

10.3389/fimmu.2023.1128196

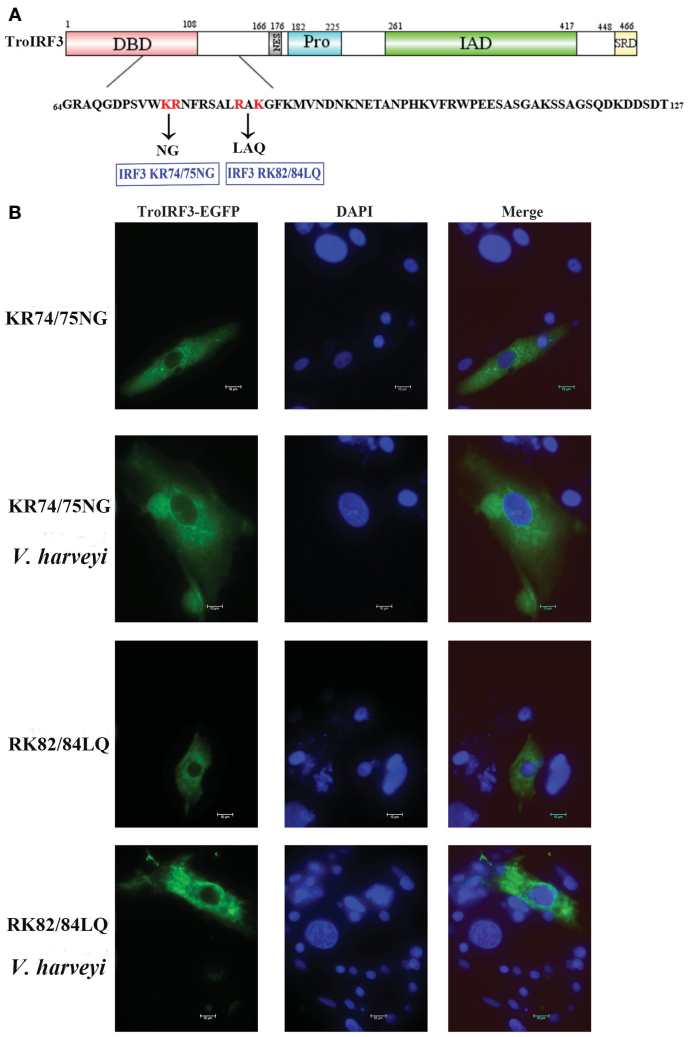

FIGURE 5
Subcellular distribution of nuclear import of TroIRF3 variants. **(A)** Schematic presentation of different TroIRF3-GFP variants. **(B)** The subcellular distribution of TroIRF3 variants with or without *V. haveyi* infection. GPS cells seeded overnight on a microscope in 24-well plates were transiently transfected with TroIRF3 variants for 48 h. The cells were stimulated by *V. haveyi* for 6 h, followed by inverted fluorescence microscopy imaging. DAPI was used to stain the nuclei of cells.

the Osteichthyes species and higher vertebrates cluster into two major groups. TroIRF3 is closely related to *S. lalandi dorsalis* IRF3, which belongs to Perciformes. Given its conserved structure and evolutionary history, TroIRF3 may play a conserved role in the immune response against pathogens.

Studies have found that IRF3 is predominantly expressed in the immune organs of several species, including *Squaliobarbus curriculus* and *E. coioides* (32, 50). In this study, TroIRF3 was most prominent in the gill and liver while relatively low in the spleen and blood. The gill and liver play a role in immunology or act as entry points for pathogens. TroIRF3 showed the highest expression level in gill, which may account for TroIRF3 could be involvement in the early immune response. The spleen and head-kidney from *Odontobutis obscura* also showed relatively low IRF3 expression levels (51). This observation may be attributed to the fact that the mRNA expression check was conducted in healthy fish, where IRF3 was not required for upregulation in the spleen and head-kidney (51). LPS treatment induces IRF3 transcripts in some fish species, such as *L. crocea* and *Ctenopharyngodon idella* (52, 53). *In vivo*, TroIRF3 transcript levels were also significantly upregulated following *V. harveyi* treatment. According to these results, *T. ovatus*' innate immune response against *V. harveyi* may be mediated by TroIRF3.

In mammals, IRF3 plays a role in antiviral immunity. However, recent studies found that IRF3 also participates in bacterial immunity (54–56). In A549 cells, siRNA inhibiting IRF3 expression resulted in an overall increase in *Legionella* numbers (57). *Chlamydophila pneumoniae* replication was enhanced when IRF3 expression was inhibited by siRNA and attenuated by IFN-β treatment (58). Mice IRF3 deficiency leads to impaired clearance of *P. aeruginosa* from the lung (56). In this study, we showed that the bacterial load reduction in fish tissues was caused by TroIRF3 overexpression. Consistent with these findings, the inhibition of TroIRF3 expression by siTroIRF3 led to an increase in the number of bacteria. In addition, TroIRF3 upregulated key genes, such as IFNa3, MXI, TRAF6, Viperin1 and MAVS, which are involved in IFN/IRF-based signalling. IFN, MXI and Viperin have several functions that participate in the antibacterial

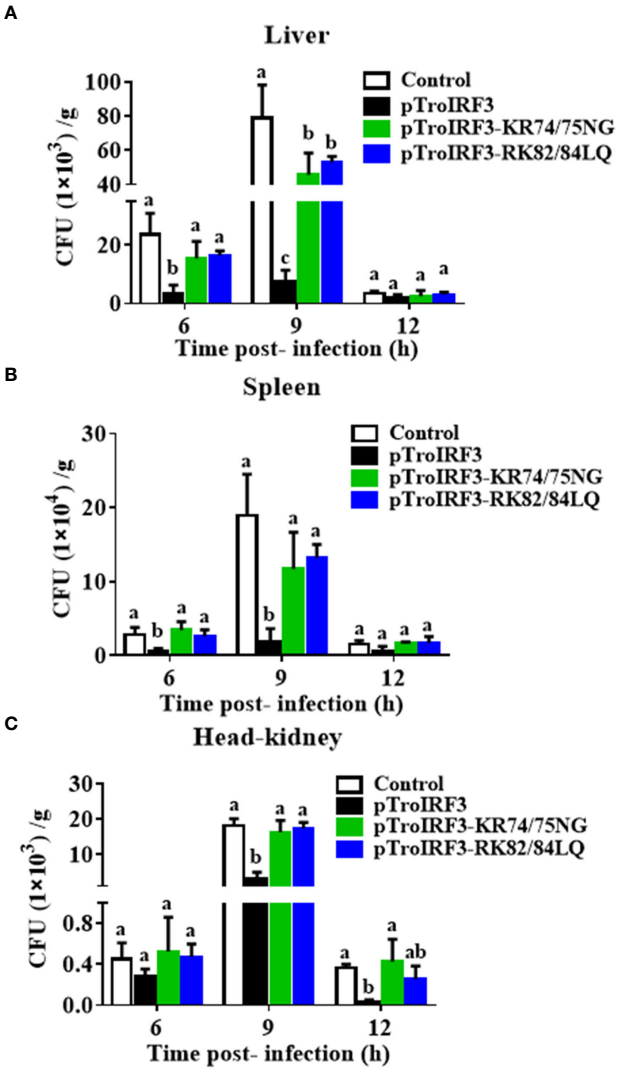

FIGURE 6
The function of NLS in antibacterial responses regulated by TroIRF3. *T. ovatus* were administered with PBS (control), pTroIRF3, pTroIRF3-KR74/75NG, or pTroIRF3-RK82/84LQ for 5 days, then injected intraperitoneally with *V. harveyi*, and the number of bacteria in the liver **(A)**, spleen **(B)**, and head-kidney **(C)** at different time points were quantified using the plate counting method. Data are expressed as means ± SD (N = 3). N, the number of fish used at each time point per group. Significant differences ($P < 0.05$) are indicated by different letters, and no significant differences are indicated by the same letters.

and antiviral immune response (59–61). Moreover, TRAF6 and MAVS participate in the activation of IRF3 (62). These findings suggested that the overexpression of TroIRF3 upregulated the expression of IFN and IFN-related genes, leading to an antibacterial state to inhibit *V. harveyi* replication.

Under healthy conditions, mice IRF3 is mostly found in the cytoplasm of cell. After infection with *P. aeruginosa*, it is phosphorylated and transported to the nuclei (56). However, fish IRF3 localization varies. *C. auratus L.* IRF3 was located in the cytoplasm without stimuli but was observed in the nuclei after a poly I: C challenge (33). *Oncorhynchus mykiss* IRF3 is localized in both cytoplasm and nuclei with or without poly I: C and no apparent transfer from the cytoplasm to the nucleus was observed (63). When no bacterial infection is present, TroIRF3 initially resides in the GPS cells' cytoplasm but undergoes nuclear translocation upon bacterial stimulation. The result suggests that TroIRF3 originally resided in the cytoplasm in an inactive form when no bacterial contamination was present, but when bacteria stimulated the cell, it was activated and translocated into the nucleus. Therefore, TroIRF3 is involved in antibacterial immunity.

IRF proteins contain both NLSs and NESs, so their subcellular distribution can be controlled to manage the IRF function (25). Before bacterial infection, TroIRF3 is predominantly localized in the cytoplasm, suggesting that nuclear export dominates nuclear import. As a result of bacterial infection, TroIRF3 resides mainly in the nucleus, which indicates that nuclear import dominates when TroIRF3 is activated. TroIRF3's NLS was mapped to aa 64–127, which contains an α-helical pattern. The basic amino acids KR74/75 and RK82/84 are integral to TroIRF3's nuclear import. KR74/75 and RK82/84 are 90° amino acids apart, which makes a spatial distance of one amino acid between these two clusters that interact with the binding sites in importin-α (Figure S3). Similarly, mice IRF3 localizes to the nucleus through a bipartite NLS located at the RK86/87 and KR77/78 sites (45). These results revealed that the amino acids that affected IRF3 nuclear localisation were conserved.

We further analysed the role of NLS in TroIRF3-mediated antibacterial responses and type I IFN expression. Our results showed that KR74/75 and RK82/84 in the NLS of TroIRF3 are involved in antibacterial immunity and immune gene (*IFNa3*, *MXI*, *TRAF6*, *Viperin1* and *MAVS*) upregulation induced by TroIRF3. Similarly, mice IRF3 NLS plays an important role in the IFN response and antiviral immunity mediated by IRF3 (45). Our findings revealed that the NLSs enforced the nuclear localisation of TroIRF3 and were essential to antibacterial immunity in *T. ovatus*.

In DNA or RNA viral infection defence, vertebrate IRF3 is the key transcription factor in the signalling of type I interferon-dependent immune responses (18, 64, 65). Mammalian IRF3 has been shown to bind to the promoters of IFN and ISG and activate their transcription (66). As shown by the luciferase activity, the ectopic expression of TroIRF3 activated the TroIFNa3 promoter. The activation was dependent on the TroIRF3 concentration and further enhanced by *V. harveyi* stimulation. These results may reveal that TroIRF3 can activate TroIFNa3-mediated antibacterial responses. Similar results were also obtained in other species, such as *Miichthys miiuy*, *Lateolabrax japonicus* and *Oreochromis niloticus*. The IRF3 protein of *O. niloticus* enhances the activity of the IFN-β promoter, which plays a role in regulating the IFN response (67). *M. miiuy* IRF3 can activate the IFNα promoter, and the expressions increased with the increase in mmIRF3 quality (68). *L. japonicus* IRF3 overexpression significantly increased the promoter activity of zebrafish IFN1 (69). Furthermore, the amino acid residues KR74/75 and RK82/84 in TroIRF3's NLS were essential for activating TroIFNa3-p2. These results showed that TroIRF3 acted as a transcription activator in immune responses and that the amino acid residues KR74/75 and RK82/84 are important to the immune regulation of TroIRF3.

In summary, the present study cloned and characterised TroIRF3. *V. harveyi* infection significantly increased TroIRF3 expression and shuttled it from the cytoplasm into the nucleus. TroIRF3 played an important role in the antibacterial immune response. Basic amino

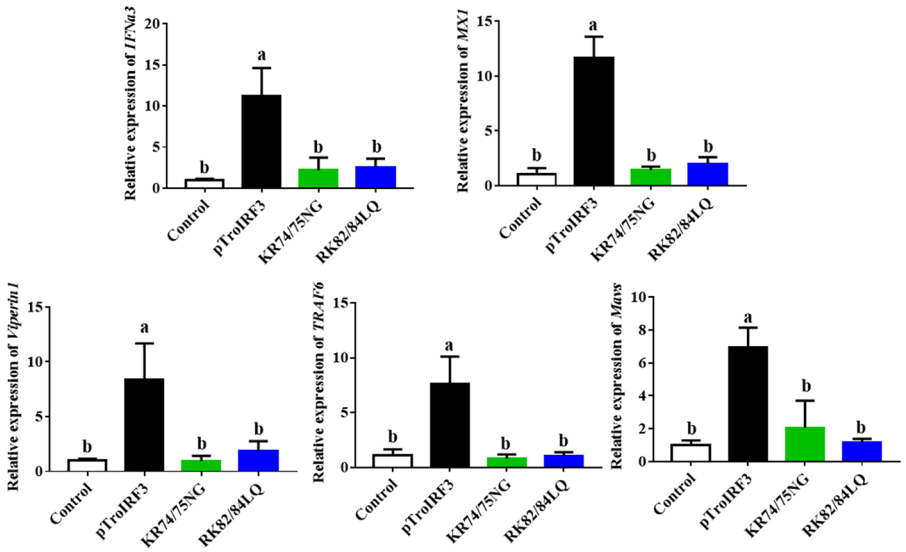

FIGURE 7
The function of NLS in the expression of interferon signaling molecules induced by TroIRF3. Golden pompano injected with pTroIRF3, pTroIRF3-KR74/75NG, pTroIRF3-RK82/84LQ, or PBS (control). After five days, the expression level of interferon signaling molecules in the spleen was detected. The results represent the mean ± SD (N=3), and N indicates the number of fish used per group. Significant differences ($P < 0.05$) are indicated by different letters, and no significant differences are indicated by the same letters.

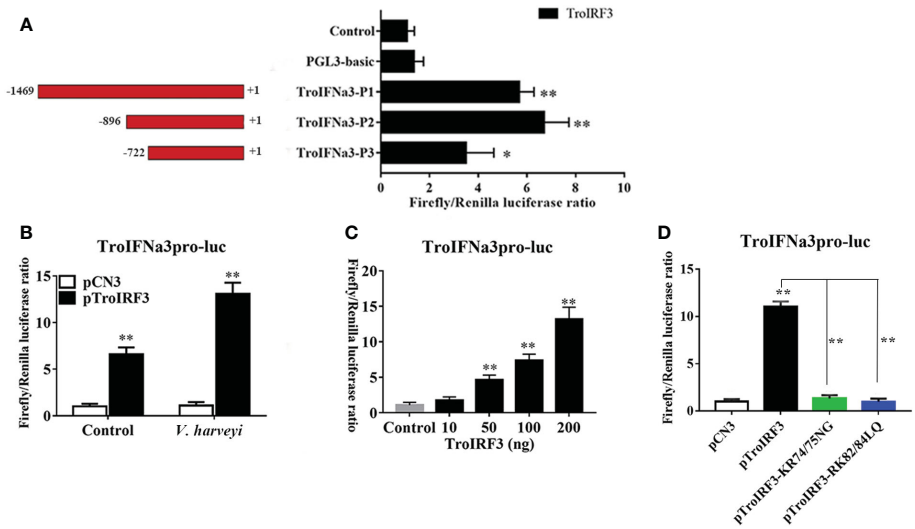

FIGURE 8
TroIRF3 regulated the activity of the TroIFNa3 promoter. **(A)** Three truncates of the TroIFNa3 promoter were constructed and transfected with pTroIRF3 into HEK 293T cells for 24 h, then harvested for detection of luciferase activity. **(B)** Activation of the TroIFNa3 promoter by TroIRF3. HEK293T cells seeded in 24-well plates were co-transfected with three plasmid sets: pCN3 (0.25 μg), pGL4-TroIFNa3-pro (0.25 μg), and pRL-TK; pTroIRF3 (0.25 μg), pGL4-TroIFNa3-pro (0.25 μg) and pRL-TK (0.025 μg). Cells were stimulated with or without *V. harveyi* after 24 h post-transfection, then harvested for detection of luciferase activity. **(C)** HEK293T cells seeded in 24-well plates were transfected with 0, 10, 50, 100, and 200 ng of pTroIRF3 along with pGL4-TroIFNa3-pro (0.25 μg) and pRL-TK (0.025 μg), then harvested for detection of luciferase activity. **(D)** The effect of NLS on TroIFNa3 promoter activation induced by TroIRF3. HEK293T cells seeded in 24-well plates were co-transfected with TroIFNa3 promoter (0.25 μg), as well as with pCN3, pTroIRF3, pTroIRF3-KR74/75NG, or pTroIRF3-RK82/84LQ (0.25 μg), plus 0.025 mg of pRL-CMV as an internal control. Cells were stimulated with *V. harveyi* for 12 h after 24 h post-transfection, then harvested for detection of luciferase activity. The values are represented as mean ± SD (N = 3). N, parallel experiments. $*P < 0.05$, $**P < 0.01$.

acids KR74/75 and RK82/84 were required for the efficient nuclear import of TroIRF3 and played a key role in the antibacterial immune response and upregulation of immune genes induced by TroIRF3. Furthermore, TroIRF3 activated the promoter of TroIFNa3, and the key amino acids KR74/75 and RK82/84 were essential for TroIFNa3-p2 activation induced by TroIRF3.

Data availability statement

The original contributions presented in the study are included in the article/Supplementary Material. Further inquiries can be directed to the corresponding authors.

Ethics statement

The animal study was reviewed and approved by Animal Care and Use Committee of the Hainan University.

Author contributions

YS, ZC, YW, and YZ designed the research. PZ, CW, YS, and WY analyzed the data. YW and YZ supervised the study. YS, YW, ZC, and JL performed the research, analyzed the data, and wrote the manuscript with support from all authors. All authors contributed to the article and approved the submitted version.

Funding

This research was funded by the National Natural Science Foundation of China (U22A20534, 42066007), and the Nanhai Famous Youth Project.

Conflict of interest

The authors declare that the research was conducted in the absence of any commercial or financial relationships that could be construed as a potential conflict of interest.

Publisher's note

Supplementary material

The Supplementary Material for this article can be found online at: https://www.frontiersin.org/articles/10.3389/fimmu.2023.1128196/full#supplementary-material

References

1. Stetson DB, Medzhitov R. Type I interferons in host defense. *Immunity* (2006) 25:373–81. doi: 10.1016/j.immuni.2006.08.007

2. Gonzalez-Navajas JM, Lee J, David M and Raz E. Immunomodulatory functions of type I interferons. *Nat Rev Immunol* (2012) 12:125–35. doi: 10.1038/nri3133

3. Ivashkiv LB, Donlin LT. Regulation of type I interferon responses. *Nat Rev Immunol* (2014) 14:36–49. doi: 10.1038/nri3581

4. Zou J, Tafalla C, Truckle J and Secombes CJ. Identification of a second group of type I IFNs in fish sheds light on IFN evolution in vertebrates. *J Immunol* (2007) 179:3859–71. doi: 10.4049/jimmunol.179.6.3859

5. Lopez-Munoz A, Roca FJ, Meseguer J and Mulero V. New insights into the evolution of IFNs: zebrafish group II IFNs induce a rapid and transient expression of IFN-dependent genes and display powerful antiviral activities. *J Immunol* (2009) 182:3440–9. doi: 10.4049/jimmunol.0802528

6. Zou J, Gorgoglione B, Taylor NGH, Summathed T, Lee PT, Panigrahi A, et al. Salmonids have an extraordinary complex type I IFN system: Characterization of the IFN oocus in rainbow trout *Oncorhynchus mykiss* reveals two novel IFN subgroups. *J Of Immunol* (2014) 193:2273–86. doi: 10.4049/jimmunol.1301796

7. Gan Z, Chen SN, Huang B, Zou J and Nie P. Fish type I and type II interferons: Composition, receptor usage, production and function. *Rev In Aquacult* (2020) 12:773–804. doi: 10.1111/raq.12349

8. Lu MM, Yang CY, Li MJ, Yi QL, Lu GX, Wu YC, et al. A conserved interferon regulation factor 1 (IRF-1) from pacific oyster *Crassostrea gigas* functioned as an activator of IFN pathway. *Fish Shellfish Immunol* (2018) 76:68–77. doi: 10.1016/j.fsi.2018.02.024

9. Stein C, Caccamo M, Laird G and Leptin M. Conservation and divergence of gene families encoding components of innate immune response systems in zebrafish. *Genome Biol* (2007) 8:R251. doi: 10.1186/gb-2007-8-11-r251

10. Panne D, Maniatis T and Harrison SC. An atomic model of the interferon-β enhanceosome. *Cell* (2007) 129:1111–23. doi: 10.1016/j.cell.2007.05.019

11. Panne D, McWhirter SM, Maniatis T and Harrison SC. Interferon regulatory factor 3 is regulated by a dual phosphorylation-dependent switch. *J Biol Chem* (2007) 282:22816–22. doi: 10.1074/jbc.M703019200

12. Clement JF, Bibeau-Poirier A, Gravel SP, Grandvaux N, Bonneil E, Thibault P, et al. Phosphorylation of IRF-3 on ser 339 generates a hyperactive form of IRF-3 through regulation of dimerization and CBP association. *J Virol* (2008) 82:3984–96. doi: 10.1128/JVI.02526-07

13. Bergstroem B, Johnsen IB, Nguyen TT, Hagen L, Slupphaug G, Thommesen L, et al. Identification of a novel *in vivo* virus-targeted phosphorylation site in interferon regulatory factor-3 (IRF3). *J Biol Chem* (2010) 285:24904–14. doi: 10.1074/jbc.M109.084822

14. Lin R, Heylbroeck C, Pitha PM, Hiscott J. Virus-dependent phosphorylation of the IRF-3 transcription factor regulates nuclear translocation, transactivation potential, and proteasome-mediated degradation. *Mol Cell Biol* (1998) 18:2986–96. doi: 10.1128/mcb.18.5.2986

15. Honda K, Takaoka A and Taniguchi T. Type I interferon gene induction by the interferon regulatory factor family of transcription factors. *Immunity* (2006) 25:349–60. doi: 10.1016/j.immuni.2006.08.009

16. Ding Y, Ao JQ, Huang XH, Chen XH. Identification of two subgroups of type I IFNs in perciforme fish large yellow croaker *Larimichthys crocea* provides novel insights into function and regulation of fish type I IFNs. *Front In Immunol* (2016) 7:343. doi: 10.3389/Fimmu.2016.00343

17. Rajput A, Kovalenko A, Bogdanov K, Yang SH, Kang TB, Kim JC, et al. RIG-I RNA helicase activation of IRF3 transcription factor is negatively regulated by caspase-8-Mediated cleavage of the RIP1 protein. *Immunity* (2011) 34:340–51. doi: 10.1016/j.immuni.2010.12.018

18. Honda K, Taniguchi T. IRFs: master regulators of signalling by toll-like receptors and cytosolic pattern-recognition receptors. *Nat Rev Immunol* (2006) 6:644–58. doi: 10.1038/nri1900

19. Takaoka A, Wang Z, Choi MK, Yanai H, Negishi H, Ban T, et al. DAI (DLM-1/ZBP1) is a cytosolic DNA sensor and an activator of innate immune response. *Nature* (2007) 448:501–5. doi: 10.1038/nature06013

20. Leulier F, Lemaitre B. Toll-like receptors–taking an evolutionary approach. *Nat Rev Genet* (2008) 9:165–78. doi: 10.1038/nrg2303

21. Suzuki N, Suzuki S and Yeh WC. IRAK-4 as the central TIR signaling mediator in innate immunity. *Trends Immunol* (2002) 23:503–6. doi: 10.1016/s1471-4906(02)02298-6

22. Janssens S, Beyaert R. Functional diversity and regulation of different interleukin-1 receptor-associated kinase (IRAK) family members. *Mol Cell* (2003) 11:293–302. doi: 10.1016/s1097-2765(03)00053-4

23. Lazear HM, Lancaster A, Wilkins C, Suthar MS, Huang A, Vick SC, et al. IRF-3, IRF-5, and IRF-7 coordinately regulate the type I IFN response in myeloid dendritic cells downstream of MAVS signaling. *PloS Pathog* (2013) 9:e1003118. doi: 10.1371/journal.ppat.1003118

24. Tamura T, Yanai H, Savitsky D and Taniguchi T. The IRF family transcription factors in immunity and oncogenesis. *Annu Rev Immunol* (2008) 26:535–84. doi: 10.1146/annurev.immunol.26.021607.090400

25. Lange A, Mills RE, Lange CJ, Stewart M, Devine SE, Corbett AH. Classical nuclear localization signals: definition, function, and interaction with importin α. *J Biol Chem* (2007) 282:5101–5. doi: 10.1074/jbc.R600026200

26. Servant MJ, Grandvaux N and Hiscott J. Multiple signaling pathways leading to the activation of interferon regulatory factor 3. *Biochem Pharmacol* (2002) 64:985–92. doi: 10.1016/s0006-2952(02)01165-6

27. Yoneyama M, Suhara W, Fukuhara Y, Fukuda M, Nishida E and Fujita T. Direct triggering of the type I interferon system by virus infection: activation of a transcription factor complex containing IRF-3 and CBP/p300. *EMBO J* (1998) 17:1087–95. doi: 10.1093/emboj/17.4.1087

28. Doyle S, Vaidya S, O'Connell R, Dadgostar H, Dempsey P, Wu T, et al. IRF3 mediates a TLR3/TLR4-specific antiviral gene program. *Immunity* (2002) 17:251–63. doi: 10.1016/s1074-7613(02)00390-4

29. Doyle SE, O'Connell R, Vaidya SA, Chow EK, Yee K and Cheng G. Toll-like receptor 3 mediates a more potent antiviral response than toll-like receptor 4. *J Immunol* (2003) 170:3565–71. doi: 10.4049/jimmunol.170.7.3565

30. Kawai T, Takeuchi O, Fujita T, Inoue J, Muhlradt PF, Sato S, et al. Lipopolysaccharide stimulates the MyD88-independent pathway and results in activation of IFN-regulatory factor 3 and the expression of a subset of lipopolysaccharide-inducible genes. *J Immunol* (2001) 167:5887–94. doi: 10.4049/jimmunol.167.10.5887

31. Sakaguchi S, Negishi H, Asagiri M, Nakajima C, Mizutani T, Takaoka A, et al. Essential role of IRF-3 in lipopolysaccharide-induced interferon-β gene expression and endotoxin shock. *Biochem Biophys Res Commun* (2003) 306:860–6. doi: 10.1016/s0006-291x(03)01049-0

32. Huang Y, Huang X, Cai J, OuYang Z, Wei S, Wei J, et al. Identification of orange-spotted grouper (*Epinephelus coioides*) interferon regulatory factor 3 involved in antiviral immune response against fish RNA virus. *Fish Shellfish Immunol* (2015) 42:345–52. doi: 10.1016/j.fsi.2014.11.025

33. Sun F, Zhang YB, Liu TK, Gan L, Yu FF, Liu Y, et al. Characterization of fish IRF3 as an IFN-inducible protein reveals evolving regulation of IFN response in vertebrates. *J Of Immunol* (2010) 185:7573–82. doi: 10.4049/jimmunol.1002401

34. Zhang J, Li YX, Hu YH. Molecular characterization and expression analysis of eleven interferon regulatory factors in half-smooth tongue sole, *Cynoglossus semilaevis*. *Fish Shellfish Immunol* (2015) 44:272–82. doi: 10.1016/j.fsi.2015.02.033

35. Iliev DB, Sobhkhez M. Fremmerlid K and Jorgensen J b, MyD88 interacts with interferon regulatory factor (IRF) 3 and IRF7 in Atlantic salmon (*Salmo salar*): Transgenic SsMyD88 modulates the IRF-induced type I interferon response and accumulates in aggresomes. *J Biol Chem* (2011) 286:42715–24. doi: 10.1074/jbc.M111.293969

36. Yao CL, Huang XN, Fan Z, Kong P and Wang ZY. Cloning and expression analysis of interferon regulatory factor (IRF) 3 and 7 in large yellow croaker. *Larimichthys crocea Fish Shellfish Immunol* (2012) 32:869–78. doi: 10.1016/j.fsi.2012.02.015

37. Ohtani M, Hikima J, Hwang SD, Morita T, Suzuki Y, Kato G, et al. Transcriptional regulation of type I interferon gene expression by interferon regulatory factor-3 in Japanese flounder. *Paralichthys olivaceus Dev Comp Immunol* (2012) 36:697–706. doi: 10.1016/j.dci.2011.10.008

38. Tu Z, Li H, Zhang X, Sun Y and Zhou Y. Complete genome sequence and comparative genomics of the golden pompano (*Trachinotus ovatus*) pathogen, *Vibrio harveyi* strain QT520. *PeerJ* (2017) 5:e4127. doi: 10.7717/peerj.4127

39. Chen Y, Zhou Y, Yang X, Cao Z, Chen X, Qin Q, et al. Insulin-like growth factor binding protein 3 gene of golden pompano (TroIGFBP3) promotes antimicrobial immune defense. *Fish Shellfish Immunol* (2020) 103:47–57. doi: 10.1016/j.fsi.2020.04.002

40. Wu Y, Zhou Y, Cao Z, Sun Y, Chen Y, Xiang Y, et al. Comparative analysis of the expression patterns of IL-1β, IL-11, and IL-34 in golden pompano (*Trachinotus ovatus*) following different pathogens challenge. *Fish Shellfish Immunol* (2019) 93:863–70. doi: 10.1016/j.fsi.2019.08.018

41. Zhu KC, Zhang N, Liu BS, Guo L, Guo HY, Jiang SG, et al. Functional analysis of IRF1 reveals its role in the activation of the type I IFN pathway in golden pompano, *Trachinotus ovatus* (Linnaeus 1758). *Int J Of Mol Sci* (2020) 21:2652. doi: 10.3390/Ijms21072652

42. Wu Y, Zhou Y, Cao Z, Chen X, Du H and Sun Y. Interferon regulatory factor 7 contributes to the host response during *Vibrio harveyi* infection in the golden pompano *Trachinotus ovatus*. *Dev Comp Immunol* (2021) 117:103959. doi: 10.1016/j.dci.2020.103959

43. Yu Y, Wei S, Wang Z, Huang X, Huang Y, Cai J, et al. Establishment of a new cell line from the snout tissue of golden pompano *Trachinotus ovatus*, and its application in virus susceptibility. *J Fish Biol* (2016) 88:2251–62. doi: 10.1111/jfb.12986

44. Chen XJ, Zhang XQ, Huang S, Cao ZJ, Qin QW, Hu WT, et al. Selection of reference genes for quantitative real-time RT-PCR on gene expression in golden pompano (*Trachinotus ovatus*). *Polish J Of Veterinary Sci* (2017) 20:583–94. doi: 10.1515/pjvs-2017-0071

45. Zhu M, Fang T, Li S, Meng K and Guo D. Bipartite nuclear localization signal controls nuclear import and DNA-binding activity of IFN regulatory factor 3. *J Immunol* (2015) 195:289–97. doi: 10.4049/jimmunol.1500232

46. Ysebrant de Lendonck L, Martinet V and Goriely S. Interferon regulatory factor 3 in adaptive immune responses. *Cell Mol Life Sci* (2014) 71:3873–83. doi: 10.1007/s00018-014-1653-9

47. Csumita M, Csermely A, Horvath A, Nagy G, Monori F, Goczi L, et al. Specific enhancer selection by IRF3, IRF5 and IRF9 is determined by ISRE half-sites, 5 ' and 3 ' flanking bases, collaborating transcription factors and the chromatin environment in a combinatorial fashion. *Nucleic Acids Res* (2020) 48:589–604. doi: 10.1093/nar/gkz1112

48. Petro TM. IFN regulatory factor 3 in health and disease. *J Immunol* (2020) 205:1981–89. doi: 10.4049/jimmunol.2000462

49. Hiscott J. Triggering the innate antiviral response through IRF-3 activation. *J Biol Chem* (2007) 282:15325–9. doi: 10.1074/jbc.R700002200

50. Wang R, Li Y, Zhou Z, Liu Q, Zeng L and Xiao T. Involvement of interferon regulatory factor 3 from the barbel chub *Squaliobarbus curriculus* in the immune response against grass carp reovirus. *Gene* (2018) 648:5–11. doi: 10.1016/j.gene.2018.01.048

51. Li Z, Chen J, Li P, Li XY, Lu L and Li S. Functional characterization of dark sleeper (*Odontobutis obscura*) IRF3 in IFN regulation. *Fish Shellfish Immunol* (2019) 89:411–19. doi: 10.1016/j.fsi.2019.04.019

52. Yu N, Xu X, Qi G, Liu D, Chen X, Ran X, et al. *Ctenopharyngodon idella* TBK1 activates innate immune response *via* IRF7. *Fish Shellfish Immunol* (2018) 80:521–27. doi: 10.1016/j.fsi.2018.06.045

53. Zou PF, Shen JJ, Li Y, Zhang ZP, Wang YL. TRAF3 enhances TRIF-mediated signaling *via* NF-κB and IRF3 activation in large yellow croaker *Larimichthys crocea*. *Fish Shellfish Immunol* (2020) 97:114–24. doi: 10.1016/j.fsi.2019.12.024

54. Juang YT, Lowther W, Kellum M, Au WC, Lin R, Hiscott J, et al. Primary activation of interferon a and interferon b gene transcription by interferon regulatory factor 3. *Proc Natl Acad Sci U.S.A.* (1998) 95:9837–42. doi: 10.1073/pnas.95.17.9837

55. Yamashiro T, Sakamoto N, Kurosaki M, Kanazawa N, Tanabe Y, Nakagawa M, et al. Negative regulation of intracellular hepatitis c virus replication by interferon regulatory factor 3. *J Gastroenterol* (2006) 41:750–7. doi: 10.1007/s00535-006-1842-x

56. Carrigan SO, Junkins R, Yang YJ, Macneil A, Richardson C, Johnston B, et al. IFN regulatory factor 3 contributes to the host response during *Pseudomonas aeruginosa* lung infection in mice. *J Immunol* (2010) 185:3602–9. doi: 10.4049/jimmunol.0903429

57. Opitz B, Vinzing M, van Laak V, Schmeck B, Heine G, Gunther S, et al. *Legionella pneumophila* induces IFNβ in lung epithelial cells *via* IPS-1 and IRF3, which also control bacterial replication. *J Biol Chem* (2006) 281:36173–9. doi: 10.1074/jbc.M604638200

58. Buss C, Opitz B, Hocke AC, Lippmann J, van Laak V, Hippenstiel S, et al. Essential role of mitochondrial antiviral signaling, IFN regulatory factor (IRF)3, and IRF7 in *Chlamydophila pneumoniae*-mediated IFN-β response and control of bacterial replication in human endothelial cells. *J Immunol* (2010) 184:3072–8. doi: 10.4049/jimmunol.0902947

59. Helbig KJ, Teh MY, Crosse KM, Monson EA, Smith M, Tran EN, et al. The interferon stimulated gene viperin, restricts shigella. *flexneri vitro Sci Rep* (2019) 9:15598. doi: 10.1038/s41598-019-52130-8

60. Boxx GM, Cheng G. The roles of type I interferon in bacterial infection. *Cell Host Microbe* (2016) 19:760–9. doi: 10.1016/j.chom.2016.05.016

61. Teles RM, Graeber TG, Krutzik SR, Montoya D, Schenk M, Lee DJ, et al. Type I interferon suppresses type II interferon-triggered human anti-mycobacterial responses. *Science* (2013) 339:1448–53. doi: 10.1126/science.1233665

62. Chen H, Jiang Z. The essential adaptors of innate immune signaling. *Protein Cell* (2013) 4:27–39. doi: 10.1007/s13238-012-2063-0

63. Holland JW, Bird S, Williamson B, Woudstra C, Mustafa A, Wang T, et al. Molecular characterization of IRF3 and IRF7 in rainbow trout, *Oncorhynchus mykiss*: Functional analysis and transcriptional modulation. *Mol Immunol* (2008) 46:269–85. doi: 10.1016/j.molimm.2008.08.265

64. Au WC, Moore PA, LaFleur DW, Tombal B, Pitha PM. Characterization of the interferon regulatory factor-7 and its potential role in the transcription activation of interferon a genes. *J Biol Chem* (1998) 273:29210–7. doi: 10.1074/jbc.273.44.29210

65. Taniguchi T, Takaoka A. A weak signal for strong responses: Interferon-α/β revisited. *Nat Rev Mol Cell Biol* (2001) 2:378–86. doi: 10.1038/35073080

66. Paun A, Pitha PM. The IRF family, revisited. *Biochimie* (2007) 89:744–53. doi: 10.1016/j.biochi.2007.01.014

67. Gu YF, Wei Q, Tang SJ, Chen XW, Zhao JL. Molecular characterization and functional analysis of IRF3 in tilapia (*Oreochromis niloticus*). *Dev Comp Immunol* (2016) 55:130–7. doi: 10.1016/j.dci.2015.10.011

68. Shu C, Chu Q, Bi D, Wang Y and Xu T. Identification and functional characterization of miiuy croaker IRF3 as an inducible protein involved regulation of IFN response. *Fish Shellfish Immunol* (2016) 54:499–506. doi: 10.1016/j.fsi.2016.04.136

69. Zhang W, Li Z, Jia P, Liu W, Yi M and Jia K. Interferon regulatory factor 3 from sea perch (*Lateolabrax japonicus*) exerts antiviral function against nervous necrosis virus infection. *Dev Comp Immunol* (2018) 88:200–05. doi: 10.1016/j.dci.2018.07.014

frontiers | Frontiers in Immunology

TYPE Original Research
PUBLISHED 03 February 2023
DOI 10.3389/fimmu.2023.1098455

OPEN ACCESS

EDITED BY
Sun Yun,
Hainan University, China

REVIEWED BY
Bei Wang,
Guangdong Ocean University, China
Yu Huang,
Guangdong Ocean University, China

*CORRESPONDENCE
Aijun Lv
lajand@126.com

†These authors have contributed equally to this work

SPECIALTY SECTION
This article was submitted to Molecular Innate Immunity, a section of the journal Frontiers in Immunology

RECEIVED 14 November 2022
ACCEPTED 11 January 2023
PUBLISHED 03 February 2023

CITATION
Huo J, Hu X, Bai J and Lv A (2023) Multiomics analysis revealed miRNAs as potential regulators of the immune response in *Carassius auratus* gills to *Aeromonas hydrophila* infection. *Front. Immunol.* 14:1098455. doi: 10.3389/fimmu.2023.1098455

Multiomics analysis revealed miRNAs as potential regulators of the immune response in *Carassius auratus* gills to *Aeromonas hydrophila* infection

Jiaxin Huo†, Xiucai Hu†, Jie Bai and Aijun Lv*

Tianjin Key Lab of Aqua-Ecology and Aquaculture, College of Fisheries, Tianjin Agricultural University, Tianjin, China

The gill of fish is an important immune organ for pathogen defense, but its microRNA (miRNA) expression and regulatory mechanism remain unclear. In this study, we report on the histopathological and immunohistochemical features of the gills of the crucian carp *Carassius auratus* challenged with *Aeromonas hydrophila*. Small RNA libraries of the gills were constructed and sequenced on the Illumina HiSeq 2000 platform. A total of 1,165 differentially expressed miRNAs (DEMs) were identified in gills, of which 539 known and 7 unknown DEMs were significantly screened ($p < 0.05$). Gene Ontology (GO) and Kyoto Encyclopedia of Genes and Genomes (KEGG) enrichment analyses revealed that the potential target genes/proteins were primarily involved in 33 immune-related pathways, in which the inflammatory responses were focused on the Toll-like receptor (TLR), mitogen-activated protein kinase (MAPK), and nuclear factor kappa B (NF-κB) signaling pathways. Moreover, the expression levels of 14 key miRNAs (e.g., miR-10, miR-17, miR-26a, miR-144, miR-145, and miR-146a) and their target genes (e.g., *TNFα*, *TLR4*, *NF-κB*, *TAB1*, *PI3K*, and *IRAK1*) were verified. In addition, the protein levels based on isobaric tags for relative and absolute quantification (iTRAQ) were significantly associated with the results of the quantitative real-time PCR (qRT-PCR) analysis ($p < 0.01$). miR-17/pre-miR-17 were identified in the regulation expression of the NF-κB target gene, and the phylogenetic tree analysis showed that the pre-miR-17 of *C. auratus* with the closest similarity to the zebrafish *Danio rerio* is highly conserved in teleosts. This is the first report of the multi-omics analysis of the miRNAs and proteins in the gills of *C. auratus* infected with *A. hydrophila*, thus enriching knowledge on the regulation mechanism of the local immune response in Cyprinidae fish.

KEYWORDS

Carassius auratus, miRNA, iTRAQ, immune response, histopathology, gills

Highlights

Multi-omics analysis of the miRNAs and iTRAQ profiles was first performed in the gills of *C. auratus* upon *A. hydrophila* infection.

The miRNAs (e.g., miR-17, miR-26a, miR-144, and miR-146a) play crucial roles in the gill local immune response of *C. auratus* to bacterial infection.

The target genes of miRNAs are involved in signaling pathways such as TLR, MAPK, and NF-κB inflammatory responses.

Introduction

MicroRNAs (miRNAs) are small endogenous non-coding RNAs with a length of approximately 20–24 bases that can bind to the 3′ untranslated region (3′-UTR) of messenger RNAs (mRNAs), thereby guiding the degradation of the target genes or inhibiting translation to negatively regulate the gene expression (1, 2). Since their first discovery in *Caenorhabditis elegans*, miRNAs have encompassed cellular functions in diverse biological processes, such as cell growth, proliferation and differentiation, development, immunity, and apoptosis (3, 4). In the past decades, some studies combined molecular immunity to prove that miRNAs are pivotal regulators of the inflammatory response (5–7). Furthermore, high-throughput sequencing has been widely used for miRNA expression profiling analysis in fish (3, 8). The innate immune system involves different signaling pathways that are regulated by complex mechanisms, most of the miRNAs of which are still unclear in fish (9, 10). In teleosts, recent studies have suggested that miR-21 targets *IRAK4* to inhibit excessive immune response (11), that miR-146 shows immune-related inducible expression in the zebrafish *Danio rerio* after *Aeromonas hydrophila* infection (12), and that miR-144 is differentially expressed to modulate the host response in the bacteria-infected miiuy croaker *Miichthys miiuy* (13). In addition, several miRNAs (e.g., miR-122, miR-192, and miR-148) have been identified to regulate the target genes that participate in innate immunity (14–16). Accumulating evidence demonstrated that, in the immune response process against bacterial infection, most miRNAs focus on regulating the gene expression in the Toll-like receptors (TLRs), C-type lectin receptors (CLR, mitogen-activated protein kinases (MAPKs) and MyD88-mediated nuclear factor kappa B (NF-κB) signaling pathways (4, 13, 16, 17). Recently, some miRNAs have been found to be involved in the regulation of signal transduction, growth, and immunity in the crucian carp *Carassius auratus* (5, 18). However, the regulation mechanisms of miRNA-mediated bacterial infection are still poorly studied in teleosts.

As a primary immune organ, the gill is considered a large mucosal surface with a variety of functions for respiration, osmotic regulation, and toxicological response (19). Recent studies have reported the gene expression patterns of gills after infection and investigated their immune response at different molecular levels (20, 21), in which immune-related genes (e.g., *TLR4*, *IRAK1*, *TNF*, and *IL-1β*) were found to be differentially expressed in the gills of teleosts (22–24). Notably, the miRNA (e.g., miR-135b, miR-146, and miR-10a-5p) expression in the gills of the Atlantic killifish *Fundulus heteroclitus* and the grass carp *Ctenopharyngodon idella* infected with *A. hydrophila*, as well as the zebrafish *D. rerio* after *Staphylococcus aureus* infection, has verified their roles in the gene regulatory network (20, 25, 26). Although previous studies have shown that gills play important roles in the immune system as the first line of defense against the invasion of pathogens, the mechanisms of the gill immune response of the miRNAs and target genes regulating bacterial infection remain unclear in fish.

The crucian carp *C. auratus* is a major freshwater species cultured for human consumption in China (5, 18). Nevertheless, the outbreak of bacterial diseases of *C. auratus* is has become a serious problem, causing economic losses (8, 18, 27). As an important Gram-negative opportunistic pathogen, *A. hydrophila* is widely distributed in the water environment (27). Recently, the characterization of the miRNAs and target genes in the internal organs (e.g., kidney, spleen, and liver) and skin of *C. auratus* has been performed using deep sequencing analysis (5, 18). Moreover, proteomic analyses (e.g., iTRAQ and 2-DE/MS) were performed in zebrafish gills and crucian carp skin after *A. hydrophila* infection (19, 28). However, the miRNA expression and its regulatory mechanism in the gills of *C. auratus* are still unclear. The present study used conventional histopathological examination, multi-omics analysis of the mRNA and protein profiles, and the high-throughput small RNA (sRNA) transcriptome sequencing technique to construct an sRNA library of the gills of *C. auratus* infected with *A. hydrophila* based on the Illumina HiSeq 2000 platform. The results of this study provide a scientific basis for elucidating the miRNAs and target genes involved in the molecular mechanisms of the gill immune response of teleost fish.

Materials and methods

Sample and challenge

C. auratus (average weight, 50 g) were obtained from Tianshi Fisheries Development Co., Ltd., Tianjin, China. Prior to the bacterial infection, the fish were acclimatized at a temperature of approximately 25°C in freshwater tanks (45 L) for 2 weeks and fed commercial dried pellets (Tongwei Co., Ltd., Chengdu, China) twice daily. In the infection experiment, the fish were immersed in *A. hydrophila* culture with a final concentration of 1×10^8 cfu/ml and then quickly transferred into freshwater after immersion for 3 h, in accordance with a previous report by Wang et al. (27). A total of 60 control and infected fish at 0, 6, and 12 h were randomly selected and aseptically excised for the collection of gill tissue samples. Three mixed gill samples were immediately frozen in liquid nitrogen and stored in a refrigerator at −80°C for later extraction of RNA. The gill samples in the control and infected groups were labeled mGC and mGT, respectively.

Pathology, immunohistochemistry, and phagocytic activity analysis

Fish were randomly selected and dissected for histopathological examination. After deep anesthesia with MS-222 (200 mg/l), the mucosal (i.e., gill, skin, and intestine) and visceral (i.e., liver, kidney, and spleen) tissue samples were fixed in 10% neutral buffered formalin for at least 24 h, then dehydrated using ascending concentrations of 70%–100% ethanol, cleared in xylene, and finally embedded in paraffin wax. Tissue sections of 5-μm thickness were cut on a microtome

(Leica RM 2125, Wetzlar, Germany), stained with hematoxylin and eosin (H&E), and examined using a light microscope (Leica DM 5000, Wetzlar, Germany). For the preparation of the rabbit polyclonal antibody, inactivated *A. hydrophila* bacteria were used as antigens to immune rabbits. The antigen was prepared using equal amounts of Freund's adjuvant (Sigma, St. Louis, MO, USA) according to the manufacturer's guidelines. Two rabbits were immunized with five hypodermic injections. Three days after the fifth injection, the rabbits were bled and the antiserum was detected and stored at −80°C. Immunohistochemical (IHC) staining experiments were performed using a Solarbio kit (Beijing, China) following the manufacturer's protocols. Phagocytosis assays were performed as described by Santos et al. (29). Briefly, 0.5 ml of blood was drawn by caudal puncture using a disposable syringe with a 0.7 × 25-mm needle, slightly moistened with diluted heparin solution (5,000 IU heparin in 50 ml of saline, 0.7%), and then immediately utilized for determination of the phagocytic activity.

Total RNA extraction

Gill samples were extracted using the RNAeasy™ Animal RNA Isolation Kit with Spin Column (code no. R0026; Beyotime, Shanghai, China) according to the manufacturer's instructions. The NanoPhotometer® spectrophotometer (NanoDrop, Wilmington, DE, USA) and agarose gel electrophoresis were utilized to check the purity of the RNA. The integrity and quality of RNA for the construction of the sRNA libraries were examined using the Agilent Bioanalyzer 2100 system (Agilent Technologies, Santa Clara, CA, USA) to ensure that high-quality samples were used for sequencing.

Illumina sequencing

According to the conventional method (29), a total of 3 μg of total RNA per sample was used as the input material for the RNA sample preparations. Two sRNA libraries (i.e., mGC and mGT) were constructed from the gill samples of the control group and the infected fish group. The NEBNext® Multiplex Small RNA Library Prep Set for Illumina® (NEB, Ipswich, MA, USA) was used to generate a sequencing library, and the TruSeq SR Cluster Kit v3-CBOT-HS (Illumina, San Diego, CA, USA) was utilized to execute the index code samples on the CBOT Cluster generation system. After clustering, the library was sequenced on the Illumina HiSeq 2000 platform, and a 50-bp single-ended read was produced by BGI Genomics Co., Ltd. (Shenzhen, China).

Analysis of the sequencing data and annotation of sRNAs

According to the recent report by Bai et al. (18), after completion of the high-throughput sRNA sequencing, overlapping and contaminated sequences and low-quality reads from the original data were removed and the length distribution of the sRNAs was determined. Non-coding RNAs such as ribosomal RNA (rRNA), transfer RNA (tRNA), and small nuclear RNA (snRNA) were identified by comparing with the Rfam database and GenBank, and the known miRNAs in the sample were identified by comparing with the miRNAs in the specified range in miRBase. sRNAs related to the repeat sequence were identified by alignment with the repeat sequence, and the mRNA degradation fragments were identified by comparison with the exons and introns. Moreover, the sRNAs were classified and annotated according to priority, and MIREAP was used to predict novel miRNAs and to determine the step ring or hairpin structure.

Differential expression and phylogenetic analysis of miRNAs

To analyze the differential expression of the miRNAs, their expression levels were standardized to calculate the expression in transcripts per million (TPM) for each library, as described by He et al. (7). The expression levels of the miRNAs in the control and infected samples (mGC/mGT) were determined with the DEGseq program. The Benjamini–Hochberg method was used for multiple verification and correction. By default, a correction p-value <0.05 was set as the threshold for significant differential expression.

The pre-miR-17 sequence of the crucian carp *C. auratus* was obtained using high-throughput sequencing. The sequences of 26 different species from the miRBase database were selected for molecular identification analysis, including the annotations, corresponding species names, and precursor sequences (Supplementary Table S1). MEGA 7.0 software was used for multiple sequence alignment of pre-miR-17, and maximum likelihood estimation (MLE) was utilized for the pre-miR-17 phylogenetic tree (bootstrap = 1,000).

Protein extraction, iTRAQ, and screening of DEPs

Protein extraction of the gill samples and isobaric tags for relative and absolute quantification (iTRAQ) labeling were performed as previously described (19). The protein concentration was determined using a BCA protein assay kit (Sangon Biotech, Shanghai, China), and the proteins were visualized with SDS-PAGE to determine their quality. In the iTRAQ analysis, protein identification and quantification were performed at Genomics Co., Ltd. (Shenzhen, China). For protein quantitation, those with ratios with $p < 0.05$ and fold change >1.2 were considered significant differentially expressed proteins (DEPs).

GO and KEGG enrichment analyses

Gene Ontology (GO) and Kyoto Encyclopedia of Genes and Genomes (KEGG) functional enrichment analyses were performed for the miRNA candidate target genes with differential expression. The commonly used prediction algorithms miRanda, pITA, and RNA hybridization were used to predict the potential miRNA targets (18).

qRT-PCR analysis of the miRNAs and target genes

The miRNAs were extracted using the RNAeasy™ Animal Small RNA Extraction Kit (code no. R0028; Beyotime, Shanghai, China),

and the Mir-X miRNA First-Strand Synthesis Kit (code no. 638315; Takara, Dalian, China) was used to synthesize the complementary DNAs (cDNAs). The candidate miRNAs were selected from the differentially expressed miRNAs (DEMs), and the cDNAs of the fish in the control and infected groups were selected as templates, with each sample containing three repeats. Quantitative real-time PCR (qRT-PCR) reaction was carried out with tail primers and universal primers and with 5.8S rRNA as the internal reference gene, verifying the expression of the DEMs. According to the results of the qRT-PCR and RNA-seq, changes in the expression of the miRNAs after infection were analyzed. Supplementary Table S2 lists the primer sequences used for the qRT-PCR analysis. In addition, the RNAhybrid software was used to predict the potential target genes. The experiment was repeated with the previously obtained RNA samples. Furthermore, using *β-actin* as the internal reference gene, the spatiotemporal expression was determined for the immune-related genes in both control and infected fish.

Results

Pathological and immunohistochemical features of the gills of *C. auratus* infected with *A. hydrophila* and hemocyte phagocytic activity

Clinically diseased *C. auratus* infected with *A. hydrophila* exhibited hyperemia, hemorrhage, and inflammatory lesion of the mucosal tissues in the gills, skin, and intestine, as well as congestion of the visceral organs. Compared with the gills of control fish, histopathological examination of the infected fish revealed high inflammatory cell infiltration in the base of the secondary gill lamellae, and the respiratory epithelial cells of the secondary lamellae showed hyperplasia, sloughing, and necrosis (Figures 1A, B). Severely damaged intestinal villi, atrophic change, and extensive vacuolization with hemorrhage in the intestinal mucosa were also

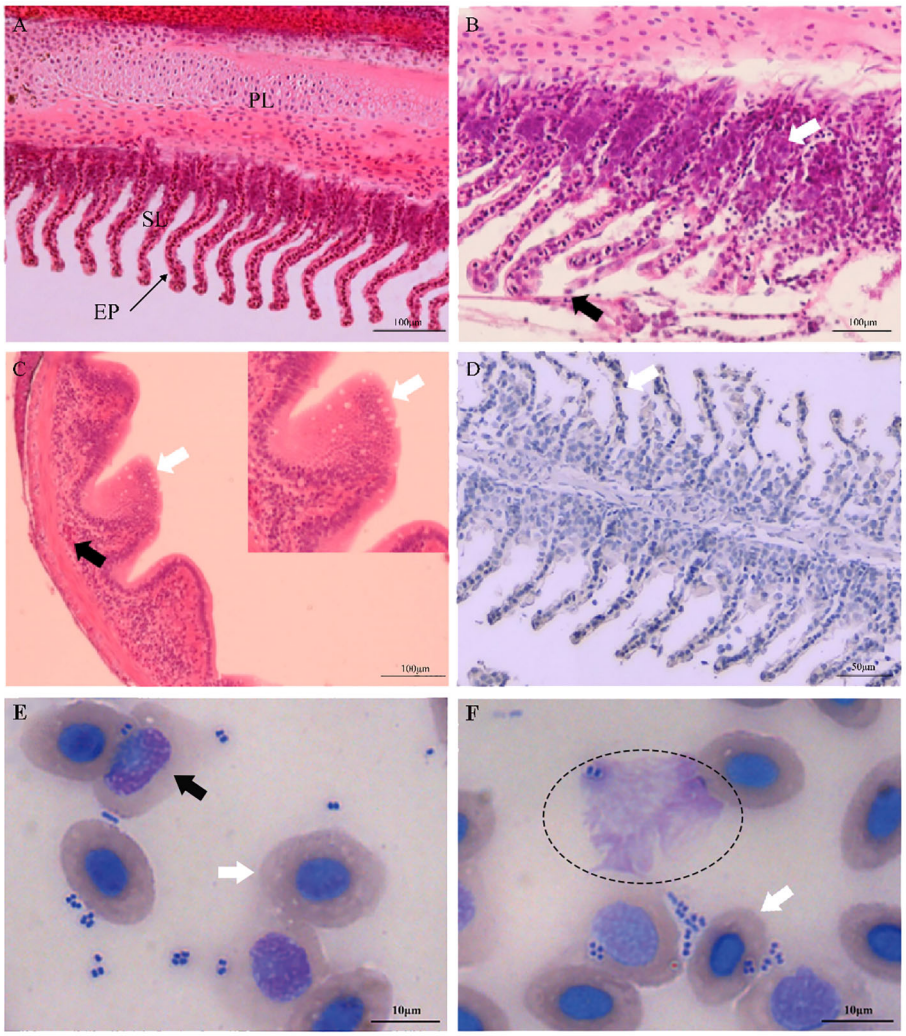

FIGURE 1
Histopathological changes and hemocyte phagocytosis of *Carassius auratus* infected with *Aeromonas hydrophila*. **(A)** Gills of the unexposed control fish. *PL*, primary lamellae; *SL*, secondary lamellae; *EP*, epithelial cell. **(B)** Exfoliation and necrosis of gill respiratory epithelial cells (*black arrow*) and extensive inflammatory cell infiltration (*white arrow*). **(C)** Intestinal villus atrophy, dehydration, vacuolization, and necrosis (*white arrow*), and lamina propria submucosa hemorrhage (*black arrow*). **(D)** Immunohistochemical staining of the gill tissues of *A hydrophila*, with positive staining appearing brown (*white arrow*). **(E, F)** Hemocyte phagocytosis of *C auratus* infected with *A hydrophila*. Phagocytic activity of *A hydrophila* is displayed by neutrophils (*black arrow*), macrophages (*elliptic circle*), and blood cells (*white arrow*).

detected (Figure 1C). In addition, the primary manifestations on the skin were hyperplasia of the epidermal mucus cells with hemorrhagic lesions, and different degrees of pathological changes such as hyperemia, hemorrhage, and inflammatory cell infiltration that occurred in the liver, kidney, and spleen. Immunohistochemical staining in the gills also revealed positive signals that were mainly distributed in the secondary gill epithelial cells (Figure 1D). In the peripheral blood of *C. auratus*, different types of leukocytes and hemocytes could phagocytize bacteria *in vitro*. Most of the *A. hydrophila* were observed to adhere to the surface of hemocytes and leukocytes, and some bacterial cells were phagocytized in hemocytes, particularly with the macrophages and neutrophils producing pseudopodia or forming emboli (Figures 1E, F).

Summary of the miRNA transcriptome in the gills of *C. auratus*

In order to investigate the miRNAs related to bacterial infection and mucosal immune response, the sRNA libraries from the gills of

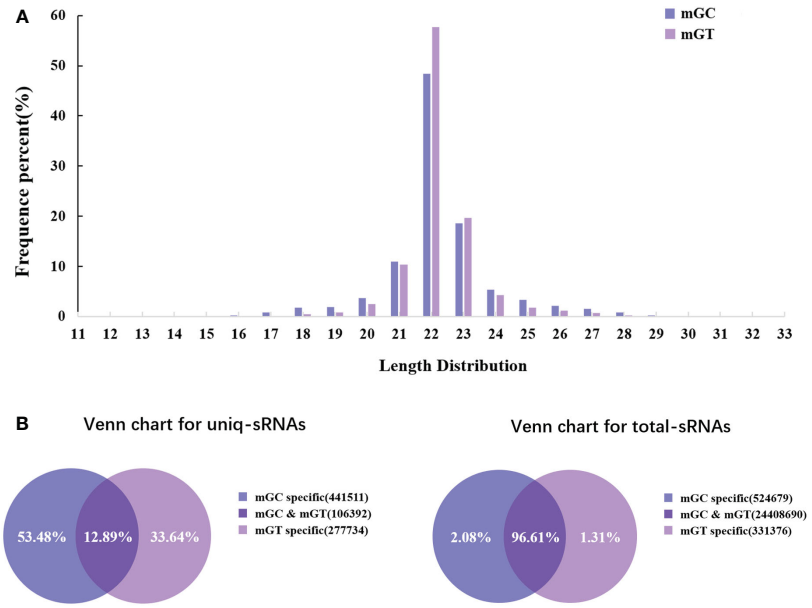

FIGURE 2
Overview of the small RNA (sRNA) sequencing libraries of the gills. **(A)** Length distribution of the sRNAs from control and infected *Carassius auratus*. **(B)** Common and specific sRNA sequences in the two libraries. Unique sRNAs (*left*) and total sRNAs (*right*).

TABLE 1 Categorization of the non-coding and organellar small RNAs in the gills of *Carassius auratus*.

Type of sRNA	mGC		mGT	
	No. of reads	Percentage	No. of reads	Percentage
miRNA	65,706	11.99	47,614	12.4
rRNA	32,334	5.9	28,211	7.34
snRNA	2,508	0.46	1,736	0.45
snoRNA	963	0.18	614	0.16
tRNA	8,944	1.63	7,212	1.88
Unannotated	412,968	75.37	281,067	73.17
Exon: antisense	3,018	0.55	1,569	0.41
Exon: sense	19,268	3.52	14,908	3.88
Intron: antisense	967	0.18	514	0.13
Intron: sense	1,227	0.22	681	0.18
Total	547,903	100	384,126	100

miRNA, microRNA; rRNA, ribosomal RNA; snRNA, small nuclear RNA; snoRNA, small nucleolar RNA; tRNA, transfer RNA.

C. auratus in the control and infected groups were constructed using the Illumina HiSeq 2000 platform. The results showed that a total of 25,628,924 original reads were generated, with 12,411,378 (98.13% of raw reads) and 12,853,367 (99.71% of raw reads) clean reads obtained from the control and infected gills, respectively (Supplementary Table S3). To further assess the changes in the sRNAs of *C. auratus*, we examined the length distribution of all sRNA reading fragments in the two libraries (mGC and mGT). Most of the unique sRNAs from the gills were between 20 and 24 nt, with a peak distribution of 22 nt, which is consistent with the typical size of products processed using Dicer (Figure 2A).

In addition, 547,903 and 384,126 sRNA sequences were obtained in the control and infected gills, respectively. Of these, 65,706 (11.99%) and 47,614 (12.4%) were identified as miRNAs in the gills. The remaining sequences comprised other types of RNAs, including rRNA, snRNA, small nucleolar RNA (snoRNA), and tRNA (Table 1). To examine the overall consistency of the sequencing data of the miRNAs, the unique and total distributions of the common and unique sequences in the mGT and mGC libraries were calculated (Figure 2B). The proportion of common sequences was 106,392 (12.89%), and the total common sequences accounted for 24,408,690 (96.61%) of the total clean reads. To establish the sRNA genome map of

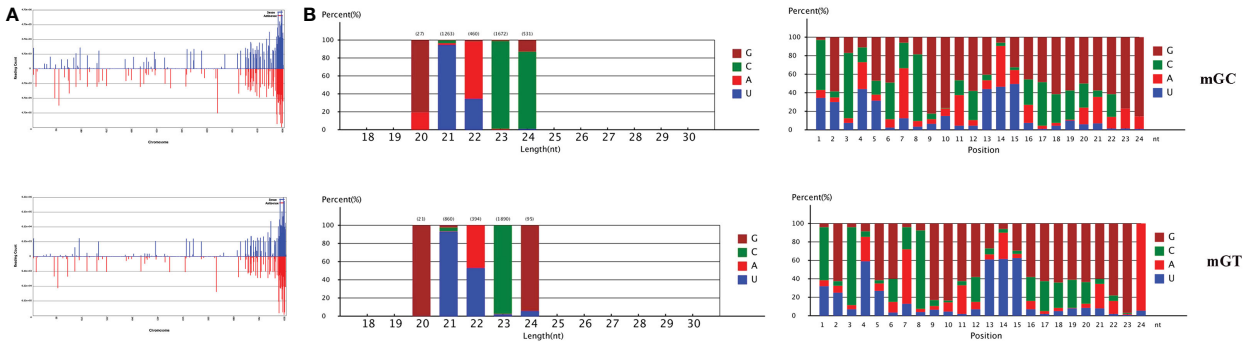

FIGURE 3
Distribution of the microRNAs (miRNAs) in *Carassius auratus* gills. **(A)** Fragments on each chromosome. **(B)** Analysis of first nucleotide bias (*left*) and position nucleotide bias (*right*).

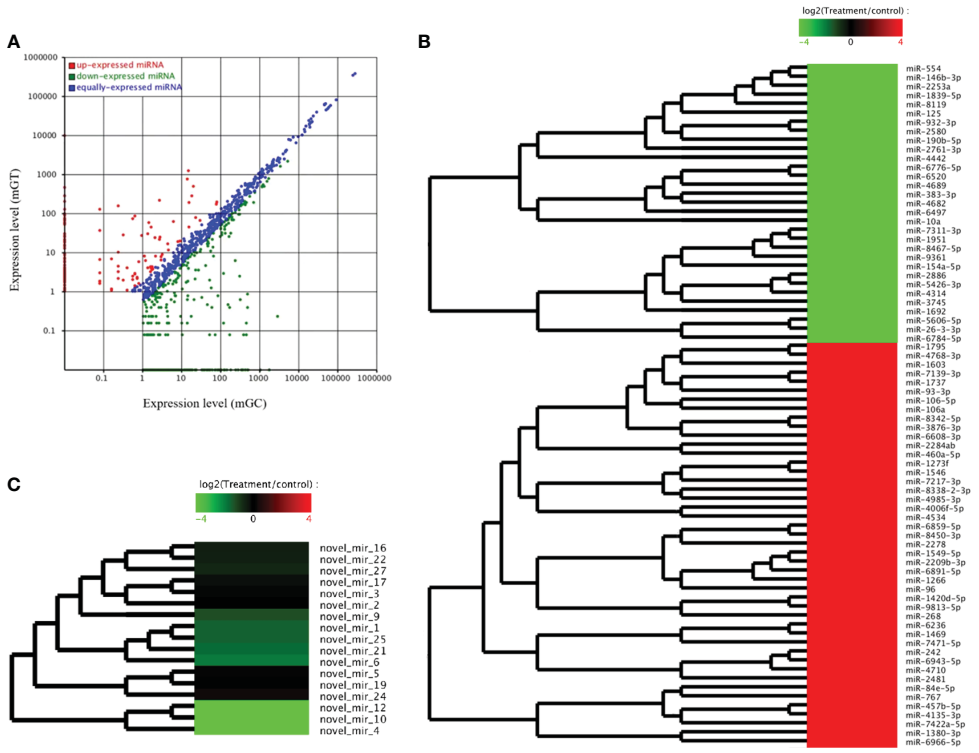

FIGURE 4
Analysis of the differentially expressed miRNAs (DEMs) in the gills of *Carassius auratus* infected with *Aeromonas hydrophila*. **(A)** Scatter plots of the DEMs. *Each point* represents one miRNA, and the *abscissa* and *ordinate values* indicate the expression levels of the miRNAs in the control and infected fish, respectively. **(B, C)** Cluster analysis of the partially known miRNAs **(B)** and the novel miRNAs **(C)** with similar expression patterns.

C. auratus, their expression and distribution in the genome were predicted, and then the miRNAs were compared to the corresponding precursors of *C. auratus* and *D. rerio* species in miRBase constructed to obtain the repertoire of the miRNAs in the gills. The results showed that 9,210,212 (74.21%) and 10,144,917 (78.93%) sRNA bands and 57,972 (10.58%) and 41,768 (10.87%) specific sRNAs were located in the genome of *C. auratus* (Figure 3A). In mGC and mGT, analysis of the first nucleotide bias showed that the content of cytosine (C) was dominant in all known miRNA sites, with a proportion of more than 50% (Figure 3B, left), while nucleotide bias analysis of the known miRNA locations showed that guanine (G) content was dominant in the gills (Figure 3B, right).

Differential expression profiling of the miRNAs and screening and identification of the key DEMs in the gills of *C. auratus*

The DEMs were screened for *C. auratus* following *A. hydrophila* infection and the results revealed the differential expression profiles of 1,165 DEMs associated with the gill immune response of *C. auratus* (Figure 4A). Of these, 539 DEMs screened from 1,148 known DEMs were observed as significant ($p < 0.05$). Cluster analysis was performed on both known and novel miRNAs that showed similar expression patterns, which indicated that the expression of several known miRNAs (e.g., miR-10a, miR-26-3-3p, miR-125, miR-146b-3p, miR-154a-5p, miR-190b-5p, miR-383-3p, miR-554, and miR-932-3p) was significantly downregulated (Figure 4B). In addition, 17 unknown miRNAs were obtained after infection, of which seven representative novel miRNAs (i.e., novel-miR-1, novel-miR-4, novel-miR-6, novel-miR-10, novel-miR-12, novel-miR-21, and novel-miR-25) showed significant differential expression out of all those downregulated in gills ($p < 0.05$) (Figure 4C). To further verify the results of the transcriptome analysis, we selected 14 key DEMs for detection in the qRT-PCR assay, and the changes in their relative expression were compared with those of the RNA-seq expression profile analysis. The results showed that the expression levels of miR-1, miR-27a, miR-145, miR-146a, miR-150, and miR-100a-2-3p were upregulated, while those of miR-10, miR-17, miR-21, and miR-26a were downregulated, which is consistent with the regulation direction of the RNA-seq expression (Figure 5A). On the other hand, the spatiotemporal expression patterns of miR-17, miR-26a, miR-144, and miR-146a in the gills were further examined, and the results showed that these four miRNAs were significantly expressed in all detected tissues, such as the gill, liver, spleen, and muscle, with particularly high expression in the intestine (Figure 5B). The "up–down–up" trend in expression was observed in the infected gills at the early [0–6 hours post-infection (hpi)], middle (12–36 hpi), and late (48–72 hpi) stages, with the expression levels being concurrently highest at 6 and 48 hpi (Figure 5C). The differential expression of the selected 20 known DEMs, including miR-10, miR-21, miR-100, miR-145, miR-148, miR-192, and miR-27b-3p, was significantly detected after *A. hydrophila* infection, indicating that

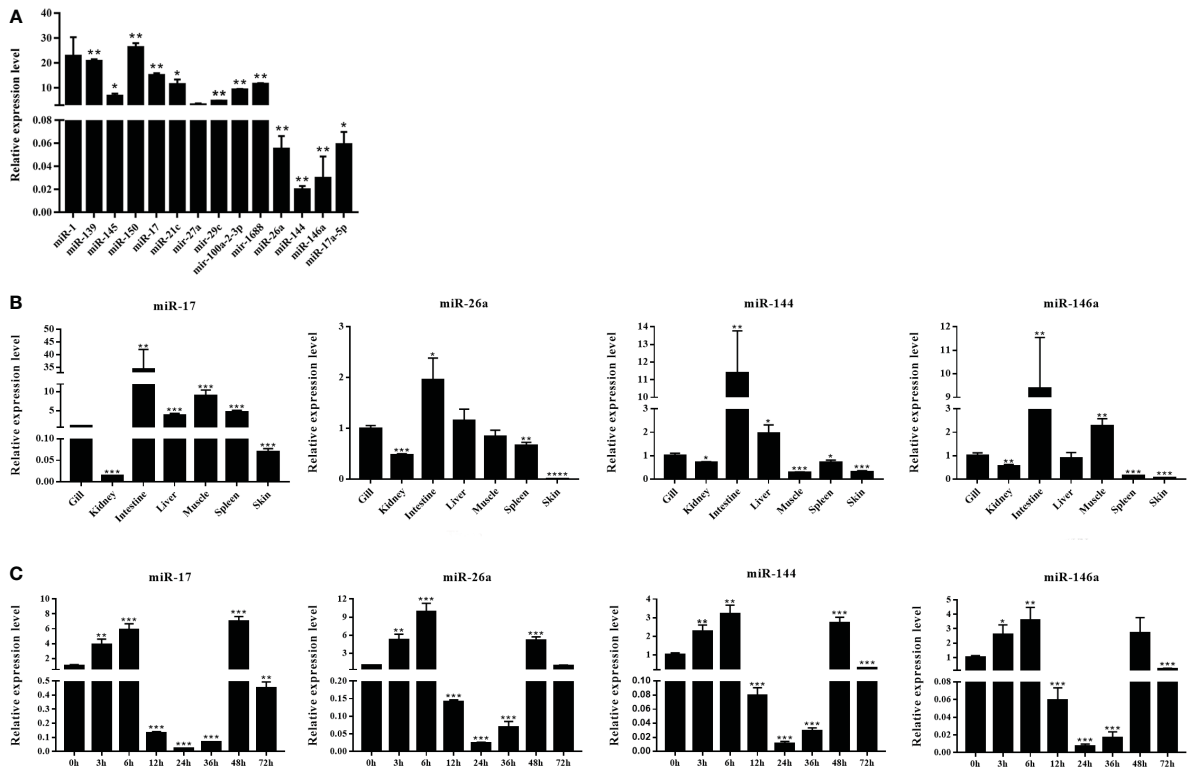

FIGURE 5
Expression analysis of the differentially expressed miRNAs (DEMs) in normal and *Aeromonas hydrophila*-infected *Carassius auratus*. **(A)** Validation of the relative expression using quantitative real-time PCR (qRT-PCR) of the 14 DEMs in the gills. **(B)** Tissue distribution of four DEMs—miR-17, miR-144, miR-146a, and miR-26a—in healthy *C auratus*. **(C)** Temporal expression of the four key miRNAs in infected gill tissues. All data were from three independent triplicate experiments (*$p < 0.05$, **$p < 0.01$). ***P<0.001, ****P<0.0001.

these miRNAs were involved in the gill immune response process. The significant differential expression levels of the representative DEMs are shown in Table 2 (Supplementary Table S4).

Moreover, the results of the key miRNA–mRNA analysis based on the relationship between negative expression and target gene prediction showed that miR-17, miR-26a, miR-144, and miR-146a bound to the 3′-UTR of the target genes *NF-κB*, *TLR4*, *TAB1*, and *IRAK1*, respectively (Figure 6A). Based on the evaluation of the multi-sequence alignment lineal homology for miRNAs, the miR-17 precursor sequence was comprehensively analyzed, which showed that the miR-17 precursor sequence of *C. auratus* had high similarity to the other 14 fish species, which is highly conserved in teleosts (Supplementary Figure S1). The phylogenetic tree results also showed that the miR-17 of *C. auratus* was closely clustered into one group with the zebrafish *D. rerio*, the common carp *C. carpio*, and the channel catfish *Ictalurus punctatus* (Figure 6B). To further analyze the evolutionary relationship of miR-17, we constructed MLE phylogenetic trees for the pre-miR-17 from 26 species, and similar results were observed for the evolutionary relationship in Cypriniformes (Figure 6C). In the miR-17 family, cau-miR-17 was very similar to dre-miR-17a-1, ccr-miR-17, and ipu-miR-17a, which were classified into the same branch within the phylogenetic tree. This revealed the sequence conservation of the miRNA precursor sequences of the same family among the different species of Cyprinid fish.

GO and KEGG enrichment analyses of the target genes and proteins

In order to further investigate the function of the DEMs in the gill immune response of *C. auratus*, GO and KEGG enrichment analyses

TABLE 2 Differential expression of the known and unknown miRNAs in the gills of *Carassius auratus* challenged with *Aeromonas hydrophila*.

miR_name	Fold change	*p*-value	Species	Target gene	Reference
miR-10	−6.05	6.75e−37	Sea cucumber (*Apostichopus japonicus*)	*TBC1D5*	30
miR-21	−0.20	0	Miiuy croaker (*Miichthys miiuy*)	*IRAK4*	11
miR-27b-3p	−0.98	5.28e−134	Common carp (*Cyprinus carpio*)	*CYP1B1*	31
miR-29c	−0.34	1.43e−04	Mouse (*Mus musculus*); human (*Homo sapiens*)	*RAG1*	32
miR-100	0.12	1.44e−06	Human (*Homo sapiens*)	*ATM*	33
miR-128	−0.31	2.67e−174	Miiuy croaker (*Miichthys miiuy*)	*TAB2*	34
miR-132-2p	−0.92	1.84e−22	Mouse (*Mus musculus*)	*SIRT1*	35
miR-142a-3p	−0.89	9.04e−28	Grass carp (*Ctenopharyngodon idella*)	*TLR5*	36
miR-145	1.14	8.35e−40	Human (*Homo sapiens*)	*PAK4*	37
miR-145-5p	0.14	0.004	Miiuy croaker (*Miichthys miiuy*)	*MDA5*	38
miR-148	−0.27	4.19e−28	Miiuy croaker (*Miichthys miiuy*)	*MyD88*	16
miR-150	0.10	4.57e−09	Japanese flounder (*Paralichthys olivaceus*)	*LMP2L*	39
miR-155	−0.85	1.13e−17	Channel catfish (*Ictalurus punctatus*)	*SOCS1*	40
miR-200a	−0.57	2.12e−160	Wuchang bream (*Megalobrama amblycephala*)	*MAPK1*	41
miR-206	−0.23	0	Human (*Homo sapiens*)	*FAIM*	42
miR-210	−0.98	1.35e−65	Miiuy croaker (*Miichthys miiuy*)	*RIPK2*	43
miR-17	−13.28	0	Crucian carp (*C. auratus*)	*NF-κB*	This study
miR-26a	−0.14	7.78e−21	Crucian carp (*C. auratus*)	*TLR4*	This study
miR-144	0.16	1.11e−05	Crucian carp (*C. auratus*)	*TAB1*	This study
miR-146a	0.13	6.15e−199	Crucian carp (*C. auratus*)	*IRAK1*	This study
novel-miR-1	−1.53	3.96e−06	Crucian carp (*C. auratus*)	Unknown	This study
novel-miR-4	−9.52	7.96e−29	Crucian carp (*C. auratus*)	Unknown	This study
novel-miR-6	−1.92	0.002	Crucian carp (*C. auratus*)	Unknown	This study
novel-miR-10	−7.60	3.83e−08	Crucian carp (*C. auratus*)	Unknown	This study
novel-miR-12	−6.92	2.30e−05	Crucian carp (*C. auratus*)	Unknown	This study
novel-miR-21	−1.70	0.004	Crucian carp (*C. auratus*)	Unknown	This study
novel-miR-25	−1.53	1.07e−11	Crucian carp (*C. auratus*)	Unknown	This study

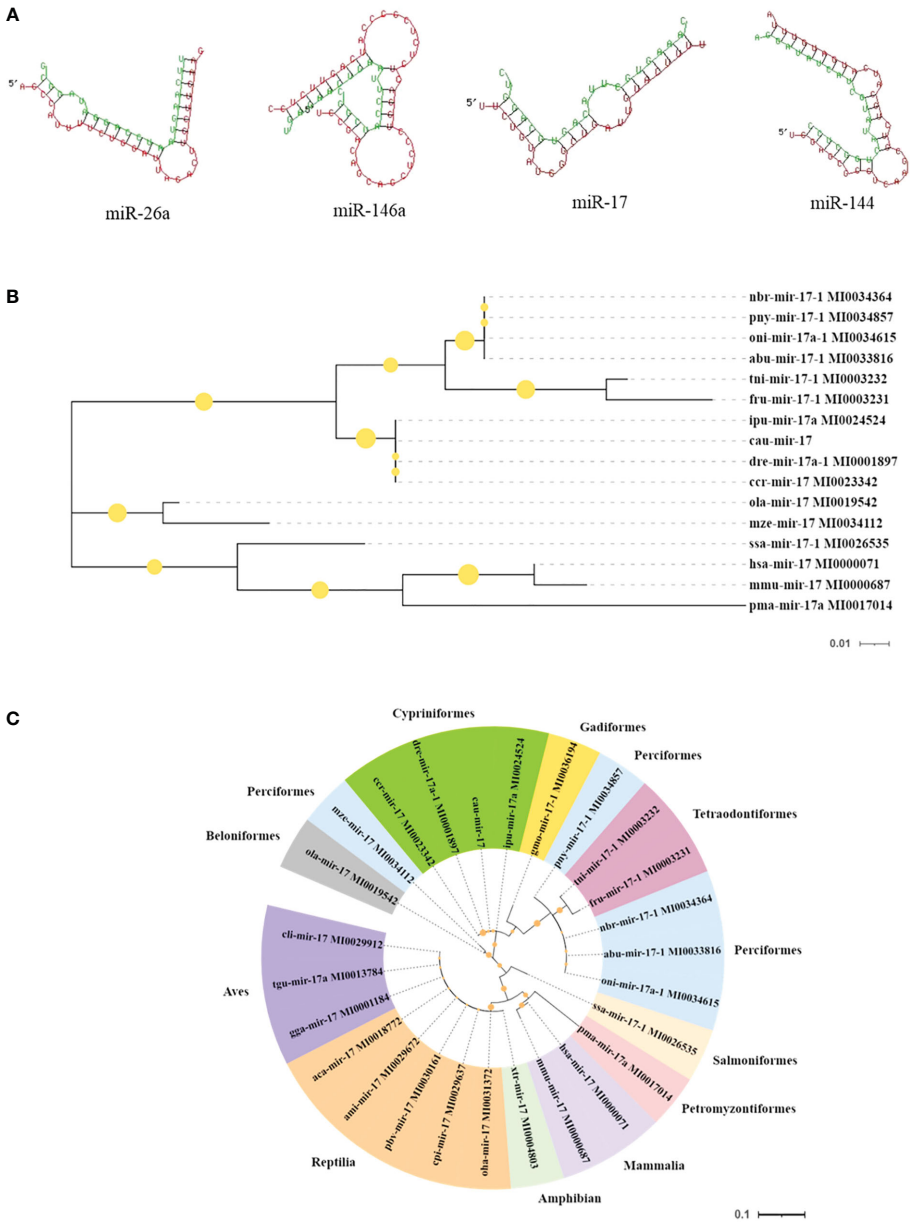

FIGURE 6
Molecular characteristics of the microRNAs (miRNAs) identified in the gills. **(A)** Predicted target sites of miR-17, miR-144, miR-146a, and miR-26a. **(B)** Species genetic relationship of miR-17 sequences. **(C)** Phylogenetic tree analysis of pre-miR-17 from the 26 species.

were performed to predict potential target genes and signaling pathways. A total of 104,211 putative target genes and 539 known miRNAs were screened in the gills. In addition, 17 unknown miRNAs and 45,326 target gene sequences were annotated in GO. These were mainly involved in biological regulation, cellular processes, metabolic processes, and biological adhesion processes. In the biological process GO terms, most of the genes were related to the cellular process, while the single-organism process, metabolic process, biological regulation, rhythmic process, and cell killing were lower. Regarding the cellular components, most genes were related to cells and cellular components, followed by organelle and macromolecular complex. In terms of molecular function, binding involved the most, followed by catalytic activity, enzyme regulator activity, molecular transducer activity, and nucleic acid binding transcription factor activity (Figure 7).

KEGG enrichment analysis mainly focused on 306 signaling pathways, of which 33 were related to gill immunity, including metabolic pathways, cell adhesion molecules (CAMs), TLRs, NOD-like receptors (NLRs), natural killer cell-mediated cytotoxicity (NKCC), RIG-I-like receptor (RLRs), MAPK, Janus kinase signal transducer and activator of transcription (JAK-STAT), NF-κB, p53, Fc gamma receptor (FcγR)-mediated phagocytosis, T-cell receptor (TCR), and B-cell receptor (BCR) signaling pathways (Table 3). At the protein level, in order to identify the biological pathways that play key roles in the response to *A. hydrophila* infection, we performed iTRAQ and KEGG analyses of the DEPs. The significantly enriched immune pathways found included bacterial invasion of epithelial cells (14), complement and coagulation cascades (15), regulation of actin cytoskeleton (14), focal adhesion (8), antigen processing and

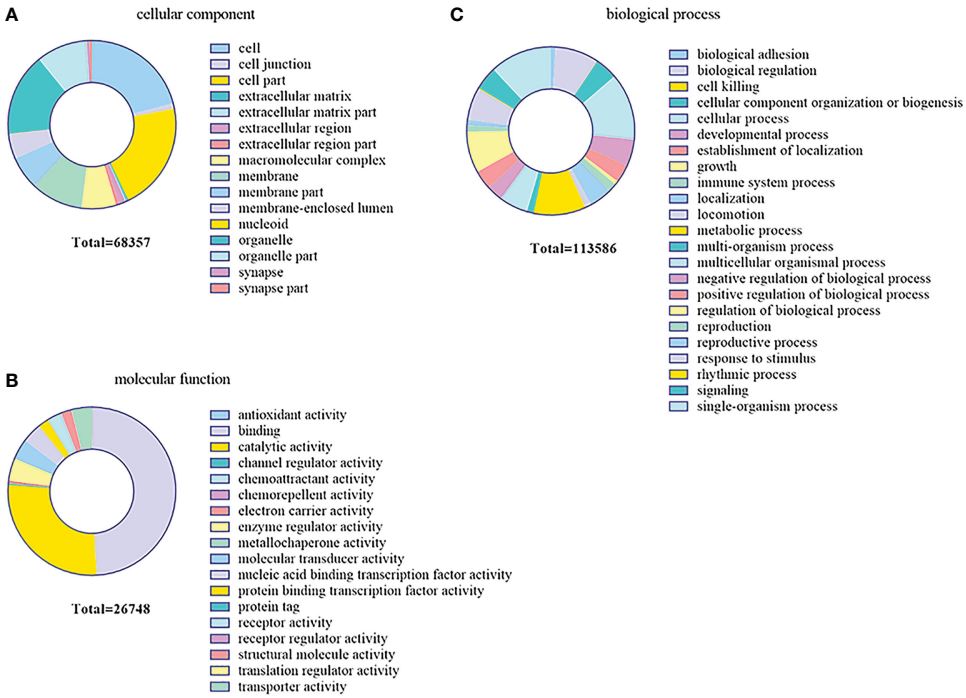

FIGURE 7
Gene Ontology (GO) enrichment analysis of the target genes predicted for the differentially expressed miRNAs (DEMs) in the gills. **(A)** Cellular component. **(B)** Biological process. **(C)** Molecular function.

presentation (10), FcγR-mediated phagocytosis (5), phagosome (14), pathogenic *Escherichia coli* infection (19), endocytosis (11), NF-κB and MAPK (6), and insulin signaling pathway (5) of DEPs (Supplementary Table S5). Notably, the network pathways for the association of the identified DEPs in the bacterial invasion of epithelial cells and endocytosis were significantly downregulated at the protein level in the gills (Figure 8).

Spatiotemporal expression and regulation analysis of the key miRNAs/target genes

The tissue distribution analysis of the miRNA-mediated target genes (e.g., *TLR4*, *TAB1*, *NF-κB*, *IRAK1*, *PKC*, *FASL*, and *CD48*) showed that the 12 immune-related genes exhibited tissue-specific expression and presented different expression levels in the examined tissues (Figure 9A). Furthermore, temporal expression analysis of the miRNA primary target genes within the TLR, NKCC, MAPK, and NF-κB signaling pathways showed that several of them, including *TLR4*, *2B4*, *FASL*, *CD48*, and *TAB1*, were mostly downregulated 72 h after *A. hydrophila* infection, with the expression levels of *TLR4*, *TAB1*, *CD48*, and *2B4* at 3 hpi at the lowest points. On the other hand, the expression levels of *NF-κB* and *IRAK1* were upregulated during the challenge, with the highest expressions at 24 and 72 hpi being 1.69 and 2.39 fold change, respectively. The expression levels of *PKC*, *MKK7*, and *PAK* in the gills showed a trend of early decline, middle rise, and late decline, in which the lowest expression was shown by *MKK7* and *PAK* at 3 hpi and the highest expression of the three genes was at 24 hpi. Furthermore, *TNF-α* and *PI3K* showed an upward trend within 72 hpi. The expression of *TNF-α* was the highest at 72 hpi, that of *PI3K* was 3.39-fold at 24 hpi, and that of *FASL* was at 12 hpi in the gills of *C. auratus* (Figure 9B). It is worth noting that the expression characteristics of the *PI3K* gene were positively associated with those of *TAB1*, *NF-κB*, and *IRAK1* (Figures 9C, D, Supplementary Figure S2). The qRT-PCR data of the detected candidate genes exhibited similar expression trends to the proteins in the iTRAQ analysis, which showed a significant correlation (Pearson's correlation coefficient of 0.70, $p < 0.01$). The protein–protein interaction (PPI) analysis revealed that the potential key miRNA target proteins (e.g., TLR4, IRAK1, TAB1, NF-κB, MyD88, TRAF3/6, MAPK, IRF3/7, FASL, TNF, and CD4) showed significant correlation in the interaction network of the infected gills of *C. auratus* (Figure 10A). Thus, it was speculated that the molecular mechanism of the gill immune response in *C. auratus* against *A. hydrophila* infection might be the regulation of the production of cytokines and inhibition of excessive inflammatory response. Further insight into the regulation mechanism of the key miRNAs (i.e., miR-26a, miR-146a, miR-144, and miR-17), which were involved in the gill local immune regulation of the TLR, MAPK, and NF-κB signaling pathways, was also drawn (Figure 10B).

Discussion

With the development of intensive aquaculture in China, the outbreak of bacterial diseases of the crucian carp *C. auratus* has become a serious problem, causing economic losses (18, 27). Recently, the spotlight on miRNA biomarkers, target genes, and immune regulation has been of great significance for the prevention and treatment of diseases in teleost fish (5, 7, 8). Mucosal immunity

10.3389/fimmu.2023.1098455

TABLE 3 Immune-related Kyoto Encyclopedia of Genes and Genomes (KEGG) pathways enriched by the target genes in the gills of *Carassius auratus* challenged with *Aeromonas hydrophila*.

Pathway	Target genes[a]	Pathway ID
Metabolic pathways	4,123 (10.49%)	ko01100
Pathways in cancer	2,007 (5.11%)	ko05200
Regulation of actin cytoskeleton	1,746 (4.44%)	ko04810
Focal adhesion	1,635 (4.16%)	ko04510
MAPK signaling pathway	1,337 (3.4%)	ko04010
Chemokine signaling pathway	1,071 (2.73%)	ko04062
RNA transport	939 (2.39%)	ko03013
Phagosome	930 (2.37%)	ko04145
Biosynthesis of secondary metabolites	908 (2.31%)	ko01110
Salmonella infection	881 (2.24%)	ko05132
Fc gamma R-mediated phagocytosis	860 (2.19%)	ko04666
Ubiquitin-mediated proteolysis	813 (2.07%)	ko04120
Leukocyte transendothelial migration	806 (2.05%)	ko04670
Cell adhesion molecules (CAMs)	784 (1.99%)	ko04514
Cytokine–cytokine receptor interaction	784 (1.99%)	ko04060
Calcium signaling pathway	766 (1.95%)	ko04020
T-cell receptor signaling pathway	733 (1.87%)	ko04660
Natural killer cell-mediated cytotoxicity	688 (1.75%)	ko04650
Cell cycle	687 (1.75%)	ko04110
NOD-like receptor signaling pathway	679 (1.73%)	ko04621
NF-kappa B signaling pathway	675 (1.72%)	ko04064
JAK-STAT signaling pathway	661 (1.68%)	ko04630
B-cell receptor signaling pathway	563 (1.43%)	ko04662
Vibrio cholerae infection	523 (1.33%)	ko05110
Fc epsilon RI signaling pathway	472 (1.2%)	ko04664
Toll-like receptor signaling pathway	465 (1.18%)	ko04620
Apoptosis	450 (1.14%)	ko04210
Antigen processing and presentation	430 (1.09%)	ko04612
p53 signaling pathway	391 (0.99%)	ko04115
mTOR signaling pathway	368 (0.94%)	ko04150
RIG-I-like receptor signaling pathway	348 (0.89%)	ko04622
PPAR signaling pathway	298 (0.76%)	ko03320
Complement and coagulation cascades	255 (0.65%)	ko04610

*Target genes indicated with pathway annotation (39302).

(i.e., gills, skin, and intestine) is the host's first line of defense against pathogen infection (3, 18, 27), which involves different signaling pathways that are regulated by complex mechanisms; however, most of the miRNAs are still unclear in fish (8, 9). As essential regulatory factors of gene expression in the biological process, miRNAs play important roles in cell differentiation, organ development, and immune progression (9, 44). Previous studies on the miRNAs of teleosts showed that they are pivotal regulators of the inflammatory response in teleosts (45–47), indicating that they are involved in the regulation of early development, organogenesis, cell differentiation and homeostasis, growth, reproduction, and immunity (48, 49). Characterization of the miRNAs and their target genes in the internal organs (e.g., kidney, spleen, and liver) and skin of *C. auratus* was subsequently performed using deep sequencing

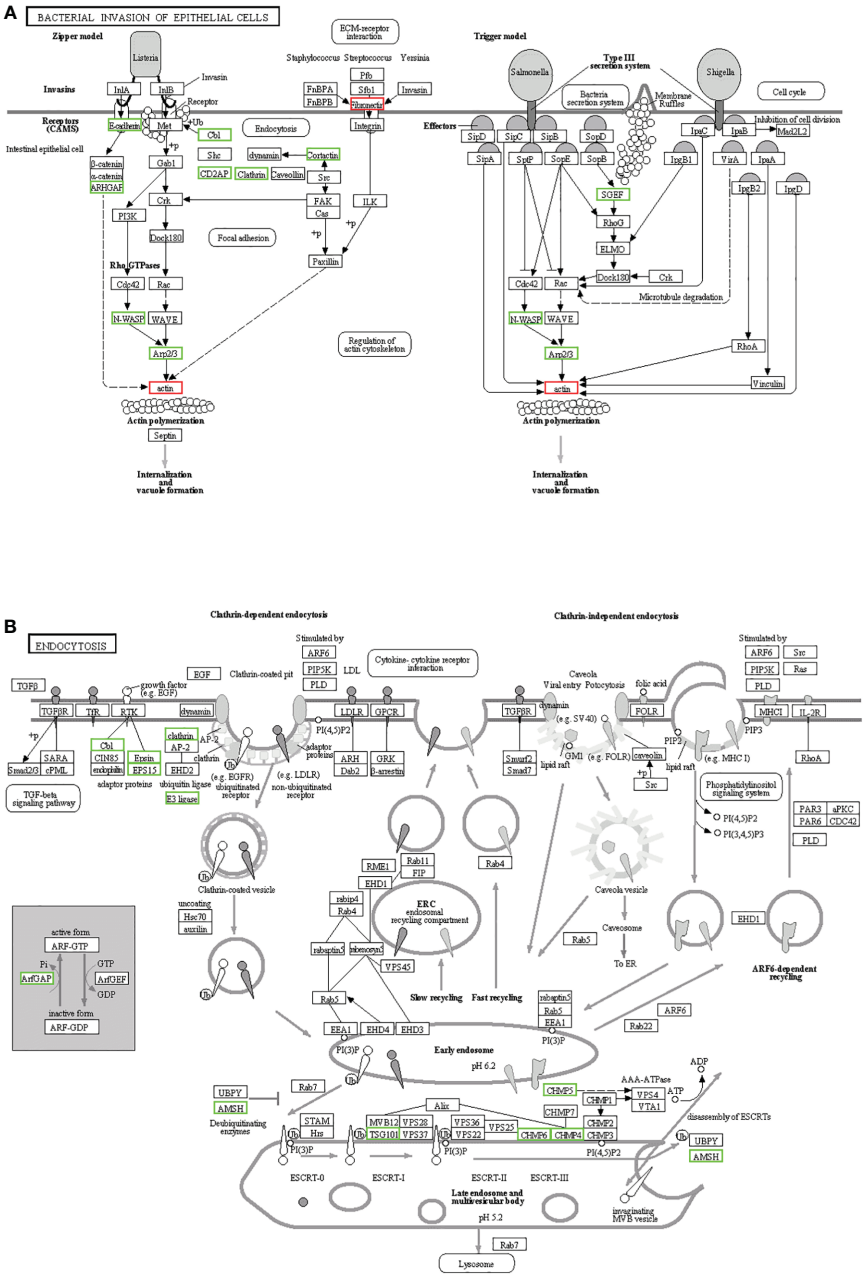

FIGURE 8
Kyoto Encyclopedia of Genes and Genomes (KEGG) pathways for the negative association of the identified proteins in the gills. **(A)** Bacterial invasion of epithelial cells. **(B)** Endocytosis. The differentially expressed proteins (DEPs) of the different pathways were upregulated (*red*) and downregulated (*green*).

analysis (5, 18). The miRNA expression and its regulatory mechanism in the gills remain unclear in *C. auratus*. The present study used a high-throughput sRNA transcriptome sequencing technique to construct an sRNA library from the gills of *C. auratus* infected with *A. hydrophila* based on the Illumina HiSeq 2000 platform. The results of this study provide a scientific basis for the elucidation of the miRNAs and target genes involved in the molecular mechanisms in the gill mucosal immune response of teleost fish.

Current evidence in fish has demonstrated miRNAs to be key regulators that play essential roles in immune response and negatively regulate the expression of genes at the posttranscriptional level (47, 50). In the crucian carp *C. auratus*, characterization of the conserved and novel miRNAs (e.g., miR-10, miR-17, and miR-122) has been recently performed using deep sequencing and prediction of miRNA targets (5). Previous studies demonstrated that the significant upregulation of miR-21, miR-146a, and miR-200a indicates their involvement in the process of skin mucosal immune response in *C. auratus* infected with *A. hydrophilic* (18). miRNAs (e.g., miR-21, miR-145, and miR-146a) are also involved in the inflammatory and immune responses to the miiuy croaker *M. miiuy* and the zebrafish *D. rerio* (11, 51), and several miRNAs (e.g., miR-21, miR-122, and miR-192-5p) were found to be differentially expressed in the *Vibrio anguillarum*-challenged *M. miiuy* (14, 15). Recent miRNA expression analysis of *D. rerio* infected with *Vibrio*

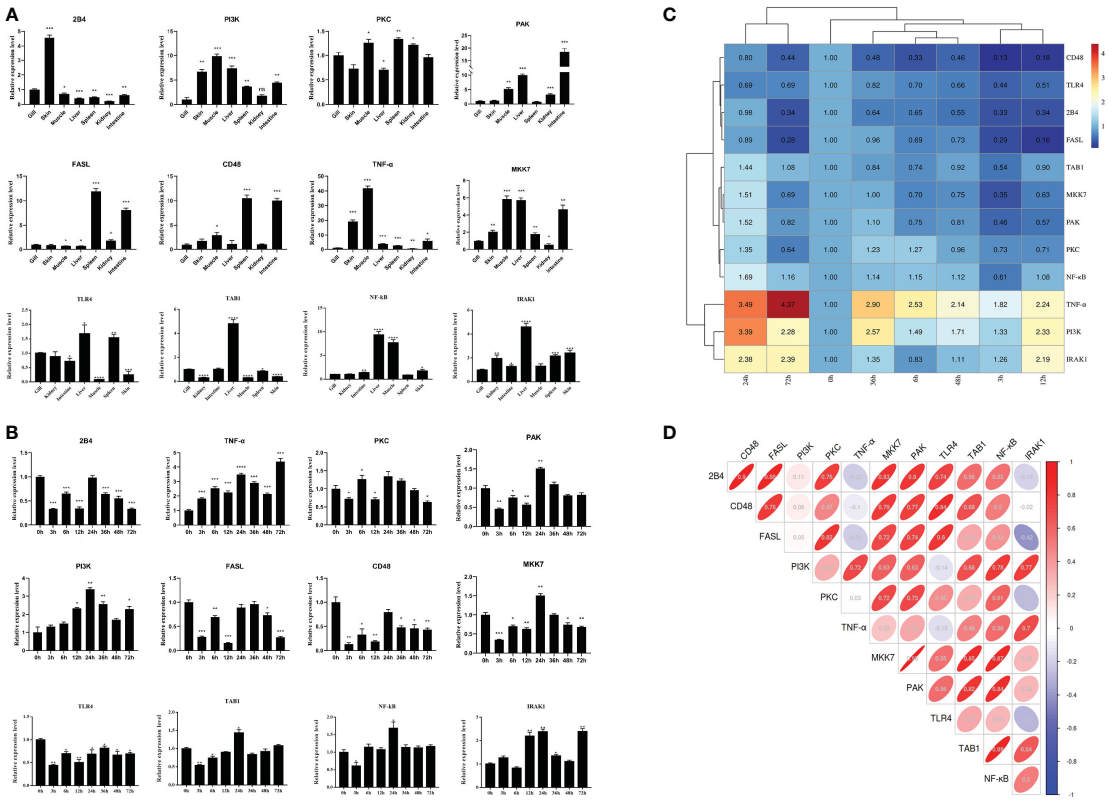

FIGURE 9
Expression changes of the immune-related target genes within the Toll-like receptor (TLR), mitogen-activated protein kinase (MAPK), and nuclear factor kappa B (NF-κB) inflammatory pathways of *Carassius auratus*. **(A)** Tissue distribution of the 12 microRNA (miRNA)-mediated potential target genes. **(B)** Temporal expression changes of the target genes in the gills. **(C)** Heat map analysis of the relative expression. **(D)** Correlation analysis of the selected target genes. Toll-like receptor 4 (*TLR4*), interleukin-1 receptor-associated kinase 1 (*IRAK1*), TGF-beta-activated kinase 1 and MAP3K7-binding protein 1 (*TAB1*), protein kinase C lambda (*PKC*), Fas ligand (*FASL*), nuclear factor kappa-B kinase subunit alpha-like (*NF-κB*), P21-activated kinase (*PAK*), phosphatidylinositol 3-kinase (*PI3K*), MAP kinase kinase 7 (*MKK7*), CD48 molecule (*CD48*), CD244 molecule (*2B4*), and tumor necrosis factor-α (*TNF-α*), which were determined by quantitative real-time PCR (qRT-PCR) assay. All data were from three independent triplicate experiments (*$p < 0.05$, **$p < 0.01$, ***$p < 0.001$, ****$p < 0.0001$).

parahaemolyticus has indicated that 37 known miRNAs (e.g., dre-miR-141-5p, dre-miR-200a-5p, and dre-miR-192) were differentially expressed, which regulate signal conduction, hematopoiesis, and protein synthesis (52). The miRNA genes in the Atlantic cod *Gadus morhua* determined by qRT-PCR analysis showed that several miRNAs (e.g., miR-144, miR-26a, and miR-200a) were overexpressed and were mainly involved in the regulation of growth, metabolism, and immune response (48). In this study on the gills of *C. auratus* challenged with *A. hydrophila*, a total of 1,148 known and 17 unknown miRNAs were obtained using the high-throughput Illumina HiSeq 2000 sequencing platform, with some of the miRNAs (e.g., miR-10, miR-106a, miR-146b-3p, miR-202-5p, miR-17, and miR-145) found to be significantly differentially expressed. Notably, the expression levels of miR-144, miR-145, and miR-146a were significantly upregulated, while those of miR-17, miR-21, miR-26a, miR-122, and miR-200a were downregulated, thereby indicating that they could serve the function of regulating the expression of the target genes in the gill mucosal immune response. Furthermore, the phylogenetic analysis revealed that the miR-17 of *C. auratus* showed a highly conservative evolution in teleost; however, some of the known miRNAs (e.g., miR-10, miR-145, and miR-155) and several novel miRNAs (e.g., novel-miR-4, novel-miR-10, and novel-miR-12), which may have resulted from differences in the species specificity of teleosts, still require further research.

Fish innate immunity is the first line of host defense and mainly comprises pattern recognition receptor signaling pathways (13, 53). The recently identified miRNAs play important roles in the regulation of the inflammatory and immune responses, indicating a miRNA-mediated TLR/NF-κB signaling pathway (54, 55). In teleost fish, it is worth noting that the miRNAs were significantly related to immune defense, such as the NLR, apoptosis, JAK-STAT, and MAPK singling pathways that are involved in various biological processes (8, 56), consistent with the results of this study on *C. auratus*. Recent research has found that miR-7a participates in PI3K regulation (17), and miR-145-5p and miR-122 have been proven to regulate the RLR signaling pathway (38, 57). We previously reported on miRNAs in the skin of *C. auratus* infected with *A. hydrophila*, indicating that the skin immune response involved the TLR, MAPK, JAK-STAT, and phagosome pathways (27). The present study also found that a lot of the miRNAs and their target genes (i.e., *TLR4*, *TAB1*, *IRAK1*, and *NF-κB*) in the gills of *C. auratus* infected with *A. hydrophila* were focused on inflammatory and immune responses, such as the TLR, MAPK, and NF-κB inflammatory pathways. Thereby, it was suggested that these key miRNAs and their target genes may be

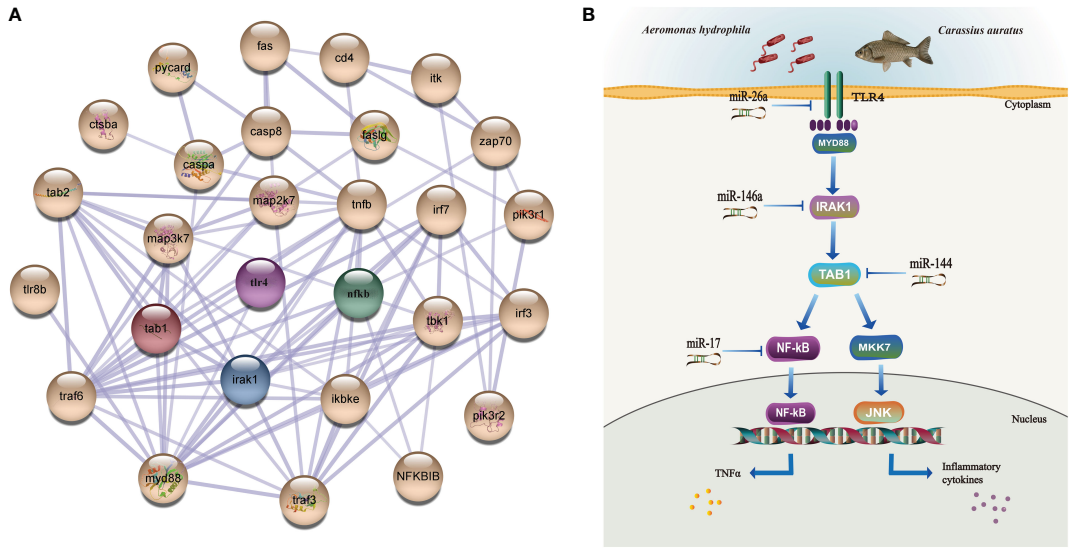

FIGURE 10
Interaction network analysis and illustration of the regulation mechanisms of the key miRNAs/target genes in the gills of *Carassius auratus* infected with *Aeromonas hydrophila*. **(A)** Interaction analysis of the protein–protein interaction (PPI) networks. *Different colored balls* represent the differentially expressed proteins (DEPs), the *node* indicates representative proteins of the corresponding pathway, and the *line thickness* denotes the strength of the predicted functional interactions. **(B)** Illustration of the regulation mechanism of the key miRNAs/target genes in the gills. miR-26a, miR-146a, miR-144, and miR-17 were identified in the gills, which were involved in the local immune regulation of the Toll-like receptor (TLR), mitogen-activated protein kinase (MAPK), and nuclear factor kappa B (NF-κB) signaling pathways by targeting Toll-like receptor 4 (*TLR4*), interleukin-1 receptor-associated kinase 1 (*IRAK1*), TGF-beta-activated kinase 1 and MAP3K7-binding protein 1 (*TAB1*), and nuclear factor kappa-B kinase subunit alpha-like (*NF-κB*).

involved in the immunomodulatory process in the gill mucosal signaling pathways, promoting immune response and protecting the organism against overwhelming inflammation after bacterial infection. However, the roles of the miRNAs in teleost gills in relation to pathogens still need to be further studied in the future.

In addition, the miRNAs interacting with the target genes and proteins were not only associated with immune response (7, 45) but also played important roles in regulating the regulators of the immune network (28, 58). In *M. miiuy* infected with *Vibrio harveyi*, miR-148 targeted and negatively regulated the expression of the *MyD88* gene, and overexpression of miR-148 inhibited the inflammatory cytokine production of both *IL-6* and *IL-1β* (16). miR-21 also upregulated and targeted the gene *IRAK4* (11), thereby preventing excessive inflammation response. In *M. miiuy* infected with *V. anguillarum*, miR-200a-3p was shown to be involved in the modulation of *TLR1* expression (57). In the gills of *D. rerio* after *A. hydrophila* and *Edwardsiella piscicida* infection (12), miR-146a suppressed the expression of the immune-related genes and was involved in the regulation of excess inflammatory responses (e.g., *TLR4*, *IL-1β*, and *TNF-α*), and it also promoted viral replication by targeting *TRAF6* in the orange-spotted grouper *Epinephelus coioides* (59). In vertebrates, several studies verified the involvement of *NOD1* in the regulation of the antibacterial immune response (60, 61), while miR-144 and miR-217-5p targeted and sequentially inhibited the gene expression of *NOD1* (13). Studies on the liver of zebrafish indicated that miR-731 served the function of directly targeting *DKK3b*, while several miRNAs (e.g., miR-200b-5p, miR-146b, and miR-731) and their target genes (i.e., *IL10*, *IRAK1*, and *TRAF6*) regulated the immune response in the spleen after *Streptococcus parauberis* infection (24, 62). The regulation of NF-κB revealed that miR-144 negatively regulated signaling transduction by targeting the *IL-1κ* gene (49). Moreover, several miRNAs (e.g., miR-122, miR-192, and miR-148) have been identified for the regulation of the target genes that participate in innate immunity (14–16). In this study on the gills of *C. auratus* infected with *A. hydrophila*, we found four miRNAs (e.g., miR-26a, miR-144, miR-146a, and miR-17) that were significantly differentially expressed in the gills, which might regulate their target genes involved in the TLR, MAPK, and NF-κB inflammatory pathways. These results present new ideas for further studies of the miRNA regulatory mechanism in the gill immune response of carp against infections.

Conclusion

To our knowledge, this is the first study on the multi-omics analysis of the miRNAs and the protein profiles in the gills of the crucian carp *C. auratus* after *A. hydrophila* infection. Based on conventional histopathological and immunohistochemical studies, the expression profiling and target gene analysis revealed that the miRNAs were significantly differentially expressed in the gills, thereby indicating that the key miRNAs (i.e., miR-17, miR-26a, miR-144, and miR-146a) play crucial roles in the local immune response of *C. auratus* against bacterial infection. The target genes of the miRNAs involved in multiple signaling pathways mainly included TLR, MAPK, and NF-κB inflammatory responses. This study provides a detailed description of the mechanism of the regulation of miRNAs in the gills and contributes to the understanding of the miRNA-mediated local immune response in Cyprinidae fish.

Data availability statement

The data presented in the study are deposited in the NCBI sequence read archive (SRA) repository, accession number: PRJNA923102.

Ethics statement

The animal study was reviewed and approved by the Tianjin Agricultural University Institutional Animal Care and Use Committee (TJAU-IACUC).

Author contributions

AL conceived the project. XH and AL provided the experimental instruments, reagents, and animals. JH and JB conducted the animal experiments. JH analyzed the data and wrote the manuscript. AL revised the manuscript. All authors contributed to the article and approved the submitted version.

Funding

This study was supported by the Natural Science Foundation of China (no. 32273182), Key Scientific Research Project Universities and Colleges in Tianjin (no. 2019ZD14), and the Natural Science Foundation of Tianjin City (nos. 18JCYBJC29900 and 21YDTPJC00510).

Conflict of interest

The authors declare that the research was conducted in the absence of any commercial or financial relationships that could be construed as a potential conflict of interest.

Publisher's note

Supplementary material

The Supplementary Material for this article can be found online at: https://www.frontiersin.org/articles/10.3389/fimmu.2023.1098455/full#supplementary-material

SUPPLEMENTARY FIGURE 1
The multiple sequences alignments of precursor miR-17 sequences.

SUPPLEMENTARY FIGURE 2
Cloning analysis of target-gene PI3K in *C. auratus*. **(A)** PCR amplification electrophoresis and positive clone detection. **(B)** Prediction of PI3K secondary structure. **(C)** Prediction of PI3K tertiary structure. **(D)** Phylogenetic tree of PI3K amino acid sequence. M is DNA standard DL 2000 bp; lane 1 is PI3K-1, lane 9 is PI3K-2, lanes 2-8 are pMD18-T PI3K-1 positive clones, lanes 10-13 are pMD18-T PI3K-2 positive clones.

SUPPLEMENTARY TABLE 1
Selected miR-17 sequences for 26 different species from the miRBase database.

SUPPLEMENTARY TABLE 2
Primers for qRT-PCR method detection of crucian carp *Carassius auratus*.

SUPPLEMENTARY TABLE 3
Summary of high-throughput sequencing from gill libraries of *C. auratus* infected with *A. hydrophila*.

SUPPLEMENTARY TABLE 4
Summary of sequenced miRNAs in the gills of *C. auratus*.

SUPPLEMENTARY TABLE 5
The iTRAQ analysis of enriched KEGG pathways in the gills of *C. auratus* challenged with *A. hydrophila*.

References

1. Bushati N, Cohen SM. microRNA functions. *Annu Rev Cell Dev Biol* (2007) 23:175–205. doi: 10.1146/annurev.cellbio.23.090506.123406

2. Lima SA, Pasquinelli AE. Identification of miRNAs and their targets in c. elegans. *Adv Exp Med Biol* (2014) 825:431–50. doi: 10.1007/978-1-4939-1221-6_12

3. Bizuayehu TT, Babiak I. MicroRNA in teleost fish. *Genome Biol Evol* (2014) 6 (8):1911–37. doi: 10.1093/gbe/evu151

4. Xie X, Ma R, Qian D, Yu Y, Liu X, Lei Y, et al. MicroRNA regulation during *Nibea albiflora* immuno-resistant against *Cryptocaryon irritans* challenge in fish skin. *Aquaculture* (2019) 507:211–21. doi: 10.1016/j.aquaculture.2019.04.034

5. Huang Y, Gao XC, Ren HT, Xiong JL, Sun XH. Characterization of conserved and novel miRNAs using deep sequencing and prediction of miRNA targets in crucian carp (*Carassius auratus*). *Gene* (2017) 635:61–8. doi: 10.1016/j.gene.2017.09.013

6. Mori R, Tanaka K, Shimokawa I. Identification and functional analysis of inflammation-related miRNAs in skin wound repair. *Dev Growth differ* (2018) 60 (6):306–15. doi: 10.1111/dgd.12542

7. Ramberg S, Krasnov A, Colquhoun D, Wallace C, Andreassen R. Expression analysis of *Moritella viscosa*-challenged atlantic salmon identifies disease-responding genes, microRNAs and their predicted target genes and pathways. *Int J Mol Sci* (2022) 23 (19):11200. doi: 10.3390/ijms231911200

8. Zhang C, Tu J, Zhang YA. MicroRNA regulation of viral replication in teleost fish: A review. *Rev Aquac* (2021) 13(3):1367–78. doi: 10.1111/raq.12526

9. Zhou Z, Lin Z, Pang X, Shan P, Wang J. MicroRNA regulation of toll-like receptor signaling pathways in teleost fish. *Fish shellfish Immunol* (2018) 75:32–40. doi: 10.1016/j.fsi.2018.01.036

10. Chu Q, Xu T. MicroRNA regulation of toll-like receptor, RIG-i-like receptor and nod-like receptor pathways in teleost fish. *Rev Aquac* (2020) 12(4):2177–93. doi: 10.1111/raq.12428

11. Chu Q, Yan X, Liu L, Xu T. The inducible microRNA-21 negatively modulates the inflammatory response in teleost fish *via* targeting IRAK4. *Front Immunol* (2019) 10:1623. doi: 10.3389/fimmu.2019.01623

12. Liyanage TD, Nikapitiya C, Lee J, De Zoysa M. Potential immune regulatory role of miR-146a upon *Aeromonas hydrophila* and *Edwardsiella piscicida* infections in zebrafish. *Braz J Microbiol* (2020) 51(3):931–7. doi: 10.1007/s42770-020-00237-w

13. Chu Q, Bi D, Zheng W, Xu T. MicroRNA negatively regulates NF-κB-mediated immune responses by targeting NOD1 in the teleost fish *Miichthys miiuy*. *Sci China Life Sci* (2021) 64(5):803–15. doi: 10.1007/s11427-020-1777-y

14. Cui J, Chu Q, Xu T. miR-122 involved in the regulation of toll-like receptor signaling pathway after vibrio anguillarum infection by targeting TLR14 in miiuy croaker. *Fish shellfish Immunol* (2016) 58:67–72. doi: 10.1016/j.fsi.2016.09.027

15. Xu G, Han J, Xu T. Comparative analysis of the small RNA transcriptomes of miiuy croaker revealed microRNA-mediated regulation of TLR signaling pathway response to *Vibrio anguillarum* infection. *Fish shellfish Immunol* (2016) 52:248–57. doi: 10.1016/j.fsi.2016.03.011

16. Chu Q, Gao Y, Bi D, Xu T. MicroRNA-148 as a negative regulator of the common TLR adaptor mediates inflammatory response in teleost fish. *Sci Rep* (2017) 7(1):4124. doi: 10.1038/s41598-017-04354-9

17. Liu Y, Liu Y, Han M, Du X, Liu X, Zhang Q, et al. *Edwardsiella tarda*-induced miR-7a functions as a suppressor in PI3K/AKT/GSK3β signaling pathway by targeting insulin receptor substrate-2 (IRS2a and IRS2b) in *Paralichthys olivaceus*. *Fish shellfish Immunol* (2019) 89:477–85. doi: 10.1016/j.fsi.2019.03.076

18. Bai J, Hu X, Wang R, Lü A, Sun J. MicroRNA expression profile analysis of skin immune response in crucian carp (*Carassius auratus*) infected by *Aeromonas hydrophila*. *Fish shellfish Immunol* (2020) 104:673–85. doi: 10.1016/j.fsi.2020.05.077

19. Lü A, Hu X, Wang Y, Shen X, Li X, Zhu A, et al. iTRAQ analysis of gill proteins from the zebrafish (*Danio rerio*) infected with *Aeromonas hydrophila*. *Fish shellfish Immunol* (2014) 36(1):229–39. doi: 10.1016/j.fsi.2013.11.007

20. Zhang QL, Dong ZX, Luo ZW, Jiao YJ, Guo J, Deng XY, et al. MicroRNA profile of immune response in gills of zebrafish (*Danio rerio*) upon *Staphylococcus aureus* infection. *Fish shellfish Immunol* (2019) 87:307–14. doi: 10.1016/j.fsi.2019.01.026

21. Chen J, Luo Y, Cao J, Xie L. Fluoride exposure changed the expression of microRNAs in gills of male zebrafish (*Danio rerio*). *Aquat Toxicol (Amsterdam Netherlands)* (2021) 233:105789. doi: 10.1016/j.aquatox.2021.105789

22. Lu C, Ling F, Ji J, Kang YJ, Wang GX. Expression of immune-related genes in goldfish gills induced by dactylogyrus intermedius infections. *Fish shellfish Immunol* (2013) 34(1):372–7. doi: 10.1016/j.fsi.2012.11.004

23. Liao X, Yang L, Zhang Q, Chen J. microRNA expression changes after lipopolysaccharide treatment in gills of amphioxus branchiostoma belcheri. *Dev Comp Immunol* (2017) 70:39–44. doi: 10.1016/j.dci.2017.01.007

24. Liyanage TD, Nikapitiya C, Lee J, De Zoysa M. Molecular insight into regulation of miRNAs in the spleen of zebrafish (*Danio rerio*) upon pathogenic *Streptococcus parauberis* infection. *Fish shellfish Immunol* (2020) 106:898–909. doi: 10.1016/j.fsi.2020.08.045

25. Goodale BC, Hampton TH, Ford EN, Jackson CE, Shaw JR, Stanton BA, et al. Profiling microRNA expression in Atlantic killifish (*Fundulus heteroclitus*) gill and responses to arsenic and hyperosmotic stress. *Aquat Toxicol (Amsterdam Netherlands)* (2019) 206:142–53. doi: 10.1016/j.aquatox.2018.11.009

26. Xu XY, Shen YB, Fu JJ, Lu LQ, Li JL. Determination of reference microRNAs for relative quantification in grass carp (*Ctenopharyngodon idella*). *Fish shellfish Immunol* (2014) 36(2):374–82. doi: 10.1016/j.fsi.2013.12.007

27. Wang R, Hu X, Lü A, Liu R, Sun J, Sung YY, et al. Transcriptome analysis in the skin of *Carassius auratus* challenged with *Aeromonas hydrophila*. *Fish shellfish Immunol* (2019) 94:510–6. doi: 10.1016/j.fsi.2019.09.039

28. Li X, Hu X, Lv A, Guan Z. Skin immune response to *Aeromonas hydrophila* infection in crucian carp *Carassius auratus* revealed by multi-omics analysis. *Fish shellfish Immunol* (2022) 127:866–75. doi: 10.1016/j.fsi.2022.07.036

29. Santos AA, Egami MI, Ranzani-Paiva MJT, Juliano Y. Hematological parameters and phagocytic activity in fat snook (*Centropomus parallelus*): Seasonal variation, sex and gonadal maturation. *Aquaculture* (2009) 296(3-4):359–66. doi: 10.1016/j.aquaculture.2009.08.023

30. Tian Y, Shang Y, Guo R, Ding J, Li X, Chang Y. miR-10 involved in salinity-induced stress responses and targets TBC1D5 in the sea cucumber, *Apostichopus japonicas*. *Comp Biochem Physiol Part B Biochem Mol Biol* (2020) 242:110406. doi: 10.1016/j.cbpb.2019.110406

31. Liu Q, Wang W, Zhang Y, Cui Y, Xu S, Li S. Bisphenol a regulates cytochrome P450 1B1 through miR-27b-3p and induces carp lymphocyte oxidative stress leading to apoptosis. *Fish shellfish Immunol* (2020) 102:489–98. doi: 10.1016/j.fsi.2020.05.009

32. Kumari R, Roy U, Desai S, Nilavar NM, Van Nieuwenhuijze A, Paranjape A, et al. MicroRNA miR-29c regulates RAG1 expression and modulates V(D)J recombination during b cell development. *Cell Rep* (2021) 36(2):109390. doi: 10.1016/j.celrep.2021.109390

33. Sun Y, Wang H, Luo C. MiR-100 regulates cell viability and apoptosis by targeting ATM in pediatric acute myeloid leukemia. *Biochem Biophys Res Commun* (2020) 522 (4):855–61. doi: 10.1016/j.bbrc.2019.11.156

34. Ren X, Cui J, Xu T, Sun Y. microRNA-128 inhibits the inflammatory responses by targeting TAB2 in miiuy croaker, miichthysmiiuy. *Dev Comp Immunol* (2021) 117:103976. doi: 10.1016/j.dci.2020.103976

35. Han S, Lin F, Ruan Y, Zhao S, Yuan R, Ning J, et al. miR-132-3p promotes the cisplatin-induced apoptosis and inflammatory response of renal tubular epithelial cells by targeting SIRT1 *via* the NF-κB pathway. *Int Immunopharmacol* (2021) 99:108022. doi: 10.1016/j.intimp.2021.108022

36. Xu XY, Shen YB, Fu JJ, Yu HY, Huang WJ, Lu LQ, et al. MicroRNA-induced negative regulation of TLR-5 in grass carp, *Ctenopharyngodon idella*. *Sci Rep* (2016) 6:18595. doi: 10.1038/srep18595

37. Wang Z, Zhang X, Yang Z, Du H, Wu Z, Gong J, et al. MiR-145 regulates PAK4 *via* the MAPK pathway and exhibits an antitumor effect in human colon cells. *Biochem Biophys Res Commun* (2012) 427(3):444–9. doi: 10.1016/j.bbrc.2012.06.123

38. Han J, Sun Y, Song W, Xu T. microRNA-145 regulates the RLR signaling pathway in miiuy croaker after poly(I:C) stimulation *via* targeting MDA5. *Dev Comp Immunol* (2017) 68:79–86. doi: 10.1016/j.dci.2016.11.021

39. Sun YL, Li XP, Sun L. Pol-miR-150 regulates anti-bacterial and viral infection in Japanese flounder (*Paralichthys olivaceus*) *via* the lysosomal protein LMP2L. *Comp Biochem Physiol Part B Biochem Mol Biol* (2021) 254:110578. doi: 10.1016/j.cbpb.2021.110578

40. Tang X, Fu J, Tan X, Shi Y, Ye J, Guan W, et al. The miR-155 regulates cytokines expression by SOSC1 signal pathways of fish *in vitro* and *in vivo*. *Fish shellfish Immunol* (2020) 106:28–35. doi: 10.1016/j.fsi.2020.07.042

41. Song C, Liu B, Xu P, Ge X, Li H, Tang Y, et al. miR-144 is the epigenetic target for emodin to ameliorate oxidative stress induced by dietary oxidized fish oil *via* Nrf2 signaling in wuchang bream, *Megalobrama amblycephala*. *Aquaculture* (2021) 534:736357. doi: 10.1016/j.aquaculture.2021.736357

42. Coccia E, Masanas M, López-Soriano J, Segura MF, Comella JX, Pérez-García MJ. FAIM is regulated by miR-206, miR-1-3p and miR-133b. *Front Cell Dev Biol* (2020) 8:584606. doi: 10.3389/fcell.2020.584606

43. Su H, Chang R, Zheng W, Sun Y, Xu T. MicroRNA-210 and microRNA-3570 negatively regulate NF-κB-mediated inflammatory responses by targeting RIPK2 in teleost fish. *Front Immunol* (2021) 12:617753. doi: 10.3389/fimmu.2021.617753

44. Bartel DP, Chen CZ. Micromanagers of gene expression: The potentially widespread influence of metazoan microRNAs. nature reviews. *Genetics* (2004) 5 (5):396–400. doi: 10.1038/nrg1328

45. Andreassen R, Høyheim B. miRNAs associated with immune response in teleost fish. *Dev Comp Immunol* (2017) 75:77–85. doi: 10.1016/j.dci.2017.02.023

46. Smith NC, Umasuthan N, Kumar S, Woldemariam NT, Andreassen R, Christian SL, et al. Transcriptome profiling of *Atlantic salmon* adherent head kidney leukocytes reveals that macrophages are selectively enriched during culture. *Front Immunol* (2021) 12:709910. doi: 10.3389/fimmu.2021.709910

47. Zhou W, Xie Y, Li Y, Xie M, Zhang Z, Yang Y, et al. Research progress on the regulation of nutrition and immunity by microRNAs in fish. *Fish shellfish Immunol* (2021) 113:1–8. doi: 10.1016/j.fsi.2021.03.011

48. Andreassen R, Rangnes F, Sivertsen M, Chiang M, Tran M, Worren MM. Discovery of miRNAs and their corresponding miRNA genes in atlantic cod (*Gadus morhua*): Use of stable miRNAs as reference genes reveals subgroups of miRNAs that are highly expressed in particular organs. *PloS One* (2016) 11(4):e0153324. doi: 10.1371/journal.pone.0153324

49. Mennigen JA. Micromanaging metabolism-a role for miRNAs in teleost energy metabolism. *Comp Biochem Physiol Part B Biochem Mol Biol* (2016) 199:115–25. doi: 10.1016/j.cbpb.2015.09.001

50. Yan X, Cui J, Liu X, Xu T. microRNA-144 regulates the NF-κB signaling in miiuy croaker *via* targeting IL1β. *Dev Comp Immunol* (2019) 96:47–50. doi: 10.1016/j.dci.2019.02.018

51. Ordas A, Kanwal Z, Lindenberg V, Rougeot J, Mink M, Spaink HP, et al. MicroRNA-146 function in the innate immune transcriptome response of zebrafish embryos to *Salmonella typhimurium* infection. *BMC Genomics* (2013) 14:696. doi: 10.1186/1471-2164-14-696

52. Ji C, Guo X, Ren J, Zu Y, Li W, Zhang Q. Transcriptomic analysis of microRNAs-mRNAs regulating innate immune response of zebrafish larvae against *Vibrio parahaemolyticus* infection. *Fish shellfish Immunol* (2019) 91:333–42. doi: 10.1016/j.fsi.2019.05.050

53. Kawai T, Akira S. The role of pattern-recognition receptors in innate immunity: update on toll-like receptors. *Nat Immunol* (2010) 11(5):373–84. doi: 10.1038/ni.1863

54. Zheng W, Chu Q, Xu T. The long noncoding RNA NARL regulates immune responses *via* microRNA-mediated NOD1 downregulation in teleost fish. *J Biol Chem* (2021) 296:100414. doi: 10.1016/j.jbc.2021.100414

55. Shankaran ZS, Walter CEJ, Ramanathan A, Dandapani MC, Selvaraj S, Kontham SS, et al. microRNA-146a gene polymorphism alters human colorectal cancer susceptibility and influences the expression of its target genes in toll-like receptor (TLR) pathway. *Meta Gene* (2020) 24:100654. doi: 10.1016/j.mgene.2020.100654

56. Gao C, Fu Q, Yang N, Song L, Tan F, Zhu J, et al. Identification and expression profiling analysis of microRNAs in Nile tilapia (*Oreochromis niloticus*) in response to *Streptococcus agalactiae* infection. *Fish shellfish Immunol* (2019) 87:333–45. doi: 10.1016/j.fsi.2019.01.018

57. Han J, Chu Q, Huo R, Xu T. Inducible microRNA-122 modulates RIG-I signaling pathway *via* targeting DAK in miiuy croaker after poly(I:C) stimulation. *Dev Comp Immunol* (2018) 78:52–60. doi: 10.1016/j.dci.2017.09.011

58. Lü A, Hu X, Wang Y, Ming Q, Zhu A, Shen L, et al. Proteomic analysis of differential protein expression in the skin of zebrafish [*Danio rerio* (Hamilton 1822)] infected with *Aeromonas hydrophila*. *J Appl Ichthyol* (2014) 30(1):28–34. doi: 10.1111/jai.12318

59. Ni S, Yu Y, Wei J, Zhou L, Wei S, Yan Y, et al. MicroRNA-146a promotes red spotted grouper nervous necrosis virus (RGNNV) replication by targeting TRAF6 in orange spotted grouper, *Epinephelus coioides*. *Fish shellfish Immunol* (2018) 72:9–13. doi: 10.1016/j.fsi.2017.10.020

60. Chuphal B, Rai U, Roy B. Teleost NOD-like receptors and their downstream signaling pathways: A brief review. *Fish Shellfish Immunol Rep* (2022) 100056:1–14. doi: 10.1016/j.fsirep.2022.100056

61. Rajendran KV, Zhang J, Liu S, Kucuktas H, Wang X, Liu H, et al. Pathogen recognition receptors in channel catfish: I. identification, phylogeny and expression of NOD-like receptors. *Dev Comp Immunol* (2012) 37(1):77–86. doi: 10.1016/j.dci.2011.12.005

62. Huang Y, Huang CX, Wang WF, Liu H, Wang HL. Zebrafish miR-462-731 is required for digestive organ development. *Comp Biochem Physiol Part D Genomics Proteomics* (2020) 34:100679. doi: 10.1016/j.cbd.2020.100679

frontiers | Frontiers in Immunology

TYPE Original Research
PUBLISHED 07 February 2023
DOI 10.3389/fimmu.2023.1092824

OPEN ACCESS

EDITED BY
Heng Chi,
Ocean University of China, China

REVIEWED BY
Jian Zhang,
Yantai University, China
Jia Cai,
Guangdong Ocean University, China

*CORRESPONDENCE
Qiwei Qin
qinqw@scau.edu.cn
Jingguang Wei
weijg@scau.edu.cn

SPECIALTY SECTION
This article was submitted to Molecular Innate Immunity, a section of the journal Frontiers in Immunology

RECEIVED 08 November 2022
ACCEPTED 16 January 2023
PUBLISHED 07 February 2023

CITATION
Zhang L, Zhang X, Liao J, Xu L, Kang S, Chen H, Sun M, Wu S, Xu Z, Wei S, Qin Q and Wei J (2023) Grouper cGAS is a negative regulator of STING-mediated interferon response.
Front. Immunol. 14:1092824.
doi: 10.3389/fimmu.2023.1092824

Grouper cGAS is a negative regulator of STING-mediated interferon response

Luhao Zhang[1], Xin Zhang[1], Jiaming Liao[1], Linting Xu[1], Shaozhu Kang[1], Hong Chen[1], Mengshi Sun[1], Siting Wu[1], Zhuqing Xu[1], Shina Wei[1,2], Qiwei Qin[1,3,4,5]* and Jingguang Wei[1,6]*

[1]College of Marine Sciences, South China Agricultural University, Guangdong Laboratory for Lingnan Modern Agriculture, Guangzhou, China, [2]Guangdong Provincial Key Laboratory of Aquatic Animal Disease Control and Healthy Culture, Zhanjiang, China, [3]Laboratory for Marine Biology and Biotechnology, Qingdao, China, [4]Pilot National Laboratory for Marine Science and Technology, Qingdao, China, [5]Southern Marine Science and Engineering Guangdong Laboratory, Zhuhai, China, [6]Department of Biological Sciences, National University of Singapore, Singapore, Singapore

Cyclic GMP-AMP synthase (cGAS) is one of the classical pattern recognition receptors that recognizes mainly intracytoplasmic DNA. cGAS induces type I IFN responses to the cGAS-STING signaling pathway. To investigate the roles of cGAS-STING signaling pathway in grouper, a cGAS homolog (named EccGAS) was cloned and identified from orange-spotted grouper (*Epinephelus coioides*). The open reading frame (ORF) of EccGAS is 1695 bp, encodes 575 amino acids, and contains a Mab-21 typical structural domain. EccGAS is homologous to *Sebastes umbrosus* and humans at 71.8% and 41.49%, respectively. EccGAS mRNA is abundant in the blood, skin, and gills. It is uniformly distributed in the cytoplasm and colocalized in the endoplasmic reticulum and mitochondria. Silencing of EccGAS inhibited the replication of Singapore grouper iridovirus (SGIV) in grouper spleen (GS) cells and enhanced the expression of interferon-related factors. Furthermore, EccGAS inhibited EcSTING-mediated interferon response and interacted with EcSTING, EcTAK1, EcTBK1, and EcIRF3. These results suggest that EccGAS may be a negative regulator of the cGAS-STING signaling pathway of fish.

KEYWORDS

Epinephelus coioides, CGAS, SGIV, virus replication, STING

1 Introduction

Groupers are one of the main economic fishes on the southeast coast of China and Southeast Asia. With the expansion of grouper aquaculture, the pollution in the water and the corresponding disease outbreaks are detrimental, threatening the aquaculture industry. In particular, the emergence of a major viral pathogen, Singapore Grouper Iridovirus (SGIV) has caused huge losses to aquaculture. SGIV belongs to *Iridoviridae*, the frog iridovirus genus (*Ranavirus*), and is a large cytoplasmic DNA virus, and can cause bleeding and swelling of the spleen of the fish. When grouper infected SGIV, the lethality rate can reach > 90% in a week (1).

The innate immune system is the host defense mechanism that plays a critical role against damage caused by microorganisms, pathogens, and other harmful agents (2). When pathogens invade a host, the pattern recognition receptors (PRRs), as part of the host innate immune response, identify pathogen-associated molecular patterns (PAMPs), subsequently activating pro-inflammatory cytokines and interferons through a series of signaling cascades to suppress damage (2). PRRs are broadly classified into five classes: DNA receptors, Toll-like receptors (TLRs), NOD-like receptors, RIG-I-like receptors (RLRs), and C-type lectin receptors (3–5). Among them, DNA receptors are an important class of PRRs that recognize foreign cytoplasmic DNA. The genetic material of many organisms, including viruses, is double-stranded DNA (dsDNA), thus DNA receptors recognize this foreign DNA in the cytoplasm, which is important in the intrinsic host immunity against viruses. Several host proteins have been identified as capable of recognizing double-stranded DNA, including TLR9 (6), Z-nucleic acid binding protein (DAI) (7), DEAD-box helicase (DDX)60 (8), DDX41 (9), Interferon gamma inducible protein 16 (IFI16) (10), and cGAS (cyclic guanosine-adenylate synthase) (11).

A widely recognized DNA receptor, cGAS, has been recognized in recent studies as a member of the nucleotidyltransferase (NTase) family (11). Notably, cGAS recognizes almost all double-stranded DNA as it does not depend on the nucleotide sequence. In mammals, cGAS consists of a nucleotidyltransferase domain and two DNA-binding domains at the N-terminal, the nucleotidyltransferase domain in the middle-conserved fragment, and the C-terminal Mab21 domain (11, 12). When cGAS recognizes foreign DNA, the DNA is attracted by its positive surface charge and zinc finger structure, forming a 2:2 dimer between two cGAS and two dsDNA (12). In turn, cGAS is activated, resulting in its conformational change, and thus promoting the production of cGAMP from ATP and GTP (13). Subsequently, cGAMP binds to the interferon gene-stimulating protein STING, which translocates cGAMP from the endoplasmic reticulum to the Golgi apparatus, and, in turn, recruits TANK-binding kinase 1 (TBK1), phosphorylates IRF3 and nuclear factor-κB (NF-κB) to promote their entry into the nucleus. When IRF3 and NF-κB are translocated from the cytoplasm to the nucleus, IFN-β is expressed, and a large number of inflammatory factors and interleukins are produced (14, 15).

In previous studies, a large number of expressed sequence tags (EST) were found in the transcriptome of the grouper spleen before and after infection with SGIV (14, 15). In this study, a cGAS homolog from orange-spotted grouper (EccGAS) was cloned, and its roles in the innate immune response were investigated. The results will provide new and more effective insights for the prevention and treatment of viral infection.

2 Materials and methods

2.1 Fish, cells and virus

Juvenile grouper (40-50 g in weight) were obtained from the fishery in Yangjiang City, China. They were stored in a recirculating seawater system at 24-28°C and fed twice daily for two weeks. Then three groupers were randomly selected to detect whether the fish was infected with bacteria or viruses. Twelve tissues were extracted from 6 healthy fish, immediately frozen in liquid nitrogen, and stored at -80°C.

Grouper spleen (GS) cells were constructed in our laboratory and are currently kept in our laboratory. GS cells were grown in Leibovitz L15 medium (Wibco, Waltham, MA, USA) containing 10% fetal bovine serum and placed in a 28°C incubator (14, 15). SGIV was isolated from diseased groupers and cultured as previously described (1, 16). Viral cultures were maintained at -80°C.

2.2 Antibodies

Rabbit monoclonal anti-green fluorescent protein (GFP) antibody was purchased from Sigma (Burlington, MA, USA), and mouse monoclonal anti-HA antibody was also purchased from Sigma (Burlington, MA, USA). Rabbit monoclonal β-tubulin antibody was purchased from Proteintech (Rosemont, IL, USA). Polyclonal antibody to SGIV protein MCP was prepared in our laboratory. Horseradish peroxidase-labeled goat anti-rabbit antibody as secondary antibody was purchased from KPL (USA).

2.3 Cloning of EccGAS and bioinformatic analysis

Primers used to amplify the open reading frame (ORF) of EccGAS were designed according to the EST sequences of cGAS in the grouper spleen transcriptome (1, 16). The ORF of EccGAS was amplified from the tissue cDNA of healthy grouper. Sequences of EccGAS were analyzed using the BLAST program (http://www.ncbi.nlm.nih.gov/blast), and the conservative domains were predicted using the conservative domain database (https://www.ncbi.nlm.nih.gov/cdd/) of NCBI. SignalP 4.1 was used to predict signal peptides and TMHMM Server V. 2.0 was used to predict transmembrane regions. GeneDoc and Clustal X1.83 were used for amino acid sequences alignment of cGAS, and MEGA version 6.0 was used for phylogenetic tree analysis.

2.4 RNA isolation and qRT-PCR

Total RNA was performed using the SV Total RNA Isolation System (Promega, United States) following the manufacturer's instructions. cDNA synthesis was performed with the ReverTra Ace qPCR RT Kit (Toyobo, Osaka, Japan) according to the manufacturers' instructions. SYBR® Green Real-Time PCR Master Mix (Toyobo) was used to perform the quantitative real-time PCR (qRT-PCR) in an Applied Biosystems QuantStudio 5 Real-Time PCR System (Thermo Fisher, Waltham, MA, USA), as previously described (17). Briefly, each assay was performed in triplicate with the cycling conditions as follows: 95°C for 1 min for activation, followed by 40 cycles of 95°C for 15 s, 60°C for 15 s, and 72°C for 45 s. The primers of target genes are listed in Table 1, and β-actin was

used as the internal reference gene. The expression levels were calculated using the $2^{-\Delta\Delta CT}$ method.

2.5 Preparation of antiserum of EccGAS

Primers were designed to amplify the ORF of EccGAS (Table 1). The PCR product was digested with BamH I and EcoR I (Takara) and subsequently subcloned into the expression vector pET-B2M. Positive clones were incubated at 37°C, and shaked at 220 rpm in a 150 mL LB medium with 100 mg/mL ampicillin. The vector pET-B2M was used as a negative control. When OD600 of the medium reached 0.6, IPTG inducer (final concentration 0.5 mM) was added, and the culture was shaken at 37°C for 3 h. Recombinant EccGAS fusion proteins (named rEccGAS) were purified. The concentration of purified rEccGAS protein was determined *via* Bradford's method (18). The purified rEccGAS proteins were then used to immunize the New Zealand white rabbits to obtain polyclonal antibodies against EccGAS according to conventional methods (19). Western blot was used to detect the specificity of the antiserum.

2.6 Cell transfection

Cell transfection was performed with Lipofectamine 2000 (Invitrogen, USA) according to the manufacturer's instructions. Briefly, cells were seeded into plates and changed to serum-free medium after the cell density had spread to 80%. Lipofectamine 2000 and plasmids were diluted with Opti-MEM (Gibco, USA) in two separate sterile tubes. After a 5-min incubation at 25°C, Lipofectamine 2000 with the diluted plasmids were mixed gently and thoroughly. The mixture was then incubated at 25°C for 25 min before being added dropwise to the cells. After 5-6 h, the medium was changed to serum medium to continue the culture (20).

2.7 Cell localization analysis

GS cells were seeded into 6-well plates containing coverslips (10 mm×10 mm). When the cell density is appropriate, the plasmids are transfected. After 24 h, cells were washed with phosphate-buffered saline and fixed with 4% paraformaldehyde or methanol for 1 h. Cells were permeabilized with anhydrous ethanol for 15 min at -20°C and then blocked with 2% BAS (ready-to-use) for 2 h at 25°C. Cells were incubated with 1% BSA diluted with rabbit polyclonal anti-EccGAS antibody (1:150) or mouse monoclonal anti-HA antibody (1:150) for 2 h. Cells were incubated for 2 h with 1% BSA diluted with rabbit polyclonal anti-EccGAS antibody (1:150) or mouse monoclonal anti-HA antibody (1:150). Cells were then washed with phosphate-buffered saline. FITC-conjugated goat anti-rabbit or goat anti-mouse antibodies were diluted (1:200) with 1% BSA and incubated for 1 h. Cells were then washed with phosphate-buffered saline and treated with 6-dibutylamino-2-phenylindole (DAPI) for 10 min in the dark, and observed under a fluorescence microscope (Leica, Wetzlar, Germany).

TABLE 1 Primers used for host and viral genes expression analysis.

Primers	Sequences (5′-3′)
IRF3-RT-F	GACAACAAGAACGACCCTGCTAA
IRF3-RT-R	GGGAGTCCGCTTGAAGATAGACA
IRF7-RT-F	CAACACCGGATACAACCAAG
IRF7-RT-R	GTTCTCAACTGCTACATAGGG
ISG15-RT-F	CCTATGACATCAAAGCTGACGAGAC
ISG15-RT-R	GTGCTGTTGGCAGTGACGTTGTAGT
ISG56-RT-F	CAGGCATGGTGGAGTGGAAC
ISG56-RT-R	CTCAAGGTAGTGAACAGCGAGGTA
Viperin-RT-F	TCTGGGTAAATTAGTCCAGTTC
Viperin-RT-R	AGGTGTTGATGACCGAGTTG
IL-1β-RT–PF	AACCTCATCATCGCCACACA
IL-1β-RT-PR	AGTTGCCTCACAACCGAACAC
IL-8-RT-PF	GCCGTCAGTGAAGGGAGTCTAG
IL-8-RT-PR	ATCGCAGTGGGAGTTTGCA
TNFα-RT-F	GTGTCCTGCTGTTTGCTTGGTA
TNFα-RT-R	CAGTGTCCGACTTGATTAGTGCTT
PKR-F	GACCTTGGCTCTGTTGGACC
PKR-R	ATGCTTGGCTTCTTTCTTGT
IFN1-RT-F	GTGTCCTTCCCGAATCATCT
IFN1-RT-R	ACAGCCTGCCTGCTTACAAC
IFN2-RT-F	TACAGCCAGGCGTCCAAAGCATC
IFN2-RT-R	CAGTACAGGAGCGAAGGCCGACA
EccGAS-RT-F	CGGGTTTCATTCTCTCAT
EccGAS-RT-R	AGGCACTCCAGTCTGTGT
Actin-RT-R	TACGAGCTGCCTGACGGACA
Actin-RT-F	GGCTGTGATCTCCTTCTGCA
MCP-RT-F	GCACGCTTCTCTCACCTTCA
MCP-RT-R	AACGGCAACGGGAGCACTA
ICP18-RT-F	ATCGGATCTACGTGGTTGG
ICP18-RT-R	CCGTCGTCGGTGTCTATTC
VP19-RT-F	TCCAAGGGAGAAACTGTAAG
VP19-RT-R	GGGGTAAGCGTGAAGACT

2.8 Virus infection assay

Three siRNAs targeting EccGAS mRNA were designed to evaluate the mechanism of EccGAS on SGIV infection in GS cells (Table 2). Cells were transfected with the same volume of siRNA or control. The cells were infected with SGIV 24 hours later. The cells were then collected at 24 h and 36 h after SGIV infection. The expression levels of SGIV ICP18, VP19, and MCP were analyzed using qRT-PCR (Table 1). The expression of SGIV MCP protein was analyzed using western blotting.

TABLE 2 Primers used for silencing EccGAS.

Primers	Sequences (5´-3´)
NC-F	UUCUUCGAACGUGUCACGUTT
NC-R	ACGUGACACGUUCGGAGAATT
EccGAS-siRNA-174-F	GGAGAAGCCGUCUCUUCAATT
EccGAS-siRNA-174-R	UUGAAGAGACGGCUUCUCCTT
EccGAS-siRNA-1042-F	GCAGUGACCCUGACCACAATT
EccGAS-siRNA-1042-R	UUGUGGUCAGGGUCACUGCTT
EccGAS-siRNA-1191-F	GCGAAUGCCGUAUUAUCUUTT
EccGAS-siRNA-1191-R	AAGAUAAUACGGCAUUCGCTT

2.9 Dual-luciferase reporter assay

GS cells were plated in 24-well plates. When the cell density is appropriate, a total of 200 ng of zebrafish IFN1-LUc, human NF-κB-Luc, or human ISRE-Luc plasmids were co-transfected with 30 ng of the internal control PRL-sv40 reninase vectors and 600 ng of the target plasmids. After 36 h, cells were collected, and the luciferase activity was detect by the Dual-Luciferase® Reporter Assay System (Promega).

2.10 Co-immunoprecipitation assays

GS cells were passaged into cell culture dishes (10cm×10cm). When the cell density is appropriate, co-transfected with relevant the target plasmids. After 36 h, cells were harvested and lysed in RIPA buffer containing protease and phosphatase inhibitors. Samples were processed using the Double Bead™ Protein G Immunoprecipitation Kit (Invitrogen).

10% SDS-PAGE was used to separate immunoprecipitates or whole cell extracts. Separated immunoprecipitates or whole cell extracts were then transferred to Immobilon-P polyvinylidene difluoride membranes (Millipore, St. Louis, MO, USA). The membranes were blocked in 5% skim milk incubated with antibodies for 2 h at 25°C or overnight at 4 °C, washed 3 times with PBST, and incubated with secondary antibodies for 1 h at 25°C. After washing three times with PBST, the immunoreactive protein was visualized by an enhanced chemiluminescence detection kit (Bio-Rad, Irvine, CA, USA). The band intensity was calculated using Quantity-one software (21).

2.11 Statistical analysis

GraphPad Prism (version 8.0.2) was used to perform statistical analysis. Data analysis results are shown as mean ± standard error of the mean of three independent experiments. The statistically significant differences were evaluated by the T-Test with a P value (*$P < 0.05$ and **$P < 0.01$).

3 Results

3.1 Amplification and sequence analysis of cGAS gene in grouper

The ORF of grouper cGAS (EccGAS) was 1695 bp in length, encoding 575 amino acids, with a molecular weight of approximately 63.05 kDa and an isoelectric point of 9.47. SMART analysis revealed that EccGAS contains the Mab-21 typical structural domain, while the signal peptide and transmembrane region were absent.

Aligning the cGAS proteins of other organisms with EccGAS revealed that the sequences of each species were relatively conserved in the Mab-21 typical structural domain, indicating that cGAS may have similar functions. The cGAS sequences of 11 species were selected for homology comparison, and the multiple sequence alignments were performed with Clustal X (Figure 1A). The phylogenetic tree showed that the EccGAS and cGAS of *Sebastes umbrosus* (XP_037637334.1) were more closely related and clustered together (Figure 1B).

The expression of EccGAS in healthy grouper tissues showed that EccGAS was expressed in all exacted tissues, with higher expression in blood, skin, and gills (Figure 2A). After SGIV infection, the transcriptional expression level of EccGAS in GS cells gradually increased and peaked at 36 h.p.i (Figure 2B), suggesting that EccGAS may play an important role in the activation of host antiviral innate immunity.

3.2 Bioassay of recombinant protein of EccGAS

The recombinant protein of EccGAS was analyzed by SDS-PAGE. A band of 57 kDa was visible using Komas Brilliant Blue staining (Figure 3A). The fused recombinant EccGAS protein (rEccGAS) was purified by affinity chromatography with nickel-nitrilotriacetic acid-agarose (QIAGEN, Germany) according to the manufacturer's instructions (Figure 3B). Immunosera were then prepared by immunizing rabbits with rEccGAS protein. rEccGAS protein was specifically recognized by the EccGAS polyclonal antibody, and no bands were detected in the negative control (Figure 3C), indicating that the anti-EccGAS antibody specifically recognized the purified EccGAS protein.

3.3 Intracellular localization of EccGAS

The expression vectors for full-length EccGAS, structural domain Mab21, and removal of the structural domain were constructed and named EccGAS(EccGAS), EccGAS-Mab21, and EccGAS-delete-mab21. Subsequently, the plasmids were transfected into GS cells, and intracellular localization of EccGAS was determined. The results showed that the green fluorescence of pEGFP-C1 was distributed in the cytoplasm and nucleus of GS cells, while the pEGFP-EccGAS and pEGFP-EccGAS-delete-mab21 were distributed uniformly in the cytoplasm, and pEGFP-EccGAS-Mab21 was distributed in the cytoplasm in an aggregated manner (Figure 4A). We next examined the intracellular localization of EccGAS in GS cells by immunofluorescence assay with anti-EccGAS serum. In GS cells, the green and red fluorescences of EccGAS were mainly localized in the cytoplasm by anti-EccGAS serum (Figure 4B), which is consistent with the results of subcellular localization.

To explore whether EccGAS co-localizes with organelles, plasmids pEGFP-EccGAS were co-transfected with pDsRed2-ER (endoplasmic reticulum) or pDsRed2-Mito (mitochondria) into GS

cells and their localization was examined. The results showed that EccGAS partially co-localized with the endoplasmic reticulum and mitochondria (Figure 4C).

3.4 EccGAS affected SGIV replication

We designed three siRNAs based on the ORF sequence of EccGAS. siRNAs were transfected into GS cells, and qRT-PCR was used to detect the expression of endogenous EccGAS after 24 hours. The results showed that all three siRNAs silenced the expression of endogenous EccGAS in GS cells, of which siRNA2 had the highest interference efficiency (Figure 5A). Next, we used siRNA2 to conduct the following experiments. After siRNA2 was transfected into GS cells and infected with SGIV, the expression of SGIV MCP, SGIV ICP18, and SGIV VP19 were examined by qRT-PCR. The expression of SGIV MCP protein was detected by western blot. The results showed that EccGAS knockdown by siRNA2 significantly inhibited the transcript expression of SGIV genes (Figure 5B). Moreover, the results of western blot showed that knockdown EccGAS by siRNA2 significantly reduced the expression of MCP protein (Figure 5C). These results suggest that EccGAS may promote SGIV replication in GS cells.

3.5 EccGAS inhibited interferon immune response

The regulatory effects of EccGAS on host immune factors were evaluated by qRT-PCR. As shown in Figure 6, EccGAS knockdown by siRNA2 potentiated the transcription of IFN1, IFN2, PKR, Viperin, ISG15, ISG56, IL-1β, IL-8, and TNFα in GS cells. Thus, the results suggested that EccGAS negatively regulated the interferon immune response *in vitro*.

3.6 EccGAS inhibits EcSTING-mediated interferon immune response

In mammals, cGAS has been reported to produce cGAMP after DNA sensing to stimulate STING, which in turn activates interferon

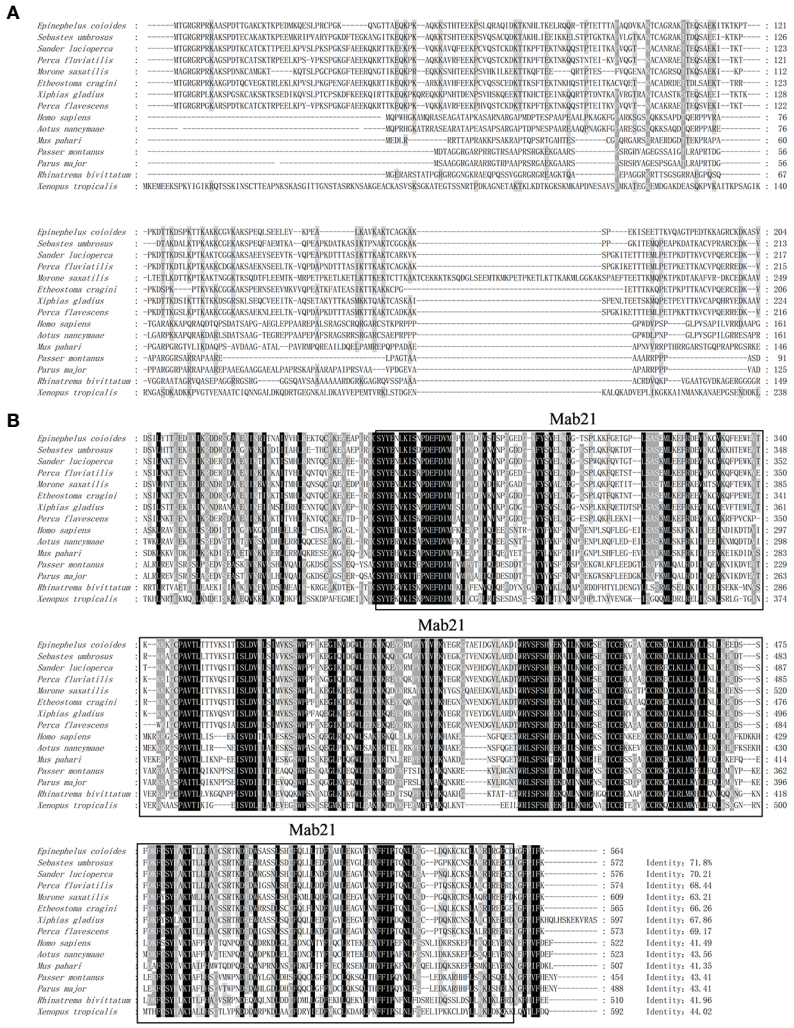

FIGURE 1
Sequence analysis and phylogenetic tree construction of EccGAS. **(A)** Multiple sequence comparison of the amino acid of EccGAS and cGAS proteins from other organisms. The predicted conserved structural domain of Mab21 is shown. **(B)** Phylogenetic tree of EccGAS proteins. The numbers on the nodes indicate bootstrap values for 1000 replicates. Scale bars represent 0.1 change per site.

production and innate immunity. We aimed to determine whether EccGAS is involved in EcSTING-mediated interferon immune response. As shown in Figure 7A, when EccGAS was co-transfected with EcSTING, EcTBK1, EcTAK1, and EcIRF3, the activities of IFN1, ISRE, and NF-κB promoters were significantly reduced, suggesting that EccGAS may be involved in EcSTING-mediated interferon immune responses. Next we investigated whether EccGAS interacts with EcSTING, EcTBK1, EcTAK1 and EcIRF3. Confocal microscopy results showed that the green fluorescence of pEGFP-EcSTING, pEGFP-EcTBK1, pEGFP-EcTAK1, and pEGFP-EcIRF3 colocalized with the red fluorescence of EccGAS (Figure 7B). We further verified the experimental results by CO-IP assay. The plamids of pcDNA3.1-EccGAS was co-transfected with pEGFP-EcSTING, pEGFP-EcTBK1, pEGFP-EcTAK1, pEGFP-EcIRF3, and pEGFP-C1, respectively, followed by immunoprecipitation (IP) and immunoblotting (IB) of whole cell lysates (WCLs). The results showed that EccGAS was detected in the IP products of EcSTING, EcTAK1, EcTBK1, and EcIRF3, but not in pEGFP-C1 (Figures 7C–E). Therefore, EccGAS inhibited EcSTING-mediated interferon immune response and interacted with EcSTING, EcTAK1, EcTBK1, and EcIRF3.

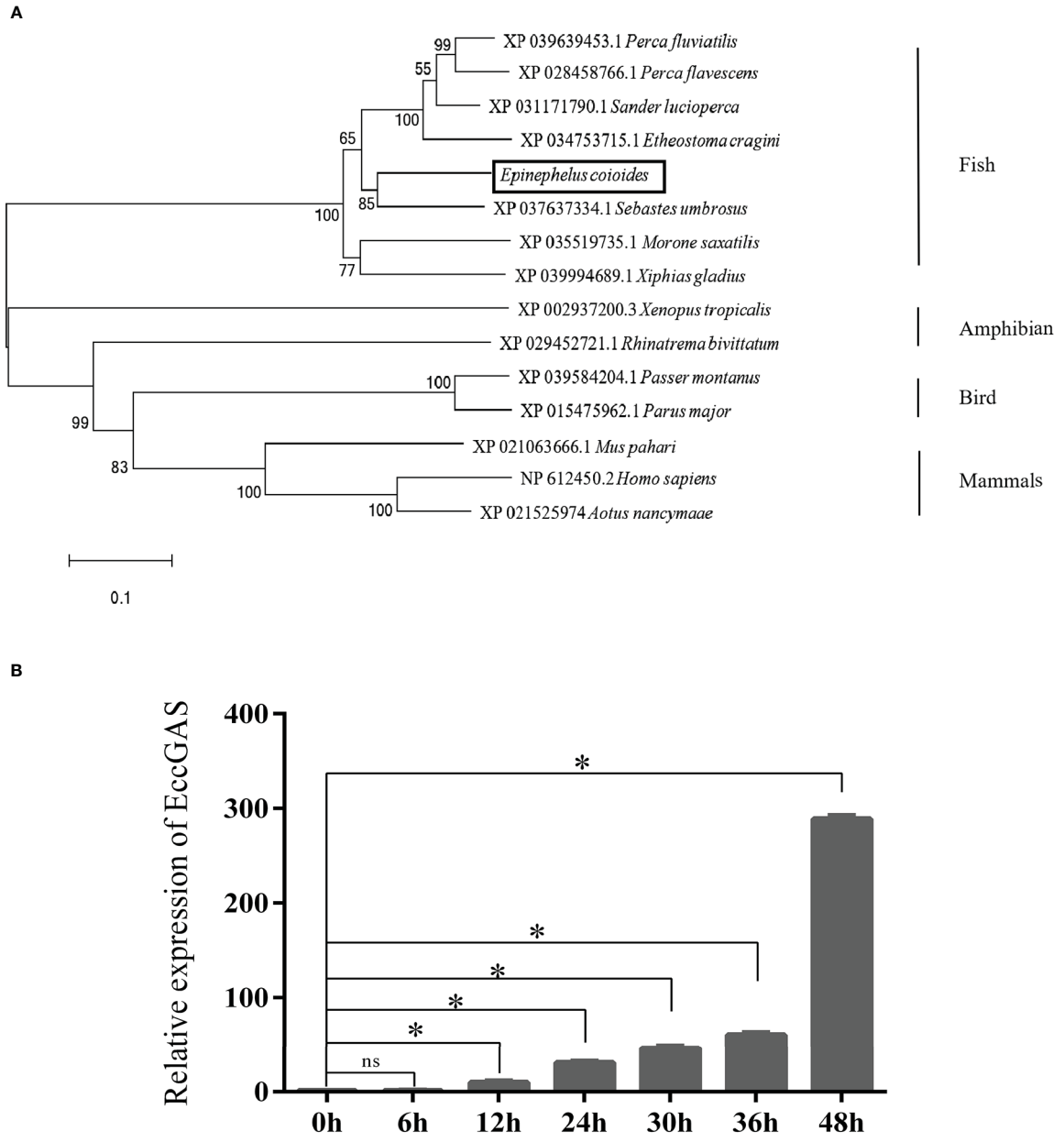

FIGURE 2
Expression pattern analysis of EccGAS. **(A)** Expression of EccGAS in different tissues of healthy groupers. Data were expressed as a ratio of the tissue value to the EccGAS mRNA expression in liver. β-actin were used as the internal control for the normalization across tissues. **(B)** Expression profiles of EccGAS in GS cells after SGIV infection. β-actin was used as an internal control. *P < 0.05. ns means no significance.

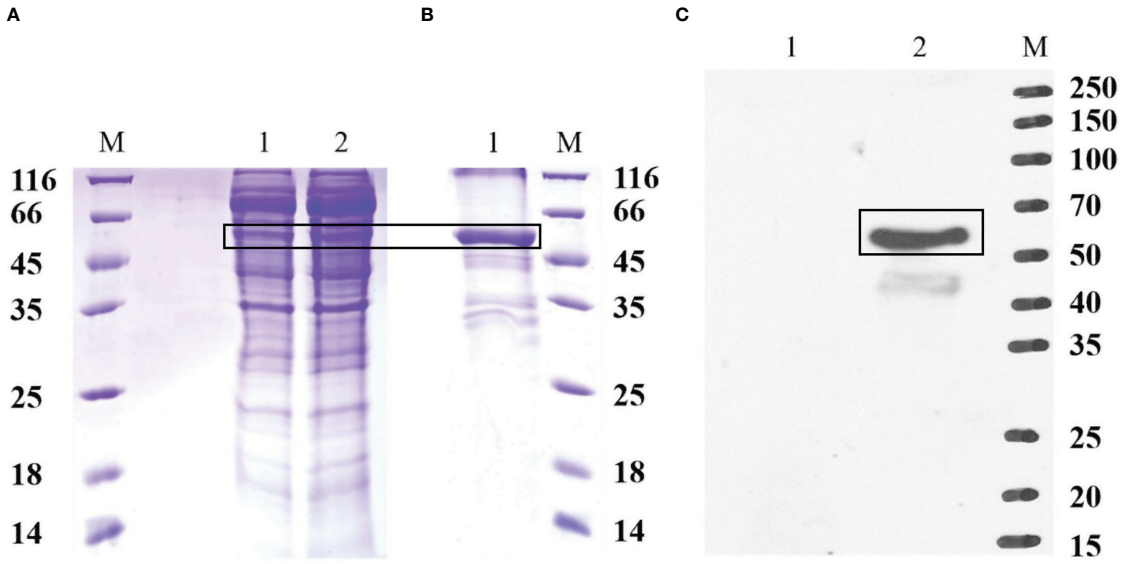

FIGURE 3
Production of recombinant EccGAS and anti-EccGAS serum. **(A)** Expression of recombinant EccGAS. M: protein molecular quality standard; 1: supernatant of pET-EccGAS induced by sonication; 2: microspheres of pET-EccGAS induced by sonication. **(B)** Purification of recombinant EccGAS. M: protein molecular quality standard; 1:purified recombinant pET-EccGAS protein. **(C)** Preparation of anti-EccGAS serum. M: protein molecular quality standard; 1: purified recombinant pET-EccGAS protein incubated with preimmune mouse serum; 2: purified recombinant pET-EccGAS protein incubated with anti-EccGAS serum (1:5000). Bands of EcCGA protein were boxed.

4 Discussion

Cytoplasmic DNA receptors, as part of the PRRs, play important roles in the innate immune response. One of the major cytoplasmic DNA receptors in humans is cGAS. It is homologous to oligoadenosine synthase, independent of nucleotide sequence, and thus able to recognize a variety of DNA viruses that invade the cytoplasm, including endogenous or threatening exogenous DNA (22–24). Currently, the function of cGAS is rarely reported in fish. In this study, a cGAS homolog from orange-spotted grouper *Epinephelus coioides* (EccGAS) was cloned and its role in the innate immune system during viral infection was studied. The results showed that

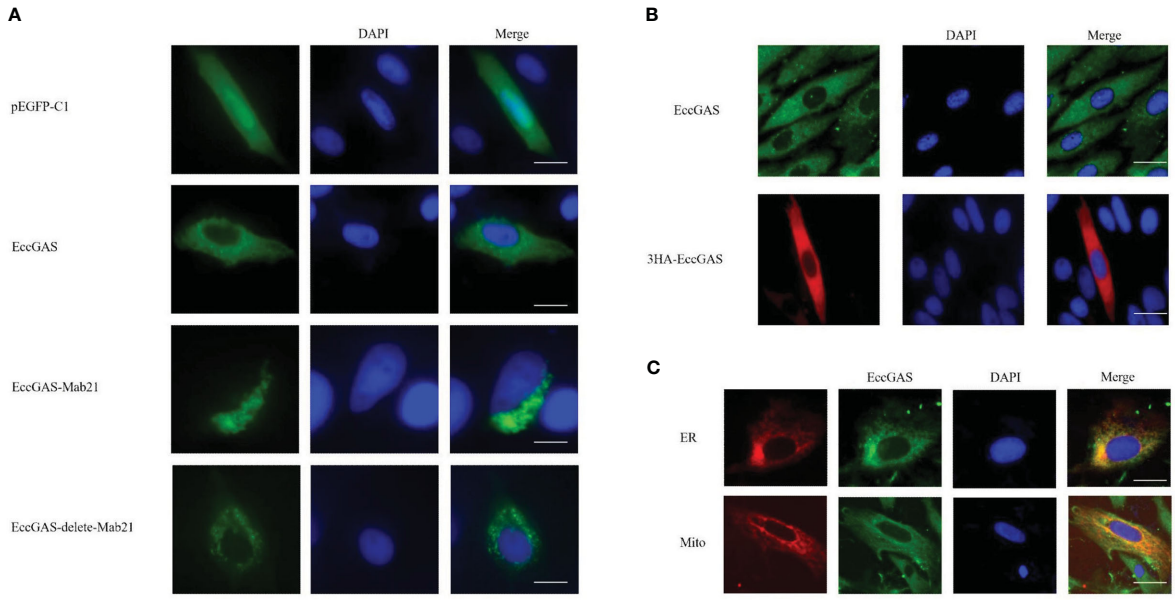

FIGURE 4
Cellular localization of EccGAS. **(A)** Subcellular localization of the EccGAS structural domain Mab21 and the deletion of the structural domain in GS cells. GS cells were transfected with pEGFP-C1, pEGFP-EccGAS, pEGFP-EccGAS-Mab21 and pEGFP-EccGAS-delete-Mab21 plasmids using Liposome 2000. After transfection for 24 h, the cells were fixed with 4% paraformaldehyde for 2 h at 25 °C, and were stained with DAPI and examined under confocal laser scanning microscopy. Scale bars shown as 20 μm. **(B, C)** Immunofluorescence and colocalization with endoplasmic reticulum and mitochondria. GS cells were inoculated and transfected with pcDNA3.1-EccGAS or pDsRed2-ER and pDsRed2-Mito, primary antibody with rabbit polyclonal anti-EccGAS antibody (1:150) or mouse monoclonal anti-HA antibody (1:150) incubated for 2 h at 25 °C and secondary antibody with FITC-conjugated goat anti-rabbit or goat anti-mouse (1:200). Subsequently, the cells were incubated for 1 h and examined by confocal microscopy. Scale bars are shown as 20 μm.

cGAS is a negative regulator of STING-mediated IFN response in grouper.

In mammals, only one type of cGAS is typically found and plays an important role in the activation of type I IFN (25, 26). In fish, due to genome duplication events (27), two paralogs of cGAS were found in grass carp and zebrafish (28, 29). However, only one cGAS has been recorded in grouper. Several reports indicate that the C-terminus is highly conserved among cGAS homologs from fish to humans, whereas the N-terminal exhibits great diversity in length and sequence among the cGAS homologs (30). BLAST analysis showed that EccGAS had the highest similarity (71.8%) with *Sebastes umbrosus* and the lowest similarity with mammals. SMART prediction revealed that EccGAS has a highly conserved Mab21 domain, suggesting that it belongs to the MAB21 family. This domain was originally discovered in *Cryptobacterium showyeri* and plays a key role in DNA binding of cGAS (31).

Recently, mammalian cGAS was identified as a ubiquitous sensor of cytosolic dsDNA. However, the role of fish cGAS in innate immune regulation has not been elucidated. Previous studies reported that cGAS is widely expressed in different tissues. cGAS was highly expressed in the spleen and intestines of pigs and chickens (32, 33). cGAS was also highly expressed in the liver and intestine of grass carp (34). The liver and gut are the major sites of interferon-stimulated gene (ISG) expression during viral infection in fish (29); therefore, cGAS may play an important role in antiviral innate immunity in fish. In the present study, EccGAS was predominantly expressed in the blood, skin, and gills. Therefore, we speculate that the high expression of cGAS at these sites may be a strategy to balance the antiviral immune response to avoid over-induction of ISGs. After SGIV infection, the expression of EccGAS increased with the time of virus infection, suggesting that EccGAS is involved in the innate immune response. Similarly, grass carp cGASa was up-regulated

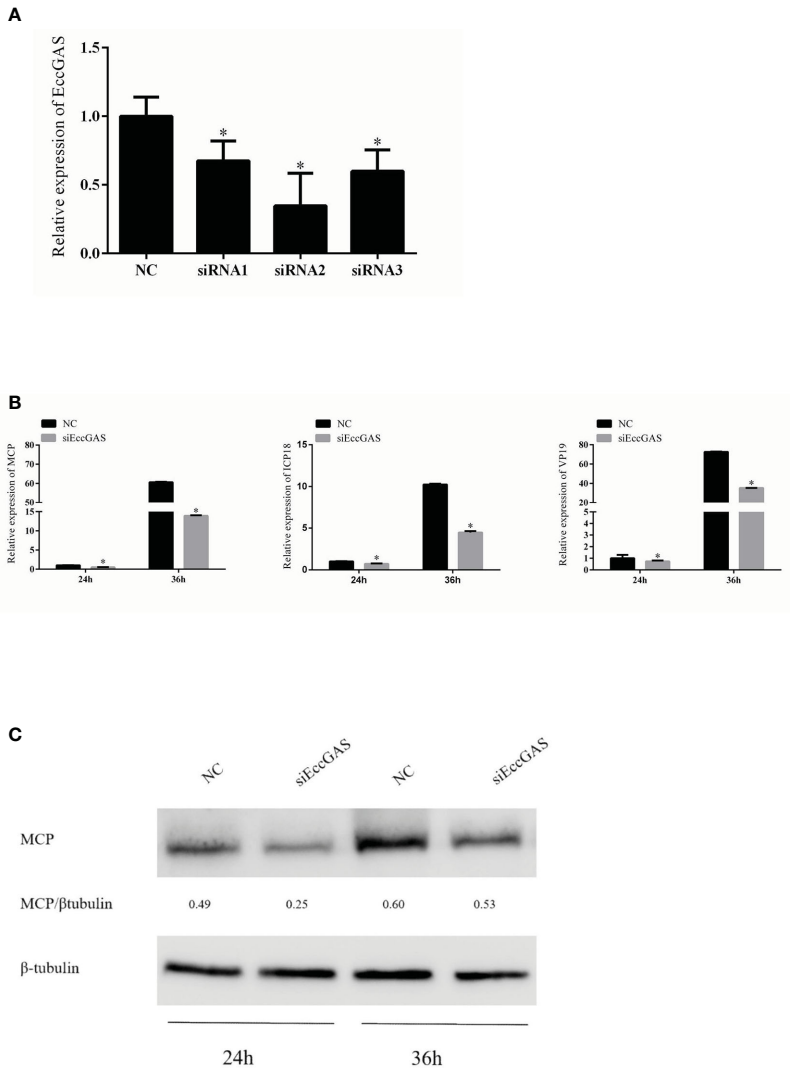

FIGURE 5
Effect of EccGAS silencing on viral replication. **(A)** Three siRNA sequences were designed based on the sequence of EccGAS and assayed for interference effects. **(B)** EccGAS knockout and control cells were infected with SGIV and collected at 24 h and 36 h to measure the relative expression levels of the viral genes. Relative expression levels of the viral genes were measured by qRT-PCR (n = 3, mean ± SD). *$P < 0.05$. **(C)** Silencing of EccGAS in GS cells infected with SGIV and protein samples collected for 24 h and 36 h. Expression of MCP protein was detected by western blotting. β-tubulin was used as an internal control. Quantity-one software was used to calculate band intensities and assess the MCP/β-tubulin ratio.

under GCRV or poly dA:dT treatment (28), and grass carp cGASb was up-regulated under GCRV, poly dA:dT or poly I:C treatment (28, 35). Meanwhile, the Japanese medaka cGAS was significantly induced under *Edwardsiella tarda* treatment (36).

Studies have reported that cGAS activates the intrinsic antimicrobial defenses of cells and promotes autophagic targeting of *Mycobacterium tuberculosis* (37). Mice deficient in cGAS or STING exhibited lower type I IFN levels and higher viral loads (38). In crucian carp and grass carp, CacGAS and CicGAS reduced the CiRIG-I-mediated cellular antiviral response and promoted viral replication (39). After silencing EccGAS, the transcription levels of SGIV genes of MCP, ICP18, and VP19 were significantly inhibited, and the levels of MCP protein were increased, suggesting that EccGAS may promote SGIV replication. Knockdown of EccGAS potentiated the transcription of endogenous IFN1, IFN2, PKR, Viperin, ISG15, ISG56, IL-1β, IL-8, and TNFα in GS cells. EccGAS also inhibited the activation of IFN1, ISRE, and NF-κB promoters in GS cells. These results suggested that EccGAS is involved in the regulation of virus-induced IFN signaling.

Many studies have shown that cGAS is distributed in the cytoplasm of humans, pigs, chickens, and grass carp (11, 32–34). In our study, EccGAS and Mab21 were uniformly distributed in the cytoplasm, suggesting that grouper cGAS may have similar functions to mammalian cGAS. Several studies have shown that STING proteins in the endoplasmic reticulum were activated to recruit and bind with MAVS located in the mitochondria (10, 40); thus, they recruit TBK1 and activate IRF3 and NF-κB phosphorylation. In our previous study, EcSTING is distributed in the endoplasmic reticulum (41). In the present study, EccGAS is highly distributed in both the endoplasmic reticulum and mitochondria. Therefore, EccGAS may play an important role in the innate immune system by interacting with STING. In grass carp, cGASL interacts with STING and inhibits STING-mediated activation of gcIFN1pro (34). EccGAS can inhibit EcSTING-induced activation of IFN1, ISRE and NF-κB promoter activities. Furthermore, EcCGAS can colocalize with EcSTING. EccGAS and EcSTING can also interact, which is independent of the Mab21 domain. These results suggest that EccGAS could interact with STING and inhibit STING-mediated activation of IFN.

As important components of the cGAS-STING signaling pathway, EcTBK1, EcTAK1, and EcIRF3 are expressed in grouper and play important roles in antiviral innate immunity (42–44). We then investigated the roles of EccGAS in EcTBK1-, EcTAK1-, and EcIRF3-mediated activation of IFN. The results showed that EccGAS inhibited the activities of IFN1, ISRE and NF-κB promoters induced

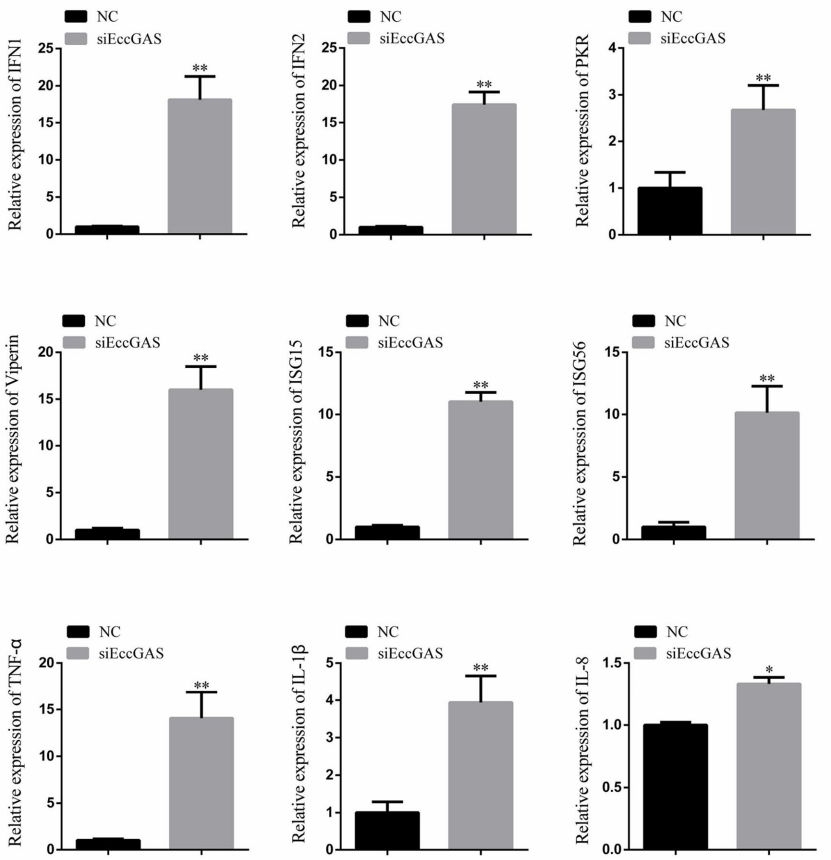

FIGURE 6
Silencing of EccGAS promoted the expression of host interferon-related genes and inflammation-related factors. Data are expressed as ratio to the control group. Error bars represent mean ± SD; *$P < 0.05$; **$P < 0.01$.

10.3389/fimmu.2023.1092824

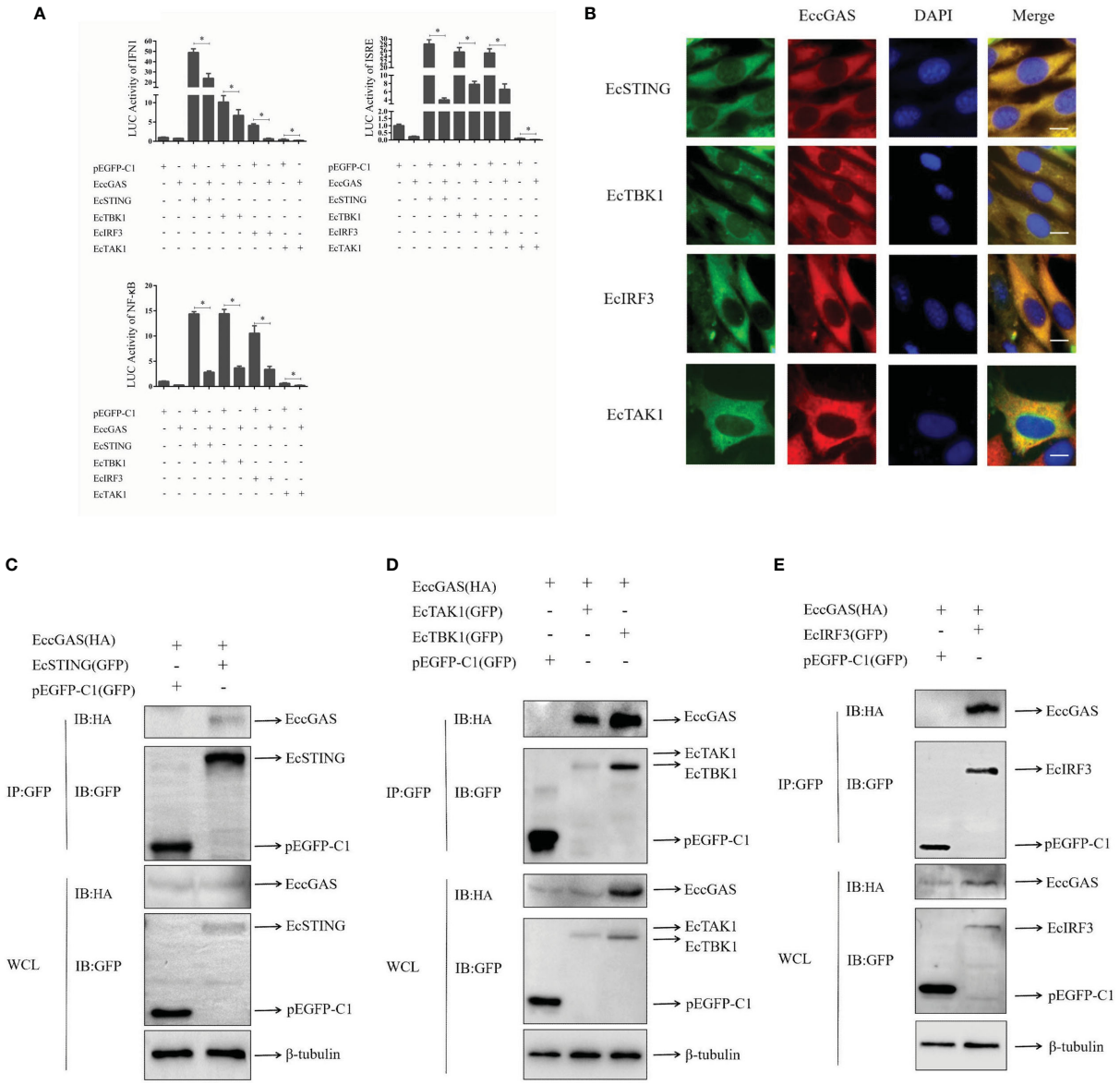

FIGURE 7
EccGAS negatively regulates EcSTING-mediated immune responses. **(A)** EccGAS inhibits the activation of IFN1, ISRE, and NF-κB promoter induced by EcSTING, EcTBK1, EcTAK1 and EcIRF3. pEGFP-EcSTING, pEGFP-EcTBK1, pEGFP-EcTAK1, and pEGFP-EcIRF3 were transfected into GS cells at a ratio of 1:1:1 with pEGFP-EccGAS and IFN1-Luc, respectively. Cells were harvested for detection of luciferase activity at 36 h after transfection.The error bars indicate mean ± SD; *P < 0.05. ISRE and NF-κB promoter activities were tested in the same way. **(B)** EccGAS colocalized with EcSTING, EcTBK1, EcTAK1 and EcIRF3, respectively. The plasmid pcDNA3.1-Red-EccGAS was co-transfected with pEGFP-EcTBK1, pEGFP-EcTAK1 and pEGFP-EcIRF3 in GS cells, respectively. Imaged by confocal microscopy, scale bars are shown at 20 μm. **(C–E)** EccGAS interacts with EcSTING, EcTBK1, EcTAK1 and EcIRF3, respectively. pEGFP-C1, pEGFP -EcSTING, pEGFP-EcTAK1, pEGFP-EcTBK1, and pEGFP-EcIRF3 were cotransfected with pcDNA3.1-EccGAS in GS cells, respectively. Samples were processed by immunoprecipitation and western blotting. β-tubulin was used as an internal control.

by EcTBK1, EcTAK1 and EcIRF3. Confocal microscopy showed that EcTBK1, EcTAK1, and EcIRF3 colocalized with EccGAS. Co-IP showed that EccGAS interacted with EcTBK1, EcTAK1, and EcIRF3. Thus, EccGAS inhibits STING-mediated interferon immune responses and interacts with STING, TAK1, TBK1, and IRF3.

In summary, a cGAS homolog of grouper (EccGAS), which contains a typical Mab21 structural domain, was identified for the first time. EccGAS was evenly distributed in the cytoplasm and partially co-located in the endoplasmic reticulum and mitochondria. EccGAS could promote SGIV replication. EccGAS negatively regulates EcSTING-mediated interferon immune responses and interacts with EcSTING, EcTAK1, EcTBK1, and EcIRF3. These findings contribute insights and methods for the prevention and treatment of viral infections.

Data availability statement

The original contributions presented in the study are included in the article/supplementary material. Further inquiries can be directed to the corresponding authors.

Ethics statement

The animal study was reviewed and approved by The Animal Care and Use Committee of College of Marine Sciences, South China Agricultural University.

Author contributions

Conceptualization, JW and QQ. Methodology, LZ. Software, LZ. Validation, XZ, JL and LX. Investigation, SK, JL, HC, MS, STW, ZX, SW. Writing-original draft preparation, LZ. Writing-review and editing, JW, QQ. Supervision, QQ. Funding acquisition, QQ, JW, SW. All authors have read and agreed to the published version of the manuscript.

Funding

This research was funded by the National Key Research and Development Program of China (2022YFD2400501), Key-Area Research and Development Program of Guangdong Province (2021B0202040002), Laboratory of Lingnan Modern Agriculture Project (NT2021008), the China Agriculture Research System of MOF and MARA(CARS-47-G16), the Agricultural Science and Technology Cooperation Project of Institute of New Rural Development of South China Agricultural University (2021XNYNYKJHZGJ042), and Open Fund of Guangdong Provincial Key Laboratory of Aquatic Animal Disease Control and Healthy culture (PBEA2020YB01).

Conflict of interest

The authors declare that the research was conducted in the absence of any commercial or financial relationships that could be construed as a potential conflict of interest.

Publisher's note

References

1. Qin QW, Chang SF, Ngoh-Lim GH, Gibson-Kueh S, Shi C, Lam TJ. Characterization of a novel ranavirus isolated from grouper epinephelus tauvina. *Dis Aquat Organ* (2003) 53:1–9. doi: 10.3354/dao053001

2. Morchikh M, Cribier A, Raffel R, Amraoui S, Cau J, Severac D, et al. HEXIM1 and NEAT1 long non-coding RNA form a multi-subunit complex that regulates DNA-mediated innate immune response. *Mol Cell* (2017) 67:387–99. doi: 10.1016/j.molcel.2017.06.020

3. Chen SN, Zou PF, Nie P. Retinoic acid-inducible gene I (RIG-i)-like receptors (RLRs) in fish: current knowledge and future perspectives. *Immunology* (2017) 151:16–25. doi: 10.1111/imm.12714

4. Yoneyama M, Onomoto K, Jogi M, Akaboshi T, Fujita T. Viral RNA detection by RIG-i-like receptors. *Curr Opin Immunol* (2015) 32:48–53. doi: 10.1016/j.coi.2014.12.012

5. Hoffmann HH, Schneider WM, Rice CM. Interferons and viruses: an evolutionary arms race of molecular interactions. *Trends Immunol* (2015) 36:124–38. doi: 10.1016/j.it.2015.01.004

6. Hemmi H, Takeuchi O, Kawai T, Kaisho T, Sato S, Sanjo H, et al. A toll-like receptor recognizes bacterial DNA. *Nature* (2000) 408:740–5. doi: 10.1038/35047123

7. Takaoka A, Wang Z, Choi MK, Yanai H, Negishi H, Ban T, et al. DAI (DLM-1/ZBP1) is a cytosolic DNA sensor and an activator of innate immune response. *Nature* (2007) 448:501–5. doi: 10.1038/nature06013

8. Miyashita M, Oshiumi H, Matsumoto M, Seya T. DDX60, a DEXD/H box helicase, is a novel antiviral factor promoting RIG-i-like receptor-mediated signaling. *Mol Cell Biol* (2011) 31:3802–19. doi: 10.1128/MCB.01368-10

9. Zhang Z, Yuan B, Bao M, Lu N, Kim T, Liu YJ. The helicase DDX41 senses intracellular DNA mediated by the adaptor STING in dendritic cells. *Nat Immunol* (2011) 12:959–65. doi: 10.1038/ni.2091

10. Unterholzner L, Keating SE, Baran M, Horan KA, Jensen SB, Sharma S, et al. IFI16 is an innate immune sensor for intracellular DNA. *Nat Immunol* (2010) 11:997–1004. doi: 10.1038/ni.1932

11. Sun L, Wu J, Du F, Chen X, Chen ZJ. Cyclic GMP-AMP synthase is a cytosolic DNA sensor that activates the type I interferon pathway. *Science* (2013) 339:786–91. doi: 10.1126/science.1232458

12. Gao P, Ascano M, Wu Y, Barchet W, Gaffney BL, Zillinger T, et al. Cyclic [G(2',5')pA(3',5')p] is the metazoan second messenger produced by DNA-activated cyclic GMP-AMP synthase. *Cell* (2013) 153:1094–107. doi: 10.1016/j.cell.2013.04.046

13. Ablasser A, Goldeck M, Cavlar T, Deimling T, Witte G, Rohl I, et al. cGAS produces a 2'-5'-linked cyclic dinucleotide second messenger that activates STING. *Nature* (2013) 498:380–4. doi: 10.1038/nature12306

14. Huang Y, Huang X, Yan Y, Cai J, Ouyang Z, Cui H, et al. Transcriptome analysis of orange-spotted grouper (Epinephelus coioides) spleen in response to Singapore grouper iridovirus. *BMC Genomics* (2011) 12:556. doi: 10.1186/1471-2164-12-556

15. Xu D, Wei J, Cui H, Gong J, Yan Y, Lai R, et al. Differential profiles of gene expression in grouper epinephelus coioides, infected with Singapore grouper iridovirus, revealed by suppression subtractive hybridization and DNA microarray. *J Fish Biol* (2010) 77:341–60. doi: 10.1111/j.1095-8649.2010.02676.x

16. Qin QW, Lam TJ, Sin YM, Shen H, Chang SF, Ngoh GH, et al. Electron microscopic observations of a marine fish iridovirus isolated from brown-spotted grouper, epinephelus tauvina. *J Virol Methods* (2001) 98:17–24. doi: 10.1016/s0166-0934(01)00350-0

17. Zhang X, Liu Z, Li C, Zhang Y, Wang L, Wei J, et al. Grouper TRADD mediates innate antiviral immune responses and apoptosis induced by Singapore grouper iridovirus (SGIV) infection. *Front Cell Infect Microbiol* (2019) 9:329. doi: 10.3389/fcimb.2019.00329

18. Wei J, Gao P, Zhang P, Guo M, Xu M, Wei S, et al. Isolation and function analysis of apolipoprotein a-I gene response to virus infection in grouper. *Fish Shellfish Immunol* (2015) 43:396–404. doi: 10.1016/j.fsi.2015.01.006

19. Sambrook JE, Maniatis TE, Fritsch EF. Molecular cloning: A laboratory manual. *2nd* ed (New York: Cold Spring Harbor Laboratory Press). (1989).

20. Li C, Wang L, Zhang X, Wei J, Qin Q. Molecular cloning, expression and functional analysis of Atg16L1 from orange-spotted grouper (Epinephelus coioides). *Fish Shellfish Immunol* (2019) 94:113–21. doi: 10.1016/j.fsi.2019.09.004

21. Li C, Liu J, Zhang X, Wei S, Huang X, Huang Y, et al. Fish autophagy protein 5 exerts negative regulation on antiviral immune response against iridovirus and nodavirus. *Front Immunol* (2019) 10:517. doi: 10.3389/fimmu.2019.00517

22. Li T, Chen ZJ. The cGAS-cGAMP-STING pathway connects DNA damage to inflammation, senescence, and cancer. *J Exp Med* (2018) 215:1287–99. doi: 10.1084/jem.20180139

23. Dhanwani R, Takahashi M, Sharma S. Cytosolic sensing of immuno-stimulatory DNA, the enemy within. *Curr Opin Immunol* (2018) 50:82–7. doi: 10.1016/j.coi.2017.11.004

24. Chen Q, Sun L, Chen ZJ. Regulation and function of the cGAS-STING pathway of cytosolic DNA sensing. *Nat Immunol* (2016) 17:1142–9. doi: 10.1038/ni.3558

25. Gratia M, Rodero MP, Conrad C, Bou SE, Maurin M, Rice GI, et al. Bloom syndrome protein restrains innate immune sensing of micronuclei by cGAS. *J Exp Med* (2019) 216:1199–213. doi: 10.1084/jem.20181329

26. Aarreberg LD, Esser-Nobis K, Driscoll C, Shuvarikov A, Roby JA, Gale MJ. Interleukin-1beta induces mtDNA release to activate innate immune signaling *via* cGAS-STING. *Mol Cell* (2019) 74:801–15. doi: 10.1016/j.molcel.2019.02.038

27. Taylor JS, Van de Peer Y, Braasch I, Meyer A. Comparative genomics provides evidence for an ancient genome duplication event in fish. *Philos Trans R Soc Lond B Biol Sci* (2001) 356:1661–79. doi: 10.1098/rstb.2001.0975

28. Xu X, Li M, Deng Z, Jiang Z, Li D, Wang S, et al. cGASa and cGASb from grass carp (Ctenopharyngodon idellus) play opposite roles in mediating type I interferon response. *Dev Comp Immunol* (2021) 125:104233. doi: 10.1016/j.dci.2021.104233

29. Liu ZF, Ji JF, Jiang XF, Shao T, Fan DD, Jiang XH, et al. Characterization of cGAS homologs in innate and adaptive mucosal immunities in zebrafish gives evolutionary insights into cGAS-STING pathway. *FASEB J* (2020) 34:7786–809. doi: 10.1096/fj.201902833R

30. Tao J, Zhang XW, Jin J, Du XX, Lian T, Yang J, et al. Nonspecific DNA binding of cGAS n terminus promotes cGAS activation. *J Immunol* (2017) 198:3627–36. doi: 10.4049/jimmunol.1601909

31. Civril F, Deimling T, de Oliveira MC, Ablasser A, Moldt M, Witte G, et al. Structural mechanism of cytosolic DNA sensing by cGAS. *Nature* (2013) 498:332–7. doi: 10.1038/nature12305

32. Wang J, Ba G, Han YQ, Ming SL, Wang MD, Fu PF, et al. Cyclic GMP-AMP synthase is essential for cytosolic double-stranded DNA and fowl adenovirus serotype 4 triggered innate immune responses in chickens. *Int J Biol Macromol* (2020) 146:497–507. doi: 10.1016/j.ijbiomac.2020.01.015

33. Wang J, Chu B, Du L, Han Y, Zhang X, Fan S, et al. Molecular cloning and functional characterization of porcine cyclic GMP-AMP synthase. *Mol Immunol* (2015) 65:436–45. doi: 10.1016/j.molimm.2015.02.002

34. Zhou Y, Lu L, Lu X, Li S, Zhang Y. Grass carp cGASL negatively regulates fish IFN response by targeting MITA. *Fish Shellfish Immun* (2019) 94:871–9. doi: 10.1016/j.fsi.2019.10.010

35. Zhou Y, Lu LF, Zhang C, Chen DD, Zhou XY, Li ZC, et al. Grass carp cGASL negatively regulates interferon activation through autophagic degradation of MAVS. *Dev Comp Immunol* (2021) 115:103876. doi: 10.1016/j.dci.2020.103876

36. Murakami S, Morimoto N, Kono T, Sakai M, Hikima JI. Molecular characterization and expression of the teleost cytosolic DNA sensor genes cGAS, LSm14A, DHX9, and DHX36 in Japanese medaka, oryzias latipes. *Dev Comp Immunol* (2019) 99:103402. doi: 10.1016/j.dci.2019.103402

37. Watson RO, Bell SL, MacDuff DA, Kimmey JM, Diner EJ, Olivas J, et al. The cytosolic sensor cGAS detects mycobacterium tuberculosis DNA to induce type I interferons and activate autophagy. *Cell Host Microbe* (2015) 17:811–9. doi: 10.1016/j.chom.2015.05.004

38. Cheng WY, He XB, Jia HJ, Chen GH, Jin QW, Long ZL, et al. The cGas-sting signaling pathway is required for the innate immune response against ectromelia virus. *Front Immunol* (2018) 9:1297. doi: 10.3389/fimmu.2018.01297

39. Zhou Y, Lei Y, Lu LF, Chen DD, Zhang C, Li ZC, et al. cGAS is a negative regulator of RIG-I-Mediated IFN response in cyprinid fish. *J Immunol* (2021) 207:784–98. doi: 10.4049/jimmunol.2100075

40. Kato H, Takahasi K, Fujita T. RIG-i-like receptors: cytoplasmic sensors for non-self RNA. *Immunol Rev* (2011) 243:91–8. doi: 10.1111/j.1600-065X.2011.01052.x

41. Huang Y, Ouyang Z, Wang W, Yu Y, Li P, Zhou S, et al. Antiviral role of grouper STING against iridovirus infection. *Fish Shellfish Immun* (2015) 47:157–67. doi: 10.1016/j.fsi.2015.09.014

42. Hu Y, Huang Y, Liu J, Zhang J, Qin Q, Huang X. TBK1 from orange-spotted grouper exerts antiviral activity against fish viruses and regulates interferon response. *Fish Shellfish Immunol* (2018) 73:92–9. doi: 10.1016/j.fsi.2017.12.010

43. Huang Y, Huang X, Cai J, OuYang Z, Wei S, Wei J, et al. Identification of orange-spotted grouper (Epinephelus coioides) interferon regulatory factor 3 involved in antiviral immune response against fish RNA virus. *Fish Shellfish Immunol* (2015) 42:345–52. doi: 10.1016/j.fsi.2014.11.025

44. Zhang L, Kang S, Chen H, Liao J, Sun M, Wu S, et al. The roles of grouper TAK1 in regulating the infection of Singapore grouper iridovirus. *Fish Shellfish Immunol* (2022) 124:164–73. doi: 10.1016/j.fsi.2022.04.006

frontiers | Frontiers in Immunology

TYPE Original Research
PUBLISHED 07 February 2023
DOI 10.3389/fimmu.2023.1124322

OPEN ACCESS

EDITED BY
Heng Chi,
Ocean University of China, China

REVIEWED BY
Changwei Shao,
Yellow Sea Fisheries Research Institute (CAFS), China
Qingguo Meng,
Nanjing Normal University, China

*CORRESPONDENCE
Yunji Xiu
yunji16@163.com

†These authors have contributed equally to this work and share first authorship

SPECIALTY SECTION
This article was submitted to Molecular Innate Immunity, a section of the journal Frontiers in Immunology

RECEIVED 15 December 2022
ACCEPTED 09 January 2023
PUBLISHED 07 February 2023

CITATION
Li Y, Su L, Liu X, Guo H, Zhou S and Xiu Y (2023) Immunity of turbot Induced by inactivated vaccine of *Aeromonas salmonicida* from the perspective of DNA methylation.
Front. Immunol. 14:1124322.
doi: 10.3389/fimmu.2023.1124322

Immunity of turbot Induced by inactivated vaccine of *Aeromonas salmonicida* from the perspective of DNA methylation

Yingrui Li†, Lin Su†, Xiaofei Liu, Huimin Guo, Shun Zhou and Yunji Xiu*

Institute of Marine Science and Engineering, Qingdao Agricultural University, Qingdao, China

Introduction: DNA methylation was one of the most important modification in epigenetics and played an important role in immune response. Since the introduction of *Scophthalmus maximus*, the scale of breeding has continued to expand, during which diseases caused by various bacteria, viruses and parasites have become increasingly serious. Therefore, the inactivated vaccines have been widely researched and used in the field of aquatic products with its unique advantages. However, the immune mechanism that occurred in turbot after immunization with inactivated vaccine of *Aeromonas salmonicida* was not clear.

Methods: In this study, differentially methylated regions (DMRs) were screened by Whole Genome Bisulfite Sequencing (WGBS) and significantly differentially expressed genes (DEGs) were screened by Transcriptome sequencing. Double luciferase report assay and DNA pull-down assay were further verified the DNA methylation state of the gene promoter region affected genes transcriptional activity after immunization with inactivated vaccine of *Aeromonas salmonicida*.

Results: A total of 8149 differentially methylated regions (DMRs) were screened, in which there were many immune-related genes with altered DNA methylation status. Meanwhile, 386 significantly differentially expressed genes (DEGs) were identified, many of which were significantly enriched in Toll-like receptor signaling pathway, NOD-like receptor signaling pathway and C-type lectin receptor signaling pathway. Combined analysis of WGBS results and RNA-seq results, a total of 9 DMRs of negatively regulated genes are located in the promoter region, including 2 hypermethylated genes with lower expression and 7 hypomethylated genes with higher expression. Then, two immune-related genes C5a anaphylatoxin chemotactic receptor 1-like (*C5ar1-Like*) and Eosinophil peroxidase-like *(EPX-Like)*, were screened to explore the regulation mechanism of DNA methylation modification on their expression level. Moreover, the DNA methylation state of the gene promoter region affected genes transcriptional activity by inhibiting the binding of transcription factors, which lead to changes in the expression level of the gene.

Discussion: We jointly analyzed WGBS and RNA-seq results and revealed the immune mechanism that occurred in turbot after immunized with inactivated vaccine of *A. salmonicida* from the perspective of DNA methylation.

KEYWORDS

DNA methylation, *Scophthalmus maximus*, *Aeromonas salmonicida*, inactivated vaccine, Whole Genome Bisulfite Sequencing, transcriptome sequencing

1 Introduction

Epigenetics, including DNA methylation, histone modification, and the regulation of noncoding RNAs, could cause heritable change in gene function without changes in DNA sequence, which produce heritable phenotypic changes eventually. As the most widely characterized epigenetic modification, DNA methylation was produced *via* 5-methylcytosine (5mC) binding a methyl group (CH_3) to the cytosine with the help of DNA methyltransferases (DNMTs) (1). DNA methylation has been widely reported to regulate gene expression, which was mostly conducted by inhibiting the binding of transcription factors on the promoters. Previous studies confirmed that DNA methylation was involved in immune response modulation. Abnormal DNA methylation was closely related to the occurrence and development of many cancers and immune diseases (2). With the development of research, the role of DNA methylation modification on immune process of aquatic animals has also been extensively explored. For example, *Ctenopharyngodon idella Retinoic acid-inducible gene I* (*CiRIG-I*) that was modified by methylation was extremely related with the resistance to grass carp reovirus (GCRV) and may be a negative regulator of *CiRIG-I* antiviral transcription (3). Besides, analysis of genome-wide DNA methylation in the spleen of resistant and susceptible Nile tilapia (*Oreochromis niloticus*) infected with *Streptococcus agalactiae* found that the methylation status was higher in the spleen samples from resistant fish than in the susceptible group (4). The above-mentioned studies indicate that DNA methylation participated in the immune defense mechanism of aquatic animals through regulating gene expression.

Scophthalmus maximus, an economically valuable flatfish, is widely distributed from Norway to the Mediterranean and China (5). The turbot is characterized with the advantages of low temperature resistance, grows fast and tastes delicious, which makes the turbot aquaculture industry develop rapidly (6). However, with the expansion of culture scale, the diseases caused by various bacteria, viruses, parasites and other pathogens have become more and more serious, causing great threats and destruction to the breeding industry. Compared with parasitic diseases and viral diseases, bacterial diseases have caused serious economic losses due to their wide spread, fast spread, strong pathogenicity and high mortality. For example, turbot could be infected by *A. salmonicida* to cause furunculosis (7), resulting in ulcerate in the infected skin area, oral bleeding, ulceration of fin edges and subcutaneous hemorrhage at the bottom, which eventually lead to the death of turbot. The traditional prevention and control methods of bacterial diseases in the turbot breeding process mainly relied on antibiotics and chemical drugs. However, the frequent use of these drugs could lead to the production of drug-resistant bacteria and immunosuppression of fish. In addition, the residual drugs existing in the turbot and in the aquaculture water might threaten human health. In fact, in the process of aquaculture, inactivated vaccines have been widely studied for its advantages such as high security, easy preparation and storage, non-pollution and easy production of combined vaccines or multivalent vaccines. On the one hand, vaccination significantly reduced the relative abundance values of potential opportunistic pathogens such as Aeromonas, Escherichia-Shigella, and Acinetobacter in teleost. On the other hand, combined with the enhancement of immune function after vaccination, inactivated Aeromonas vaccination had a protective effect against the pathogen infection of teleost. In the previous research, the relative immune protection rate of inactivated vaccine of *A. salmonicide* was up to 72.72% after inoculation with the *A. salmonicide* inactivated vaccine. Besides, turbot could achieve effective immune protection and induced immune responses by the immunization of inactivated vaccine of *A. salmonicida* (8).

The regulation of DNA methylation on immune response and the immune mechanism triggered by inactivated vaccines were widely reported in aquatic animals. For example, the immune-related genes of aquatic animals could be effectively activated by inactivated vaccines. Bacteria-mediated immune response was often closely related to aberrant DNA methylation. According to the current research, the potential link between vaccines and DNA methylation has emerged. Previous studies have found that Bacillus Calmette Guerin Vaccine injection induced a persistent change in DNA methylation, which was involved in antibacterial response (9) and pneumococcal vaccines leaded to changes in DNA methylation, which was associated with immune response activation (10). Balb/c mice vaccinated with a protective vaccine could cause changes in the DNA methylation level of gene promoters in livers, which ultimately improve the survival of the mice after infection with *P. chabaudi* (11). However, the effect of inactivated vaccines on DNA methylation patterns in fish and the mechanism by which DNA methylation was involved in the immune response *in vivo* were unclear.

In this study, whole-genome bisulfite sequencing (WGBS) and transcriptome sequencing were performed on turbot kidney tissue during the immunization of *A. salmonicide* inactivated vaccine, after which the expression changes of immune-related genes and genome-wide DNA methylation profiles were revealed. The sequencing results of the two groups were jointly analyzed and obtained differentially methylated regions (DMRs) and differentially expressed genes (DEGs) related to immune response. Besides, qRT-PCR and the double luciferase reporter assay was conducted and confirmed that DNA methylation inhibited gene expression by repressing the transcriptional activity of gene promoters. DNA pull down and Mass Spectrometry (MS) illustrated that DNA methylation effected binding of transcription factors to immune-related gene the and further influenced the expression of immune-related gene. In a word, our study revealed the potential relationship between DNA methylation levels and gene expression levels during the immunization of inactivated vaccines, which reveals the regulatory effect of inactivated vaccine on the immune mechanism of turbot from the perspective of DNA methylation, and provides new ideas for disease resistance breeding of turbot.

2 Methods and materials

2.1 Experimental fish, vaccine immunity and sample collection

Healthy turbot with an average weight of 80 ± 10 g was ordered from Haiyang Yellow Sea Aquatic Product Co.,Ltd., and kept in the laboratory until the inactivated vaccine of *A. salmonicida* was injected. Preparation of inactivated vaccines was performed as

described previously (8). The formaldehyde-inactivated vaccine of *A. salmonicida* (1×10^9 CFU/ml) was prepared at a concentration of 5‰ at 4 °C for 24 h. The turbot was immunized by intraperitoneal injected with 0.1 ml of inactivated vaccine (LD_{50} = 2.63×10^6 CFU/mL). Nine healthy turbot kidney tissue were randomly selected as the control group (named as NVSm) before vaccination, and nine challenged kidney tissue were randomly selected as the experimental group (named as AsVSm) after 30 days of inactivated vaccine immunization. In order to ensure the authenticity of the experimental results, we mixed the kidney tissue of 3 fish as a sample, and each group had 3 biological replicates. The tissue samples were quickly frozen in liquid nitrogen and then transferred to -80 °C refrigerator for storage.

2.2 Transcriptome sequencing and bioinformatics analysis

The TRIzol reagents were used to extract the total RNA from turbot kidney tissue in accordance with the manufacturer's instructions (Invitrogen, USA). After purification and quantification, a total of 1 μg of RNA per sample was utilized for the RNA sample preparations. Using the NEBNext® UltraTM RNA Library Prep Kit for Illumina® (NEB, USA) in accordance with the manufacturer's instructions, sequencing libraries were generated. The mRNA containing polyA tails was enhanced using oligo (dT) magnetic beads, and the resulting mRNA was then randomly interrupted in NEB Fragmentation Buffer. The M-MuLV reverse transcriptase system was used to create the first strand of cDNA using fragmented mRNA as a template and random oligonucleotides as primers. The RNA strand was then broken down using RNaseH, and the DNA polymerase I apparatus was utilized to create the second strand of cDNA utilizing dNTPs as the starting material. The end of the purified double-stranded cDNA was repaired, an A-tail was inserted, and a sequencing adaptor was attached. To create the library, the 250–300 bp cDNA was first screened with AMPure XP beads, followed by PCR amplification and further purification of the PCR products with AMPure XP beads. Use a Qubit2.0 Fluorometer to first measure the library, then diluted it to 1.5 ng/μL. The Agilent 2100 bioanalyzer then identified the insert size of the library and carried out qRT-PCR to precisely measure the library's effective concentration and guarantee the library's quality. After the library was validated, the various libraries were combined based on the intended offline data volume and effective concentration. Following that, Illumina sequencing was carried out, and a 150bp paired-end reading was produced.

Raw data were initially treated using in-house perl scripts to gain clean reads. The clean data for Q20, Q30, and GC content were evaluated simultaneously. The clear data with high-quality served as the foundation for all downstream studies. Hisat2 v2.0.5 was used to build index of the reference genome and aligned paired-end clean reads to the reference genome. The number of reads that were mapped to each gene was counted using FeatureCounts v1.5.0-p3. The length of each gene and the number of reads mapped to this gene were used to calculate the FPKM of each gene. Using the DESeq2 R software (1.16.1), differential expression analysis of two groups (three biological replicates per condition) was carried out. The Benjamini and Hochberg method for reducing the false discovery rate was used to modify the resulting *P*-values. Genes identified by DESeq2 as having differential expression were those with an adjusted *P*-value < 0.05. The clusterProfiler R package was used to implement the Gene Ontology (GO) enrichment analysis of DEGs, and gene length bias was addressed. GO terms were deemed to be substantially enriched by differentially expressed genes when the adjusted *P*-value < 0.05. Additionally, the statistical enrichment of differentially expressed genes in KEGG pathways was examined using the clusterProfiler R program. WGBS Library Construction, Sequencing and Bioinformatics Analysis

2.3 WGBS library construction, sequencing and bioinformatics analysis

Using the OMEGA Tissue DNA Kit, genomic DNA was extracted from the harvested kidney tissue and examined on agarose gels for deterioration and contamination. Using the Qubit® 2.0 Flurometer (Life Technologies, CA, USA) and NanoPhotometer® spectrophotometer (IMPLEN, CA, USA), respectively, the DNA purity and concentration were assessed. The subsequent procedure form a DNA library from the genomic DNA of the turbot kidney tissue. 5.2 μg of genomic DNA spiked with 26 ng of lambda DNA was sonicated into 200-300 bp-sized pieces using a Covaris S220. Then, using the EZ DNA Methylation-GoldTM Kit (Zymo Research, China), these DNA fragments were subjected to two rounds of bisulfite treatment. The resultant single-strand DNA fragments were then amplified using KAPA HiFi HotStart Uracil + ReadyMix (2X). The Agilent Bioanalyzer 2100 system was used to measure the insert size, and the DNA library concentration was measured using the Qubit® 2.0 Flurometer (Life Technologies, CA, USA) and quantitative PCR.

On the Illumina Hiseq 4000 platform, the library preparations were sequenced, and 150 bp paired-end reads were produced. The basis of information analysis is the quality control of the data to produce qualified data. Using FastQC (fastqc v0.11.5), basic statistics on the caliber of the raw readings were calculated. All following studies were dependent on the quality of the cleandata reads, which were first obtained by pre-processing the raw reads sequence using the parameters program. Basic statistics on the quality of the clean data readings were performed using FastQC. The reads to a reference genome were then carried out using Bismark software (version 0.16.3) (12). The two alignment procedures created a unique best alignment of sequence reads, and by comparing it to the typical genomic sequence, it is possible to deduce the methylation status of any place containing cytosine in the read. For IGV browser display, the methylation extractor data were converted to bigWig format (13). The sequence was then separated into several bins that were each 10 kb in size to determine the sequence's methylation level (14).

The DMRs were located using the DSS program (15). We define genes associated to DMRs as genes whose genomic area (from TSS to TES) or the promoter region (upstream 2kb from the TSS) coincides with DMRs in accordance with the distribution of DMRs in the genome. The GOseq R package (16), which corrects for gene length bias, was then used to execute Gene Ontology (GO) enrichment analysis of genes associated with DMRs. DMR-related genes were thought to substantially enrich GO terms with a corrected *P*-value < 0.05. The statistical enrichment of DMR-related genes in KEGG pathways was examined using KOBAS software (17).

2.4 Quantitative real-time PCR

Using the BIORAD CFX96 Touch fluorescence quantitative PCR equipment, qPCR was carried out using β-actin as an internal standard after the mRNA was transformed to cDNA using a PrimeScriptTM RT reagent Kit (TaKaRa, China) (Bio-Rad Laboratories, CA, USA). The reaction system was composed of 10 L of ddH2O, 5 L of TB Green Premix Ex Taq II (2×)(Takara, China), 0.4 L of a particular forward/reverse primer, and 0.8 L of cDNA. The primers were listed in Table 1. The following were the conditions for quantitative PCR: 95 °C for 30s, 35 cycle of 95 °C for 5 s and 60 °C for 1 min. The following conditions were used during the melting curve to confirm the amplicons' specificity: 95 °C for 10 s, 65 °C for 5 s and up to 95 °C at a rate of 0.5 °C/cycle. Each sample was made three biological replicates to reduce deviation. Using the $2^{-\triangle\triangle Ct}$ method, gene expression was evaluated in relation to β-actin expression.

2.5 Bisulfite sequencing PCR

The Tissue DNA Kit (OMEGA, China) was used to extract genomic DNA from kidney samples from the AsVSm group and NVSm group, each group contains 3 biological repetition. The genomic DNA of the three samples of the AsVSm group and the NVSm group were mixed in equal amounts (1 μg) and used as a template. According to the manufacturer's instructions, the EZ DNA Methylation-Gold^{TM} Kit (ZYMO RESEARCH, USA) was used for bisulfite modification. The reaction system was 50 μL including methylation modified DNA 4 μL, 10×EpiTaq PCR Buffer (Mg^{2+} free) 5 μL, 25mM $MgCl_2$ 6 μL, dNTP Mixture 4 μL, BSP forward/reverse primer 5 μL, TaKaRa EpiTaq HS (5 U/μL) (TaKaRa, China) 0.3 μL and ddH_2O. The BSP primers were produced using the MethPrimer program, which is available online at http://www.urogene.org/methprimer/. Table 1 contains the sequence details. The following steps were taken in order to execute the BS-PCR: 3 min at 98°C, then 35 cycles of 10 s of denaturation at 98°C, 30 s of annealing at 55°C, and 30 s of extension at 72°C, with a final extension at 72°C for 7 min. The PCR products were assembled on the pEASY-T1 Cloning Vector after being gel purified using the TaKaRa MiniBEST Agarose Gel DNA Extraction Kit Ver.4.0 (TaKaRa, China) (TransGen, China). The recombinant plasmid was transferred into *Trans1*-T1 competent cells (TransGen, China) according to the manufacturer's instructions of the *pEASY*-T1 Cloning Kit (TransGen, China). At least 10 different positive clones of each subject were randomly selected for sequencing. The final sequence results were processed by online BiQ-Analyzer (https://biq-analyzer.bioinf.mpi-inf.mpg.de/).

2.6 *In vitro* methylation modification and dual luciferase reporter assay

The dual luciferase reporter assay was used to verify the effect of DNA methylation modification on the gene expression. The DMR from the promoter region was amplified with different length to explore the effect of different promoter fragments on gene expression. Primer 5 was used to design specific primers (Table 1). The 12.5 μL 2×Taq PCR Mix, 2μL of DNA Template, 0.5μL of a particular forward/reverse primer, and 25μL of ddH_2O made up the PCR reaction system. The following steps were used to carry out the PCR: 5 min at 94°C, then 34 cycles of 30 s of denaturation at 94°C, 30 s of annealing at 55°C, and 1 min of extension at 72°C, with a final extension lasting 7 min at 72°C. The qualified target fragments were then retrieved after the 1% agarose gel electrophoresis was used to confirm the PCR results. The construction of dual luciferase reporter recombinant plasmid was constructed as follows: First of all, the restriction enzymes *Hind* III and *Kpn* I were used to double digest the target fragment and the empty pGL3-basic vector. Then, the recovered and purified vector and the target fragment were ligated at a molar ratio of 1:10 using T4 DNA ligase overnight at 16 °C to obtain recombinant plasmids. The recombinant plasmids were transferred into *Trans1*-T1 competent cells according to the previous method, and then the positive clones were selected and sequenced. The competent cells were cultivated overnight to amplify the recombinant plasmid verified by sequencing, and then extract the endotoxin-free recombinant plasmid according to the manufacturer's instructions of Endo-free Plasmid Mini Kit II(OMEGA, China).

CpG methyltransferase (M.Sss I) was used to modify recombinant plasmids methylation *in vitro*. M.Sss I can specifically mimic the modification mode of higher eukaryotic genomes, which will specifically modify the "CG" site on double-stranded DNA with the help of S-adenosylmethionine (SAM). The reaction system was as follows: 1 μg recombinant plasmid, 1 μL M.Sss I methylase, 2 μL SAM (1600 μM), 2 μL 10×NEBuffer 2 and added with Nuclease-free water for a final volume of 20 μL. Then, the reaction system was incubated at 37 °C for 1 h and terminated at 65 °C for 20 min. The *Hpa* II restriction endonuclease was used to verify the *in vitro* methylation modification of recombinant plasmid. The *Hpa* II can cut the unmethylated CG site, and the *in vitro* methylation modification of recombinant plasmid can be identified according to whether the digested product produces fragments of different lengths. The reaction system was as follows: 1 μL *Hpa* II, 1 μg recombinant plasmids with methylation modification, 5 μL 10×NEBuffer and added with ddH_2O for a final volume of 50 μL. Then, the restriction enzyme reaction system was incubated at 37 °C for 15 min and terminated at 80 °C for 20 min. The results of methylation modification *in vitro* were verified by 1% agarose gel electrophoresis.

In vitro, the recombinant plasmids methylation was transfected into HEK293 cells according to the instructions of the manufacturer of the Lipo6000^{TM} Transfection Reagent (Beyotime, China). The pRL-TK plasmid was used as an internal reference plasmid. The recombinant plasmids methylation and pRL-TK plasmid were co-transfected into HEK293T cells and cultured for 48h to detect the fluorescence activity. At the same time, the unmethylated recombinant plasmid was co-transfected with pRL-TK plasmid as a control, and the pGL3-basic empty vector was co-transfected with pRL-TK plasmid as a negative control, with 3 replicates in each group. According to the instructions provided by the manufacturer of the Dual-LumiTM II Luciferase Reporter Gene Assay Kit, Renilla luciferase and firefly luciferase activity were found in the cell lysate (Beyotime, China). The activity of renilla luciferase was used to standardize the activity of firefly luciferase in individual transfections.

TABLE 1 List of the primers used in this manuscript.

Gene name	Primer name	Primer sequence (5′ – 3′)	Assay
C5ar1-Like	*C5ar1-Like*-qRT-F	TCGTGGGATTCTTCCTCCCT	qPCR
	C5ar1-Like-qRT-R	GGAAGTCCAAGACGTGCAGA	
EPX-Like	*EPX-Like*-qRT-F	ACCAGAACCACTACAGCACG	
	EPX-Like-qRT-R	TTCAGCCGGAGAAGTGTGTC	
Smβ-actin	Smβ-actin-qRT-F	AATGAGCTGAGAGTTGCCCC	
	Smβ-actin-qRT-R	AGCTTGGATGGCAACGTACA	
C5ar1-Like	*C5ar1-Like*-BSP-F	ATTTTAATTTATAGGTTTAGTGGT	Bisulfite sequencing PCR
	C5ar1-Like-BSP-R	CAAATAAATATTATAAACAAATTATAAAC	
EPX-Like	*EPX-Like*-BSP-F	GTGTTTTTGTAAATTTTTTTAAAAA	
	EPX-Like-BSP-R	AAATTTCCTTTAACACAAAAAAAA	
C5ar1-Like	C5ar1-Like-F1	CGGGGTACCGAGTTTATATTTGGGA	Dual luciferase report assay
	C5ar1-Like-R1	CCCAAGCTTCTTACAGGCTCAGTGG	
	C5ar1-Like-F2	CGGGGTACCGTTGTAAGCAGGTTGTAG	
	C5ar1-Like-R2	CCCAAGCTTTATTTCAACTTACAGGCT	
EPX-Like	EPX-Like-F1	CGGGGTACCGCCATAAGCACAAGAAAACTCCC	
	EPX-Like-R1	CCCAAGCTTTGTCCCTGTAAACCCCCCCAAAA	
	EPX-Like-F2	CGGGGTACCTCAAAATGTAAGAAACTGCT	
	EPX-Like-R2	CCCAAGCTTGAAAATCTCATTACCAGTGT	
	EPX-Like-F3	CGGGGTACCCTTCACCTGGACAACCCT	
	EPX-Like-R3	CCCAAGCTTAAATCTCATTACCAGTGT	
pGL3-basic	RVP3	CTAGCAAAATAGGCTGTCCC	
	GLP2	CTTTATGTTTTTGGCGTCTTCCA	
SmC5ar1-Like-F	CGTGTGCGTCCGGGACGGGCGAAGTATAAAAACTCACCGAAAAGCAGAAGAGCTCCATAACTTCCAGCGAGCGGTGAGGACACAACGTTGACCG		DNA pull down
SmC5ar1-Like-R	CGGTCAACGTTGTGTCCTCACCGCTCGCTGGAAGTTATGGAGCTCTTCTGCTTTTCGGTGAGTTTTTATACTTCGCCCGTCCCGGACGCACACG		
met-SmC5ar1-Like methylation probes	CGTGTGCGTCCGGGACGGGCGAAGTATAAAAACTCACCGAAAAGCAGAAGAGCTCCATAACTTCCAGCGAGCGGTGAGGACACAACGTTGACCG		

10.3389/fimmu.2023.1124322

2.7 DNA pull down and mass spectrometry

The protein potentially binds to the DNA probe of DMR was identified by the DNA pull down technology. Using DMR of *C5ar1-Like* gene as the target sequence, the primers were designed to synthesize specific probes (control group, SmC5ar1-Like) and methylation probes (experimental group, met-SmC5ar1-Like) respectively, and labeled with biotin (Table 1). A 500 μL system comprised of 200 pmol biotin-labeled DNA, nucleic acid incubation buffer, and beaver magnetic beads was incubated for 1 hour at room temperature to create a DNA-magnetic bead combination. DNA-magnetic bead complex was magnetically separated after being rinsed twice with pre-cooled nucleic acid incubation buffer and protein incubation buffer. The HEK293 cell protein extract and the protein incubation buffer were formed into a 500 μL system and then incubated with DNA-magnetic bead complex at 4 °C overnight to form a protein-DNA-magnetic bead complex. The protein-DNA-magnetic bead complex was centrifuged and rinsed with pre-cooled protein incubation buffer. The precipitate added100 μL of protein elution buffer. Then, the mixture was heated for 5 min in a 95°C water bath and centrifuged at 12000 rpm for 15min. Supernatant was taken for WB and MS analysis.

The protein solution of met-SmC5ar1-Like experimental group and SmC5ar1-Like control group were subjected to MS respectively to screen the differential proteins, after which the different proteins in the experimental group was selected. The gel was chopped and decolorized with a decolorizing solution (50mM NH4HCO3 and ACN (1:1)), and was dehydrated by adding acetonitrile and vacuum dried. The proteins were then alkylated by 55 mM IAM in the darkroom for 1 hour after being reduced with DTT at 37°C for 1 hour. After dehydration, 0.01 μg/μL Trypsin was added and the mixture was reacted at 37 °C overnight and centrifuged to collect the supernatant of the enzymatic hydrolysis. The remaining micelles were added to acetonitrile and vortexed for 5 min, and centrifuged to collect the supernatant of the enzymatic hydrolysis. In addition, 0.1% FA was added to the remaining micelles and collected the supernatant of the enzyme hydrolysis. All supernatants were collected in the same centrifugal tube for vacuum lyophilization and stored at -20°C.The mobile phase A liquid (100% mass spectrometry water, 0.1% formic acid) and B liquid (80% acetonitrile, 0.1% formic acid) were prepared, respectively. The lyophilized powder were dissolved in 10 μL of A liquid, and centrifuged at 14000 g for 20 min at 4 °C. Then, 1 μg of the supernatant was collected for liquid quality detection. Data acquisition occurred by MS. The MS1 scans were acquired over a range of 300–1500 m/z at a resolution of 120 000 at m/z 200, with an automated gain control (AGC) target of 2×10^5, and a maximum ion injection time of 50 ms. The precursor ions were fragmented using the high energy collision cracking (HCD) method, and then detected by the secondary mass spectrometry. The MS2 precursors was set to 15000 (200 m/z) with the AGC of 5×10^4, and the maximum ion injection time of 45 ms. Precursors were fragmented by high-energy collision dissociation at a collision energy of 30% to generate the original data of the MS detection.

3 Result

3.1 Analysis of transcriptome sequencing results

Transcriptome sequencing was performed on the samples of the AsVSm group and the NVSm group to explore the impact of the inactivated vaccine of *A. salmonicida* on the immunity of turbot. The raw reads of the AsVSm group and NVSm group samples were filtered to obtain a total of 32.26G and 28.42G of clean reads, respectively (Table 2). Sequencing error rate distribution check results reflected that the quality of sequencing data meets the requirements of subsequent analysis. The clean reads were aligned to the reference genome, and the results were shown in Table 3. More than 91.11% of the clean reads were aligned to the reference genome in all 6 samples, and the unique alignment rate was between 88.62% and 89.2%. It shows that the tested species was consistent with the reference genome, the sequencing results were very accurate and credible. The gene expression level was compared to screen the DEGs after quantitative analysis of the gene expression level of the AsVSm group and NVSm group samples. A total of 14,995 differential genes were screened, including 14,432 genes shared by the AsVSm group and the NVSm group, as well as 317 unique genes of the AsVSm group and 246 unique genes of the NVSm group (Figure 1A). Then, using |log2 (FoldChange)|> 0 & padj <0.05 as the screening threshold, 386 significantly DEGs were screened, including 194 genes with up-regulation and 192 genes with down-regulation (AsVSm vs NVSm) (Figure 1B). The cluster analysis was carried out by taking the union of significantly DEGs of each comparison group, and the results were shown in Figure 1C. The gene expression patterns between biologically duplicated samples were very similar, while the expression patterns of DEGs

TABLE 2 The summary of sample data quality.

Sample	Raw_reads	Clean_reads	Clean_bases	Error_rate(%)	Q30(%)	GC_pct(%)
NVSm_1	52550964	51640142	7.75G	0.02	94.99	50.3
NVSm_2	78598000	77295498	11.59G	0.02	95.17	51.08
NVSm_3	61550178	60511312	9.08G	0.02	94.69	49.46
AsVSm_1	69415734	68532074	10.28G	0.02	94.72	50.74
AsVSm_2	72174578	71086780	10.66G	0.02	95.21	50.73
AsVSm_3	76623394	75498176	11.32G	0.02	95.08	50.69

10.3389/fimmu.2023.1124322

TABLE 3 The statistics of comparison samples and reference genomes.

Sample	NVSm_1	NVSm_2	NVSm_3	AsVSm_1	AsVSm_2	AsVSm_3
total_reads	51640142	77295498	60511312	68532074	71086780	75498176
total_map	47135061 (91.28%)	70962598 (91.81%)	55134031 (91.11%)	62631841 (91.39%)	65200633 (91.72%)	69181075 (91.63%)
unique_map	45814685 (88.72%)	68945071 (89.2%)	53651116 (88.66%)	60736194 (88.62%)	63292839 (89.04%)	67204082 (89.01%)

between the AsVSm group and NVSm group showed significant differences.

In order to discover the functions of DEGs and the interaction mechanism between DEGs, the functional enrichment analysis was carried out. The GO enrichment analysis showed that in terms of biological process, DEGs were significantly enriched in negative regulation of signal transduction, negative regulation of response to stimulus, immune response and immune system process. In terms of cellular component, DEGs were significantly enriched in extracellular region, transmembrane transporter complex and integral component of plasma membrane. In terms of molecular function, DEGs were significantly enriched in NAD^+ ADP-ribosyltransferase activity, transferase activity, transferring pentosyl groups, phosphofructokinase activity and carbohydrate kinase activity (Figure 1D). These results showed that the genes involved in immune response and signal transduction were enriched in turbot after immunization with inactivated vaccine of *A. salmonicida*, which promoted the activation of immune-related signaling pathways and the regulation of immune response. The results of KEGG enrichment showed that DEGs were significantly enriched in a number of immune-related signaling pathways, such as the TGF-beta signaling pathway, Toll-like receptor signaling pathway, NOD-like receptor signaling pathway and C-type lectin receptor signaling pathway (Figure 1E). To sum up, the result of functional enrichment analysis suggested that after immunization with inactivated vaccine of *A. salmonicida*, lots of the DEGs were enriched in a variety of immune-related signaling pathways.

3.2 Analysis of whole genome bisulfite sequencing

The inactivated vaccine of *A. salmonicida* was injected into turbot to induce the changes of methylation pattern, which were investigated by WGBS technology. The raw data of each sequenced sample was

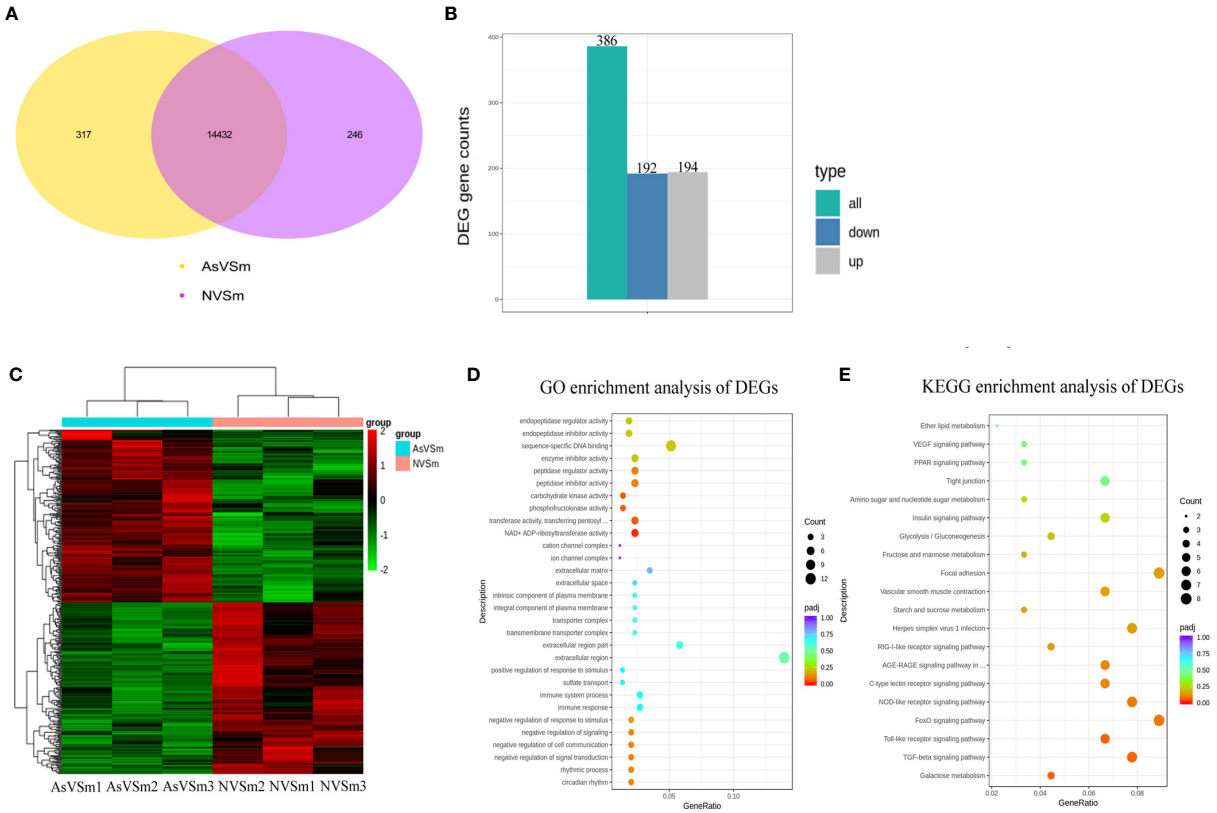

FIGURE 1
Screening of differential genes by transcriptome sequencing. **(A)** Venn diagram showed differential gene in the comparison of AsVSm and NVSm. **(B)** The bar chart showed statistics of the number of significantly DEGs. **(C)** Clustering heat map of significantly DEGs. The abscissa represents the sample name, and the ordinate represents the value of fpkm after homogenization. Red means high expression and green means low expression. **(D)** GO enrichment analysis of significantly DEGs. **(E)** Scatter plot of KEGG enrichment. The most significantly enriched top 20 pathways of significantly DEGs in AsVSm vs NVSm.

120 million. After sequencing and quality control, the average clean ratio (clean reads/raw reads) in the AsVSm and NVSm samples was 97.48% and 97.24%, respectively. The Q30 value of each sequenced sample was higher than 89.61%, indicating that the sequencing result was credible and subsequent bioinformatics analysis could be carried out. BS Conversion Rate measures the success rate of bisulfite treatment of samples, and the results show that the conversion rate of each sample is above 99.7% (Table 4). The clean reads of six samples (AsVSm1-3, NVSm1-3) were compared to the reference genome (Table 5), and the unique mapping ratio were between 77.79% and 80.15%, and the duplication rates were below 17.96%, indicating that the sequencing has high quality and reliability. At the genome-wide level, the proportion of methylated C sites (mC) in different sequence environments (CG, CHG, CHH) was less different in both the AsVSm group and NVSm group, in which the average percentage of mC, mCG, mCHG and mCHH were 11.33%, 85.63%, 0.16% and 0.15% in NVSm group and were 11.07%, 85.67%, 0.20%, 0.17% in AsVSm group, respectively. (Table 6). Besides, the proportion of methylated C sites (mCG) in the mC sequence environment, which the average percentage of mCG was 98.54% in NVSm group and 98.76% in AsVSm group, was also the highest among the four sequence environments. (Table 7). These results showed that the methylation in turbot kidney tissue was mainly concentrated in the CG sequence environment, and more than 85.5% of the CG in genome-wide level and more than 98.5% of the CG in mC sequence environment was modified by methylation.

The distribution of methylation levels in the upstream and downstream of regions was shown in Figure 2A. The highest average methylation level was shown in the CG sequence environment. In detail, the upstream2k regions were down-methylated compared to the of gene body regions, in which the methylation level gradually declined to a minimum at the transcription start site (TSS). Although the levels of CHG and CHH methylation were low in genome-wide level, the CHG and CHH methylation levels similar to mCG with consistent trends. Heat map analysis were used for more specific location analysis of the mCG

TABLE 4 Output Data quality of WGBS.

Sample name	Raw Reads	Clean Reads	Q30(%)	GC Content(%)	BS Conversion Rate(%)
NVSm_1	120000000	116381500	89.61	24.13	99.739
NVSm_2	120000000	116928214	90.1	23.5	99.755
NVSm_3	120000000	116755983	89.65	23.68	99.768
AsVSm_1	120000000	116236185	90.96	23.78	99.729
AsVSm_2	120000000	117169760	91.46	23.69	99.731
AsVSm_3	120000000	117543645	91.64	23.94	99.743

TABLE 5 Ratio of reads to the reference genome in WGBS.

Samples	Total reads	Mapped reads	Mapping rate(%)	Duplication rate(%)
NVSm_1	116381500	90533168	77.79	14.7
NVSm_2	116928214	91964040	78.65	10
NVSm_3	116755983	91373232	78.26	10.78
AsVSm_1	116236185	92128800	79.26	14.39
AsVSm_2	117169760	92610978	79.04	11.4
AsVSm_3	117543645	94211231	80.15	17.96

TABLE 6 Genome-wide methylation level.

Samples	mC percent(%)	mCpG percent(%)	mCHG percent(%)	mCHH percent(%)
NVSm1	11.05%	85.71%	0.17%	0.15%
NVSm2	11.01%	85.5%	0.15%	0.14%
NVSm3	11.04%	85.68%	0.16%	0.15%
AsVSm1	11.05%	85.64%	0.17%	0.16%
AsVSm2	11.08%	85.69%	0.21%	0.18%
AsVSm3	11.07%	85.68%	0.21%	0.18%

10.3389/fimmu.2023.1124322

TABLE 7 The number and percentage distribution of mC.

Samples	mC Quantity and Ratio	mCG Quantity and Ratio	mCHG Quantity and Ratio	mCHH Quantity and Ratio
AsVSm1	24553255(100%)	24227051(98.67%)	87507(0.35%)	238697(0.97%)
AsVSm2	24618989(100%)	24241083(98.46%)	105825(0.42%)	272081(1.1%)
AsVSm3	24607157(100%)	24239064(98.5%)	103954(0.42%)	264139(1.07%)
NVSm1	24557640(100%)	24246585(98.73%)	83991(0.34%)	227064(0.92%)
NVSm2	24479029(100%)	24187260(98.8%)	78507(0.32%)	213262(0.87%)
NVSm3	24541005(100%)	24238210(98.76%)	81627(0.33%)	221168(0.9%)

sequence environment (Figure 2B). The result showed that CG methylation levels were lowest in the regions of promoter and 5'UTR around TSS, which are similar results as for Figure 2A.

DSS software was used to identify differentially methylated domains. A total of 8,149 DMRs were obtained in in the AsVSm and NVSm groups, including 4,377 hypermethylated domains (AsVSm/NVSm) and 3,772 hypomethylated domains (AsVSm/NVSm). The promoter is a DNA sequence that RNA polymerase recognized, bound and transcribed, which is generally located upstream of the TSS. Therefore, the analysis of the DMRs in the promoter region is very important to explore the regulation of DNA methylation on gene expression. The statistics of DMRs related genes anchored in the promoter regions were performed, and the results were shown in Figure 2C. The DMRs in the promoter region mainly exist in the environment of CG sequence, and among them, there were 665 DMGs that were unique in CG sequence. This phenomenon indicated that in the promoter region, the occurrence of DNA methylation was mainly concentrated in the environment of the CG sequence. Heat map analysis showed the differences between DMGs among different groups (Figure 2D). In the CG sequence environment, the DMR methylation levels of the AsVSm group and the NVSm group were significantly different. In the CHG and CHH sequence environment, although the comparison between the AsVSm group and the NVSm group showed significant differences in some regions, due to the low overall methylation level, we mainly focused on the CG sequence environment for subsequent analysis.

GO and KEGG enrichment analysis of DMRs were carried out. The DMGs were most significantly enriched in biological processes, including immune system process and regulation of Wnt signaling (Figure 2E). Besides, The DMRs were significant enriched in the immune-related signaling pathways, such as MAPK signaling pathway, Wnt pathway, Focal adhesion, Adhesion junction

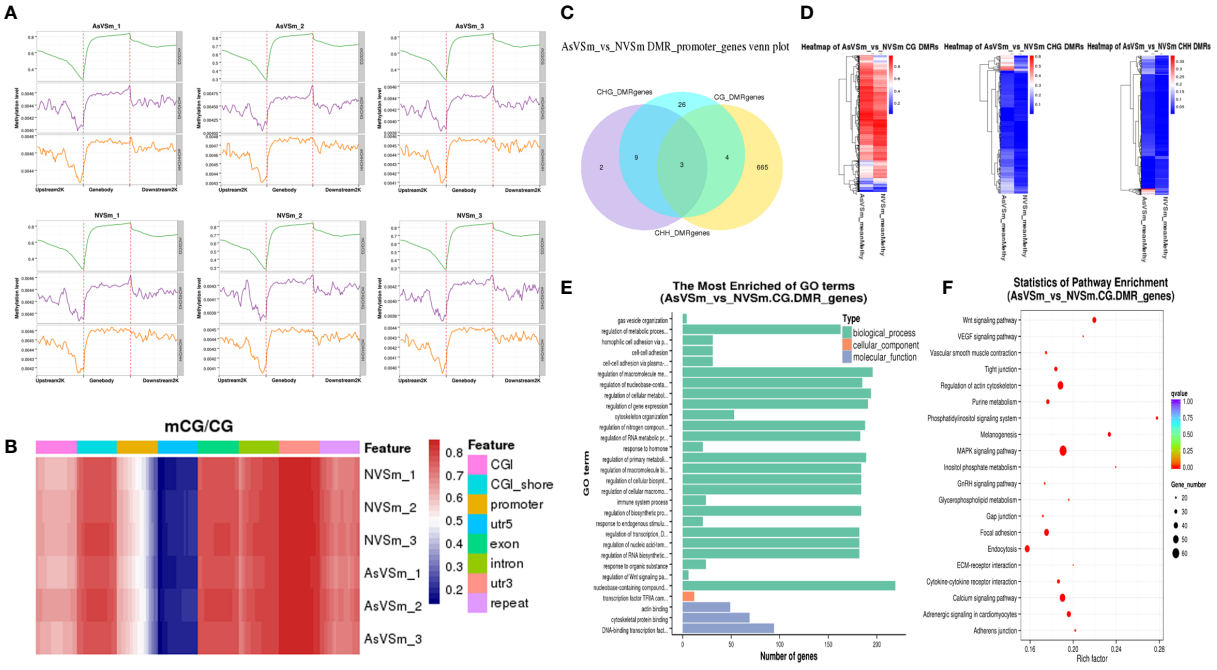

FIGURE 2
Screening of DMR and related genes by whole genome bisulfite sequencing. **(A)** The distribution of methylation level of samples at 2K upstream and downstream of gene region. **(B)** The results of thermographic analysis of methylation level of gene functional region in mCG sequence environment. **(C)** The number of intersections or unique gene sets of DMGs anchoring promoter regions in different sequence contexts (CG, CHG, CHH). **(D)** Clustering heatmap of DMR methylation levels in different sequence contexts (CG, CHG, CHH). **(E)** Go enrichment analysis of DMGs in the context of CG sequence. **(F)** The top 20 pathways significantly enriched for DMGs in the context of CG sequences.

(Figure 2F). The analysis results confirmed that turbot immunized with inactivated vaccine changed the function of many immune related genes by altering methylation level, which might played a role in the immune process by affecting the gene expression level.

3.3 Association analysis between WGBS and transcriptome sequencing

The expression level of DEGs was divided into four levels: none, low, medium, and high, and their corresponding methylation level in the CG sequence environment was calculated. The results showed that DEGs in the AsVSm group and the NVSm group had similar DNA methylation patterns. In the environment of CG sequence, there was a significant negative correlation between the methylation level and the expression level of DEGs, and the negative regulatory was more significant with the closer distance to the TSS site (Figure 3A). In a word, the expression of hypomethylated genes was increased and the expression of hypermethylated genes was decreased. The results of combined analysis of DMGs and DEGs were shown in Figure 3B. There were a total of 42 negative regulatory genes located in the gene body region, in which 9 genes were hypermethylated with down-regulated expression, 33 genes were hypomethylated with up-regulated expression. And there were a total of 9 negative regulatory genes located in the promoter region, in which 2 genes were hypermethylated with down-regulated expression, and 7 genes were hypomethylated with up-regulated expression. We focused on the overlapping genes in the promoter region for GO enrichment analysis, the results were shown in Figure 3C. The hypermethylated genes with lower expression were mainly enriched in terms related to transport and localization in biological processes, membrane part in cellular components, and enzymatic activity in molecular functions. The hypomethylated genes with higher expression were mainly enriched in terms related to cell death in biological processes, organelles in cellular components, and transmembrane transport in molecular functions. Besides, GO enrichment analysis found that there were only 5 hypomethylation-high expression genes in the promoter region, including Eosinophil peroxidase-like (*EPX-Like*), Angiopoietin-related protein 5-like, C5a anaphylatoxin chemotactic receptor 1-like (*C5ar1-Like*), Arginase-2 mitochondrial, Hypothetical protein. KEGG enrichment analysis showed that hypermethylated genes with lower expression and hypomethylated genes with higher expression were significantly enriched in different signaling pathways (Figure 3D). In particular, many hypomethylated genes with higher expression were enriched in immune-related pathways, such as TGF-beta signaling pathway, MAPK signaling pathway and NOD-like receptor signaling pathway. Therefore, further study will focus on hypomethylated genes with higher expression to study their immune regulatory mechanisms.

3.4 DNA methylation negatively regulates gene expression

According to combined analysis, we selected two immune-related genes, *C5ar1-Like* and *EPX-Like*, with lower methylation in the promoter region and higher expression level as candidate genes to verify the reliability of WGBS result and transcriptomic results. Real-time PCR was used to detect the relative expression levels of *C5ar1-Like* and *EPX-Like* genes in AsVSm group and NVSm group. Experimental results showed that the expression level of *C5ar1-Like* and *EPX-Like* genes in AsVSm group was significantly higher than that in NVSm group ($P < 0.05$) (Figure 4A, C). The verification results proved that the expression level of *C5ar1-Like* and *EPX-Like* genes was consistent with the transcriptome sequencing. BSP sequencing results showed that the average methylation level of the promoter

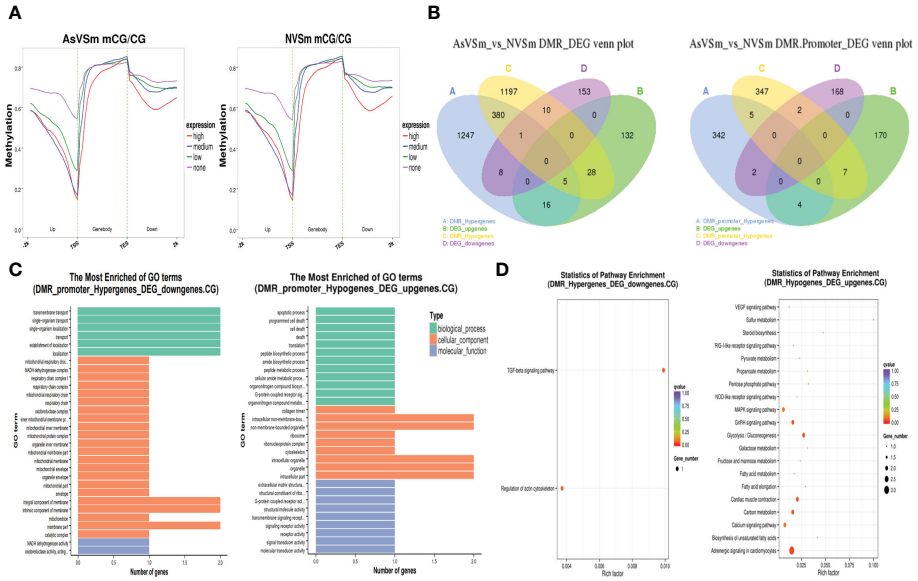

FIGURE 3
Regulation of methylation modification on gene expression level. **(A)** Distribution of gene expression level and methylation level in CG sequence environments. **(B)** Statistics of overlapping genes between DMGs and DEGs. **(C)** GO enrichment analysis of overlapping gene in promoter region CG sequence environment. **(D)** Significantly enriched pathway statistics for methylation negatively regulated genes.

10.3389/fimmu.2023.1124322

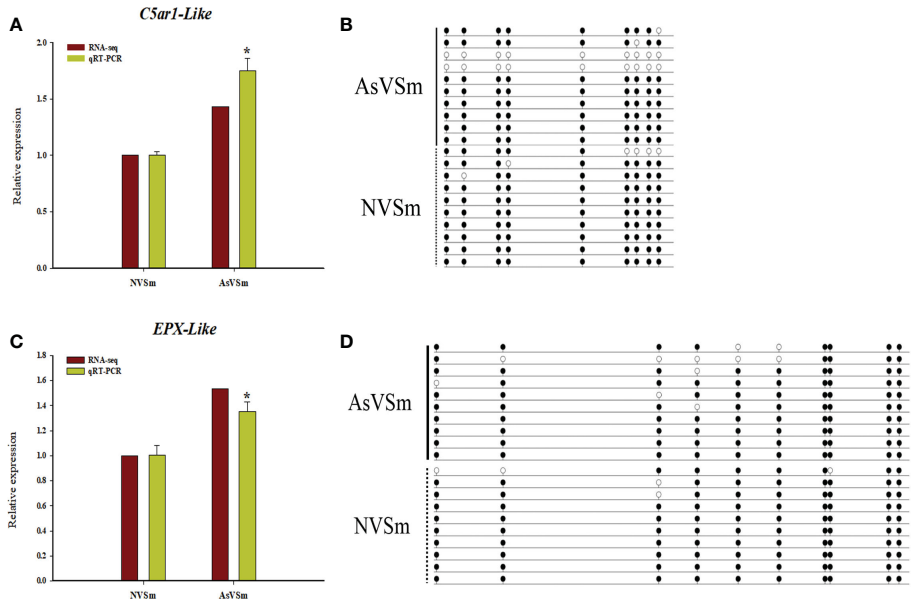

FIGURE 4
DNA methylation negatively regulated gene expression. **(A)** The relative expression levels of *C5ar1-Like* gene in AsVSm group and NVSm group. **(B)** The average methylation level of the promoter regions of the *C5ar1-Like* gene in AsVSm group and NVSm group. **(C)** The relative expression levels of *EPX-Like* gene in AsVSm group and NVSm group. **(D)** The average methylation level of the promoter regions of the *EPX-Like* gene in AsVSm group and NVSm group. *p<0.05.

regions of the *C5ar1-Like* and *EPX-Like* genes in the AsVSm group was significantly lower than that in the NVSm group, indicating that the BSP sequencing results were consistent with the WGBS sequencing results (Figure 4B, D). Methylation and expression level verification experiments demonstrated that the expression level of *C5ar1-Like* and *EPX-Like* genes was increased, and the methylation level was decreased after the turbot was injected with the inactivated vaccine of *A. salmonicida*.

3.5 The mechanism of DNA methylation inhibited immune-related gene expression

We constructed a series of dual luciferase reporter gene recombinant plasmids (pGL3-C5ar1-Like1, pGL3-C5ar1-Like2 and pGL3-EPX-Like1, pGL3-EPX-Like2, pGL3-EPX-Like3) around the DMR in the promoter regions of *C5ar1-Like* and *EPX-Like* genes to perform methylation modification *in vitro* (Figure 5A). The results of the dual luciferase report experiment showed that the effects of C5ar1-Like and EPX-Like promoter methylation on gene expression were similar to the above results (Figure 5B,C). One side, compared with the pGL3-basic empty vector (Control), the relative luciferase activity of the unmethylated recombinant plasmid (Unmethylation treatment) was significantly increased, proving that the recombinant promoter sequence has transcriptional activity. Other side, compared with the unmethylated recombinant plasmid, the relative luciferase activity of the methylated recombinant plasmid (Methylation treatment) was significantly reduced. In detail, the transcriptional activity of C5ar1-like2 was lower than that of C5ar1-like1, but the same trend was observed in C5ar1-like1 and C5ar1-like2, which indicates that methylation could effectively inhibit the transcriptional activity of both. Similarly, the transcriptional activity of EPX-Like2 was lower than that of EPX-Like2, but the same trend was observed in EPX-Like1 and EPX-Like2, which indicates that methylation could also effectively inhibit the transcriptional activity of both. In particular, no significant changes in luciferase activity of EPX-Like3 promoter were observed in unmethylation treatment group compared with control group, indicating EPX-Like3 transcription inactivation. Therefore, there was also no significant change in fluorescence activity of EPX-Like3 promoter in methylation treatment group compared with control group. These results showed that the transcriptional activity of EPX-Like3 promoter were not impacted by the methylated modification because of EPX-Like3 transcription inactivation. According to the experimental results, we speculated that the DNA methylation directly modified the promoter of *C5ar1-Like* and *EPX-Like* genes and inhibited the transcriptional activity of the promoters, thereby inhibited the expression of genes.

The interaction proteins with the probes of met-SmC5ar1-Like and the SmC5ar1-Like were screened by DNA pull down. The nuclear protein of HEK293T cells was extracted for sodium dodecyl sulfate Polycrylamide gel electrophoresis (SDS-PAGE) (Figure 5D) and DNA pull down (Figure 5E). Then, the interacting proteins with the met-SmC5ar1-Like and the SmC5ar1-Like were verified by WB. The silver staining results of enriched proteins showed that there were obvious different bands between the met-SmC5ar1-Like and the SmC5ar1-Like, which indicated that the interacting proteins with the met-SmC5ar1-Like had obvious changes compared with the SmC5ar1-Like (Figure 5E). Then, all ofthe interacting proteins with the met-SmC5ar1-Like and the SmC5ar1-Like were identified by MS. Using Homo sapiens database as a reference database, and the Proteome Discoverer 2.4 software was used to retrieve the database to determine the properties of interacting proteins. MS results showed that a total of 1,097 interacting proteins were identified, including 911 common interacting proteins, 159 the met-SmC5ar1-Like specific binding

10.3389/fimmu.2023.1124322

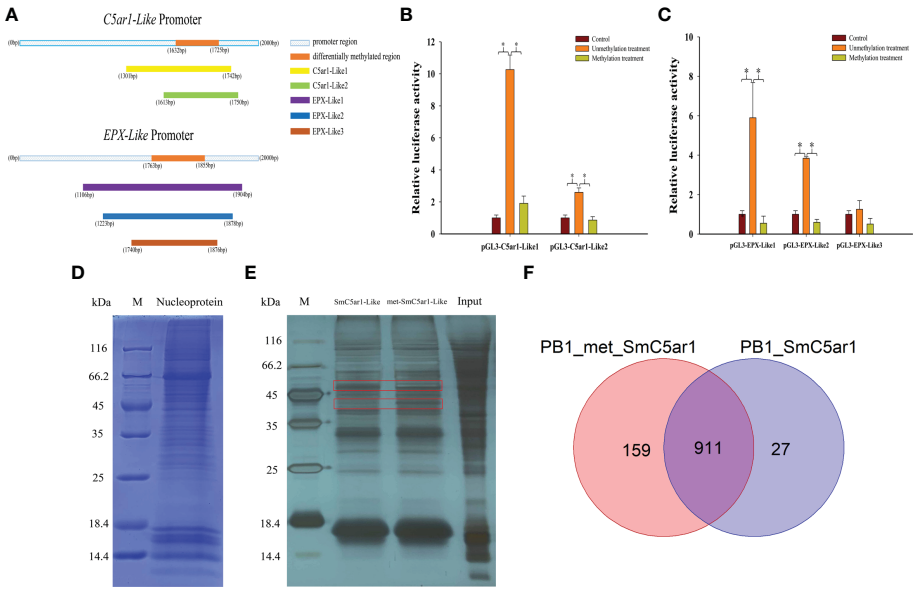

FIGURE 5
The mechanism of DNA methylation inhibited immune-related gene expression. **(A)** Amplified fragments from *C5ar1-Like* and *EPX-Like* promoter regions. The different colors represent different gene fragments. **(B)** Effects of DNA methylation modifications on fluorescent activity of *C5ar1-Like* promoter regions. **(C)** Effects of DNA methylation modifications on fluorescent activity of *EPX-Like* promoter regions.*Representative significant difference ($P < 0.05$). **(D)** Coomassie blue staining of HEK293T nuclear proteins. **(E)** Silver staining of DNA pull down enriched proteins. The red box shows the different bands between the met-SmC5ar1-Like and the SmC5ar1-Like. **(F)** Total number of the met-SmC5ar1-Like and the SmC5ar1-Like interacting proteins identified by MS.

proteins and 27 the SmC5ar1-Like specific binding proteins (Figure 5F). The relevant information of met-SmC5ar1-Like and SmC5ar1-Like specific binding proteins can be found in the Supplementary Table S1 and Supplementary Table S2, respectively. The result indicated that DNA methylation effected binding of the interaction proteins to the promoter region of SmC5ar1-Like and further influenced the gene expression and immune responses.

4 Discussion

DNA methylation was generally considered to have a regulatory effect on gene expression. Therefore, the combined analysis of WGBS and transcriptome sequencing has been widely conducted in the related research of mammal (18, 19). Besides, this combined analysis also has been widely reported in aquatic animals. In growth and development, RNA-seq and WGBS sequencing results association analysis was conducted in common carp, and the results showed that the expression levels of PUFA-related genes in muscle tissue were significantly correlated with their methylation status (20). However, this research model has hardly been applied in the immune response of turbot. In this study, the combined analysis of WGBS and transcriptome sequencing was used for the first time to explore the DNA methylation pattern and gene expression pattern of in kidney tissue of control and inactivated vaccine-infected turbot. We found no significant changes in the genome-wide DNA methylation pattern in the kidney tissue of turbot after immunization with inactivated vaccine of *A. salmonicida*. However, analysis of the WGBS results revealed a total of 4,377 hypermethylated domains and 3,772 hypomethylated domains in the AsVSm group. This phenomenon reflected that the change of DNA methylation pattern of AsVSm group samples was not the change of overall DNA methylation level, but the change of DNA methylation level of a large number of genes. In general, DNA methylation was thought to occur universally in vertebrates, and CG sites were hypermethylated in genome-wide, also in turbot. DNA methylation was rare in the context of CHG and CHH sequences and was only present in some specialized tissues, such as the brain and embryonic stem cells (21, 22), speculating that CHG and CHH methylation patterns may play a role in special tissues. Our data showed that in the AsVSm group and the NVSm group, methylated C sites accounted for about 11% of the total C sites, mCG accounted for about 98% of the total methylated C sites, and mCG accounted for about 85% of the total CG sites. Combined with the results of gene methylation level distribution, it was not difficult to find that mCG was mainly distributed in the genebody and its downstream 2K region, and the methylation level was low in the promoter region, especially in the region near the TSS. Obviously, most of the CG sites near TSS were not methylated. This situation might be due to the distribution of many CpG islands (CGI) with high CpG sequence density in the promoter region. According to statistics, about 70% of vertebrate annotated gene promoters are related to CGI (23, 24) and CG sites in CGI are generally in a non-methylated state, while CG sites located outside CGI are more easily modified by methylation, so the methylation level of promoter regions was significantly lower than that of other gene functional elements (25). When CGI undergo methylation modification, the methylation level of promoter region changes and generally accompanied by the inhibition of gene transcription, resulting in gene silencing (26, 27). The distribution of upstream and downstream methylation levels of genes indicated high methylation levels in this genomic region, which

is common in mammalian, especially in aquatic animals, and negatively regulated the level of gene expression (28, 29). These results indicated that the spontaneous DNA methylation pattern in turbot was similar to other species, indicating that the DNA methylation patterns among vertebrates are relatively conserved to a certain extent.

In addition, the injection of inactivated vaccine of *A. salmonicida* changed the methylation level of several genes in turbot kidney tissue. It was found from the WGBS results that many DMGs were significantly enriched in multiple immune-related pathways, such as MAPK signaling pathway, Wnt signaling pathway. Among them, MAPK signaling pathway plays a key role in apoptosis and the interaction between bacteria and host in cancer and immune system (29, 30). At the same time, a large number of immune-related DEGs were screened and analyzed from the transcriptome sequencing results. Multiple immune related DEGs, such as Toll-like receptor 7 (TLR7), transcription factor activator protein 1 (AP-1), Signal transducer and activator of transcription (STAT), Tumor necrosis factor receptor superfamily member 5 (TNFSF5), Mitogen-activated protein kinase 14A (MAPK14A) and Anthrax toxin receptor 1 (Antxr1), were significantly enriched in multiple immune-related pathways, including the two most significant pathways, Toll-like receptor signaling pathway and NOD-like receptor signaling pathway. Toll-like receptor (TLR) family was an important pathogen-related molecular pattern recognition receptor, which could activate downstream NF-κB and mediated the expression of transcription factor AP-1 to induce the expression of inflammatory cytokines such as tumor necrosis factor, interleukins, and interferon, triggering inflammatory response and playing an important role in immune response (31–33). NOD-like receptor family could recognized pathogen-mediated damage signals and activated NF-κB and MAPK signaling pathways to participate in inflammatory and immune responses (34). In general, after immunization with inactivated vaccine, the changes of methylation level modified expression level of immune-related genes, and finally triggered the immune response in turbot.

Specific relationships between inactivated vaccines-mediated DNA methylation and immune responses were demonstrated by combined analysis of WGBS and RNA-seq. Two immune-related negative regulatory genes, *C5ar1-Like* and *EPX-Like*, were screened from the immune-related genes in the combined analysis of DMRs-DEGs. C5a anaphylatoxin as a potent soluble mediator triggered chemotactic inflammation and the innate immune response *via* effecting inflammatory cell chemotaxis, chemokine release, phagocytosis as well as recruiting neutrophils and macrophages (35, 36). As a specific receptor of C5a, C5ar could cause pro-inflammatory activation after specific binding with C5a in grass carp and zebrafish (37, 38). Studies have shown that in the vaccinated rainbow trout, the expression of C5ar gene was up-regulated and enhance the binding of C5ar to C5a, inducing chemotactic response in granulocytes and immune response in response to *Yersinia ruckeri* (39). Eosinophil peroxidase (EPX) as a major cationic protein found in immune cell of human and mouse was highly conserved (40). In fish, EPX has been reported that was a vital component of the immune system of starry flounder (*Platichthys stellatus*), showing significant antibacterial and antiviral activity against *Streptococcus parauberis* and viral *haemorrhagic septicaemia* virus infection (41). In this study, the methylation level of *C5ar1-Like* gene and *EPX-Like* gene in the AsVSm group were significantly lower than that in the NVSm group, and the expression level in the AsVSm group was significantly higher than that in the NVSm group. Therefore, we inferred that DNA methylation was very likely to negatively regulate the expression of the *C5aR1-Like* and *EPX-Like* gene. In order to accurately verify the methylation modification site in the promoter region of the *C5aR1-Like* and *EPX-Like* gene, the dual-luciferase reporter assay was conducted. The results showed that methylation modification significantly inhibited the fluorescent activity of *C5aR1-Like* and *EPX-Like* in the promoter region. Meanwhile, the methylation modification of the *EPX-like* promoter region significantly reduced its expression level. These finding confirmed that DNA methylation directly modified the promoter of *C5ar1-Like* and *EPX-Like* genes and might inhibit the transcriptional activity of the promoters, thereby inhibited the expression of genes.

In order to prove that DNA methylation modification regulated gene expression by affecting transcription factor binding, the differential binding proteins of *C5ar1-Like* gene promoter were identified and screened by DNA pull down and MS. We found that compared with met-SmC5ar1-Like, SmC5ar1-Like has 27 unique interacting proteins, indicating that these proteins were unable to bind to the *C5ar1-Like* promoter after DNA methylation modification. These specific binding transcription factors included transcription-related transcription factors, translation-related transcription factors, signaling-related transcription factors, and also included some immune-related transcription factors such as eukaryotic translation initiation factor 2B (eIF-2B), talin-1 (TLN1), immunoglobulin heavy constant mu (IGHM). Among them, eIF-2B could affect the initiation phase of mRNA translation and was essential for modulating white matter disease in zebrafish (42). TLN1 could induce heart disease *via* suppressing the PI3K/AKT signaling pathway in zebrafish (43). The overexpression of IGHM could activate the immune response during bacterial and parasite infection in *Labrus bergylta* (44). The absence of these transcription factors greatly affected the immune response. Therefore, DNA methylation effected binding of transcription factors to the gene promoter regions and further influenced the transcription factors to regulate immune response.

In conclusion, a number of DNA methylation and the gene expression in turbot kidney tissue was changed after vaccination with inactivated vaccine of *A. salmonicida*. In addition, the result of dual luciferase reporting experiment and DNA pull down confirmed that DNA methylation modification in gene promoter region can affect gene expression *via* inhibiting the binding of transcription factors with gene promoter region. Our results reveal that inactivated vaccine affected the level of DNA methylation and gene expression in turbot kidney tissue, which explored the potential application of DNA methylation in turbot resistance breeding, and provided a new idea for genetic improvement of turbot.

Data availability statement

The datasets presented in this study can be found in online repositories. The names of the repository/repositories and accession number(s) can be found below: https://doi.org/10.6084/m9.figshare.21821160.v1.

Ethics statement

All fish experimental procedures were carried out in accordance with the National Institutes of Health's Guide for the Care and Use of Laboratory Animals, as implemented by Qingdao Agricultural University. The convention has been ratified by the IACUC Committee on the Ethics of Animal Experiments at Qingdao Agricultural University (Institutional Animal Care and Use Committee).

Author contributions

YX contributed to conception and design of the study. YL analyzed the data, and drafted manuscript. LS provided helpful discussions, XL and HG organized the database. SZ commented on the manuscript. All authors contributed to manuscript revision, read, and approved the submitted version.

Funding

These studies were supported by National Natural Science Foundation of China (No. 32002421), the Advanced Talents Foundation of QAU (Grant No. 6651118016), Fish Innovation Team of Shandong Agriculture Research System (SDAIT-12-06), Aquatic Animal Immunologic Agents Engineering Research Center of Shandong Province, "First class fishery discipline" programme in Shandong Province.

Conflict of interest

The authors declare that the research was conducted in the absence of any commercial or financial relationships that could be construed as a potential conflict of interest.

Publisher's note

Supplementary material

The Supplementary Material for this article can be found online at: https://www.frontiersin.org/articles/10.3389/fimmu.2023.1124322/full#supplementary-material

References

1. Shi G, Feng J, Jian LY, Fan XY. DNA Hypomethylation promotes learning and memory recovery in a rat model of cerebral Ischemia/Reperfusion injury. *Neural Regeneration Res* (2023) 18(4):863–8. doi: 10.4103/1673-5374.353494

2. Zhang L, Lu Q, Chang C. Epigenetics in health and disease. *Adv Exp Med Biol* (2020) 1253:3–55. doi: 10.1007/978-981-15-3449-2_1

3. Shang X, Wan Q, Su J, Su J. DNA Methylation of cirig-I gene notably relates to the resistance against gcrv and negatively-regulates mrna expression in grass carp, ctenopharyngodon idella. *Immunobiology* (2016) 221(1):23–30. doi: 10.1016/j.imbio.2015.08.006

4. Hu Q, Ao Q, Tan Y, Gan X, Luo Y, Zhu J. Genome-wide DNA methylation and rna analysis reveal potential mechanism of resistance to streptococcus agalactiae in gift strain of Nile tilapia (*Oreochromis niloticus*). *J Immunol (Baltimore Md 1950)* (2020) 204 (12):3182–90. doi: 10.4049/jimmunol.1901496

5. Pereiro P, Figueras A, Novoa B. Turbot (*Scophthalmus maximus*) vs. *Vhsv (Viral Hemorrhagic Septicemia Virus): A Review. Front Physiol* (2016) 7:192. doi: 10.3389/fphys.2016.00192

6. He X, Song X, Cao H, Zhou Q, Zhang J, Yue H, et al. Glaesserella parasuis induces il-17 production might through pkc-Erk/Mapk and Iκb/Nf-κb signaling pathways. *Veterinary Microbiol* (2022) 273:109521. doi: 10.1016/j.vetmic.2022.109521

7. Liu X, Wang B, Gao C, Xue T, Liu Z, Su B, et al. Characterization and the potential immune role of class a scavenger receptor member 4 (Scara4) in bacterial infection in turbot (*Scophthalmus maximus l.*). *Fish shellfish Immunol* (2022) 120:590–8. doi: 10.1016/j.fsi.2021.12.041

8. Huimin; G, Yuanyuan; D, Hao; W, Xujia; Z, Yunji; X, Shun Z. Preparation of *Aeromonas salmonicida* inactivated vaccine and test of its immunological efficacy in *Scophthalmus maximus*. *J Fisheries China* (2021) 45(9):1574–83. doi: 10.11964/jfc.20210612932

9. Ansell BRE, Bahlo M, Bannister S, Kim B, Domínguez-Andrés J, Vlahos A, et al. Neonatal bcg vaccination is associated with a long-term DNA methylation signature in circulating monocytes. *Sci Adv* (2022) 8(31):eabn4002. doi: 10.1126/sciadv.abn4002

10. Fairfax BP, Martinon-Torres F, Pischedda S, O'Connor D, Pollard AJ, Salas A, et al. Changes in epigenetic profiles throughout early childhood and their relationship to the response to pneumococcal vaccination. *Clin Epigenet* (2021) 13-25(1):29. doi: 10.1186/s13148-021-01012-w

11. Al-Quraishy S, Dkhil MA, Abdel-Baki AS, Ghanjati F, Erichsen L, Santourlidis S, et al. Protective vaccination and blood-stage malaria modify DNA methylation of gene promoters in the liver of Balb/C mice. *Parasitol Res* (2017) 116(5):1463–77. doi: 10.1007/s00436-017-5423-0

12. Farrell C, Thompson M. Bisulfite bolt: A bisulfite sequencing analysis platform. *GigaScience* (2021) 10(5):1–8. doi: 10.1093/gigascience/giab033

13. Langmead B, Salzberg SL. Fast gapped-read alignment with bowtie 2. *Nat Methods* (2012) 9(4):357–9. doi: 10.1038/nmeth.1923

14. Lister R, Mukamel EA, Nery JR, Urich M, Puddifoot CA, Johnson ND, et al. Global epigenomic reconfiguration during mammalian brain development. *Sci (New York NY)* (2013) 341(6146):1237905. doi: 10.1126/science.1237905

15. Park Y, Wu H. Differential methylation analysis for bs-seq data under general experimental design. *Bioinf (Oxford England)* (2016) 32(10):1446–53. doi: 10.1093/bioinformatics/btw026

16. Young MD, Wakefield MJ, Smyth GK, Oshlack A. Gene ontology analysis for rna-seq: Accounting for selection bias. *Genome Biol* (2010) 11(2):R14–26. doi: 10.1186/gb-2010-11-2-r14

17. Wang LJ, Qiu BQ, Yuan MM, Zou HX, Gong CW, Huang H, et al. Identification and validation of dilated cardiomyopathy-related genes *Via* bioinformatics analysis. *Int J Gen Med* (2022) 15:3663–76. doi: 10.2147/ijgm.s350954

18. Zhang D, Wu S, Zhang X, Ren S, Tang Z, Gao F. Coordinated transcriptional and post-transcriptional epigenetic regulation during skeletal muscle development and growth in pigs. *J Anim Sci Biotechnol* (2022) 13(1):146–60. doi: 10.1186/s40104-022-00791-3

19. Ju Z, Jiang Q, Wang J, Wang X, Yang C, Sun Y, et al. Genome-wide methylation and transcriptome of blood neutrophils reveal the roles of DNA methylation in affecting transcription of protein-coding genes and mirnas in e. *Coli-Infected Mastitis Cows. BMC Genomics* (2020) 21(1):102–16. doi: 10.1186/s12864-020-6526-z

20. Zhang H, Xu P, Jiang Y, Zhao Z, Feng J, Tai R, et al. Genomic, transcriptomic, and epigenomic features differentiate genes that are relevant for muscular polyunsaturated fatty acids in the common carp. *Front Genet* (2019) 10:217. doi: 10.3389/fgene.2019.00217

21. Lister R, Pelizzola M, Dowen RH, Hawkins RD, Hon G, Tonti-Filippini J, et al. Human DNA methylomes at base resolution show widespread epigenomic differences. *Nature* (2009) 462(7271):315–22. doi: 10.1038/nature08514

22. Feng S, Cokus SJ, Zhang X, Chen PY, Bostick M, Goll MG, et al. Conservation and divergence of methylation patterning in plants and animals. *Proc Natl Acad Sci United States America* (2010) 107(19):8689–94. doi: 10.1073/pnas.1002720107

23. Saxonov S, Berg P. Brutlag DL A genome-wide analysis of cpg dinucleotides in the human genome distinguishes two distinct classes of promoters. *Proc Natl Acad Sci United States America* (2006) 103(5):1412–7. doi: 10.1073/pnas.0510310103

24. Ma Z, Wang Y, Quan Y, Wang Z, Liu Y, Ding Z. Maternal obesity alters methylation level of cytosine in cpg island for epigenetic inheritance in fetal umbilical cord blood. *Hum Genomics* (2022) 16(1):34–45. doi: 10.1186/s40246-022-00410-2

25. Cardenas H, Fang F, Jiang G, Perkins SM, Zhang C, Emerson RE, et al. Methylomic signatures of high grade serous ovarian cancer. *Epigenetics* (2021) 16(11):1201–16. doi: 10.1080/15592294.2020.1853402

26. Zou Z, Zhang Y, Huang Y, Wang J, Min W, Xiang M, et al. Integrated genome-wide methylation and expression analyses provide predictors of diagnosis and early response to antidepressant in panic disorder. *J Affect Disord* (2023) 322:146–55. doi: 10.1016/j.jad.2022.10.049

27. Xu J, Zhang W, Zhong S, Xie X, Che H, Si W, et al. Microcystin-Leucine-Arginine affects brain gene expression programs and behaviors of offspring through paternal epigenetic information. *Sci total Environ* (2023) 857(Pt 1):159032. doi: 10.1016/j.scitotenv.2022.159032

28. Yang L, Liu L, Cheng J, Wu Z, Bao W, Wu S. Association analysis of DNA methylation and the Tissue/Developmental expression of the Fut3 gene in meishan pigs. *Gene* (2023) 851:147016. doi: 10.1016/j.gene.2022.147016

29. Liu Z, Zhou T, Gao D. Genetic and epigenetic regulation of growth, reproduction, disease resistance and stress responses in aquaculture. *Front Genet* (2022) 13:994471. doi: 10.3389/fgene.2022.994471

30. Yin C, Gu J, Gu D, Wang Z, Ji R, Jiao X, et al. The salmonella T3ss1 effector ipaj is regulated by itra and inhibits the mapk signaling pathway. *PloS Pathog* (2022) 18(12): e1011005. doi: 10.1371/journal.ppat.1011005

31. O'Neill LA, Golenbock D, Bowie AG. The history of toll-like receptors - redefining innate immunity. *Nat Rev Immunol* (2013) 13(6):453–60. doi: 10.1038/nri3446

32. Kawai T, Akira S. The role of pattern-recognition receptors in innate immunity: Update on toll-like receptors. *Nat Immunol* (2010) 11(5):373–84. doi: 10.1038/ni.1863

33. DiDonato JA, Mercurio F, Karin M. Nf-κb and the link between inflammation and cancer. *Immunol Rev* (2012) 246(1):379–400. doi: 10.1111/j.1600-065X.2012.01099.x

34. Cao X. Self-regulation and cross-regulation of pattern-recognition receptor signalling in health and disease. *Nat Rev Immunol* (2016) 16(1):35–50. doi: 10.1038/nri.2015.8

35. Mateu-Borrás M, González-Alsina A, Doménech-Sánchez A, Querol-García J, Fernández FJ, Vega MC, et al. *Pseudomonas aeruginosa* adaptation in cystic fibrosis patients increases C5a levels and promotes neutrophil recruitment. *Virulence* (2022) 13 (1):215–24. doi: 10.1080/21505594.2022.2028484

36. Roewe J, Walachowski S, Sharma A, Berthiaume KA, Reinhardt C, Bosmann M. Bacterial polyphosphates induce Cxcl4 and synergize with complement anaphylatoxin C5a in lung injury. *Front Immunol* (2022) 13:980733. doi: 10.3389/fimmu.2022.980733

37. Li L, Yang W, Shen Y, Xu X, Li J. The evolutionary analysis of complement component C5 and the gene Co-expression network and putative interaction between C5a and C5a anaphylatoxin receptor (C5ar/Cd88) in human and two cyprinid fish. *Dev Comp Immunol* (2021) 116:103958. doi: 10.1016/j.dci.2020.103958

38. Pandey MK, Trivedi VS, Magnusen AF, Rani R, Marsili L. Targeting the complement-sphingolipid system in covid-19 and gaucher diseases: Evidence for a new treatment strategy. *Int J Mol Sci* (2022) 23(22):103390. doi: 10.3390/ijms232214340

39. Raida MK, Buchmann K. Bath vaccination of rainbow trout (*Oncorhynchus mykiss walbaum*) against *Yersinia ruckeri*: Effects of temperature on protection and gene expression. *Vaccine* (2008) 26(8):1050–62. doi: 10.1016/j.vaccine.2007.12.029

40. Percopo CM, Krumholz JO, Fischer ER, Kraemer LS, Ma M, Laky K, et al. Impact of eosinophil-peroxidase (Epx) deficiency on eosinophil structure and function in mouse airways. *J Leukocyte Biol* (2019) 105(1):151–61. doi: 10.1002/jlb.3ab0318-090rr

41. Choi KM, Joo MS, Kang G, Woo WS, Kim KH, Jeong SH, et al. First report of eosinophil peroxidase in starry flounder (*Platichthys stellatus*): Gene identification and gene expression profiling. *Fish Shellfish Immunol* (2021) 118:155–9. doi: 10.1016/j.fsi.2021.08.021

42. Kang HC, Kim CH, Kim D, Lee YR, Choi TI, Kim SH, et al. Comparative proteome research in a zebrafish model for vanishing white matter disease. *Int J Mol Sci* (2021) 22 (5):2707–19. doi: 10.3390/ijms22052707

43. Yu B, Yao S, Liu L, Li H, Zhu J, Li M, et al. The role of polypeptide Pdtln1 in suppression of Pi3k/Akt signaling causes cardiogenetic disorders in vitro and in vivo. *Life Sci* (2022) 289:120244. doi: 10.1016/j.lfs.2021.120244

44. Zhou W, Krogdahl Å, Sæle Ø, Chikwati E, Løkka G, Kortner TM. Digestive and immune functions in the intestine of wild ballan wrasse (*Labrus bergylta*). *Comp Biochem Physiol Part A Mol Integr Physiol* (2021) 260:111011. doi: 10.1016/j.cbpa.2021.111011

frontiers | Frontiers in Immunology

TYPE Original Research
PUBLISHED 14 February 2023
DOI 10.3389/fimmu.2023.1126843

OPEN ACCESS

EDITED BY
Francesca Granucci,
University of Milano-Bicocca, Italy

REVIEWED BY
Weiwei Zhang,
Ningbo University, China
Jingguang Wei,
South China Agricultural University, China
Min Zhang,
Qingdao Agricultural University, China

*CORRESPONDENCE
Yun Sun
syshui207@126.com

†These authors contributed equally to this work

SPECIALTY SECTION
This article was submitted to Molecular Innate Immunity, a section of the journal Frontiers in Immunology

RECEIVED 18 December 2022
ACCEPTED 25 January 2023
PUBLISHED 14 February 2023

CITATION
Du H, Zhou Y, Du X, Zhang P, Cao Z and Sun Y (2023) Insulin-like growth factor binding protein 5b of *Trachinotus ovatus* and its heparin-binding motif play a critical role in host antibacterial immune responses *via* NF-κB pathway. *Front. Immunol.* 14:1126843. doi: 10.3389/fimmu.2023.1126843

Insulin-like growth factor binding protein 5b of *Trachinotus ovatus* and its heparin-binding motif play a critical role in host antibacterial immune responses *via* NF-κB pathway

Hehe Du[1,2†], Yongcan Zhou[1,2,3†], Xiangyu Du[2], Panpan Zhang[2], Zhenjie Cao[2] and Yun Sun[1,2,3*]

[1]State Key Laboratory of Marine Resource Utilization in South China Sea, Hainan University, Haikou, China, [2]Hainan Provincial Key Laboratory for Tropical Hydrobiology and Biotechnology, College of Marine Science, Hainan University, Haikou, China, [3]Collaborative Innovation Center of Marine Science and Technology, Hainan University, Haikou, China

Introduction: Insulin-like growth factor binding protein 5 (IGFBP5) exerts an essential biological role in many processes, including apoptosis, cellular differentiation, growth, and immune responses. However, compared to mammalians, our knowledge of IGFBP5 in teleosts remains limited.

Methods: In this study, TroIGFBP5b, an IGFBP5 homologue from golden pompano (*Trachinotus ovatus*) was identified. Quantitative real-time PCR (qRT-PCR) was used to check its mRNA expression level in healthy condition and after stimulation. *In vivo* overexpression and RNAi knockdown method were performed to evaluate the antibacterial profile. We constructed a mutant in which HBM was deleted to better understand the mechanism of its role in antibacterial immunity. Subcellular localization and nuclear translocation were verified by immunoblotting. Further, proliferation of head kidney lymphocytes (HKLs) and phagocytic activity of head kidney macrophages (HKMs) were detected through CCK-8 assay and flow cytometry. Immunofluorescence microscopy assay (IFA) and dual luciferase reporter (DLR) assay were used to evaluate the activity in nuclear factor-κB (NF-κβ) pathway.

Results: The TroIGFBP5b mRNA expression level was upregulated after bacterial stimulation. *In vivo*, TroIGFBP5b overexpression significantly improved the antibacterial immunity of fish. In contrast, TroIGFBP5b knockdown significantly decreased this ability. Subcellular localization results showed that TroIGFBP5b and TroIGFBP5b-δHBM were both present in the cytoplasm of GPS cells. After stimulation, TroIGFBP5b-δHBM lost the ability to transfer from the cytoplasm to the nucleus. In addition, rTroIGFBP5b promoted the proliferation of HKLs and phagocytosis of HKMs, whereas rTroIGFBP5b-δHBM, suppressed these facilitation

effects. Moreover, the *in vivo* antibacterial ability of TroIGFBP5b was suppressed and the effects of promoting expression of proinflammatory cytokines in immune tissues were nearly lost after HBM deletion. Furthermore, TroIGFBP5b induced NF-κβ promoter activity and promoted nuclear translocation of p65, while these effects were inhibited when the HBM was deleted.

Discussion: Taken together, our results suggest that TroIGFBP5b plays an important role in golden pompano antibacterial immunity and activation of the NF-κβ signalling pathway, providing the first evidence that the HBM of TroIGFBP5b plays a critical role in these processes in teleosts.

KEYWORDS

IGFBP5, HBM, subcellular localizations, antibacterial immunity, NF-κB pathway

Introduction

The insulin-like growth factor (IGF) system is mainly composed of IGF-I/II, IGF receptors, and IGF-binding proteins (IGFBPs) (1). IGFBPs act as IGF carriers and regulate their biological distribution (2). The IGF signaling pathway has been proven to be crucial for the onset and progression of numerous diseases as well as the control of cellular activities (1, 3). Given the extensive evidence regarding the significance of IGF, the IGFBP family, which was identified and designated IGFBP1 to IGFBP6, has attracted much attention in recent years (4, 5). IGFBP5 belongs to one of the most diverse groups in the biologically active IGFBP family (6). It was first found in human bone extracts (7). Since then, IGFBP5 has been cloned from a wide range of species and has the highest level of sequence similarity among the IGFBP family (8–10).

In mammals, IGFBP5 plays a variety of functions in cellular activities and has been reported to be associated with many diseases (1, 4). Studies found that the expression of IGFBP5 may stimulate retinal pigment epithelium (RPE) cell fibrosis, leading to the progression of proliferative vitreoretinopathy (11, 12). It was discovered that the expression of IGFBP5 was downregulated in kidney renal papillary renal cell carcinoma patients, could strengthen tissue regeneration, and had an anti-inflammatory effect by maintaining immune homeostasis (13–15).

Overall, IGFBP5 remains poorly understood in teleosts compared with mammals. To date, few studies have focused on the immune response of the IGF system in fish, and even fewer ones have focused on the function of IGFBP5. Several IGFBP5 sequences in fine flounder (*Paralichthys adspersus*), zebrafish (*Danio rerio*), grass carp (*Ctenopharyngodon idella*), salmon, and rainbow trout (*Oncorhynchus mykiss*) have been cloned and characterized (8, 16–19). These studies mainly focused on the aspects of evolution, function in growth, muscle or embryonic development, and hormonal regulation (20, 21).

IGFBP5 contains a nuclear localization signal (NLS) in the C-terminal domain which is suggested to help IGFBP5 translocate to the nucleus and activate many transcription factors in the nucleus of cells involved in immune and inflammatory reactions (22, 23). Recently, many studies have focused on IGFBP5 nuclear trafficking and demonstrated that its subcellular compartmentalization affects its functions—for example, NLS-mutated IGFBP5 is mainly located in the cytoplasm, and it can enhance proliferation and migration (24). IGFBP5 induces Egr-1 and binds to each other in the nucleus, resulting in the promotion of fibrotic gene transcription (25). Moreover, according to some reports, the NLS domain contains a heparin-binding motif (HBM; ^{206}KRKQCK^{211}) that appears to be key in determining the various functions of IGFBP5 (26–29).

Vibrio harveyi is the main threat to the large-scale farming of *Trachinotus ovatus*, an important commercial fish in China (30, 31). In the present study, TroIGFBP5b was cloned and identified, and its different expression patterns were examined. To assess whether HBM deficiency affects its subcellular location and influences its function, we generated a mutant containing a truncated form of TroIGFBP5b in which the HBM motif of the NLS domain was deleted. The findings provide insight into the mechanisms underlying the immune function of TroIGFBP5b.

Materials and methods

Fish and cells

T. ovatus (average weight 18.5 g) from Hainan Province was temporarily reared for 1 week before the experiments. Golden pompano snout (GPS) cells, kindly provided by Professor Qin, were cultured in L-15 medium [containing 10% fetal bovine serum (FBS, Gibco), 100 U/ml penicillin, and 100 U/ml streptomycin] at 26°C (32). Human embryonic kidney (293T) cells were incubated in Dulbecco's modified Eagle's medium with 10% FBS and incubated at 37°C (5% CO_2 incubator).

Pathogenic bacteria and challenge experiment

V. harveyi that was isolated by our laboratory from golden pompano was used as the pathogen and cultured in Luria–Bertani

(LB) medium (containing 100 μg/ml ampicillin, Amp) at 30°C (31). The suspension was diluted to 3×10^7 colony-forming units (CFU)/ml when the OD_{600} value reached approximately 0.6. The fish were intraperitoneally injected with 0.1 ml of the suspension, and the same volume of phosphate-buffered saline (PBS) was injected as the control. The liver, spleen, and head kidney were collected at 6, 9, 12, and 24 h post-infection (hpi). Three separate samples were prepared as well.

Quantitative real-time PCR

Total RNA of tissues and cells was extracted using E.A.N.A. Total RNA Extraction Kit (OMEGA, USA) and digested with DNase (OMEGA, USA). cDNAs were synthesized using Eastep® RT Master Mix Kit (Promega, USA). qRT-PCR was performed to quantify the target gene mRNA level using SYBR ExScript qRT-PCR Kit (Promega, China). *Beta-2-microglobulin* was used as the housekeeping gene, and data were analyzed by the $2^{-\Delta\Delta CT}$ method (33). The primers used are listed in Supplementary Table S1.

Gene cloning and analysis

The full open reading frame of the TroIGFBP5b sequence was amplified with primers TroIGFBP5b-F1/TroIGFBP5b-R1 by using *T. ovatus* liver cDNA as the template. The TroIGFBP5b sequence was blasted at the National Center for Biotechnology Information (NCBI, http://www.ncbi.nlm.nih.gov/blast). The structural domain was predicted at SMART online (http://smart.embl-heidelberg.de/). The three-dimensional (3D) structure prediction of TroIGFBP5b was carried out on the SWISS-MODEL website, and the visualization of the predicted protein 3D structure was achieved using PyMOL software. The phylogenetic tree constructed by MEGA 7.0 employed the neighbor-joining (NJ) method.

Plasmid construction and small interfering RNA synthesis

The TroIGFBP5b sequence, except for the signal peptide (SP) domain, was amplified with primer TroIGFBP5b-F2/TroIGFBP5b-R1, using the pEASY-T-TroIGFBP5b plasmid as a template by PCR, and named TroIGFBP5b-ΔSP. Subsequently, two HBM-deleted mutants (^{215}RKGFFKRKQCKPSRGRKR^{232} to ^{215}RKGFFPSRGRKR^{226}, delete ^{220}KRKQCK^{225}) of TroIGFBP5b were amplified with full-length TroIGFBP5b or TroIGFBP5b-ΔSP using the primer pairs TroIGFBP5b-F1/TroIGFBP5b-R3 or TroIGFBP5b-F2/TroIGFBP5b-R3 and TroIGFBP5b-F3/TroIGFBP5b-R1 by overlap PCR assay and named TroIGFBP5b-ΔHBM and TroIGFBP5b-Δ(HBM+SP), respectively.

To construct a eukaryotic expression vector for overexpressing IGFBP5 *in vivo*, TroIGFBP5b and TroIGFBP5b-ΔHBM were inserted into the pCN3 vector, which expresses the human cytomegalovirus immediate-early promoter, at the *EcoR* V site, resulting in pTroIGFBP5b and pTroIGFBP5b-ΔHBM (34). pEGFPX-N3 was used for subcellular localization and was reformed from the pEGFP-N3 vector (35). Recombinant GFP plasmids were constructed by connecting TroIGFBP5b, TroIGFBP5b-ΔSP, TroIGFBP5b-ΔHBM, and TroIGFBP5b-Δ(HBM+SP) to pEGFPX-N3 at the *Sma*I site, resulting in pTroIGFBP5b-WT-N3, pTroIGFBP5b-ΔHBM-N3, pTroIGFBP5b-ΔSP-N3, and pTroIGFBP5b-Δ(HBM+SP)-N3, respectively. To obtain biologically active recombinant TroIGFBP5b-ΔSP and TroIGFBP5b-Δ(HBM+SP) proteins, pET-32a, which could express a His-tag and a thioredoxin protein (Trx), was used and linearized at the *Eco*RV site. All of the above-mentioned positive constructs were confirmed by colony PCR and sequencing. The plasmids used in the cell-related experiments, as well as those injected into the fish body, were endotoxin-free plasmids harvested using Plasmid Extraction Kit (TransGen, China) according to the supplier's instructions.

The siRNA synthesis followed the instructions of RiboMAX™ Express RNAi System (Promega, USA) as described (36). Briefly, two pairs of primers, siTroIGFBP5b-P1/siTroIGFBP5b-P2 and siTroIGFBP5b-P3/siTroIGFBP5b-P4, were designed to obtain two DNA oligonucleotides after incubation at 95°C for 5 min. The templates were allowed to cool slowly to room temperature (RT). Next, these two DNA oligonucleotides were used to separately synthesize the sense strand RNA or the antisense strand RNA templates at 37°C for 2 h. Afterwards, the DNA template was removed from the separate short RNA strands by digestion with DNase, and then the two RNA strands were mixed to synthesize the siRNA. Finally, the synthesized siRNA was purified following the manufacturer's instructions. The control siRNA (siTroIGFBP5b-C) was synthesized with siTroIGFBP5b- C-P1/P2 and siTroCCL4-C-P3/P4 as described above. The primers used in this study are listed in Supplementary Table S1.

In vivo overexpression and knockdown of TroIGFBP5b

To evaluate the *in vivo* role of TroIGFBP5b, the fish were intramuscularly injected with 15 μg (0.1 ml) overexpression plasmids (pTroIGFBP5b and pCN3). The knockdown of TroIGFBP5b was achieved by an intramuscular injection of 15 μg siTroIGFBP5b or siTroIGFBP5b-C into the fish. For these experiments, 0.1 ml PBS was injected as a control. To further study the function of HBM on bacterial infection *in vivo*, the pTroIGFBP5b-ΔHBM plasmid was also injected into the fish as described above, and the pTroIGFBP5b, pCN3, and PBS groups were repeated to compare differences.

In vivo antibacterial ability assay

After the post-injection of overexpressing plasmids for 5 days and the post-injection of siRNA for 12 h, 0.1 ml of *V. harveyi* (2×10^7 CFU/ml) suspension was injected into all groups intraperitoneally. The appropriate size of the liver, spleen, and head kidney tissue blocks was determined aseptically at 6, 9, and 12 hpi. The weighed tissue blocks were ground in 300 μl PBS, and 700 μl PBS was added. In total, 100 μl homogenate was spread evenly onto LB plates (containing 100

μg/ml Amp) to measure the bacterial loads of the different tissues. Finally, the number of colonies per gram was calculated.

Subcellular localization

GPS cells were cultivated to analyze the subcellular localization of TroIGFBP5b according to the method of Chen et al. (33). Briefly, before transfection, GPS cells were grown in six-well plates overnight until reaching 60% confluence. pTroIGFBP5b-WT-N3, pTroIGFBP5b-ΔHBM-N3, pTroIGFBP5b-ΔSP-N3, pTroIGFBP5b-Δ(HBM+SP)-N3, and pEGFPX-N3 (4 μg) were transfected into GPS cells using LipoFiter3.0 (Hanbio, Shanghai, China). At 48 h post-transfection, the cells were fixed for 15 min with 4% (v/v) paraformaldehyde at RT. 4′,6-Diamidino-2-phenylindole (1 μg/ml) was used to stain the nuclei for 20 min, and rhodamine B was used to highlight the whole cell. Finally, the cells were washed with PBS until the cleaning solution became colorless, and the cells were observed using an inverted microscope. To monitor the localization of TroIGFBP5b after stimulation, *V. harveyi* (1×10^5 CFU/ml) or lipopolysaccharide (LPS; 100 ng/ml) was added to the transfected cells (TroIGFBP5b-WT and TroIGFBP5b-ΔHBM) for 4 h after transfection for 48 h. The ensuing steps were the same as those described above.

Protein expression and purification

Recombinant TroIGFBP5b (rTroIGFBP5b), HBM mutant (rTroIGFBP5b-ΔHBM), and rTrx were purified as described in a previous report (33). After exploring the induction conditions, the optimum induction condition was determined by incubating at 20°C for 8 h after adding isopropyl β-d-1-thiogalactopyranoside (0.5 mM). After purification by a Ni Sepharose column, PBS was used to dialyze the recombinant proteins which were concentrated with PEG8000. The concentration of the purified recombinant protein was measured by the Bradford method.

Phagocytic activity detection of head kidney macrophages through flow cytometry

T. ovatus head kidneys were collected and rinsed with PBS three times aseptically. Density gradient centrifugation was used to obtain head kidney macrophages (HKMs) from *T. ovatus* as previously described with Percoll (GE Healthcare, USA) (37). The isolated cells were added to a six-well plate (1×10^7 cells/well) containing L-15 medium for 2 h, and then 100 μl each of 200 μg/ml rTroIGFBP5b, rTroIGFBP5b-ΔHBM, and rTrx was infused into each well; the mixture was incubated at 26°C overnight. Green fluorescent microspheres (Aladdin, China) were diluted to 1% (w/v) L-15 (containing 10% FBS) medium and then added to each well at 26°C in the dark for 2 h. Before being subjected to Guava easyCyte™ Flow Cytometer (Millipore, USA), the cells were washed and resuspended in L-15 to 1×10^9 cells/ml. The experiment was performed in triplicate.

Proliferation detection of head kidney lymphocytes by CCK-8 assay

T. ovatus head kidneys were collected and rinsed aseptically with PBS three times. Density gradient centrifugation was used to obtain head kidney lymphocytes (HKLs) from *T. ovatus* as previously described by Percoll (GE Healthcare, USA) (36). The prepared HKLs resuspended in L-15 medium with 10% FBS were added (90 μl) to a 96-well culture plate (1×10^5 cells/well). Subsequently, 10 μl of rTroIGFBP5b and rTroIGFBP5b-ΔHBM (final concentrations of 10, 50, 100, 200, and 300 μg/ml) or rTrx (300 μg/ml) was incubated for 12 h at 26°C, and PBS was added as a control. As per the instructions, Cell Counting Kit-8 (CCK8) (Hanbio, Shanghai, China) was applied to measure the proliferation of HKLs. The results were calculated as follows: (A_{450} of protein-treated cells – A_{450} of the empty well)/(A_{450} of control cells – A_{450} of the empty well). The empty well contained only medium and CCK-8 solution. The experiment was repeated in triplicate.

Immunofluorescence microscopy assay

293T cells were transfected with pTroIGFBP5b, pTroIGFBP5b-ΔHBM, and pCN3 as described above. The immunofluorescence microscopy assay was performed as previously described (38). The primary antibody used was an anti-p65 polyclonal antibody (Bioss, Beijing, China) at 1/200 dilution.

Western blot assay

GPS cells were transfected with pTroIGFBP5b-WT-N3, pTroIGFBP5b-ΔHBM-N3, pTroIGFBP5b-ΔSP-N3, pTroIGFBP5b-Δ(HBM+SP)-N3, or pEGFPX-N3 in 10-cm-diameter culture dishes. Nuclear and Cytoplasmic Extraction Reagent Kit (Beyotime, Beijing, China) was used to separately extract nuclear and cytoplasmic proteins. After protein separation by 15% SDS-PAGE and transfer to a PVDF membrane (Millipore, Germany), the membrane was blocked with 5% BSA for 1 h. Then, the membrane was incubated with anti-EGFP (1/2,000 dilution, Bioss, Beijing, China) at 4°C overnight. After 10 min of washing with TBST three times, the secondary antibody (HRP-conjugated goat anti-mouse IgG and 1/2000 dilution) was added and incubated for 1 h at RT. Anti-β tubulin and anti-Histone H3 (Bioss, Beijing, China) were used as the nuclear and cytoplasmic internal references, respectively. The experiment was performed in triplicate.

Dual-luciferase reporter assay

A DLR assay was performed to examine the activation of NF-κB. GPS and 293T cells (1×10^6 cells/well) were seeded in a 24-well plate. A total of 0.2 mg of NF-κB-specific firefly luciferase reporter vector, the pGL4.32 vector (luc2P/NF-κB, Promega, USA), 0.05 mg of pRL-CMV (a control vector), and 0.2 mg of pTroIGFBP5b or pTroIGFBP5b-ΔHBM were co-transfected into cells using

LipoFiter3.0 (Hanbio, Shanghai, China). After transfection for 48 h, the firefly and Renilla luciferase activities in the cell lysates were measured using Dual-Luciferase Reporter Assay Kit (Promega, USA). All experiments were conducted three times independently.

Statistical analysis

All data in this study were statistically processed using GraphPad Prism (version 8.0.2). Statistically significant differences were evaluated by the *t*-test, with the *P*-value indicated (*$P < 0.05$, **$P < 0.01$).

Results

Sequence characterization of TroIGFBP5b

TroIGFBP5b is 801 bp in length and encodes 266 amino acids (a.a.) (NCBI GenBank accession number OP712620). According to SMART prediction analysis, TroIGFBP5b is composed of a signal peptide (SP) (1–20 a.a.), an insulin growth factor-binding (IB) domain (23–100 a.a.), and a thyroglobulin type I repeat (TY) domain (210–261 a.a.) (Figure 1A). In addition, TroIGFBP5b contains a highly conserved HBM (220–226 a.a.) in the NLS sequence (215–232 a.a.) of the C-terminal domain (Figure 1B). The

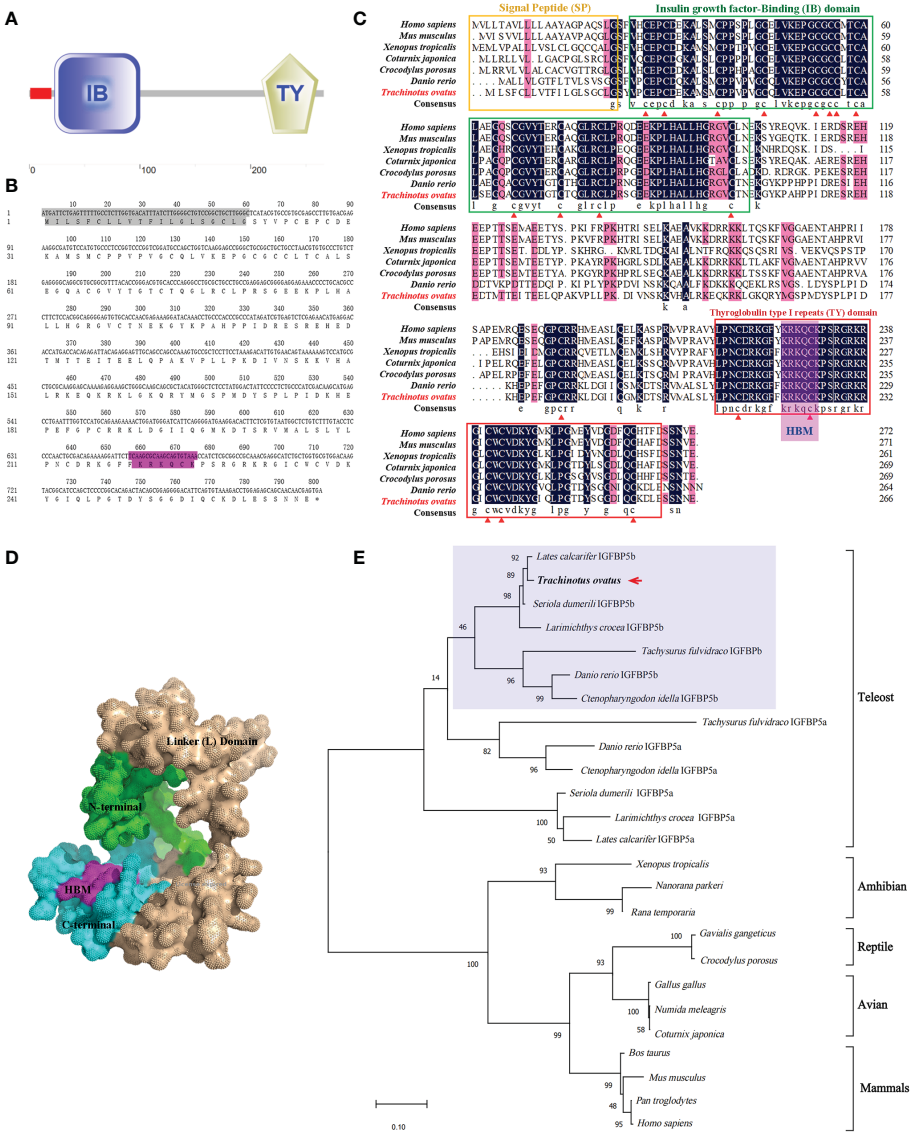

FIGURE 1
Predicted domains, multiple alignments, and phylogenetic tree for TroIGFBP5b amino acid sequence. **(A)** The domains were predicted by SMART. The red box was a signal peptide (SP) as detected by the SignalP v4.0 program. **(B)** The TroIGFBP5b sequence **in** the background shown in gray was the SP, and the purple color indicated the heparin-binding motif (HBM) sequence. **(C)** Multiple sequence alignment analyses of TroIGFBP5b. The consensus and ≥75% identical residues were in black and pink among the aligned sequences. The putative SP, insulin growth factor-binding, and thyroglobulin type I repeat regions were marked by the yellow, green, and red boxes, respectively. The red triangles indicated the 18 conserved cysteine residues. **(D)** Surface view of the TroIGFBP5b 3D structure. The N-terminal and C-terminal were marked with green and blue colors, respectively, and the purple region represented the HBM. **(E)** Phylogenetic tree. The selected protein sequences are listed in Table 1. The newly characterized TroIGFBP5b was marked with an arrow.

10.3389/fimmu.2023.1126843

sequence alignment analysis showed that the IB and TY domains of TroIGFBP5b were very highly conserved among vertebrates, including mammals (*Homo sapiens* and *Mus musculus*), amphibians (*Xenopus tropicalis*), reptiles (*Chelonia mydas*), avians (*Gallus gallus)*, and teleosts (*D. rerio*), suggesting its conservation during species evolution. The N-domain contains 12 conserved cysteine residues, and the C-domain contains six, which contributed to the structural stability by intradomain disulfide bonds between cysteine residues (Figure 1C). From the 3D predicted structure, HBM is located in the cavity formed by the C- and N- termini (Figure 1D). Identities with mammals, avians, reptiles, and amphibians are relatively lower, ranging from 51.66% to 58.74%. According to the multiple sequence alignment analysis, identities vary in teleosts, ranging from 60.15% to 97.38%. TroIGFBP5b shows a high identity with IGFBP5b in *Seriola dumerili* (97.38%), *Lates calcarifer* (94.91%), and *Larimichthys crocea* (92.54%) (Table 1). A phylogenetic tree was constructed using the NJ algorithm, showing that TroIGFBP5b clusters with IGFBP5b of other teleosts and resembles *Lates calcarifer* IGFBP5b, the closest phylogenetically, with a bootstrap value of 92 (Figure 1E).

TABLE 1 Identities of TroIGFBP5b with other species.

Species	Accession number	Identities (%)
Crocodylus porosus	XP_019409774.1	51.66
Gavialis gangeticus	XP_019378195.1	51.85
Pan troglodytes	XP_003309513.1	53.85
Homo sapiens	NP_000590.1	53.85
Xenopus tropicalis	XP_031748507.1	54.28
Bos taurus	NP_001098797.1	54.41
Gallus gallus	XP_422069.3	54.81
Mus musculus	NP_034648.2	55.15
Numida meleagris	XP_021254294.1	55.19
Coturnix japonica	XP_015724280.1	55.19
Nanorana parkeri	XP_018408077.1	58.27
Rana temporaria	XP_040214133.1	58.74
Danio rerio IGFBP5b	NP_001119935.1	78.07
Danio rerio IGFBP5a	NP_001092224.1	69.37
Lates calcarifer IGFBP5b	XP_018552191.1	94.91
Lates calcarifer IGFBP5a	XP_018516555.1	64.68
Seriola dumerili IGFBP5b	XP_022596386.1	97.38
Seriola dumerili IGFBP5a	XP_022617333.1	65.06
Larimichthys crocea IGFBP5b	XP_010732591.1	92.54
Larimichthys crocea IGFBP5a	XP_010740884.1	62.59
Tachysurus fulvidraco IGFBP5b	XP_027020371.1	70.22
Tachysurus fulvidraco IGFBP5a	XP_026989260.1	60.15
Ctenopharyngodon idella IGFBP5b	APX54482.1	77.53
Ctenopharyngodon idella IGFBP5a	APX54481.1	71.59

The expression profiles of TroIGFBP5b were regulated by *V. harveyi* infection

The expression pattern of *TroIGFBP5b* in *T. ovatus* was detected in 11 tissues using qRT-PCR: heart, stomach, brain, liver, skin, head kidney, intestine, spleen, gills, blood, and muscle. The results showed that it was the lowest in the muscle, set as 1. In contrast to the set criterion of muscle, the expression levels of the other tissues ranking from high to low were as follows: liver (134.44-fold), spleen (33.19-fold), brain (30.43-fold), gill (27.51-fold), head kidney (17.69-fold), intestine (17.18-fold), stomach (12.67-fold), skin (10.12-fold), blood (5.51-fold), and heart (5.11-fold) (Figure 2A). The results for the expression of *TroIGFBP5b* during *V. harveyi* infection in the three main immune organs all displayed a significant enhancement with a similar expression pattern, which tended to decrease after an initial increase. The time points at which the peaks appeared were different. In the liver, the expression peak was at 9 hpi with a 6.86-fold change, and it was also at 9 hpi with a 4.64-fold change in the head kidney. For the spleen, the highest expression (10.93-fold) was observed at 12 hpi (Figure 2B).

In vivo antibacterial ability after TroIGFBP5b overexpression and knockdown

To explore the function of TroIGFBP5b in response to bacterial infection, TroIGFBP5b was overexpressed *in vivo* by injection with pTroIGFBP5b, pCN3, or PBS (as a control). On the 5th day after the plasmid injection, the expression levels of TroIGFBP5b in the liver, spleen, and head kidney of fish treated with pTroIGFBP5b were significantly higher than in the control using qRT-PCR analysis, indicating that the overexpression of TroIGFBP5b was successful (Supplementary Figure S2). In the liver of the pTroIGFBP5b overexpression group, the bacterial load decreased by 1.7- and 1.85-fold compared with that of the control at 9 and 12 hpi, respectively. In the spleen, it was decreased by 1.05-fold and 2.23-fold in the pTroIGFBP5b group compared with the control group at the two time points. Furthermore, the pTroIGFBP5b group had an approximately 1.46- and 1.67-fold reduction in head kidney bacterial load at 9 and 12 hpi, respectively (Figure 3A).

In vivo siRNA technology was used to further analyze the effect of TroIGFBP5b against pathogen infection. The qRT-PCR analysis showed that the expression levels of TroIGFBP5b in the liver, spleen, and head kidney of fish treated with pTroIGFBP5b were significantly decreased than in the control group using qRT-PCR analysis, indicating that the knockdown of TroIGFBP5b was successful after siRNA injection for 12 h (Supplementary Figure S3). After being challenged by *V. harveyi*, the liver bacterial counts were approximately 1.90-, 1.50-, and 1.55-fold higher in the siTroIGFBP5b-injected group at 6, 9, and 12 hpi than in the control group, respectively. On the other hand, at 6, 9, and 12 hpi, the splenic bacterial load after siTroIGFBP5b injection was approximately 1.97-, 1.87-, and 1.69-fold higher than that in the control group. In the head kidney, the bacterial loads increased by 1.63-, 1.54-, and 1.94-fold compared with the control at 6, 9, and 12 hpi, respectively (Figure 3B).

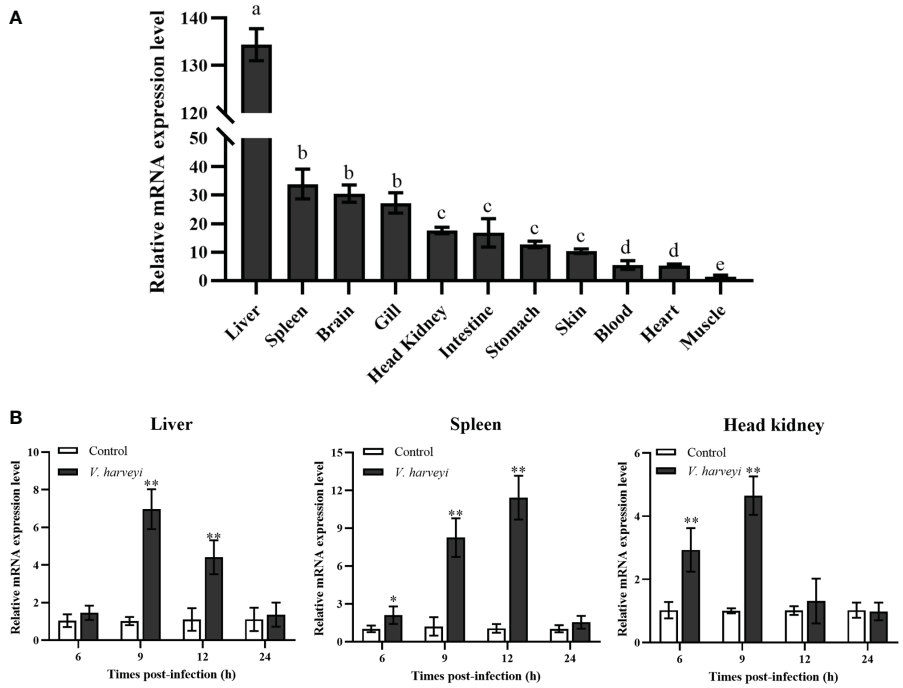

FIGURE 2
Relative mRNA expression levels of *TroIGFBP5b*. **(A)** The mRNA expressions of *TroIGFBP5b* were detected in 11 tissues using qRT-PCR, and the muscle was set as 1. Groups with the same letters are not significantly different from each other ($P < 0.05$). **(B)** The IGFBP5 expressions of different times infected with *V. harveyi* in the liver, spleen, and head kidney were determined by qRT-PCR, and phosphate-buffered-saline-injected group—as the control—was set as 1. *Beta-2-microglobulin* was used as a reference gene in normalizing. Data were presented as means ± SD (*N*, number of fish used; $N = 3$). *$P < 0.05$, **$P < 0.01$.

Subcellular localization of TroIGFBP5b WT and HBM- and SP-deficient mutants

As mentioned above, TroIGFBP5b contains an SP sequence and an HBM in its NLS domain. To explore the role of these two motifs in the subcellular localization characteristics of TroIGFBP5b, recombinant plasmids containing TroIGFBP5b wild type, HBM-deleted TroIGFBP5b, SP-deleted TroIGFBP5b, and both HBM- and SP-deleted TroIGFBP5b were constructed based on pEGFPX-N3, which were named TroIGFBP5b-WT, TroIGFBP5b-ΔHBM, TroIGFBP5b-

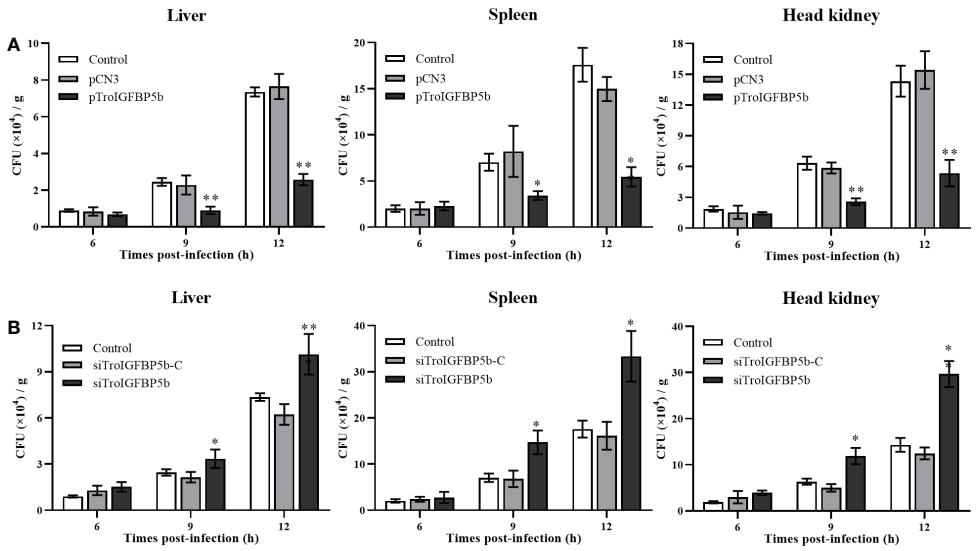

FIGURE 3
Antibacterial ability after TroIGFBP5b overexpression and knockdown. The bacteria colony counts in the liver, spleen, and head kidney were detected after the overexpression plasmid was injected for 5 days **(A)** and siRNA was injected for 12 h **(B)**. Data were shown as means ± SD ($N = 3$), and the statistical significance was indicated. *$P < 0.05$, **$P < 0.01$.

ΔSP, and TroIGFBP5b-Δ(HBM+SP), respectively (Figure 4A). GPS cells were transfected using LipoFiter3.0. The inverted fluorescence microscopy results showed IGFBP5-WT and IGFBP5-ΔHBM to be mainly observed in the cytoplasm, indicating that TroIGFBP5b might be localized in the cytoplasm of GPS cells. While in the absence of the SP sequence its localization changed, the main localization was transferred from the cytoplasm to the nucleus (Figure 4B). The protein level displayed by the green fluorescence was consistent with those observed by fluorescence microscopy (Figure 4C).

IGFBP5-ΔHBM altered the intracellular actions of TroIGFBP5b *in vitro*

Although the subcellular localization of IGFBP5-WT and IGFBP5-ΔHBM did not seem different through observation, we wondered if the HBM deficiency would affect the subcellular localization under pathogen stimulation. To explore this postulate, GPS cells transfected with TroIGFBP5b-WT and TroIGFBP5b-ΔHBM were treated with LPS or *V. harveyi*. According to the results, green fluorescence could be observed in the nucleus after stimulation in the TroIGFBP5b-WT transfected cells. However, the cells transfected with TroIGFBP5b-ΔHBM did not undergo such transfer, suggesting that the deletion of HBM would result in the loss of nuclear transfer reaction in response to stimulation (Figure 5A). We also evaluated the green fluorescence at the protein level, and the results were in agreement with the results mentioned above (Figure 5B).

In vitro effects on the lymphocytes and macrophages of rTroIGFBP5b and rTroIGFBP5b-ΔHBM

Since TroIGFBP5b was involved in defense against the pathogen *in vivo*, we wonder whether TroIGFBP5b had any effect on immune cell activities and if HBM contributed to the processes. To prove this opinion, rTroIGFBP5b, rTroIGFBP5b-ΔHBM, and rTrx (control) were purified, and the lymphocytes and macrophage cells were extracted from the head kidney. According to the CCK-8 assay results, rTroIGFBP5b enhanced HKL proliferation in a dose-dependent manner, and it was shown that 200 mg/ml exhibited the best effect, compared with the cells incubated with PBS and rTrx, while rTroIGFBP5b-ΔHBM had no effects on HKL proliferation (Figure 6A). From the results derived by checking using a flow cytometer, it was shown that the phagocytosis rate of the rTroIGFBP5b group was extremely higher than that in the rTrx and rTroIGFBP5b-ΔHBM cells, while the phagocytic activity of those cells that were treated with rTroIGFBP5b-ΔHBM was comparable with that of the rTrx-treated group (Figure 6B).

TroIGFBP5b overexpression could activate the NF-κB pathway, while TroIGFBP5b-ΔHBM could not

A dual-luciferase reporter assay was performed to determine the role of TroIGFBP5b in the NF-κB pathway. It was found that the overexpression of TroIGFBP5b significantly activated the NF-κB luciferase reporter activity in a dose-dependent manner, while the activating effects on the NF-κB signaling did not occur in the TroIGFBP5b-ΔHBM overexpression cells in both 293T and GPS cells (Figures 7A, B). This indicated that HBM was important in TroIGFBP5b activation to the NF-κB pathway. The immunofluorescence staining results proved that TroIGFBP5b overexpression promoted the nuclear translocation of p65 in 293T cells. However, this p65 translocation was blocked by overexpressing TroIGFBP5b-ΔHBM in 293T cells (Figure 7C). However, due to the poor specificity of the p65 antibody in GPS cells, we did not achieve satisfactory results (data not shown). These results demonstrated that the HBM of TroIGFBP5b seemed to function as a key for activating the NF-κB pathway.

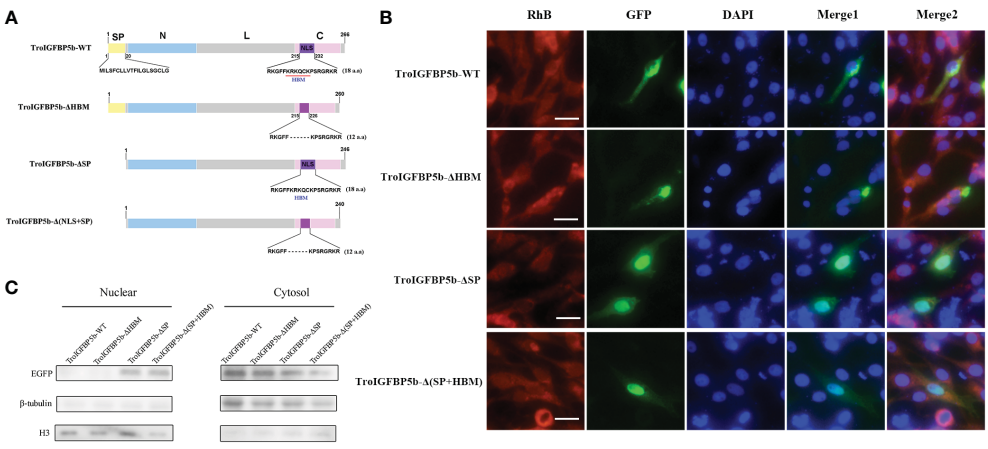

FIGURE 4
Subcellular localization of TroIGFBP5b and its mutants in golden pompano snout (GPS) cells. **(A)** Schematic diagrams of the structural domain comparison between the TroIGFBP5b wild type (TroIGFBP5b-WT), heparin-binding motif (HBM)-deleted TroIGFBP5b (IGFBP5-ΔHBM), signal peptide (SP)-deleted TroIGFBP5b (IGFBP5-ΔSP), and both HBM- and SP-deleted TroIGFBP5b [IGFBP5-Δ(HBM+SP)]. Different colors represented different structural domains. **(B)** GPS cells transfected with pTroIGFBP5b-N3 and mutants were observed under fluorescence microscopy. Bar = 20 μm. **(C)** Western blot analysis of the nuclear and cytoplasmic protein extracted from the cells mentioned above.

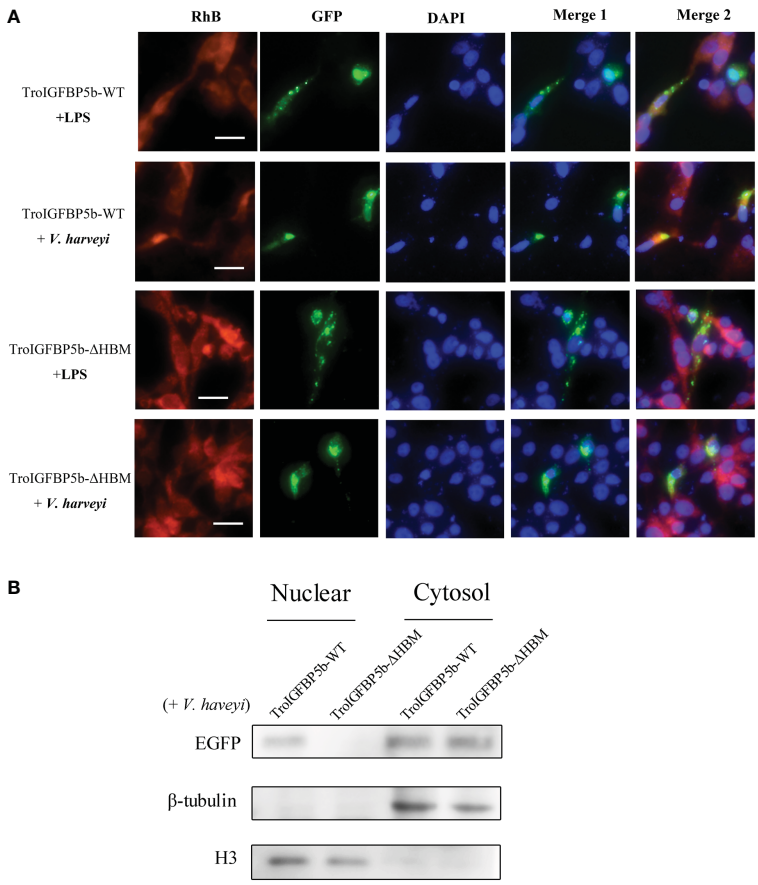

FIGURE 5
IGFBP5-ΔHBM subcellular localization after stimulations. **(A)** After being transfected with pTroIGFBP5b-WT-N3 and pTroIGFBP5b-ΔHBM-N3 for 48 h, golden pompano snout cells were stimulated with lipopolysaccharide and *V. haveyi*. Bar = 20 μm. **(B)** The Western blot analysis of the nuclear and cytoplasmic protein extracted from the cells mentioned above was stimulated by *V. haveyi* for 4 h.

IGFBP5-ΔHBM lost the antibacterial and activated immune-related gene abilities *in vivo*

Since the HBM sequence could affect the nuclear transfer of TroIGFBP5b protein in response to pathogenic stimulation, we further investigated whether it could affect its antimicrobial activity *in vivo*. Taking the same approach as before, the fish were injected with overexpression plasmids pTroIGFBP5b-WT, pTroIGFBP5b-ΔHBM, pCN3, or PBS (control), respectively. After having been infected with *V. harveyi* for 9 and 12 h, the bacterial loads in the liver, spleen, and head kidney of the pTroIGFBP5b-ΔHBM group were all significantly higher than that in the pTroIGFBP5b group. In the head kidney, the bacterial load in the mutant group was not any different from that of the control group, while in the liver the bacterial load was lower than the control at 9 and 12 hpi, and in the spleen, it was shown to be lower at 12 hpi (Figure 8A).

Furthermore, the *in vivo* function mechanism after the overexpression of TroIGFBP5b and TroIGFBP5b-ΔHBM was figured out by examining the expression of immune-related genes using qRT-PCR. According to the results, TroIGFBP5b overexpression could significantly raise the expression level of the selected immune-related genes (p65, *IKBα*, *IL-8*, *IL-10*, *IL-1β*, and *TNF-α*). TroIGFBP5b-ΔHBM could also affect some genes compared with pCN3, such as *TNF-α*, *IKBα*, *IL-8*, and *IL-1β* in the liver and *IL-8* and *IL-1β* in the spleen. However, compared with the TroIGFBP5b group, the upregulated effect on those genes was significantly decreased in TroIGFBP5b-ΔHBM. To sum up, the upregulated expression of immune-related genes induced by TroIGFBP5b was practically shut down in the absence of HBM (Figures 8B–D).

Discussion

IGF is instrumental in growth regulation, development, and immune response (1, 4, 39). Meanwhile, IGFBPs have crucial roles due to their high binding affinity to IGFs (3, 40). In this study, a teleost IGFBP5 of golden pompano, TroIGFBP5b, was cloned, and its expression and biological properties were analyzed accordingly.

Similar to other members of the IGFBP family, TroIGFBP5b was found to have a highly conserved structure containing N- and C-terminal domains, suggesting that IGFBP5 might present as highly conservative during structural and functional evolution (8, 16, 29, 41). Similar to other reported IGFBP5, the NLS sequence of TroIGFBP5b also included a putative classical HBM (^{206}KRKQCK^{211}), which might be critical in the diverse functions of IGFBP5 (26–28, 42). Due to the teleost-specific whole-genome duplication, some fish were reported to retain two copies of IGFBP5 (IGFBP5a and IGFBP5b), such as

10.3389/fimmu.2023.1126843

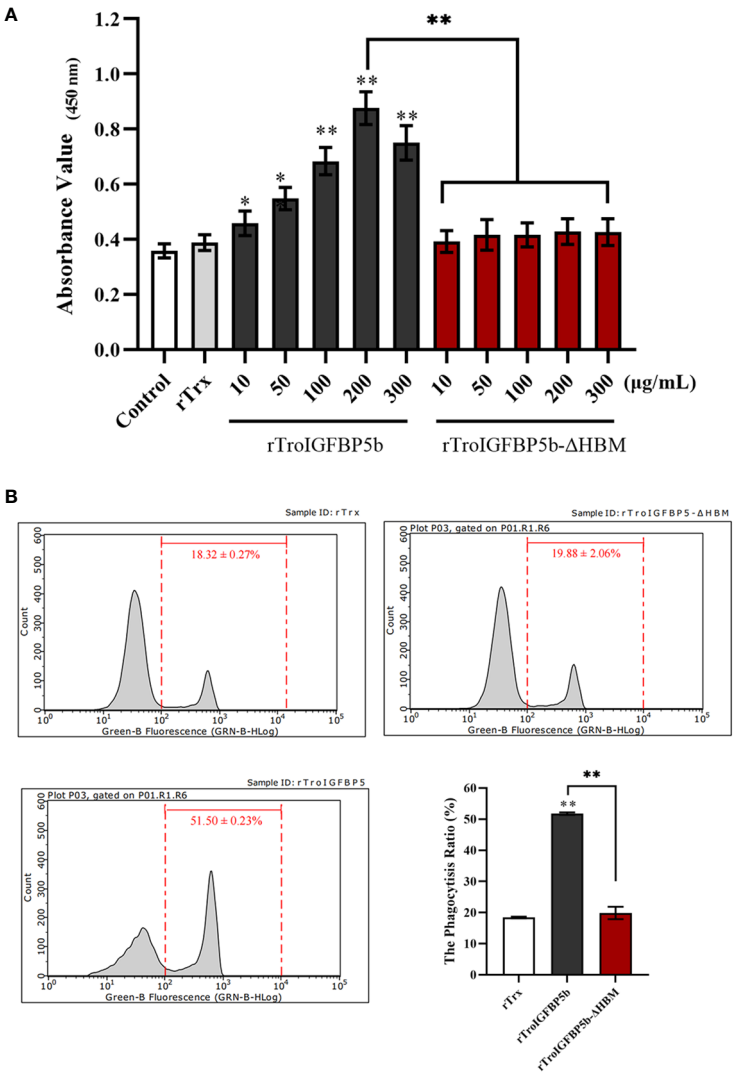

FIGURE 6
Effect of TroIGFBP5b and heparin-binding motif mutant recombinant proteins on the proliferation of head kidney lymphocytes (HKLs) and phagocytosis of head kidney macrophages (HKMs). **(A)** The proliferation of HKLs was examined by CCK8 assay after incubation with different concentrations of rTroIGFBP5b or rTroIGFBP5b-ΔHBM. **(B)** The phagocytic activity of HKMs treated with recombinant proteins was examined with a flow cytometer after incubating with fluorescent microsphere for 2 h Values are shown as means ± SD ($N = 3$). *N*, number of times the experiment was performed. The statistical significance was indicated (*$P < 0.05$, **$P < 0.01$).

zebrafish, grass carp, and Atlantic salmon (8, 16, 17). In this study, the phylogenetic tree results suggested that TroIGFBP5b clustered with IGFBP5b of other teleosts and had the closest phylogenetic relationship with *Lates calcarifer* IGFBP5b. This indicated that IGFBP5 was an evolutionarily conserved protein, and the duplication of the IGFBP5a/b subfamily probably occurred during fish evolution from a genome duplication event. There might be TroIGFBP5ba in the golden pompano genome waiting for us to discover.

A number of studies have reported the tissue-specific expression of IGFBP5. According to these reports, IGFBP5 has been identified in multiple tissues and different types of cells not only in humans and mice (13, 22, 43–46) but also in teleost and invertebrates (8, 16, 19, 47, 48). In mammals, the transcription levels of other IGFBPs were usually more abundant in the liver, while IGFBP5 was different and was more abundant in the kidney (49, 50). In teleosts, the duplicated IGFBP5 showed different expression patterns in the tested tissues. The IGFBP5b mRNA of zebrafish was detected in the brain, gill, eye, heart, gut, kidney, and gonad, while IGFBP5a was detected with a high level in the brain and gill but could not be detected in the liver and muscle (8). Compared with the expression in grass carp, GcIGFBP5b was markedly present in the liver and brain as well as in the heart, skin, and muscles at low levels (16). In the current study, TroIGFBP5b expression was most abundant in immune organs. The top five tissues with the highest expression level were the liver, spleen, brain, gill, and head kidney. In humans, IGFBP5 was closely related to many diseases, such as colorectal cancer, chronic rhinosinusitis, sarcopenia, and so on (51–55), and pathogen infection induced a significantly higher expression of IGFBP5 in mammals—for example, IGFBP5 expression was significantly upregulated after *Salmonella enterica* stimulation in pigs (56). In our study, *V. harveyi* caused a significant induction of TroIGFBP5b in the liver, spleen, and head kidney. All of these suggested that TroIGFBP5b was involved in antimicrobial immunity.

Studies proved that IGFBP5 was a secreted protein, while it was also found in the nucleus to interact with nuclear proteins (23, 44, 57). The

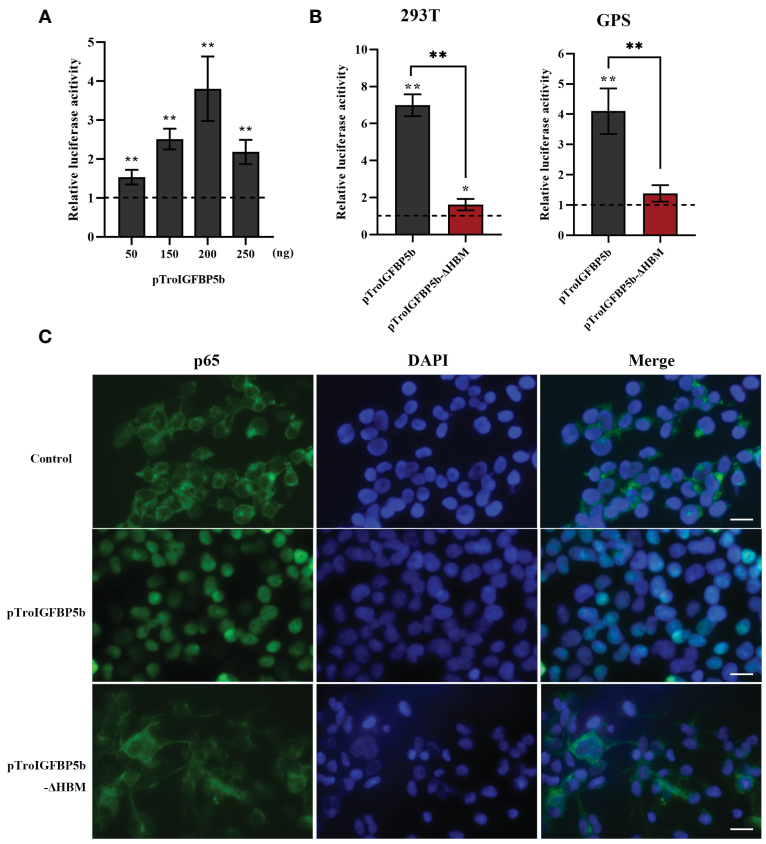

FIGURE 7
Effects of TroIGFBP5b overexpression on the activity of NF-κB pathways *in vitro*. **(A)** pTroIGFBP5b (50, 150, 200, and 250 ng/well) was co-transfected with pGL4.32 (Luc2P/NF-κB) and pRL-CMV into 293T cells incubated in a 24-well cell plate. **(B)** pTroIGFBP5b (200 ng/well) and pTroIGFBP5b-ΔHBM (200 ng/well) were co-transfected with 200 ng/well pGL4.32 (Luc2P/NF-κB) and 50 ng/well pRL-CMV into 293T and golden pompano snout cells incubated in a 24-well cell plate, respectively. After 48 h post-transfection, firefly and renilla luciferase activities were detected in the cell lysates. The data were shown as means ± SD ($N = 3$). *N*, number of times the experiment was performed. **(C)** 293T cells transfected with pCN3, pTroIGFBP5b, and pTroIGFBP5b-ΔHBM were stained with anti-p65 antibody and AlexaFluor-488. Bar = 30 μm. The experiment was done in triplicate, and one of them was displayed. The statistical significance was indicated (*$P < 0.05$, **$P < 0.01$).

nucleus IGFBP5 was detected in the breast cancer cell line (T47D), lung fibroblasts from idiopathic pulmonary fibrosis patients, and vascular smooth muscle cells (25, 41, 58). Various studies also reported that the localization of IGFBP determines its roles, and the NLS domain was crucial for its subcellular location (24, 28, 58, 59). In MDA-MB-435 cells (a kind of breast cancer cell), wild-type IGFBP5 could translocate to the nucleus and inhibit cell proliferation and migration; on the contrary, NLS-mutant was mainly detected in the cytoplasm and enhanced the proliferation and migration of cells (24). In MCF-7 (breast) and LnCaP (prostate) cells, IGFBP2 possessed a functional NLS sequence, and the activation of VEGF expression and subsequent angiogenesis required the nuclear IGFBP2 (60). HBMs are found in many secreted proteins and responsible for binding to heparan sulfate proteoglycans which take part in a variety of biological processes, including signal transduction, cell adhesion, and blood coagulation (61, 62). Furthermore, the HBM in the NLS domain of IGFBP5 C-terminal domain was functional heparin binding motif (42). In teleosts, studies on the relationship between localization and functions of IGFBP are very limited. In zebrafish, the subcellular localizations of IGFBP5a and IGFBP5b were different. IGFBP5a was only found in the nucleus, and IGFBP5b was found in both the nucleus and the cytoplasm (8). Our results showed that TroIGFBP5b with SP was mostly in the cytoplasm, and mature TroIGFBP5b without SP was found in both the nucleus and the cytoplasm. In mammary epithelium, the overexpression of mature IGFBP5 resulted in nuclear localization, whereas upon expression of the secreted form, no nuclear localization was observed under physiological conditions (63). Previous studies proved that the location of protein always affected its role. In the present study, TroIGFBP5b was transferred from the cytoplasm to the nucleus after being stimulated by LPS or *V. harveyi*, while the phenomenon of TroIGFBP5b-ΔHBM that was to be found in the cytoplasm did not occur. Similar findings were found in T47D breast cancer cells, which provided the necessary NLS residues for nuclear accumulation (23). It was interesting that, in mammary epithelium cells, it was found that intracellular trafficking of IGFBP5 would be restricted to vesicular structures in the cytoplasm and not be uptaken into the nucleus unless the integrity of the plasma membrane was compromised (63). In our results, TroIGFBP5b nuclear uptake occurred probably due to the cell membrane damage after LPS or bacteria stimulation, leading to the loss of membrane integrity (64). Our results indicated that HBM plays a key role in the trigger of the TroIGFBP5b translocation to the nucleus upon stimulation.

In mammals, many studies revolved around the function of IGFBP5 in modulating cell migration and proliferation and in regulating immune processes (65). The recombinant IGFBP5 could

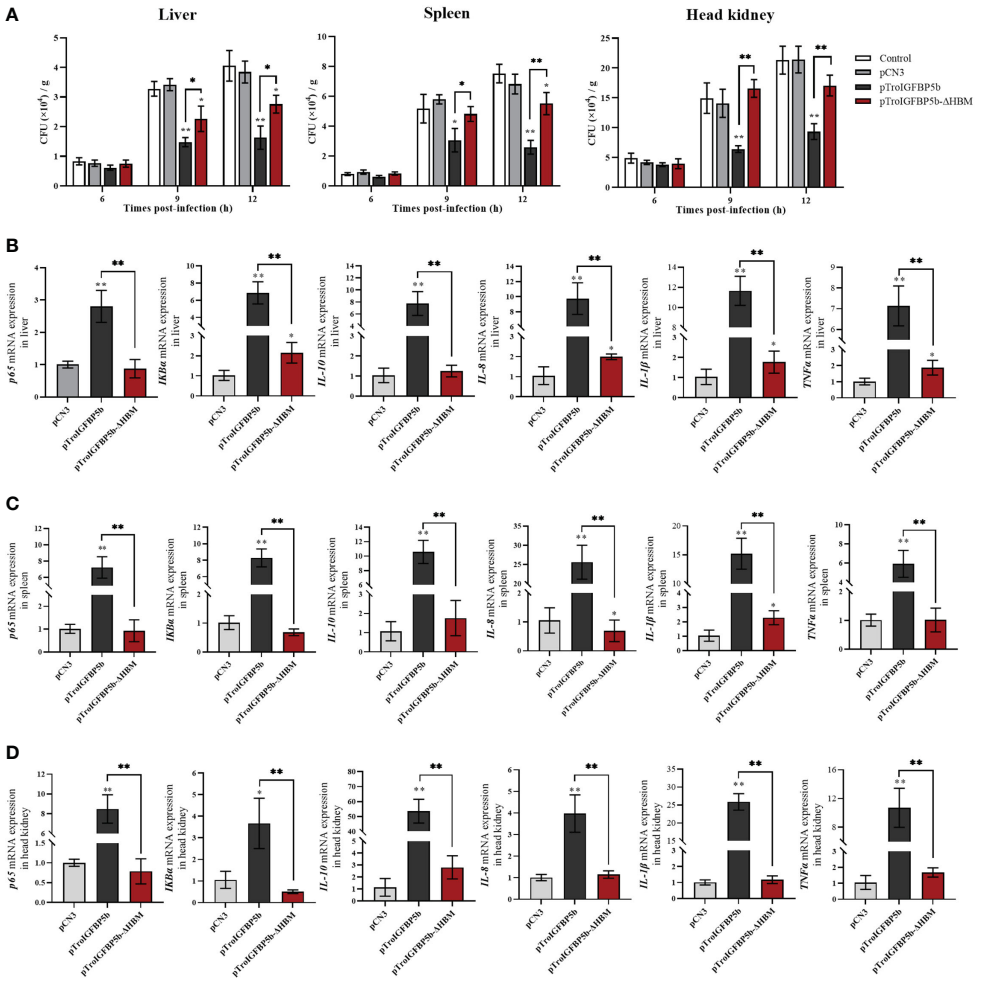

FIGURE 8
In vivo antibacterial ability of IGFBP5-ΔHBM. **(A)** *T. ovatus*, which was injected with pTroIGFBP5b, pTroIGFBP5b-ΔHBM, pCN3, and phosphate-buffered saline (control) for 5 days, was infected with *V. harveyi*; then, the bacterial load in the tissues was determined. Effect of TroIGFBP5b and TroIGFBP5b-ΔHBM on the expressions of proinflammatory cytokines in the liver **(B)**, spleen **(C)**, and head kidney **(D)** at 5 days after the injection of pTroIGFBP5b and pTroIGFBP5b-ΔHBM. The data were shown as means ± SD (N = 3), and the statistical significance was indicated (*P < 0.05, **P < 0.01).

increase human RPE cell proliferation, promote periodontal tissue regeneration, and reduce local inflammation (43, 66, 67). Multiple studies showed that IGFBP5 could directly affect inflammation mediated by immune cells and suggested that IGFBP5 exerts anti-inflammatory effects by maintaining immune homeostasis (14, 43). In the current study, the biological properties of TroIGFBP5b were analyzed. The *in vitro* assays showed that rTroIGFBP5b enhanced the cell proliferation of PBLs in a dose-dependent manner and significantly enhanced HKM phagocytic activity, suggesting that rTroIGFBP5b could induce the activation of some immune cells. In contrast, rTroIGFBP5b-ΔHBM was significantly reduced in the activation of PBLs and HKMs. Furthermore, *in vivo* overexpression and knockdown experiments confirmed the role of TroIGFBP5b in fish disease resistance. However, after the HBM of TroIGFBP5b was deleted, its antibacterial ability after overexpression was inhibited. These results further confirmed the role of TroIGFBP5b in antibacterial immune response, and HBM played an important role in antibacterial immunity. However, the underlying mechanisms by which IGFBP and HBM participate in immune response remained an area that has not been thoroughly studied and thus needed more research. Relative reports suggested that the IGF system regulated the immune function and represented an important switch governing immune responses (68).

The NF-κB signaling pathway was the main regulator of inflammatory responses to pathogens, and p65, which belonged to the five NF-κB monomers, would translocate from the cytoplasm to the nucleus after activation (69, 70). Nowadays, many studies found that the IGFBP family got its job done *via* the NF-κB signaling pathway, such as IGFBP2, which promotes PDAC cell invasion and metastasis through the NF-κB pathway (69). In prostate cancer cells, rIGFBP-3 significantly suppressed the NF-κB activity (71). IGFBP5 was proven to inhibit the phorbol myristate acetate-induced NF-κB activity and IL-6 expression in U-937 cells (72). The novel findings in this study showed that, in both 293T and GPS cells, TroIGFBP5b showed a significant upregulation effect in NF-κB activity, while overexpression of TroIGFBP5b-ΔHBM did not. Similar results were also discovered in stimulating the transfer of p65 to the nucleus. On the other hand, activating the NF-κB pathway can regulate the expression of related genes, especially inflammatory cytokines (73–75). In our study, the *in vivo* analysis showed that, after the injection

with pTroIGFBP5b, the mRNA transcriptions of NF-κB-related genes (p65 and ikBα) and several cytokines were significantly induced, including *IL-8*, *IL-10*, *IL-1β*, and *TNF-α*. However, after the HBM of TroIGFBP5b was deleted, its function of upregulating the expression of inflammatory cytokines in immune tissues was almost lost. Therefore, these results demonstrated that TroIGFBP5b could not only activate the NF-κB activity and p65 nuclear translocation but also increase the proinflammatory cytokine level, and this indicated that the HBM domain of TroIGFBP5b seemed to function a key role in these processes.

To sum up, the TroIGFBP5b was cloned and identified in this study. TroIGFBP5b was expressed higher *in vivo* in some immune-related tissues and showed a significant upregulated response after the bacterial infection. Overexpressing TroIGFBP5b could improve the body's antibacterial immunity significantly. In contrast, this ability was decreased after its knockdown. An HBM-deficient mutation of TroIGFBP5b was constructed to better understand the mechanism of its antibacterial immunity. The *in vitro* studies demonstrated that TroIGFBP5b could promote PBL proliferation, stimulated macrophage activation, induced the NF-κB promoter activity, and promoted the nuclear translocation of p65, while the HBM mutant, compared with the wild type, failed to function with those abilities. Overall, the results showed that TroIGFBP5b was essential in the antimicrobial immunity of golden pompano and that HBM was also of great importance in the NF-κB pathway activation.

Data availability statement

The datasets presented in this study can be found in online repositories. The names of the repository/repositories and accession number(s) can be found in the article/Supplementary Material.

Ethics statement

The animal study was reviewed and approved by Animal Care and Use Committee of the Hainan University. Written informed consent was obtained from the owners for the participation of their animals in this study.

Author contributions

HD and YZ conceived and designed the experiments and wrote the manuscript draft. XD, PZ, and ZC performed the experiments and analyzed the data. YS was responsible for forming the hypothesis, project development, data coordination, and writing, finalizing, and submitting the manuscript. All authors contributed to the article and approved the submitted version.

Funding

This research was funded by the National Natural Science Foundation of China (U22A20534), Hainan Province Science and Technology Special Fund (ZDYF2021XDNY298), and Nanhai Famous Youth Project.

Conflict of interest

The authors declare that the research was conducted in the absence of any commercial or financial relationships that could be construed as a potential conflict of interest.

Publisher's note

Supplementary material

The Supplementary Material for this article can be found online at: https://www.frontiersin.org/articles/10.3389/fimmu.2023.1126843/full#supplementary-material

References

1. Song F, Zhou XX, Hu Y, Li G, Wang Y. The roles of insulin-like growth factor binding protein family in development and diseases. *Adv Ther* (2021) 38(2):885–903. doi: 10.1007/s12325-020-01581-x

2. Kiepe D, Ulinski T, Powell DR, Durham SK, Mehls O, Tonshoff B. Differential effects of insulin-like growth factor binding proteins-1, -2, -3, and -6 on cultured growth plate chondrocytes. *Kidney Int* (2002) 62(5):1591–600. doi: 10.1046/j.1523-1755.2002.00603.x

3. Nguyen DV, Li Calzi S, Shaw LC, Kielczewski JL, Korah HE, Grant MB. An ocular view of the IGF-IGFBP system. *Growth Horm IGF Res* (2013) 23(3):45–52. doi: 10.1016/j.ghir.2013.03.001

4. Firth SM, Baxter RC. Cellular actions of the insulin-like growth factor binding proteins. *Endocrine Rev* (2002) 23(6):824–54. doi: 10.1210/er.2001-0033

5. Baxter Robert C. Insulin-like growth factor (IGF)-binding proteins: interactions with IGFs and intrinsic bioactivities. *Am J Physiol* (2000) 278(6):E967–76. doi: 10.1152/ajpendo.2000.278.6.E967

6. Duan C, Allard JB. Insulin-like growth factor binding protein-5 in physiology and disease. *Front Endocrinol (Lausanne)* (2020) 11:100. doi: 10.3389/fendo.2020.00100

7. Andress DL, Birnbaum RS. A novel human insulin-like growth factor binding protein secreted by osteoblast-like cells. *Biochem Biophys Res Commun* (1991) 176 (1):213–8. doi: 10.1016/0006-291x(91)90911-p

8. Wei D, Hiroyasu K, Yang Z, Jun D, Zhou D, Cunming D. Duplicated zebrafish insulin-like growth factor binding protein-5 genes with split functional domains: evidence for evolutionarily conserved IGF binding, nuclear localization, and transactivation activity. *FASEB J* (2010) 24(6):2020–9. doi: 10.1096/fj.09-149435

9. Allander SV, Coleman M, Luthman H, Powell DR. Chicken insulin-like growth factor binding protein (IGFBP)-5: conservation of IGFBP-5 structure and expression during evolution. *Comp Biochem Physiol Part B Biochem Mol Biol* (1997) 116(4):477. doi: 10.1016/s0305-0491(96)00289-1

10. Rehman MS, Mushtaq M, Hassan FU, Zia-Ur R, Mushahid M, Shokrollahi B. Comparative genomic characterization of insulin-like growth factor binding proteins in cattle and buffalo. *BioMed Res Int* (2022) 2022:5893825. doi: 10.1155/2022/5893825

11. Hiscott P, Sheridan C, Magee RM, Grierson I. Matrix and the retinal pigment epithelium in proliferative retinal disease. *Prog Retinal Eye Res* (1999) 18(2):167–90. doi: 10.1016/s1350-9462(98)00024-x

12. Simon CM RS, Gunnersen JM, Holtmann B, Drepper C, Dombert B, Braga M, et al. Dysregulated IGFBP5 expression causes axon degeneration and motoneuron loss in diabetic neuropathy. *Acta Neuropathol* (2015) 130(3):373–87. doi: 10.1007/s00401-015-1446-8

13. Wang S, Hong Q, Geng X, Chi K, Cai G, Wu D. Insulin-like growth factor binding protein 5–a probable target of kidney renal papillary renal cell carcinoma. *BioMed Res Int* (2019) 2019:1–10. doi: 10.1155/2019/3210324

14. Zhu M, Han H, Hu L, Cao Y, Fan Z. Insulin-binding protein-5 down-regulates the balance of Th17/Treg. *Front Immunol* (2022) 13:1019248. doi: 10.3389/fimmu.2022.1019248

15. Liu D, Wang Y, Jia Z, Wang L, Wang J, Yang D, et al. Demethylation of IGFBP5 by histone demethylase KDM6B promotes mesenchymal stem cell-mediated periodontal tissue regeneration by enhancing osteogenic differentiation and anti-inflammation potentials. *Stem Cells (Dayton Ohio)* (2015) 33(8):2523–36. doi: 10.1002/stem.2018

16. Zheng GD, Zhou CX, Lin ST, Chen J, Jiang XY, Zou SM. Two grass carp (*Ctenopharyngodon idella*) insulin-like growth factor-binding protein 5 genes exhibit different yet conserved functions in development and growth. *Comp Biochem Physiol B Biochem Mol Biol* (2017) 204:69–76. doi: 10.1016/j.cbpb.2016.11.008

17. Macqueen DJ, Garcia de la serrana D, Johnston IA. Evolution of ancient functions in the vertebrate insulin-like growth factor system uncovered by study of duplicated salmonid fish genomes. *Mol Biol Evol* (2013) 30(5):1060–76. doi: 10.1093/molbev/mst017

18. Kamangar BB, Gabillard JC, Bobe J. Insulin-like growth factor-binding protein (IGFBP)-1, -2, -3, -4, -5, and -6 and IGFBP-related protein 1 during rainbow trout postvitellogenesis and oocyte maturation: molecular characterization, expression profiles, and hormonal regulation. *Endocrinology* (2006) 147(5):2399–410. doi: 10.1210/en.2005-1570

19. Safian D, Fuentes EN, Valdés JA, Molina A. Dynamic transcriptional regulation of autocrine/paracrine igfbp1, 2, 3, 4, 5, and 6 in the skeletal muscle of the fine flounder during different nutritional statuses. *J Endocrinol* (2012) 214(1):95–108. doi: 10.1530/joe-12-0057

20. Garcia de la Serrana D, Macqueen DJ. Insulin-like growth factor-binding proteins of teleost fishes. *Front Endocrinol* (2018) 9:80. doi: 10.3389/fendo.2018.00080

21. Wood AW, Duan C, Bern HA. Insulin-like growth factor signaling in fish. *Int Rev Cytol* (2005) 243:215–85. doi: 10.1016/s0074-7696(05)43004-1

22. Assassi S, Su Y, Nishimoto T, Feghali-Bostwick C. IGFBP-5 promotes fibrosis independently of its translocation to the nucleus and its interaction with nucleolin and IGF. *PloS One* (2015) 10(6):e0130546. doi: 10.1371/journal.pone.0130546

23. Schedlich LJ, Le Page SL, Firth SM, Briggs LJ, Jans DA, Baxter RC. Nuclear import of insulin-like growth factor-binding protein-3 and -5 is mediated by the importin beta subunit. *J Biol Chem* (2000) 275(31):23462–70. doi: 10.1074/jbc.M002208200

24. Akkiprik M, Hu L, Sahin A, Hao X, Zhang W. The subcellular localization of IGFBP5 affects its cell growth and migration functions in breast cancer. *BMC Cancer* (2009) 9:103. doi: 10.1186/1471-2407-9-103

25. Yasuoka H, Hsu E, Ruiz XD, Steinman RA, Choi AM, Feghali-Bostwick CA. The fibrotic phenotype induced by IGFBP-5 is regulated by MAPK activation and egr-1-dependent and -independent mechanisms. *Am J Pathol* (2009) 175(2):605–15. doi: 10.2353/ajpath.2009.080991

26. Abrass CK, Berfield AK, Andress DL. Heparin binding domain of insulin-like growth factor binding protein-5 stimulates mesangial cell migration. *Am J Physiol* (1997) 273(6):F899–906. doi: 10.1152/ajprenal.1997.273.6.F899

27. Shand JH, Beattie J, Song H, Phillips K, Kelly SM, Flint DJ, et al. Specific amino acid substitutions determine the differential contribution of the n- and c-terminal domains of insulin-like growth factor (IGF)-binding protein-5 in binding IGF-I. *J Biol Chem* (2003) 278(20):17859–66. doi: 10.1074/jbc.M300526200

28. Allan GJ, Tonner E, Szymanowska M, Shand JH, Kelly SM, Phillips K, et al. Cumulative mutagenesis of the basic residues in the 201-218 region of insulin-like growth factor (IGF)-binding protein-5 results in progressive loss of both IGF-I binding and inhibition of IGF-I biological action. *Endocrinology* (2006) 147(1):338–49. doi: 10.1210/en.2005-0582

29. Beattie J, Allan GJ, Lochrie JD, Flint DJ. Insulin-like growth factor-binding protein-5 (IGFBP-5): a critical member of the IGF axis. *Biochem J* (2006) 395(1):1–19. doi: 10.1042/BJ20060086

30. Ni X, Li X, Ran G, Chen J, Jiang X, Sun J, et al. Determination of the geographical origin of *Trachinotus ovatus and Pampus argenteus* in China by multi-element and stable isotope analysis. *Food Chem* (2022) 394:133457. doi: 10.1016/j.foodchem.2022.133457

31. Tu Z, Li H, Zhang X, Sun Y, Zhou Y. Complete genome sequence and comparative genomics of the golden pompano (*Trachinotus ovatus*) pathogen, *Vibrio harveyi* strain QT520. *PeerJ* (2017) 5:e4127. doi: 10.7717/peerj.4127

32. Yu Y, Wei S, Wang Z, Huang X, Huang Y, Cai J, et al. Establishment of a new cell line from the snout tissue of golden pompano trachinotus ovatus, and its application in virus susceptibility. *J Fish Biol* (2016) 88(6):2251–62. doi: 10.1111/jfb.12986

33. Chen Y, Zhou Y, Yang X, Cao Z, Chen X, Qin Q, et al. Insulin-like growth factor binding protein 3 gene of golden pompano (TroIGFBP3) promotes antimicrobial immune defense. *Fish Shellfish Immunol* (2020) 103:47–57. doi: 10.1016/j.fsi.2020.04.002

34. Jiao XD, Zhang M, Hu YH, Sun L. Construction and evaluation of DNA vaccines encoding *Edwardsiella tarda* antigens. *Vaccine* (2009) 27(38):5195–202. doi: 10.1016/j.vaccine.2009.06.071

35. Diao Q, Du H, Zhao N, Wu Y, Du X, Sun Y, et al. Cathepsin C (CTSC) contributes to the antibacterial immunity in golden pompano *Trachinotus ovatus*. *Fish Shellfish Immunol* (2022) 128:316–26. doi: 10.1016/j.fsi.2022.07.078

36. Sun B, Lei Y, Cao Z, Zhou Y, Sun Y, Wu Y, et al. TroCCL4, a CC chemokine of *Trachinotus ovatus*, is involved in the antimicrobial immune response. *Fish Shellfish Immunol* (2018) 86:525–35. doi: 10.1016/j.fsi.2018.11.080

37. Yun S, Sun L, Yolande R. CsBAFF, a teleost b cell activating factor, promotes pathogen-induced innate immunity and vaccine-induced adaptive immunity. *PloS One* (2015) 10(8):e0136015. doi: 10.1371/journal.pone.0136015

38. Du H, Cao Z, Liu Z, Wang G, Wu Y, Du X, et al. *Cromileptes altivelis* microRNA transcriptome analysis upon nervous necrosis virus (NNV) infection and the effect of cal-miR-155 on cells apoptosis and virus replication. *Viruses* (2022) 14(10):2184. doi: 10.3390/v14102184

39. LeRoith D, Holly JMP, Forbes BE. Insulin-like growth factors: Ligands, binding proteins, and receptors. *Mol Metab* (2021) 52:101245. doi: 10.1016/j.molmet.2021.101245

40. Waters JA, Urbano I, Robinson M, House CD. Insulin-like growth factor binding protein 5: Diverse roles in cancer. *Front Oncol* (2022) 12:1052457. doi: 10.3389/fonc.2022.1052457

41. Xu Q, Li S, Zhao Y, Maures TJ, Yin P, Duan C. Evidence that IGF binding protein-5 functions as a ligand-independent transcriptional regulator in vascular smooth muscle cells. *Circ Res* (2004) 94(5):E46–54. doi: 10.1161/01.Res.0000124761.62846.Df

42. Song H, Shand JH, Beattie J, Flint DJ, Allan GJ. The carboxy-terminal domain of IGF-binding protein-5 inhibits heparin binding to a site in the central domain. *J Mol Endocrinol* (2001) 26(3):229–39. doi: 10.1677/jme.0.0260229

43. Yasuoka H, Yamaguchi Y, Feghali-Bostwick CA. The pro-fibrotic factor IGFBP-5 induces lung fibroblast and mononuclear cell migration. *Am J Respir Cell Mol Biol* (2009) 41(2):179–88. doi: 10.1165/rcmb.2008-0211OC

44. Schedlich LJ, Muthukaruppan A, O'Han MK, Baxter RC. Insulin-like growth factor binding protein-5 interacts with the vitamin D receptor and modulates the vitamin D response in osteoblasts. *Mol Endocrinol* (2007) 21(10):2378–90. doi: 10.1210/me.2006-0558

45. Moralez AM, Maile LA, Clarke J, Busby WHJr., Clemmons DR. Insulin-like growth factor binding protein-5 (IGFBP-5) interacts with thrombospondin-1 to induce negative regulatory effects on IGF-I actions. *J Cell Physiol* (2005) 203(2):328–34. doi: 10.1002/jcp.20343

46. Schneider MR, Wolf E, Hoeflich A, Lahm H. IGF-binding protein-5: flexible player in the IGF system and effector on its own. *J Endocrinol* (2002) 172(3):423–40. doi: 10.1677/joe.0.1720423

47. Sharker MR, Kim SC, Hossen S, Kho KH. Characterization of insulin-like growth factor binding protein-5 (IGFBP-5) gene and its potential roles in ontogenesis in the pacific abalone, *Haliotis discus* hannai. *Biol (Basel)* (2020) 9(8):216. doi: 10.3390/biology9080216

48. Fan S, Wang Z, Yu D, Xu Y. Molecular cloning and expression profiles of an insulin-like growth factor binding protein IGFBP5 in the pearl oyster, *Pinctada fucata*. *J Appl Anim Res* (2018) 46(1):1395–402. doi: 10.1080/09712119.2018.1517647

49. Schuller AG, Groffen C, van Neck JW, Zwarthoff EC, Drop SL. cDNA cloning and mRNA expression of the six mouse insulin-like growth factor binding proteins. *Mol Cell Endocrinol* (1994) 104(1):57–66. doi: 10.1016/0303-7207(94)90051-5

50. Shimasaki S, Shimonaka M, Zhang HP, Ling N. Identification of five different insulin-like growth factor binding proteins (IGFBPs) from adult rat serum and molecular cloning of a novel IGFBP-5 in rat and human. *J Biol Chem* (1991) 266(16):10646–53. doi: 10.1016/S0021-9258(18)99272-0

51. Deng Y, Yang X, Hua H, Zhang C. IGFBP5 is upregulated and associated with poor prognosis in colorectal cancer. *Int J Gen Med* (2022) 15:6485–97. doi: 10.2147/ijgm.S370576

52. Sanada F, Taniyama Y, Muratsu J, Otsu R, Shimizu H, Rakugi H, et al. IGF binding protein-5 induces cell senescence. *Front Endocrinol (Lausanne)* (2018) 9:53. doi: 10.3389/fendo.2018.00053

53. Mueller SK, Nocera AL, Workman A, Libermann T, Dillon ST, Stegmann A, et al. Significant polyomic and functional upregulation of the PAPP-A/IGFBP-4/5/IGF-1 axis in chronic rhinosinusitis with nasal polyps. *Int Forum Allergy Rhinol* (2020) 10(4):546–55. doi: 10.1002/alr.22512

54. Bayol S, Loughna PT, Brownson C. Phenotypic expression of IGF binding protein transcripts in muscle, *in vitro* and *in vivo*. *Biochem Biophys Res Commun* (2000) 273(1):282–6. doi: 10.1006/bbrc.2000.2667

55. Spangenburg EE, Abraha T, Childs TE, Pattison JS, Booth FW. Skeletal muscle IGF-binding protein-3 and -5 expressions are age, muscle, and load dependent. *Am J Physiol Endocrinol Metab* (2003) 284(2):E340–50. doi: 10.1152/ajpendo.00253.2002

56. Davis BL, Fraser JN, Burkey TE, Skjolaas KA, Dritz SS, Johnson BJ, et al. Oral inoculation with salmonella enterica serovar typhimurium or choleraesuis promotes divergent responses in the somatotropic growth axis of swine. *J Anim Sci* (2010) 88(5):1642–8. doi: 10.2527/jas.2009-2259

57. Amaar YG, Thompson GR, Linkhart TA, Chen ST, Baylink DJ, Mohan S. Insulin-like growth factor-binding protein 5 (IGFBP-5) interacts with a four and a half LIM protein 2 (FHL2). *J Biol Chem* (2002) 277(14):12053–60. doi: 10.1074/jbc.M110872200

58. Schedlich LJ, Young TF, Firth SM, Baxter RC. Insulin-like growth factor-binding protein (IGFBP)-3 and IGFBP-5 share a common nuclear transport pathway in T47D human breast carcinoma cells. *J Biol Chem* (1998) 273(29):18347–52. doi: 10.1074/jbc.273.29.18347

59. Poreba E, Durzynska J. Nuclear localization and actions of the insulin-like growth factor 1 (IGF-1) system components: Transcriptional regulation and DNA damage response. *Mutat Res* (2020) 784:108307. doi: 10.1016/j.mrrev.2020.108307

60. Azar WJ, Zivkovic S, Werther GA, Russo VC. IGFBP-2 nuclear translocation is mediated by a functional NLS sequence and is essential for its pro-tumorigenic actions in cancer cells. *Oncogene* (2014) 33(5):578–88. doi: 10.1038/onc.2012.630

61. Nesterenko AM, Orlov EE, Ermakova GV, Ivanov IA, Semenyuk PI, Orlov VN, et al. Affinity of the heparin binding motif of Noggin1 to heparan sulfate and its visualization in the embryonic tissues. *Biochem Biophys Res Commun* (2015) 468(1-2):331–6. doi: 10.1016/j.bbrc.2015.10.100

62. Li JP, Kusche-Gullberg M. Heparan sulfate: Biosynthesis, structure, and function. *Int Rev Cell Mol Biol* (2016) 325:215–73. doi: 10.1016/bs.ircmb.2016.02.009

63. Jurgeit A, Berlato C, Obrist P, Ploner C, Massoner P, Schmolzer J, et al. Insulin-like growth factor-binding protein-5 enters vesicular structures but not the nucleus. *Traffic* (2007) 8(12):1815–28. doi: 10.1111/j.1600-0854.2007.00655.x

64. Nova Z, Skovierova H, Calkovska A. Alveolar-capillary membrane-related pulmonary cells as a target in endotoxin-induced acute lung injury. *Int J Mol Sci* (2019) 20(4):831. doi: 10.3390/ijms20040831

65. Ha YM, Nam JO, Kang YJ. Pitavastatin regulates ang II induced proliferation and migration *via* IGFBP-5 in VSMC. *Korean J Physiol Pharmacol* (2015) 19(6):499–506. doi: 10.4196/kjpp.2015.19.6.499

66. Samuel W, Kutty RK, Vijayasarathy C, Pascual I, Duncan T, Redmond TM. Decreased expression of insulin-like growth factor binding protein-5 during n-(4-hydroxyphenyl)retinamide-induced neuronal differentiation of ARPE-19 human retinal pigment epithelial cells: regulation by CCAAT/enhancer-binding protein. *J Cell Physiol* (2010) 224(3):827–36. doi: 10.1002/jcp.22191

67. Han N, Zhang F, Li G, Zhang X, Lin X, Yang H, et al. Local application of IGFBP5 protein enhanced periodontal tissue regeneration *via* increasing the migration, cell proliferation and osteo/dentinogenic differentiation of mesenchymal stem cells in an inflammatory niche. *Stem Cell Res Ther* (2017) 8(1):210. doi: 10.1186/s13287-017-0663-6

68. Smith TJ. Insulin-like growth factor-I regulation of immune function: a potential therapeutic target in autoimmune diseases? *Pharmacol Rev* (2010) 62(2):199–236. doi: 10.1124/pr.109.002469

69. Gao S, Sun Y, Zhang X, Hu L, Liu Y, Chua CY, et al. IGFBP2 activates the NF-kappaB pathway to drive epithelial-mesenchymal transition and invasive character in pancreatic ductal adenocarcinoma. *Cancer Res* (2016) 76(22):6543–54. doi: 10.1158/0008-5472.CAN-16-0438

70. Dorrington MG, Fraser IDC. NF-kappaB signaling in macrophages: Dynamics, crosstalk, and signal integration. *Front Immunol* (2019) 10:705. doi: 10.3389/fimmu.2019.00705

71. Han J, Jogie-Brahim S, Harada A, Oh Y. Insulin-like growth factor-binding protein-3 suppresses tumor growth *via* activation of caspase-dependent apoptosis and cross-talk with NF-kappaB signaling. *Cancer Lett* (2011) 307(2):200–10. doi: 10.1016/j.canlet.2011.04.004

72. Hwang JR, Huh JH, Lee Y, Lee SI, Rho SB, Lee JH. Insulin-like growth factor-binding protein-5 (IGFBP-5) inhibits TNF-alpha-induced NF-kappaB activity by binding to TNFR1. *Biochem Biophys Res Commun* (2011) 405(4):545–51. doi: 10.1016/j.bbrc.2011.01.064

73. Singh S, Singh TG. Role of nuclear factor kappa b (NF-κB) signalling in neurodegenerative diseases: An mechanistic approach. *Curr Neuropharmacol* (2020) 18 (10):918–35. doi: 10.2174/1570159x18666200207120949

74. Nilsson BO. Mechanisms involved in regulation of periodontal ligament cell production of pro-inflammatory cytokines: Implications in periodontitis. *J Periodontal Res* (2021) 56(2):249–55. doi: 10.1111/jre.12823

75. Gallucci GM, Alsuwayt B, Auclair AM, Boyer JL, Assis DN, Ghonem NS. Fenofibrate downregulates NF-κB signaling to inhibit pro-inflammatory cytokine secretion in human THP-1 macrophages and during primary biliary cholangitis. *Inflammation* (2022) 45(6):2570–81. doi: 10.1007/s10753-022-01713-1

frontiers | Frontiers in Immunology

TYPE Original Research
PUBLISHED 20 February 2023
DOI 10.3389/fimmu.2023.1128138

OPEN ACCESS

EDITED BY
Sun Yun,
Hainan University, China

REVIEWED BY
Xianghui Kong,
Henan Normal University, China
Zhi Liu,
Huazhong University of Science and Technology, China

*CORRESPONDENCE
Yong-An Zhang
yonganzhang@mail.hzau.edu.cn
Xu-Jie Zhang
xujiezhang@mail.hzau.edu.cn

SPECIALTY SECTION
This article was submitted to Molecular Innate Immunity, a section of the journal Frontiers in Immunology

RECEIVED 20 December 2022
ACCEPTED 02 February 2023
PUBLISHED 20 February 2023

CITATION
Liu X, Hu Y-Z, Pan Y-R, Liu J, Jiang Y-B, Zhang Y-A and Zhang X-J (2023) Comparative study on antibacterial characteristics of the multiple liver expressed antimicrobial peptides (LEAPs) in teleost fish.
Front. Immunol. 14:1128138.
doi: 10.3389/fimmu.2023.1128138

Comparative study on antibacterial characteristics of the multiple liver expressed antimicrobial peptides (LEAPs) in teleost fish

Xun Liu[1], Ya-Zhen Hu[1], Yi-Ru Pan[1], Jia Liu[1], You-Bo Jiang[1], Yong-An Zhang[1,2]* and Xu-Jie Zhang[1]*

[1]State Key Laboratory of Agricultural Microbiology, Hubei Hongshan Laboratory, Engineering Research Center of Green Development for Conventional Aquatic Biological Industry in the Yangtze River Economic Belt, Ministry of Education, College of Fisheries, Huazhong Agricultural University, Wuhan, China, [2]Guangdong Laboratory for Lingnan Modern Agriculture, Guangzhou, China

Antimicrobial peptides are important components of the host innate immune system, forming the first line of defense against infectious microorganisms. Among them, liver-expressed antimicrobial peptides (LEAPs) are a family of antimicrobial peptides that widely exist in vertebrates. LEAPs include two types, named LEAP-1 and LEAP-2, and many teleost fish have two or more *LEAP-2s*. In this study, *LEAP-2C* from rainbow trout and grass carp were discovered, both of which are composed of 3 exons and 2 introns. The antibacterial functions of the multiple LEAPs were systematically compared in rainbow trout and grass carp. The gene expression pattern revealed that rainbow trout and grass carp *LEAP-1*, *LEAP-2A*, *LEAP-2B* and/or *LEAP-2C* were differentially expressed in various tissues/organs, mainly in liver. After bacterial infection, the expression levels of *LEAP-1*, *LEAP-2A*, *LEAP-2B* and/or *LEAP-2C* in the liver and gut of rainbow trout and grass carp increased to varying degrees. Moreover, the antibacterial assay and bacterial membrane permeability assay showed that rainbow trout and grass carp LEAP-1, LEAP-2A, LEAP-2B and LEAP-2C all have antibacterial activities against a variety of Gram-positive and Gram-negative bacteria with varying levels through membrane rupture. Furthermore, cell transfection assay showed that only rainbow trout LEAP-1, but not LEAP-2, can lead to the internalization of ferroportin, the only iron exporter on cell surface, indicating that only LEAP-1 possess iron metabolism regulation activity in teleost fish. Taken together, this study systematically compared the antibacterial function of LEAPs in teleost fish and the results suggest that multiple LEAPs can enhance the immunity of teleost fish through different expression patterns and different antibacterial activities to various bacteria.

KEYWORDS

rainbow trout, grass carp, LEAP-1, LEAP-2, expression pattern, antibacterial activity

Introduction

Antimicrobial peptides (AMPs) are widely found in organisms and are considered to be the first line of host defense against pathogens (1, 2). With the increasing resistance of bacteria to traditional antibiotics, AMPs have gradually become one of the important alternatives to antibiotics (3, 4). There are two main antibacterial mechanisms of AMPs: direct sterilization and immune regulation, and the sterilization mechanism can be divided into membrane targeting and non-membrane targeting (5). In addition to their broad-spectrum antibacterial activities, AMPs can also inhibit fungi, viruses and parasites (6). Compared with other species, some AMPs derived from fish, shrimp, crabs and other aquatic animals have unique structures and functions (7, 8).

Liver-expressed antimicrobial peptide (LEAP) is a class of antibacterial peptides expressed and secreted by liver, including LEAP-1 and LEAP-2. Both LEAP-1 and LEAP-2 can be separated and purified from human plasma (9, 10). *LEAP-1* exists as a single gene in the vast majority of mammals, which is highly expressed in the liver, followed by heart and brain (9). Because of its dual functions of antibacterial and iron regulation, LEAP-1 is also known as hepcidin. LEAP-1 mainly binds to ferroportin (Fpn), the only known iron exporter on the surface of cells (11), to facilitate its internalization, thus affecting the absorption and release of iron ion in iron storage cells (12–14). Fish have two hepcidin isoforms, hamp1 and hamp2; however, hamp1 is found to exist in both ray-finned and lobe-finned fish, while hamp2 is only found to exist in ray-finned fish, and the tissue distribution of hepcidin in most teleost fish is polymorphic (15–17).

Mammalian *LEAP-2* is a single gene, which is mainly expressed by the liver, and to a certain extent by other tissues (18). For example, mouse *LEAP-2* is mainly expressed in the liver and small intestine (18). Studies have shown that the mature peptide 38-77 of human LEAP-2 has different killing effects on both Gram-positive and Gram-negative bacteria, while its cleaved form 44-77 loses antibacterial activity but participates in the blood circulation of the body (19). Therefore, LEAP-2 may have other physiological functions besides sterilization. However, unlike mammals with a single *LEAP-2*, three *LEAP-2s* have been discovered in fish species, including *LEAP-2A*, *LEAP-2B* and *LEAP-2C* (20–23), and the tissue expression patterns in different fish species are also different (22, 24). Teleost LEAP-2 can enhance the bacterial killing efficiency of monocytes/macrophages (25, 26) and has a synergistic effect with antibiotics on the killing of drug-resistant bacteria (27).

So far, systematic comparative studies on the antibacterial functions of LEAPs are still blank. Therefore, this study was devoted to analyzing the antibacterial functions of LEAPs and conducting a systematic comparative study to lay a theoretical foundation for their use as feed additives to prevent bacterial diseases in fish.

Materials and methods

Experimental fish and cells

Rainbow trout (*Oncorhynchus mykiss*) (30 ± 5 g) and grass carp (*Ctenopharyngodon idella*) (200 ± 20 g) were purchased from Dujiang Dam Rainbow Trout Farm (Chengdu, China) and Xiantao Hatchery (Xiantao, China) respectively. They were maintained and acclimated to the laboratory conditions for at least two weeks before experiments. All animal experiments in this study were approved by the Committee on the Ethics of Animal Experiments at Huazhong Agricultural University.

Human embryonic kidney 293T (HEK293T) cells were cultured in 5% CO_2 at 37°C. Dulbecco's modified Eagle's medium (DMEM) (HyClone) was supplemented with 10% fetal bovine serum (FBS) (Gibco), 100 g/mL penicillin (Sigma-Aldrich), and 100 g/mL streptomycin (Sigma-Aldrich).

Searching, identification, and localization of *LEAPs* in rainbow trout and grass carp genome

The chromosome-level genome of grass carp was assembled by our laboratory and deposited in the NCBI BioProjects with the accession number PRJNA745929 (28). The published fish *LEAPs*, especially zebrafish *LEAPs*, were used to search against the grass carp genome using the Basic Local Alignment Search Tool (BLAST). Interestingly, in addition to *LEAP-2A* and *LEAP-2B*, *LEAP-2C* was found in grass carp. The grass carp *LEAP-2C* was cloned and submitted to the GenBank database (https://www.ncbi.nlm.nih.gov/genbank/) under the accession number OQ026323. Similarly, the rainbow trout *LEAP-2C* was cloned and submitted to the GenBank database under the accession number GQ870279.1.

Sequence alignment and phylogenetic analysis

The signal peptide of the deduced amino acid sequences was predicted using the SignalP 5.0 Server (https://services.healthtech.dtu.dk/service.php?SignalP-5.0). The *LEAPs* gene organizations, including exon, intron and UTR were determined by aligning the cDNA sequences with the gene sequences. The protein sequence identity was calculated using the BioEdit software (version 7.0.9). Multiple sequence alignment was conducted with the ClustalX program (version 3.0), and phylogenetic tree was constructed based on the alignments using the neighbour-joining method with 1000 bootstrap times using the MEGA program (version 4.1). All the sequences used for multiple sequence alignment and phylogenetic analysis were listed in Table 1.

10.3389/fimmu.2023.1128138

TABLE 1 LEAP sequences used in this study.

Species	Protein	GenBank accession no.
Homo sapiens	LEAP-1	NP_066998.1
Oryctolagus cuniculus	LEAP-1	XP_008247717.1
Mus musculus	LEAP-1	NP_115930.1
Strigops habroptila	LEAP-1	XP_030330703.1
Xenopus laevis	LEAP-1	XP_018097982.2
Zootoca vivipara	LEAP-1	XP_034976619.1
Oncorhynchus mykiss	LEAP-1	ADU85830.1
Ctenopharyngodon idella	LEAP-1	AEZ51835.1
Danio rerio	LEAP-1	NP_991146.1
Salmo salar	LEAP-1	NP001134321.1
Scophthalmus maximus	LEAP-1	AAX92670.1
Dicentrarchus labrax	LEAP-1	KJ890391.1
Homo sapiens	LEAP-2	AJ306405.1
Oryctolagus cuniculus	LEAP-2	NP_001164729.1
Mus musculus	LEAP-2	AJ409055.1
Gallus gallus	LEAP-2	AAS99322.1
Strigops habroptila	LEAP-2	XP_030360362.1
Xenopus laevis	LEAP-2	NC_054375.1
Zootoca vivipara	LEAP-2	XP_034961285.1
Oncorhynchus mykiss	LEAP-2A	AAR11766.1
Oncorhynchus mykiss	LEAP-2B	AAR11767.1
Oncorhynchus mykiss	LEAP-2C	GQ870279.1
Ctenopharyngodon idella	LEAP-2A	ACR54299.1
Ctenopharyngodon idella	LEAP-2B	AOG20830.1
Ctenopharyngodon idella	LEAP-2C	OQ026323
Danio rerio	LEAP-2A	BC162807.1
Danio rerio	LEAP-2B	AL918619.1
Danio rerio	LEAP-2C	NP_001373333.1

The mRNA expression of *LEAPs* in rainbow trout and grass carp tissues

Four healthy rainbow trout and grass carp were anesthetized with MS222 (1:10000), then the blood was removed from the body by cardiac perfusion using phosphate-buffered saline (PBS; pH 7.4; Gibco). The head kidney, spleen, gut, gill, skin, liver, heart, and muscle were collected, and the total RNA was extracted using the TRIzol Reagent (Takara). The cDNA was synthesized using the PrimeScript™ RT Reagent Kit contains gDNA Eraser (Takara). The mRNA expression levels of *LEAPs* were detected by quantitative real-time PCR (qPCR) using the CFX Connect™ Real-Time System (Bio-Rad). The primers used are listed in Table 2. The reaction mixture (20 μl) contained 1 μl cDNA, 10 μl SsoAdvanced™ SYBR Green Supermix (Bio-Rad), 1 μl forward primer (10 μM each) and 1 μl reverse primer (10 μM each). The amplification program was as follows: 95°C for 5 min, 45 cycles of amplification (95°C for 5 s and 60°C for 30 s), and then 65°C for 5 s. The tissue expression levels of *LEAPs* were determined using $2^{-\Delta Ct}$ method with *β-actin* as the internal reference.

Bacterial infection

To detect the immune responses of LEAPs during infection, rainbow trout and grass carp were intraperitoneally injected with 100 μL *Aeromonas salmonicida* BG1 (29) suspension culture (1×10^7 CFU/mL) and 200 μL *Aeromonas hydrophila* XS91-4-1 (30) suspension culture (8×10^6 CFU/mL) respectively, while the control fish were intraperitoneally injected with PBS instead after anesthetized with MS222 (1:10000). At 12 h, 1 d, 3 d, 5 d, and 7 d post-injection, the liver and gut of four individuals were sampled from each group. After the RNA extraction and cDNA synthesis, the expression levels of *LEAPs* in infected and control fish were determined by qPCR. The expression changes of *LEAPs* after infection were calculated using the $2^{-\Delta\Delta Ct}$ method, with *β-actin* as the internal reference.

Peptide synthesis

The mature peptides of rainbow trout and grass carp LEAPs were synthesized by GL Biochem Ltd. The purity was confirmed to be higher than 95% by HPLC and MALDI-TOF mass spectroscopy. All peptides were stored at -80°C for later use.

Antibacterial activity assay

Six Gram-negative bacterial strains (*Escherichia coli* ATCC25922, *A. hydrophila* XS91-4-1, *A. salmonicida* BG1, *A. sobria* CR79-1-1, *Edwardsiella ictaluri* HSN-1, and *Vibrio fluvialis* WY91-24-3) and two Gram-positive bacterial strains (*Micrococcus luteus* ATCC10240 and *Streptococcus agalactiae* ATCC13813) were used in the antibacterial activity assay. Radial-diffusion assay (RDA) was conducted as previously described (31, 32). Briefly, 5 mL underlay agarose gel containing 0.03% (wt/vol) TSB, 1% (wt/vol) low electroendosmosis (EEO) agarose (Aladdin), 0.02% (vol/vol) Tween 20 (Amresco), and 4×10^6 CFU bacteria was added into each sterile petri dish (90 mm diameter). After the solidification of the agarose, 4 mm diameter wells were punched in the agar using a sterile steel borer. Then 6 μL peptide (125 μM) was added to each well, and sterile water was added as control. Agar plates were incubated for 3 h at the optimum bacterial growth temperature (28°C for *A. hydrophila*, *A. salmonicida*, *A. sobria* and *E. ictaluri* or 37°C for *E. coli, V. fluvialis, M. luteus* and *S. agalactiae*) to diffuse the peptides. Each plate was added 5 mL sterilized overlay agarose gel (containing 6% TSB and 1% low EEO agarose) and incubated for 24 h at the optimum bacterial growth temperature. The diameter of the clearance zone around each well was measured.

10.3389/fimmu.2023.1128138

TABLE 2 Primers used in this study.

Name	Sequence (5′→3′)	Application
rtLEAP-1-QF	CATTTCAGGTTCAAGCGTCAGA	Real-time PCR
rtLEAP-1-QR	ATTTGCAGCAGAAGCCACAGC	Real-time PCR
rtLEAP-2A-QF	CTGCCAGCCCTGTTCCATCT	Real-time PCR
rtLEAP-2A-QR	CATCCGCTTCAGTGCCCTCT	Real-time PCR
rtLEAP-2B-QF	TGGTGGCTCTGATTCTTATGCA	Real-time PCR
rtLEAP-2B-QR	TCATGCGGGTTCTCCGTTCC	Real-time PCR
rtLEAP-2C-QF	GAATACTCTGAAGCCCGTTGG	Real-time PCR
rtLEAP-2C-QR	ATTTGGTCCCGCACTCGTCG	Real-time PCR
gcLEAP-1-QF	ACAGCAGGAGCAGGATGAGC	Real-time PCR
gcLEAP-1-QR	TATCCACAGCCTTTGTTACGAC	Real-time PCR
gcLEAP-2A-QF	TGGTGATTGTCCAGCAGGTGA	Real-time PCR
gcLEAP-2A-QR	GTAATGGTTCTGGCAGTAGGC	Real-time PCR
gcLEAP-2B-QF	GTATCTACTGTGCCATTAGCGA	Real-time PCR
gcLEAP-2B-QR	GACATTCGTATCTTGCGGTGC	Real-time PCR
gcLEAP-2C-QF	CGGCACCCGTAGATACTGAC	Real-time PCR
gcLEAP-2C-QR	GTGTTCCATCGCCATAGTAAAG	Real-time PCR
rtβ-actin-QF	ACAGGTCATCACCATCGGCA	Real-time PCR
rtβ-actin-QR	GGTCTCGTGGATACCGCAAG	Real-time PCR
gcβ-actin-QF	AGCCATCCTTCTTGGGTATG	Real-time PCR
gcβ-actin-QR	GGTGGGGCGATGATCTTGAT	Real-time PCR
pEGFP-Fpn-F	CGGGGTACCGATGGATAACGCGGGACCTAAG	Expression
pEGFP-Fpn-R	TCCCCCCGGGACACCGTGGTGGGAAGCAA	Expression

The restriction enzyme sites are underlined. F, forward; R, reverse.

Bacterial membrane permeability assay

The membrane permeability of bacteria after the treatment of peptides was assessed by flow cytometry as previously described (33) with minor modifications. In brief, *V. fluvialis* WY91-24-3 were cultured to mid-logarithmic phase, then washed twice and resuspended to 10^6 CFU/ml with 10 mM NaPB (pH 7.4). Thereafter, 40 μl of peptides diluted in NaPB was added to 160 μl of *V. fluvialis* to give a final concentration of 8 μM. LL37 and NaPB was used as the positive and negative control, respectively. After being incubated at 37°C for 1 h, propidium iodide (PI; Sigma-Aldrich) was added to the bacterial suspension at a final concentration of 9 μM. The PI positive bacterial cells were detected using the flow cytometer FACSVerse (BD Biosciences) at 3,000 events and the data were analyzed using the FlowJo software v10 (Tree Star).

Plasmid construction and transfection

The *Fpn* of rainbow trout (GenBank: XM_021579209.2) was amplified using the cDNAs reverse-transcribed from liver RNA using the primers listed in Table 2. The PCR product was digested with restriction enzymes (Kpn 1and Xma 1), followed by ligation into pEGFP-N1 to construct pEGFP-Fpn. The plasmid pEGFP-Fpn was extracted from the Trans5α cells using an E.Z.N.A. Plasmid Maxi Kit (Omega). The extracted plasmid was transfected into the HEK293T cells using the TransIntro EL transfection reagents (TransGen Biotech) according to the manufacturer's instructions. At 24 h after transfection, cycloheximide (Aladdin) was added to the HEK293T cells to give a final concentration of 75 μg/mL. After incubation for 3 h, the synthetic rainbow trout LEAPs were added to give a final concentration of 1 μM and incubated for 24 h. The changes in the position of Fpn-EGFP in the cells were investigated using a live cell station (Leica AF6000).

Statistical analysis

The statistic p value was calculated using the SPSS Statistics (version 19, IBM) by one-way ANOVA with a Dunnett *post hoc* test. A p value < 0.05 was considered statistically significant while a p value < 0.01 was considered highly significant.

Results

Homology comparison of LEAPs

Homologous sequence alignment showed that all LEAPs consist of a signal peptide, a propeptide and a mature peptide. The sequences of the mature peptides are more conserved than those of the signal peptides and propeptides. The mature peptide of LEAP-1 and LEAP-2 possessed eight and four conserved cysteines, respectively. Interestingly, from fish to mammals, the signature of the cleavage site (RXXR) between the propeptide and the mature peptide of LEAPs are conserved in evolution (Figure 1).

Gene structure and phylogenetic analyses of LEAPs

LEAP-1 and *LEAP-2* have the same gene structure, which is composed of 3 exons and 2 introns. The 5' and 3' UTR of rainbow

10.3389/fimmu.2023.1128138

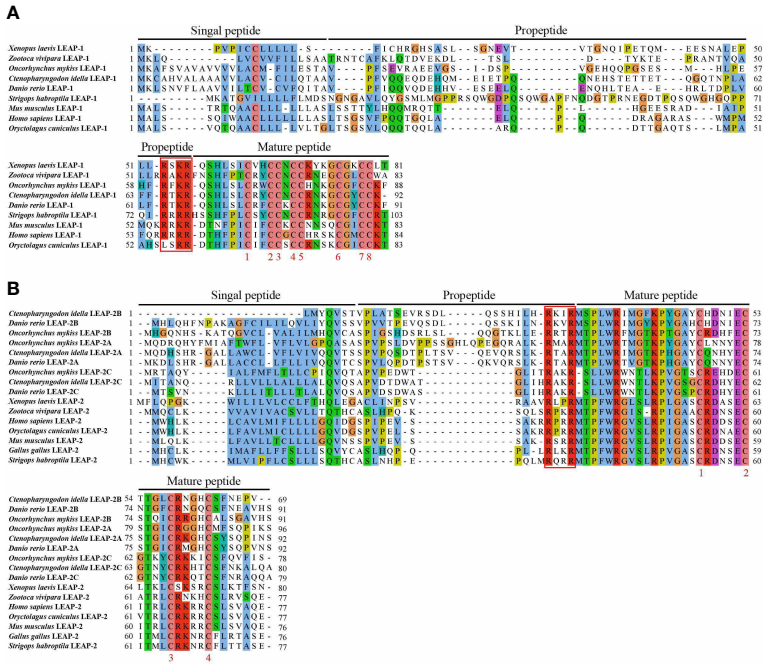

FIGURE 1
Amino acid sequence and domain organization of LEAP-1 **(A)** and LEAP-2 **(B)** from mammals, birds, amphibians, reptiles, and fish. The signal peptide, propeptide and mature peptide are denoted above the alignment. GenBank accession numbers of the selected sequences are listed in Table 1.

trout and grass carp *LEAP-1* are longer than those of *LEAP-1s* from other species analyzed. The two introns of grass carp *LEAP-2C* are longer than those of *LEAP-2Cs* from other species analyzed (Figure 2A).

In the phylogenetic tree constructed using the amino acid sequences of the LEAP-1 and LEAP-2 precursors (Figure 2B), the LEAP-1 sequences branched apart from the LEAP-2 sequences. Teleost LEAPs were distinguished from those of other vertebrates. LEAP-2 of grass carp, rainbow trout and zebrafish contain three members, named LEAP-2A, LEAP-2B and LEAP-2C.

Expression of *LEAPs* in rainbow trout and grass carp tissues

The mRNA expression levels of the *LEAPs* were evaluated in several healthy rainbow trout (Figure 3A) and grass carp (Figure 3B) tissues. Rainbow trout (rt) and grass carp (gc) *LEAPs* were differentially expressed in various tissues and organs, with an overall predominance of *LEAP-1*. In general, the *LEAPs* were highly expressed in the liver and lowly expressed in the gill, heart, and muscle. *LEAP-2A* was significantly expressed in the gut and skin of rainbow trout and grass carp, and the expression of *LEAP-2C* in the gut of rainbow trout was higher than that in the liver.

Induced expression of *LEAPs* by pathogenic bacteria

Expression of the total transcripts of *rtLEAP-1* and *rtLEAP-2* in the liver (Figure 4A) and gut (Figure 4B) of rainbow trout induced by *A. salmonicida* was studied. The expression level of *rtLEAP-1* increased significantly in the liver from 12 h to 1 d, and in the gut from 12 h to 3 d after infection. The expression level of *rtLEAP-2A* increased significantly in the gut at 12 h after infection. The expression level of *rtLEAP-2B* increased significantly in the liver from 1 d to 5 d, and in the gut from 3 d to 7 d after infection. However, the expression level of *rtLEAP-2C* decreased significantly in the gut from 3 d to 7 d after infection.

Expression of the total transcripts of *gcLEAP-1* and *gcLEAP-2* in the liver (Figure 4C) and gut (Figure 4D) of grass carp induced by *A. hydrophila* was studied. The expression levels of *gcLEAP-1* and *gcLEAP-2s* increased from 12 h to 3 d after infection, and then gradually returned to normal level, with *gcLEAP-2A* increased most significantly in the liver and *gcLEAP-1* increased most significantly in the gut.

Antibacterial activities of LEAPs

To investigate the antimicrobial properties of rainbow trout and grass carp LEAPs, we synthesized the mature peptides of rainbow trout and grass carp LEAPs and tested their antibacterial activities against a variety of bacterial strains. The results showed that all of the rainbow trout and grass carp LEAPs were antibacterial to Gram-negative (*E. coli*, *A. hydrophila*, *A. salmonicida*, *A. sobria*, *E. ictaluri*, and *V. fluvialis*) and Gram-positive bacteria (*M. luteus* and *S. agalactiae*) (Figures 5A, B). For the same bacterium, the antibacterial activities of different LEAPs are different. Interestingly, rainbow trout and grass carp LEAP-2C showed significant inhibitory effects on *A. hydrophila*, a common and harmful pathogen in fish farming.

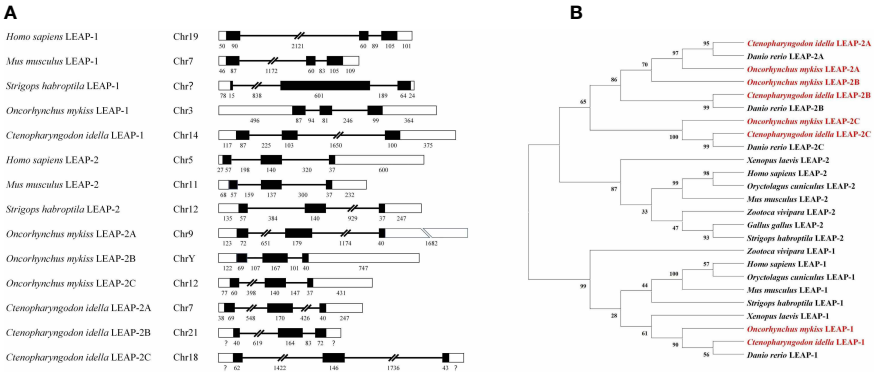

FIGURE 2
Gene structure and phylogenetic relationship of vertebrate LEAPs. **(A)** Gene structure of LEAPs from *Homo sapiens*, *Mus musculus*, *Strigops habroptila*, *Oncorhynchus mykiss*, and *Ctenopharyngodon idella*. The rectangles represent the exons, and the lines between them indicate the introns. Black and white areas indicate the coding regions and untranslated regions, respectively. The sizes of the exons and introns are shown by the numbers below. GenBank accession numbers of the selected sequences are listed in Table 1. The question mark means the length is unknown. **(B)** Phylogenetic relationship of LEAPs. A neighbour-joining phylogenetic tree was generated using the MEGA program with 1000 bootstrap replications. Rainbow trout and grass carp LEAPs are in red. GenBank accession numbers of the selected sequences are listed in Table 1.

Antibacterial mechanism of LEAPs

To clarify the antibacterial mechanism of LEAPs, we detected the integrity of cell membrane by bacterial membrane permeability assay. The results showed that rainbow trout and grass carp LEAPs could significantly increase the permeability of the cell membrane of *V. fluvialis* within 1 h, and rtLEAP-1 had the most significant effect, which was similar to human AMP LL-37 (Figures 6A–K), suggesting that LEAPs kill bacteria through membrane permeabilizing action.

Comparison of the ability of LEAPs to internalize Fpn

Through the amino acid sequence alignment of the LEAP-1 mature peptides in rainbow trout, grass carp, zebrafish, European sea bass, Atlantic salmon, and turbot, the Q-S/I-H-L/I-S/A-L motif was found in the N-terminus of the mature peptides (Figure 7A). To compare the ability of LEAPs to internalize Fpn, rtLEAPs were added to the cells expressing Fpn-EGFP, and the changes in the position of Fpn-EGFP in the cells were investigated using a live cell station. The results showed that only rtLEAP-1 resulted in the loss of cell surface Fpn-EGFP and the presence of intracellular Fpn-EGFP (Figure 7B), indicating that only rtLEAP-1 can cause the internalization of Fpn, while rtLEAP-2A, rtLEAP-2B and rtLEAP-2C cannot.

Discussion

Just as in tetrapods, there are also LEAP-1 and LEAP-2 in fish, but the difference is that fish LEAP-1 and LEAP-2 contain multiple genes. This is most likely due to the genome duplications and positive selection in fish, which suggests that different LEAPs may perform different functions. Multiple *LEAPs* existing in fish may be contributed to the immune defense of fish, which live in a complex aquatic environment.

Through amino acid sequence alignment, it was found that the LEAP-1 sequences of rainbow trout and grass carp were similar to other species, and the identity between rainbow trout and grass carp is 87.5%. Previous studies have shown that the LEAP-2 of rainbow trout (20) and grass carp (34) contains two genes, *LEAP-2A* and *LEAP-2B*, but in the current study we found that *LEAP-2C* also exists in these two species. Phylogenetic analysis indicated that LEAP-2 has evolved separately from LEAP-1 in vertebrates, resulting in LEAP-1 having iron regulation function, while LEAP-2 doing not.

As in many fish species and other vertebrates (19, 35–37), though predominantly expressed in the liver, both *LEAP-1* and

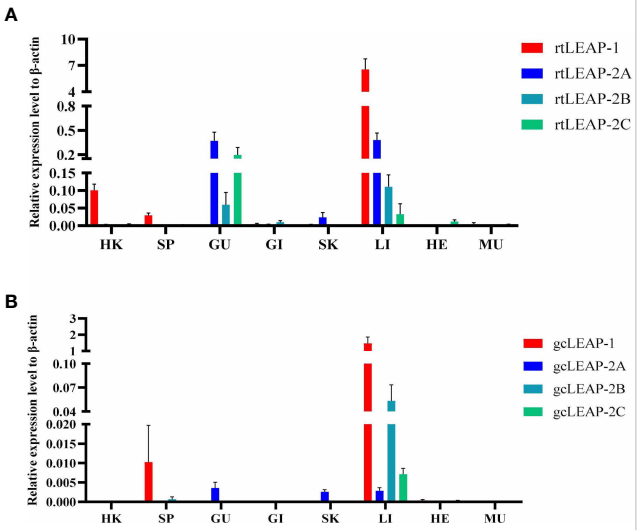

FIGURE 3
Expression patterns of rainbow trout **(A)** and grass carp **(B)** *LEAPs* in various tissues. The expression levels of *LEAPs* in lymphoid and non-lymphoid tissues were analyzed by qPCR and normalized against the expression of *β-actin* using the $2^{-\Delta Ct}$ method. Abbreviations for tissues are as follows: HK, head kidney; SP, spleen; GU, gut; GI, gill; SK, skin; LI, liver; HE, heart; MU, muscle. Data for rainbow trout represent the mean ± SEM of four individuals, and data for grass carp represent the mean ± SEM of five individuals.

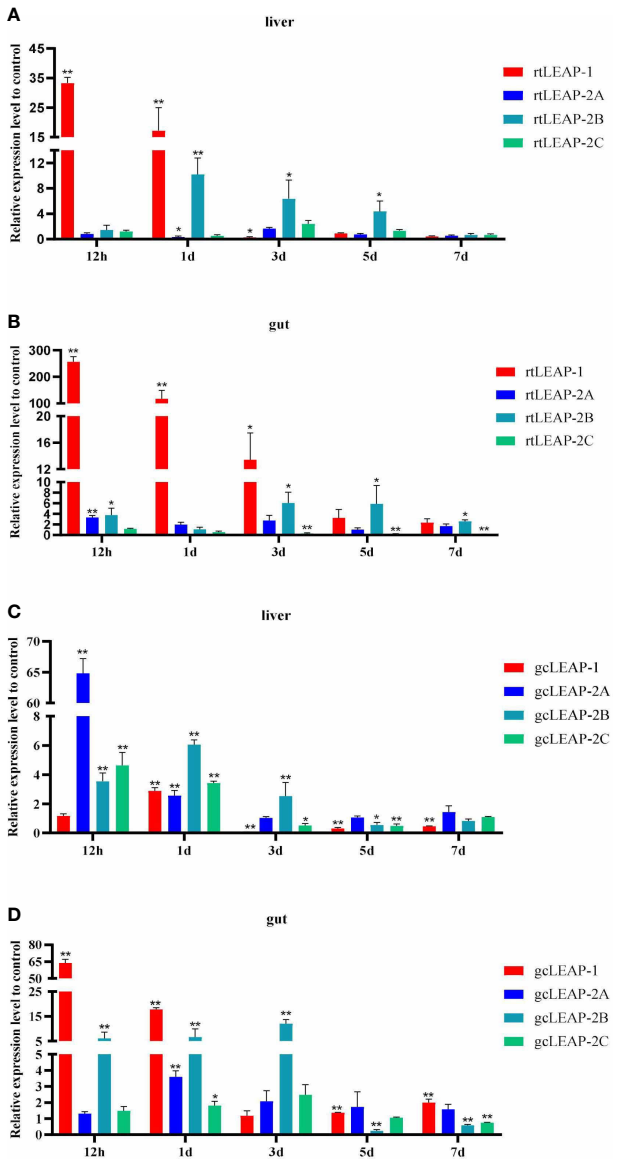

FIGURE 4
Induced expressions of *rtLEAPs* **(A, B)** and *gcLEAPs* **(C, D)** in the liver and gut under the condition of infection. Fold changes were calculated by comparing the infected group with the control group (defined as 1) using the $2^{-\Delta\Delta Ct}$ method. Data represent the mean ± SEM of four fish individuals. The *p* value was calculated by one-way ANOVA with a Dunnett *post hoc* test (*$p < 0.05$, **$p < 0.01$).

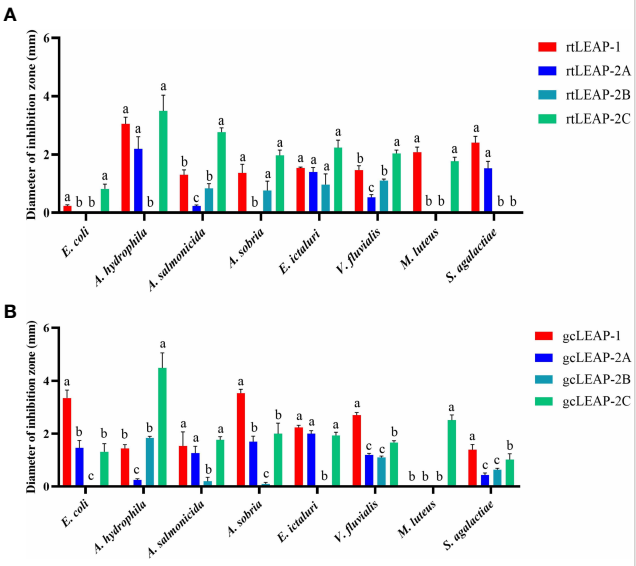

FIGURE 5
Antibacterial activities of rainbow trout **(A)** and grass carp **(B)** LEAPs against various bacteria. The underlay agarose gel containing *E. coli* ATCC25922, *A. hydrophila* XS91-4-1, *A. salmonicida* BG1, *A. sobria* CR79-1-1, *E. ictaluri* HSN-1, *V. fluvialis* WY91-24-3, *M. luteus* ATCC10240 and *S. agalactiae* ATCC13813 respectively was poured into sterile petri dishes. After the solidification, 4 mm diameter wells were punched in the agarose gel. Then 6 μL LEAP (125 μM) was added to each well, and sterile water was added as the control. Plates were incubated at the optimum bacterial growth temperature (28℃ for *A. hydrophila, A. salmonicida, A. sobria* and *E. ictaluri* or 37℃ for *E. coli, V. fluvialis, M. luteus* and *S. agalactiae*) for 3 h, and then the underlay agarose gel was covered with overlay agarose gel. The diameter of the inhibition zone around each well was measured after 24 h of incubation at the optimum bacterial growth temperature. Data represent the mean ± SEM of three independent experiments. Different letters indicate significant differences ($p<0.05$).

LEAP-2 were differentially expressed in other tissues and organs of rainbow trout and grass carp. A notable phenomenon was that *LEAP-2A* was significantly expressed in the gut and skin of rainbow trout and grass carp and *LEAP-2B* and *LEAP-2C* were significantly expressed in the gut of rainbow trout. Similar results were reported in blunt snout bream, whose *LEAP-2* mRNA expression level was highest in the gut (38). Research has shown that common carp *LEAP-2A* mRNA expression level increased in the gut, gills and skin after infection (22). These suggest that LEAPs of teleost fish may play important roles in both systemic and mucosal immunity, respectively.

A significant induction of *LEAP* was observed after experimental bacterial challenge, with *LEAP-1* being the most responsive gene in the liver and gut of both rainbow trout and grass carp. In rainbow trout, *LEAP-1* expression increased significantly in the early stage of infection, and *LEAP-2B* expression increased significantly in the late stage of infection. In grass carp, the gene expression of all *LEAPs* increased after infection, and then gradually returned to normal levels. These results suggest that rtLEAPs may function for a longer period after pathogen infection to maintain robust immunity. Similar induced expression of *LEAPs* was reported in other fish species after bacterial infection. It is worth noting that the tissue expression patterns of *LEAPs* in different fish species have specificity, and different pathogens are likely to induce the expression of different LEAPs (35, 39–42). All of these studies, however, shared the same idea that multiple LEAPs in hosts perform important antimicrobial functions.

Rainbow trout and grass carp LEAPs have broad spectrum antibacterial activities against a various type of bacteria. Notably, gcLEAP-2A has antibacterial activity against several bacterial strains, including *E. coli*, which is different from the previous report that gcLEAP-2A has no antibacterial activity against *E. coli* (34). Our results suggest that the antibacterial immunity of fish was enhanced through LEAP expansion. Although LEAP-1 and LEAP-2 belong to different types, their bactericidal mechanisms are roughly the same. Rainbow trout and grass carp LEAPs kill bacteria by disrupt the cell membranes, which is similar to previous study on other species that

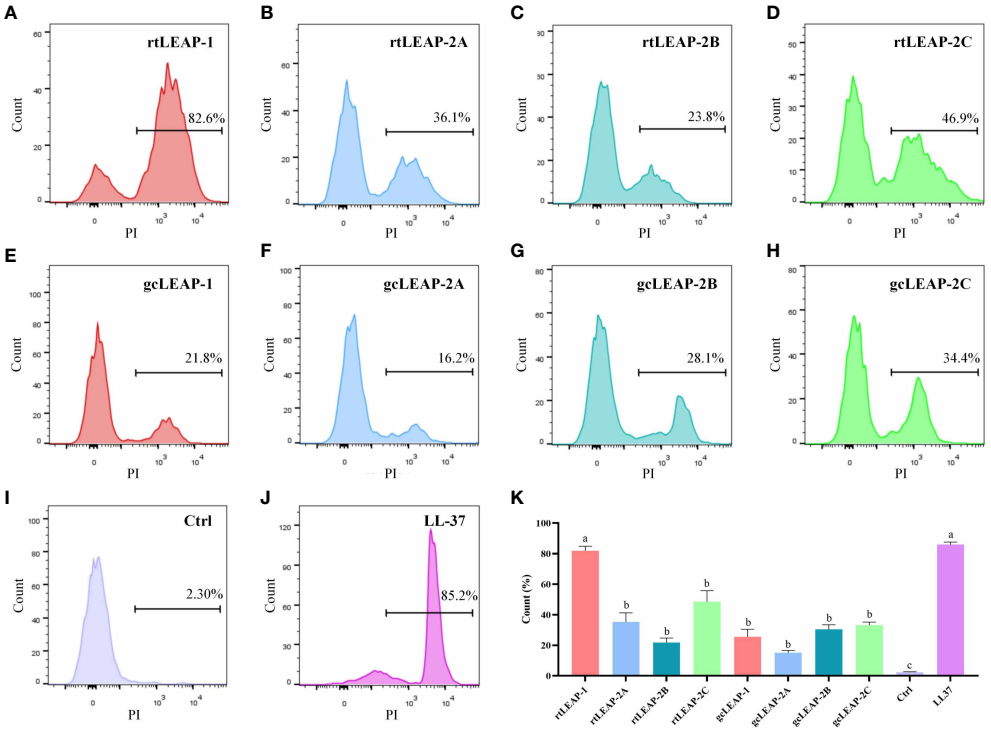

FIGURE 6
Antibacterial mechanisms of LEAPs. **(A–J)** Membrane permeability of *V. fluvialis* treated with LEAPs. The bacteria were incubated with LEAPs (8 μM) at 37°C for 1 h, and a bacterial suspension without peptide was included as a control (Ctrl). Then PI (9 μM) was added and the influx of PI was detected by flow cytometry. Data are representative results of three independent experiments. **(K)** The data in **(A–J)** were analyzed statistically. The *p* value was calculated by one-way ANOVA with a Dunnett *post hoc* test. Different letters indicate significant differences ($p<0.05$).

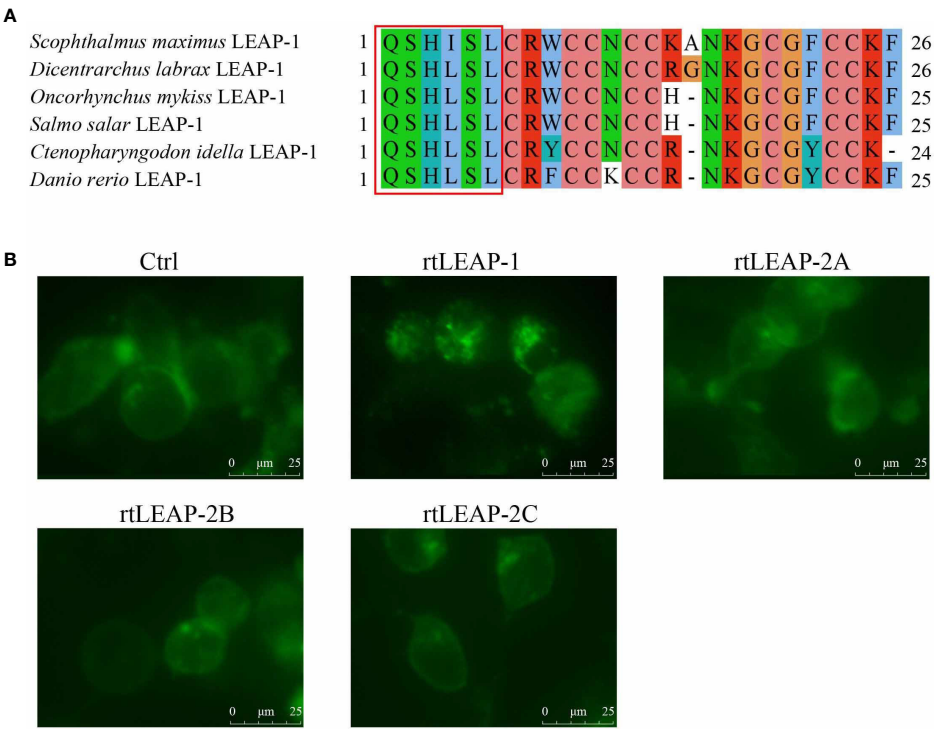

FIGURE 7
The effects of LEAPs on Fpn internalization. **(A)** Amino acid sequence alignment of LEAP-1 mature peptides in rainbow trout, grass carp, zebrafish, European sea bass, Atlantic salmon, and turbot. The Q-S/I-H-L/I-S/A-L motif at the N-terminus of the mature peptides are indicated with a red rectangle. GenBank accession numbers of the selected sequences are listed in Table 1. **(B)** The ability of LEAPs to internalize Fpn. HEK293T cells were seeded in 6-well plates and transfected with pEGFP-Fpn. After 24 h, cycloheximide (75 ug/mL) was added for 3 h, and then cells were incubated with rtLEAPs (1 μM) and PBS (blank control [Ctrl]) for 24 h. The images of cells were captured using a live cell station.

LEAPs form multiple pairs of disulfide bonds through cysteine residues and form a stable β-sheet structure, which can destroy bacterial cell membrane, promote its permeability, and cause the leakage of cell contents and the death of bacterial cells, thus killing pathogenic bacteria (10, 43).

Previous study has shown that the expression of LEAP-1 is directly or indirectly regulated by iron storage anemia, hypoxia, inflammation, pathological conditions, cytokines, and other signals (44, 45). Under normal physiological conditions, the expression of LEAP-1 is negatively correlated with iron level (46–48). The conserved sequence Q-S/I-H-L/I-S/A-L, which is associated with iron regulation activity (49), is present at the N-terminus of the mature peptide of LEAP-1, but not LEAP-2, suggesting that LEAP-1 and LEAP-2 play different roles in iron regulation. Our results further confirm that only LEAP-1 has the ability to internalize Fpn. On the one hand, this reaction maintains the homeostasis of iron in teleost fish; on the other hand, it leads to the obstruction of iron outflow from cells and reduces the available iron content of extracellular pathogens (13, 50).

In conclusion, this study first reported the existence of the *LEAP-2C* in rainbow trout and grass carp and systematically compared the antibacterial function of LEAPs in these teleost fish, which suggested that multiple LEAPs can enhance the immunity of teleost fish through different expression patterns and different antibacterial activities to various bacteria. This enhanced our understanding of host innate immunity and provided new evidence and insights for systematically analyzing the antibacterial function of LEAPs in teleost fish.

Data availability statement

The data presented in the study are deposited in the GenBank repository (https://www.ncbi.nlm.nih.gov/genbank/), accession numbers GQ870279.1 and OQ026323.

Ethics statement

The animal study was reviewed and approved by the Committee on the Ethics of Animal Experiments at Huazhong Agricultural University. Written informed consent was obtained from the owners for the participation of their animals in this study.

Author contributions

XL performed most of the experiments, analyzed most of the data, and wrote the preliminary manuscript. Y-ZH searched the *LEAP-2C* in the grass carp genome and helped with the date analysis. Y-RP helped with the gene structure analysis. JL helped with the sampling of infection experiments. Y-BJ participated in the radial-diffusion assay. Y-AZ helped with the experiment design and revised the manuscript. X-JZ designed the research, analyzed some of the data, and revised the manuscript. All authors contributed to the article and approved the submitted version.

Funding

This work was supported by the National Key Research and Development Program of China (2018YFD0900505), the Laboratory of Lingnan Modern Agriculture Project (NT2021008), the China Agriculture Research System (CARS-46), and the Youth Talent Project of Engineering Research Center of Green Development for Conventional Aquatic Biological Industry in the Yangtze River Economic Belt (2662021SSSY004).

Acknowledgments

The authors are grateful to Zi-You Ma and Tao-Zhen Lu for their help in fish challenge experiments and sampling.

Conflict of interest

The authors declare that the research was conducted in the absence of any commercial or financial relationships that could be construed as a potential conflict of interest.

Publisher's note

References

1. Kosciuczuk EM, Lisowski P, Jarczak J, Strzalkowska N, Jozwik A, Horbanczuk J, et al. Cathelicidins: Family of antimicrobial peptides. *A Review. Mol Biol Rep* (2012) 39 (12):10957–70. doi: 10.1007/s11033-012-1997-x

2. Yeaman MR, Yount NY. Mechanisms of antimicrobial peptide action and resistance. *Pharmacol Rev* (2003) 55(1):27–55. doi: 10.1124/pr.55.1.2

3. Epand RM, Vogel HJ. Diversity of antimicrobial peptides and their mechanisms of action. *Bba-Biomembranes* (1999) 1462(1-2):11–28. doi: 10.1016/S0005-2736(99)00198-4

4. Zasloff M. Antimicrobial peptides of multicellular organisms. *Nature* (2002) 415 (6870):389–95. doi: 10.1038/415389a

5. Won HS, Kang SJ, Lee BJ. Action mechanism and structural requirements of the antimicrobial peptides, gaegurins. *Bba-Biomembranes* (2009) 1788(8):1620–9. doi: 10.1016/j.bbamem.2008.10.021

6. Huan YC, Kong Q, Mou HJ, Yi HX. Antimicrobial peptides: Classification, design, application and research progress in multiple fields. *Front Microbiol* (2020) 11:582779. doi: 10.3389/fmicb.2020.582779

7. Bachere E, Destoumieux D, Bulet P. Penaeidins, antimicrobial peptides of shrimp: A comparison with other effectors of innate immunity. *Aquaculture* (2000) 191(1-3):71–88. doi: 10.1016/S0044-8486(00)00419-1

8. Chen YC, Yang Y, Zhang C, Chen HY, Chen FY, Wang KJ. A novel antimicrobial peptide Sparamosin(26-54) from the mud crab *Scylla paramamosain* showing potent antifungal activity against *Cryptococcus neoformans*. *Front Microbiol* (2021) 12:746006. doi: 10.3389/fmicb.2021.746006

9. Krause A, Neitz S, Magert HJ, Schulz A, Forssmann WG, Schulz-Knappe P, et al. LEAP-1, a novel highly disulfide-bonded human peptide, exhibits antimicrobial activity. *FEBS Lett* (2000) 480(2-3):147–50. doi: 10.1016/S0014-5793(00)01920-7

10. Krause A, Sillard R, Kleemeier B, Kluver E, Maronde E, Conejo-Garcia JR, et al. Isolation and biochemical characterization of LEAP-2, a novel blood peptide expressed in the liver. *Protein Sci* (2003) 12(1):143–52. doi: 10.1110/ps.0213603

11. Donovan A, Lima CA, Pinkus JL, Pinkus GS, Zon LI, Robine S, et al. The iron exporter Ferroportin/Slc40a1 is essential for iron homeostasis. *Cell Metab* (2005) 1 (3):191–200. doi: 10.1016/j.cmet.2005.01.003

12. Qiao B, Sugianto P, Fung E, del-Castillo-Rueda A, Moran-Jimenez MJ, Ganz T, et al. Hepcidin-induced endocytosis of ferroportin is dependent on ferroportin ubiquitination. *Cell Metab* (2012) 15(6):918–24. doi: 10.1016/j.cmet.2012.03.018

13. Nemeth E, Tuttle MS, Powelson J, Vaughn MB, Donovan A, Ward DM, et al. Hepcidin regulates cellular iron efflux by binding to ferroportin and inducing its internalization. *Science* (2004) 306(5704):2090–3. doi: 10.1126/science.1104742

14. Ramey G, Deschemin JC, Durel B, Canonne-Hergaux F, Nicolas G, Vaulont S. Hepcidin targets ferroportin for degradation in hepatocytes. *Haematol-Hematol J* (2010) 95(3):501–4. doi: 10.3324/haematol.2009.014399

15. Hilton KB, Lambert LA. Molecular evolution and characterization of hepcidin gene products in vertebrates. *Gene* (2008) 415(1-2):40–8. doi: 10.1016/j.gene.2008.02.016

16. Padhi A, Verghese B. Evidence for positive Darwinian selection on the hepcidin gene of perciform and pleuronectiform fishes. *Mol Divers* (2007) 11(3-4):119–30. doi: 10.1007/s11030-007-9066-4

17. Serna-Duque JA, Cuesta A, Esteban MA. Massive gene expansion of hepcidin, a host defense peptide, in gilthead seabream (*Sparus aurata*). *Fish Shellfish Immunol* (2022) 124:563–71. doi: 10.1016/j.fsi.2022.04.032

18. Mani BK, Puzziferri N, He ZY, Rodriguez JA, Osborne-Lawrence S, Metzger NP, et al. LEAP2 changes with body mass and food intake in humans and mice. *J Clin Invest* (2019) 129(9):3909–23. doi: 10.1172/Jci125332

19. Sang Y, Ramanathan B, Minton JE, Ross CR, Blecha F. Porcine liver-expressed antimicrobial peptides, hepcidin and LEAP-2: Cloning and induction by bacterial infection. *Dev Comp Immunol* (2006) 30(4):357–66. doi: 10.1016/j.dci.2005.06.004

20. Zhang YA, Zou J, Chang CI, Secombes CJ. Discovery and characterization of two types of liver-expressed antimicrobial peptide 2 (LEAP-2) genes in rainbow trout. *Vet Immunol Immunopathol* (2004) 101(3-4):259–69. doi: 10.1016/j.vetimm.2004.05.005

21. Li HX, Lu XJ, Li CH, Chen J. Molecular characterization and functional analysis of two distinct liver-expressed antimicrobial peptide 2 (LEAP-2) genes in Large yellow croaker (*Larimichthys crocea*). *Fish Shellfish Immun* (2014) 38(2):330–9. doi: 10.1016/j.fsi.2014.04.004

22. Yang GW, Guo HY, Li H, Shan SJ, Zhang XQ, Rombout JHWM, et al. Molecular characterization of LEAP-2 cDNA in common carp (*Cyprinus carpio* l.) and the differential expression upon a *Vibrio anguillarum* stimulus; indications for a significant immune role in skin. *Fish Shellfish Immun* (2014) 37(1):22–9. doi: 10.1016/j.fsi.2014.01.004

23. Zhang SH, Xu QQ, Du H, Qi ZT, Li YS, Huang J, et al. Evolution, expression, and characterisation of liver-expressed antimicrobial peptide genes in ancient chondrostean sturgeons. *Fish Shellfish Immun* (2018) 79:363–9. doi: 10.1016/j.fsi.2018.05.023

24. Li HX, Lu XJ, Li CH, Chen J. Molecular characterization of the liver-expressed antimicrobial peptide 2 (LEAP-2) in a teleost fish, plecoglossus altivelis: Antimicrobial activity and molecular mechanism. *Mol Immunol* (2015) 65(2):406–15. doi: 10.1016/j.molimm.2015.02.022

25. Chen J, Chen Q, Lu XJ, Chen J. The protection effect of LEAP-2 on the mudskipper (*Boleophthalmus pectinirostris*) against edwardsiella tarda infection is associated with its immunomodulatory activity on Monocytes/Macrophages. *Fish Shellfish Immun* (2016) 59:66–76. doi: 10.1016/j.fsi.2016.10.028

26. Chen J, Lv YP, Dai QM, Hu ZH, Liu ZM, Li JH. Host defense peptide LEAP-2 contributes to Monocyte/Macrophage polarization in barbel steed (*Hemibarbus labeo*). *Fish Shellfish Immun* (2019) 87:184–92. doi: 10.1016/j.fsi.2019.01.015

27. Chen Y, Wu J, Cheng HL, Dai Y, Wang YP, Yang HL, et al. Anti-infective effects of a fish-derived antimicrobial peptide against drug-resistant bacteria and its synergistic effects with antibiotic. *Front Microbiol* (2020) 11:602412. doi: 10.3389/fmicb.2020.602412

28. Wu CS, Ma ZY, Zheng GD, Zou SM, Zhang XJ, Zhang YA. Chromosome-level genome assembly of grass carp (*Ctenopharyngodon idella*) provides insights into its genome evolution. *BMC Genomics* (2022) 23(1):271. doi: 10.1186/s12864-022-08503-x

29. Long M, Zhao J, Li T, Tafalla C, Zhang Q, Wang X, et al. Transcriptomic and proteomic analyses of splenic immune mechanisms of rainbow trout (*Oncorhynchus mykiss*) infected by *Aeromonas salmonicida* subsp. *Salmonicida*. *J Proteomics* (2015) 122:41–54. doi: 10.1016/j.jprot.2015.03.031

30. Lu T-Z, Liu X, Wu C-S, Ma Z-Y, Wang Y, Zhang Y-A, et al. Molecular and functional analyses of the primordial costimulatory molecule CD80/86 and its receptors CD28 and CD152 (CTLA-4) in a teleost fish. *Front Immunol* (2022) 13:885005. doi: 10.3389/fimmu.2022.885005

31. Nordahl EA, Rydengard V, Nyberg P, Nitsche DP, Morgelin M, Malmsten M, et al. Activation of the complement system generates antibacterial peptides. *Proc Natl Acad Sci USA* (2004) 101(48):16879–84. doi: 10.1073/pnas.0406678101

32. Pasupuleti M, Walse B, Nordahl EA, Morgelin M, Malmsten M, Schmidtchen A. Preservation of antimicrobial properties of complement peptide C3a, from invertebrates to humans. *J Biol Chem* (2007) 282(4):2520–8. doi: 10.1074/jbc.M607848200

33. Hu YZ, Ma ZY, Wu CS, Wang J, Zhang YA, Zhang XJ. LECT2 is a novel antibacterial protein in vertebrates. *J Immunol* (2022) 208(8):2037–53. doi: 10.4049/jimmunol.2100812

34. Liu F, Li JL, Yue GH, Fu JJ, Zhou ZF. Molecular cloning and expression analysis of the liver-expressed antimicrobial peptide 2 (LEAP-2) gene in grass carp. *Veterinary Immunol Immunopathology* (2010) 133(2-4):133–43. doi: 10.1016/j.vetimm.2009.07.014

35. Wang Y, Liu X, Ma L, Yu Y, Yu H, Mohammed S, et al. Identification and characterization of a hepcidin from half-smooth tongue sole *Cynoglossus semilaevis*. *Fish Shellfish Immunol* (2012) 33(2):213–9. doi: 10.1016/j.fsi.2012.04.011

36. Yang M, Chen B, Cai JJ, Peng H, Ling C, Yuan JJ, et al. Molecular characterization of hepcidin as-Hepc2 and as-Hepc6 in black porgy (*Acanthopagrus schlegelii*): Expression pattern responded to bacterial challenge and in vitro antimicrobial activity. *Comp Biochem Physiol B Biochem Mol Biol* (2011) 158(2):155–63. doi: 10.1016/j.cbpb.2010.11.003

37. Zhou JG, Wei JG, Xu D, Cui HC, Yan Y, Ou-Yang ZL, et al. Molecular cloning and characterization of two novel hepcidins from orange-spotted grouper. *Epinephelus Coioides*. *Fish Shellfish Immunol* (2011) 30(2):559–68. doi: 10.1016/j.fsi.2010.11.021

38. Liang T, Ji W, Zhang GR, Wei KJ, Feng K, Wang WM, et al. Molecular cloning and expression analysis of liver-expressed antimicrobial peptide 1 (LEAP-1) and LEAP-2 genes in the blunt snout bream (*Megalobrama amblycephala*). *Fish Shellfish Immunol* (2013) 35(2):553–63. doi: 10.1016/j.fsi.2013.05.021

39. Bao BL, Peatman E, Xu P, Li P, Zeng H, He CB, et al. The catfish liver-expressed antimicrobial peptide 2 (LEAP-2) gene is expressed in a wide range of tissues and developmentally regulated. *Mol Immunol* (2006) 43(4):367–77. doi: 10.1016/j.molimm.2005.02.014

40. Chen SL, Xu MY, Ji XS, Yu GC, Liu Y. Cloning, characterization, and expression analysis of hepcidin gene from red Sea bream (*Chrysophrys major*). *Antimicrob Agents Ch* (2005) 49(4):1608–12. doi: 10.1128/Aac.49.4.1608-1612.2005

41. Pereiro P, Figueras A, Novoa B. A novel hepcidin-like in turbot (*Scophthalmus maximus* l.) highly expressed after pathogen challenge but not after iron overload. *Fish Shellfish Immunol* (2012) 32(5):879–89. doi: 10.1016/j.fsi.2012.02.016

42. Kim YO, Park EM, Nam BH, Kong HJ, Kim WJ, Lee SJ. Identification and molecular characterization of two hepcidin genes from black rockfish (*Sebastes schlegelii*). *Mol Cell Biochem* (2008) 315(1-2):131–6. doi: 10.1007/s11010-008-9796-3

43. Rodrigues PNS, Vazquez-Dorado S, Neves JV, Wilson JM. Dual function of fish hepcidin: Response to experimental iron overload and bacterial infection in Sea bass (*Dicentrarchus labrax*). *Dev Comp Immunol* (2006) 30(12):1156–67. doi: 10.1016/j.dci.2006.02.005

44. Zhao N, Zhang AS, Enns CA. Iron regulation by hepcidin. *J Clin Invest* (2013) 123 (6):2337–43. doi: 10.1172/JCI67225

45. Neves JV, Caldas C, Vieira I, Ramos MF, Rodrigues PN. Multiple hepcidins in a teleost fish, *Dicentrarchus labrax*: Different hepcidins for different roles. *J Immunol* (2015) 195(6):2696–709. doi: 10.4049/jimmunol.1501153

46. Nemeth E, Ganz T. Regulation of iron metabolism by hepcidin. *Annu Rev Nutr* (2006) 26:323–42. doi: 10.1146/annurev.nutr.26.061505.111303

47. Vyoral D, Jiri P. Therapeutic potential of hepcidin - the master regulator of iron metabolism. *Pharmacol Res* (2017) 115:242–54. doi: 10.1016/j.phrs.2016.11.010

48. Ward DM, Kaplan J. Ferroportin-mediated iron transport: Expression and regulation. *Biochim Biophys Acta* (2012) 1823(9):1426–33. doi: 10.1016/j.bbamcr.2012.03.004

49. Robertson LS, Iwanowicz LR, Marranca JM. Identification of centrarchid hepcidins and evidence that 17beta-estradiol disrupts constitutive expression of hepcidin-1 and inducible expression of hepcidin-2 in largemouth bass (*Micropterus salmoides*). *Fish Shellfish Immunol* (2009) 26(6):898–907. doi: 10.1016/j.fsi.2009.03.023

50. Hu YZ, Kurobe T, Liu XL, Zhang YA, Su JG, Yuan GL. Hamp type-1 promotes antimicrobial defense *Via* direct microbial killing and regulating iron metabolism in grass carp (*Ctenopharyngodon idella*). *Biomolecules* (2020) 10(6):825. doi: 10.3390/biom10060825

frontiers | Frontiers in Immunology

TYPE Review
PUBLISHED 21 February 2023
DOI 10.3389/fimmu.2023.1065357

OPEN ACCESS

EDITED BY
Chunsheng Liu,
Hainan University, China

REVIEWED BY
Qingpi Yan,
Jimei University, China
Jian Zhang,
Yantai University, China

*CORRESPONDENCE
Zhixia Zhou
zhou_zhixia@qdu.edu.cn
Shoushi Wang
wangshoushi1226@126.com
Peifeng Li
peifli@qdu.edu.cn

SPECIALTY SECTION
This article was submitted to Molecular Innate Immunity, a section of the journal Frontiers in Immunology

RECEIVED 09 October 2022
ACCEPTED 06 February 2023
PUBLISHED 21 February 2023

CITATION
Zhou Z, Leng C, Wang Z, Long L, Lv Y, Gao Z, Wang Y, Wang S and Li P (2023) The potential regulatory role of the lncRNA-miRNA-mRNA axis in teleost fish. *Front. Immunol.* 14:1065357. doi: 10.3389/fimmu.2023.1065357

The potential regulatory role of the lncRNA-miRNA-mRNA axis in teleost fish

Zhixia Zhou[1*], Cuibo Leng[2], Zhan Wang[2], Linhai Long[1], Yiju Lv[1], Ziru Gao[1], Yin Wang[1], Shoushi Wang[2*] and Peifeng Li[1*]

[1]Institute for Translational Medicine, The Affiliated Hospital of Qingdao University, College of Medicine, Qingdao University, Qingdao, China, [2]The Affiliated Qingdao Central Hospital of Qingdao University, The Second Affiliated Hospital of Medical College of Qingdao University, Qingdao, China

Research over the past two decades has confirmed that noncoding RNAs (ncRNAs), which are abundant in cells from yeast to vertebrates, are no longer "junk" transcripts but functional regulators that can mediate various cellular and physiological processes. The dysregulation of ncRNAs is closely related to the imbalance of cellular homeostasis and the occurrence and development of various diseases. In mammals, ncRNAs, such as long noncoding RNAs (lncRNAs) and microRNAs (miRNAs), have been shown to serve as biomarkers and intervention targets in growth, development, immunity, and disease progression. The regulatory functions of lncRNAs on gene expression are usually mediated by crosstalk with miRNAs. The most predominant mode of lncRNA-miRNA crosstalk is the lncRNA-miRNA-mRNA axis, in which lncRNAs act as competing endogenous RNAs (ceRNAs). Compared to mammals, little attention has been given to the role and mechanism of the lncRNA-miRNA-mRNA axis in teleost species. In this review, we provide current knowledge about the teleost lncRNA-miRNA-mRNA axis, focusing on its physiological and pathological regulation in growth and development, reproduction, skeletal muscle, immunity to bacterial and viral infections, and other stress-related immune responses. Herein, we also explored the potential application of the lncRNA-miRNA-mRNA axis in the aquaculture industry. These findings contribute to an enhanced understanding of ncRNA and ncRNA-ncRNA crosstalk in fish biology to improve aquaculture productivity, fish health and quality.

KEYWORDS

lncRNA, miRNA, teleost, reproduction, immunity, infection

1 Introduction

Over the past two decades, the primary function of RNA is no longer what was once thought to be a mere intermediate molecule of genetic information from DNA to protein because the RNA pool contains thousands of noncoding RNA (ncRNA) transcripts that have little or no ability to form proteins (1, 2). Although ncRNAs are not directly involved

in gene coding and protein synthesis, they can act as regulators to regulate gene expression at the epigenetic, transcriptional, posttranscriptional, translational, and posttranslational levels (3, 4). Therefore, an increasing number of ncRNAs, especially microRNAs (miRNAs) and long noncoding RNAs (lncRNAs), have been identified for their important roles in cellular physiology or pathological processes in various species, including teleost fish (5–7).

miRNAs, one of the most abundant and most studied natural single-stranded small ncRNAs, are 21 to 24 nucleotides in length and are generally highly conserved from yeast to vertebrates (8). miRNA can bind to the 3'- and 5′-untranslated region (UTR), promoter region and coding region of the messenger RNA (mRNA) target by base-pairing with complementary sites, thereby inhibiting the translation of mRNA into protein or inducing mRNA degradation (9, 10). In mammals, more than 60% of mRNAs have been predicted to be regulated by miRNAs, which are involved not only in various physiological processes but also in the pathophysiological processes of various diseases (11–13). In teleost fish, miRNAs were first discovered in zebrafish (*Danio rerio*, *D. rerio*) and were soon identified in various fish species, such as rainbow trout (*Oncorhynchus mykiss*, *O. mykiss*), bighead carp (*Aristichthys nobilis*, *A. nobilis*), silver carp (*Hypophthalmichthys molitrix*, *H. molitrix*), common carp (*Cyprinus carpio*, *C. carpio*), channel catfish (*Ictalurus punctatus*, *I. punctatus*), flounder (*Paralichthys olivaceus*, *P. olivaceus*) and large yellow croaker (*Larimichtly crocea*, *L. crocea*) (14–17). Similar to mammals, fish miRNAs have also been shown to be involved in fish development, nutrition, immune and inflammatory responses, and their roles and molecular mechanisms have gradually been revealed (15, 18–22).

lncRNA is another of the most widely studied ncRNAs with lengths generally more than 200 nt, which plays an important role in growth and development, and its dysregulation is associated with a variety of diseases (23, 24). Compared with miRNAs, most lncRNAs have lower sequence conservation across species, but they can regulate gene expression at almost all levels (25). In addition, probably because of their lower conservation, their expression patterns in cells or tissues are more specific than miRNAs or even mRNAs (19). lncRNAs act as molecular signaling activators, decoys, guides, or scaffolds that interact with a range of DNAs, RNAs, and proteins to influence their function, especially miRNAs (23, 26–29). At least four patterns of lncRNA-miRNA interactions have been identified in mammals as follows: 1) lncRNAs act as competing endogenous RNAs (ceRNA)/sponges or decoys to bind miRNAs and release their target mRNAs; 2) lncRNAs as precursors are one of the sources of miRNAs; 3) lncRNAs compete with miRNAs to bind directly to mRNAs; and 4) miRNAs induce the degradation of lncRNAs (19, 29–31). Among these RNAs, the first is the most predominant mode of interaction between lncRNAs and miRNAs, which is termed the lncRNA-miRNA-mRNA ceRNA network mode, as shown in Figure 1. Undoubtedly, most lncRNA functions are mediated by their ceRNA networks. In fish, similar to miRNAs, lncRNAs have also been found in a variety of fish and have been shown to be involved in fish liver metabolism (32, 33), growth and development (34–38), as well as immune responses to various stresses, such as netting and chasing (39), hypoxia (40), bacteria (40–43), and viruses (44, 45). However, compared with fish miRNAs, the identification, function and mechanisms of fish lncRNAs are still relatively poorly studied, including the signaling pathways associated with the lncRNA-miRNA-mRNA regulatory network.

Herein, we provide a brief overview of recent advances in the regulatory roles of the lncRNA-miRNA-mRNA network in teleost fish physiological and pathological processes, mainly including teleost growth and development, reproduction, immune response to infection, and other immune-related biological processes. Furthermore, we explored the potential application of the lncRNA-miRNA-mRNA axis as a biomarker or intervention target in fish domestication, farming or disease treatment. This may help to elucidate the fish lifestyle related to the regulation of the lncRNA-miRNA-mRNA network and provide new ideas for ncRNA, targeting fish growth, breeding, or disease treatment strategies to improve the sustainable development of fisheries.

2 The regulatory roles of the lncRNA-miRNA-mRNA axis in teleost physiology and pathology

Similar to mammals, the regulatory functions of miRNA-related lncRNAs in fish are mediated mainly by the lncRNA-miRNA-mRNA axis. Different axes have been found in different tissues of different fish species, involving many lncRNAs and miRNAs, which may further suggest the specificity advantage of less conserved lncRNAs. The lncRNAs can be constitutively present in normal cells to maintain cellular homeostasis or regulated in specific stress responses and diseases to induce innate or specific immunity, as shown in Table 1 and Figure 2.

2.1 Regulation in growth and development

2.1.1 Brain and Nerves

Different expression profiles of mRNA, lncRNA and miRNA were identified in the brain of grass carp (*Ctenopharyngodon Idella*, *C. Idella) at* different growth rates by whole transcriptome

Abbreviations: AANC, rantiviral-associated long noncoding RNA; BncRNA, B chromosome long noncoding RNA; Bs, B chromosomes; ceRNA, competitive endogenous RNA; CIK, grass carp kidney; CNS, central nervous system; IB, intermuscular bone; IRF3, interferon regulatory factor 3; lncRNA, long noncoding RNA; IRAK4, interleukin-1 receptor-related kinase 4; IRL, IRAK4-related lncRNA; MAVS, mitochondrial antiviral signaling protein; MARL, MAVS antiviral-related lncRNA; miRNA, microRNA; MICs, miiuy croaker intestines cells; mRNA, messenger RNA; ncRNA, noncoding RNA; mTOR, mammalian target of rapamycin; NAFLD, nonalcoholic fatty liver disease; NARL, antibacterial and antiviral-related lncRNA; NF-κB, nuclear transcription factor-κB; NOD1, nucleotide oligomerization domain 1; POMV, orthomyxovirus; SCRV, siniperca chuatsi rhabdovirus; Se, selenium; SELJA, selenoprotein Ja; TGF-β, transforming growth factor-beta; TLR, Toll-like receptor; RNAi, RNA interference; Wnt, wingless-type MMTV integration site family.

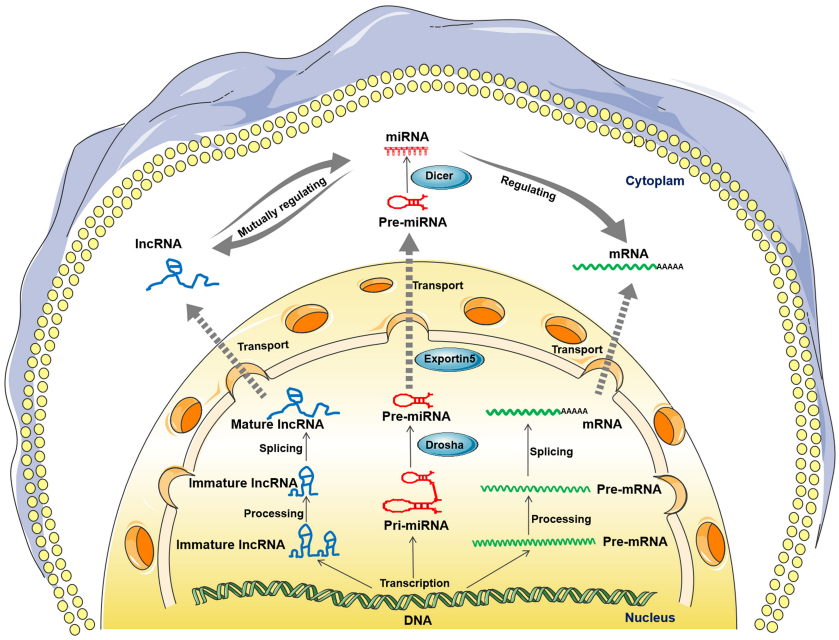

FIGURE 1
Biogenesis of the long noncoding RNA (lncRNA)-microRNA (miRNA)-messenger RNA (mRNA) axis. (lncRNA, left) Immature lncRNAs are transcribed from the intergene, exon or distal protein coding region of the genome and become stable immature lncRNAs after posttranscriptional processing. Then, most lncRNAs undergo alternative splicing and become mature lncRNAs. Mature lncRNAs can exist in the nucleus or be transported to the cytoplasm. (miRNA, middle) Primary miRNAs (pri-miRNAs) transcribed from the genome are converted into precursor miRNAs (pre-miRNAs) by Drosha cleavage. Then, the premiRNAs were transferred to the cytoplasm in an Exportin-5-dependent manner. Finally, mature miRNAs are produced from premiRNAs after Dicer1 cleavage. (mRNA, right) The initial transcription products of mRNAs are high molecular weight precursor RNAs (pre-mRNAs). Then, the premRNAs are transformed into mature mRNA after posttranscriptional processing, alternative splicing and RNA modification. Subsequently, the mRNAs are transported into the cytoplasm and translated. In the cytoplasm, lncRNA can interact with miRNA, acting mainly on miRNA as a competing endogenous RNA (ceRNA), thus regulating its target molecule mRNA and inducing its translation repression or decoy.

sequencing (80). The hub mRNAs and hub ncRNAs in the brain with increased growth rates were associated with many biological processes, including immune, endocrine, and growth hormone signaling pathways, and processes such as amino acid and carbohydrate metabolism. In the lncRNA-miRNA-mRNA ceRNA networks of the brain based on hub mRNAs and hub ncRNAs, the MSTRG.6764-miR-27a-3p-lpxn (leupaxin) and MSTRG.50349-miR-206-axpm (abnormal spindle-like microcephaly associated) axes were identified. All lncRNAs and mRNAs in these two ceRNA networks were determined to be upregulated, while all miRNAs were downregulated. The expression levels of these lncRNAs and mRNAs were further confirmed to be positively correlated with the growth of *C. Idella*, while miR-27a-3p or miR-206 expression was negatively correlated with *C. Idella* growth (80). These data suggest that the difference in grass carp growth rate may be related to the development of the central nervous system of the brain regulated by the ceRNA network.

In addition, recent studies have found that lncRNAs can not only serve as miRNA precursors or ceRNAs but can also be silenced as miRNA targets in fish (46). Lee reported that miRNAs primarily targeted and silenced the 5' caps and 3' poly(A)-tails of lncRNAs in *D. rerio* at the posttranscriptional and translational levels. The mRNA-like lncRNA (containing a 5' cap, 3' poly(A)-tail, and canonical miRNA target sites) was inhibited by miRNA at both the RNA and ribosomal levels during the early developmental stages of *D. rerio* embryos, whereas the nonmRNA-like long noncoding RNA (containing miRNA target sites, but no 5' cap and 3' poly(A)-tail) was not strongly inhibited by miRNA and may act as a miRNA decoy (46, 59). Cyrano is a miRNA-regulated lncRNA whose expression and function are repressed by miR-7 (59). Cyrano was confirmed to be parentally inherited lncRNA in *D. rerio* and was proven to play an important role in the symmetric development of neuronal structures by interacting with miR-7 (59). In addition, knockdown of Cyrano without altering zygotic Cyrano resulted in changes in zebrafish brain morphology, suggesting that inherited Cyrano is critical for brain development (59). These data indicated that fish lncRNAs and miRNAs have a reciprocal regulatory relationship, which in turn affects the expression and function of growth- or development-related mRNAs.

2.1.2 Immune organs

Similarly, the expression and interaction of lncRNAs, miRNAs and mRNAs was explored in the hepatopancreas, gill, intestine, liver, kidney, and spleen in fish by using high-throughput sequencing technology (47, 80, 81). A total of 10,270 lncRNAs and 7720 mRNAs were identified in gill, intestine, liver and kidney tissues of *P. olivaceus*. The mRNA-miRNA interaction network confirmed that one-third of mRNAs were predicted to be targeted for regulation by more than one miRNA (47). In contrast, 975 lncRNAs and 163 mature miRNAs were found in the liver, kidney, and spleen of coho salmon (*Oncorhynchus kisutch*, *O. kisutch*). Among these RNAs, 1339 lncRNAs putatively interacted with 148

TABLE 1 LncRNA-miRNA-mRNA axis regulation in teleost fish.

Regulated biological process	Related fish species	Related Organs/ Cells	Stimulus	Mainly related lncRNAs	Mainly related miRNAs	Mainly related genes	Mainly related signaling pathways	Refs
Growth and development	*Ctenopharyngodon idella*	Brain	None	MSTRG.6764; MSTRG.50349	miR-27a-3p; miR-206	*lpxn*; *axpm*	Actin cytoskeleton; Ras; Chemokine; Immunity	(46)
	Danio rerio	Embryos	None	Cyrano	miR-7	UN	Neurodevelopment	(47)
	Ctenopharyngodon idella	Hepatopancreas	None	MSTRG.35807; MSTRG.21503; MSTRG.25056; MSTRG.41999	miR-13b-5p; miR-22a-5; miR-10b-5p	*cel*; *amy2a*; *repe2*; *cbp1*; *celf1*; *ela3l*; *cpa2*	Biosynthesis; Immunity; Pancreatic secretion; Peroxisome; Ras; Nutrient metabolism	(46)
	Oncorhynchus kisutch	Liver; Kidney; Spleen	None	NL	NL	NL	TGF-β; NF-κB; Cytokines; Immunity; Adherens junction	(48)
	Paralichthys olivaceus	Gill; Liver; Kidney; Intestine	None	NL	NL	NL	Antigen processing and presentation; TLRs; Immunity	(49)
	Paralichthys olivaceus	Skeletal muscle	None	TCONS_00003213; TCONS_00006684; TCONS_00023918	miR-133-5p; miR-221-3p; miR-124-5p;	GS-010675; GS-018639; GS-016120	Actin cytoskeleton; Tight junction; Focal adhesion	(50)
	Sparus aurata	Fast skeletal muscle	None	lncRNA20194	miR-133; miR-206; miR-20	*myod1*	Myoblast proliferation	(51)
	Oncorhynchus mykiss	Muscle	None	Omy500041161; Omy400178299	mir-26a; mir-4185; mir-10b-mature 3'; mir-181d-mature 5'	GSONMT00080511001; GSONMT00041090001	TGF-β; Protein catabolism/anabolism; Immunity	(52)
	Megalobrama amblycephala	Intermuscular bone	None	LNC_017705; LNC_007210; LNC_011298	miR-24b-3p; miR-193b-3p	*zip1*; *C6*; MamblycephalaGen-e23275	Osteoblast differentiation; $Ca2^{+}$ deposition	(53)
	Astatotilapia latifasciata	B chromosomes	None	BncRNA	miR-129-3p; miR-9-5p; miR-153a-5p	UN	Maintenance and segregation of B chromosome	(54)
Reproduction	*Diplodus puntazzo*	Infemale gonads	None	DP-novel-07606; DP-novel-06984; DP-novel-07767	miR-122-1; miR-7a; miR-129; miR-125c	XR_003984576.1; XR_003429050.1; XR_001814721.1	Gonad maturation	(55)
	Paralichthys olivaceus	Ovary; Testis	None	TCONS-00021450; TCONS-00058013; TCONS-00058894	miR-20a; let-7; miR-82155_166	*dnah1*; *dnah11*; *dnah12*	Steroidogenesis; Spermatogenesis	(56)
	Paralichthys olivaceus	Ovary; Liver	None	LNC-001695; LNC-007947; LNC-002362; LNC-003418	novel_103; novel_120; novel_125; novel_167	ARMC6; PCCA; TANC2; TNR5; MMP28	Steroid biosynthesis; Metabolism; Immunity; Signal transduction	(57)

(Continued)

10.3389/fimmu.2023.1065357

TABLE 1 Continued

Regulated biological process	Related fish species	Related Organs/ Cells	Stimulus	Mainly related lncRNAs	Mainly related miRNAs	Mainly related genes	Mainly related signaling pathways	Refs
Bacterial infection	*Salmo salar*; *Sebastes schlegelii*	Gill; Spleen	*Aeromonas salmonicida*	TCONS_00079020; LOC106564649; TCONS_00022856; LNC_00116154	miR-155-5p; miR-551-3p; miR-8157-3p; novel_264	*atm*; *tp53*; *mdm4*; NLRC3	P53; Wnt/β-catenin; mTOR; Metabolism; Immunity; Phagocytosis; TLRs; Degradation	(58, 59)
	Paralichthys olivaceus; *Miichthys miiuy*; *Nibea diacanthus*; *Larimichthys crocea*	Spleen; MICs; EPCs; Kidney cells	*Vibrio anguillarum*	lncRNA-IRL	miR-27c-3p	IRAK4	Pathogen recognition and killing; NF-κB; Apoptosis; Immunity	(60, 61)
	Paralichthys olivaceus	Intestine; HEK293T	*Edwardsiella tarda*	LNC_001979	novel_171	*potusc2*; *podad1*	Autophagy; PPAR, Endocytosis; MAPK, Notch; Phagosomes; Immunity	(62)
	Ctenopharyngodon idella	Spleen; Muscle; Brain; Heart; Fin; Gill; CIKs	*Aeromonas hydrophila*	lncRNA-WAS; lncRNA-C8807; lncRNA-SUMO3; lncRNA-HDMO13; LncRNA-ANAPC2; lncRNA-NEFM	miR-142a-3p; miR-21; miR-451	*ccr7*; *glut3*; *jnk*; *tnfaip2*; *npr2*; *hdac8*	NF-kB; MAPK; Immunity	(63–65)
	Oreochromis niloticus	Spleen; Kidney	*Streptococcus agalactiae*	MSTRG.2496.2; MSTRG.204071.1; MSTRG.61707.9; MSTRG.129013.3	miR-265; miR-574; miR-466; miR-2305; miR-7082; miR-4739	ON_73287; ON_86194; PB_14857; PB_1748; PB_10169; EN_09656	Cytokines; TLRs; Endocytosis; Lysosomal metabolic; Immunity	(66)
	Epinephelus coioides	Spleen	*Pseudomonas plecoglossicida*	c115058_g1-i1; c125321_g1-i1; c132960_g1-i1; C202650_g1-i1	miR-731; miR-16b; miR-375; miR-15a-3p	*cela1*; *cela2*; *ctrb*; *prss*	Immunity; Chemokine; Cytokine; Antigen processing and presentation	(67–70)
Viral infection	*Miichthys miiuy*	Liver; Spleen, Kidney; Brain, Heart; Gill; Intestine; MICs	SCRV	AANCR; MARL; NOD1; NARL; MIR2187HG; MIR122HG	miR-210; miR-122; miR-217-5p; miR-2187-3p; miR-122-5p	MITA; MAVS; NOD1; TBK1; TAK1	Cell proliferation; NF-κB; IRF3; Immunity	(71–75)
	Salmo salar	Gill	POMV	MSTRG.13941.1	miRNA-30e-3-3p	*selja*	Selenium transport	(76)
Others	*Oreochromis niloticus*; *Oncorhynchus mykiss*	Brain; Skin; Heart; Gill; Intestine; Head kidney;	Hypoxia; Cold; Alkalinity; Salinity; Acute heat;	TCONS_00151992; MSTRG.11484.2; MSTRG.32014.1; MSTRG.29012.1	miR-128-5p; C-5p-43254_34; PC-3p-28352_70; bta-miR-11987_L-1R-1_1ss8TA	*ifih1*; *dhx58*; *irf3*	MAPK; Phagosome; Immunity; NOD-like receptor; RIG-I-like receptor, ...	(77–79)

NL, not listed; UN, unknown.

10.3389/fimmu.2023.1065357

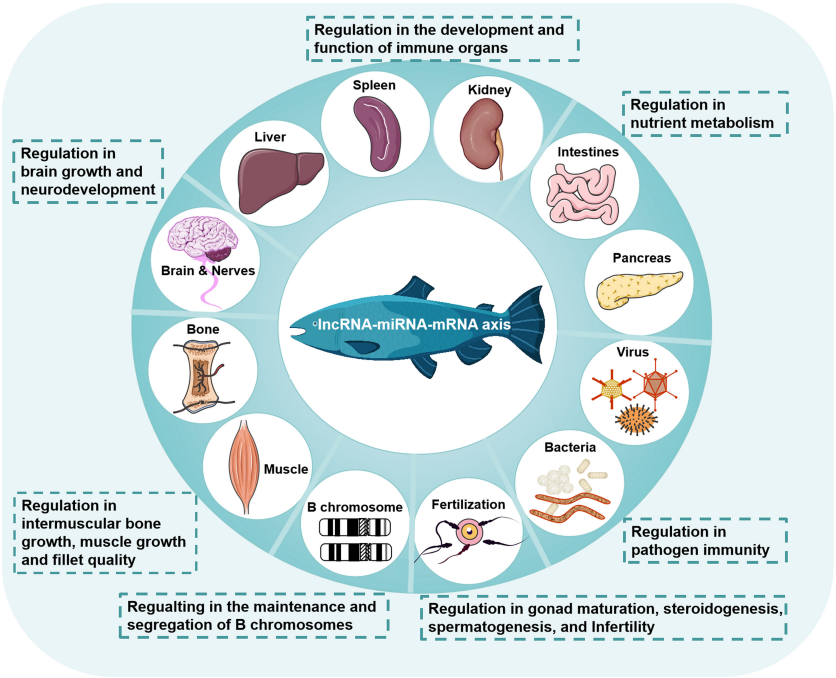

FIGURE 2
Regulation of the lncRNA-miRNA-mRNA axis in teleost fish. The lncRNA-miRNA-mRNA axis is widely involved in the physiological and pathological processes of fish, including the development and function of immune organs, nutrient metabolism, brain growth and neurodevelopment, intermuscular bone growth, muscle growth and fillet quality, the maintenance and segregation of B chromosomes, gonad maturation, steroidogenesis, spermatogenesis, infertility, and pathogen immunity.

miRNAs, while 6 lncRNAs were identified as precursors of 16 miRNAs (81). These data support that ceRNAs are the most common mode of relationship between ncRNAs. The central ceRNA networks of the hepatopancreas are formed by 4 lncRNAs, 3 miRNAs and 7 mRNAs in grass carp (80). Fourteen hub lncRNAs and 28 hub miRNAs were both expressed in the liver and head kidney of coho salmon (81). This finding indicates that the two main immune organs of fish have relatively similar ncRNA expression patterns, supporting ncRNAs as biomarkers of tissue/organ-specific expression and developmental stages of organisms (48, 81). Moreover, the pathways of the target genes of these ncRNAs are concentrated in 12 pathways, such as the transforming growth factor-beta (TGF-β) signaling pathway, cytokine-cytokine receptor interaction, adherens junction, and nuclear transcription factor (NF)-κB signaling pathway (81), suggesting that ncRNAs and their interactions play important regulatory roles in the development or function of fish immune organs.

2.1.3 Skeletal muscles

Regarding skeletal muscle, different expression profiles of lncRNAs and mRNAs were identified in different developmental stages of Japanese flounder (62). These lncRNAs were then predicted to take part in skeletal muscle development *via* cis- or trans-acting mechanisms. In addition, coexpression networks of the lncRNA-miRNA-mRNA axis showed that most lncRNAs interact with one or two predicted miRNAs. Some lncRNAs can even interact with at least three target miRNAs, such as TCONS_00093971, TCONS_00096817, and TCONS_00032744 (62). Similarly, a total of 290 lncRNAs are differentially expressed in juvenile and adult fast skeletal muscle of gilthead sea bream (*Sparus aurata*, *S. aurata*), and the number of differential lncRNAs is greater in juveniles than in adults, indicating that most of the differential lncRNAs play a role in the muscle growth of juveniles (49). In addition, most of the differential lncRNAs (such as lncRNA20194) were more active in myoblast proliferation and were downregulated during the fusion process, which may play a promoting role in myoblast proliferation by acting as sponges for miR-133, miR-206 and miR-208 (49). Moreover, the different expression profiles of mRNAs and lncRNAs were identified in fish families with different phenotypes of rainbow trout (49, 82). In the constructed lncRNA-miRNA-mRNA network, 3 lncRNAs (Omy500041161, Omy400178299, and Omy500089619) were coexpressed with mRNAs known to be associated with whole body weight (WBW), muscle yield and fat content, such as lipoprotein lipase (LIPL) and TGF-β, to impact muscle quality traits. Moreover, 44 lncRNAs were able to interact with miRNAs as sponges to control mRNAs belonging to protein catabolic/anabolic pathways, affecting muscle mass characteristics and fast/effective growth rates (82). These data demonstrate the regulatory role of lncRNAs and their ceRNA networks in muscle growth and development and in the characteristics of muscle growth and fillet quality.

2.1.4 Intermuscular bone

Intermuscular bone (IB) is a small spicul-like bone present in the muscular septum of teleost fish that adversely affects the food and economic value of fish (83). The expression profiles of mRNAs

and ncRNAs (lncRNAs and miRNAs) were different in blunt snout bream (*Megalobrama amblycephala*, *M. amblycephala*) at two intermuscular bone (IB) growth stages (1 and 3 years old) (50). The slow-growing IB-3 was found to possibly be due to the reduced osteoblast differentiation and Ca^{2+} deposition caused by ZIP1 downregulation. In addition, 14 ceRNA axes related to the growth of IBs were identified with 10 lncRNAs, 7 miRNAs, and 10 mRNAs (50). Among these RNAs, dre-miR-24b-3p and dre-miR-193b-3p were confirmed to be core miRNAs that could interact with 4 lncRNAs (LNC_007210, LNC_011298, LNC_001774, and LNC_017705) and 3 mRNAs (iron-regulated transporter (IRT)-like protein (ZIP), complement component 6 (C6), and *M. amblycephala* Gene 23275). In particular, the lnc017705-miR-24a-3p-ZIP1 axis is likely to regulate the development of IB (50), which suggests their regulatory roles in the growth of IB in *M. amblycephala*.

2.1.5 B chromosomes

B chromosomes (Bs) are predominantly found in karyotype species of eukaryotic taxa and are considered extra or redundant chromosomes (84). Recently, Bs in fish were found to also be able to generate lncRNAs, termed B chromosome long noncoding RNA (BncRNA) (67). BncRNA is transcribed from a transcriptionally active repetitive DNA (BncDNA) that is highly expressed on all B chromosomes in the cichlid fish (*Astatotilapia latifasciata*, *A. latifasciata)*. In addition, BncRNA was predicted to be involved in the maintenance and segregation of the B chromosome during cell division by interacting with miRNAs on the B chromosome, including miR-129-3p, miR-9-5p, and miR-153a-5p (67), possibly leading to a new understanding of B chromosomes and lncRNA-miRNA regulatory networks in fish development.

2.2 Regulation in reproduction

2.2.1 Gonad maturation

ncRNAs, including lncRNAs, miRNAs, rRNAs, and piRNAs, have been found to show differential expression between mature and immature gonads of infemale sharpsnout seabream (*Diplodus puntazzo*, *D. puntazzo*) (51). The study found that 8 of the 10 lncRNAs that were identified in the National Center for Biotechnology Information (NCBI) basic local alignment search tool (BLAST) hit were highly expressed in immature fish, while 8 of the 10 identified miRNAs were highly expressed in mature fish (51). Furthermore, putative lncRNA-miRNA-mRNA hybridizations were constructed, which included 3 lncRNAs (DP-novel-07606, DP-novel-06984, and DP-novel-07767), 5 miRNAs (miR-122-1, miR-129, miR-125c, miR-7a, and ENSGACT00000282061), and 3 mRNAs (XR_003984576.1, XR_003429050.1, and XR_001814721.1) (51). Most miRNAs in these networks have been proven to be associated with a broad range of physiological processes, including gonad maturation. For example, miR-125c can inhibit the maturation of immature females by inhibiting the expression or proteolysis of vitellogenins and yolk proteins (68). In addition, follicle-stimulating hormone receptor (FSHR) is a target of miR-125c, which is a critical gene for the growth of the primary ovarian follicle (69), suggesting that lncRNAs highly expressed in immature gonads may promote gonad maturation by regulating the miRNA-mRNA pathway.

2.2.2 Steroidogenesis and Spermatogenesis

Similarly, ncRNAs also showed differential expression between gonads of different sexes in gynogenetic Japanese flounder. A total of 6772 differentially expressed mRNAs (3541 testis-biased and 3231 ovary-biased), 2284 lncRNAs (1870 testis-biased and 414 ovary-biased), and 244 miRNAs (146 testis-biased and 98 ovary-biased) were obtained between gynoenetic female ovaries and sex-reversed neomale testes (52). Clearly, the numbers of differentially expressed mRNAs and lncRNAs were significantly higher in the testis than in the ovaries, suggesting that ncRNAs function more actively in the neomale testis, especially lncRNAs. Furthermore, the lncRNA-miRNA-mRNA interaction network was constructed with 91 mRNAs, 64 lncRNAs, and 98 miRNAs. In this network, some hub miRNAs interact with many lncRNAs. For example, ovary-biased let-7 binds to 18 lncRNAs and targets dnah1, testis-biased miR-20a interacts with 14 DElncRNAs and targets dnah11, while the novel miRNA-82155_166 can cooperate with 57 lncRNAs to target most large mRNAs. These miRNA-associated regulatory axes involve numerous steroid biogenesis- and sperm motility-related genes and pathways, such as the cytoskeleton, microtubule cytoskeleton, cytoplasmic dynein complex, tubulin and actin binding (52). These data suggest the regulatory roles of the lncRNA-miRNA-mRNA network in steroidogenesis and sexual spermatogenesis in *P. olivaceus*.

2.2.3 Infertility

Moreover, the lncRNA-miRNA-mRNA ceRNA network was proven to be involved in the mechanism underlying infertility in fish. The liver is essential for fish fertility because it can synthesize vitelline and the precursor of vitelline, which is required for oocyte development and maturation (53, 85). Compared with fertile fish livers, sterile fish livers were found to have fewer vacuoles and significantly lower serum vitellogenin levels in *P. olivaceus* (86). Moreover, ncRNAs (mRNAs, lncRNAs, circular RNAs, and miRNAs) were differentially expressed in infertile and fertile individuals *P. olivaceus*). The lncRNA-miRNA-mRNA ceRNA network was constructed with 92 lncRNAs, 14 mRNAs, and 4 miRNAs, which included the identified potentially functional ncRNAs in steroid biosynthesis pathways, such as pol-miR-133-3p, pol-miR-221-3p, XLOC_008437, XLOC_015293, and XLOC_019323. Among the target genes, armadillo repeat-containing protein 6 (ARMC6), propionyl-CoA carboxylase alpha chain (PCCA), tetratricopeptide repeat, ankyrin repeat and coiled-coil containing 2 (TANC2), transposable DNA element 5 (TNR5), and matrix metalloproteinase 28 (MMP28) were associated mainly with metabolism (fat and glycerophospholipid), signal transduction (complement and coagulation cascades), and immunity (RIG-I-like receptor signaling pathway) (86). These results indicate that fish infertility is related not only to histological structure, hormone secretion, and the steroid biosynthesis pathway but also to liver

metabolism, immunity, and signal transduction, which may all be regulated by ncRNAs and their ceRNA network.

2.3 Regulation in bacterial infection

Infection is a life-and-death struggle between host and pathogen (54), in which host must mobilize its immune system to win (55). Similar to other vertebrates, the immune response of organisms to the invasion of foreign pathogens in teleost fish usually involves the regulation of ncRNAs, especially lncRNAs and miRNAs (19, 20). In fish infected by various types of bacteria or viruses, many immune-related lncRNA-miRNA-mRNA regulatory networks have been identified and play an antibacterial, antiviral or opposite role, as shown in Figure 3.

2.3.1 Aeromonas hydrophila (A. hydrophila)

lncRNA-WAS, lncRNA-C8807, lncRNA-SUMO3, lncRNA-HDMO13, lncRNA-ANAPC2 and lncRNA-NEFM were recently identified in grass carp (*C. idella*) and are constitutively expressed in all tested tissues, including the spleen, muscle, brain, heart, fin, and gill (66, 70, 87). However, their expression levels in grass carp kidney (CIK) cells after infection by *A. hydrophila* were found to increase during the initial infection but began to decline and even returned to normal levels later, suggesting their response to *A. hydrophila* infection in cells. Furthermore, overexpression of these lncRNAs was found to significantly promote the cell activity of NF-κB and inflammatory factors, including tumor necrosis factor (TNF)-α, IL-1β, IL-6, IL-8, IL-12, and TGF-β (66, 70, 87). Furthermore, lncRNA-WAS and lncRNA-C8807 were shown to interact with miR-142a-3p to regulate the expression of its targets tnfaip2 and glut3 (70). lncRNA-SUMO3 and lncRNA-HDMO13 may act as sponges to regulate miR-21 and miR-142a-3 to affect their target genes, c-Jun N-terminal kinase (jnk) and CC-chemokine receptor 7 (ccr7), glucosetranspoter isoform (glut3), and tumor necrosis factor alpha induced protein 2 (tnfaip2) (66). LncRNAANAPC2 and lncRNA-NEFM interact with miR-451 to target histone deacetylase 8 (hdac8) and natriuretic peptide receptor 2 (npr2) (87). These network targeting genes tnfaip2, jnk, cc7, glut3, npr2 and hdac8 were all proven to induce inflammatory responses associated with the NF-kB or MAPK pathway (56, 60, 61, 71, 88). These data suggest that the lncRNA-miRNA-mRNA networks mediated by lncRNA-WAS, lncRNA-C8807, lncRNA-SUMO3, lncRNA-HDMO13, lncRNAANAPC2 and lncRNA-NEFM play positive regulatory roles in the inflammatory response of grass carp to *A. hydrophila* challenge.

2.3.2 Aeromonas salmonicida (A. salmonicida)

Based on the identified lncRNAs, miRNAs, and mRNAs that were differentially expressed in gills of Atlantic salmon (*Salmo salar*, *S. salar*) infected with *A. salmonicida*, an immune-related lncRNA-miRNA-mRNA ceRNA network was constructed (72). This network includes 32 lncRNAs, 10 miRNAs, and 16 mRNAs, which are associated with many immune-related signaling pathways, such as p53, (Wnt)/β-chain protein (β-catenin), mammalian target of rapamycin (mTOR), Janus kinase (JAK)/signal transducer and activators of transcription (STAT), and Toll-like receptor (TLR). In addition, three typical lncRNA-miRNA-mRNA axes were found: TCONS_00079020- miR-155-5p- atm (*ataxia telangiectasia*-mutated gene), LOC106564649-miR-551-3p- tp53, and TCONS_00022856- miR-8157-3p- mdm4 (murine double minute 4), which were all included in the p53

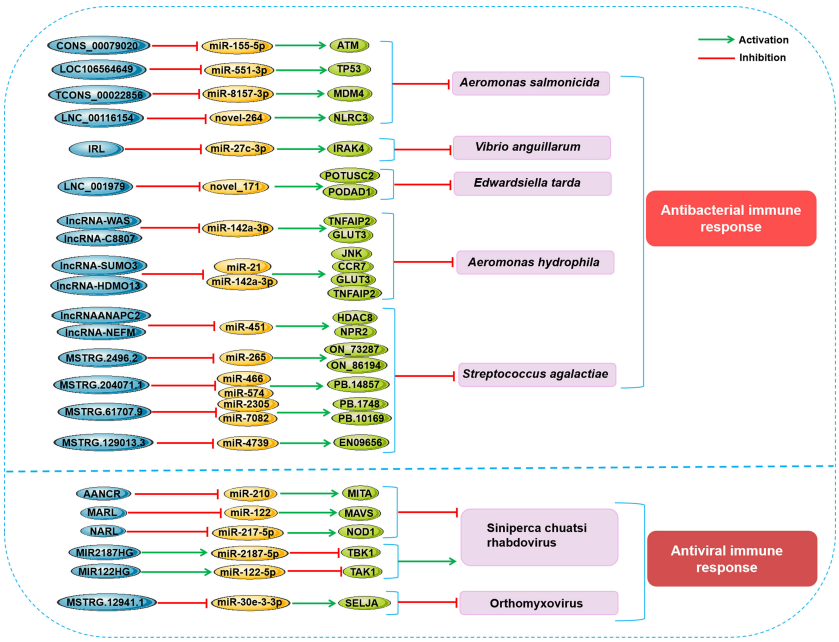

FIGURE 3
Schematic presentation of the main lncRNA-miRNA-mRNA axes involved in the fish antipathogen immune response. (up) Main lncRNA-miRNA-mRNA axes related to the antibacterial immune response in fish. (down) Main lncRNA-miRNA-mRNA axes related to antiviral immune response in fish.

signaling pathway (85). Meanwhile, 1091 lncRNA-miRNA-mRNA network axes were constructed in black rockfish (*Sebastes schlegelii*, *S.schlegelii*) spleen infected with *A. salmonicida*, which included 400 lncRNAs, 69 miRNAs, and 70 mRNAs (73). The main immune-related signaling pathways involved in the network axis were nutrient metabolism, cell adhesion molecules (CAMs), phagocytosis, and degradation. In the regulatory networks, NLRC3-like genes can be regulated by 17 lncRNAs but only one miRNA (novel_264) at the same time. The key ceRNA triple regulatory network was focused on the LNC_00116154-novel-264-NLRC3 pathway, which may play an important immune regulatory role in the resistance of black rockfish against *A. salmonicida* infection (73). These results indicate the regulatory roles of the lncRNA-miRNA-mRNA network in the immune response of teleost fish against *A. salmonicida* infection.

2.3.3 Edwardsiella tarda (E. tarda)

A total of 115 differentially expressed lncRNAs were identified in the intestine of olive flounder infected by *E. tarda* (89). Among these RNAs, 64 lncRNAs together with 31 miRNAs and 1,766 mRNAs constituted the lncRNA-miRNA-mRNA regulatory network. Many immune-related processes or signaling pathways are involved in the miRNA-mRNA regulatory network mediated by these lncRNAs, such as the signaling pathways of autophagy, peroxisome proliferator-activated receptor (PPAR), endocytosis, mitogen-activated protein kinase (MAPK), Notch, and phagosomes. In addition, two potential ceRNA regulatory networks were preliminarily identified: LNC_001979- novel_171- Potusc2 and LNC_001979- novel_171- Podad1 in the intestine of olive flounder, suggesting their roles in anticeRNA regulatory networks (89). Both tusc2 (tumor suppressor candidate 2) and dad1 (defender against cell death 1) could encode multifunctional proteins associated with cellular processes (57, 90), which suggests that Potusc2- and Podad1-tagged ceRNA regulatory networks may play an important role in regulating the antibacterial immune response against *E. tarda* in olive flounder.

2.3.4 Pseudomonas plecoglossicida (P. plecoglossicida)

In addition, the network of lncRNA-miRNA-mRNA relationships was also proven to be involved in the regulation of immune responses in the spleen of *Epinephelus coioides* (*E. coioides*) infected by *P. plecoglossicida* (63, 64, 91, 92). Compared with the wild-type strain of *P. plecoglossicida*, infection with the L321_RS19110-RNAi (RNA interference) strains, sigX-RNAi strains, L321_20267-RNAi strains, or L321_RS15240-RNAi strains resulted in a delayed onset time, a 20%-50% reduction in the mortality rate of *E. coioides*, and a reduction in symptoms in the spleen, suggesting that L321_RS19110, sigX, and L321_20267, and L321_RS15240 are important disease-causing genes for *P. plecoglossicida* (63, 64, 91, 92). Moreover, these RNAi strains had significant effects on immune-related genes in *P. plecoglossicida*-infected *E. coli*, which were associated with the expression of many lncRNAs. Many upregulated mRNAs are involved in important immune response processes in the spleen, including chemokine or cytokine signaling pathways, receptor-ligand interactions, and antigen processing and presentation (63, 64, 91, 92). For example, chymotrypsin-like elastase family member (cela) 1 was associated with 16 lncRNAs and 4 miRNAs, cela2 was associated with 20 lncRNAs and 5 miRNAs, chymotrypsin B (ctrb) was associated with 24 lncRNAs and 18 miRNAs, and trypsinogen (prss) was associated with 15 lncRNAs and 19 miRNAs (91). In addition, these immune genes are predicted to be regulated by miRNAs and lncRNAs in complex ways, including the formation of lncRNA-miRNA-mRNA ceRNA networks (63, 91, 92). These results suggest that upregulation of immune response-related regulatory lncRNA-miRNA-mRNA networks in *P. plecoglossicida-infected E. coli* may enhance the body's antibacterial capacity.

2.3.5 Streptococcus agalactiae (S. agalactiae)

In *S. agalactiae*-challenged tilapia (*Oreochromis niloticus*, *O. niloticus)*, 1281 lncRNAs were found to be differentially expressed during infection (65). Among the constructed lncRNA-miRNA-mRNA ceRNA networks, 4 lncRNA (MSTRG.2496.2, MSTRG.204071.1, MSTRG.61707.9, and MSTRG.129013.3)-mediated networks were highly correlated in the spleen and kidney, the main target organs of *S. agalactiae*. In addition, these four lncRNA-mediated ceRNA networks included 6 miRNAs (miR-265, miR-574, miR-466, miR-2305, miR-7082, and miR-4739) and 6 mRNAs (ON_73287, ON_86194, PB_14857, PB_1748, PB_10169, and EN_09656), which were involved in several key immune signaling pathways, such as the cytokine-cytokine receptor interaction pathway, Toll-like receptor signaling, endocytosis pathway, and lysosomal metabolic pathway (65). These data further illustrate the role of lncRNAs and their mediated ceRNA networks in innate immunity against bacterial infection in tilapia.

2.3.6 Vibrio anguillarum (V. anguillarum)

In *Vibrio anguillarum* (*V. anguillarum*)-infected Japanese flounder, 414 lncRNAs were identified that exhibited differential expression, of which 36 lncRNAs acted as competing endogenous RNAs (ceRNAs) interacting with 16 miRNAs and 37 mRNAs (93). Mainly 10 immune pathways were involved in the ceRNA regulatory networks, such as pathogen recognition and killing, NF-κB-regulated inflammation response, apoptosis, and adaptive immunity (93). This finding supports the relationship between the identified ceRNA networks and antibacterial immunity in *V. anguillarum*-treated flounder. Similarly, many lncRNAs were also identified in the spleen tissues of Miiuy croaker (*Miichthys miiuy*, *M. miiuy*) challeged with *V. anguillarum* (94). Interleukin-1 receptor-related kinase (IRAK)-4-related lncRNA (IRL) is one of the significantly upregulated lncRNAs induced by *V. anguillarum*. Knockdown of IRL significantly inhibited the expression levels of tumor necrosis factor (TNF)-α, interleukin (IL)-6, IL-8, and IL-1β in miiuy croaker intestines cells (MICs) upon lipopolysaccharide (LPS) stimulation. In addition, IRL knockdown increased apoptosis but decreased the viability of LPS-treated MICs. Furthermore, IRL was found to act as a sponge for miR-27c-3p to enhance IRAK4 expression, which is a critical regulator involved in the TLR-dependent immune response, thus inhibiting the innate

antibacterial response mediated by the production of inflammatory cytokines resulting from activation of the TLR-nuclear transcription factor (NF)-κB signaling pathway. Moreover, the IRL-miR-27c-3p-IRAK4 ceRNA network 4 was shown widely in other teleost fish, including *Nibea diacanthus* (*N. diacanthus*) and *Larimichthys crocea* (*L. crocea*), suggesting the relative conservation of the existence and function of this axis in fish species (94). These results indicate that IRL is a positive regulator of antibacterial responses in fish species by sponging miR-27c-3p.

2.4 Regulation of viral infection

2.4.1 Siniperca chuatsi rhabdovirus (SCRV)

The lncRNA-miRNA-mRNA regulation mechanism also exists in the innate antiviral responses of Miiuy croaker to SCRV. Xu reported that a total of 897 lncRNAs were differentially expressed in SCRV-infected spleen samples of miiuy croaker, including the newly identified upregulated lncRNAs antiviral-associated long noncoding RNA (AANCR), mitochondrial antiviral signaling protein (MAVS) antiviral-related lncRNA (MARL), nucleotide oligomerization domain 1 (NOD1) antibacterial and antiviral-related lncRNA (NARL), MIR2187HG and MIR122HG (58, 74, 95–97). Among these RNAs, AANCR, MARL and NARL were subsequently shown to function as positive regulators to counteract the enhancement of SCRV replication. Knockdown of AANCR, MARL, or NARL can promote SCRV replication in SCRV-treated MICs and reduce the expression levels of antiviral-related immune genes, including type I interferon (IFN-1), TNF-α, myxovirus resistance protein 1 (MX1), interferon-stimulated gene 15 (ISG15) and viperin. In addition, their silencing also inhibited cell proliferation in SCRV-treated MICs, whereas their overexpression significantly promoted cell proliferation (74, 95, 96). Mechanistically, AANCR, MARL and NARL were shown to act as ceRNAs by sponging miR-210, miR-122 or miR-217-5p, respectively, to relieve their repressive effects on antiviral gene expression of stimulator of interferon genes (MITA), MAVS or nucleotide oligomerization domain receptor 1 (NOD1), thereby maintaining the stability of the antiviral response of the body and ensuring an appropriate inflammatory response (74, 95, 96). In contrast, MIR2187HG and MIR122HG were proven to be negative regulators to counteract the enhancement of SCRV replication (58, 97). MIR2187HG was identified as a developmental reservoir or as premiR-2187 of miR-2187-3p to increase its expression in SCRV-treated miiuy croaker, thereby inhibiting intracellular TANK-binding kinase 1 (TBK1) expression and TBK1-mediated signaling of NF-κB and interferon regulatory Factor 3 (IRF3) (97). MIR122HG was found to decrease the transforming growth factor-β-activated kinase 1 (TAK1)-triggered NF-κB and IRF3 signaling pathways by acting as a precursor of miR-122-5p (58). These results suggest that the upregulated lncRNAs in miiuy croaker infected by SCRV can positively or negatively regulate the body's antiviral immune response by interacting with miRNAs, which can not only maintain the stability of the response but also avoid an excessive response to maintain a stable and appropriate antiviral immune response.

2.4.2 Orthomyxovirus (POMV)

In POMV-infected Atlantic salmon, Samsing found that a total of 86 lncRNAs and 478 miRNAs were aberrantly expressed in the gill tissues of infected fish (75). Through the analysis of the ceRNA network constructed between miRNAs, lncRNAs and mRNAs, noncoding RNAs targeting mRNAs were found to be concentrated mainly on genes involved in the immune response process. Among them, the pathway consisting of lncRNA MSTRG.13941.1, miRNA-30e-3-3p and selenoprotein Ja (selja) attracted attention. MSTRG.13941.1 is one of the lncRNAs that rarely changes in fish in the late stage of virus infection. The predicted target genes of miRNA-30e-3-3p include not only fish genes but also virus genes, while the expression level of selja involved in selenium (Se) transport was significantly reduced in late-stage infected fish (75). Selenium is an essential micronutrient for a variety of organisms and has important physiological functions, such as promoting immunity and antioxidation (76), suggesting that the MSTRG.13941.1/miRNA-30e-3-3p/Selja pathway may be involved in virus clearance and homeostasis restoration by regulating selenium metabolism in fish, which requires further study.

2.5 Regulation in other stress responses

In an expression analysis of ncRNAs in Nile tilapia (*Oreochromis niloticus*, *O. niloticus*) under at least 15 different tissues and different stress conditions (e.g., hypoxia, cold, alkalinity, salinity, and *Streptococcus agalactiae (S. agalactiae)* infection), 1955 tissue-specific lncRNAs and 99 stress-related lncRNAs were identified (98). Ninety-nine stress-related lncRNAs were predicted to bind to 448 miRNAs, of which 10 lncRNAs contained a motif complementary to 17 mature miRNAs, including the TCONS_00151992-dre-miR-128-5p pair (98). Similarly, when rainbow trout were exposed to acute heat stress, a total of 2605 lncRNAs, 214 miRNAs and 5608 mRNAs were found to be differentially expressed in the head kidney (77). Then, a lncRNA-miRNA-mRNA ceRNA interaction network was constructed based on these differentially expressed lncRNAs, which were significantly enriched in the innate immune response. Immune-related ceRNAs may regulate the acute heat stress-induced response mainly by the MAPK signaling pathway (77). In addition, comparing the whole transcriptome of skin in wild-type rainbow trout, a total of 1630 lncRNAs, 50 miRNAs and 2448 mRNAs were differentially expressed in the skin of yellow mutant rainbow trout, which involved numerous key innate immune-related signaling pathways (78). In the immune-related lncRNA-mediated ceRNA network, the lncRNAs MSTRG.11484.2, MSTRG.32014.1 and MSTRG.29012.1 together with PC-5p-43254_34, PC-3p-28352_70 and bta-miR-11987_L-1R-1_1 ss8TA were identified to regulate at least 3 immune-related genes, interferon-induced helicase C domain-containing protein 1 (ifih1), DEXH (Asp-Glu-X-His) box polypeptide 58 (dhx58) and irf3 (78). These results suggest that the lncRNA-mediated ceRNA network is involved in the fish immune response to various stresses.

3 Potential application of the lncRNA-miRNA-mRNA axis in fish

Regarding the above description of lncRNA-miRNA-mRNA interactions in fish, we can speculate that this regulatory mode is highly conserved in biological genetic evolution, although the conservation of lncRNAs is considered to be much lower than the conservation of miRNAs, suggesting that similar to mammals, the lncRNA-miRNA-mRNA axis may also be a potential disease or nondisease biomarker in fish and also suggesting that strategies used in mammals to modulate lncRNAs or miRNAs as molecular targets (silencing or activation) may also be useful in the diagnosis and treatment of fish domestication or disease treatment. Even though lncRNAs are less conserved in fish, targeting the regulation of miRNAs targeted by lncRNA sponges is also a valuable tool for the development of novel therapeutics and high-value biotechnological products for fish. Currently, well-established biotechnologies for lncRNA or miRNA inhibition in mammals include the use of oligonucleotides, RNA interference or small molecule inhibitors, nucleic acid restriction, and clustered regularly interspersed short palindromic repeats (CRISPR)–Cas9 (79, 99–101). In contrast, biotechnologies targeting lncRNA or miRNA overexpression use mainly mimics or viral vector-based gene restoration, transcriptional upregulation, and therapeutic manipulation of ncRNA promoters (102, 103).

In addition, the expression profiles of lncRNAs and mRNAs were found to be altered in the intestine of rainbow trout fed a probiotic diet, suggesting that diet can alter the expression patterns of noncoding RNAs and genes *in vivo* (104). Furthermore, feeding shrimp with bacteria expressing shrimp miR-34 could significantly increase the expression level of miR-34 or mja-miR-35 in shrimp, thereby exerting an antiviral effect against white spot syndrome virus (WSSV) infection. These shrimp were then cooked and fed to a human tumor xenograft mouse model, and the lung metastatic ability of the tumor was significantly reduced in these mice (105, 106). Moreover, dietary miRNA absorption was confirmed to indeed occur in the stomach mediated by mammalian systemic RNA interference defective-1 (SID1) transmembrane family member 1 (SIDT1), which is a key transporter enriched in the stomach (105, 107). These results suggest that dietary or oral administration is an efficient way of delivering ncRNAs *in vivo* for the treatment of diseases such as viral infections or tumors. Using a simple and convenient dietary ncRNA approach to alter nutritional or reproductive strategies regulated by the lncRNA-miRNA-mRNA network would be an effective strategy to improve feeding/breeding efficiency and fishery production.

4 Conclusions and discussion

Over the past 20 years, ncRNA-related research has expanded dramatically, especially in the context of human disease. In fish, novel rearing/reproduction strategies targeted by noncoding RNAs have attracted attention to achieve the intriguing goal of optimizing fish growth while maintaining high nutritional value. In recent years, a variety of ncRNAs have been identified and molecules in fish, their functions and molecular mechanisms have gradually become clear, and several fish ncRNA databases have been established, such as FishDB (http://fishdb.ihb.ac.cn) (108). However, compared with the available information for mammals, the amount of information about teleost ncRNAs is still limited. The expression patterns, regulatory functions and molecular mechanisms of ncRNAs in fish need to be further studied. Here, we review the composition and role of the lncRNA-mediated miRNA-mRNA regulatory network in fish growth and development (brain, hepatopancreas, immune organs, skeletal muscles, intermuscular bone, B chromosomes), reproduction (gonad maturation, steroidogenesis, spermatogenesis and infertility), bacterial infection (*A. salmonicida, V. anguillarum, E. tarda, A. hydrophila, S. agalactiae, and E. coioides*), viral infection (SCRV and POMV), and other biological processes, as shown in Table 1. These data allow us to better understand the molecular regulatory mechanisms of lncRNA-miRNA-mRNA regulatory networks in fish responses to various environmental stress stimuli and provide new ideas for fish domestication, breeding and feeding, as well as the diagnosis, prevention and treatment of diseases. Interestingly, we found that the regulation of LNC RNA-miRNA-mRNA regulatory networks on the abovementioned fish physiological or pathological processes is basically related to immunity, which further indicates the importance of the fish immune system and immune response in fish growth and development.

However, many lncRNA-miRNA-mRNA axes are limited to the prediction of biological information, and their regulatory relationships, regulatory effects on fish processes and molecular mechanisms have yet to be verified. In addition, the regulatory role of lncRNAs mediated by miRNAs may also be involved in other biological processes, but the composition and molecular mechanism of the lncRNA-miRNA-mRNA axis need to be confirmed. For example, the differential expression of miRNAs and lncRNAs was also found in tiger pufferfish (*Takifugu rubripes*, *T. rubripes*) of different sexes (109). Compared with female gonads, 79 lncRNAs were upregulated and 51 were downregulated in male gonads, while 3 mature miRNAs were upregulated and 3 mature miRNAs were downregulated. Moreover, several lncRNAs and miRNAs were also predicted to regulate the expression of sex-related genes in *T. rubripes* gonads, such as lnc_000338, lnc_000690, lnc_000370, fru-miR-15b, novel-167, and novel-318 (109). In the central nervous system (CNS) of the weakly electric brown ghost knifefish (*Apteronotus leptorhynchus*, *A. leptorhynchus*), a broad variety of ncRNAs were identified, including lncRNAs, miRNAs, snRNAs, snoRNAs, and other ncRNA sequences (110). These ncRNAs appear to be involved in neurodevelopmental processes such as neurogenesis, neuroregeneration, neuronal differentiation and the neural basis of behavior (110, 112). In addition, in adult zebrafish fed a high-cholesterol diet, the ncRNA regulatory network was shown to be associated with nonalcoholic fatty liver disease (NAFLD) (113). Thirty-two hub lncRNAs, 5 hub miRNAs, and 8 hub mRNAs were identified to be associated with NAFLD-related regulation (113). These results suggest that the regulation of ncRNAs in fish sex determination and differentiation, CNS development, and liver metabolism in fish may be mediated by lncRNA-miRNA-mRNA ceRNA networks, which need to be studied further.

Overall, the available data on the lncRNA-miRNA-mRNA regulatory network in teleost fish, acting as a regulator in physiology and pathology, support its critical role in maintaining cellular homeostasis and functions. However, many regulatory axes are still limited to biological predictions, and more *in vivo* and *in vitro* studies are needed to confirm their composition and function. Additionally, there are still many obstacles that need to be overcome in the research process of noncoding regulatory genes in fish, such as novel ncRNA-based biotechnology tools, screening of core molecular markers, precise intervention strategies, and development of specific ncRNA-related modulators. Therefore, solving the above problems will be an important direction for future fish species research and will further promote the development of selective breeding and sustainable aquaculture.

Author contributions

ZZ and PL designed the review and contributed to manuscript preparation. ZZ wrote the manuscript. LL, YL and ZG provided technical and administrative support. ZZ and ZW prepared the figures. ZZ, CL, YW and SW revised the manuscript. All authors contributed to the article and approved the submitted version.

Funding

This study was supported by the Natural Science Foundation of Shandong Province of China (ZR2020MH250), and the National Natural Science Foundation of China (91849209 and 81502063).

Conflict of interest

The authors declare that the research was conducted in the absence of any commercial or financial relationships that could be construed as a potential conflict of interest.

Publisher's note

References

1. Santosh B, Varshney A, Yadava PK. Non-coding RNAs: Biological functions and applications. *Cell Biochem Funct* (2015) 33:14–22. doi: 10.1002/cbf.3079

2. Djebali S, Davis CA, Merkel A, Dobin A, Lassmann T, Mortazavi A, et al. Landscape of transcription in human cells. *Nature* (2012) 489:101–8. doi: 10.1038/nature11233

3. Esteller M. Non-coding RNAs in human disease. *Nat Rev Genet* (2011) 12:861–74. doi: 10.1038/nrg3074

4. Ali SA, Peffers MJ, Ormseth MJ, Jurisica I, Kapoor M. The non-coding RNA interactome in joint health and disease. *Nat Rev Rheumatol* (2021) 17:692–705. doi: 10.1038/s41584-021-00687-y

5. Wang ZY Z, Xu H, Zhang Y, Zhang Y. Exosomal noncoding RNAs in central nervous system diseases: Biological functions and potential clinical applications. *Front Mol Neurosci* (2022) 15:1004221. doi: 10.3389/fnmol.2022.1004221

6. Zuo Y, Zhang R, Tian J, Lv X, Li R, Li S, et al. Ferroptosis in cancer progression: Role of noncoding RNAs. *Int J Biol Sci* (2022) 18:1829–43. doi: 10.7150/ijbs.66917

7. Andreassen B. Høyheim, miRNAs associated with immune response in teleost fish. *Dev Comp Immunol* (2017) 75:77–85. doi: 10.1016/j.dci.2017.02.023

8. Bartel DP. MicroRNAs: Genomics, biogenesis, mechanism, and function. *Cell* (2004) 116:281–97. doi: 10.1016/S0092-8674(04)00045-5

9. Lee I, Ajay SS, Yook JI, Kim HS, Hong SH, Kim NH, et al. New class of microRNA targets containing simultaneous 5'-UTR and 3'-UTR interaction sites. *Genome Res* (2009) 19:1175–83. doi: 10.1101/gr.089367.108

10. Schnall-Levin M, Rissland OS, Johnston WK, Perrimon N, Bartel DP, Berger B. Unusually effective microRNA targeting within repeat-rich coding regions of mammalian mRNAs. *Genome Res* (2011) 21:1395–403. doi: 10.1101/gr.121210.111

11. Friedman RC, Farh KKH, Burge CB, Bartel DP. Most mammalian mRNAs are conserved targets of microRNAs. *Genome Res* (2009) 19:92–105. doi: 10.1101/gr.082701.108

12. Krol J, Loedige I, Filipowicz W. The widespread regulation of microRNA biogenesis, function and decay. *Nat Rev Genet* (2010) 11:597–610. doi: 10.1038/nrg2843

13. Loh YH, Yi SV, Streelman JT. Evolution of microRNAs and the diversification of species. *Genome Biol Evol* (2011) 3:55–65. doi: 10.1093/gbe/evq085

14. Lim LP, Glasner ME, Yekta S, Burge CB, Bartel DP. Vertebrate microRNA genes. *Science* (2003) 299:1540. doi: 10.1126/science.1080372

15. Zhou W, Xie Y, Li Y, Xie M, Zhang Z, Yang Y, et al. Research progress on the regulation of nutrition and immunity by microRNAs in fish. *Fish Shellfish Immunol* (2021) 113:1–8. doi: 10.1016/j.fsi.2021.03.011

16. Bizuayehu TT, Babiak I. MicroRNA in teleost fish. *Genome Biol Evol* (2014) 6:1911–37. doi: 10.1093/gbe/evu151

17. Best C, Ikert H, Kostyniuk DJ, Craig PM, Navarro-Martin L, Marandel L, et al. Epigenetics in teleost fish: From molecular mechanisms to physiological phenotypes. *Comp Biochem Physiol B Biochem Mol Biol* (2018) 224:210–44. doi: 10.1016/j.cbpb.2018.01.006

18. Zhou Z, Lin Z, Pang X, Shan P, Wang J. MicroRNA regulation of toll-like receptor signaling pathways in teleost fish. *Fish Shellfish Immunol* (2018) 75:32–40. doi: 10.1016/j.fsi.2018.01.036

19. Abo-Al-Ela HG. The emerging regulatory roles of noncoding RNAs in immune function of fish: MicroRNAs versus long noncoding RNAs. *Mol Genet Genomics* (2021) 296:765–81. doi: 10.1007/s00438-021-01786-x

20. Andreassen R, Hoyheim B. miRNAs associated with immune response in teleost fish. *Dev Comp Immunol* (2017) 75:77–85. doi: 10.1016/j.dci.2017.02.023

21. Alvi SM, Zayed Y, Malik R, Peng C. The emerging role of microRNAs in fish ovary: A mini review. *Gen Comp Endocrinol* (2021) 311:113850. doi: 10.1016/j.ygcen.2021.113850

22. Xie D, Chen C, Dong Y, You C, Wang S, Monroig O, et al. Regulation of long-chain polyunsaturated fatty acid biosynthesis in teleost fish. *Prog Lipid Res* (2021) 82:101095. doi: 10.1016/j.plipres.2021.101095

23. Clark MB, Mattick JS. Long noncoding RNAs in cell biology. *Semin Cell Dev Biol* (2011) 22:366–76. doi: 10.1016/j.semcdb.2011.01.001

24. Mattick JS. Long noncoding RNAs in cell and developmental biology. *Semin Cell Dev Biol* (2011) 22:327. doi: 10.1016/j.semcdb.2011.05.002

25. Li T, Mo X, Fu L, Xiao B, Guo J. Molecular mechanisms of long noncoding RNAs on gastric cancer. *Oncotarget* (2016) 7:8601–12. doi: 10.18632/oncotarget.6926

26. Zhou Z, Wang Z, Gao J, Lin Z, Wang Y, Shan P, et al. Noncoding RNA-mediated macrophage and cancer cell crosstalk in hepatocellular carcinoma. *Mol Ther Oncolytics* (2022) 25:98–120. doi: 10.1016/j.omto.2022.03.002

27. Zhou Z, Lin Z, He Y, Pang X, Wang Y, Ponnusamy M, et al. The long noncoding RNA D63785 regulates chemotherapy sensitivity in human gastric cancer by targeting miR-422a. *Mol Ther Nucleic Acids* (2018) 12:405–19. doi: 10.1016/j.omtn.2018.05.024

28. Lin ZJ, Zhou ZX, Guo H, He YQ, Pang X, Zhang XM, et al. Long noncoding RNA gastric cancer-related lncRNA1 mediates gastric malignancy through miRNA-885-3p and cyclin-dependent kinase 4. *Cell Death Dis* (2018) 9:607. doi: 10.1038/s41419-018-0643-5

29. Wang KC, Chang HY. Molecular mechanisms of long noncoding RNAs. *Mol Cell* (2011) 43:904–14. doi: 10.1016/j.molcel.2011.08.018

30. Zhang F, Zhang L, Zhang C. Long noncoding RNAs and tumorigenesis: Genetic associations, molecular mechanisms, and therapeutic strategies. *Tumour Biol* (2016) 37:163–75. doi: 10.1007/s13277-015-4445-4

31. Shetty A, Venkatesh T, Kabbekodu SP, Tsutsumi R, Suresh PS. LncRNA-miRNA-mRNA regulatory axes in endometrial cancer: A comprehensive overview. *Arch Gynecol Obstet* (2022) 306:1431–1447. doi: 10.1007/s00404-022-06423-5

32. Barbosa DA, Araujo BC, Branco GS, Simeone AS, Hilsdorf AWS, Jabes DL, et al. Transcriptomic profiling and microsatellite identification in cobia (Rachycentron canadum), using high-throughput RNA sequencing. *Mar Biotechnol (NY)* (2022) 24:255–62. doi: 10.1007/s10126-021-10081-0

33. Xu H, Cao L, Sun B, Wei Y, Liang M. Transcriptomic analysis of potential "lncRNA-mRNA" interactions in liver of the marine teleost cynoglossus semilaevis fed diets with different DHA/EPA ratios. *Front Physiol* (2019) 10:331. doi: 10.3389/fphys.2019.00331

34. Wang J, Fu L, Koganti PP, Wang L, Hand JM, Ma H, et al. Identification and functional prediction of Large intergenic noncoding RNAs (lincRNAs) in rainbow trout (Oncorhynchus mykiss). *Mar Biotechnol (NY)* (2016) 18:271–82. doi: 10.1007/s10126-016-9689-5

35. He Z, Ye L, Yang D, Ma Z, Deng F, He Z, et al. Identification, characterization and functional analysis of gonadal long noncoding RNAs in a protogynous hermaphroditic teleost fish, the ricefield eel (Monopterus albus). *BMC Genomics* (2022) 23:450. doi: 10.1186/s12864-022-08679-2

36. Song F, Wang L, Zhu W, Dong Z. Long noncoding RNA and mRNA expression profiles following igf3 knockdown in common carp, cyprinus carpio. *Sci Data* (2019) 6:190024. doi: 10.1038/sdata.2019.24

37. Castro-Arnau J, Chauvigne F, Gomez-Garrido J, Esteve-Codina A, Dabad M, Alioto T, et al. Developmental RNA-seq transcriptomics of haploid germ cells and spermatozoa uncovers novel pathways associated with teleost spermiogenesis. *Sci Rep* (2022) 12:14162. doi: 10.1038/s41598-022-18422-2

38. Basu S, Hadzhiev Y, Petrosino G, Nepal C, Gehrig J, Armant O, et al. The tetraodon nigroviridis reference transcriptome: Developmental transition, length retention and microsynteny of long non-coding RNAs in a compact vertebrate genome. *Sci Rep* (2016) 6:33210. doi: 10.1038/srep33210

39. Dettleff P, Hormazabal E, Aedo J, Fuentes M, Meneses C, Molina A, et al. Identification and evaluation of long noncoding RNAs in response to handling stress in red cusk-eel (Genypterus chilensis) *via* RNA-seq. *Mar Biotechnol (NY)* (2020) 22:94–108. doi: 10.1007/s10126-019-09934-6

40. Wang M, Jiang S, Wu W, Yu F, Chang WG, Li PF, et al. Non-coding RNAs function as immune regulators in teleost fish. *Front Immunol* (2018) 9:2801. doi: 10.3389/fimmu.2018.02801

41. Sun Q, Wang J, Wang G, Wang H, Liu H. Integrated analysis of lncRNA and mRNA in liver of megalobrama amblycephala post aeromonas hydrophila infection. *BMC Genomics* (2021) 22:653. doi: 10.1186/s12864-021-07969-5

42. Yang N, Wang B, Yu Z, Liu X, Fu Q, Cao M, et al. Characterization of a novel lncRNA (SETD3-OT) in turbot (Scophthalmus maximus l.). *Fish Shellfish Immunol* (2020) 102:145–51. doi: 10.1016/j.fsi.2020.04.010

43. Liu S, Yu T, Zhang Y, Pan C, Cai L, Yang M. Integrated analysis of mRNA and long non-coding RNA expression profiles reveals the potential roles of lncRNA-mRNA network in carp macrophage immune regulation. *In Vitro Cell Dev Biol Anim* (2021) 57:835–47. doi: 10.1007/s11626-021-00610-5

44. Valenzuela-Munoz V, Pereiro P, Alvarez-Rodriguez M, Gallardo-Escarate C, Figueras A, Novoa B. Comparative modulation of lncRNAs in wild-type and rag1-heterozygous mutant zebrafish exposed to immune challenge with spring viraemia of carp virus (SVCV). *Sci Rep* (2019) 9:14174. doi: 10.1038/s41598-019-50766-0

45. Pereiro P, Lama R, Moreira R, Valenzuela-Munoz V, Gallardo-Escarate C, Novoa B, et al. Potential involvement of lncRNAs in the modulation of the transcriptome response to nodavirus challenge in European Sea bass (Dicentrarchus labrax l.). *Biol (Basel)* (2020) 9:165. doi: 10.3390/biology9070165

46. Lee KT, Nam JW. Post-transcriptional and translational regulation of mRNA-like long non-coding RNAs by microRNAs in early developmental stages of zebrafish embryos. *BMB Rep* (2017) 50:226–31. doi: 10.5483/BMBRep.2017.50.4.025

47. Xiu Y, Li Y, Liu X, Li C. Full-length transcriptome sequencing from multiple immune-related tissues of paralichthys olivaceus. *Fish Shellfish Immunol* (2020) 106:930–7. doi: 10.1016/j.fsi.2020.09.013

48. Kern C, Wang Y, Chitwood J, Korf I, Delany M, Cheng H, et al. Genome-wide identification of tissue-specific long non-coding RNA in three farm animal species. *BMC Genomics* (2018) 19:684. doi: 10.1186/s12864-018-5037-7

49. Garcia-Perez I, Molsosa-Solanas A, Perello-Amoros M, Sarropoulou E, Blasco J, Gutierrez J, et al. The emerging role of long non-coding RNAs in development and function of gilthead Sea bream (Sparus aurata) fast skeletal muscle. *Cells* (2022) 11:428. doi: 10.3390/cells11030428

50. Chen Y, Wan S, Li Q, Dong X, Diao J, Liao Q, et al. Genome-wide integrated analysis revealed functions of lncRNA-miRNA-mRNA interaction in growth of intermuscular bones in megalobrama amblycephala. *Front Cell Dev Biol* (2020) 8:603815. doi: 10.3389/fcell.2020.603815

51. Papadaki M, Kaitetzidou E, Mylonas CC, Sarropoulou E. Non-coding RNA expression patterns of two different teleost gonad maturation stages. *Mar Biotechnol (NY)* (2020) 22:683–95. doi: 10.1007/s10126-020-09991-2

52. Cheng J, Yang F, Liu S, Zhao H, Lu W, Zhang Q. Transcriptomic analysis reveals functional interaction of mRNA-lncRNA-miRNA in steroidogenesis and spermatogenesis of gynogenetic Japanese flounder (Paralichthys olivaceus). *Biol (Basel)* (2022) 11:213. doi: 10.3390/biology11020213

53. Baumann L, Holbech H, Keiter S, Kinnberg KL, Knorr S, Nagel T, et al. The maturity index as a tool to facilitate the interpretation of changes in vitellogenin production and sex ratio in the fish sexual development test. *Aquat Toxicol* (2013) 128:34–42. doi: 10.1016/j.aquatox.2012.11.016

54. Tang Y, Xin G, Zhao L, Huang L, Qin Y, Su Y, et al. Novel insights into host-pathogen interactions of large yellow croakers (Larimichthys crocea) and pathogenic bacterium pseudomonas plecoglossicida using time-resolved dual RNA-seq of infected spleens. *Zoological Res* (2020) 41:314–327. doi: 10.24272/j.issn.2095-8137.2020.035.

55. Yuan B, Zhao L, Zhuang Z, Wang X, Fu Q, Huang H, et al. Transcriptomic and metabolomic insights into the role of the flgK gene in the pathogenicity of pseudomonas plecoglossicida to orange-spotted grouper (Epinephelus coioides). *Zoological Res* (2022) 43:952–65. doi: 10.24272/j.issn.2095-8137.2022.216

56. Watanabe M, Abe N, Oshikiri Y, Stanbridge EJ, Kitagawa T. Selective growth inhibition by glycogen synthase kinase-3 inhibitors in tumorigenic HeLa hybrid cells is mediated through NF-kappaB-dependent GLUT3 expression. *Oncogenesis* (2012) 1:e21. doi: 10.1038/oncsis.2012.21

57. Zhang Y, Cui C, Lai ZC. The defender against apoptotic cell death 1 gene is required for tissue growth and efficient n-glycosylation in drosophila melanogaster. *Dev Biol* (2016) 420:186–95. doi: 10.1016/j.ydbio.2016.09.021

58. Zheng W, Chang R, Luo Q, Liu G, Xu T. The long noncoding RNA MIR122HG is a precursor for miR-122-5p and negatively regulates the TAK1-induced innate immune response in teleost fish. *J Biol Chem* (2022) 298:101773. doi: 10.1016/j.jbc.2022.101773

59. Sarangdhar MA, Chaubey D, Srikakulam N, Pillai B. Parentally inherited long non-coding RNA cyrano is involved in zebrafish neurodevelopment. *Nucleic Acids Res* (2018) 46:9726–35. doi: 10.1093/nar/gky628

60. Gomez-Nicola D, Pallas-Bazarra N, Valle-Argos B, Nieto-Sampedro M. CCR7 is expressed in astrocytes and upregulated after an inflammatory injury. *J Neuroimmunol* (2010) 227:87–92. doi: 10.1016/j.jneuroim.2010.06.018

61. Wang P, Zhao Z, Zhang Z, Cai Z, Liao J, Tan Q, et al. Genome-wide identification and analysis of NPR family genes in brassica juncea var. tumida. *Gene* (2021) 769:145210. doi: 10.1016/j.gene.2020.145210

62. Wu S, Zhang J, Liu B, Huang Y, Li S, Wen H, et al. Identification and characterization of lncRNAs related to the muscle growth and development of Japanese flounder (Paralichthys olivaceus). *Front Genet* (2020) 11:1034. doi: 10.3389/fgene.2020.01034

63. Tang R, Luo G, Zhao L, Huang L, Qin Y, Xu X, et al. The effect of a LysR-type transcriptional regulator gene of pseudomonas plecoglossicida on the immune responses of epinephelus coioides. *Fish Shellfish Immunol* (2019) 89:420–7. doi: 10.1016/j.fsi.2019.03.051

64. Luo G, Zhao L, Xu X, Qin Y, Huang L, Su Y, et al. Integrated dual RNA-seq and dual iTRAQ of infected tissue reveals the functions of a diguanylate cyclase gene of pseudomonas plecoglossicida in host-pathogen interactions with epinephelus coioides. *Fish Shellfish Immunol* (2019) 95:481–90. doi: 10.1016/j.fsi.2019.11.008

65. Shen Y, Liang W, Lin Y, Yang H, Chen X, Feng P, et al. Single molecule real-time sequencing and RNA-seq unravel the role of long non-coding and circular RNA in the regulatory network during Nile tilapia (Oreochromis niloticus) infection with streptococcus agalactiae. *Fish Shellfish Immunol* (2020) 104:640–53. doi: 10.1016/j.fsi.2020.06.015

66. Li L, Jia X, Liu Y, He Y, Pang Y, Shen Y, et al. lncRNA-SUMO3 and lncRNA-HDMO13 modulate the inflammatory response by binding miR-21 and miR-142a-3p in grass carp. *Dev Comp Immunol* (2021) 121:104082. doi: 10.1016/j.dci.2021.104082

67. Ramos E, Cardoso AL, Brown J, Marques DF, Fantinatti BE, Cabral-de-Mello DC, et al. The repetitive DNA element BncDNA, enriched in the b chromosome of the cichlid fish astatotilapia latifasciata, transcribes a potentially noncoding RNA. *Chromosoma* (2017) 126:313–23. doi: 10.1007/s00412-016-0601-x

68. He Y, Huang CX, Chen N, Wu M, Huang Y, Liu H, et al. The zebrafish miR-125c is induced under hypoxic stress *via* hypoxia-inducible factor 1 alpha and functions in cellular adaptations and embryogenesis. *Oncotarget* (2017) 8:73846–59. doi: 10.18632/oncotarget.17994

69. Zhang Z, Lau SW, Zhang L, Ge W. Disruption of zebrafish follicle-stimulating hormone receptor (fshr) but not luteinizing hormone receptor (lhcgr) gene by TALEN leads to failed follicle activation in females followed by sexual reversal to males. *Endocrinology* (2015) 156:3747–62. doi: 10.1210/en.2015-1039

70. Fan K, Shen Y, Xu X, Tao L, Bao T, Li J. LncRNA-WAS and lncRNA-C8807 interact with miR-142a-3p to regulate the inflammatory response in grass carp. *Fish Shellfish Immunol* (2021) 111:201–7. doi: 10.1016/j.fsi.2021.02.003

71. Wu J, Zhang L, Feng Y, Khadka B, Fang Z, Liu J. HDAC8 promotes daunorubicin resistance of human acute myeloid leukemia cells *via* regulation of IL-6 and IL-8. *Biol Chem* (2021) 402:461–8. doi: 10.1515/hsz-2020-0196

72. Xia YQ, Cheng JX, Liu YF, Li CH, Liu Y, Liu PF. Genome-wide integrated analysis reveals functions of lncRNA-miRNA-mRNA interactions in Atlantic salmon challenged by aeromonas salmonicida. *Genomics* (2022) 114:328–39. doi: 10.1016/j.ygeno.2021.12.013

73. Gao C, Cai X, Ma L, Li C. Identification of mRNA-miRNA-lncRNA regulatory network associated with the immune response to aeromonas salmonicides infection in the black rockfish (Sebastes schlegelii). *Dev Comp Immunol* (2022) 130:104357. doi: 10.1016/j.dci.2022.104357

74. Chu Q, Xu T, Zheng W, Chang R, Zhang L. Long noncoding RNA MARL regulates antiviral responses through suppression miR-122-dependent MAVS downregulation in lower vertebrates. *PloS Pathog* (2020) 16:e1008670. doi: 10.1371/journal.ppat.1008670

75. Samsing F, Wynne JW, Valenzuela-Munoz V, Valenzuela-Miranda D, Gallardo-Escarate C, Alexandre PA. Competing endogenous RNA-networks reveal key regulatory microRNAs involved in the response of Atlantic salmon to a novel orthomyxovirus. *Dev Comp Immunol* (2022) 132:104396. doi: 10.1016/j.dci.2022.104396

76. Avery JC, Hoffmann PR. Selenium, selenoproteins, and immunity. *Nutrients* (2018) 10:1203. doi: 10.3390/nu10091203

77. Zhou CQ, Ka W, Yuan WK, Wang JL. The effect of acute heat stress on the innate immune function of rainbow trout based on the transcriptome. *J Therm Biol* (2021) 96:102834. doi: 10.1016/j.jtherbio.2021.102834

78. Wu S, Huang J, Li Y, Liu Z, Zhao L. Integrated analysis of lncRNA and circRNA mediated ceRNA regulatory networks in skin reveals innate immunity differences between wild-type and yellow mutant rainbow trout (Oncorhynchus mykiss). *Front Immunol* (2022) 13:802731. doi: 10.3389/fimmu.2022.802731

79. Arun G, Diermeier SD, Spector DL. Therapeutic targeting of long non-coding RNAs in cancer. *Trends Mol Med* (2018) 24:257–77. doi: 10.1016/j.molmed.2018.01.001

80. Ye W, Duan Y, Zhang W, Cheng Y, Shi M, Xia XQ. Comprehensive analysis of hub mRNA, lncRNA and miRNA, and associated ceRNA networks implicated in grass carp (Ctenopharyngodon idella) growth traits. *Genomics* (2021) 113:4004–14. doi: 10.1016/j.ygeno.2021.10.001

81. Leiva F, Rojas-Herrera M, Reyes D, Bravo S, Garcia KK, Moya J, et al. Identification and characterization of miRNAs and lncRNAs of coho salmon (Oncorhynchus kisutch) in normal immune organs. *Genomics* (2020) 112:45–54. doi: 10.1016/j.ygeno.2019.07.015

82. Ali A, Al-Tobasei R, Kenney B, Leeds TD, Salem M. Integrated analysis of lncRNA and mRNA expression in rainbow trout families showing variation in muscle growth and fillet quality traits. *Sci Rep* (2018) 8:12111. doi: 10.1038/s41598-018-30655-8

83. Danos N, Ward AB. The homology and origins of intermuscular bones in fishes: phylogenetic or biomechanical determinants? *Biol J Linn Soc* (2012) 106:607–22. doi: 10.1111/j.1095-8312.2012.01893.x

84. Kocher TD. Adaptive evolution and explosive speciation: The cichlid fish model. *Nat Rev Genet* (2004) 5:288–98. doi: 10.1038/nrg1316

85. Ferre LE, Medesani DA, Garcia CF, Grodzielski M, Rodriguez EM. Vitellogenin levels in hemolymph, ovary and hepatopancreas of the freshwater crayfish cherax quadricarinatus (Decapoda: Parastacidae) during the reproductive cycle. *Rev Biol Trop* (2012) 60:253–61. doi: 10.15517/rbt.v60i1.2759

86. Mang Q, Hou J, Han T, Wang G, Wang Y, Liu Y, et al. The effect of infertility on the liver structure, endocrinology, and gene network in Japanese flounder. *Anim (Basel)* (2021) 11:936. doi: 10.3390/ani11040936

87. Pang Y, Li L, Yang Y, Shen Y, Xu X, Li J. LncRNA-ANAPC2 and lncRNA-NEFM positively regulates the inflammatory response *via* the miR-451/npr2/ hdac8 axis in grass carp. *Fish Shellfish Immunol* (2022) 128:1–6. doi: 10.1016/j.fsi.2022.07.014

88. Zhao D, Deng SC, Ma Y, Hao YH, Jia ZH. miR-221 alleviates the inflammatory response and cell apoptosis of neuronal cell through targeting TNFAIP2 in spinal cord ischemia-reperfusion. *Neuroreport* (2018) 29:655–60. doi: 10.1097/WNR.0000000000001013

89. Xiu Y, Li Y, Liu X, Su L, Zhou S, Li C. Identification and characterization of long non-coding RNAs in the intestine of olive flounder (Paralichthys olivaceus) during edwardsiella tarda infection. *Front Immunol* (2021) 12:623764. doi: 10.3389/fimmu.2021.623764

90. Yan Q, Si J, Cui X, Peng H, Jing M, Chen X, et al. GmDAD1, a conserved defender against cell death 1 (DAD1) from soybean, positively regulates plant resistance against phytophthora pathogens. *Front Plant Sci* (2019) 10:107. doi: 10.3389/fpls.2019.00107

91. Zhang B, Luo G, Zhao L, Huang L, Qin Y, Su Y, et al. Integration of RNAi and RNA-seq uncovers the immune responses of epinephelus coioides to L321_RS19110 gene of pseudomonas plecoglossicida. *Fish Shellfish Immunol* (2018) 81:121–9. doi: 10.1016/j.fsi.2018.06.051

92. Sun Y, Luo G, Zhao L, Huang L, Qin Y, Su Y, et al. Integration of RNAi and RNA-seq reveals the immune responses of epinephelus coioides to sigX gene of pseudomonas plecoglossicida. *Front Immunol* (2018) 9:1624. doi: 10.3389/fimmu.2018.01624

93. Ning X, Sun L. Identification and characterization of immune-related lncRNAs and lncRNA-miRNA-mRNA networks of paralichthys olivaceus involved in vibrio anguillarum infection. *BMC Genomics* (2021) 22:447. doi: 10.1186/s12864-021-07780-2

94. Zheng W, Chu Q, Xu T. Long noncoding RNA IRL regulates NF-kappaB-mediated immune responses through suppression of miR-27c-3p-dependent IRAK4 downregulation in teleost fish. *J Biol Chem* (2021) 296:100304. doi: 10.1016/j.jbc.2021.100304

95. Chu Q, Xu T, Zheng W, Chang R, Zhang L. Long noncoding RNA AANCR modulates innate antiviral responses by blocking miR-210-dependent MITA downregulation in teleost fish, miichthys miiuy. *Sci China Life Sci* (2021) 64:1131–48. doi: 10.1007/s11427-020-1789-5

96. Zheng W, Chu Q, Xu T. The long noncoding RNA NARL regulates immune responses *via* microRNA-mediated NOD1 downregulation in teleost fish. *J Biol Chem* (2021) 296:100414. doi: 10.1016/j.jbc.2021.100414

97. Chang R, Zheng W, Sun Y, Geng S, Xu T. Long noncoding RNA MIR2187HG suppresses TBK1-mediated antiviral signaling by deriving miR-2187-3p in teleost fish. *J Virol* (2022) 96:e0148421. doi: 10.1128/JVI.01484-21

98. Li BJ, Jiang DL, Meng ZN, Zhang Y, Zhu ZX, Lin HR, et al. Genome-wide identification and differentially expression analysis of lncRNAs in tilapia. *BMC Genomics* (2018) 19:729. doi: 10.1186/s12864-018-5115-x

99. Corsini LR, Bronte G, Terrasi M, Amodeo V, Fanale D, Fiorentino E, et al. The role of microRNAs in cancer: diagnostic and prognostic biomarkers and targets of therapies. *Expert Opin Ther Targets* (2012) 16 Suppl 2:S103–109. doi: 10.1517/14728222.2011.650632

100. Singh D, Khan MA, Siddique HR. Emerging role of long non-coding RNAs in cancer chemoresistance: Unravelling the multifaceted role and prospective therapeutic targeting. *Mol Biol Rep* (2020) 47:5569–85. doi: 10.1007/s11033-020-05609-x

101. Shalaby KE, Aouida M, Gupta V, Abdesselem H, El-Agnaf OMA. Development of non-viral vectors for neuronal-targeted delivery of CRISPR-Cas9 RNA-proteins as a therapeutic strategy for neurological disorders. *Biomater Sci* (2022) 10:4959–77. doi: 10.1039/D2BM00368F

102. Bhan A, Soleimani M, Mandal SS. Long noncoding RNA and cancer: A new paradigm. *Cancer Res* (2017) 77:3965–81. doi: 10.1158/0008-5472.CAN-16-2634

103. Yan Y, Liu XY, Lu A, Wang XY, Jiang LX, Wang JC. Non-viral vectors for RNA delivery. *J Control Release* (2022) 342:241–79. doi: 10.1016/j.jconrel.2022.01.008

104. Nunez-Acuna G, Detree C, Gallardo-Escarate C, Goncalves AT. Functional diets modulate lncRNA-coding RNAs and gene interactions in the intestine of rainbow trout oncorhynchus mykiss. *Mar Biotechnol (NY)* (2017) 19:287–300. doi: 10.1007/s10126-017-9750-z

105. Cui Y, Wan H, Zhang X. miRNA in food simultaneously controls animal viral disease and human tumorigenesis. *Mol Ther Nucleic Acids* (2021) 23:995–1006. doi: 10.1016/j.omtn.2021.01.011

106. Chen Y, Zhang S, Cao J, Zhang X. Shrimp antiviral mja-miR-35 targets CHI3L1 in human M2 macrophages and suppresses breast cancer metastasis. *Front Immunol* (2018) 9:2071. doi: 10.3389/fimmu.2018.02071

107. Chen Q, Zhang F, Dong L, Wu H, Xu J, Li H, et al. SIDT1-dependent absorption in the stomach mediates host uptake of dietary and orally administered microRNAs. *Cell Res* (2021) 31:247–58. doi: 10.1038/s41422-020-0389-3

108. Yang L, Xu Z, Zeng H, Sun N, Wu B, Wang C, et al. FishDB: an integrated functional genomics database for fishes. *BMC Genomics* (2020) 21:801. doi: 10.1186/s12864-020-07159-9

109. Yan HW, Liu Q, Jiang JM, Shen XF, Zhang L, Yuan Z, et al. Identification of sex differentiation-related microRNA and long non-coding RNA in takifugu rubripes gonads. *Sci Rep-Uk* (2021) 11:7459. doi: 10.1038/s41598-021-83891-w

110. Salisbury JP, Sirbulescu RF, Moran BM, Auclair JR, Zupanc GK, Agar JN. The central nervous system transcriptome of the weakly electric brown ghost knifefish (Apteronotus leptorhynchus): de novo assembly, annotation, and proteomics validation. *BMC Genomics* (2015) 16:166. doi: 10.1186/s12864-015-1354-2

111. Morris KV, Mattick JS. The rise of regulatory RNA. *Nat Rev Genet* (2014) 15:423–37. doi: 10.1038/nrg3722

112. Liu W, Liu X, Wu C, Jiang L. Transcriptome analysis demonstrates that long noncoding RNA is involved in the hypoxic response in larimichthys crocea. *Fish Physiol Biochem* (2018) 44:1333–47. doi: 10.1007/s10695-018-0525-x

113. An HJ, Lee YJ, Choe CP, Cho HK, Song DH. Long noncoding RNAs associated with nonalcoholic fatty liver disease in a high cholesterol diet adult zebrafish model. *Sci Rep* (2021) 11:23005. doi: 10.1038/s41598-021-02455-0

frontiers | Frontiers in Immunology

TYPE Original Research
PUBLISHED 01 March 2023
DOI 10.3389/fimmu.2023.1142488

OPEN ACCESS

EDITED BY
Jun Li,
Lake Superior State University,
United States

REVIEWED BY
Jianguo Su,
Huazhong Agricultural University, China
Xue-Peng Li,
Yantai University, China

*CORRESPONDENCE
Shuai Jiang
sjiang@qdio.ac.cn
Li Sun
lsun@qdio.ac.cn

SPECIALTY SECTION
This article was submitted to Molecular Innate Immunity, a section of the journal Frontiers in Immunology

RECEIVED 11 January 2023
ACCEPTED 15 February 2023
PUBLISHED 01 March 2023

CITATION
Li X, Jiang S and Sun L (2023) Tongue sole creatine kinases function as DAMP and activate antimicrobial immunity *via* TLR2. *Front. Immunol.* 14:1142488. doi: 10.3389/fimmu.2023.1142488

Tongue sole creatine kinases function as DAMP and activate antimicrobial immunity *via* TLR2

Xin Li[1,2,3], Shuai Jiang[1,2,3]* and Li Sun[1,2,3]*

[1]CAS and Shandong Province Key Laboratory of Experimental Marine Biology, Institute of Oceanology, CAS Center for Ocean Mega-Science, Chinese Academy of Sciences, Qingdao, China, [2]Laboratory for Marine Biology and Biotechnology, Pilot National Laboratory for Marine Science and Technology, Qingdao, China, [3]College of Earth and Planetary Sciences, University of Chinese Academy of Sciences, Beijing, China

Creatine kinase (CK) is an enzyme that regulates adenosine triphosphate (ATP) metabolism to maintain energy homeostasis. Although CK has been reported to be involved in pathogen infection, the immune function of CK remains elusive. In this study, we identified two muscle-type CK from the teleost tongue sole *Cynoglossus semilaevis* (designated CsCKM-1 and CsCKM-2). Bacterial infection modulated CsCKM-1/2 expression in tongue sole tissues and induced the release of CsCKM-1/2 into serum. Recombinant CsCKM-1/2 (rCsCKM-1/2) exhibited robust kinase activity and bound to bacterial pathogens and pathogen-associated molecular patterns. rCsCKM-1/2 also bound to tongue sole peripheral blood leukocytes (PBLs) and promoted PBLs to uptake bacterial pathogens, inhibit bacterial proliferation, and express proinflammatory cytokines. When co-expressed in HEK293T cells, CsCKM-1/2 were found to interact with the leucine rich domain of toll-like receptor 2 (TLR2). The presence of TLR2 antagonist significantly reduced CsCKM-1/2-induced immune response and antibacterial effect. Taken together, these results indicated that tongue sole creatine kinases function as damage-associated molecular pattern (DAMP) molecules and play an important role in antimicrobial immunity *via* TLR2.

KEYWORDS

creatine kinase, tongue sole, teleost, toll-like receptor 2, antimicrobial immunity

1 Introduction

Creatine kinase (CK) is a class of proteins belonging to the phosphagen kinase family (1). CK exists widely in animals, ranging from sponge, fish to human (2). In vertebrates, there are four types of CK, including two cytosolic isoenzymes, i.e., M-CK (muscle type) and B-CK (brain type), and two mitochondrial isoenzymes, i.e., Mi_u-CK (ubiquitous type) and Mi_s-CK (sarcomeric type) (2). The cytosolic type CKs function as homodimer (MM-CK and BB-CK) or heterodimer (MB-CK), while the mitochondrial CKs function as octamer. The CK monomers share similar structure, which is composed of a small N-terminal domain constituted solely by α-helix and a large C-terminal domain comprising

an antiparallel β-sheet core and several external α-helices. The two domains form a cleft in their interface and therein accommodate the active site (2–6). CK catalyzes the reversible conversion of phosphocreatine and adenosine diphosphate (ADP) to creatine and adenosine triphosphate (ATP) (4). CK and its substrates/products constitute an energy buffer system enabling replenishment of ATP, the primary fuel of biological activities. Thus, CK plays a vital role in the physiological processes requiring high energy turnover, such as skeletal muscle contraction (2–6).

In human and mouse, accumulating reports indicate that CK is also involved in immunity. For instance, B-CK could modulate thymocyte differentiation and T cell activation (7). The abrogation of B-CK impaired TCR-mediated activation of mTORC1 signaling and compromised $CD8^+$ T cell expansion in response to infection (8). The blockade of CK pathway impaired the expression of GSK3-targeted genes and the upstream genes of Wnt signaling (9). B-CK could interact with the NS4A protein of hepatitis C virus (HCV) and affect viral replication (10). Moreover, CK can be released into the extracellular milieu during physiological stress (11–13). In clinical diagnostics, the CK level in body fluid has been widely employed as a biomarker for many pathological conditions, such as exertional muscle damage (14), acute pulmonary tuberculosis (15), acute myocardial infarction (16) and bacterial infection (17, 18).

In teleost, evidence shows that CK is involved in anti-bacterial immunity. For example, in zebrafish *Danio rerio*, the protein level of CK in gill was elevated during *Aeromonas hydrophila* infection (19). In juvenile Nile tilapia *Oreochromis niloticus*, the activities of branchial cytosolic CK and mitochondrial CK decreased upon *Providencia rettgeri* infection (20). In silver catfish *Rhamdia quelen*, the activities of cytosolic and mitochondrial CK were regulated by *Aeromonas caviae* and *Citrobacter freundii* infection (21, 22). In addition, it has been observed that the extracellular level of teleost CK changed upon bacterial infection (23). However, the immunological function and mechanism of CK in teleost remain largely unknown.

Half-smooth tongue sole (*Cynoglossus semilaevis*) is an economically valuable marine flatfish (24). In the present work, we identified and characterized two M-CK homologues from *C. semilaevis* (named CsCKM-1 and CsCKM-2). The immune function and the molecular mechanism of CsCKM-1/2 in antimicrobial immunity were examined. We found that bacterial infection induced extracellular release of CsCKM-1/2, and recombinant CsCKM-1/2 stimulated the activity of peripheral blood leukocytes (PBLs) and exerted antimicrobial effects in a manner that required Toll-like receptor 2 (TLR2). Our results revealed novel immune functions of CK in teleost.

2 Materials and methods

2.1 Fish, bacteria, and cells

Tongue sole were purchased from a local fish farm in Shandong Province. The fish were reared at 20°C in tanks filled with aerated seawater, fed daily with commercial feed and confirmed to be clinically healthy as described previously (25, 26). Fish with average weight of 500g were used to collect peripheral blood leukocytes (PBLs). Fish with average weight of 20g were used in the bacterial infection experiment. The fish were euthanized with tricaine methane sulfonate (Sigma, St. Louis, USA) at the dose of 0.1 g/l before tissue collection. The bacterial pathogens *Edwardsiella tarda*, *Vibrio anguillarum, Vibrio harveyi* and *Streptococcus iniae* have been reported previously (27–30) *V. anguillarum, V. harveyi* and *E. tarda* were cultured in Luria-Bertani broth (LB) at 28°C to an OD_{600} of 0.8, *S. iniae* was cultured in tryptic soy broth (TSB) at 28°C to an OD_{600} of 0.8. HEK293T cells were cultured in Dulbecco's modified Eagle's medium as reported previously (31). Tongue sole peripheral blood leukocytes (PBLs) were prepared by Percoll gradient centrifugation as described previously (32). Briefly, the blood was placed on top of 61% Percoll and centrifuged at 400 g for 15 min. The white layer of PBLs in the interface was collected, washed twice with PBS and resuspended in L-15 medium.

2.2 Sequence and phylogenetic analysis

The sequence analysis was performed with Clustal W Multiple Alignment program (33). The phylogenetic tree was constructed using the Maximum likelihood method of MEGA-X with 1500 bootstrap replications, and edited with iTOL (34). The sequences of creatine kinase isoforms were obtained from National Center for Biotechnology Information (NCBI). The GenBank accession numbers are as follows: *Homo sapiens* M-CK, NP_001815. 2; *H. sapiens* B-CK isoform 1, NP_001814.2; *H. sapiens* B-CK isoform 2, NP_001349460.1; *H. sapiens* Mi_s-CK, NP_001093205.1; *H. sapiens* Mi_u-CK, NP_001015001.1; *Oryzias latipes* M-CK, XP_004076079.1; *O. latipes* B-CK, XP_023808469.1; *O. latipes* Mi_u-CK, XP_004069454.3; *O. latipes* Mi_s-CK, XP_023816157.1; *Mus musculus* M-CK, NP_031736.1; *M. musculus* B-CK, NP_067248.1; *M. musculus* Mi_s-CK, NP_940807.1; *M. musculus* Mi_u-CK, NP_001341998.1; *Danio rerio* M-CK b, NP_001099153.1; *D. rerio* M-CK a, NP_571007.2; *D. rerio* B-CK a, NP_001070631.1; *D. rerio* B-CK b, NP_775329.1; *D. rerio* Mi_s-CK, NP_956991.1; *Cynoglossus semilaevis* M-CK-1, XP_008307091.1; *C. semilaevis* M-CK-2, XP_008330730.1.

2.3 Expression of CsCKM-1/2 in tongue sole tissues and cells

Expressions of CsCKM-1/2 in tissues under different conditions were determined by quantitative real time reverse transcription-PCR (qRT-PCR). Heart, liver, spleen, head kidney, brain, gill, intestine, skin, and muscle were taken aseptically from three tongue sole for total RNA extraction with Trizol reagent. cDNA synthesis and qRT-PCR were performed as described previously (35) The expression levels of CsCKM-1/2 were analyzed using comparative threshold cycle method ($2^{-\Delta\Delta CT}$). To examine the expression of CsCKM-1/2 in response to infection, tongue sole were randomly divided into three groups and injected intraperitoneally with 50 μl *V. anguillarum* (1×10^8 CFU/ml), *E. tarda* (2×10^8 CFU/ml) or PBS. Three fish were taken at 6, 12, 24 or

48 h post-infection (hpi), and CsCKM-1/2 expressions in liver, spleen and head kidney were determined as above. To examine CsCKM-1/2 expression in PBLs in response to bacterial infection, tongue sole PBLs were incubated with *V. anguillarum* or *E. tarda* (multiplicity of infection (MOI) = 4) for 2, 4, or 6 h, and the expression levels of CsCKM-1/2 were determined by qRT-PCR as above. β-actin was used as an internal reference as reported previously (36). The primers used for PCR are listed in Table S1.

2.4 Recombinant protein purification, polyclonal antibody preparation, and creatine kinase activity assay

The coding sequences of CsCKM-1/2 were amplified by PCR with primers listed in Table S1. The pET30a (+) vector (Novagen, Madison, WI, USA) was digested with the restriction endonucleases NdeI and XhoI. The PCR products were ligated with the linearized vector. The recombinant pET30a (+) vectors expressing CsCKM-1/2 were introduced into *Escherichia coli* Transetta (DE3) (TransGen, Beijing, China) by transformation. The transformants were cultured in LB medium at 37°C to mid-logarithmic phase, and isopropyl-β-D-thiogalactopyranoside was added to the medium to a final concentration of 0.1 mM. After an additional 12 h incubation at 16°C, the bacteria were harvested by centrifugation and lysed on ice by ultrasonication. The recombinant CsCKM-1/2 (rCsCKM-1/2) in the supernatant were purified with Ni-NTA agarose (QIAGEN, Valencia, USA). Triton X-114 was added to the washing buffer to remove endotoxin. The endotoxin levels of the recombinant proteins were determined using Toxin SensorTM Endotoxin Detection System (GenScript). The endotoxin concentrations of rCsCKM-1&2 were 0.24 and 0.17 EU/mg, respectively. The eluted proteins were dialyzed and concentrated as described previously (30). The proteins were analyzed by SDS-PAGE and stained with Coomassie brilliant blue R-250. Mouse anti-rCsCKM-1/2 antiserum was prepared as reported previously (37). Recombinant Trx was prepared as described previously (38). The enzyme activity of recombinant CKs was measured as reported previously (6). Briefly, substrate chromogenic solution was prepared as follows: creatine (25mM), $MgAC_2{\cdot}4H_2O$ (5mM), thymol blue (0.01%), Gly-NaOH (pH 9.0, 5mM), and $ATP{\cdot}Na_2$ (5mM). NaOH (1 mol/L) was used to carefully adjust the color of the solution to dark purple (pH 8.5). rCsCKM-1/2 was then added to the chromogenic solution and the absorption at 597nm was recorded every 30s.

2.5 The *in vivo* and *in vitro* detection of CsCKM-1/2 release

To examine the release of CsCKM-1/2 into serum, tongue sole (average 20 g) were randomly divided into three groups and injected intraperitoneally with 50 μl *V. anguillarum* (1×10^8 CFU/ml), *E. tarda* (2×10^8 CFU/ml) or PBS. Blood was collected at 6, 12 and 24 hpi (three fish per group at each time point), and the serum was separated by centrifugation at 2000 g, 4°C for 15 minutes. The serum was subjected to SDS-PAGE, and the proteins were transferred onto nitrocellulose membranes (Millipore, MA, USA). The membrane was blocked with 5% BSA for 1 h, and mouse anti-rCsCKM-1/2 antiserum (1:1000 dilution) were added. After incubation for 1 h, the membranes were washed with PBS for three times. The membranes were further incubated with HRP goat anti-mouse IgG (1:4000 dilution) for 1h, and then washed as above. The protein bands were visualized using an ECL kit (Sparkjade Biotechnology Co. Ltd., Shandong, China). To examine the release of CsCKM-1/2 to culture medium, PBLs (1×10^7 cells/ml) were incubated with *V. anguillarum* (2×10^7 CFU/ml), *E. tarda* (1×10^7 CFU/ml), or PBS for 1 h. The supernatants were collected and precipitated using TCA as reported previously (31). The proteins released by PBLs were detected by immunoblotting as above.

2.6 Interaction of rCsCKM-1/2 with bacteria

The binding between bacteria and rCsCKM-1/2 was determined by enzyme-linked immunosorbent assay (ELISA) as reported previously (39). The binding of rCsCKM-1/2 to pathogen-associated molecular patterns (PAMPs), including lipopolysaccharides, peptidoglycan, glucan and mannan, was examined as follows. PAMPs (0.1 mg/ml) were diluted in coating buffer (15 mM Na_2CO_3 and 35 mM $NaHCO_3$, pH 9.6) and placed into 96-well microtiter ELISA plates. The plates were incubated at 4°C overnight. After blocking with 5% skim milk at 37°C for 1 h, the plates were washed with PBS for three times. The plates were incubated with different concentrations (1, 5, or 10 μM) of rCsCKM-1/2, followed by incubating with mouse anti-His tag antibody and HRP-conjugated goat anti-mouse IgG as described above. To examine the effect of rCsCKM-1/2 on bacterial growth, rCsCKM-1/2 (85 μg/ml), rTrx (85 μg/ml) or PBS was mixed with bacteria (1×10^5 CFU/ml) in LB medium. The bacteria were incubated at 22°C, and bacterial growth was recorded every hour by measuring absorbance at OD_{600}.

2.7 The interaction of rCsCKM-1/2 with PBLs

The interaction between rCsCKM-1/2 and PBLs were performed as reported previously (35). Briefly, 1×10^6 cells in 100 μl PBS were settled on the cell culture dish (NEST Biotechnology, Wuxi, China). The dish was blocked with 5% BSA for 1 h and washed with PBS for three times. Then cells were incubated with rCsCKM-1/2 (42.5 μg/ml) or rTrx (42.5 μg/ml) for 1 h and washed as above. Mouse anti-His tag antibody (1:1000 dilution) was added to the dish, and the dish was incubated for 1 h and washed. Goat anti-mouse IgG Alexa Flour 488 (1:2000 dilution) was added to the dish, and the dish was incubated and washed as above. The cells were stained with DAPI and observed with a confocal microscope (Carl Zeiss, Oberkochen, Germany).

2.8 The effect of rCsCKM-1/2 on immune gene expression and bacterial infection

Tongue sole were divided randomly into four groups and injected intraperitoneally with 50 μl rCsCKM-1/2 (85 μg/ml), rTrx (85 μg/ml) or PBS. At 6 h post-injection, liver and spleen were taken (three fish per group at each time point) for RNA extraction and cDNA synthesis as described above. cytokine and antimicrobial peptide expression was determined by qRT-PCR with primers listed in Table S1. β-actin was used as the internal reference. To examine cytokine expression in PBLs, tongue sole PBLs were incubated with rCsCKM-1/2 (85 μg/ml), rTrx (85 μg/ml) or PBS for 1, 3 and 6 h. RNA extraction and cDNA synthesis were performed as above, and the expression of cytokines and antimicrobial peptides was determined by qRT-PCR as above. To examine the effect of rCsCKM-1/2 on the antimicrobial activity of PBLs, PBLs were pretreated with rCsCKM-1/2 (85 μg/ml), rTrx (85 μg/ml) or PBS for 2 h, followed by incubation with *E. tarda* (MOI=4) for 2 h. Extracellular bacteria were killed by gentamicin (400 μg/ml) for 30 minutes. The cells were placed in fresh medium (this time point was set as 0 h) and incubated for 2 and 4 h. The cells were counted and lysed as reported previously (35). The lysate was diluted and plated on LB agar plates. After incubation at 28°C for 48 h, the colony number was recorded.

2.9 The effect of TLR2 antagonist on CsCKM-1/2-induced immune response

Tongue sole PBLs were pretreated with DMSO (control) or different concentrations (1 and 10 μM) of CU-CPT22 (TLR2 specific antagonist) (Selleck.cn, Houston, TX, USA) for 2 h, followed by incubation with rCsCKM-1/2 (85 μg/ml), rTrx (85 μg/ml) or PBS for 1 h. After incubation, the expression levels of IL-1β, IL-6 and TNF-α were determined by qRT-PCR as above. To examine the effect of CU-CPT22 on phagocytosis, tongue sole PBLs in L-15 medium were settled on 24-well plates (Corning Incorporated, Costar) and treated with CU-CPT22 (10 μM) or DMSO (control) for 2 h. The cells were then incubated with rCsCKM-1/2 (85 μg/ml), rTrx (85 μg/ml) or PBS for 2 h as above. *E. tarda* (MOI=4) was added and incubated for another 2 h. After killing the extracellular bacteria, the number of intracellular bacteria was counted by spread plate method as described above.

2.10 The interaction between CsCKM-1/2 and TLR2

Confocal microscopy and co-immunoprecipitation were performed to examine the interaction between CsCKM-1/2 and TLR2. For confocal microscopy, recombinant pmCherry-N1 vectors expressing CsCKM-1/2 were constructed as follows. The coding sequences of CsCKM-1/2 were amplified by PCR. The pmCherry-N1 vector was digested with the restriction endonucleases HindIII and BamHI. The PCR products were ligated with the linearized vector. The recombinant vectors were introduced into *E. coli* Trelief 5α (Tsingke Biological Technology, Beijing, China) by transformation. The pEGFP-C1 vector expressing TLR2 leucine rich domain (LRR) was constructed as follows. The coding sequence of TLR2-LRR was amplified by PCR and inserted into the pEGFP-C1 vector at between the HindIII and BamHI sites. HEK293T cells were transfected with vectors expressing mCherry-tagged CsCKM-1/2 or GFP-tagged TLR2-LRR alone, or co-transfected mCherry-tagged CsCKM-1/2 with vector expressing GFP-tagged TLR2-LRR using PolyJet Transfection Reagent (SignaGen, USA). At 24 h after transfection, the cells were observed with a confocal microscope as above. For co-immunoprecipitation, pCS2-6Myc vectors expressing CsCKM-1/2 and TLR2-LRR were constructed as follows. The coding sequences of CsCKM-1/2 and TLR2-LRR were amplified by PCR. The pCS2-6Myc vector was digested with the restriction endonucleases EcoRI and XbaI. The PCR products were ligated with the linearized vector. The pCMV-N-Flag vectors expressing CsCKM-1/2 and TLR2-LRR were constructed as follows: the coding sequences of CsCKM-1/2 and TLR2-LRR were amplified by PCR. The pCMV-N-Flag vector was digested with the restriction endonucleases EcoRI and NheI. The PCR products were ligated with the linearized vector. HEK293T cells were transfected with Flag-tagged CsCKM-1/2 and Myc-tagged TLR2-LRR, or Myc-tagged CsCKM-1/2 and Flag-tagged TLR2-LRR for 24 h. The cells were lysed and incubated with pretreated anti-Flag affinity gel (Beyotime, Shanghai) at 4°C overnight and washed with PBS for seven times. The samples were boiled and used for immunoblotting with HRP-conjugated mouse anti-Myc-tag IgG and HRP-conjugated mouse anti-Flag-tag IgG. The blot was visualized using the ECL kit. All the PCR primers used are listed in Table S1.

2.11 Statistical analysis

All statistical analysis were carried out with GraphPad Prism 8.4.0 (GraphPad Software, La Jolla, CA, USA). The significance between groups was analyzed with student's t-test, and statistical significance was defined as $P < 0.05$.

3 Results

3.1 Tongue sole possesses two M-CKs with phosphotransferase activity

By searching the genomic database, we identified two creatine kinases (CKs) from tongue sole *C. semilaevis*. The two CKs share high sequence identity with each other, and share 85.4% and 85.8% sequence identities with human M-CK, respectively (Figure S1). Phylogenetic analysis showed that the tongue sole CKs were phylogenetically grouped together with teleost (*Danio rerio* and *Oryzias latipes*) and human the M-CKs (Figure 1A). Based on these results, the two tongue sole CKs were named muscle type CKs (CsCKM-1/2). To examine the activity of CsCKM-1/2, recombinant CsCKM-1/2 (rCsCKM-1/2) were prepared (Figure S2). rCsCKM-1/2 exhibited robust phosphotransferase activity in a manner that

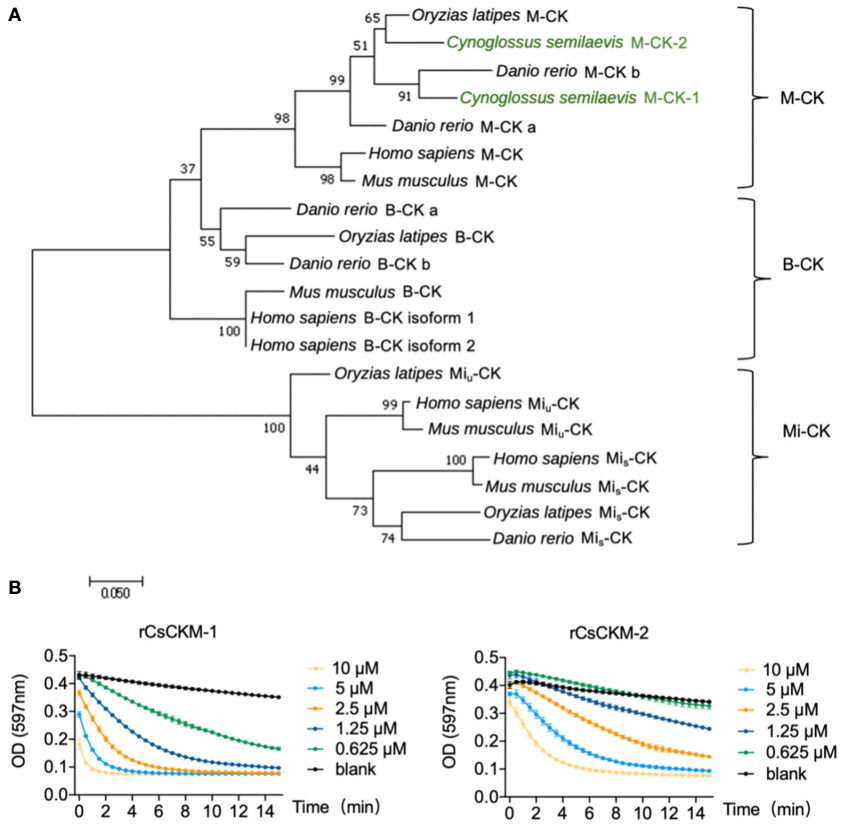

FIGURE 1
Phylogenetic and activity analyses of CsCKM-1/2. **(A)** Phylogenetic analysis of CK homologs. The numbers indicate bootstrap values based on 1500 replications. M-CK, muscle type CK; B-CK, brain type CK; Mi-CK, mitochondrial type CK; Mi_u-CK, ubiquitous type Mi-CK; Mi_s-CK, sarcomeric type Mi-CK. **(B)** rCsCKM-1/2 at different concentrations were incubated with the substrates. The enzymatic reaction was recorded every 30 seconds by monitoring the absorbance of thymol blue (pH indicator) at 597 nm, because creatine kinase catalysis generates hydrogen ions.

positively correlated with the concentration of rCsCKM-1/2 (Figure 1B).

3.2 Bacterial infection stimulates the expression and extracellular release of CsCKM-1/2

Under normal physiological condition, CsCKM-1 expression was detected in muscle, skin, heart, liver, head kidney, brain, spleen, gill and intestine (Figure S3). The expression pattern of CsCKM-2 was largely similar to that of CsCKM-1. When tongue sole were infected with *Edwardsiella tarda*, the expression of CsCKM-1/2 significantly increased at 6 to 24 hpi in liver and spleen, and at 12 or 24 hpi in head kidney (Figure 2A). When the fish were infected with *Vibrio anguillarum*, CsCKM-1 expression significantly increased in liver (6 to 48 hpi) and spleen (6 and 24 hpi), but decreased in head kidney at 6 hpi; CsCKM-2 expression significantly increased in liver (12 and 24 hpi) and decreased in spleen (6 and 12 hpi) and head kidney (6 hpi) (Figure 2B). In tongue sole PBLs, both *E. tarda* and *V. anguillarum* infections significantly enhanced CsCKM-1/2 expression at 4 and 6 hpi (Figure 2C). Furthermore, *E. tarda* and *V. anguillarum* infections caused extracellular production of CsCKM-1/2 (Figure 2D). Consistently, *in vivo* study showed that both *E. tarda* and *V. anguillarum* infections induced secretion of CsCKM-1/2 into tongue sole serum (Figure 2E).

3.3 CsCKM-1/2 bind bacterial pathogens and pathogen-associated molecular patterns (PAMPs)

To examine whether bacteria-induced production of CsCKM-1/2 had any role in immune defense against bacterial pathogens, we determined the potential of CsCKM-1/2 to interact with bacteria. The results showed that rCsCKM-1/2 exhibited dose-dependent binding to the fish bacterial pathogens *E. tarda*, *V. anguillarum*, *Vibrio harveyi* and *Streptococcus iniae* (Figure 3A). rCsCKM-1/2 also exhibited strong binding to PAMPs, including lipopolysaccharides (LPS), peptidoglycan (PGN), glucan (Glu) and mannan (Man) (Figure 3B). rCsCKM-1/2 had no apparent effect on the growth of *E. tarda*, *V. anguillarum*, *V. harveyi* and *S. iniae* (Figure S4).

10.3389/fimmu.2023.1142488

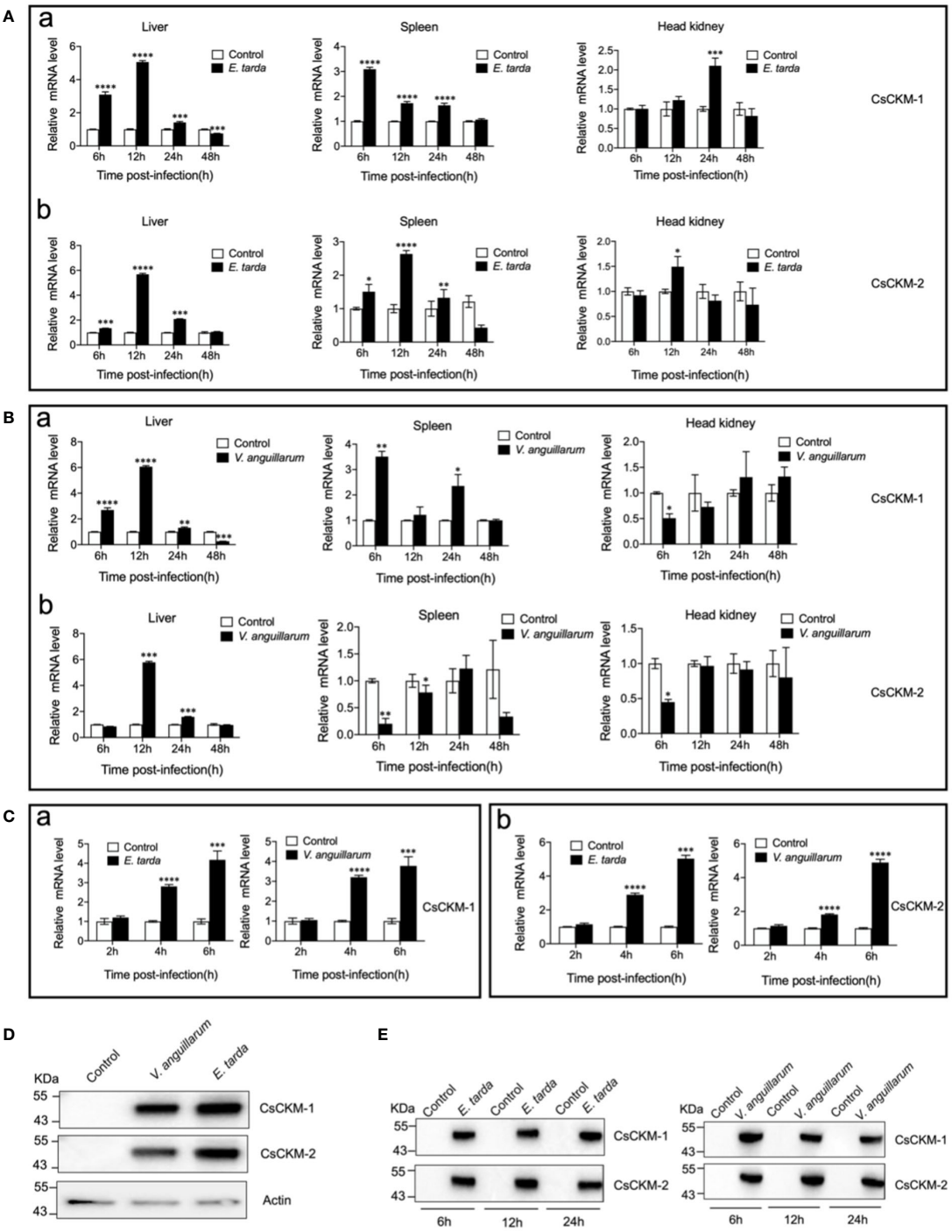

FIGURE 2
The effect of bacterial infection on CsCKM-1/2 expression and extracellular release. **(A, B)** Tongue sole were infected with or without (control) *Edwardsiella tarda* **(A)** or *Vibrio anguillarum* **(B)**, and the expression levels of CsCKM-1 (a) and CsCKM-2 (b) in liver, spleen and head kidney were determined by qRT-PCR at various time points. **(C)** Tongue sole PBLs were infected with or without (control) *E. tarda* or *V. anguillarum*, and the expression of CsCKM-1(a) and CsCKM-2 (b) was determined by qRT-PCR. In all panels, the expression level in the control fish/cells was set as 1. Values are the means of triplicate assays and shown as means ± SD. *P < 0.05; **P < 0.01; ***P < 0.001; ****P < 0.0001. **(D)** Tongue sole PBLs were infected with or without (control) *E. tarda* or *V. anguillarum*. Extracellular release of CsCKM-1/2 was detected by immunoblotting using anti-CsCKM-1/2 antibodies. β-actin was used as a loading control. **(E)** Tongue sole were infected with or without (control) *E. tarda* or *V. anguillarum* for 6 to 24 h. CsCKM-1/2 in serum were determined by immunoblotting as above.

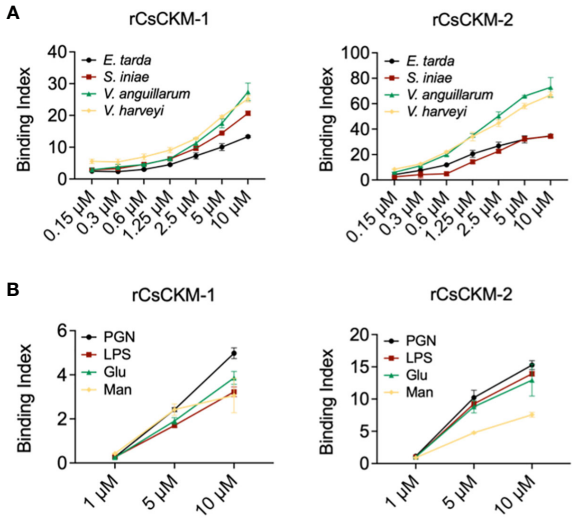

FIGURE 3
Binding of CsCKM-1/2 to bacteria and bacterial cell surface components. **(A)** rCsCKM-1/2 in different concentrations were incubated with *Edwardsiella tarda*, *Vibrio anguillarum*, *Vibrio harveyi* and *Streptococcus iniae*, and the binding was determined by ELISA. **(B)** The binding of rCsCKM-1/2 to different pathogen-associated molecular patterns (PAMPs) was determined by ELISA. LPS, lipopolysaccharides; PGN, peptidoglycan; Glu, glucan; Man, mannan. Values are the means of triplicate assays and shown as means ± SD.

3.4 CsCKM-1/2 promote proinflammatory cytokine expression and reduce bacterial infection

Since CsCKM-1/2 were released by PBLs during bacterial infection, we examined whether CsCKM-1/2 were able to interact with PBLs. The result showed that following incubation with PBLs, rCsCKM-1/2 were found to bind to PBLs (Figure 4A) and significantly upregulated the expression of IL-1β, IL-6 and TNF-α (Figure 4B). IL-1β and TNF-α were significantly induced by rCsCKM-1 at 1 hpi and by rCsCKM-2 at 1 and 3 hpi; IL-6 was significantly induced by rCsCKM-1/2 at 1 to 6 hpi. In addition, we found that both CsCKM-1 and CsCKM-2 significantly up-regulated the expression of hepcidin and down-regulated the expression of NK-lysin and saposin (Figure 4C). Compared to control cells, rCsCKM-1/2-treated PBLs exhibited enhanced ability to uptake *E. tarda* and inhibit the intracellular replication of *E. tarda* (Figures 4D, E). *In vivo* study showed that in tongue sole, rCsCKM-1 significantly upregulated IL-6 and TNF-α expression in liver and spleen, and significantly upregulated IL-1β expression in liver; rCsCKM-2 significantly upregulated IL-6 expression in liver and TNF-α expression in spleen (Figure 4F).

3.5 TLR2 is required for CsCKM-1/2-mediated immune response

In order to explore the molecular mechanism of CsCKM-1/2-induced immune response, we investigated whether TLR2 was involved in CsCKM-1/2-induced cytokine expression. The result showed that when PBLs were pretreated with the TLR2 antagonist CU-CPT22, which inhibited TLR2 signaling (40), rCsCKM-1/2-induced expression of IL-1β, IL-6 and TNF-α was significantly suppressed (Figures 5A, B). Similarly, the boosting effect of rCsCKM-1/2 on phagocytosis was abolished (Figure S5). When expressed in HEK293T cells, CsCKM-1/2 and TLR2 leucine-rich domain (LRR) were evenly distributed in the cytoplasm (Figure 5C). When CsCKM-1/2 were co-expressed with TLR2-LRR, co-localization of CsCKM-1/2 with TLR2-LRR was detected by microscopy (Figure 5D). Consistently, CsCKM-1/2 were co-immunoprecipitated with TLR2-LRR (Figure 5E), suggesting interaction between CsCKM-1/2 and TLR2-LRR.

4 Discussion

CK exists in all vertebrates and reversibly catalyzes the reaction of ATP production and consumption (2, 41). Different CK isoenzymes have distinct patterns of tissue specific expression and subcellular localization, which is important to maintain energy homeostasis (42, 43). In teleost, the transcription of CK can respond to various stimulations including temperature, salinity, muscle damage and bacterial infection (19, 44–46). The activity and content of intracellular creatine kinase vary upon bacterial infection in fish such as zebrafish, rainbow trout and Nile tilapia (19, 20, 23, 47). In this study, we found that the two muscle type CKs from tongue sole *C. semilaevis* share over 80% identities with human M-CK, suggesting conserved function of CK in vertebrates. Consistently, rCsCKM-1/2 exhibited robust kinase activity. CsCKM-1/2 expression was detected at high levels in muscle, where CK may provide support for energy homeostasis. CsCKM-1/2 also expressed in immune organs, including spleen and liver, in which the expression of CsCKM-1/2 was significantly elevated after *E. tarda* or *V. anguillarum* infection, suggesting involvement of CK in fish antibacterial immunity.

10.3389/fimmu.2023.1142488

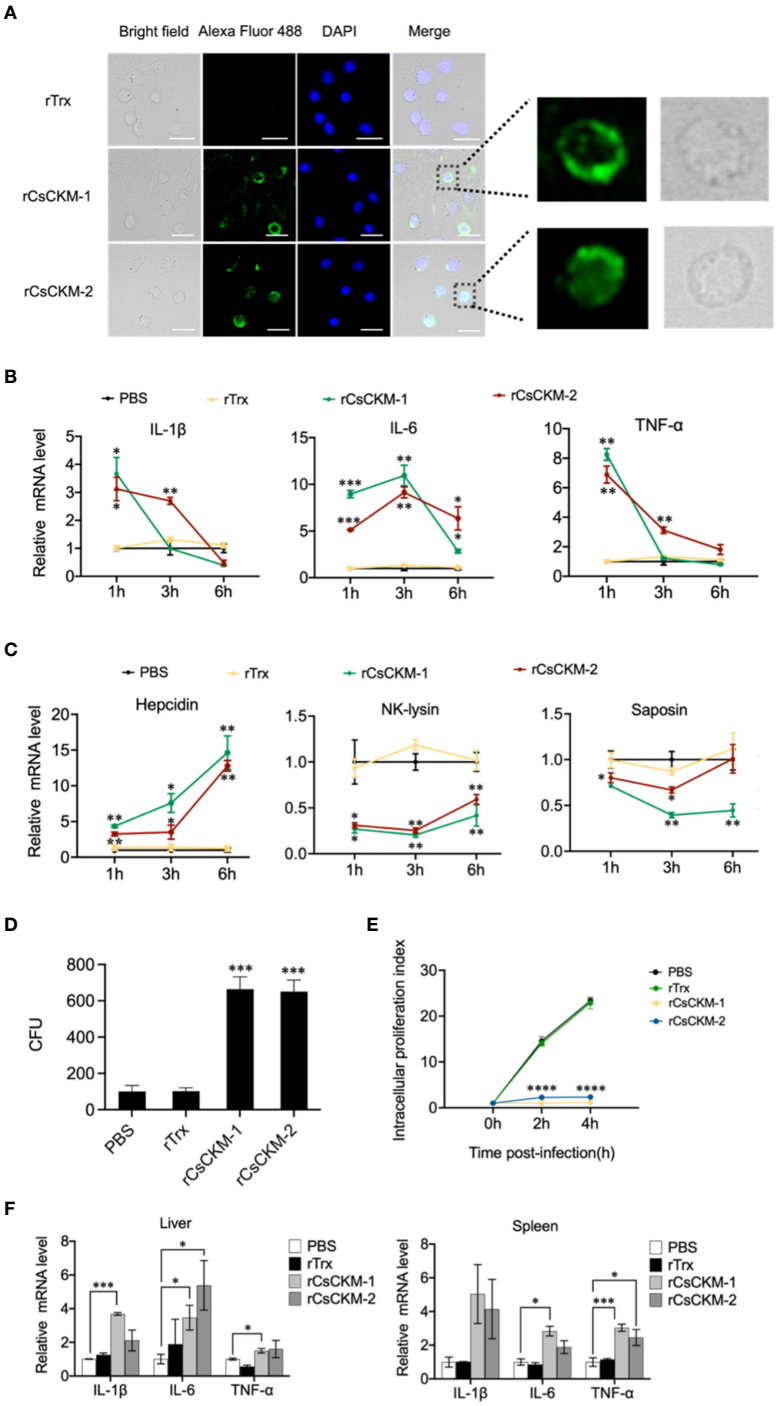

FIGURE 4
The effect of CsCKM-1/2 on IL-1β, IL-6 and TNF-α expression and *Edwardsiella tarda* infection. **(A)** His-tagged rCsCKM-1/2 or rTrx was incubated with tongue sole PBLs for 1 h. The cells were stained with DAPI and treated with anti-His tag antibody and Alexa Fluor 488-labeled secondary antibody. The distribution of rCsCKM-1/2 in one cell was shown in the enlarged images. Scale bar, 10 μm. **(B)** The expression of IL-1β, IL-6 and TNF-α in PBLs treated with rCsCKM-1/2, rTrx, or PBS (control) was determined at different times by qRT-PCR. **(C)** The expression of hepcidin, NK-lysin and saposin in PBLs treated with rCsCKM-1/2, rTrx, or PBS (control) was determined as above. **(D)** PBLs were pretreated with rCsCKM-1/2, rTrx, or PBS (control) for 2 h, and then incubated with *E. tarda* for 2 h. The number of phagocytosed bacteria was determined. **(E)** PBLs were pretreated with rCsCKM-1/2, rTrx, or PBS (control) and then infected with *E. tarda*. Intracellular bacteria replication at different hours was determined. **(F)** Tongue sole were infected with rCsCKM-1/2, rTrx, or PBS (control), and the expression of IL-1β, IL-6 and TNF-α in spleen and liver was determined by qRT-PCR. For **(B–D)**, values are the means of triplicate assays and shown as means ± SD. **P* < 0.05; ***P* < 0.01; ****P* < 0.001, *****P* < 0.001.

10.3389/fimmu.2023.1142488

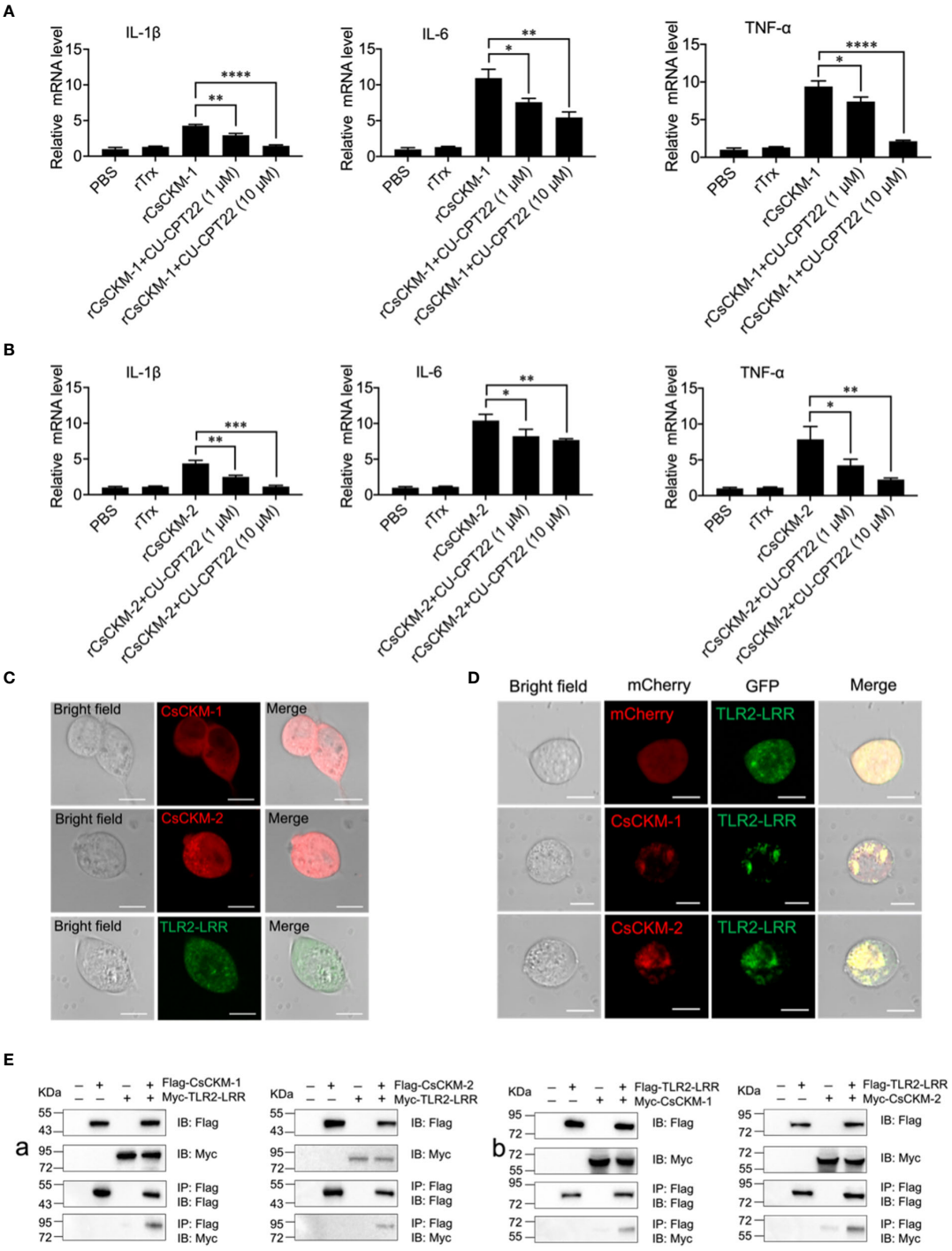

FIGURE 5
The involvement of TLR2 in CsCKM-1/2-induced immune response. **(A)** Tongue sole PBLs were incubated with PBS, rTrX, rCsCKM-1, or rCsCKM-1 plus different concentrations of CU-CPT22 for 2 h. The expression of IL-1β, IL-6 and TNF-α was determined by qRT-PCR. **(B)** PBLs were incubated with PBS, rTrX, rCsCKM-2, or rCsCKM-2 plus different concentrations of CU-CPT22 for 2 h. Gene expression was determined as above. For both **(A, B)**, values are the means of triplicate assays and shown as means ± SD. *P < 0.05; **P < 0.01; ***P < 0.001, ****P < 0.0001. **(C)** HEK293T cells were transfected with mCherry-tagged CsCKM-1/2 or GFP-tagged TLR2-LRR and observed with a confocal microscope. **(D)** HEK293T cells co-expressed GFP-tagged TLR2-LRR and the mCherry tag, or co-expressed TLR2-LRR and mCherry-tagged CsCKM-1/2. Protein colocalization was observed with a confocal microscope. Scale bar, 10 μm. **(E)** Flag-tagged CsCKM-1/2 and Myc-tagged TLR2-LRR (Ea), or Myc-tagged CsCKM-1/2 and Flag-tagged TLR2-LRR (Eb) were co-expressed in HEK293T cells for 24 h. Co-immunoprecipitation and immunoblotting were performed with antibodies against Myc-tag and Flag-tag.

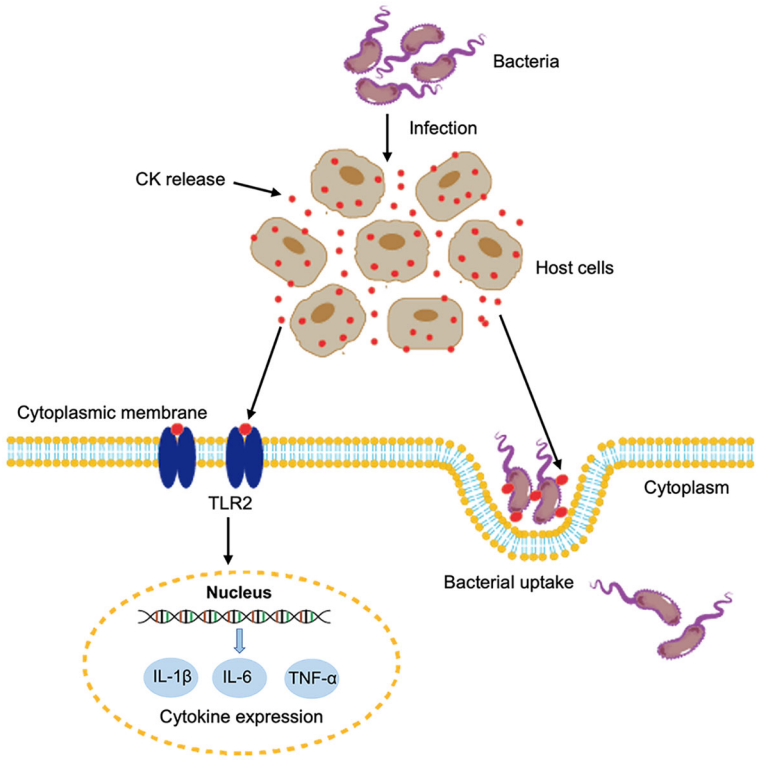

FIGURE 6
A proposed model of the immune function of CsCKM-1/2. Bacterial infection induces the release of CsCKM-1/2. CsCKM-1/2 interact with TLR2 and activate TLR2-mediated signaling, which induces cytokine expression and likely inhibits bacterial infection. In addition, CsCKM-1/2 bind to the bacterial pathogen and enhance bacterial uptake by host cells.

Under normal physiological conditions, CKs are mainly distributed in the cytoplasm, whereas under pathological conditions, they are released into the extracellular environment. Hence, CKs have been widely used as biomarkers in the early diagnosis of various diseases, including myocardial infarction, Alzheimer's Disease and seizure disorders (13, 48, 49). In human, bacterial infection could induce the release of CK into serum (17). Similar results were observed in teleost. In rainbow trout, CK was the most upregulated enzyme in the serum during *Aeromonas salmonicida* infection (50). However, the function of CK in serum remains elusive. In mammals, it has been proposed that extracellular CK could modulate purinergic signaling, which is associated with the antimicrobial mechanisms of host immune cells (51, 52). In amphioxus *Branchiostoma belcheri*, CK was able to bind *E. coli* and inhibit bacterial growth through a mechanism similar to that of lectin (53). In speckled hind (*Epinephelus drummondhayi*), the branchial muscle-type CK could interact with the envelope proteins of *Edwardsiella tarda* (54). In our study, we found that under the normal conditions, CsCKM-1/2 could not be detected in serum. However, during the infection of *E. tarda* or *V. anguillarum*, CsCKM-1/2 were detected in serum, indicating bacteria-induced release of CsCKM-1/2. rCsCKM-1/2 exhibited apparent binding capacity to fish pathogens, including *E. tarda*, *V. anguillarum, V. harveyi* and *S. iniae*, probably through interaction with microbial surface PAMPs, such as LPS and PGN. rCsCKM-1/2 lacked bactericidal activity but enhanced the phagocytosis of PBLs, suggesting that extracellular CsCKM-1/2 likely function to promote the antimicrobial activity of PBLs. In addition, as the phosphagen kinases that regulate ATP/ADP homeostasis, the released serum CsCKs might also exert immune effects *via* ATP. Previous studies reported that there existed conserved extracellular ATP-activated signaling pathways in fish, which activated innate immunity and induced cell apoptosis, whereas the hydrolytic product of extracellular ATP, adenosine, exhibited inhibitory effect on the immunity (55, 56). It is possible that serum CsCKs might modulate tongue sole immunity *via* the regulation of the purinergic signaling pathway.

In addition to binding bacteria, CsCKM-1/2 also bound PBLs and upregulated the expression of IL-1β, IL-6 and TNF-α. Similarly, *in vivo* administration of CsCKM-1/2 increased the expression of these cytokines in tongue sole tissues. These results indicated that CsCKM-1/2 probably function as damage-associated molecular patterns (DAMPs) that were released into the extracellular environment in response to bacterial infection and acted as a warning signal to the immune system. Previous studies showed that HMGB1, a classical and widely studied DAMP molecule, mediates sepsis by transferring LPS to CD14, which facilitates the activation of TLR4 (57). In the present study, we

found that PBLs pretreated with rCsCKM-1/2 exhibited enhanced phagocytosis and inhibition of the intracellular proliferation of *E. tarda*, indicating an immune activation capacity of CsCKM-1/2.

Host immune response depends on various receptors to recognize extracellular signals, and the evolutionarily conserved pattern recognition receptors (PRRs) play important roles in this process (58). Previous studies showed that certain PRRs (e.g., TLRs) can be activated by DAMPs (59) and initiate downstream signaling pathways, such as the NF-κB, MAPK, cGAS and RIG-I signaling pathways, which result in cytokine production and immune activation (59–61). In human, TLR2/MAPKs signaling pathway is crucial for microbicidal phagocytosis (62). In tongue sole, cell membrane TLR2 was reported to play an important role in cytokine expression and phagocytosis of bacteria (24). In our present study, we found that inhibition of TLR2 signaling significantly decreased CsCKM-1/2-induced proinflammatory cytokine expression and bacterial uptake, indicating involvement of TLR2 in CsCKM-1/2-induced immune response. Consistently, CsCKM-1/2 were found to be co-localized with TLR2-LRR and were co-immunoprecipitated with TLR2-LRR, suggesting that TLR2 likely serves as a receptor for CsCKM-1/2 as DAMPs. The findings collectively suggested a possibility that the bacterial binding ability of CsCKs may facilitate CsCKs to effectively target the bacteria-bound immune cells and interact with the cell surface TLR2, leading to enhanced phagocytosis and other immune response.

In conclusion, we demonstrated that two fish CKs were released extracellularly during bacterial infection. The extracellular CsCKM-1/2 could bind to bacterial pathogens and promote bacterial phagocytosis by immune cells. Moreover, CsCKM-1/2 could function as DAMPs and activate antimicrobial immunity probably *via* interaction with TLR2 (Figure 6). These findings provided new insights into the immune function and regulation of CK in teleost.

Data availability statement

The original contributions presented in the study are included in the article/Supplementary Material. Further inquiries can be directed to the corresponding authors.

Ethics statement

The animal study was reviewed and approved by Ethics Committee of Institute of Oceanology, Chinese Academy of Sciences.

Author contributions

SJ, LS, and XL designed the study; XL conducted the experiments, analyzed the data, and wrote the first draft of the manuscript; LS and SJ edited the manuscript. All authors contributed to the article and approved the submitted version.

Funding

This work was supported by the grants from the National Key Research and Development Program of China (2018YFD0900500), the Youth Innovation Promotion Association CAS (2021204), and the Taishan Scholar Program of Shandong Province (2018 and 2021).

Conflict of interest

The authors declare that the research was conducted in the absence of any commercial or financial relationships that could be construed as a potential conflict of interest.

Publisher's note

Supplementary material

The Supplementary Material for this article can be found online at: https://www.frontiersin.org/articles/10.3389/fimmu.2023.1142488/full#supplementary-material

References

1. Wallimann T, Tokarska-Schlattner M, Schlattner U. The creatine kinase system and pleiotropic effects of creatine. *Amino Acids* (2011) 40(5):1271–96. doi: 10.1007/s00726-011-0877-3

2. McLeish MJ, Kenyon GL. Relating structure to mechanism in creatine kinase. *Crit Rev Biochem Mol* (2005) 40(1):1–20. doi: 10.1080/10409230590918577

3. Leydier C, Andersen JS, Couthon F, Forest E, Marcillat O, Denoroy L, et al. Proteinase K processing of rabbit muscle creatine kinase. *J Protein Chem* (1997) 16 (1):67–74. doi: 10.1023/A:1026347129083

4. He HW, Zhang J, Zhou HM, Yan YB. Conformational change in the c-terminal domain is responsible for the initiation of creatine kinase thermal aggregation. *Biophys J* (2005) 89(4):2650–8. doi: 10.1529/biophysj.105.066142

5. Eder M, Fritz-Wolf K, Kabsch W, Wallimann T, Schlattner U. Crystal structure of human ubiquitous mitochondrial creatine kinase. *Proteins* (2000) 39(3):216–25. doi: 10.1002/(Sici)1097-0134(20000515)39:3<216::Aid-Prot40>3.0.Co;2-#

6. Bong SM, Moon JH, Nam KH, Lee KS, Chi YM, Hwang KY. Structural studies of human brain-type creatine kinase complexed with the Adp-Mg2+-No3–creatine transition-state analogue complex. *FEBS Lett* (2008) 582(28):3959–65. doi: 10.1016/j.febslet.2008.10.039

7. Zhang YF, Li H, Wang XM, Gao X, Liu XL. Regulation of T cell development and activation by creatine kinase b. *PLoS One* (2009) 4(4):e5000. doi: 10.1371/journal.pone.0005000

8. Samborska B, Roy DG, Rahbani JF, Hussain MF, Ma EH, Jones RG, et al. Creatine transport and creatine kinase activity is required for Cd8(+) T cell immunity. *Cell Rep* (2022) 38(9):110446. doi: 10.1016/j.celrep.2022.110446

9. Benajiba L, Alexe G, Su A, Raffoux E, Soulier J, Hemann MT, et al. Creatine kinase pathway inhibition alters Gsk3 and wnt signaling in Evi1-positive aml. *Leukemia* (2019) 33(3):800–4. doi: 10.1038/s41375-018-0291-x

10. Hara H, Aizaki H, Matsuda M, Shinkai-Ouchi F, Inoue Y, Murakami K, et al. Involvement of creatine kinase b in hepatitis c virus genome replication through

interaction with the viral Ns4a protein. *J Virol* (2009) 83(10):5137–47. doi: 10.1128/Jvi.02179-08

11. Ozawa E, Hagiwara Y, Yoshida M. Creatine kinase, cell membrane and duchenne muscular dystrophy. *Mol Cell Biochem* (1999) 190(1-2):143–51. doi: 10.1023/A:1006974613418

12. Baird MF, Graham SM, Baker JS, Bickerstaff GF. Creatine-kinase- and exercise-related muscle damage implications for muscle performance and recovery. *J Nutr Metab* (2012) 2012:960363. doi: 10.1155/2012/960363

13. Roberts R, Sobel BE. Creatine kinase isoenzymes in the assessment of heart disease. *Am Heart J* (1978) 95(4):521–8. doi: 10.1016/0002-8703(78)90245-4

14. Clarkson PM, Kearns AK, Rouzier P, Rubin R, Thompson PD. Serum creatine kinase levels and renal function measures in exertional muscle damage. *Med Sci Sport Exer* (2006) 38(4):623–7. doi: 10.1249/01.mss.0000210192.49210.fc

15. Essone PN, Adegbite BR, Mbadinga MJM, Mbouna AV, Lotola-Mougeni F, Alabi A, et al. Creatine kinase-(Mb) and hepcidin as candidate biomarkers for early diagnosis of pulmonary tuberculosis: A proof-of-Concept study in lambarene, Gabon. *Infection* (2022) 50(4):897–905. doi: 10.1007/s15010-022-01760-8

16. Adams JE, Schechtman KB, Landt Y, Ladenson JH, Jaffe AS. Comparable detection of acute myocardial-infarction by creatine-kinase Mb isoenzyme and cardiac troponin-I. *Clin Chem* (1994) 40(7):1291–5. doi: 10.1093/clinchem/40.7.1291

17. Nakafusa J, Misago N, Miura Y, Kayaba M, Tanaka T, Narisawa Y. The importance of serum creatine phosphokinase level in the early diagnosis, and as a prognostic factor, of vibrio vulnificus infection. *Brit J Dermatol* (2001) 145(2):280–4. doi: 10.1046/j.1365-2133.2001.04347.x

18. Liu YL, Sun XH, Wang YQ, Xing CH, Li L, Zhou SY. Evaluation of associated markers of neonatal pathological jaundice due to bacterial infection. *Iran J Public Health* (2021) 50(2):333–40. doi: 10.18502/ijph.v50i2.5394

19. Lu AJ, Hu XC, Wang Y, Shen XJ, Li X, Zhu AH, et al. Itraq analysis of gill proteins from the zebrafish (Danio rerio) infected with aeromonas hydrophila. *Fish Shellfish Immun* (2014) 36(1):229–39. doi: 10.1016/j.fsi.2013.11.007

20. Baldissera MD, Souza CF, Descovi SN, Verdi CM, Santos RCV, da Silva AS, et al. Impairment of branchial energy transfer pathways in disease pathogenesis of providencia rettgeri infection in juvenile Nile tilapia (Oreochromis niloticus): Remarkable involvement of creatine kinase activity. *Aquaculture* (2019) 502:365–70. doi: 10.1016/j.aquaculture.2018.12.074

21. Baldissera MD, Souza CF, Junior GB, Verdi CM, Moreira KLS, da Rocha MIUM, et al. Aeromonas caviae alters the cytosolic and mitochondrial creatine kinase activities in experimentally infected silver catfish: Impairment on renal bioenergetics. *Microb Pathogenesis* (2017) 110:439–43. doi: 10.1016/j.micpath.2017.07.031

22. Baldissera MD, Souza CF, Junior GB, Moreird KLS, da Veiga ML, da Rocha MIUM, et al. Citrobacter freundii impairs the phosphoryl transfer network in the gills of rhamdia quelen: Impairment of bioenergetics homeostasis. *Microb Pathogenesis* (2018) 117:157–61. doi: 10.1016/j.micpath.2018.02.040

23. Rivas-Aravena A, Fuentes-Valenzuela M, Escobar-Aguirre S, Gallardo-Escarate C, Molina A, Valdes JA. Transcriptomic response of rainbow trout (Oncorhynchus mykiss) skeletal muscle to flavobacterium psychrophilum. *Comp Biochem Phys D* (2019) 31:100596. doi: 10.1016/j.cbd.2019.100596

24. Li XP, Sun L. Toll-like receptor 2 of tongue sole cynoglossus semilaevis: Signaling pathway and involvement in bacterial infection. *Fish Shellfish Immunol* (2016) 51:321–8. doi: 10.1016/j.fsi.2016.03.001

25. Li M-F, Wang C, Sun L. Edwardsiella tarda mlic, a lysozyme inhibitor that participates in pathogenesis in a manner that parallels ivy. *Infection Immun* (2015) 83 (2):583–90. doi: 10.1128/IAI.02473-14

26. Sun BG, Hu YH. Evaluation of potential internal references for quantitative real-time rt-pcr normalization of gene expression in red drum (Sciaenops ocellatus). *Fish Physiol Biochem* (2015) 41(3):695–704. doi: 10.1007/s10695-015-0039-8

27. Cheng S, Hu YH, Jiao XD, Sun L. Identification and immunoprotective analysis of a streptococcus iniae subunit vaccine candidate. *Vaccine* (2010) 28(14):2636–41. doi: 10.1016/j.vaccine.2010.01.016

28. Sun K, Zhang WW, Hou JH, Sun L. Immunoprotective analysis of Vhhp2, a vibrio harveyi vaccine candidate. *Vaccine* (2009) 27(21):2733–40. doi: 10.1016/j.vaccine.2009.03.012

29. Yu LP, Hu YH, Zhang XH, Sun BG. Development of a triplex loop-mediated isothermal amplification method for rapid on-site detection of three vibrio species associated with fish diseases. *Aquaculture* (2013) 414:267–73. doi: 10.1016/j.aquaculture.2013.08.016

30. Zhang M, Sun K, Sun L. Regulation of autoinducer 2 production and luxs expression in a pathogenic edwardsiella tarda strain. *Microbiol (Reading)* (2008) 154(Pt 7):2060–9. doi: 10.1099/mic.0.2008/017343-0

31. Xu H, Jiang S, Yu C, Yuan ZH, Sun L. Gsdmea-mediated pyroptosis is bi-directionally regulated by caspase and required for effective bacterial clearance in teleost. *Cell Death Dis* (2022) 13(5):491. doi: 10.1038/s41419-022-04896-5

32. Li YQ, Sun L, Li J. Macropinocytosis-dependent endocytosis of Japanese flounder igm(+) b cells and its regulation by Cd22. *Fish Shellfish Immun* (2019) 84:138–47. doi: 10.1016/j.fsi.2018.09.068

33. Zhang P, Sun BG. Cryptochrome 1 is involved in anti-bacterial immunity in Japanese flounder (Paralichthys olivaceus). *Aquaculture* (2022) 561:738675. doi: 10.1016/j.aquaculture.2022.738675

34. Letunic I, Bork P. Interactive tree of life (Itol) V5: An online tool for phylogenetic tree display and annotation. *Nucleic Acids Res* (2021) 49(W1):W293–W6. doi: 10.1093/nar/gkab301

35. Yu C, Zhang P, Li XP, Sun L. Japanese Flounder paralichthys olivaceus interleukin 21 induces inflammatory response and plays a vital role in the immune defense against bacterial pathogen. *Fish Shellfish Immun* (2020) 98:364–73. doi: 10.1016/j.fsi.2020.01.043

36. Long H, Chen C, Zhang J, Sun L. Antibacterial and antiviral properties of tongue sole (Cynoglossus semilaevis) high mobility group B2 protein are largely independent on the acidic c-terminal domain. *Fish Shellfish Immunol* (2014) 37(1):66–74. doi: 10.1016/j.fsi.2014.01.013

37. Jiang S, Gu H, Zhao Y, Sun L. Teleost gasdermin e is cleaved by caspase 1, 3, and 7 and induces pyroptosis. *J Immunol* (2019) 203(5):1369–82. doi: 10.4049/jimmunol.1900383

38. Wang T, Sun L. Cssap, a teleost serum amyloid p component, interacts with bacteria, promotes phagocytosis, and enhances host resistance against bacterial and viral infection. *Dev Comp Immunol* (2016) 55:12–20. doi: 10.1016/j.dci.2015.10.002

39. Li M, Wu M, Sun Y, Sun L. Edwardsiella tarda trat is an anti-complement factor and a cellular infection promoter. *Commun Biol* (2022) 5(1):637. doi: 10.1038/s42003-022-03587-3

40. Cheng K, Wang XH, Zhang ST, Yin H. Discovery of small-molecule inhibitors of the Tlr1/Tlr2 complex. *Angew Chem Int Edit* (2012) 51(49):12246–9. doi: 10.1002/anie.201204910

41. Suzuki T, Mizuta C, Uda K, Ishida K, Mizuta K, Sona S, et al. Evolution and divergence of the genes for cytoplasmic, mitochondrial, and flagellar creatine kinases. *J Mol Evol* (2004) 59(2):218–26. doi: 10.1007/s00239-004-2615-x

42. Trask RV, Billadello JJ. Tissue-specific distribution and developmental regulation of m and b creatine kinase mrnas. *Biochim Biophys Acta* (1990) 1049 (2):182–8. doi: 10.1016/0167-4781(90)90039-5

43. Payne RM, Strauss AW. Expression of the mitochondrial creatine-kinase genes. *Mol Cell Biochem* (1994) 133:235–43. doi: 10.1007/Bf01267957

44. Ji LQ, Jiang KY, Liu M, Wang BJ, Han LJ, Zhang MM, et al. Low temperature stress on the hematological parameters and hsp gene expression in the turbot scophthalmus maximus. *Chin J Oceanol Limn* (2016) 34(3):430–40. doi: 10.1007/s00343-016-4367-z

45. Weng CF, Chiang CC, Gong HY, Chen MHC, Lin CJF, Huang WT, et al. Acute changes in gill na+-K+-Atpase and creatine kinase in response to salinity changes in the euryhaline teleost, tilapia (Oreochromis mossambicus). *Physiol Biochem Zool* (2002) 75 (1):29–36. doi: 10.1086/338283

46. Rojas V, Morales-Lange B, Avendano-Herrera R, Poblete-Morales M, Tapia-Cammas D, Guzman F, et al. Detection of muscle-specific creatine kinase expression as physiological indicator for Atlantic salmon (Salmo salar l) skeletal muscle damage. *Aquaculture* (2018) 496:66–72. doi: 10.1016/j.aquaculture.2018.07.006

47. Kurpe SR, Sukhovskaya IV, Borvinskaya EV, Morozov AA, Parshukov AN, Malysheva IE, et al. Physiological and biochemical characteristics of rainbow trout with severe, moderate and asymptomatic course of vibrio anguillarum infection. *Animals-Basel* (2022) 12(19):2642. doi: 10.3390/ani12192642

48. Wyllie E, Lueders H, Pippenger C, Vanlente F. Postictal serum creatine-kinase in the diagnosis of seizure disorders. *Arch Neurol-Chicago* (1985) 42(2):123–6. doi: 10.1001/archneur.1985.04060020033010

49. . The creatine Kinase/Creatine connection to alzheimer's disease: Ck inactivation, app-ck complexes, and focal creatine deposits. *J BioMed Biotechnol* (2006) 2006(3):35936. doi: 10.1155/Jbb/2006/35936

50. Racicot JG, Gaudet M, Leray C. Blood and liver-enzymes in rainbow-trout (Salmo-gairdneri rich) with emphasis on their diagnostic use - study of Ccl4 toxicity and a case of aeromonas infection. *J Fish Biol* (1975) 7(6):825–&. doi: 10.1111/j.1095-8649.1975.tb04653.x

51. Coutinho-Silva R, Savio LEB. Purinergic signalling in host innate immune defence against intracellular pathogens. *Biochem Pharmacol* (2021) 187:114405. doi: 10.1016/j.bcp.2021.114405

52. Brewster LM. Extracellular creatine kinase may modulate purinergic signalling. *Purinerg Signal* (2020) 16(3):305–12. doi: 10.1007/s11302-020-09707-0

53. An Y, Fan NN, Zhang SC. Creatine kinase is a bacteriostatic factor with a lectin-like activity. *Mol Immunol* (2009) 46(13):2666–70. doi: 10.1016/j.molimm.2009.04.001

54. Liu Y, Zhang HL, Liu YJ, Li H, Peng XX. Determination of the heterogeneous interactome between edwardsiella tarda and fish gills. *J Proteomics* (2012) 75(4):1119–28. doi: 10.1016/j.jprot.2011.10.022

55. Li S, Zhang T, Feng Y, Sun J. Extracellular atp-mediated purinergic immune signaling in teleost fish: A review. *Aquaculture* (2021) 537:736511. doi: 10.1016/j.aquaculture.2021.736511

56. Baldissera MD, de Freitas Souza C, Val AL, Baldisserotto B. Involvement of purinergic signaling in the Amazon fish pterygoplichthys pardalis subjected to handling stress: Relationship with immune response. *Aquaculture* (2020) 514:734481. doi: 10.1016/j.aquaculture.2019.734481

57. Ciesielska A, Matyjek M, Kwiatkowska K. Tlr4 and Cd14 trafficking and its influence on lps-induced pro-inflammatory signaling. *Cell Mol Life Sci* (2021) 78 (4):1233–61. doi: 10.1007/s00018-020-03656-y

58. Arancibia SA, Beltran CJ, Aguirre IM, Silva P, Peralta AL, Malinarich F, et al. Toll-like receptors are key participants in innate immune responses. *Biol Res* (2007) 40 (2):97–112. doi: 10.4067/s0716-97602007000200001

59. Chen GY, Nunez G. Sterile inflammation: Sensing and reacting to damage. *Nat Rev Immunol* (2010) 10(12):826–37. doi: 10.1038/nri2873

60. Lau CM, Broughton C, Tabor AS, Akira S, Flavell RA, Mamula MJ, et al. Rna-associated autoantigens activate b cells by combined b cell antigen Receptor/Toll-like receptor 7 engagement. *J Exp Med* (2005) 202(9):1171–7. doi: 10.1084/jem.20050630

61. Qin C, Zhou J, Gao Y, Lai W, Yang C, Cai Y, et al. Critical role of P2y12 receptor in regulation of Th17 differentiation and experimental autoimmune encephalomyelitis pathogenesis. *J Immunol* (2017) 199(1):72–81. doi: 10.4049/jimmunol.1601549

62. Lin Y, Cong H, Liu K, Jiao Y, Yuan Y, Tang G, et al. Microbicidal phagocytosis of nucleus pulposus cells against staphylococcus aureus *Via* the Tlr2/Mapks signaling pathway. *Front Immunol* (2019) 10:1132. doi: 10.3389/fimmu.2019.01132

frontiers | Frontiers in Immunology

TYPE Original Research
PUBLISHED 18 May 2023
DOI 10.3389/fimmu.2023.1168517

OPEN ACCESS

EDITED BY
Heng Chi,
Ocean University of China, China

REVIEWED BY
Yan Zhao,
Tsinghua University, China
Jhon Carlos Castaño,
University of Quindío, Colombia

*CORRESPONDENCE
Dongling Zhang
zhangdongling@jmu.edu.cn

RECEIVED 17 February 2023
ACCEPTED 04 May 2023
PUBLISHED 18 May 2023

CITATION
Chen M, Lin N, Liu X, Tang X, Wang Z and Zhang D (2023) A novel antimicrobial peptide screened by a *Bacillus subtilis* expression system, derived from *Larimichthys crocea* Ferritin H, exerting bactericidal and parasiticidal activities. *Front. Immunol.* 14:1168517. doi: 10.3389/fimmu.2023.1168517

A novel antimicrobial peptide screened by a *Bacillus subtilis* expression system, derived from *Larimichthys crocea* Ferritin H, exerting bactericidal and parasiticidal activities

Meiling Chen[1], Nengfeng Lin[2], Xiande Liu[1], Xin Tang[1], Zhiyong Wang[1] and Dongling Zhang[1]*

[1]Key Laboratory of Healthy Mariculture for the East China Sea, Ministry of Agriculture and Rural Affairs, Jimei University, Xiamen, China, [2]Institute of Biotechnology, Fujian Academy of Agricultural Sciences, Fuzhou, China

Antimicrobial peptides (AMPs) may be the most promising substitute for antibiotics due to their effective antimicrobial activities and multiple function mechanisms against pathogenic microorganisms. In this study, a novel AMP containing 51 amino acids, named Lc1687, was screened from the large yellow croaker (*Larimichthys crocea*) *via* a *B. subtilis* system. Bioinformatics and circular dichroism (CD) analyses showed that Lc1687 is a novel anionic amphiphilic α-helical peptide, which was derived from the C-terminal of a Ferritin heavy subunit. The recombinant Lc1687 (named rLc1687) purified from *Escherichia coli* exhibited strong activities against Gram-positive (Gram+) bacterium *Staphylococcus aureus*, Gram-negative (Gram-) bacteria *Vibrio vulnificus, V. parahaemolyticus*, and *Scuticociliatida*. Scanning electron microscope (SEM) and transmission electron microscopy (TEM) revealed the possible function mechanisms of this peptide, which is to target and disrupt the bacterial cell membranes, including pore-forming, loss of fimbriae, and cytoplasm overflow, whereas gel retardation assay revealed that peptide Lc1687 cannot bind bacterial DNA. The peptide stability analysis showed that rLc1687 acts as a stable antimicrobial agent against Gram+ and Gram- bacteria at temperatures ranging from 25 to 100°C, pH 3-12, and UV radiation time ranging from 15 to 60 min. A hemolytic activity assay confirmed that this peptide may serve as a potential source for clinical medicine development. Taken together, Lc1687 is a novel AMP as it is a firstly confirmed Ferritin fragment with antimicrobial activity. It is also a promising agent for the development of peptide-based antibacterial and anti-parasitic therapy.

KEYWORDS

antimicrobial peptide, *Bacillus subtilis*, antibacterial, antiparasite, Ferritin heavy subunit, *Larimichthys crocea*.

1 Introduction

The discovery and use of antibiotics is one of the most important breakthroughs in medical history. However, the widespread use and misuse of antibiotics have led to the continuous acquisition of new genetic traits and resistance genes by bacteria. Furthermore, drug residues in food and the environment pose a great threat to human public health. These problems have become a major obstacle to the healthy development of aquaculture. In various substrates of mariculture farms, antibiotics resistance genes have extremely high abundances and pose potential ecological health risks (1, 2). Additionally, recently, the World Health Organization (WHO) highlighted that most antibiotic candidates are merely modifications of existing molecules and do not target drug-resistant Gram-negative (Gram-) bacteria. Nevertheless, infectious diseases in aquaculture are primarily caused by multi-resistant Gram- bacteria, and the water environment in which fish live is more conducive to the survival of bacteria and other microorganisms. Accordingly, the search for alternatives to synthetic antibiotics in aquaculture has become essential.

Antimicrobial peptide (AMP), as a native host defense peptide, is widely distributed in animals, plants, and microorganisms. It is routinely described as a class of small-molecular peptides (within 100 amino acids in length) with significant activities against bacteria, parasites, viruses, fungi, tumor cells, and inflammation (3). Most AMPs are cationic peptides, containing 2 to 13 positive charges, with a high proportion of hydrophobic residues (typically 50%) (4). These features allow AMPs to interact with negatively charged bacterial surfaces *via* electrostatic attraction and hydrophobic insertion causing membrane disorganization by inducing toroidal pore (i.e., wormhole), barrel-stave, and carpet model phenomena and, eventually, cell death (5). Besides these, some AMPs can penetrate the cell membrane to reach the interior of the cell, where they block critical cell processes, such as disturbing protein/nucleic acids synthesis, protein/enzyme activity, cell division, protein proper folding, etc. (6). In addition to killing bacteria directly, AMPs affect the host response to infection in multiple ways, including the modulation of chemokine and cytokine production, angiogenesis, endotoxin neutralization, and wound healing (7, 8). Furthermore, AMPs can affect the maintenance of the integrity of the intestinal barrier by stimulating mucus synthesis and promoting the production of tight junction proteins and the repair of the endothelium (9, 10). Interestingly, accumulating evidence shows the synergistic effects between AMPs or between AMPs and antibiotics, and these combinations can significantly reduce bacterial resistance (11–13). Owing to these favorable characteristics with infrequent drug resistance, broad-spectrum antimicrobial activities, rapid killing effects, and high capacity for synergies, AMPs have been considered attractive candidates for alternative antibiotics.

AMPs can be rapid screened from the natural source through various chromatography and high throughput sequence methods (14, 15). However, these methods are relatively complicated, and the predictions are not accurate enough. *Bacillus subtilis* is generally recognized as a safe (GRAS) food-grade microbial system. Due to its clear inherited background, simple and diverse genetic manipulation systems, high growth rate, short fermentation time, strong secretory ability, and accumulative fermentation experience, *B. subtilis* has been widely used as a cell factory for the microbial production of chemicals, enzymes, and antimicrobial materials in industry, agriculture, and medicine.

The large yellow croaker (*Larimichthys crocea or L. crocea*) is an important marine economic fish and is one of the traditional "four marine products" in China. *L. crocea* is extremely susceptible to bacteria and parasites, which lead to enormous economic damage (16, 17). Currently, there are numerous problems surrounding the culture of *L. crocea*, including bacterial multi-resistance, the absence of effective drugs against parasites, food drug residues, and environmental contamination of antibiotics. Therefore, there is an urgent need to develop natural antimicrobial agents.

In the current study, a novel AMP was identified from *L. crocea* using a *B. subtilis* expression system, and further studies were performed to explore their antibacterial and anti-parasitic activities. To determine the basis of the host–pathogen interaction, the mechanism of action of AMP was investigated, and the stabilities and safety of this peptide were also estimated.

2 Materials and methods

2.1 Pathogen cultures and fish tissue collection

Staphylococcus aureus, Pseudomonas plecoglossicida, Vibrio vulnificus, and *V. parahaemolyticus* were preserved in our laboratory. *B. subtilis* SCK46 was presented by Professor Wubei Dong from Huazhong Agricultural University in Wuhan, China. All bacteria were cultured on Luria-Bertani (LB) media at 37 °C or 28 °C. *Scuticociliatida* was isolated from *L. crocea* by our team and maintained in our laboratory. Specifically, in mid-April 2019, the infected fish was obtained from Fuding City, Fujian Province, China. The fish was dissected, and the gills were put into a plate full of seawater. *Scuticociliatida* swam in seawater and were then drawn into a 6-well plate. The parasites were cultured at 16 °C and fed *Escherichia coli* once every day.

Health *L. crocea* (~10 g) was obtained from a Guanjingyang Company Limited in Ningde, Fujian province, China. The fish was acclimatized in the filtered and aerated seawater (25 °C) and fed a commercial feed twice daily for two weeks before conducting the experiments. The immersion method was used in the challenge experiment. The *Pseudomonas plecoglossicida* was cultured for 18 hours before challenge, and the fish was exposed to bacteria at a concentration of 1×10^6 CFU/mL for 3 hours. Samples (liver, spleen, and kidney) were collected at different time points (24h, 48h, 72h) and then immediately frozen in liquid nitrogen, and saved at -80 °C.

2.2 *L. crocea* cDNA library construction

Total RNA was extracted with TransZol^{TM} Up Plus RNA Kit (Invitrogen, USA). The obtained mRNA was purified using

PolyATtract® mRNA Isolation Systems (Promega, Madison, WI, USA). The quality of total RNA and purified mRNA was detected by 1% agarose gel electrophoresis. cDNA library construction refers to Abbas' method (18). Briefly, the Double-stranded cDNA was prepared with a specific oligo(dT) primer (containing an Xba I cleavage site). Three pairs of primers containing Nde I cleavage site adaptor were added to the cDNA library. The library and a pBE-S vector were then digested with Xba I and Nde I restriction enzyme (TaKaRa, Dalian, China), followed by their ligation by T4 ligase. Finally, the ligation products were transformed into *B. subtilis* SCK6 cells and incubated at 37 °C overnight. Individual colonies were picked, colony PCR was performed using pBE-S-F and pBE-S-R primers (Table S1) to confirm the cDNA library quality, and then colonies were saved at −80 °C.

2.3 Candidate genes screening

Transformants from the cDNA library were plated on LB plates containing kanamycin (10 mg/L) and incubated at 37 °C to observe the phenotype. The strains with lethal phenotype would be validated through three repeat bacterial spotting tests, and then the strains with stable lethal phenotype were sequenced.

2.4 Crude protein extraction

We only extracted the extracellular protein because *B. subtilis* has a high capacity to secrete protein directly into the extracellular medium. The strains with stable lethal phenotype were fermented at 180 r/min, at 37 °C for 72 h. The supernatant was collected by centrifugation at 10,000 r/min, 4 °C for 30 min. Saturated ammonium sulfate solution at the final concentration of 50%-60% was slowly added into the supernatant and stirred continuously on ice for at least 20 min. The solution was then maintained at 4 °C for overnight. The next day, the separated protein was centrifuged using the aforementioned conditions-. The collected precipitation was dissolved in 25 mM PBS (pH 7.0) and dialyzed in the same PBS buffer for 24 h at 4 °C. The insoluble debris was discarded by centrifugation.

2.5 Antibacterial activity analysis of the extracellular protein

Antibacterial activity assay of the extracellular protein was performed using disk diffusion. Indicator bacteria *S. aureus, V. vulnificus*, and *V. parahaemolyticus* (1×10^8 cfu/mL) were mixed with LB media and poured over previously prepared LB plates. Then, 4 mm diameter filter paper disks were placed on the agar plates and 20 µl extracellular proteins (1000 µg/mL) were added to each filter paper. Hereafter, the plates were incubated for 12 h at the different temperatures required for the different indicator bacteria. Antibacterial activity was confirmed by measuring the diameters of inhibition zones. The extracellular protein of null vector pBE-S was set as the control.

2.6 Bioinformatics analysis and circular dichroism spectrophotometry

Homology analysis of Lc1687 was performed using the BLAST program at NCBI (http://www.ncbi.nlm.nih.gov/blast). The molecular weight (MW) and isoelectric point (pI) of protein are predicted on the EXPASY server (http://www.expasy.org/). A three-dimensional protein model was constructed using Vector NTI Suite 8 and Phyre2 (http://www.sbg.bio.ic.ac.uk/phyre2, 30 September 2019). The helical wheel analysis was performed with Heliquest. The bioinformatics results were corroborated by the findings of circular dichroism (CD).

The circular dichroism analysis was carried out using a spectropolarimeter (Chirascan V100, Applied Photophysics Ltd). The peptide was dissolved in 0.2 M PBS (pH 7.3) to a final concentration of 1.0 mg/mL, and PBS served as the control. The samples were put into 1 mm path length quartz cuvettes and the data were recorded from 190 to 260 nm. The scanning speed of the CD spectrum was 100 nm/min, with data recorded at 1.0 nm intervals. The circular dichroic absorption value was calculated using the following equation: $[\Theta]= mdeg\times M/(l0\times c\times nr)$. Where mdeg is the CD value, M is the molar mass of the peptide, c is the concentration of the peptide, and nr is the number of amino acid residues.

2.7 Expression and purification of antimicrobial peptide

Antimicrobial peptide Lc1687 was expressed using a pET-32a vector. Primers Lc1687-F/R (Table S1) with restriction sites were used to amplify the *Lc1687* gene. The target PCR fragment was inserted into the expression vector pET-32a with TRX-His-tag after being digested with EcoRI and XhoI restriction enzymes (TaKaRa, Dalian, China). The recombinant plasmid (pET-32a-Lc1687) and the parent vector pET-32a (negative control) were both transformed into *E. coli* BL21 (DE3) and expressed with IPTG induction at 20 °C for 16 h. The bacteria were harvested by centrifugation at 7,000 r/min for 20 min and resuspended in buffer A (20 mM imidazole, 10 mM Na_2HPO_4, 140 mM NaCl, 1.8 mM KH_2PO_4, 2.7 mM KCl, pH 7.4) for sonication. Afterward, the supernatant was collected by centrifugation at 12,000 g for 20 min and loaded onto a His-tag column. The His-tag column was equilibrated with buffer A, followed by washing with buffer B (40 mM imidazole, pH 7.4) to remove non-target proteins, and, finally, the target protein was collected with elution buffer (500 mM imidazole, pH 7.4). The purified protein was analyzed by 12% SDS-PAGE and dialyzed with PBS buffer (0.01M, pH 7.4) for desalination.

2.8 Antibacterial activity analysis and minimum inhibitory concentration determination of recombinant Lc1687 (rLc1687)

Antibacterial activity assay of the recombinant protein was performed using Oxford cup diffusion. The method was similar to

the previously described disk diffusion, except that the filter paper disk was replaced with an Oxford cup, the protein 50 μl (500 μg/mL) was added into the cup, and the empty vector protein was set as the control. In addition, the protein was diluted into 1000, 500, 250, 125, 62.5, 31.25, and 15.63 μg/mL with PBS (0.01 mol/L, pH 7.4) to determine the MIC. The three inhibition zones on the same solid plate are for three experimental replicates.

2.9 Scanning electron microscopy

Bacterial cell surface morphology was observed by SEM. Indicator bacteria (1.0×10^8 cfu/mL) were incubated with the same volume of antimicrobial peptide rLc1687 (500 μg/mL) at the different temperatures required for the bacteria for 2 h. The empty vector protein was substitute for rLc1687 as the control. The samples were subsequently fixed with 2.5% glutaraldehyde aqueous solution for 3 h at 4 °C and dehydrated in a series of ethanol solutions (50%, 70%, 90%, 95%, and 100%). Finally, the samples were lyophilized, gold coated, and observed using a scanning electron microscope (Hitachi S-4800, Japan).

2.10 Transmission electron microscopy

The ultrastructural changes in bacteria induced by antimicrobial peptide rLc1687 were examined by TEM. Indicator bacteria (1.0×10^8 CFU/mL) were incubated with equal volume antimicrobial peptide rLc1687 (500 μg/mL) at 28 or 37 °C for 1.5-2 h. The bacteria added to empty vector protein served as the controls. The samples were dropped onto a cropper mesh, followed by 2.0% phosphotungstic acid negative staining for 60 sec before being imaged on an H-7650 transmission electron microscope (Hitachi, Japan).

2.11 Gel retardation assay

To explore whether the AMP destroys nucleic acids of pathogenic bacteria, a gel retardation assay was performed to analyze bacterial DNA integrity. Bacterial genomes were extracted by FastPure® Bacteria DNA Isolation Mini Kit (Vazyme, Nanjing, China). AMP rLc1687 was incubated with the bacterial genome in various proportions (4:1, 3:2, 2:3, and 1:4) at room temperature for 1 h, following the DNA integrity check using 1% gel electrophoresis. The bacterial genome was used as a blank control.

2.12 Anti-parasitic activity analysis of rLc1687

The isolated *Scuticociliatida* was cultured in a petri dish at 16 °C with sterilized seawater. On the third to fourth day, when the ciliates adapted to the culture and were able to expand steadily, they were used in the following experiment. Approximately 300 ciliates were added into a 48-well plate (a total volume of 1.5 mL) containing a final concentration of 500 μg/mL rLc1687 and then incubated at 16 °C. The ciliates were observed under an ordinary light microscope at 15 min, 30 min, 1h, and 2 h. The protein purified from the null vector was substitute for rLc1687 as the control.

2.13 Stability assay of rLc1687

To explore whether the antimicrobial activity of rLc1687 is affected by environmental factors, rLc1687 was treated with gradient temperature, pH, and UV irradiation time, then its antibacterial activity was detected using the Oxford cup diffusion method. The work concentration of rLc1687 is 1000 μg/mL. For the thermal stability test, the peptide was heated at 25, 50, 75, and 100 °C for 30 min before use. For the pH assay, rLc1687 solution was adjusted with HCL and NaOH to pH 3, 5, 7, 11, and 12. For UV irradiation, the peptide was irradiated for 15, 30, 45, and 60 min.

2.14 Hemolytic activity assay of rLc1687

The hemolytic activity of rLc1687 was assessed according to the previously described method with slight modifications (19). Briefly, fresh blood was taken from the *L. crocea* tail vein and centrifuged at 3,000 r/min for 5 min to collect the erythrocytes then washed three times with a TBS buffer (0.20 M, pH 7.2) and resuspended in the same solution (1.50% v/v). The erythrocyte suspension was mixed with different concentrations of protein solutions (0, 15.625, 31.25, 62.5, 125, 250, 500, 1000 μg/mL) in equal volumes. TBS buffer was used as a negative control (no hemolysis), and double-distilled water was used as a positive control (complete hemolysis). The hemolytic activity percentage was calculated using the following equation: hemolysis (%) = [(test group A_{520} - negative control group A_{520})/(positive control group A_{520} - negative control group A_{520})] ×100%.

2.15 Statistical analysis

All experiments were performed with at least three replicates. Data were expressed as the mean ± standard error of the mean (SEM). Statistical analysis was performed by a one-way ANOVA, LSD multiple comparison test, and independent sample t-test using SPSS 20.0. $P<0.05^*$ and $P<0.01^{**}$ indicated a statistical significance between groups.

3 Results

3.1 Candidate gene from an *L. crocea* cDNA library exhibited antimicrobial potential

A high-quality *L. crocea* cDNA library was constructed (Figure S1). A total of 3,086 clones from the cDNA library were spotted on LB solid media. During initial screening, strain 1687 exhibited cell lysis at

72 h post-incubation at 37 °C (Figure 1A). Three repeat tests for the bacterial spotting plate confirmed this result (Figure 1B). These investigations suggested that the protein encoded from the inserted fragment in the 1687 strain has the potential to inhibit or kill microorganisms.

3.2 The extracellular protein in the 1687 strain exhibited antibacterial activity

Extracellular protein of the 1687 strain was extracted using the ammonium sulfate precipitation method, and its antibacterial activity was further detected using the disk diffusion method. The results revealed that the 1687 protein (named Lc1687) exhibited more significant antibacterial activity against Gram+ bacterium *S. aureus* as well as Gram- bacteria *V. vulnificus*, and *V. parahaemolyticus* compared to the control *B. subtilis* SCK6 (Figure 2). Among these, the strongest antibacterial activity exhibited by Lc1687 was against *V. vulnificus*. The results again confirmed that the *B. subtilis* 1687 strain harboring protein possesses the ability to restrict the growth of Gram + and Gram- bacteria.

3.3 Lc1687 is a novel anionic amphipathic α-helical antimicrobial peptide derived from a Ferritin heavy subunit

Lc1687 (CDFIETHYLDEQVKSIKELADWVTNLRRMGAPQ NGMAEYLFD-KHTLGKESS) is a C-terminal fragment of a Ferritin heavy subunit (Ferritin H). The tertiary structure analysis showed that Lc1687 contains long and short α-helices, whereas the whole Ferritin H in *L. crocea* has five α-helical structures (Figures 3A, B). A helical wheel analysis implied that Lc1687 is an anionic antimicrobial peptide with a total net charge of -3 at neutral pH 7.4. Moreover, Lc1687 exhibits good amphipathic properties with a hydrophobicity of 0.311 and a hydrophobicity moment of 0.217. The hydrophobic face is composed of YLCL (Tyr, Leu, Cys, Tyr), whereas the charged residues are on the hydrophilic side (Figure 3C). The calculated molecular weight (MW) of Lc1687 is 6,047.87 Da with a theoretic isoelectric point (pI) of 5.11. Additionally, circular dichroism analysis revealed that peptide Lc1687 exhibited one positive absorption peak at 190 nm and two negative absorption peaks at around 208 nm and 220 nm in PBS solution, which is a typical α-helical structural characteristic of circular dichroism (Figure 3D), and the results are consistent with foregoing structure prediction (Figure 3A). This peptide is considered to be a novel antibacterial peptide because no previous reports have revealed which Ferritin fragment has the ability to restrict bacterial growth. And it had no homology with any peptide in the antimicrobial peptide database (APD). The series analysis showed that Lc1687 is a novel anionic amphipathic α-helical antimicrobial peptide derived from Ferritin H.

3.4 Capture and purification of recombinant protein

The parent vector pET-32a and the plasmid pET-32a-Lc1687 were transformed into *E. coli* BL21 (DE3). After IPTG induction, purification, and SDS-PAGE analysis, one approximate 20 kDa (Trx tag + S tag + 6 × His tag) band was visualized (Figure 4, lane 7), and the recombinant Lc1687 (named as rLc1687) exhibited a distinct band at ~26 kDa (Figure 4, lane 4/5/8), corresponding to the prediction for Lc1687 6.05 kDa plus a 20 kDa of TRX-S-His-tag. The fusion protein mainly appeared in solution form (Figure 4-lane 5). The results indicated that rLc1687 was successfully expressed in a prokaryotic system.

3.5 rLc1687 possesses antibacterial activity in a low dose

The antibacterial activity of purified rLc1687 was checked using the Oxford cup diffusion method. The results revealed that rLc1687 displayed significant levels of inhibition against *S. aureus*, *V.*

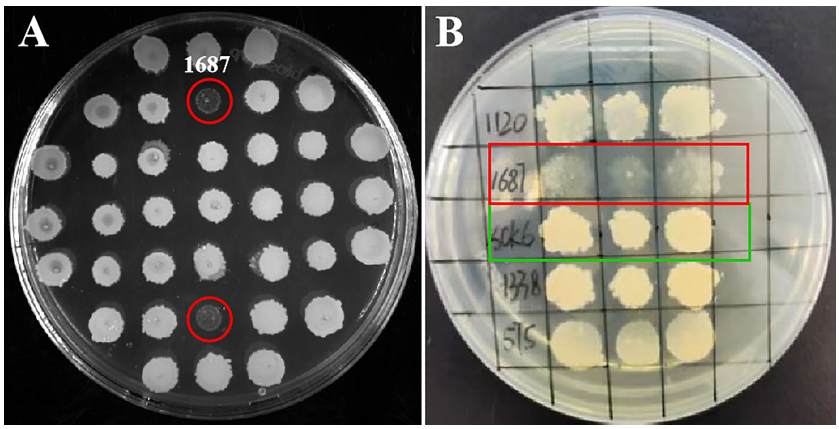

FIGURE 1
Screening antimicrobial gene from *L. crocea* cDNA library. The engineered *B. subtilis* strain 1687 (red marks) and SCK6 control (green mark) were separately spotted onto LB plates and incubated at 37 °C for 72 (h) **(A)** Initial screening of antibacterial genes; **(B)** Repeat screening of antibacterial genes (*n*=3).

10.3389/fimmu.2023.1168517

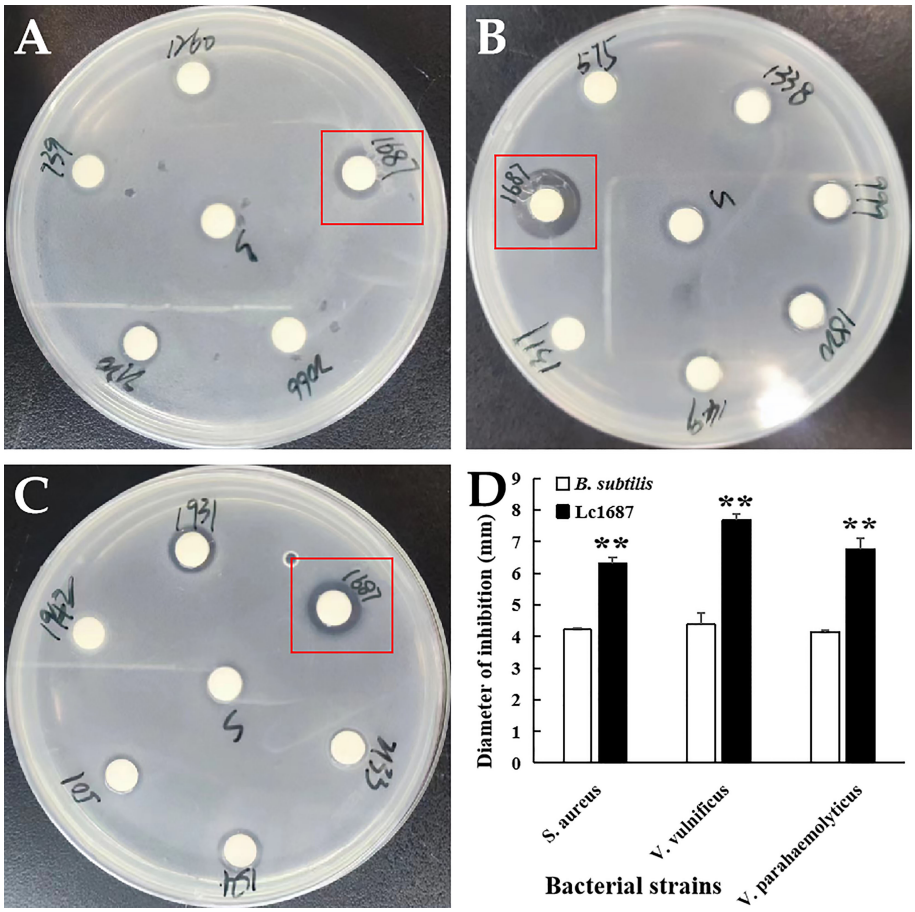

FIGURE 2
Antibacterial activity of extracellular protein Lc1687. **(A)** *S. aureus*; **(B)** *V. vulnificus*; **(C)** *V. parahaemolyticus*; **(D)** Diameter of inhibition zone. The meaning of the symbol ** is extremely significant.

vulnificus, and *V. parahaemolyticus* (Figure 5). Moreover, once again, the strongest antibacterial activity exhibited by peptide Lc1687 was confirmed to be against *V. vulnificus*, of the three indicated bacteria. The control empty vector protein exhibited no antibacterial activity against the three indicator bacteria.

A serial dilution of rLc1687 was used to measure MIC with the Oxford cup diffusion method. As shown in Figure 6, with the decrease in rLc1687 concentration, the inhibition zone diameters of various indicator bacteria also gradually decrease. The diameter of the inhibition zone against *S. aureus* was 2.10 mm at an rLc1687 concentration of 62.5 μg/mL, and the diameters against *V. vulnificus* and *V. parahaemolyticus* were, separately, 2.0 *mm* and 1.50 mm at an rLc1687 concentration of 31.25 μg/mL. No activity was observed at lower protein concentrations. In conclusion, the MICs of rLc1687 against the three indicator bacteria were 31.25-62.5, 15.625-31.25, and 15.625-31.25 μg/mL, respectively.

3.6 Antibacterial mechanisms analysis of rLc1687

The bactericidal mechanism of AMPs is commonly through the disruption of cell membranes or through targeting certain intracellular components, such as DNA. To investigate the possible mechanisms for the bactericidal function of rLc1687, firstly, we employed the SEM method to visualize bacterial surface integrity (Figure 7). The SEM results revealed that the three indicator bacteria showed noticeable membrane pore formation and cytoplasm outflow after treatment with rLc1687, but the three bacterial morphologies were different. *S. aureus* shrinks exceptionally (Figures 7A, B), and the cells became deformed and stuck together, whereas two vibrio strain (*V. vulnificus* and *V. parahaemolyticus*) surfaces became smoother, compared to the controls, due to the loss of pilis (Figures 7C–E). The bacterial ultrastructure changes were further examined by TEM; the control group bacteria had evenly distributed intact cell membranes, whereas the test group bacteria had drastic changes (Figure 8). Deformation and disruption of cell walls and cell membranes, as well as cytoplasm outflow, were observed in the test group. Finally, we wondered whether rLc1687 kills the three bacteria by targeting intracellular molecules. The results show that rLc1687 cannot bind directly to the genomic DNA of the three indicator bacteria (Figure S2). Collectively, rLc1687 kills bacteria by disrupting the membrane integrity and leading to cytoplasm overflow for both Gram+ and Gram- bacteria, without binding bacterial DNA.

10.3389/fimmu.2023.1168517

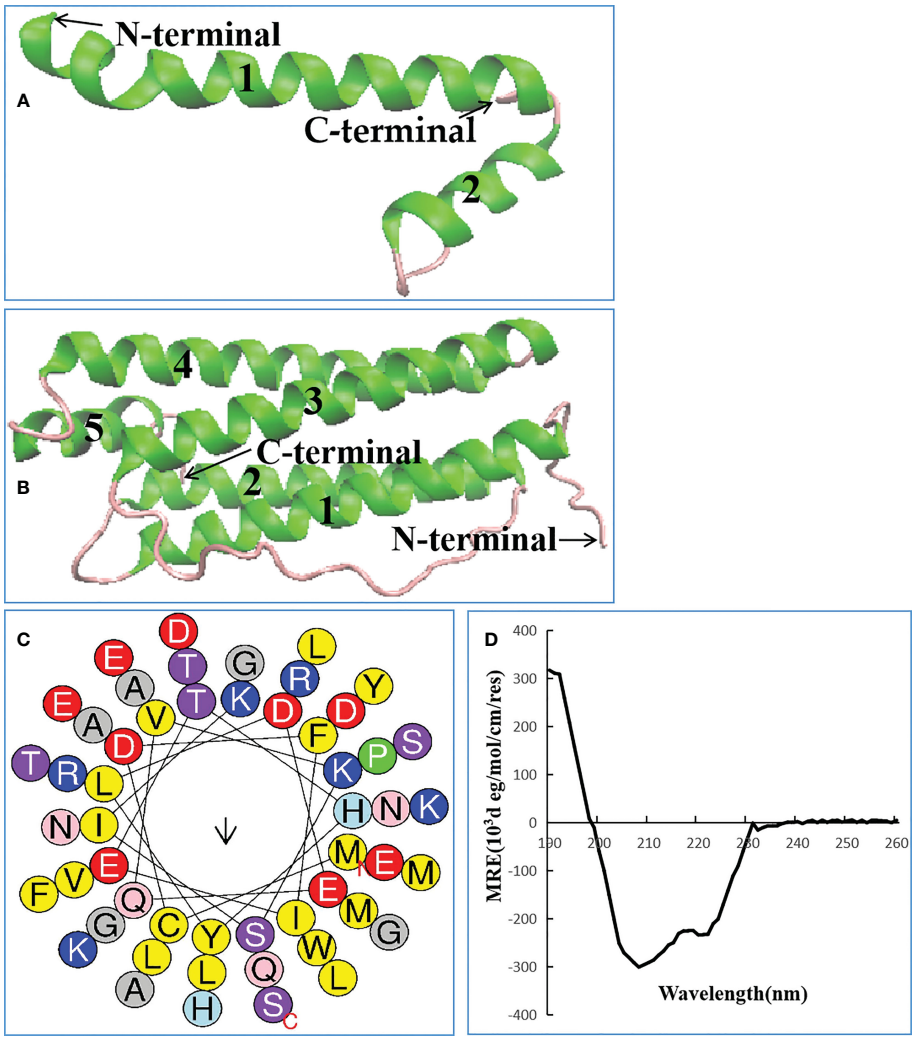

FIGURE 3
Biological characteristics of Lc1687. **(A)** Antibacterial peptide Lc1687, **(B)** *L. crocea* Ferritin (H) The numbers 1-5 represent α helical structure marked with green, and purple indicates random coil; **(C)** Helical wheel diagram. The black arrows indicate the direction of the hydrophobic moment, different kinds of residues are presented in different colors, hydrophobic residues are shown in yellow, and blue circles represent cationic residues; **(D)** Circular dichroism pattern at 25°C.

3.7 rLc1687 exhibits potent killing *Scuticociliatida* directly

In order to determine the damaging effects of recombinant rLc1687 on *Scuticociliatida*, the ciliates were incubated with the peptide and then observed using a light microscope. As shown in Figure 9, in the control group (Figure 9A), the ciliates swam freely and maintained *Helianthus annuus*-like morphology. The surface cilia were intact and internal food vacuoles were clearly visible. After incubation for 15 min (Figure 9B), the ciliates swam slowly; most of the food vacuole membranes were destroyed. After incubation for 30 min (Figure 9C), the food vacuoles completely disappeared and partial cilia disappeared. After incubation for 1 h (Figure 9D), the parasites became small and most of the cilia disappeared. After incubation for 2 h (Figure 9E), the parasite cell membranes were completely destroyed and intracellular protoplasm spilled out. There is no doubt that rLc1687 has the ability to kill *Scuticociliatida*.

3.8 rLc1687 is a relatively stable and safe antimicrobial agent for bony fish

AMPs usually have a certain resistance to various environmental factors. To investigate the possible effects, we set up several different conditions and then measured the antibacterial activity of AMPs. The results indicated that rLc1687 acts as a stable antimicrobial agent against Gram+ and Gram- bacteria at temperatures ranging from 25 to 100 °C, at pH 3-12, and under UV radiation for 15 to 60 min (Figure 10).

Hemolytic activity assays were performed on *L. crocea* blood cells. We found that the hemolysis rate of rLc1687 at the extremely

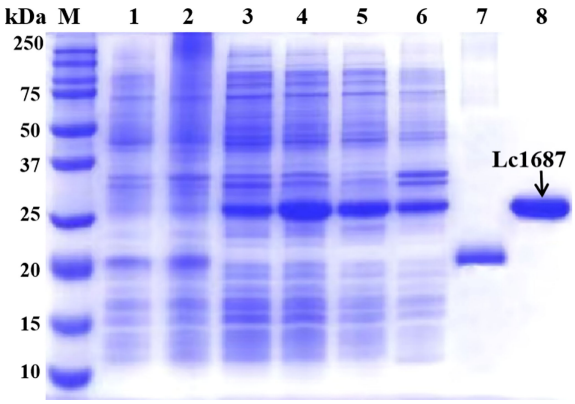

FIGURE 4
Expression and purification of recombinant Lc1687. Lane M, protein marker; 1: Non-induced empty vector pET-32a; 2: Induced empty vector pET-32a; 3: Non-induced pET-32a-Lc1687; 4: Induced pET-32a-Lc1687; 5: pET-32a-Lc1687 supernatant; 6: pET-32a-Lc1687 precipitate; 7: Purified Trx-His-tag; 8: Purified rLc1687.

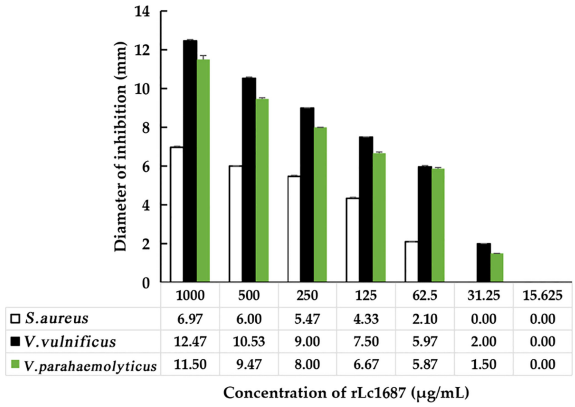

	1000	500	250	125	62.5	31.25	15.625
S.aureus	6.97	6.00	5.47	4.33	2.10	0.00	0.00
V.vulnificus	12.47	10.53	9.00	7.50	5.97	2.00	0.00
V.parahaemolyticus	11.50	9.47	8.00	6.67	5.87	1.50	0.00

FIGURE 6
MIC determination of rLc1687 antibacterial activity against three indicator bacteria.

high concentration of 1000 mg/L was 2.5% (Table 1). According to our results, no significant hemolytic activity was observed against *L. crocea* blood cells. Taken together, it is likely that this peptide is a relatively stable and safe antimicrobial agent for bony fish.

4 Discussion

In aquaculture, the accumulation of antibiotics results in the development of resistance among bacterial pathogens. As a result,

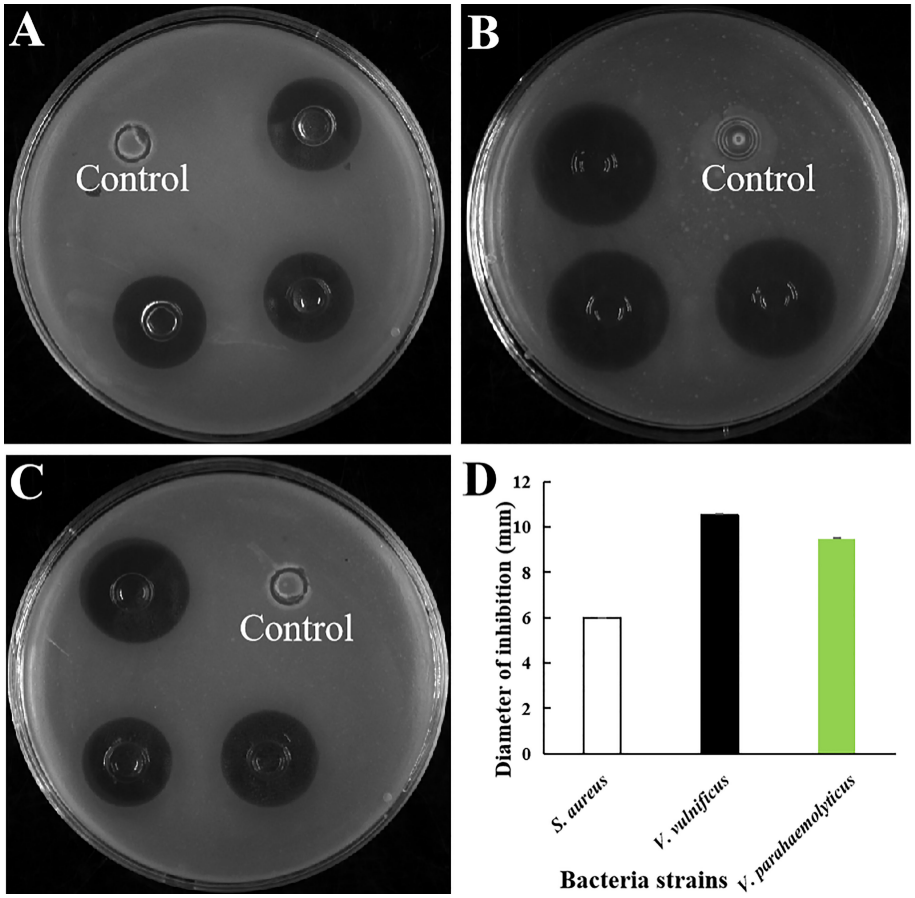

FIGURE 5
Antibacterial activity of rLc1687. **(A)** *S. aureus*; **(B)** *V. vulnificus*; **(C)** *V. parahaemolyticus*; **(D)** Diameters of inhibition zones. The empty vector protein was substitute for rLc1687 as the control. The three inhibition zones on the same solid plate served as three experimental replicates.

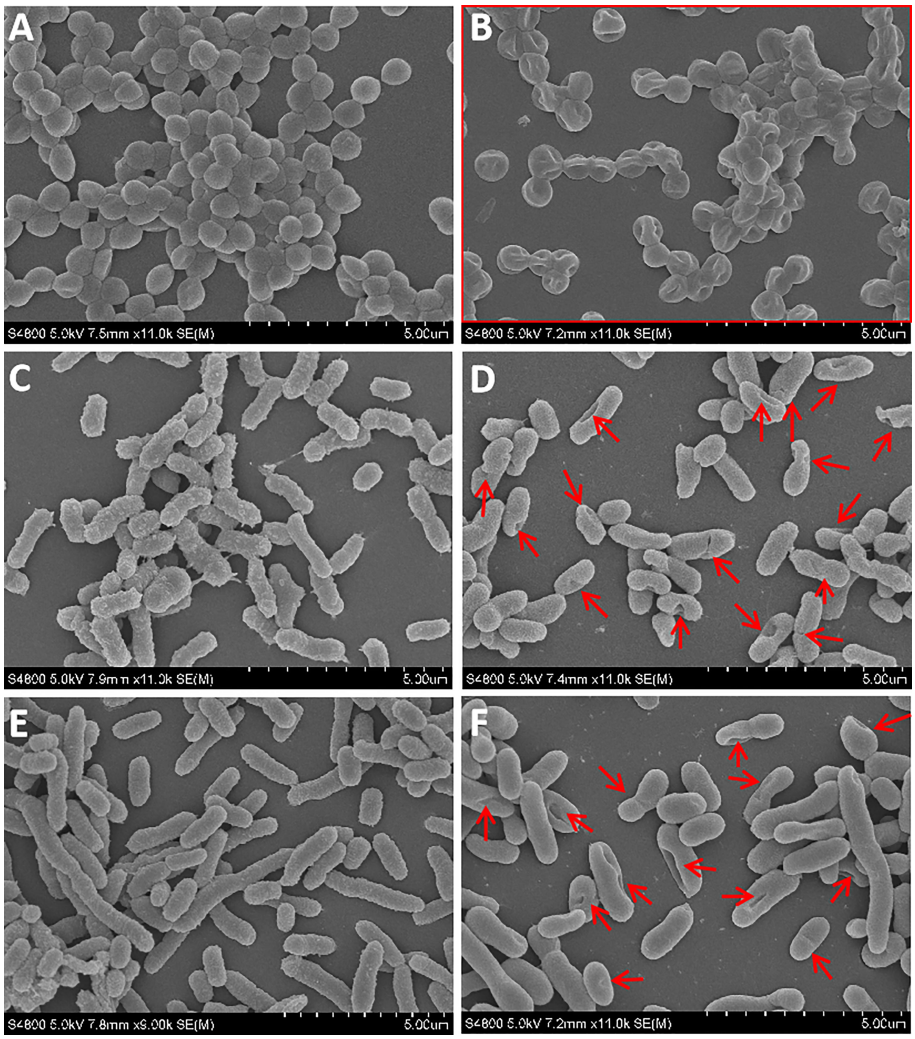

FIGURE 7
SEM observation on the damaged bacteria. **(A, C, E)** *S. aureus*, *V. vulnificus*, and *V. parahaemolyticus* blank control; **(B, D, F)** *S. aureus*, *V. vulnificus*, and *V. parahaemolyticus* were incubated with rLc1687, respectively; The rectangles and red arrows represent damaged bacteria. The empty vector protein was substitute for rLc1687 as a control.

strong efforts have to be directed toward finding AMPs as alternatives to traditional antibiotics. *B. subtilis* acts as a host cell facilitating soluble and secretory protein expression and is, therefore, particularly effective at producing peptide and protein. In the current study, we screened out a novel antibacterial peptide based on the damaging or killing of the peptide on *B. subtilis* host cells. A drawback of this method is that strong AMPs might not be selected because they kill *B. subtilis* cells too quickly to detect clones, so weakly killed AMPs are preferred. However, *B. subtilis* has a good secretory system, which may decrease the toxicity of strong AMPs. In addition, during the first few hours (12 h), the concentration of strong AMPs is possibly not high enough to kill the cells. These factors make the selection of strong AMPs feasible. In this study, the Lc1687 clone demonstrated a killing effect on *B. subtilis* at 72 h after spotting on the LB plate. Our follow-up investigation confirmed that both repeated selection and extracellular protein exhibit powerful antibacterial activity.

Blast analysis showed that Lc1687 is derived from Ferritin H and located at the C-terminal. Ferritin is a globular protein complex with 24 subunits and has a hollow shell-like structure, which can mineralize up to 4500 iron atoms. In vertebrates, it comprises two Ferritin subunits (heavy subunit-H and light subunit-L) encoded by two different genes (20). Ferritin was involved in the immune response as an acute phase reaction protein in the invasion of pathogens. The transcript level of these ferritins could be significantly induced under infection. Importantly, they were able to exhibit resistant activity to bacterial growth. Zheng et al. verified that a Ferritin in *Scapharca broughtonii* could inhibit the growth of Gram- bacterium *E. coli*, Gram+ bacteria *M. luteus*, and *S. aureus* (21). Jung et al. demonstrated that Ferritin subunits (H and M) of *Liza haematocheila* possess antibacterial activity against *E. coli* along with iron sequestration activity (22). Ding et al. also indicated that two Ferritin subunits (H and M) from *Megalobrama amblycephala* could inhibit the growth of

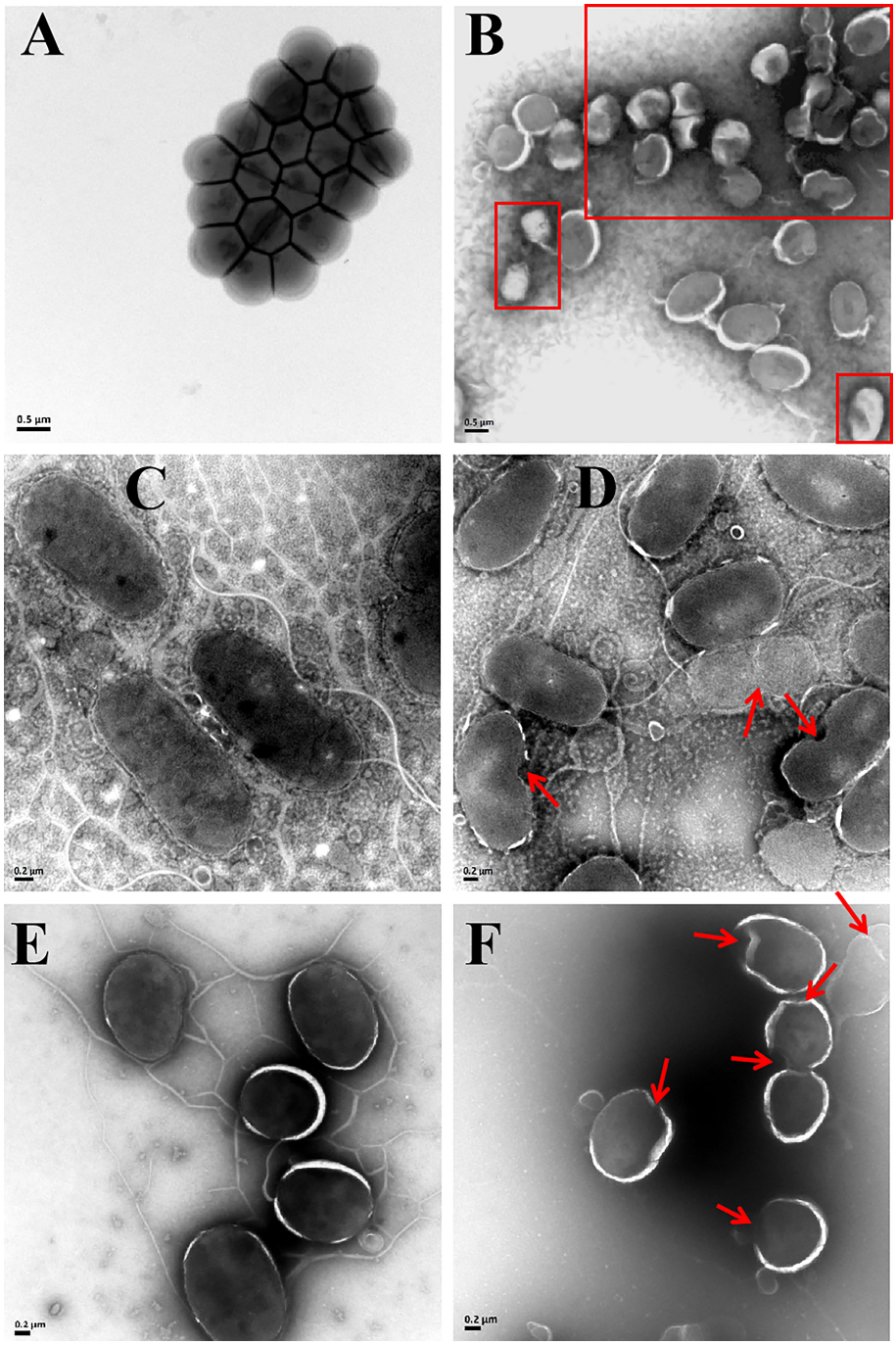

FIGURE 8
TEM images of *S. aureus* **(A, B)**, *V. vulnificus* **(C, D)**, and *V. parahaemolyticus* **(E, F)** under the empty vector protein **(A, C, E)** and rLc1687 treatments **(B, D, F)**, respectively. The rectangles and red arrows represent damaged bacteria.

Aeromonas hydrophila (23). In addition, Ferritin is also involved in the innate defense against viruses. The WSSV copy number in *ferritin*-silenced shrimp was much higher than that in the control group (24). Unfortunately, previous reports have indicated that Ferritin can serve as a bacterial growth inhibitor, whereas no direct killing effect was characterized. In the present study, the extracellular Lc1687 and recombinant rLc1687 exhibited strong bactericidal action against Gram+ bacterium *S. aureus*, Gram- bacteria *V. vulnificus*, and *V. parahaemolyticus*, as well as killing effects on parasitic *Scuticociliatida*. This peptide is considered to be a novel antimicrobial peptide, as no previous reports have revealed that Ferritin fragments are able to constrain the growth of Gram+ or Gram- bacteria.

Lc1687 is a novel anionic antibacterial peptide with α-helical and amphipathic characteristics. Anionic antimicrobial peptides (AAMP) are very rare, and it is thought that these peptides are complements of cationic antimicrobial peptides (CAMP) and have different mechanisms of action. Based on the available experimental

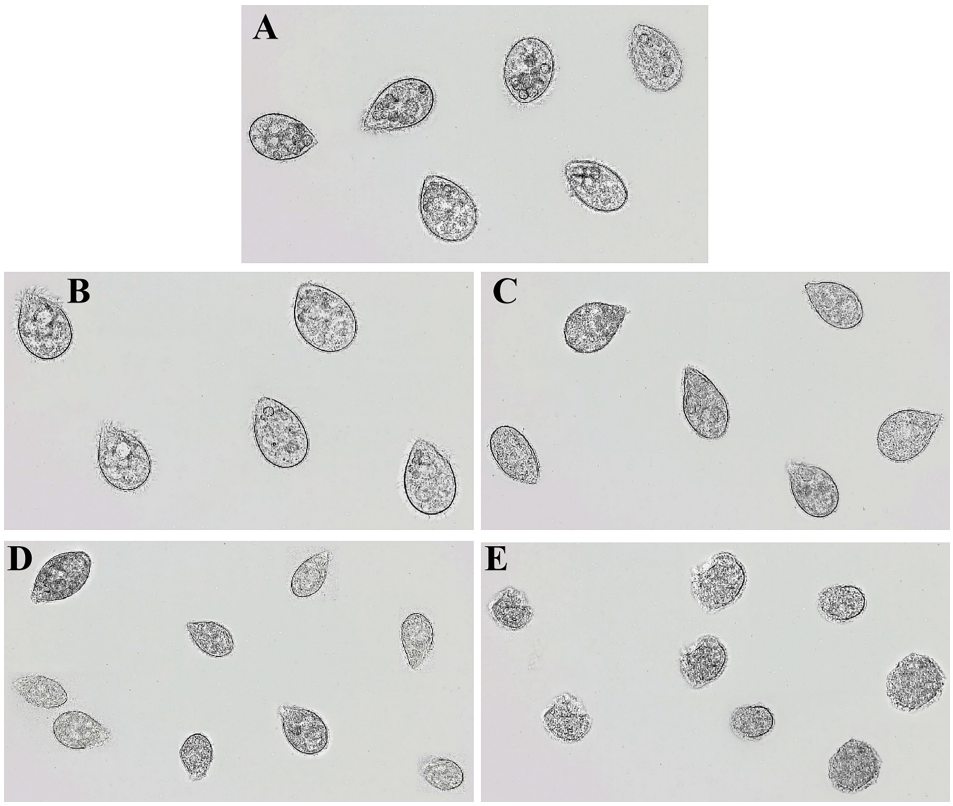

FIGURE 9
Anti-*Scuticociliatida* activity of rLc1687. The ciliates were cultured without **(A)** and with **(B–E)** rLc1687 for 15 min **(B)**, 30 min **(C)**, 1 h **(D)**, and 2 h **(E)** and then visualized under a light microscope, respectively.

evidence, membrane interaction is a key step in the antimicrobial mechanism of AAMPs, including the Shai-Huang-Matsazuki model of membrane interaction and toroidal pore formation, as well as membranolysis *via* tilted peptide formation (25, 26). For example, DCD-1L, one of the best-studied AAMPs, is able to bind to negatively charged bacterial surfaces as an amphiphilic α-helix and then assemble into an oligomeric state. The oligomerization DCD-1L has the capacity to form ion channels in the bacterial membrane, resulting in cell death (27). In addition, α-helical structure is also an important characteristic of AMP. In our study, peptide Lc1687 has the typical α-helical structural characteristics of circular dichroism. The SEM and TEM observations showed that Lc1687 resulted in bacterial cell membrane damage, including shrinkage, distortion, pore formation, and rupture. It appears that some pilis fall off from the surface of *V. vulnificus* and *V. parahaemolyticus*. We incubated this peptide with the genomes of different pathogens, but it did not cause DNA degradation. Based on these investigations, we assume that the possible mechanism of the Lc1687 peptide is to interrupt and rupture the cell membrane, as well as weaken the adhesion and motility of bacteria.

Accumulated evidence has demonstrated that AMPs have antimicrobial activities against a diverse range of pathogens. The Lc1687 peptide was consistent with previously reported AMPs due to its significant inhibitory effect against Gram+ and Gram- bacteria. The MICs for rLc1687 were 31.25-62.5 (5.17-10.33 μM), 15.625-31.25 (2.58-5.17 μM), and 15.625-31.25 (2.58-5.17 μM) μg/mL against *S. aureus*, *V. vulnificus*, and *V. parahaemolyticus*, respectively. Similarly, AAMPs Kappacins A and B, isolated from bovine milk, have been shown to exhibit activity against a range of Gram+ and Gram- oral bacteria with MICs in the 26-44 μM range (28). In contrast, maximin H5 derived from the skin of *Bombina maxima* possesses a net charge of -3 and exhibits weak activity against *S. aureus*, with an MIC of 800 μM and exhibits no activity against Gram- bacteria and fungi (29). In addition to bacterial killing effects, rLc1687 demonstrates forceful anti-parasitic activity against *Scuticociliatida* in our study.

The water environment in which fish live is extremely complex. The production of AMPs and the different forms of administration can cause some effects of the external environment on antibacterial activity. In our study, we found that rLc1687 has a high tolerance to heat, pH, and UV and that it is stable at low pH and high-temperature conditions. Furthermore, AMPs exhibit damaging effects against diverse microorganisms, but their safety in animals and humans is still an open question (30). As previously reported, some AMPs have shown low hemolytic activity against mammalian blood cells (31). In this study, low hemolytic activity in fish was observed at an extremely high peptide concentration. Therefore, we

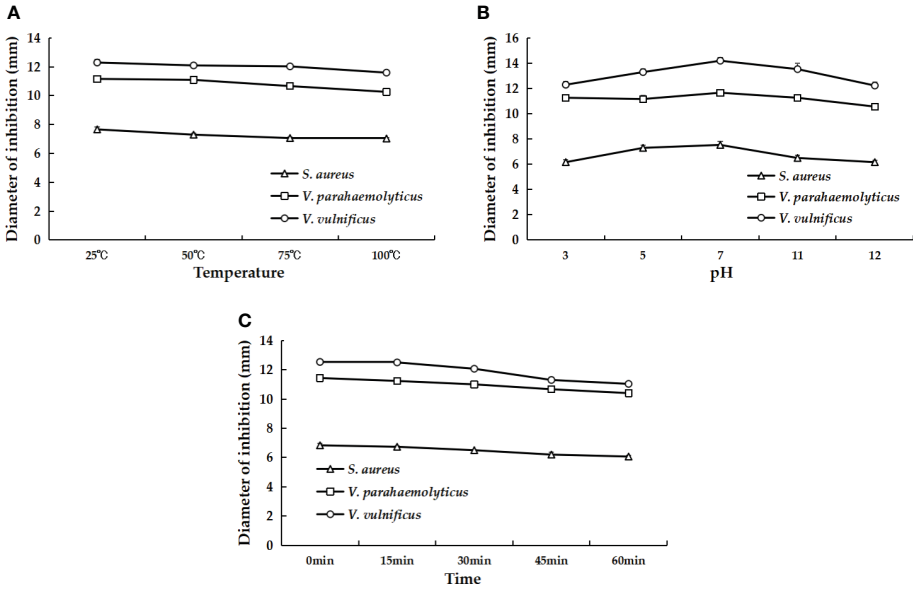

FIGURE 10
The effects of different temperatures **(A)**, pH values **(B)**, and UV irradiation times **(C)** on the antibacterial activity of rLc1687.

TABLE 1 *Hemolytic activity of* rLc1687 *against* L. crocea blood *cells.*

Treatments	Percentage hemolysis at different concentrations (μg/mL)							
	0	15.625	31.25	62.5	125	250	500	1000
Lc1687	0.00± 0.00	0.003± 0.005	0.005± 0.005	0.008± 0.007	0.017± 0.007	0.014± 0.005	0.018± 0.005	0.025± 0.005
TBS	0.00± 0.00	0.00± 0.00	0.00± 0.00	0.00± 0.00	0.00± 0.00	0.00± 0.00	0.00± 0.00	0.00± 0.00
Ultrapure water	100.00± 0.00	100.00± 0.00	100.00± 0.00	100.00± 0.00	100.00± 0.00	100.00± 0.00	100.00± 0.00	100.00± 0.00

speculated that this peptide, Lc1687, obtained from *L. crocea*, is a relatively stable and safe antimicrobial agent for fish.

In summary, in this study, we screened a novel anionic amphiphilic α-helical peptide, Lc1687, *via* a *B. subtilis* system. Lc1687 is derived from *L. crocea* Ferritin H and exhibits forceful bactericidal and parasiticidal activities, as well as neglectable toxicity to fish. Moreover, Lc1687 has stable antibacterial activity against Gram+ and Gram- bacteria over a wide range of temperatures, pH, and UV radiation time. The functional mechanism of Lc1687 involves destroying the bacterial cell wall and cell membrane. The potent activities endow Lc1687 with promising clinical application prospects against bacterial and parasite infections in fish. Based on these distinctive features, future research will mainly focus on more detailed functional mechanisms and *in-vivo* experiment verification.

Data availability statement

The datasets presented in this study can be found in online repositories. The names of the repository/repositories and accession number(s) can be found in the article/Supplementary material.

Ethics statement

All experiments were carried out following the principles and protocols of the Animal Care and Use Committee of Fisheries College, Jimei University, China.

Author contributions

Conceptualization, experimental design, and project administration: DZ and MC; methodology: MC, NL, and XT; supervision: ZW and DZ; writing of the original draft: MC writing—review and editing: XL and DZ. All authors have read and agreed to the published version of the manuscript.

Funding

This work was supported by the National Natural Science Foundation of China (32172964), key projects of the Fujian Provincial Natural Science Foundation (2022J02042).

Conflict of interest

The authors declare that the research was conducted in the absence of any commercial or financial relationships that could be construed as a potential conflict of interest.

Publisher's note

All claims expressed in this article are solely those of the authors and do not necessarily represent those of their affiliated organizations, or those of the publisher, the editors and the reviewers. Any product that may be evaluated in this article, or claim that may be made by its manufacturer, is not guaranteed or endorsed by the publisher.

Supplementary material

The Supplementary Material for this article can be found online at: https://www.frontiersin.org/articles/10.3389/fimmu.2023.1168517/full#supplementary-material

References

1. Wang JH, Lu J, Zhang YX, Wu J, Luo Y, Liu H. Metagenomic analysis of antibiotic resistance genes in coastal industrial mariculture systems. *Bioresour Technol* (2018) 253:235–43. doi: 10.1016/j.biortech.2018.01.035

2. Wang JH, Lu J, Wu J, Zhang Y, Zhang C. Proliferation of antibiotic resistance genes in coastal recirculating mariculture system. *Environ pollut* (2019) 248:462–70. doi: 10.1016/j.envpol.2019.02.062

3. Chung CR, Kuo TR, Wu LC, Lee TY, Horng JT. Characterization and identification of antimicrobial peptides with different functional activities. *Brief Bioinform* (2019) 21(3):1098–114. doi: 10.1093/bib/bbz043

4. Kumar P, Kizhakkedathu JN, Straus SK. Antimicrobial peptides: diversity, mechanism of action and strategies to improve the activity and biocompatibility. *vivo. Biomol.* (2018) 8(1):4. doi: 10.3390/biom8010004

5. Zhang R, Xu L, Dong C. Antimicrobial peptides: an overview of their structure, function and mechanism of action. *Protein Pept Lett* (2022) 29:641–50. doi: 10.2174/0929866529666220613102145

6. Le CF, Fang CM, Sekaran SD. Intracellular targeting mechanisms by antimicrobial peptides. *Antimicrob Agents Chemother* (2017) 61. doi: 10.1128/AAC.02340-16

7. Luo Y, Song Y. Mechanism of antimicrobial peptides: antimicrobial, anti-inflammatory and antibiofilm activities. *Int J Mol Sci* (2021) 22:11401. doi: 10.3390/ijms222111401

8. Noga EJ, Ullal AJ, Corrales J, Fernandes JM. Application of antimicrobial polypeptide host defenses to aquaculture: exploitation of downregulation and upregulation responses. *Comp Biochem Physiol Part D Genomics Proteomics* (2011) 6:44–54. doi: 10.1016/j.cbd.2010.06.001

9. Hu Z, Zhang C, Sifuentes-Dominguez L, Zarek CM, Propheter DC, Kuang Z, et al. Small proline-rich protein 2A is a gut bactericidal protein deployed during *Helminth* infection. *Science* (2021) 374:e6723. doi: 10.1126/science.abe6723

10. Lin Q, Fu Q, Chen D, Yu B, Luo Y, Huang Z, et al. Functional characterization of *Porcine* NK-lysin: a novel immunomodulator that regulates intestinal inflammatory response. *Molecules* (2021) 26(14):4242. doi: 10.3390/molecules26144242

11. Yu G, Baeder DY, Regoes RR, Rolff J. Combination effects of antimicrobial peptides. *Antimicrob Agents Chemother* (2016) 60:1717–24. doi: 10.1128/AAC.02434-15

12. Li Q, Yu S, Han J, Wu J, You L, Shi X, et al. Synergistic antibacterial activity and mechanism of action of nisin/carvacrol combination against *Staphylococcus aureus* and their application in the infecting pasteurized milk. *Food Chem* (2022) 380:132009. doi: 10.1016/j.foodchem.2021.132009

13. Ormondes DFJ, Resende FA, Cardoso KA, Berto RT, Dias SC. Synergistic activity and immunomodulatory potential of levofloxacin and synoeca-MP peptide against multi-resistant strains of *Klebsiella pneumoniae*. *Microb Pathog* (2022) 163:105403. doi: 10.1016/j.micpath.2022.105403

14. Zhang DL, Guan RZ, Huang WS, Xiong J. Isolation and characterization of a novel antibacterial peptide derived from hemoglobin alpha in the liver of Japanese eel. *Anguilla japonica. Fish Shellfish Immunol* (2013) 35:625–31. doi: 10.1016/j.fsi.2012

15. Yi Y, You X, Bian C, Chen S, Lv Z, Qiu L, et al. High-throughput identification of antimicrobial peptides from *Amphibious mudskippers*. *Mar Drugs* (2017) 15(11):364. doi: 10.3390/md15110364

16. Zhang ZX, Wang ZY, Fang M, Ye K, Tang X, Zhang DL. Genome-wide association analysis on host resistance against the rotten body disease in a naturally infected population of large yellow croaker. *Larimichthys crocea.* Aquaculture(2022) 548. doi: 10.1016/j.aquaculture.2021.737615

17. Tang X, Wang Z, Jiang D, Chen M, Zhang D. Expression profile, subcellular localization of MARCH4 and transcriptome analysis of its potential regulatory signaling pathway in large yellow croaker (*Larimichthys crocea*). *Fish Shellfish Immunol* (2022) 130:273–82. doi: 10.1016/j.fsi.2022.09.017

18. Abbas H, Xiang J, Ahmad Z, Wang L, Dong W. Enhanced *Nicotiana benthamiana* immune responses caused by heterologous plant genes from *Pinellia ternata*. *BMC Plant Biol* (2018) 18:357. doi: 10.1186/s12870-018-1598-5

19. Wu J, Abbas H, Li J, Yuan Y, Liu Y, Wang G, et al. Cell membrane-interrupting antimicrobial peptides from *Isatis indigotica* fortune isolated by a *Bacillus subtilis* expression system. *Biomolecules* (2019) 10(1):30. doi: 10.3390/biom10010030

20. Arosio P, Ingrassia R, Cavadini P. Ferritins: a family of molecules for iron storage, antioxidation and more. *Biochim Biophys Acta* (2009) 1790:589–99. doi: 10.1016/j.bbagen.2008.09.004

21. Zheng L, Liu Z, Wu B, Dong Y, Zhou L, Tian J, et al. Ferritin has an important immune function in the ark shell. *Scapharca broughtonii. Dev Comp Immunol* (2016) 59:15–24. doi: 10.1016/j.dci.2015.12.010

22. Jung S, Kim MJ, Lim C, Elvitigala D, Lee J. Molecular insights into two ferritin subunits from red-lip mullet (*Liza haematocheila*): detectable antibacterial activity with its expressional response against immune stimulants. *Gene* (2023) 851:146923. doi: 10.1016/j.gene.2022.146923

23. Ding Z, Zhao X, Zhan Q, Cui L, Sun Q, Wang W, et al. Comparative analysis of two ferritin subunits from blunt snout bream (*Megalobrama amblycephala*): characterization, expression, iron depriving and bacteriostatic activity. *Fish Shellfish Immunol* (2017) 66:411–22. doi: 10.1016/j.fsi.2017.05.032

24. Yang H, Liu Z, Jiang Q, Xu J, An Z, Zhang Y, et al. A novel *ferritin* gene from *Procambarus clarkii* involved in the immune defense against aeromonas hydrophila infection and inhibits WSSV replication. *Fish Shellfish Immunol* (2019) 86:882–91. doi: 10.1016/j.fsi.2018.12.022

25. Harris F, Dennison SR, Phoenix DA. Anionic antimicrobial peptides from eukaryotic organisms. *Curr Protein Pept Sci* (2009) 10:585–606. doi: 10.2174/138920309789630589

26. Dennison SR, Harris F, Mura M, Phoenix DA. An atlas of anionic antimicrobial peptides from. *Amphibians. Curr Protein Pept Sci* (2018) 19:823–38. doi: 10.2174/1389203719666180226155035

27. Paulmann M, Arnold T, Linke D, Ozdirekcan S, Kopp A, Gutsmann T, et al. Structure-activity analysis of the dermcidin-derived peptide DCD-1L, an anionic antimicrobial peptide present in human sweat. *J Biol Chem* (2012) 287:8434–43. doi: 10.1074/jbc.M111.332270

728. Dashper SG, Liu SW, Reynolds EC. Antimicrobial peptides and their potential as oral therapeutic agents. *Int J Pept Res Ther* (2007) 13:505–16. doi: 10.1007/s10989-007-9094-z

29. Lai R, Liu H, Hui LW, Zhang Y. An anionic antimicrobial peptide from toad *Bombina maxima*. *Biochem Biophys Res Commun* (2002) 295:796–99. doi: 10.1016/s0006-291x(02)00762-3

30. Li S, Wang M, Chen S, Ampomah-Wireko M, Gao C, Xia Z, et al. Development of biaromatic core-linked antimicrobial peptide mimics: substituent position significantly affects antibacterial activity and hemolytic toxicity. *Eur J Med Chem* (2023) 247:115029. doi: 10.1016/j.ejmech.2022.115029

31. Xiao X, Lu H, Zhu W, Zhang Y, Huo X, Yang C, et al. A novel antimicrobial peptide derived from bony fish IFN1 exerts potent antimicrobial and anti-inflammatory activity in mammals. *Microbiol Spectr* (2022) 10:e201321. doi: 10.1128/spectrum.02013-21

Frontiers in Immunology

Explores novel approaches and diagnoses to treat immune disorders.

The official journal of the International Union of Immunological Societies (IUIS) and the most cited in its field, leading the way for research across basic, translational and clinical immunology.

Discover the latest Research Topics

See more →

Frontiers

Avenue du Tribunal-Fédéral 34
1005 Lausanne, Switzerland
frontiersin.org

Contact us

+41 (0)21 510 17 00
frontiersin.org/about/contact